AECOM STi

Sonoma Technology, Inc.

Air Quality Research and Innovative Solutions

Environment

Utah Air Resource Management Strategy Modeling Project: Air Quality Model Performance Evaluation

AECOM

1601 Prospect Pkwy
Fort Collins, CO 80525

970.493.8878   tel
970.493.0213   fax

March 3, 2014

Leonard Herr
BLM Utah State Office
440 West 200 South, Suite 500
Salt Lake City, UT 84101

**Subject: Final Utah Air Resource Management Strategy Modeling Project: Air Quality Model
Performance Evaluation Report**

Dear Mr. Herr:

AECOM Technical Services, Inc. (AECOM) and Sonoma Technology, Inc. are pleased to submit the
final *Utah Air Resource Management Strategy Modeling Project: Air Quality Model Performance
Evaluation* (the ARMS Air Quality MPE). The ARMS Air Quality MPE Report describes the
performance of the air quality model that could be used as a reusable modeling framework for the
Utah Bureau of Land Management's (BLM) Air Resource Management Strategy (ARMS). The primary
objective of the ARMS Modeling Project is to develop an air quality management tool that is
appropriate to assess the potential air impacts from future activities occurring on BLM-administered
land in the Uinta Basin. The reusable modeling framework developed as part of the ARMS Modeling
Project also could be used to assess the potential cumulative impacts from future project-specific
NEPA actions, which will facilitate consistency and efficiency with the planning activities in the area.

Enclosed with this letter is an electronic copy of the final ARMS Air Quality MPE Report, in Adobe
format (PDF) which was developed based on input from the Resource Technical Advisory Group
(RTAG). Comments received from RTAG on the draft ARMS Air Quality MPE Report and the
responses are also included with this transmittal.

 If you have any questions relative to this report, or would like to discuss this study, please contact
Courtney Taylor (Courtney.Taylor@aecom.com) or call (970) 493-8878.

Yours sincerely,

Courtney Taylor
Project Manager
Courtney.Taylor@aecom.com

cc: Stephen Reid
     Chao-Jung Chien
     Kenneth Craig
     Marco Rodriguez
     Caitlin Shaw
     Tiffany Samuelson

Executive Summary

This report presents the Air Quality Model Performance Evaluation (MPE) for the Bureau of Land Management (BLM) Utah State Office's Air Resource Management Strategy (ARMS) Modeling Project. The ARMS Modeling Project is one of several studies that will inform and support the Utah BLM's air management strategy. As part of the ARMS, the Utah BLM, together with other state and federal agencies, has commissioned several studies to further understand and analyze current ambient air and meteorological conditions in the Uinta Basin, and to develop emissions inventories appropriate for ozone modeling applications. These studies include special monitoring studies (Energy Dynamics Laboratory 2011; Utah Department of Environmental Quality 2011) and an emissions inventory development study (AECOM 2013). The results of these studies are being used in the ARMS Modeling Project and are essential to the overall understanding of the issues affecting air quality in the Uinta Basin.

The ARMS Modeling Project is being conducted by AECOM, Inc., dba AECOM Environment (AECOM) and Sonoma Technology, Incorporated (STI) under the direction of the Utah BLM. This report is one of several documents that are being developed for the ARMS Modeling Project, including a modeling protocol, MPEs for the meteorological model and the air quality model, an emissions inventory report, and a final report documenting model-predicted future air quality impacts. The ARMS Modeling Project is not a project-specific National Environmental Policy Act (NEPA) analysis, and the modeling files and reports are not NEPA products. It also is not a policy study, analysis of regulatory actions, or an analysis of the impacts of project-specific development. Rather, the ARMS Modeling Project is a cumulative assessment of potential future air quality impacts associated with predicted oil and gas activity in the Uinta Basin. The ARMS Modeling Project will provide data, models, and estimates of future air quality impacts to facilitate BLM's future NEPA and land use planning efforts.

As described in the Protocol (AECOM 2012), a Photochemical Grid Modeling (PGM) system was used to assess base year (2010) conditions. Given the complexity and emerging understanding of wintertime ozone formation, the Utah Air Resource Technical Advisory Group (RTAG) advised the Utah BLM to investigate two state-of-the-science PGM systems in an attempt to replicate the winter ozone events and to assess cumulative impacts to air quality and air quality-related values (AQRVs) during the rest of the year. The two PGM models selected for evaluation were the: 1) Community Multi-Scale Air Quality (CMAQ) modeling system; and 2) Comprehensive Air Quality Model with Extensions (CAMx). Both CMAQ and CAMx have been run and evaluated as documented in this report. Based on evaluation and intercomparison of the models' performance, the CMAQ model is recommended for assessment of future impacts in the Uinta Basin. This recommendation is driven primarily by the fact that the CMAQ model was able to replicate wintertime ozone formation and timing in the Uinta Basin better than the CAMx model. Also CMAQ provided slightly better performance for total particulate matter with an aerodynamic diameter less than or equal to 2.5 microns ($PM_{2.5}$) in the Uinta Basin during wintertime, as well as better performance domain-wide for ozone and wet deposition.

The CMAQ and CAMx models were configured for the ARMS Modeling Project following the methods and approach detailed in the Utah Air Resource Management Strategy Air Quality Modeling and Assessment Protocol (AECOM 2012). The air quality modeling domains include a coarse domain centered on the continental United States (U.S.) at a 36-kilometer (km) horizontal grid resolution and two refined domains of 12-km and 4-km grid resolutions focused on the area of interest. The vertical grid is composed of 36 layers with thinner (more) layers in the planetary boundary layer (PBL). Thinner model layers lower in the atmosphere, within the PBL, are better able to capture boundary layer characteristics for the transport and diffusion of emitted pollutants, which is important for air quality modeling, particularly during winter inversions. Key model configuration options for both CMAQ and CAMx used for the ARMS project are listed in **Table ES-1**.

The models' results were assessed relative to the monitored ambient air quality conditions in 2010. The model performance evaluation focuses primarily on ozone and speciated $PM_{2.5}$, with analysis of other pollutants and AQRV included to provide a broader understanding of model performance. The performance of both air quality models was evaluated using identical statistical and qualitative methods over a variety of temporal and spatial scales, including statistical summaries of performance, time series comparisons, review of spatial plots, scatter plots, and bugle plots. While all available monitoring data were used for evaluating annual and seasonal model performance, selected air pollution episodes that occurred in the Uinta Basin during 2010 were further analyzed with time series and spatial plots. Results were compared with benchmarks from the U.S. Environmental Protection Agency (USEPA), when appropriate.

A detailed model inter-comparison between CAMx and CMAQ was performed using a variety of statistical and graphical analyses. These analyses were examined to understand how both models performed relative to USEPA performance benchmarks, and to each other. The analyses covered all of the key gaseous and particulate pollutant species. Model performance was analyzed on a domain-wide basis for all three modeling domains, with special attention on the models' performance within the Uinta Basin in the 4-km domain.

For ozone, both models performed well on a domain-wide basis for all three modeling domains, with biases and errors well within USEPA recommended performance criteria for all months except December, when ozone monitoring data are limited. CMAQ biases were generally smaller in magnitude than in CAMx, except during the summer months in the 4-km domain. In the Uinta Basin, both models produced enhanced ozone concentrations during the observed winter ozone episodes. Although both models under-predicted peak daily ozone concentrations, CMAQ produced higher ozone concentrations and reproduced observed maximum concentrations better than CAMx when observed ozone concentrations were highest in the Uinta Basin.

For total $PM_{2.5}$, both models performed reasonably well on a domain-wide basis for all three modeling domains. For most months, biases and errors fell within USEPA recommended performance criteria. However, in the Uinta Basin, CMAQ produced significantly higher $PM_{2.5}$ concentrations and reproduced observed concentrations better than CAMx during the winter air quality episodes. For individual particulate species, model performance tendencies varied depending on domain, season, species, and monitoring network. For both models, performance metrics consistently fell within USEPA recommended performance criteria for sulfate (SO_4), nitrate (NO_3), and ammonium (NH_4), with CMAQ producing slightly smaller annual SO_4 biases than CAMx.

Based on the detailed model inter-comparison performed between CMAQ and CAMx, CMAQ is the recommended modeling system for the ARMS Modeling Platform. The CMAQ model performance is summarized below for applicable criteria air pollutants, as well as AQRVs for visibility and atmospheric deposition in order to provide an overview of the model errors and biases identified as part of this operational MPE.

In general, the model performance for ozone was acceptable and meets the USEPA-recommended performance goals for all modeling domains, monitoring networks and seasons on a domain-wide basis, as supported by the mean normalized bias (MNB) and mean normalized gross error (MNGE) model performance statistics for daily maximum 1-hour and daily maximum 8-hour average ozone with a 60 ppb threshold. While the daily maximum modeled concentrations compare well with the monitored daily maximum values, the MNB and MNGE values for the running 8-hour average ozone concentration (with the 60 parts per billion [ppb] threshold applied) generally are outside USEPA performance criteria, indicating that although the model reproduces peak concentrations well, the timing of the daily peaks differs from monitored peaks. Importantly, in the context of assessing peak concentrations for comparison with Ambient Air Quality Standards (AAQS), statistics computed from daily maximum 8-hour ozone concentration are most important for evaluating model performance and suitability.

Table ES-1   CMAQ and CAMX Air Quality Model Configurations for Base Case

Parameter	CMAQ	CAMx	Details
Model Version	CMAQ (v.5.0)	CAMx (v.5.40)	
Horizontal Grid Mesh	36-, 12-, and 4-km (see **Figure 2-1**)	36-, 12-, and 4-km (see **Figure 2-1**)	
Vertical Grid Mesh	36 layers	36 layers	Using Weather Research and Forecasting (WRF) layers with no collapsing
Grid Interaction	One-way nesting	36-km is run with one-way nesting and the 12-km and 4-km domains are run with two-way nesting	
Initial Conditions	15 days spin-up for the 36-km domain and 7 days of spin-up for the 12-km and 4-km nested domain	15 days spin-up for the 36-km domain and 7 days of spin-up for the 12-km and 4-km nested domains	Separately run four quarters of 2010
Boundary Conditions	2010 Goddard Earth Observing System-Chemical (GEOS-Chem) data is used as boundary conditions for the 36-km domain and each domain is extracted as boundary conditions for the finer resolution domain	2010 GEOS-Chem data is used as boundary conditions for the 36-km domain and the 36-km domain is extracted as boundary conditions for the 12-km and 4-km nested domains	2010 GEOS-Chem data is extracted for CMAQ and CMAQ BC data is processed to be compatible with CAMx
Meteorological Processor	Meteorology-Chemistry Interface Processor (MCIP) (v.4.0)	WRFCAMx (version 3.3)	For processing WRF meteorology
Emissions Processor	Sparse Matrix Operator Kernel Emissions (SMOKE) (v.3.0)	CMAQ2CAMx processor	CMAQ2CAMx converter tool converts CMAQ-ready emissions inputs to CAMx-ready format
Chemistry			
Gas Phase Chemistry	Carbon Bond V (CB05)-TU	CB6	CB05-TU is CB05 with updated toluene chemistry. Both mechanisms can use the same SMOKE output

Table ES-1   CMAQ and CAMX Air Quality Model Configurations for Base Case

Parameter	CMAQ	CAMx	Details
Aerosol Chemistry	AERO5 and ISORROPIA2.1	Secondary Organic Aerosol Formation/partitioning (SOAP) and Inorganic Aerosol Thermodynamics/Partitioning (ISORROPIA) 1.6 with static 2-mode coarse/fine size distribution.	
Cloud Chemistry	RADM-type aqueous chemistry	Regional Acid Deposition Model (RADM)-type aqueous chemistry	
Numerics			
Gas Phase Chemistry Solver	Euler Backward Iterative (EBI) solver on 36-km and 12-km domains;Rosenbrock solver on 4-km domain.	EBI solver	
Horizontal Advection	YAMO scheme	PPM scheme	
Vertical Advection	VWRF scheme	Implicit scheme with vertical velocity update	
Diffusion			
Horizontal Diffusion	Multiscale	K-theory 1st order closure with K_h grid size dependence	
Vertical Diffusion	Asymmetric Convective Model Version 2 (ACM2)	K-theory approach	$K_z\_min = 0.01$ m^2/s
Deposition			
Dry Deposition	CCTM in-line	Zhang scheme	
Wet Deposition	CMAQ-specific	CAMx-specific	Rain, snow, graupel
Integration Time Step	Wind speed dependent	Wind speed dependent	

The biases calculated when monitored values exceed 60 ppb show that the model generally under-predicts daily maximum 8-hour ozone concentrations, except during the summer and fall within the 4-km domain. While some measures of bias and error exceed the USEPA-recommended goals for the Air Quality System (AQS) monitoring network during winter months, modeled values relative to the Clean Air Status and Trends Network (CASTNet) network are almost always within the USEPA-recommended goals throughout the year.

Comparison of ozone modeling results with observations in the Uinta Basin shows the model is able to capture both episodic events and seasonal trends well, although the model consistently over-predicts ozone concentrations when observed values are below 30 ppb. Importantly, the model shows good agreement with periods of elevated winter ozone in the Uinta Basin, particularly relative to the Ouray monitor, which typically monitors the highest winter ozone concentrations in the basin. In general, the model is able to capture the observed diurnal variation, but tends to under-predict ozone peaks in winter and over-predict ozone peaks in summer. Given that the applicable AAQS and the tools used to predict future impacts are based on concentrations over 60 ppb, the model is considered to be suitable for assessment of both potential project-specific and cumulative ozone impacts. Importantly, any model biases for ozone are accounted for and minimized when the Model Attainment Test Software (MATS) tool is used in the assessment of future impacts.

In general, the model performs adequately for total $PM_{2.5}$ concentrations in most locations and seasons with a tendency to under-predict total $PM_{2.5}$ and particulate matter with an aerodynamic diameter less than or equal to 10 microns (PM_{10}) concentrations. For the 12- and 4-km domain, the model systematically shows the largest under-predictions during the summer months while it tends to slightly over-predict $PM_{2.5}$ concentrations during the winter months. The model performance for total $PM_{2.5}$ is generally within the USEPA-established performance criteria for most months, monitoring networks, and modeling domains. Although model $PM_{2.5}$ errors relative to hourly measurements often do not meet USEPA-established performance criteria, the model performance relative to daily measurements are more relevant for comparison to AAQS since the standards are for 24-hour or annual averaging periods. Given the good model performance for daily $PM_{2.5}$ relative to USEPA performance criteria, the model is considered suitable for cumulative $PM_{2.5}$ impact assessments.

The model predictions of total PM_{10} are under-predicted relative to observed concentrations for all modeling domains, time periods, and most monitoring networks except during the winter relative to Interagency Monitoring of Protected Visual Environments (IMPROVE) measurements. Seasonally, the model tends to be the most accurate in winter. The model performance for PM_{10} frequently is outside the USEPA-established performance criteria.

The overall performance for $PM_{2.5}$ and PM_{10} is related to the performance of their primary chemical constituents. There is variability in the model performance of these particulate matter (PM) components; notably, the model tends to over-predict SO_4, NH_4, and fine soil (SOIL) and tends to under-predict NO_3, organic carbon (OC), elemental carbon (EC), and carbon mass (CM) in the 4-km domain. It is important to note that model biases for each chemical compound are accounted for and minimized when the MATS tool is used for predicting future impacts to $PM_{2.5}$ (AECOM 2012).

Model performance for other gas-phase criteria pollutants was carefully analyzed to provide additional information for chemically related pollutants. Model results for oxides of nitrogen (NO_x) show reasonable performance for all modeling domains, monitoring networks and seasons on a domain-wide basis. On the 4-km domain, the model under-predicts NO_x in the winter and fall and over-predicts NO_x in the spring and summer. In the Uinta Basin during winter, the model consistently under-predicts NO_x concentrations although performance is better at the Ouray site than at Redwash. Given that the model was able to reproduce the observed diurnal cycle as well as the approximate magnitude of observed concentrations, the model is believed to be appropriate for ozone impact assessments. Model-predicted concentrations of short-term and annual nitrogen dioxide (NO_2) are not considered to be representative of maximum values, and a near-field modeling demonstration will be necessary for future site-specific analyses of potential impacts for comparison to applicable AAQS.

In general, the model tends to under-predict carbon monoxide (CO) concentrations throughout the year for all the modeling domains. Spatial plots of modeled CO concentrations over two periods of interest (POIs) indicated elevated CO concentrations in the Salt Lake City area and relatively low concentrations throughout the rest of the 4-km domain. Sparsely located monitors, however, indicate a general under-prediction of CO by the model throughout the 4-km domain. Model-predicted concentrations of cumulative CO are not considered to be representative of maximum values, and a near-field modeling demonstration will be necessary for future site-specific analyses of potential impacts for comparison to applicable AAQS.

The model shows no clear trend of under-prediction or over-prediction for sulfur dioxide (SO_2) concentrations relative to the AQS network, although the model systematically over-predicts SO_2 relative to CASTNet. The AQS monitors tend to be located in the Salt Lake City metropolitan area and therefore the statistical metrics based on the AQS network may not adequately represent SO_2 model performance throughout the entire 4-km domain or the Uinta Basin study area. The modeled spatial analysis indicated localized hotspots of SO_2 concentrations scattered throughout the 4-km domain that are likely attributable to emissions from electric-generating units. Model-predicted short-term cumulative SO_2 values are usually not considered to be representative of maximum values, and near-field modeling demonstrations will be necessary to assess the potential impacts of specific sites for comparison to applicable AAQS.

The model performed well for total light extinction (b_{ext}) in both the 12- and 4-km domains. The model-predicted annual average total b_{ext} values are fairly consistent with reconstructed annual average b_{ext}. Based on the mean b_{ext} and MFB, the model tends to slightly over-predict the extinction during the winter and under-predict b_{ext} for all other seasons. The overall model performance for visibility is influenced by the contributions from individual PM species. The largest errors in the b_{ext} due to individual species are due to sea salt (SS), followed by NO_3, CM, OC, SOIL, EC, and SO_4 in decreasing order. While the model was not able to reproduce maximum reconstructed b_{ext} values due to wildfire and wind-blown dust events, the model-predicted b_{ext} was similar to reconstructed b_{ext} during most seasons. The model is considered suitable for assessing visibility impacts for this study particularly since model biases for each chemical compound are accounted for and minimized by the MATS tool, which will be used for predicting future impacts to visibility.

The modeled deposition performance was assessed for wet deposition recognizing that dry deposition model performance also is important for assessing overall model performance. However, only wet deposition measurements are available for select species. In general, for the 12- and 4-km domains the model tends to over-predict SO_4 and NH_4 wet deposition for all three domains except in the fall and winter when it tends to under-predict the wet deposition of these ions. NO_3 wet deposition does not exhibit any particular seasonal trend for the bias that might indicate any systematic over- or under-prediction for its deposition values. Generally, on an annual basis for the 4-km domain, the model is able to capture the spatial patterns as well as the magnitude of the observed precipitation. Based on the spatial variability of the wet deposition performance, the model is considered suitable for assessing wet deposition impacts; however, since wet deposition impacts are only a portion of total deposition amounts, total modeled deposition results should be interpreted with care.

In summary, the CMAQ model is considered suitable for assessing the impacts on certain pollutants (O_3, $PM_{2.5}$, regional haze [visibility], deposition). The model performance for these species typically was within the USEPA-recommended performance criteria. As part of ARMS future year impacts assessment, all results will be reported and qualified based on the findings described in this MPE.

Acronyms and Abbreviations

AAQS	Ambient Air Quality Standards
ACM2	Asymmetric Convective Model version 2
agl	above ground level
AQRVs	air quality-related values
AQS	Air Quality System
ARMS	Air Resource Management Strategy
b_{ext}	light extinction coefficient
BLM	Bureau of Land Management
BMP	Best Management Practices
CAMx	Comprehensive Air Quality Model with Extensions
CASTNet	Clean Air Status and Trends Network
CB05	Carbon Bond V
CM	carbon mass
CMAQ	Community Multi-scale Air Quality
CO	carbon monoxide
°	degrees
EA	environmental assessment
EBI	Euler Backward Iterative
EC	elemental carbon
EGU	electric generating unit
EIS	environmental impact statement
FB	fractional bias
f(RH)	relative humidity adjustment factor
g/ha/day	grams per hectare per day
GEOS-Chem	Goddard Earth Observing System-Chemical
HNO_3	nitric acid
IC/BC	initial conditions and boundary conditions
IMPROVE	Interagency Monitoring of Protected Visual Environments
ISORROPIA	Inorganic Aerosol Thermodynamics/Partitioning
°K	degrees Kelvin
kg/ha	kilogram per hectare
K_h	eddy diffusivity for heat
km	kilometer
Kv	coefficient of vertical eddy diffusion

LCC	Lambert Conformal Conic
LDT	Local Daylight Time
Ln[p]	natural log-pressure
lpm	liters per minute
LST	Local Standard Time
m^2/s	square meters per second
MATS	Modeled Attainment Test Software
mb	millibar
MCIP	Meteorology-Chemistry Interface Processor
MDT	Mountain Daylight Time
MFB	mean fractional bias
MFGE	mean fractional gross error
$\mu g/m^3$	micrograms per cubic meter
Mm^{-1}	inverse megameters
MNB	mean normalized bias
MNGE	mean normalized gross error
MOU	Memorandum of Understanding
MPE	model performance evaluation
MPES	Model Performance Evaluation Software
MST	Mountain Standard Time
MYJ	Mellor, Yamada, and Janic
NAAQS	National Ambient Air Quality Standard
NADP	National Atmospheric Deposition Program
NASA	National Aeronautics and Space Administration
NCDC	National Climate Data Center
NEPA	National Environmental Policy Act
NH_3	ammonia
NH_4	ammonium
NMB	normalized mean bias
NME	normalized mean error
NO	nitrogen oxide
NO_2	nitrogen dioxide
NO_3	nitrate
NO_X	oxides of nitrogen
NOAA	National Oceanic and Atmospheric Administration
NP	National Park

NPS	National Park Service
NTN	National Trends Network
O_3	ozone
OC	organic carbon
PAMS	Photochemical Assessment Monitoring Stations
PBL	planetary boundary layer
PGM	photochemical grid model
PIXE	particle-induced x-ray
PM	particulate matter
PM_{10}	particulate matter with an aerodynamic diameter less than or equal to 10 microns
$PM_{2.5}$	particulate matter with an aerodynamic diameter less than or equal to 2.5 microns
POI	periods of interest
ppb	parts per billion
ppbv	parts per billion by volume
ppm	parts per million
ppmv	parts per million by volume
RADM	Regional Acid Deposition Model
RPO	Regional Planning Organization
RTAG	Resource Technical Advisory Group
SMOKE	Sparse Matrix Operator Kernel Emissions
SOAP	Secondary Organic Aerosol Formation/partitioning
SO_2	sulfur dioxide
SO_4	sulfate
SS	sea salt
STI	Sonoma Technology, Incorporated
STN	Speciation Trends Network
TUV	total ultraviolet
UGRB	Upper Green River Basin
U.S.	United States
USEPA	United States Environmental Protection Agency
USGS	United States Geological Survey
UTC	Coordinated Universal Time
UV	ultraviolet
VOC	volatile organic compound
WA	wilderness area
WRAP	Western Regional Air Partnership

WRF   Weather Research and Forecasting

XRF   x-ray flourescence

Contents

List of Appendices

Appendix A – Model Sensitivity Tests

Appendix B – CAMx Model Performance Evaluation

List of Tables

List of Figures

1.0   Introduction

This report presents the Air Quality Model Performance Evaluation (MPE) for the Bureau of Land Management (BLM) Utah State Office's Air Resource Management Strategy (ARMS) Modeling Project. The ARMS Modeling Project is one of several studies that will inform and support the Utah BLM's air management strategy. As part of the ARMS, the Utah BLM, together with other state and federal agencies, has commissioned several studies to further understand and analyze current ambient air and meteorological conditions in the Uinta Basin, and to develop emissions inventories appropriate for ozone modeling applications. These studies include special monitoring studies (Energy Dynamics Laboratory [EDL] 2011, Utah Department of Environmental Quality [UDEQ] 2011) and an emissions inventory development study (AECOM 2013). The results of these studies are being used in the ARMS Modeling Project and are essential to the overall understanding of the issues affecting air quality in the Uinta Basin.

The ARMS Modeling Project is being conducted by AECOM, Inc., dba AECOM Environment (AECOM) and Sonoma Technology, Incorporated (STI) under the direction of the Utah BLM. This report is one of several documents that will be developed for the ARMS Modeling Project, including a modeling protocol, MPEs for both the meteorological model and the air quality model, an emissions inventory report, and a final report of predicted future air quality impacts.

1.1   Study Background

The BLM is required to complete a National Environmental Policy Act (NEPA) analysis (environmental impact statement [EIS] or environmental assessment [EA]) for each proposed project that would occur on BLM-administered federal land. In the recent past, there has been concern about the methods used to assess potential air quality impacts and air quality related values (AQRVs) associated with proposed oil and gas projects. This concern has lead to several procedural changes including the establishment of the national-level June 2011 Memorandum of Understanding (MOU), referred to hereafter as the National MOU, and the Utah-specific ARMS project. It is important to note that the National MOU and the ARMS Modeling Project have different objectives. The National MOU is a guidance document for multiple federal agencies to design and execute a consistent and efficient air quality analysis for a specific NEPA action. On the other hand, the ARMS is designed to develop a reusable air management tool applicable to multiple projects for activities in the Uinta Basin, an area in northeastern Utah that is projected to have extensive development of oil and gas reserves in the foreseeable future (shown in **Figure 1-1**). The ARMS modeling framework also could be used to assess the potential cumulative impacts associated with future project-specific NEPA actions, which will facilitate consistency and efficiency with the planning activities in the area. .

The Utah BLM established the Utah Air Resource Technical Advisory Group (RTAG) to provide a forum to discuss and review the results of the BLM-funded studies aimed at understanding air quality issues in Utah. RTAG participation and review supports the goals of the National MOU, including collaboration and transparency among multiple federal agencies. The ARMS Modeling Project also supports the goals of the National MOU by developing a Reusable Modeling Framework, which, in this case, is being developed for the Uinta Basin. It is expected that future NEPA actions could be evaluated with the reusable modeling framework developed by this study.

While the procedures described in the National MOU will be followed, as appropriate, during the ARMS Modeling Project, it is important to note that this particular study is not a project-specific NEPA analysis, and the modeling files and reports are not NEPA products. It also is not a policy study, analysis of regulatory actions, or an analysis of the impacts of project-specific development. Rather, the ARMS Modeling Project is a cumulative assessment of potential future air quality impact associated with predicted oil and gas activity in the Uinta Basin. The ARMS Modeling Project will provide data, models,

Legend

- City
- Study Area
- County Boundary
- BLM Field Office Boundary
- Bureau of Land Management (BLM)
- BLM Wilderness Area
- US Forest Service (USFS)
- USFS Wilderness Area
- National Park Service (NPS)
- US Fish & Wildlife (USFW) National Wildlife Refuge
- Indian Reservation (IR)
- Military Reservations and Corps of Engineers
- State
- State Parks and Recreation
- State Wildlife Reserve/Management Area
- Private
- Bankhead-Jones Land Use Lands
- Water

WYOMING

SALT LAKE F.O.

SUMMIT

DAGGETT

LITTLE SNAKE F.O.

WASATCH

MOFFAT

DUCHESNE

Vernal

UTAH

VERNAL F.O.

COLORADO

UTAH

WHITE RIVER F.O.

UINTAH

RIO BLANCO

CARBON

PRICE F.O.

EMERY

GRAND GARFIELD
MOAB F.O.
JUNCTION F.O.

0 4 8 16 24 32
Kilometers

N
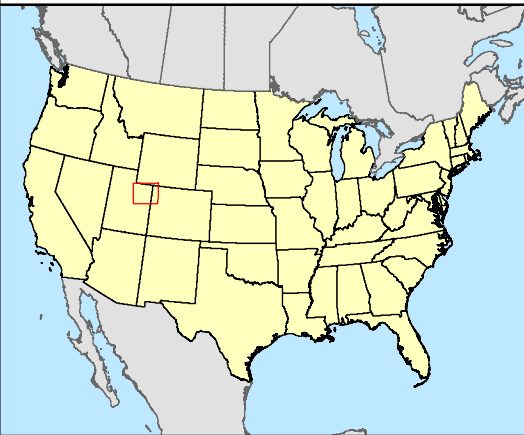
ARMS Modeling Project

**Figure 1-1
Uinta Basin
Study Area**

X:\0Projects\BLM_UTSO_ARMS_60225687\Figures\protocol\Fig_1-2_ARMS_Study_Area.mxd

and estimates of future air quality impacts to facilitate BLM's future NEPA and land use planning efforts. Therefore, the National MOU guidance applicable to project-specific emissions, impacts, and analyses will not be required as part of this study. However, while the ARMS Modeling Project is not a project-specific NEPA analysis, it may result in specific mitigation measures or Best Management Practices (BMP) applicable to future NEPA actions.

One of the main air quality concerns related to continued development of oil and gas reserves in the Uinta Basin is the elevated ozone levels measured during winter. Several winter episodes of elevated 8-hour ozone concentrations have been measured in the Uinta Basin since monitoring began in 2009. Observations of elevated winter ozone concentrations initially were detected in the winter of 2005 in the Upper Green River Basin (UGRB) in Wyoming, another area with significant oil and gas development. Since then multiple ambient air monitoring studies have been conducted in the UGRB in Wyoming and in the Uinta Basin in Utah. During the winter of 2011, maximum 8-hour average ozone concentrations in the Uinta Basin exceeded 130 ppb, which is well above the United States (U.S.) Environmental Protection Agency's (USEPA) National Ambient Air Quality Standard (NAAQS) for 8-hour average ozone concentrations of 75 parts per billion (ppb).[1] These episodes of elevated ozone concentrations typically occur in the late winter and early spring, but sustained ozone concentrations above natural background are evident in these areas during summer conditions, as well.

While continued winter monitoring studies are on-going in the Uinta Basin, air quality assessment tools are currently under development. Given the complexity and emerging understanding of wintertime ozone formation, RTAG advised the Utah BLM to investigate two state-of-the-science Photochemical Grid Modeling (PGM) systems in an attempt to replicate the winter ozone events and to assess cumulative impacts to air quality and AQRVs during the rest of the year. The two PGM models selected for evaluation are the: 1) the Community Multi-Scale Air Quality (CMAQ) modeling system; and 2) the Comprehensive Air Quality Model with Extensions (CAMx). In keeping with RTAG recommendations, both CMAQ and CAMx have been run and evaluated as documented in this report. Based on evaluation and intercomparison of the models' performance, the CMAQ model is recommended for assessment of future impacts in the Uinta Basin. Of particular importance for this recommendation, the CMAQ model is able to replicate wintertime ozone formation and timing in the Uinta Basin.

1.2   Organization of the ARMS Modeling Project Documents

As described in the Protocol (AECOM 2012), a photochemical grid modeling system is used to assess base year (2010) conditions and projected future cumulative air quality impacts. The modeling system is composed of three primary models:

- The Weather Research and Forecast (WRF) meteorological model is a state-of-science mesoscale numerical weather prediction system, which develops a four-dimensional meteorological data grid capable of supporting urban- and regional-scale photochemical, fine particulate, and regional haze regulatory modeling studies.

- The Sparse Matrix Operating Kernel Emissions (SMOKE) model is an emissions processing system that generates hourly, gridded, and speciated emissions inputs for photochemical grid models. These inputs include emissions from mobile, non-road, area, point, fire, and biogenic sources.

---

[1] It is important to note that the official form of the 8-hour ozone NAAQS is the annual fourth-highest daily maximum 8-hour ozone concentration averaged over 3 years cannot exceed 75 ppb. Three full years of ozone monitoring data have not yet been collected in the Uinta Basin as of the writing of this report, and therefore the reported 8-hour average concentrations are not directly comparable to the form of the USEPA NAAQS.

- The photochemical grid model (PGM) is a state-of-science 'One-Atmosphere' air quality model capable of addressing ozone and other criteria pollutants, visibility, and acid deposition at the regional and urban scale. As described above, two PGMs were run and evaluated for the base year: CMAQ and CAMx.

Details regarding the modeling approach and analysis techniques for the air quality impact analyses are presented in the Protocol (AECOM 2012).

Following the Protocol (AECOM 2012), the performance of the meteorological model (WRF) was evaluated as documented in the Utah ARMS Meteorological Model Performance Evaluation Report (AECOM and STI 2013). This document describes the WRF model configuration, meteorological results, and performance of the model relative to measured meteorological parameters in base year 2010. The results of the WRF model are being used in the air quality model for transport of pollutants, chemical reactions, and removal processes.

The Utah State BLM Emissions Inventory Technical Support Document (AECOM 2013a) documents the emissions inventory developed for the ARMS Modeling Project. It details the input data, processing methods, and resulting emissions for the base year (2010), as well as the future year (2021) emissions inventories. The 2010 emissions inventory is used in conjunction with the WRF results to run the 2010 air quality model simulation.

This Air Quality MPE report documents the air quality model configuration, results, and performance of the air quality models relative to measured air quality data in base year 2010. The purpose of this report is discussed further in Section 1.3.

Following the assessment of the suitability of the air quality model, as documented in this report, the air quality model results will be summarized in tables and graphical displays in the final report. The final report will summarize the results of the modeled base year (2010) and predicted cumulative future year (2021) air quality conditions.

1.3   Purpose of the Air Quality MPE

The CMAQ and CAMx models were configured for the ARMS Modeling Project, and the models' results were assessed relative to the monitored ambient air quality conditions in 2010. The model performance evaluation focuses primarily on ozone and speciated $PM_{2.5}$, with analysis of other pollutants and air quality related values (AQRV) included to provide a broader understanding of model performance.

The performance of both air quality models were evaluated using identical statistical and qualitative methods over a variety of temporal and spatial scales. While all available monitoring data were used for evaluating annual and seasonal model performance, selected air pollution episodes that occurred in the Uinta Basin during 2010 were further analyzed with time series and spatial plots. These periods of interest (POI) include:

- POI 1: January 8-January 23 (elevated ozone and $PM_{2.5}$);
- POI 2: February 21-March 8 (elevated ozone);
- POI 3: August 19-August 29 (elevated ozone and $PM_{2.5}$); and
- POI 4: September 27-October 5 (elevated $PM_{2.5}$).

The MPE includes evaluation of both model results over various spatial extents, but the analyses focus on the Uinta Basin study area when monitoring data is available.

The models' statistical results are compared with recommended benchmarks developed for photochemical grid models. Altogether this information is used to provide an assessment of the model

performance, magnitude of the errors and biases, and associated limitations. Based on this, the preferred model is recommended and model limitations are documented for the assessment of future year air impacts.

1.4   Organization of the Air Quality MPE Report

Chapter 2.0 of this report describes the PGM modeling systems, identifies the modeling domains, and outlines the models' configuration and input datasets used for the study. Chapter 3.0 describes the MPE process, statistical metrics, and tools used to conduct the MPE. Chapter 4.0 presents the results of the model simulations, compares the model results to observed measurements, and inter-compares the performance of both models. Chapter 5.0 summarizes the results and provides an assessment of model limitations. **Appendix A** presents the results of two sensitivity tests. While results from all model performance analyses are synthesized in Chapter 4.0, additional data for the CAMx model results are provided in **Appendix B**.

2.0   Air Quality Model

2.1   Air Quality Model Overview

One of the primary objectives of this study is to conduct a detailed performance evaluation of the USEPA's CMAQ (Byun and Ching 1999) and ENVIRON Corporation's CAMx (ENVIRON 2011) photochemical grid models for the period of January 1 to December 31, 2010. Both models are capable of assessing a variety of air quality metrics, including ozone, particulate matter, visibility, and atmospheric deposition. While the model performance for all these metrics is assessed for this study, the primary pollutant of concern in the Uinta Basin is ozone (for both summer and winter).

Ozone is a secondary pollutant formed through the photochemical reactions of NO_X, VOC, and sunlight. The precursors to ozone (VOC and NO_X) are emitted into the atmosphere by anthropogenic (man-made), geogenic (natural geologically occurring), and biogenic (natural biologically occurring) sources. In general, ozone concentrations fluctuate as a function of multiple factors: 1) pollution released by local emissions sources; 2) meteorological influences on transport and diffusion; 3) photochemistry and photolysis rates; 4) deposition of ozone and its precursors; and 5) transport of ozone and precursor emissions from upwind areas.

Parameterization of these important chemical and physical processes is incorporated, to varying degrees, in photochemical grid models such as CMAQ and CAMx. Although many of the same science options are generally available in both CMAQ and CAMx, each model implements the parameterizations differently. It is important to leverage each model's unique capabilities to obtain the best possible performance. Therefore, the models and their preprocessors are not always configured to be the same; rather, the models and input data are developed to enhance performance given the current understanding of the science and each model's strengths.

2.2   Modeling Domains

The air quality modeling domains include a coarse domain centered on the continental U.S. at a 36-km horizontal grid resolution and two refined domains of 12-km and 4-km grid resolutions focused on the area of interest. **Figure 2-1** shows the nested modeling domains for CMAQ and CAMx relative to the WRF meteorological model.

All modeling domains use the standard map projection from the Regional Planning Organization (RPO) unified grid, which was used by the Western Regional Air Partnership (WRAP) in its prior analyses. The RPO unified grid consists of a Lambert Conformal Conic (LCC) map projection using the map projection parameters listed in **Table 2-1**. A complete description of the model domains is provided in **Table 2-2**.

The vertical grid is composed of 36 layers with thinner (more) layers in the planetary boundary layer (PBL). Thinner model layers lower in the atmosphere, within the PBL, are better able to capture boundary layer characteristics for the transport and diffusion of emitted pollutants, which is important for air quality modeling, particularly during winter inversions. The layer structure is summarized in **Table 2-3**. The altitudes above sea level are estimated according to standard atmosphere assumptions.[1]

---

[1] Standard equations and assumptions include: surface pressure of 1,000 mb, model top at 100 mb, surface temperature of 275 degrees Kelvin (°K), and lapse rate of 50°K/ natural log-pressure (ln[p]).

Figure 2-1
Air Quality and WRF
Modeling Domains
4-km, 12-km, and 36-km

ARMS Modeling Project
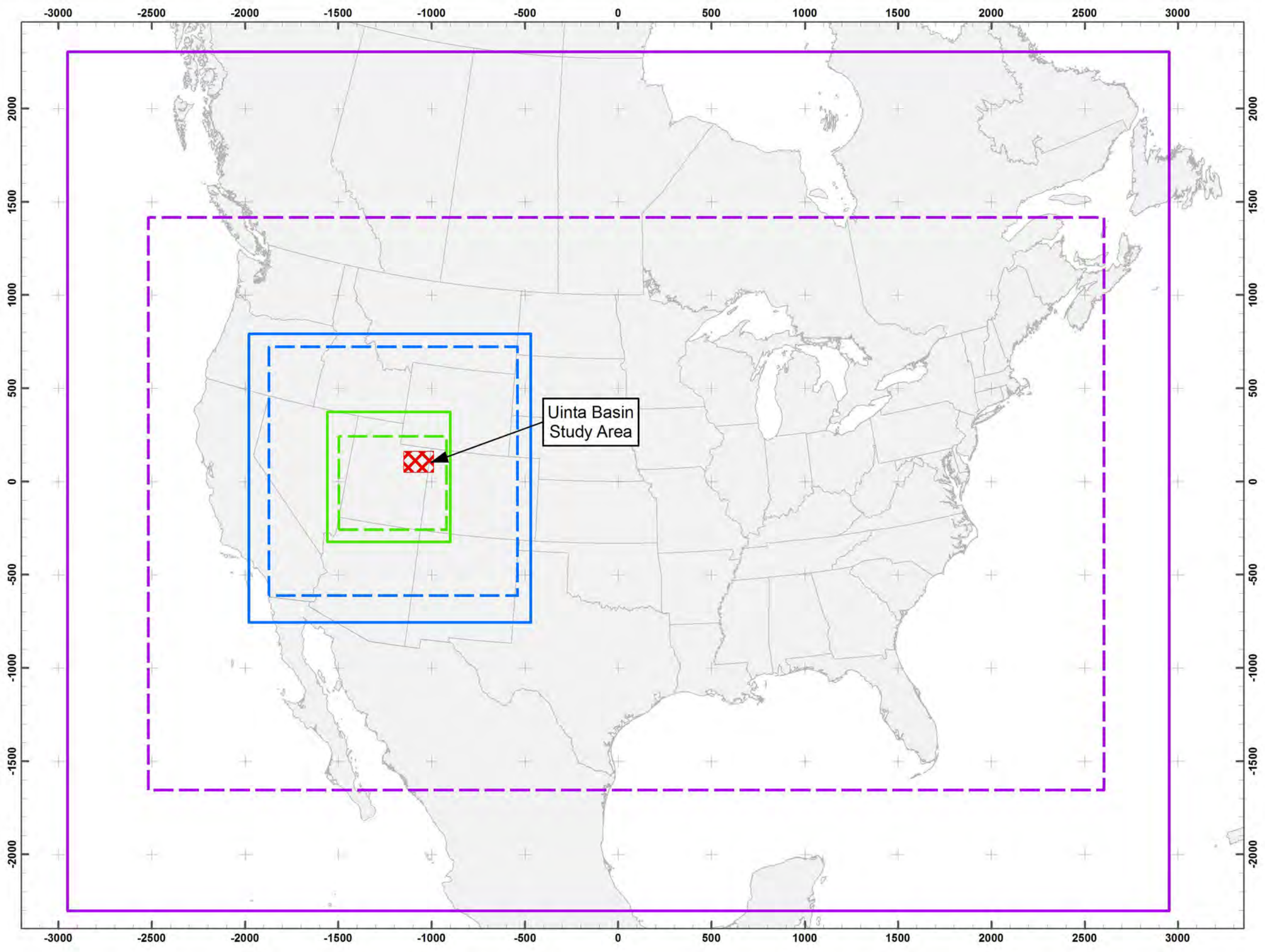
Legend

Study Area

Grid Boundaries

WRF	Air Quality Model
4 km	
12 km	
36 km	

Uinta Basin
Study Area

Table 2-1   RPO Unified Grid Definition

Parameter	Value
projection	LCC
datum	World Geodetic System 1984
alpha	33 degrees (°) latitude
beta	45° latitude
x center	97° longitude
y center	40° latitude

Table 2-2   Model Domain Dimensions

Model	Domain	Number of Grid Cells	Coordinates of Southwestern Corner of Grid (km)
CMAQ and CAMx	36-km	148 x 112	-2736, -2088
	12-km	111 x 111	-1872, -612
	4-km*	144 x 126	-1500, -264
WRF	36-km	165 x 129	-2952, -2304
	12-km	127 x 130	-1980, -756
	4-km	166 x 175	-1560, -324

*Dimensions exclude buffer cells used for CAMx

Table 2-3   Vertical Layer Structure for Meteorological and Air Quality Modeling Simulations

Model Layer	Sigma	Pressure (millibars [mb])	Height (meters)	Depth (meters)
36 – top	0.000	50	20,559	4,262
35	0.050	98	16,297	2,527
34	0.100	145	13,770	1,805
33	0.150	193	11,965	1,407
32	0.200	240	10,559	1,185
31	0.250	288	9,374	1,035
30	0.300	335	8,339	931
29	0.350	383	7,408	832
28	0.400	430	6,576	760
27	0.450	478	5,816	701
26	0.500	525	5,115	652
25	0.550	573	4,463	609
24	0.600	620	3,854	572

Table 2-3   Vertical Layer Structure for Meteorological and Air Quality Modeling Simulations

Model Layer	Sigma	Pressure (millibars [mb])	Height (meters)	Depth (meters)
23	0.650	668	3,282	540
22	0.700	715	2,741	412
21	0.740	753	2,329	298
20	0.770	782	2,032	290
19	0.800	810	1,742	188
18	0.820	829	1,554	185
17	0.840	848	1,369	182
16	0.860	867	1,188	178
15	0.880	886	1,009	175
14	0.900	905	834	87
13	0.910	915	747	85
12	0.920	924	662	85
11	0.930	934	577	85
10	0.940	943	492	83
9	0.950	953	409	83
8	0.960	962	326	83
7	0.970	972	243	81
6	0.980	981	162	41
5	0.985	986	121	41
4	0.990	991	80	20
3	0.9929	993	60	20
2	0.995	995	40	20
1	0.9976	998	20	20
0 – ground	1.000	1,000	0	0

2.3   Base Case Model Configuration

Table 2-4 lists the main CMAQ and CAMx configurations that are used in the annual 2010 Base Case simulation. To ensure the best possible air quality model performance, each of the models is configured to best-science, based on the scientific and numerical options that were available in both modeling systems at the beginning of this project.

2.3.1   CMAQ

The global mass-conserving scheme (vwrf scheme) advection solver is used to calculate horizontal and vertical advection. Horizontal diffusion is calculated using diffusion coefficient based on local wind deformation. The vertical diffusion is calculated with the Asymmetric Convective Model version 2 (ACM2).

Table 2-4   CMAQ and CAMX Air Quality Model Configurations for Base Case

Parameter	CMAQ	CAMx	Details
Model Version	CMAQ (v.5.0)	CAMx (v.5.40)	
Horizontal Grid Mesh	36/12/4 km (see **Figure 2-1**)	36/12/4 km (see **Figure 2-1**)	
Vertical Grid Mesh	36 layers	36 layers	Using WRF layers with no collapsing
Grid Interaction	One-way nesting	36-km is run with one-way nesting and the 12-km and 4-km domains are run with two-way nesting	
Initial Conditions	15 days spin-up for the 36-km domain and 7 days of spin-up for the 12-km and 4-km nested domain	15 days spin-up for the 36-km domain and 7 days of spin-up for the 12-km and 4-km nested domain	Separately run four quarters of 2010
Boundary Conditions	2010 GEOS-Chem data is used as boundary conditions for the 36-km domain and each domain is extracted as boundary conditions for the finer resolution domain	2010 GEOS-Chem data is used as boundary conditions for the 36-km domain and the 36-km domain is extracted as boundary conditions for the 12-km and 4-km nested domains	2010 GEOS-Chem data is extracted for CMAQ and CMAQ BC data is processed to be compatible with CAMx.
Meteorological Processor	MCIP (v.4.0)	WRFCAMx (version 3.3)	For processing WRF meteorology
Emissions Processor	SMOKE (v.3.0)	CMAQ2CAMx processor	CMAQ2CAMx converter tool converts CMAQ-ready emissions inputs to CAMx-ready format
Chemistry			
Gas Phase Chemistry	CB05-TU	CB6	CB05-TU is CB05 with updated toluene chemistry. Both mechanisms can use the same SMOKE output.
Aerosol Chemistry	AERO5 and ISORROPIA2.1	SOAP and ISORROPIA1.6 with static 2-mode coarse/fine size distribution.	

Table 2-4   CMAQ and CAMX Air Quality Model Configurations for Base Case

Parameter	CMAQ	CAMx	Details
Cloud Chemistry	RADM-type aqueous chemistry	RADM-type aqueous chemistry	
Numerics			
Gas Phase Chemistry Solver	Euler Backward Iterative (EBI) solver on 36-km and 12-km domains; Rosenbrock solver on 4-km domain.	EBI solver	
Horizontal Advection	YAMO scheme	PPM scheme	
Vertical Advection	VWRF scheme	Implicit scheme with vertical velocity update	
Diffusion			
Horizontal Diffusion	Multiscale	K-theory 1st order closure with K_h grid size dependence	
Vertical Diffusion	ACM2	K-theory approach	$K_z\_min = 0.01$ m^2/s
Deposition			
Dry Deposition	CCTM in-line	Zhang scheme	
Wet Deposition	CMAQ-specific	CAMx-specific	Rain, snow, graupel
Integration Time Step	Wind speed dependent	Wind speed dependent	

As shown in **Table 2-4**, the CMAQ configuration includes the CB05 gas phase photochemical mechanism with updated toluene chemistry. The CB05 gas-phase photochemical mechanism contains 205 reactions involving 80 chemical species. VOC species are treated using a lumped bond approach in which actual VOC species are represented in the CB05 mechanism by model species that are designed to represent certain carbon bond types. This approach is used to reduce the total number of VOC species represented in the photochemical model. The updated RADM aqueous-phase and AERO5/ISORROPIA2 aerosol chemistry scheme is used in the CMAQ modeling. The particulate chemistry mechanism utilizes products from the gas-phase photochemistry for production of sulfate (SO_4), nitrate (NO_3), condensable organic gases, and chloride. Mineral nitrate is included in the calculation of aerosol nitrate formation.

2.3.2   CAMx

As shown in **Table 2-4**, CMAQ and CAMx use many similar science options and input data sets. However, there are instances where the models diverge in characterizing physical and chemical processes and how the governing equations are implemented. For CAMx two-way grid nesting is used instead of the one-way nesting employed in CMAQ. The Piecewise Parabolic Method (PPM) advection solver is used along with the spatially varying horizontal diffusion approach. Vertical diffusion in CAMx is modeled by the K-theory approach.

The CAMx configuration includes the CB6 gas phase photochemical mechanism (Yarwood et al. 2010). The CB6 gas-phase photochemical mechanism contains 218 reactions involving 77 gas-phase species. While CB6 is compatible with emissions processed for CB05, CB6 extensively revises CB05 with the core inorganic chemistry updated to 2010 and major revisions to the chemistry for aromatics, isoprene, alkenes, alkanes, and oxygenates. Several long-lived and abundant VOCs are added explicitly and could be added to emission inventories. Several alpha-dicarbonyls are included because they are secondary organic aerosol (SOA) precursors. Compared to CB05, more rapid ozone formation is expected for VOC sensitive conditions with less change in ozone for NO_x-limited conditions. CB6 has greater computer requirements than CB05. CB6 can be used with CB05 format emission inventories.

CAMx algorithms to estimate ozone and PM formation include aqueous chemistry (RADM), ISORROPIA, and Secondary Organic Aerosol Formation/partitioning (SOAP) schemes. The particulate chemistry mechanism utilizes products from the gas-phase photochemistry for production of SO_4, NO_3, condensable organic gases, and chloride. Mineral nitrate is included in the calculation of aerosol nitrate formation.

2.4   Air Quality Model Inputs

Air quality models require input files that configure each simulation; define the chemical mechanism; and describe the photochemical conditions, surface characteristics, initial/boundary conditions, emissions rates, and various meteorological fields over the entire modeling domain. The air quality model inputs include:

- Three-dimensional hourly meteorological fields generated by MCIP or the WRFCAMx, the processors used to prepare input meteorology files for CMAQ and CAMx, respectively, from the WRF output;

- Emissions files generated by the SMOKE emissions processor, and

- Initial conditions (IC) and boundary conditions (BC).

The sources of data and processing steps are described in detail below.

2.4.1   Meteorological Data Processing

Meteorological model output is required in order to simulate the transport and dispersion of emissions within the air quality model. Because observed data are not available for the full gridded model domain for this study, a numerical meteorological model is required to provide these inputs. For gridded air quality models, a prognostic meteorology model is used in order to provide gridded meteorological output on the same spatial domain and grid resolutions as the air quality model.

For this study, the WRF meteorological model was used to develop the meteorological data required for both air quality models. For more detail regarding the WRF model configuration and the meteorological model results, refer to the Utah Air Resource Management Strategy Modeling Project: Meteorological Model Performance Evaluation (AECOM 2013). The outputs of the WRF model are not directly input into CMAQ/CAMx or the emissions processing model (SMOKE). The WRF model output files are processed using the most current version of either the Meteorological Chemistry Interface Processor (MCIP) or WRFCAMx. MCIP and WRFCAMx are processors used to generate meteorological files that are used for air quality simulations based on the raw WRF outputs. MCIP is used for the CMAQ model and the SMOKE model and WRFCAMx is used for CAMx model. (Additional details regarding the emissions processing are available in Section 2.4.2.)

MCIP (version 4.0) is used to pre-process the WRF meteorological output into the CMAQ-ready format. In addition to the extraction and formatting of the WRF output fields, additional parameters required by the PGM, but not always available in the meteorological files, are calculated in MCIP. These parameters include: cloud and moisture parameters for each horizontal grid cell, Monin-Obukhov length, PBL height, convective velocity scale, temperature and wind at specific heights (used for plume rise calculations when vertically distributing the emissions in the SMOKE model, and dry deposition velocities.

Table 2-5 shows the configuration used in MCIP for processing the WRF output to produce CMAQ-ready meteorology input files that is used for all CMAQ model simulations.

Table 2-5   MCIP Configuration

Module or Option	Values or Setting	Additional Information
LPV	0	Potential vorticity is not calculated or output in MCIP.
LWOUT	1	Produce outputs of vertical velocity in MCIP files.[1]
LUVCOUT	1	Produce outputs of u- and v-components of the wind speed.
LSAT	0	No satellite data is used for MCIP outputs.

[1] Note that vertical velocity is not used in CMAQ; however, review of this parameter may provide additional insight during the MPE process.

WRFCAMx (version 3.3) is used to pre-process the WRF meteorological output into the CAMx-ready format. WRFCAMx produced three 2-dimensional and four 3-dimensional daily meteorological and geophysical files in formats compatible for use in the CAMx model. The data files include three-dimensional gridded fields of horizontal wind speed, temperatures, pressure, water vapor, cloud water, cloud optical depth, precipitation, and vertical exchange coefficients. Two-dimensional gridded fields of terrain elevation, snow cover, and land use fraction also were developed.

Other meteorological parameters necessary for CAMx but not available from the WRF meteorological model (such as coefficient of vertical eddy diffusion [Kv] values and micrometeorological variables) are estimated with appropriate diagnostic algorithms in the WRFCAMx program. The Mellor, Yamada, and Janic (MYJ) method will be used to diagnose vertical diffusivities. WRFCAMx will be use a 0.01 meters

squared per second (m^2/s) Kz_min value. The diagnostic cumulus scheme is used to process the WRF 36-km and 12-km domain sub-grid cloud data and no cumulus parameterization is used for the WRF 4-km domain. The Zhang deposition option is used in the WRFCAMx processing and the fractional distribution of the 26 landuse categories is generated. The WRFCAMx processor also limits output of meteorological data from the WRF domain so that the domain in the output files precisely matches the CAMx model domain.

Table 2-6 shows the configuration to be used in WRFCAMx for processing the 2010 base year WRF output to produce CAMx-ready meteorology input files.

Table 2-6   WRFCAMx Configuration

Module or Option	Values or Setting	Additional Information
Vertical eddy diffusion [Kv] method	ACM2 (non-winter) and MYJ (winter)	Mellor-Yamada-Janic (MYJ) and Asymmetric Convective Model 2 (ACM2)
Minimum Kv	0.01	Unit is m^2/s
Projection	LCC	Same map projection as in WRF
Process snow cover	True	
Grid time zone	0	Using Coordinated Universal Time

[1] CMAQ refers to the method used to obtain values for this option.

2.4.2   Emissions Development

The meteorological output from WRF data were processed for SMOKE using MCIP. Spatially gridded and hourly varying meteorological data from MCIP were used by SMOKE to estimate emissions from biogenics, ammonia, windblown dust, and mobile sources. These emissions require meteorological input data including wind fields, humidity, temperature, clouds, and solar radiation at the surface. The SMOKE modeling system (version 2.7) is an emissions processing system that generates hourly, gridded, and speciated emissions inputs of mobile, non-road, area, point, fire, and biogenic emissions sources in a format for PGMs. The SMOKE model was used to prepare the base year and future year EIs for air quality modeling. SMOKE was configured to develop emissions files for CMAQ using the chemical mechanism Carbon Bond V (CB05), which is compatible with both CB05-TU and CB6. These files were used as the emissions input for CMAQ without further modification.

For CAMx, the CMAQ-ready input files then were merged and post-processed with the CMAQ2CAMx utility program to generate emissions in CAMx-ready format. Two-way grid nesting between the 12- and 4-km domains requires emissions data for "buffer" cells around the perimeter of the 4-km. Therefore, emissions data were post-processed to add this buffer to the 4-km domain emissions data for CAMx.

Additional details regarding the 2010 emissions data sources, processing methods, and final results are available in the Utah State BLM Emissions Inventory Technical Support Document (AECOM 2013b).

2.4.3   Initial Condition and Boundary Condition Data

Three-dimensional concentration fields of chemical species are required to initialize the PGMs, as well as provide inputs to the lateral boundaries of the 36-km grid.

The initial conditions are created by performing a model spin-up simulation. To reduce the time required for a full annual simulation, the model simulation is performed in four separate runs of 3 months each. The spin-up period eliminates effects of initial conditions. For the first 3-month period beginning

January 1, 2010, emissions and meteorology data from January 1 to 7, 2010, is used to spin-up the model since emissions and meteorological data for the end of 2009 were not readily available. For each subsequent quarter, the results of the CMAQ and CAMx spin-up simulation is used to initialize the annual CMAQ and CAMx modeling simulations, respectively. The final 15 days of the preceding quarter is used to spin-up the 36-km domain and the final 7 days of the preceding quarter is used to spin-up the 12-km and 4-km domains.

The boundary concentration data for the 36-km domain for both PGMs are derived from a 2010 Goddard Earth Observing System – Chemical (GEOS-Chem) global simulation model (Liu et al. 2006) output.

The GEOS-Chem data were provided by the U.S. Environmental Protection Agency (USEPA) (2012) in a format compatible with the CMAQ model's CB05 chemical mechanism. The BC files are then converted to CAMx-ready files using ENVIRON's CMAQ2CAMx processor. The procedure used to map BC data from the GEOS-Chem chemical species and grid definitions to values that are appropriate for the CMAQ CB05 species and CAMx CB6 species are defined in coordination with the USEPA. These data were converted to be compatible with CAMx CB6. The species mapping shown in **Table 2-7** were determined in coordination with the USEPA, and are limited to those chemical species that are different between the two models.

For CMAQ, data from the 2010 GEOS-Chem simulation are used to provide boundary conditions for the 36-km domain. Boundary conditions for the 12-km domain are extracted from the 36-km run with the CMAQ BCON processor. Similarly, the boundary conditions for the 4 km domain are extracted from the 12-km results.

For CAMx, data from the 2010 GEOS-Chem simulation are used to provide boundary conditions for the 36-km domain. Boundary conditions for the 12-km domain are extracted from the 36-km run. Due to the use of two-way nesting, boundary conditions for the 4-km domains are calculated during runtime from the 12-km domain.

Table 2-7   Species Mapping Table for the GEOS-Chem Dataset to CAMx CB6 and CMAQ CB05

GEOS-Chem CB05_AE6 Species[1]	Used for CAMx CB6-SOAP_AE Species[1]	Used for CMAQ CB05_AE5 Species[2]
NO3 + 2*N2O5	NXOY	NO3 + 2*N2O5
TOL	TOLA	TOL
XYL	XYLA	XYL
ISOP	ISP	ISOP
BENZENE	BENZ	BENZENE
SV_TOL1 + SV_XYL1 + SV_BNZ1	CG1	SV_TOL1 + SV_XYL1 + SV_BNZ1
SV_TOL2 + SV_XYL2 + SV_BNZ2	CG2	SV_TOL2 + SV_XYL2 + SV_BNZ2
SV_ISO1	CG3	SV_ISO1
SV_ISO2	CG4	SV_ISO2
SV_TRP1	CG5	SV_TRP1
SV_TRP2	CG6	SV_TRP2

Table 2-7   Species Mapping Table for the GEOS-Chem Dataset to CAMx CB6 and CMAQ CB05

GEOS-Chem CB05_AE6 Species[1]	Used for CAMx CB6-SOAP_AE Species[1]	Used for CMAQ CB05_AE5 Species[2]
SV_SQT	CG7	SV_SQT
ASO4I + ASO4J + ASO4K	PSO4	ASO4I + ASO4J + ASO4K
ANO3I + ANO3J + ANO3K	PNO3	ANO3I + ANO3J + ANO3K
ANH4I + ANH4J	PNH4	ANH4I + ANH4J
APOCI + APOCJ + APNCOMI + APNCOMJ	POA	AORGPAJ + AORGPAI + APNCOMI + APNCOMJ
AECI + AECJ	PEC	AECI + AECJ
AMGJ + AKJ + ACAJ + AFEJ + ASIJ + AOTHRJ + ATIJ + AMNJ + AALJ	FPRM	AMGJ + AKJ + ACAJ + AFEJ + ASIJ + A25J + ATIJ + AMNJ + AALJ
ACORS + ASOIL	CPRM	ACORS + ASOIL
ANAI + ANAJ + ANAK	NA	ANAI + ANAJ + ANAK
ACLI + ACLJ + ACLK	PCL	ACLI + ACLJ + ACLK
AH2OI + AH2OJ + AH2OK	PH2O	AH2OI + AH2OJ + AH2OK
ABNZ1J + ABNZ2J + ATOL1J + ATOL2J + AXYL1J + AXYL2J	SOA1	ABNZ1J + ABNZ2J + ATOL1J + ATOL2J + AXYL1J + AXYL2J
ABNZ3J + ATOL3J + AXYL3J	SOA2	ABNZ3J + ATOL3J + AXYL3J
AISO1J	SOA3	AISO1J
AISO2J + AISO3J	SOA4	AISO2J + AISO3J
ATRP1J	SOA5	ATRP1J
ATRP2J	SOA6	ATRP2J
ASQTJ	SOA7	ASQTJ
AOLGAJ	SOPA	AOLGAJ
AOLGBJ	SOPB	AOLGBJ

[1] The definitions for GEOS-Chem species are available from the GEOS-Chem User's Guide Appendix 6 at http://acmg.seas.harvard.edu/geos/doc/archive/man.v8-01-04/. The CB05 mapping is used for CB6.

[2] The differences between CAQ AE5 and AE6 species names are: AOTHRJ (AE6) is A25J(AE5), and APOCI + APOCJ (AE6) is AORGPAJ + AORGPAI (AE5)

2.4.4   Photolysis Rates and AHOMAP

The photolysis rates for NO_2 and other species have a significant effect on the rate of ozone formation, and are a function of the amount of UV radiation available. Accurate estimates of these photolysis rates are needed to accurately represent the complex chemical transformations in the atmosphere. The photolysis rates are derived for each grid cell assuming clear sky conditions as a function of five parameters: solar zenith angle, altitude, total ozone column and aerosol scattering, surface ultraviolet albedo, and atmospheric turbidity.

The surface ultraviolet albedo is calculated based on the gridded land use data using land use-specific UV albedo values. The albedo varies spatially according to the land cover distribution, but typically does not vary with time with the exception of temporally varying snow cover surface.

For CMAQ, Photolysis rates for all photolytic reactions in CMAQ modeling were calculated for each grid cell at every synchronization time step using the in-line photolysis module available in CMAQ version 5.0. The in-line photolysis module is more computationally efficient than using the JPROC look-up tables. This module also introduces an algorithm that calculates the surface albedo based on land use categories, cloud cover, zenith angle, seasonal vegetation, and snow cover.

The in-line photolysis module in CMAQ version 5.0, while capable of adjusting surface albedo based on land-use type and snow/ice coverage, tended to under-estimate the albedo over snow covered areas. This is because CMAQ adjusts the albedo explicitly based on the "sea ice" land-use category, while for other land use categories a "snow cover coefficient" is used instead. This results in very limited enhancement of the albedo and photolysis rates in areas covered by snow. These limitations to the original CMAQ version 5.0 were identified by USEPA Region 8, who provided updated code that uses alternative treatment of snow cover resulting in enhanced surface albedos. This update modifies the in-line albedo calculation to set the albedo to 0.85 times the fractional snow cover.

For CAMx, the model system includes the AHOMAP processor to prepare albedo/haze/ozone column input files for CAMx. The CAMx TUV preprocessor then calculates a table of clear-sky photolysis rates for each grid cell for a specific date. TUV accounts for environmental parameters that influence photolysis rates including solar zenith angle, altitude above the ground, surface ultraviolet albedo, aerosols (haze), and stratospheric ozone column. The ozone column data for AHOMAP is from the Ozone Monitoring Instrument (OMI) data that is a 1° longitude by 1° latitude resolution. CAMx is configured to use the in-line TUV to adjust for cloud cover. The albedo for snow covered surfaces is set to 0.5 for all CAMx domains.

2.4.5   Snow Cover Fields

The WRF snow cover fields were qualitatively assessed by comparison to actual snow and ice coverage data as part of the WRF model performance evaluation (AECOM 2013). Snow cover data available from the National Oceanic and Atmospheric Administration National (NOAA) Ice Center[2] was compared with spatial plots of the WRF snow cover fields. In general, the WRF model reproduced the observed snow cover well throughout the year and determined to be adequate for use in the PGM simulations.

For CMAQ modeling, the WRF fractional snow cover fields from all domains were extracted by MCIP and used directly for each CMAQ domain. For the CAMx modeling, the snow cover fields were extracted from the WRF model using WRFCAMx. CAMx carries snow cover data for each grid cell as a binary value (either with snow or without), and thus no variation for clean or dirty snow or partial sub-grid snow coverage is accounted for in the current CAMx model. In CAMx version 5.40, in the binary snow cover data was added to the albedo/haze/ozone column input file developed by the CAMx preprocessor, AHOMAP. CAMx uses the snow cover field to adjust the UV albedo. Separate snow cover fields were developed for the 36-km and 12-km domains. For the nested 4-km grid, all nested grid cells receive values from the master (i.e., 12-km) grid, which limits the resolution of the snow cover data. In addition, when the WRF fractional snow cover exceeds 0.5, WRFCAMx indicates that the grid cell is snow covered. This prevents "snow creep" that could occur if WRFCAMx considered a grid cell as snow covered when the WRF fractional snow coverage is less than half.

---

[2] The NOAA National Ice Center produces operational snow and ice products generated from satellite data. These products are available at the website http://www.natice.noaa.gov/ims/.

2.5   Air Quality Model Sensitivity Tests

Two sensitivity simulations, boundary condition and non-anthropogenic, were performed for the months of February and August for each model. The model sensitivity study compared the contribution of background ozone to the total predicted ozone in CAMx and CMAQ. The observed local ozone concentration is the sum of: 1) natural background ozone, 2) transported ozone generated from emissions from upwind cities and non-routine natural events such as wildfires, and 3) ozone generated from local anthropogenic emissions (STI 2006). The contribution of non-local sources of ozone was evaluated with two model sensitivity tests with CMAQ and CAMx: 1) a boundary condition test (referred to as the BC test) that follows the evolution of ozone concentrations from the 36-km lateral boundaries to the inner domains; and 2) a natural background test that follows the evolution of ozone and $PM_{2.5}$ concentrations from the lateral boundaries and from natural background (i.e., non-anthropogenic) sources. The full methodology and results from these sensitivity tests are documented in **Appendix A**. Note that these sensitivity tests do not include a test of the vertical eddy diffusivity term that was originally proposed in the protocol (AECOM 2012) since other studies found that the model was able to use the proposed minimum eddy diffusivity threshold (shown in **Table 2-4**) without difficulty.

2.5.1.1   Boundary Condition Test

The BC test examines the contribution of natural background ozone from boundary conditions to the Uinta Basin. In this set of model runs, the chemistry solvers were turned off in both models to investigate the contribution of ozone transported in from the boundary conditions provided by the GEOS-Chem global model. Both CMAQ and CAMx used the identical set of GEOS-Chem boundary conditions for the 36-km domain.

Results from the BC test showed that boundary ozone has a larger contribution to the total ozone concentration in the Uinta Basin during the summer than during the winter. Ozone from the western boundary is the largest source of ozone transported in the Uinta Basin from the boundaries during the winter, whereas ozone from both the western and northern boundaries is transported to the Uinta Basin during the summer. Both models predict boundary ozone concentrations in excess of 70 ppb at times during the summer in the Uinta Basin, suggesting that the boundary conditions may contribute to enhanced summer ozone concentrations in the Uinta Basin. Finally, results from the BC test were similar for CMAQ and CAMx, which suggest similarities in the way both models handle vertical and horizontal transport in the Uinta Basin.

2.5.1.2   Natural Background Test

The natural background test examines the background ozone concentration from natural sources by turning chemistry solvers on. In this set of simulations, all anthropogenic emissions within the modeling domain are removed leaving only biogenic emissions and wildfires.

Results from the natural background test showed that ozone concentrations predicted by both models are significantly lower than in the boundary condition test, due to the activation of chemical transformations and deposition processes, previously turned off in the boundary condition test. Ozone concentrations predicted by CAMx are slightly higher than predicted by CMAQ during the winter, but the opposite is true during the summer, indicating differences in chemistry and deposition treatment between the two models. Total $PM_{2.5}$ concentrations predicted by CMAQ are less than those predicted by CAMx, but both models predict very low concentrations of $PM_{2.5}$ from natural background sources during both summer and winter.

3.0   Air Quality Model Performance Evaluation Methodology

The purpose of the air quality MPE is to demonstrate that the base year modeling system meets the performance criteria specified in USEPA guidance documents and understand the model limitations. The air quality MPE provides an assessment of the strengths and limitations of the overall meteorology-emissions-air quality modeling system. This is an important evaluation since this system is intended to be used to estimate potential future air quality and AQRVs both within the Uinta Basin study area and at selected sensitive areas in the 12-km and 4-km modeling domains (AECOM 2012). Once the modeling system has been evaluated and demonstrates acceptable performance, the modeling system will be used to assess cumulative air conditions for 2021 for several emissions scenarios (AECOM 2013). The MPE results presented in Chapter 4.0 compare the modeled 2010 base year concentrations to observed concentrations of gas-phase and particle-phase species. The MPE has been conducted using a suite of statistical metrics and graphical analyses as described in this chapter.

3.1   Ambient Monitoring Data Used to Evaluate Model Performance

Data from ambient monitoring networks for both gas and aerosol species were used to evaluate air quality model performance. **Table 3-1** provides an overview of the ambient monitoring networks that were used. Locations of monitoring sites are shown relative to the 12- and 4-km modeling domains in **Figure 3-1**. Ambient data monitored in 2010 were compiled from each of the monitoring networks located in the states that are part of the Western Regional Air Partnership (WRAP). The WRAP states include Arizona, California, Colorado, Idaho, Montana, Nevada, New Mexico, North Dakota, Oregon, South Dakota, Utah, Washington, and Wyoming. The performance of the 36-km modeling domain was assessed in order to better assess the 36-km results that are used as boundary conditions for the CMAQ and CAMx 12-km domain. Statistical differences were calculated between the modeled concentrations and the monitored values. The statistics, time periods, and spatial extents assessed varied by the pollutant and metric of interest. In general, the model performance results are grouped into five classifications: ozone, PM, other gaseous criteria pollutants, visibility, and deposition.

3.1.1   Interagency Monitoring of Protected Visual Environments (IMPROVE) Network

The Interagency Monitoring of Protected Visual Environments (IMPROVE) monitoring network was established in 1985 and is a multiple federal agency effort designed to monitor visibility and related air quality, focused on 156 Class I visibility-sensitive regions in the U.S. (e.g., national parks) (Malm et al. 1994; Malm et al. 2002). The primary focus is on using aerosol chemical composition from a suite of filter-based measurements to reconstruct atmospheric light scattering and light absorbing properties.

The IMPROVE data are reported for actual temperature and pressure conditions at the sampling sites. The network monitors particulate matter with an aerodynamic diameter less than or equal to 2.5 microns ($PM_{2.5}$) mass, particulate matter with an aerodynamic diameter less than or equal to 10 microns (PM_{10}) mass, and $PM_{2.5}$ speciated chemical composition using four independent modules with the following design:

- Filter Module A collects $PM_{2.5}$ on a Teflon substrate. These filters are analyzed for $PM_{2.5}$ mass concentration, optical absorption, hydrogen, and trace minerals and metals via particle-induced x-ray (PIXE) and x-ray fluorescence (XRF) methods.

- Filter Module B collects $PM_{2.5}$ on a nylon substrate preceded by a sodium carbonate coated tubular aluminum denuder that removes nitric acid vapors. These filters are analyzed by ion chromatography for NO_3, chloride, sulfate, and nitrite. A subset of IMPROVE sites do not use this filter.

- Filter Module C collects $PM_{2.5}$ on a quartz substrate. These filters are analyzed for carbonaceous material using Thermal Optical Reflectance (TOR). A backup secondary filter is used to quantify volatility loss artifacts.

- Filter Module D collects PM_{10} on a Teflon substrate that is analyzed for PM_{10} mass concentration.

3.1.2   CASTNet

The Clean Air Status and Trends Network (CASTNet) is a network designed to support assessment of trends in air quality, atmospheric deposition, and ecological effects due to changes in air pollutant emissions. The CASTNet measures nitrogen, sulfur, and O_3 ambient concentrations primarily in rural environments. Nitrogen and sulfur dry deposition is estimated from measured ambient concentrations and modeled dry deposition velocities. Network sites were first established in 1987 as part of the National Dry Deposition Network. The CASTNet program started in 1991 and now comprises over 80 monitoring stations with the longest period of records in the eastern U.S.

The sampling network employs a three-stage filter pack and does not use an imposed inlet size cut; however, it is likely that coarse particles are limited through the inlet plumbing (Gego et al. 2005). The filter pack uses a first-stage Teflon filter for particle collection. The second stage collects nitric acid on a nylasorb filter, and the third stage collects sulfur dioxide (SO_2) on a potassium carbonate impregnated cellulose filter. The CASTNet minimum sampling and reporting time is 1 week (Tuesday to Tuesday integrated samples). The filters are all analyzed via ion chromatography, and data is corrected to standard temperature and pressure.

3.1.3   National Atmospheric Deposition Program

The National Atmospheric Deposition Program (NADP) monitoring network was initiated in the 1970s, with cooperation between government agencies, universities, and industry. The network initially was intended to monitor wet deposition of acidic species and related precipitation chemistry with 1-week samples. It has expanded to monitor other chemical species of interest as well as related meteorology important to atmospheric wet deposition. The network is focused on wet deposition as it relates to human health and ecological impacts. The network currently includes over 300 monitoring sites and has encompassed several sub-networks, including the National Trends Network (NTN), which are designed for specific studies.

In the NTN, the primary species of interest are precipitation amount, pH, conductance, and major ions including calcium, magnesium, sodium, potassium, SO_4, NO_3, chloride, and ammonium (NH_4). The network uses automated wet precipitation collectors that open upon precipitation and close during non-precipitating time periods. An integrated sample is collected weekly. Precipitation amounts and proper collector operation is verified with independent rain gauges.

3.1.4   Speciation Trends Network

Established in 1999, the Speciation Trends Network (STN) is a national network designed for speciated $PM_{2.5}$ data at urban and suburban U.S. sites. The network was implemented in support of maintaining the NAAQS for $PM_{2.5}$ and is operated by the USEPA and other regulatory agencies. The network consists of 53 mostly urban sites (as of July 20, 2012), with approximately 239 supplemental state and local air monitoring stations (SLAMS) that are considered part of the STN network. The network measures total $PM_{2.5}$ mass concentrations as well as $PM_{2.5}$ composition, including major ions, elemental carbon (EC), organic carbon (OC), and numerous trace metals and minerals. The STN network

generally collects samples every 1 in 3 days, although some State and Local Air Monitoring Stations site sample every 1 in 6 days. Due to the diversity of sampling sites in the network, different sampling techniques and instruments are used.

3.1.5   USEPA Air Quality System

The USEPA Air Quality System (AQS) is a publically available national database that houses ambient air quality data. The AQS is not a monitoring network in and of itself; rather, it serves as a clearinghouse for data from ambient air quality monitoring sites operated by the USEPA plus state, local, and tribal air quality networks (USEPA 2006). The database stores criteria ambient air pollutant data (including PM_{10}, $PM_{2.5}$, CO, NO_2, SO_2, lead, and O_3), speciation data, as well as meteorological data from thousands of sites across the U.S. The data is updated quarterly and conforms to the USEPA formatting and quality assurance guidelines. The USEPA Office of Air Quality Planning and Standards (OAQPS) uses AQS data to assess air quality, assist in attainment/non-attainment designations, evaluate State Implementation Plans for non-attainment areas, and perform modeling for permit review analyses, among other functions.

3.1.6   Comparisons between Monitoring Networks

Ambient air quality monitoring networks have been developed with diverse goals, including visibility monitoring, dry deposition monitoring, and NAAQS compliance assessment. Depending on the goals of the network, there are a wide range of sampling times, sampling height, sampler flow rate, sampling size cut or other inlet differences, sample collection methods analysis methods, and quality assurance protocols (see **Table 3-1**).

The diversity of methods results in a range of potential impacts on measurements and potential sampling artifacts. Even with identical methods, differences are observed with collocated samplers due to sample loss/contamination, variability in flow rate, and other sampling differences (Flanagan et al. 2006). An analysis of systematic uncertainties in monitoring networks attributed greater impacts of sample uncertainties, even between like samplers, as compared to laboratory analysis uncertainties (Flanagan et al. 2006). Nonetheless, the analysis uncertainties can at times be significant; this can particularly be the case in comparing the same species with differing analysis methods.

One important difference in the networks is potential volatility losses, which is of most concern for ammonium nitrate and potentially some OC species. These losses are a function of sample versus ambient temperature, filter face velocity of the sampling, sampling filter pressure drop, and exposure time of the filter substrates plus shipping time and temperature (Lane 1999 and references therein).

Several studies have investigated the inter-comparability of various subsets of the ambient monitoring networks of interest to this study. An early comparison by Ames and Malm (2001) examined 23 IMPROVE and CASTNet sites within approximately 50 km of each other and with overlapping data for more than 1 year for inter-comparability of SO_4 and NO_3. Whereas differences in SO_4 concentrations generally were small, differences in NO_3 concentrations varied from -9 percent at eastern U.S. sites to +56 percent in the interior mountain desert region expressed as (CASTNet-IMPROVE)/IMPROVE. While some of the differences in NO_3 concentrations potentially were related to true geographic differences in sites since they are not precisely collocated, Ames and Malm (2001) associated both volatility losses of ammonium nitrate as well as varying contributions of coarse mode NO_3 as driving factors in the poor inter-comparability for NO_3.

An inter-comparison of three major ion species from three networks (IMPROVE, CASTNet, and STN) showed reasonable yet to a lesser degree (Gego et al. 2005) agreement for SO_4 and NH_4. As a result of the differing sampling periods (hourly to weekly depending on parameter and network), the comparison by Gego et al. (2005) required averaging the data over 4- to 6-week periods for reasonable agreement to be realized. Even with doing so, the results for NO_3 for the three networks were divergent, largely attributed to the volatility of ammonium nitrate. The poor agreement for nitrate lead Gego et al. (2005) to caution against integrating NO_3 data from these networks.

A comparison of 10 collocated CASTNet and IMPROVE sites in the eastern U.S. for SO_4 and NO_3 was conducted over a 16-year period by Sickles and Shadwick (2008). This study calculated weekly IMPROVE averages from the 1 in 3 day samples and then further averaged both datasets to seasonal averages. Correlations for both anions were high, at 0.97 and 0.91 for SO_4 and NO_3, respectively. Similar to past studies, larger and more variable biases were found with NO_3 in comparing the eastern U.S. sites from the two networks. Sickles and Shadwick (2008) concluded that CASTNet measurements were biased low for NO_3 due to volatility losses, which become particularly important at low NO_3 concentrations and high ambient temperature.

Differences in network monitoring objectives and siting criteria, instrument selection, as well as inherent sampling limitations and possible artifacts are all important considerations when comparing modeling results to measurements. When model-predicted concentrations are compared to measurements from different networks and the results are similar, this provides a higher level of confidence in the findings, strengthening the weight-of-evidence approach. However, in some cases, inter-network differences may occur, which can elucidate model performance differences for different regions, such as urban versus rural/remote environments. Or inter-network differences could indicate a high level of uncertainty in the measurements themselves either due to sampling challenges, different instrumentation, or number of valid data points included in the analysis. None the less, monitoring differences add an additional level of complexity to the evaluation of the model performance which is important to acknowledge and consider as part of the assessment.

Table 3-1   Comparison of Ambient Air Quality Networks Sampling Protocols

Monitoring Network[1]	Intent and Sites	Chemical Species Measured[2,3]	Sampling Period	Sample Flow Rate[3]	Inlet Details	Sampling Height (meters agl)	Reporting Time, Units and Corrections	Analysis Method	Data Availability/Source	Notes on Networks
IMPROVE	Class I visibility areas	Filter Modules for speciated $PM_{2.5}$ and PM_{10}	1 in 3 days; 24-hour average	Critical orifice 22.8 lpm ($PM_{2.5}$); 19.1 or 16.9 lpm (PM_{10})	$PM_{2.5}$ (cyclone) and PM_{10} (size selective inlet head)	3	Midnight to midnight LDT[4] $\mu g/m^3$ (PM, ambient temperature and pressure)	S from XRF and ion chromatography; cations from stoichiometry, NO_3 from ion chromatography; HNO_3 denuder	http://vista.cira.colostate.edu/improve/Data/IMPROVE/improve_data.html	
CASTNet	Atmospheric deposition at rural sites	Filter pack for speciated $PM_{2.5}$, major ions, O_3	Approximately 1 week average for PM (Tuesday to Tuesday); hourly average for O_3	Mass flow controller 1.5 lpm (east); 3 lpm (west)	No imposed size cut	10	$\mu g/m^3$ (PM standardized to 25C and 1,013 mb), ppb (O_3), kg/ha (estimated deposition)	Ion chromatography (SO_4, NO_3), automated colorimetry (NH_4^+), ICP-AES (sodium, potassium, magnesium) UV absorption (O_3)	http://www.epa.gov/castnet/data.html	Gego et al. (2005)
NADP/NTN	Atmospheric deposition at rural sites	Wet deposition of SO_4, NO_3, NH_4, and other ions	1 week average (Tuesday to Tuesday)	N/A	Covered bucket that opens upon precipitation	1 (typical)	Tuesday to Tuesday, kg/ha (deposition)	Ion chromatography	http://nadp.sws.uiuc.edu/	
AQS (formerly Aeromatic Information Retrieval System)	Database for USEPA, state, and local compliance monitoring	CO, NO_2, NO_x, SO_2, $PM_{2.5}$, PM_{10}, and O_3	Typical hourly average	Varies	Varies	Varies	Hour beginning LST; $\mu g/m^3$ ($PM_{2.5}$, ambient temperature and pressure); ppb or ppm (all gases)	Varies	http://www.epa.gov/air/data/	
STN	Urban and suburban NAAQS compliance	Speciated $PM_{2.5}$	1 in 3 day; 24-hour average	Varies	Varies	Varies	$\mu g/m^3$ ($PM_{2.5}$, ambient temperature and pressure) midnight to midnight (LST)	Varies	http://www.epa.gov/ttn/amtic/amticpm.html	More IMPROVE like though sulfates, nitrates, ammonium via IC. Gego et al. (2005)

[1] The list of monitoring networks is slightly different than identified in the Protocol (AECOM 2012) due to the addition of the WARMS and WYVISNET networks and the removal of the Photochemical Assessment Monitoring Stations (PAMS) and NPS Gaseous Pollutant Monitoring networks. The PAMS network has been removed from the analysis due to lack of monitoring stations within proximity to the 12-km domain. The National Park Service (NPS) monitoring network has been removed from the analysis due to the lack of available monitoring data.

[2] Note that not all chemical species measured by a monitoring network are used to evaluate model performance. Only those species that are important to the parameters evaluated for this study are included in the model performance assessment.

[3] NO = nitrogen oxide; NO_x = oxides of nitrogen; lpm = liters per minute

[4] IMPROVE previously reported data in local daylight time (LDT) but has adopted to the USEPA protocol of local standard time (LST).

ARMS Modeling Project

**Figure 3-1
Air Quality Monitoring Sites
in the 12-km and 4-km
Modeling Domains**
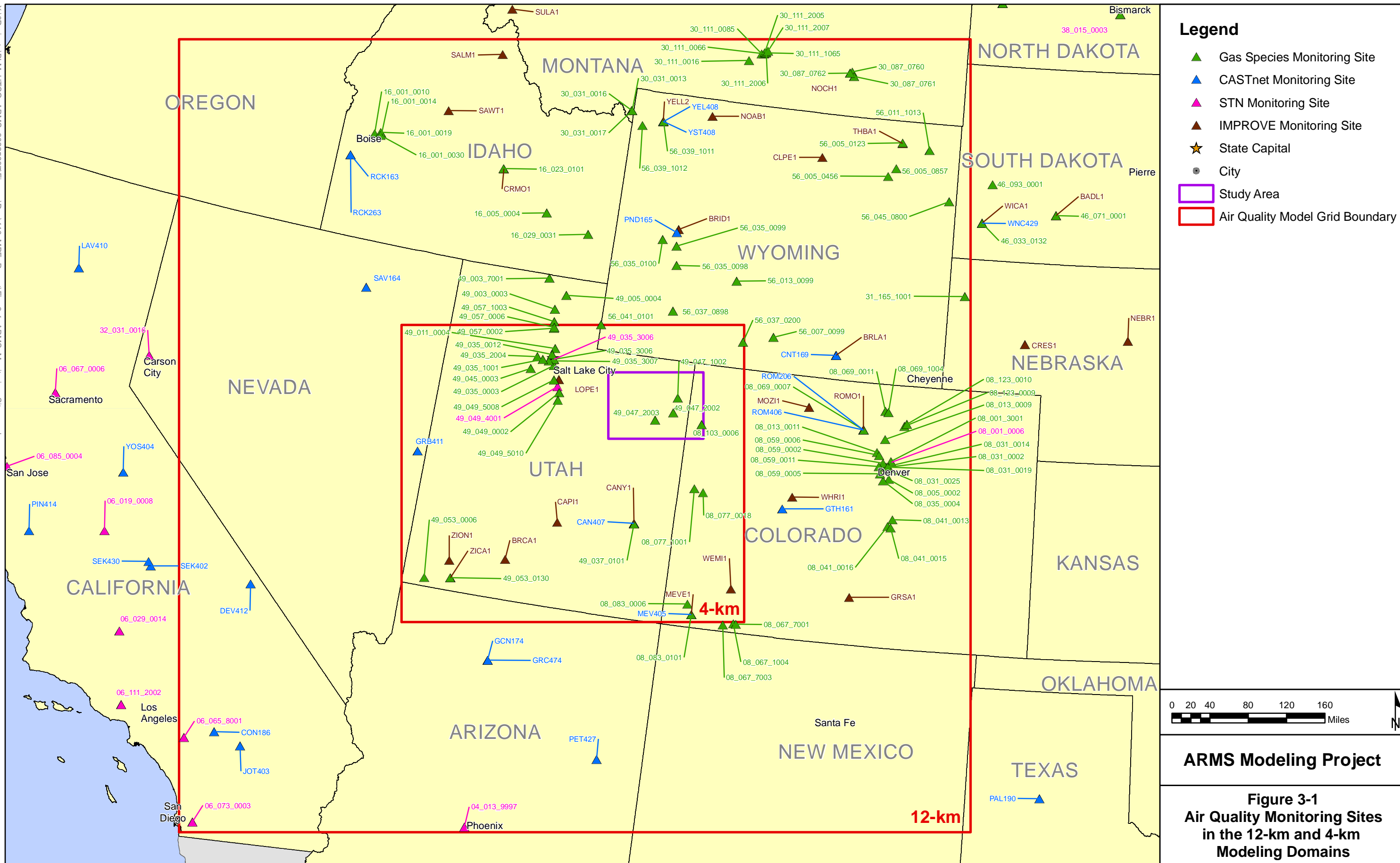
3.2   Statistical Metrics and Benchmarks

As part of the MPE, statistical performance metrics were calculated for the gas-phase species and particle-phase species discussed in Chapter 4.0. The statistical metrics were calculated for each monitoring site, and the results were processed and reported for various spatial and temporal scales. Temporally, the statistical measures were calculated for the following: 1-hour for gas-phase compounds (e.g., NO, NO_2, CO, SO_2, and O_3) and total $PM_{2.5}$ and PM_{10} when 1-hour average monitoring data were available; 8-hour for O_3; 24-hour for SO_4, NO_3, $PM_{2.5}$, PM_{10}, and other particle-phase species; and weekly for wet deposition of SO_4, NO_3, and NH_4. These results were averaged over annual, monthly, and seasonal periods for display, further analysis, and reporting. The results are presented by monitoring network for the 36-, 12-, and 4-km domains. Importantly, the number of monitors with valid data varies for each monitoring network, model domain, and season. The number of valid monitors used for calculating the statistical performance metrics is shown in **Table 3-2**. The equations for the statistical metrics calculated and analyzed as part of the MPE are shown in **Table 3-3**.

3.2.1   Ozone Statistical Measures

While all statistics in **Table 3-3** were calculated for all chemical species discussed in Chapter 4.0, not all results are reported for each pollutant and model. For assessment of ozone model performance, the primary emphasis is on the following three metrics recommended by the USEPA (2007):

- Mean Normalized Bias (MNB): This performance statistic is the average of the modeled/observed residual, paired in time, normalized by observation, over all monitor times/locations. A value close to zero is desirable; however, this also may indicate that model over-predictions and under-predictions cancel each other out.

- Mean Normalized Gross Error (MNGE): This performance statistic is the average of the absolute value of the modeled/observed residual, paired in time, normalized by observation, over all monitor times/locations. A value of zero would indicate that the model exactly matches the observed values at all points in space/time.

- Average Peak Prediction Bias and Error: These are measures of model performance that only assess the ability of the model to predict daily peak 1-hour and 8-hour O_3. They essentially are calculated the same as the MNB and MNGE, except that only daily maxima data (predicted versus observed) are considered at each monitoring location.

For assessment of O_3, the performance metrics are calculated two ways: 1) only assessing data when the ambient concentrations exceeded a 60 parts per billion (ppb) threshold, and 2) assessing all data with no cutoff threshold. These two forms of the performance metrics were further processed in to assess O_3 performance considering different time averaging periods: both hourly and 8-hours rolling averages for evaluation of model results in the form appropriate to compare with the 8-hour average NAAQS. Overall, the O_3 MPE focuses on MNB and MNGE for the following 8 metrics: 1) 1-hour average O_3 with the 60 ppb threshold, 2) 1-hour average O_3 without a threshold, 3) 1-hour average O_3 peak prediction with the 60 ppb threshold, 4) 1-hour average O_3 peak prediction without a threshold, 5) 8-hour average O_3 with the 60 ppb threshold, 6) 8-hour average O_3 without a threshold, 7) 8-hour average O_3 peak prediction with the 60 ppb threshold, and 8) 8-hour average O_3 peak prediction without a threshold.

In addition to MNB and MNGE, Normalized Mean Bias (NMB) and Normalized Mean Error (NME) are presented for all 8 ozone metrics based on recent recommendations that NMB and NME are a better statistical measure of performance (Simon, Baker, and Phillips 2012).

Table 3-2   Number of Ambient Air Quality Monitors by Network, Model Domain, and Season

Monitoring Network	Species	36-km Domain					12-km Domain					4-km Domain				
		Annual	Winter	Spring	Summer	Fall	Annual	Winter	Spring	Summer	Fall	Annual	Winter	Spring	Summer	Fall
AQS (Hourly)	CO	85	85	82	68	76	59	59	57	44	52	7	7	7	7	6
	NOx	204	186	194	194	194	55	49	52	53	53	10	8	9	10	9
	Ozone	225	28	211	213	205	174	27	165	167	159	24	3	23	23	22
	PM$_{10}$ (daily)	207	204	202	202	200	172	169	168	168	167	17	17	17	17	17
	PM$_{10}$ (hourly)	55	50	50	51	50	48	43	43	44	43	2	2	2	2	1
	PM$_{2.5}$ (daily)	128	125	124	121	120	98	95	94	91	90	16	16	16	16	16
	PM$_{2.5}$ (hourly)	77	69	68	71	71	57	51	50	53	53	8	8	7	7	8
	SO$_2$	38	38	36	37	37	28	28	27	28	28	4	4	4	4	4
CASTNET (Weekly)	Ozone	80	15	77	73	73	13	6	13	13	12	3	1	3	3	3
	All other	83	83	83	83	83	13	13	13	13	13	3	3	3	3	3
IMPROVE Concentrations (Daily)	All	160	159	160	159	158	37	37	37	37	37	7	7	7	7	7
IMPROVE Visibility (Daily)	All	157	157	157	157	155	38	38	38	38	38	7	7	7	7	7
STN (Daily)	All	20	20	20	20	20	6	6	6	6	6	1	1	1	1	1
NADP (Weekly)	All	235	214	224	214	217	41	40	37	36	40	6	6	6	6	6

Table 3-3   Definitions of Statistical Performance Metrics

Statistical Measure	Mathematical Expression	Notes
Mean Fractional Bias (MFB)	$$\frac{2}{N}\sum_{i=1}^{N}\left(\frac{P_i - O_i}{P_i + O_i}\right)$$	Reported as percent P_i = prediction at time and location i O_i = observation at time and location i N= Number of matched predictions and observations
Mean Fractional Gross Error (MFGE)	$$\frac{2}{N}\sum_{i=1}^{N}\left|\frac{P_i - O_i}{P_i + O_i}\right|$$	Reported as percent
Mean Normalized Bias (MNB)	$$\frac{1}{N}\sum_{i=1}^{N}\frac{\left(P_i - O_i\right)}{O_i}$$	Reported as percent
Mean Normalized Gross Error (MNGE)	$$\frac{1}{N}\sum_{i=1}^{N}\frac{\left|P_i - O_i\right|}{O_i}$$	Reported as percent
Normalized Mean Bias (NMB)	$$\frac{\sum_{i=1}^{N}(P_i - O_i)}{\sum_{i=1}^{N}O_i}$$	Reported as percent
Normalized Mean Error (NME)	$$\frac{\sum_{i=1}^{N}\left|P_i - O_i\right|}{\sum_{i=1}^{N}O_i}$$	Reported as percent
Coefficient of Determination (r^2)	$$\frac{\left[\sum_{i=1}^{N}(P_i - \overline{P})(O_i - \overline{O})\right]^2}{\sum_{i=1}^{N}(P_i - \overline{P})^2 \sum_{i=1}^{N}(O_i - \overline{O})^2}$$	$\overline{P}$ = arithmetic average of P_i, i=1,2,…, N; $\overline{O}$ = arithmetic average of O_i, i=1,2,…,N

Table 3-3   Definitions of Statistical Performance Metrics

Statistical Measure	Mathematical Expression	Notes
Mean Observation	$$\frac{1}{N}\sum_{i=1}^{N} O_i$$	Reported as concentration (e.g., micrograms per cubic meter [µg/m^3] or parts per million by volume [ppmv] depending on the pollutant)
Mean Prediction	$$\frac{1}{N}\sum_{i=1}^{N} P_i$$	Reported as concentration (e.g., µg/m^3 or ppmv depending on the pollutant)

3.2.2   Particulate and Visibility Statistical Measures

USEPA's (2007) PM and regional haze guidance suggested a suite of metrics for use in evaluating model performance. The standard set of statistical performance measures suggested for evaluating fine particulate models include: 1) normalized bias; 2) normalized gross (unsigned) error; 3) MFB; 4) MFGE; and 5) MFB in standard deviations. In past regional PM model evaluations (Tesche et al. 2005; Tonnesen et al. 2006), fractional bias and fractional error were found to be the most useful summary measures. Therefore, for this study, all error and bias metrics are calculated for PM species; however, the results only are analyzed for MFB and MFGE.

While all statistics in **Table 3-3** are presented for all chemical species discussed in Chapter 4.0, when assessing model performance for particle-phase species, the analysis focuses on MFB and MFGE. In Chapter 4.0, statements regarding model bias are referring to MFB and statements regarding model error are referring to MFGE for particle-phase compounds, visibility, and deposition.

As defined by Boylan and Russell (2006), the performance goals for PM species are MFB within ±30 percent and MFGE ≤50 percent. The performance criteria are MFB within ±60 percent and MFGE ≤75 percent. The performance goals are the more stringent of the two sets of metrics, and a good-performing model will achieve these goals. The performance criteria are less strict. If the criteria are equaled or exceeded, it suggests potential shortcomings with the model simulation. The goals and criteria increase at lower concentrations according to the following equations, in which C_o is the observation concentration and C_m is the model-predicted concentration:

Performance Goal:

$$FB \leq \pm 170\, e^{\frac{-0.5(\overline{C_o}+\overline{C_m})}{0.5\,\mu g/m^3}} + 30$$

$$FE \leq 150\, e^{\frac{-0.5(\overline{C_o}+\overline{C_m})}{0.75\,\mu g/m^3}} + 50$$

Performance Criteria:

$$FE \leq 125 e^{\frac{-0.5(\overline{C_o}+\overline{C_m})}{0.75\,\mu g/m^3}} + 75$$

$$FB \leq \pm 140 e^{\frac{-0.5(\overline{C_o}+\overline{C_m})}{0.5\,\mu g/m^3}} + 60$$

While the Boylan and Russell (2006) performance goals and criteria may not be achieved for this study, particularly for species that typically are difficult to model such as NO$_3$, performance goals and criteria will be

used to put the PM model performance into context and to facilitate model performance intercomparison across episodes, species, models, and sensitivity tests.

The most recent modeling guidance does not recommend specific criteria that distinguish between adequate and inadequate model performance (USEPA 2007). Instead, it is recommended that a suite of performance measures and displays be analyzed and that a "weight of evidence" approach be used to assess whether the model performs sufficiently well to be used for the intended purpose.

3.3   Model Performance Evaluation Software Tool

The University of California Riverside Model Performance Evaluation Software (MPES) (Chien et al. 2005) was developed to efficiently compute performance metrics and to present results in both tabular and graphical formats. The MPES generates the statistical measures shown in **Table 3-3** for appropriate temporal and spatial extents for each pollutant. The MPES was used to calculate the average of the model performance metrics for each month and to summarize these results using bar plots to compare the monthly average statistics for each species. In addition, statistical results were averaged over the full annual period as well as the four seasons and presented in tables in Chapter 4.0. Together, the bar plots and tabular summary provide a quick summary of the variability in seasonal model performance.

For most gas-phase compounds, the monitored ambient air concentrations can be directly compared to a single modeled chemical species. For particle-phase species and visibility, the comparison of modeled concentrations to ambient concentrations is more complicated. The PM is composed of many chemically different particle-phase species, and there are many different methods to measure these species, which makes it difficult to compare ambient concentrations to modeled concentrations. Measurements of these particle-phase species are available from several PM monitoring networks including the following: 1) IMPROVE; 2) CASTNet; 3) USEPA STN; and 4) NADP monitoring data. The comparison of modeled PM species to the monitored data must be performed in a consistent fashion. **Table 3-4** identifies the approach that was used to map measured data from each of the PM monitoring sites to the modeled PM species.

Chemical species present in the atmosphere contribute to visibility degradation by scattering and absorbing visible light. The combined effect of scattered and absorbed light is called light extinction. Total b_{ext} can be estimated based on the concentrations of atmospheric pollutants (Hand and Malm 2006) using the equation shown in **Table 3-4**, which can be re-written as the sum of the light extinction coefficients of the individual consituents of the atmosphere:

$$b_{ext} = b_{ext}SO_4 + b_{ext}NO_3 + b_{ext}OC + b_{ext}EC + b_{ext}SOIL + b_{ext}SS + b_{ext}CM + b_{ext}Rayleigh + b_{ext}NO_2$$

Where the individual light extinction coefficients are calculated by multplying the concentrations of the chemical species (binned into small and large sizes, where appropriate) with their extinction efficiency as follows:

$b_{ext}SO_4 = 2.2 \times f_s(RH) \times [Small\ SO_4] + 4.8 \times f_L(RH) \times [Large\ SO_4]$

$b_{ext}NO_3 = 2.4 \times f_s(RH) \times [Small\ NO_3] + 5.1 \times f_L(RH) \times [Large\ NO_3]$

$b_{ext}OC = 2.8 \times [Small\ OC] + 6.1 \times [Large\ OC]$

$b_{ext}EC = 10 \times [EC]$

$b_{ext}SOIL = 1 \times [SOIL]$

$b_{ext}SS = 1.7 \times f_{ss}(RH) \times [Sea\ Salt]$

$b_{ext}CM = 0.6 \times [CM]$

$b_{ext}Rayleigh = Rayleigh\ Scattering\ (value\ varies\ by\ site)$

$b_{ext}NO_2 = 0.33 \times [NO_2(ppb)]$

In a pristine atmosphere, Rayleigh scattering due to light interaction with air molecules is the primary contributor to total b_{ext}. In other environments, Rayleigh scattering is added to the estimated b_{ext} from measured concentrations of other chemical species. These chemicals include particulates composed of SO_4, NO_3, OC, EC, SOIL, SS, and CM. The concentrations of each compound are converted into an estimate of the individual contribution to b_{ext} using chemical-specific dry extinction efficiency, which is adjusted to actual conditions using relative humidity adjustment factors (f[RH]). The f(RH) values vary as a function of the relative humidity and chemical species for SO_4, NO_3, and SS and are defined as follows:

f_s(RH)= relative humidity adjustment factor for small SO_4 and NO_3

f_L(RH) = relative humidity adjustment factor for large SO_4 and NO_3

f_{ss}(RH) = relative humidity adjustment factor for SS

This equation is applied to both model-predicted pollutant concentrations and measured pollutant concentrations at IMPROVE monitoring sites within the 12- and 4-km model domains. Model-predicted visiblity is computed using the modeled concentrations of the same species. To facilitate visibility calculations using the new IMPROVE equation for MPE purposes, model results were further processed to separate SO_4, NO_3, and organic mass species into large and small groups based on the approach by Hand and Malm (2006). For the MPE, the f_s(RH), f_L(RH), and f_{ss}(RH) are based on the monitored daily relative humidity and the corresponding growth factors for small and large size SO_4 and NO_3, and total SS. To assess the model performance for visibility impacts, the daily model-predicted b_{ext} was compared to the reconstructed b_{ext} using the statistical measures in **Table 3-3**.

In addition to statistical summary tables, results are presented in graphical format to facilitate quantitative and qualitative comparisons between model predictions and measurements. Together with the statistical metrics identified in **Table 3-3**, the graphical procedures are intended to help: 1) identify flawed model simulations; 2) guide the implementation of performance improvements in the 2010 model input files in a logical, defensible manner; and 3) identify the similarities and differences between the alternative model simulations. These graphical tools were used to depict the ability of the model to predict the observed gas-phase species concentrations, as well as particle-phase concentrations for comparison to PM standards and visibility metrics.

Graphical displays include the following:

- Time-series plots during key events at monitoring locations in or near the Uinta Basin study area.

- Spatial plots of gas-phase and particulate concentration isopleths overlaid with monitoring values during key events.

- Bias and error stratified by concentration (e.g., "bugle plots") for PM composition. Bugle plots are used to show how model performance varies as a function of the PM species concentration. Monthly average error and bias are plotted in a bugle plot as a function of the species concentration on the x-axis. These plots help characterize differences in model performance for clean versus impacted conditions. These plots also include curves showing model performance goals and model performance criteria.

- Time-series of stacked bar charts showing the reconstructed b_{ext} contribution from each chemical species for both monitored and modeled species. Each plot has two parts: the top graphic shows the reconstructed b_{ext} from observations, and the bottom graphic shows the modeled contributions to visibility impairment for each of the 365 modeled days. The two graphics presented together in each plot provide a summary of temporal variability in model performance.

These graphical displays were generated with the MPES, where appropriate. Due to the large number of plots that are generated to cover all sites and all species, only selected graphical plots are presented in the MPE.

Table 3-4   Mapping of Monitored Particulate Species to Modeled Particulate Species

Compound	Monitored Species Definitions by Network[1]				CAMx Modeled Species Definitions[2]	CMAQ Modeled Species Definitions[2]
	IMPROVE	CASTNet	STN	NADP		
SO_4	3*S	TSO_4 (Teflon filter)	SO_4	wSO_4	PSO4	ASO4I + ASO4J
NO_3	NO_3	TNO_3 (Teflon filter)	NO_3	wNO_3	PNO3	ANO3I + ANO3J
Particulate NO_3+SO_4	---	0.29*TNO_3 + 0.375*TSO_4	---	---	0.29*PNO3 + 0.375*PSO4	0.29*ANO3J + 0.29*ANO3I + 0.375*ASO4J + 0.375*ASO4I
Total NO_3 (gas+particle)	---	TOTAL_NO3	---	---	PNO3 + 0.9841*2175.6* DENS*HNO3	ANO3J + ANO3I + 0.9841*2175.6*DENS*HNO3
NH_4	0.375*SO_4 + 0.29*NO_3	TNH_4 (Teflon filter)	NH_4	wNH_4	PNH4	ANH4I + ANH4J
OC	1.4*($OC1$ + OC_2 + OC_3 + OC_4 + OP)	---	OC	---	POA + SOA1 + SOA2 + SOA3 + SOA4 + SOA5 + SOA6 + SOA7 + SOPA + SOPB	0.6 * AORGAI + 0.6 * AORGAJ + 0.833 * AORGPAI + 0.833 * AORGPAJ + 0.678 * AORGBI + 0.678 * AORGBJ
EC	EC_1 + EC_2 + EC_3 - OP	---	EC	---	PEC	AECI + AECJ
Soil	2.2*Al + 2.49*Si + 1.63*Ca + 2.42*Fe + 1.94*Ti	---	---	---	FCRS + FPRM	A25I + A25J
Carbon mass (CM)	MT – FM	---	---	---	CCRS + CPRM	ACORS + ASEAS + ASOIL
Sea salt (SS)[3]	SS				NA + PCl	0.78*ANAJ + 0.78*ANAI + ACLI + ACLJ
$PM_{2.5}$	FM	---	$PM_{2.5}$	---	PSO4 + PNO3 + PNH4 + POA + SOA1 + SOA2 + SOA3 + SOA4 + SOA5 + SOA6 + SOA7 + SOPA + SOPB + PEC + FCRS + FPRM	ASO4I + ASO4J + ANO3I + ANO3J + ANH4I + ANH4J + AORGAI + AORGAJ + 1.167*(AORGPAI + AORGPAJ) + AORGBI + AORGBJ + AECI + AECJ + ANAJ + ACLJ + A25J

Table 3-4   Mapping of Monitored Particulate Species to Modeled Particulate Species

Compound	Monitored Species Definitions by Network[1]				CAMx Modeled Species Definitions[2]	CMAQ Modeled Species Definitions[2]
	IMPROVE	CASTNet	STN	NADP		
Reconstructed fine mass (reconstructed $PM_{2.5}$)	1.375*SO4 + 1.29*NO3 + EC + OC + SOIL	---	---	---	1.375*PSO4 + 1.29*PNO3 + POA + SOA1 + SOA2 + SOA3 + SOA4 + SOA5 + SOA6 + SOA7 + SOPA + SOPB + PEC + FCRS + FPRM	1.375*ASO4J + 1.375*ASO4I + 1.29*ANO3J + 1.29*ANO3I + AECJ + AECI + AORGAJ + AORGAI + AORGPAJ + AORGPAI + AORGBJ + AORGBI + A25J + A25I
PM_{10}	MT	---	---	---	$PM_{2.5}$ + CM	$PM_{2.5}$ + CM
Reconstructed light extinction coefficient (b_{ext})[4]	b_{ext} = 2.2 x f_s(RH) x [Small SO_4] + 4.8 x f_L(RH) x [Large SO_4] + 2.4 x f_s(RH) x [Small NO_3] + 5.1 x f_L(RH) x [Large NO_3] + 2.8 x [Small OC] + 6.1 x [Large OC] + 10 x [EC] + 1 x [SOIL] + 1.7 x f_{ss}(RH) x [SS] + 0.6 x [CM] + Rayleigh Scattering Site Specific + 0.33 x [NO_2 (ppb)]	---	---	---		

[1]   Monitored species names are defined differently for each individual monitoring network and are available on-line. The websites for each network are presented in Table 4-2 of the Air Quality Protocol (AECOM 2012). Compounds not measured by a network are indicated by "---."

[2]   The definitions for each modeled species are based on species definition files from USEPA's AMETv1.1.

[3]   SS generally is not a species of concern in the Uinta Basin study area; therefore, the model performance was not assessed for this particular species. However, SS was included in the calculation and evaluation of visibility for completeness.

[4]   The equation to reconstruct b_{ext} is based on the approach developed by Hand and Malm (2006).

4.0   Air Quality Model Performance Evaluation

The CMAQ and CAMx model performance was evaluated based on a comparison of the 2010 modeling results to the monitored concentrations of pollutants. The model performance was evaluated throughout the 36-, 12-, and 4-km model domains, with the primary focus on the 4-km domain and the Uinta Basin study area. Model performance was assessed for air quality pollutants (gas-phase and particle-phase pollutants) and for AQRVs (visibility and atmospheric deposition).

For each pollutant, the model was assessed using the statistical metrics discussed in Section 3.2. Seasonal and annual statistical metrics provide an overview of annual model performance and information regarding how the pollutant concentrations and model performance may vary by season. These statistics are summarized separately for the 36-, 12-, and 4-km domains.

Following the statistical summaries, annual time series plots are presented for select monitoring sites. The time series plots are informative for evaluating the model's ability to reproduce seasonal trends and monitored air quality events. Following the assessment of annual and seasonal model performance, a more detailed assessment is conducted by evaluating the model performance during the POI described in **Chapter 1**. The POI were selected for analysis based on the elevated levels of pollutant concentrations during these periods. These periods are also consistent with the POI analyzed as part of the WRF model performance evaluation (AECOM and STI 2013). A detailed analysis of these POIs is conducted by reviewing time series plots at select monitoring sites as well as spatial plots of the 4-km domain model values overlaid with observed concentrations. Both time series and spatial plots present data that are useful for qualitatively assessing model performance during these episodes in order to provide additional insight regarding the overall model performance.

The focus of this chapter is a detailed assessment of the model performance relative to observations for individual pollutants and AQRVs. Chapter 5.0 builds on this detailed information and describes the implications of the model performance results as related to the intended use of the model for ARMS.

4.1   Ozone

Based on USEPA guidance (2007), model-predicted ozone concentrations were processed in several different ways for the statistical assessment of ozone model performance, as explained in detail in **Section 3.2**. The USEPA suggests model performance goals for ozone of MNB within ±15%, and MNGE less than or equal to 35% (2007). Since biases for low observed concentrations can be inflated by the MNB and MNGE statistics, NMB and NME are recommended for consideration of model performance when no concentration threshold is applied.

The full set of 1-hour ozone model results was used to qualitatively assess model performance when evaluating time series and spatial performance.

4.1.1   Annual Ozone Model Performance

The annual and seasonal ozone model performance is assessed based on statistical evaluations as well as time series of surface concentrations. Time series of modeled annual deposition are also included for informational purposes.

4.1.1.1   Ozone Statistical Analyses for the CMAQ 36-km, 12-km, and 4-km Domains

Annual and seasonal MNB summaries are presented for 1-hour, daily maximum 1-hour, 8-hour, and daily maximum 8-hour ozone concentrations in **Table 4.1-1** for each monitoring network and modeling domain.

These statistical summaries are presented both with a 60ppb threshold and without the threshold. **Table 4.1-2** presents the MNGE for each monitoring network and modeling domain. Similarly, NMB and NME are presented in **Table 4.1-3** and **4.1-4**, respectively. A more detailed assessment of the monthly average of daily maximum 8-hour average ozone MNB for all monitoring values exceeding 60 ppb is presented in **Figure 4.1-1**.

Tables 4.1-1 and **4.1-2** show that when a 60 ppb threshold is applied to the observed data, the MNB and MNGE model performance statistics for daily maximum 1-hour and daily maximum 8-hour average ozone are well within the suggested performance criteria for all monitoring networks and seasons. **Figure 4.1-1** illustrates how well the model performs for daily maximum 8-hour average ozone on a monthly basis. Although the MNB and MNGE values for the running 8-hour average ozone concentration (with the 60 ppb threshold applied) generally fall outside the performance criteria, statistics computed from peak 8-hour ozone concentration are more important in the context of the current NAAQS. The large MNB and MNGE values in **Tables 4.1-1** and **4.1-2** that were calculated without a threshold show that the model generally does not reproduce low ozone concentrations well. However, as noted above, MNB and MNGE statistics are typically inflated for low observed concentrations. Considering the NMB and NME values instead, in **Tables 4.1-3** and **4.1-4**, the model meets the performance goals for ozone for almost all measures, both with and without a threshold. Overall, the results indicate good model performance and that the model is generally able to reproduce the timing and magnitude of observed ozone concentrations. Given that the model is performing within USEPA recommended bias and error limits for higher ozone concentrations, which are the most relevant conditions for comparison to NAAQS, the model performance is acceptable.

Examination of the statistics in **Tables 4.1-1** through **4.1-4** indicates seasonal variability in the model performance for both the AQS and CASTNet networks for all modeling domains. In general, when the 60 ppb threshold is applied, the model results show negative biases during all seasons for 1-hour and 8-hour ozone concentrations, but positive biases tend to occur during the summer and fall for the daily maximum 1-hour and 8-hour ozone concentrations. The monthly MNB for daily maximum 8-hour average ozone, displayed in **Figure 4.1-1**, shows good model performance in general for both the AQS and CASTNet networks. For the 4-km domain, biases for the AQS network exceeds the USEPA model performance limits in January and February, but biases for all other months and networks are within the recommended performance criteria.

4.1.1.2   Annual Ozone Time Series Analyses

<u>Surface Ozone</u>

Figure 4.1-2 presents time series plots of hourly ozone concentrations at monitoring locations in the Uinta Basin. The plots compare hourly average ozone concentrations at four AQS monitoring sites with model-predicted ozone concentrations from the grid cells that contain the monitors. The monitoring sites selected for analysis of ozone model performance include Dinosaur (AQS monitor 49-047-1002), Ouray (AQS monitor 49-047-2003), Rangely (AQS monitor 08-103-0006), and Redwash (AQS monitor 49-047-2002). These monitoring locations are shown in **Figure 3-1** relative to the Uinta Basin study area and model domains. The model values in each time series are shown in red (CAMx) and blue (CMAQ), while the monitor values are shown in grey. The CAMx results are discussed in the model inter-comparison presented below, while the CMAQ results are summarized in more detail here.

In general, CMAQ is able to reproduce the observed values in the Uinta Basin throughout the year, with a few notable exceptions. Specifically, the model does not reproduce the minimums and peak concentrations at Dinosaur during summer. Similarly, the model is overestimating the low concentrations at Rangely during fall. On the other hand, the model tends to underestimate the peak concentrations at Ouray during winter. This tendency is more pronounced at Redwash.

Ozone Deposition

To enhance the analysis of ozone performance, an assessment of ozone removal via a deposition pathway is conducted based on time series of CMAQ ozone deposition rates. Since no ozone deposition observations are available, information is presented to more fully understand model performance and cannot be evaluated for accuracy. While total ozone deposition values are presented and discussed, ozone deposition is exclusively due to dry deposition processes.

Figure 4.1-3 shows time series analyses of modeled annual ozone deposition at selected sites in the Uinta Basin. The sites are the same ones used for the ozone concentration time series analyses presented above. All of the time series plots display CMAQ deposition results in blue, and CAMx results in red. The annual time series (**Fig. 4.1-3**) shows that both models exhibit a seasonal cycle, with higher dry deposition rates during the summer. The seasonal cycle in CAMx is much stronger than in CMAQ, with more daily variability.

1   **Table 4.1-1   Mean Normalized Bias Summary for Ozone**

Monitoring Network	Pollutant	36-km Domain					12-km Domain					4-km Domain				
		Annual	Winter	Spring	Summer	Fall	Annual	Winter	Spring	Summer	Fall	Annual	Winter	Spring	Summer	Fall
AQS (Hourly)	1-hour O_3 (60 ppb threshold)	-6.8	-31.3	-8.1	-6.4	-3.5	-7.2	-30.4	-9.0	-6.5	-2.4	-8.2	-31.5	-9.5	-1.5	5.7
	1-hour O_3 (no threshold)	139.7	279.8	79.0	48.0	190.0	106.7	226.9	54.9	44.9	131.1	76.0	145.5	51.3	40.3	98.5
	Daily Max 1-hour O_3 (60 ppb threshold)	0.8	-9.7	-2.7	1.5	5.4	-0.9	-17.7	-4.5	0.2	3.2	0.8	-13.5	-4.0	3.3	9.4
	Daily Max 1-hour O_3 (no threshold)	17.8	28.1	11.5	14.0	20.1	13.8	22.0	8.5	11.0	15.5	14.7	36.0	5.1	10.0	14.6
	8-hour O_3 (60 ppb threshold)	-28.5	-44.5	-28.4	-27.4	-32.1	-24.0	-38.5	-23.6	-23.3	-26.0	-21.2	-41.2	-19.7	-13.7	-18.8
	8-hour O_3 (no threshold)	97.9	250.8	43.9	27.3	104.6	80.6	200.6	36.8	27.5	86.0	83.2	227.9	53.0	30.8	76.4
	Daily Max 8-hour O_3 (60 ppb threshold)	-1.9	-11.6	-5.4	-0.8	1.3	-3.7	-20.4	-7.1	-2.5	0.6	-3.6	-18.3	-7.2	1.1	4.3
	Daily Max 8-hour O_3 (no threshold)	23.2	42.3	12.7	16.6	25.0	17.3	31.1	9.0	12.6	19.6	17.7	47.6	5.1	10.5	17.5
CASTNET (Hourly)	1-hour O_3 (60 ppb threshold)	-7.9	-14.3	-9.2	-5.7	-9.6	-8.7	-16.0	-11.1	-7.6	-2.9	-4.8	-11.3	-9.9	0.6	7.8
	1-hour O_3 (no threshold)	40.8	20.4	27.0	61.2	54.4	6.3	3.7	1.5	11.5	8.1	7.9	6.1	2.4	12.4	10.7
	Daily Max 1-hour O_3 (60 ppb threshold)	-1.1	-9.3	-2.4	0.8	-2.3	-3.0	-9.4	-5.6	-1.6	2.0	-0.3	-4.5	-5.8	4.4	12.0
	Daily Max 1-hour O_3 (no threshold)	14.3	11.6	10.7	17.2	17.6	5.8	5.6	2.1	7.3	7.9	7.8	6.0	2.0	12.7	10.5
	8-hour O_3 (60 ppb threshold)	-22.0	-11.3	-22.3	-19.3	-27.1	-12.6	-12.5	-13.9	-12.2	-9.2	-8.0	NA	-12.6	-3.0	0.3
	8-hour O_3 (no threshold)	44.0	24.7	26.9	64.2	60.5	6.3	3.7	1.6	11.4	8.0	7.7	5.9	2.4	12.2	10.2
	Daily Max 8-hour O_3 (60 ppb threshold)	-2.9	-8.3	-4.9	-0.1	-4.1	-5.4	-10.0	-7.6	-4.5	0.5	-2.7	NA	-7.6	2.3	11.6
	Daily Max 8-hour O_3 (no threshold)	14.4	10.2	9.8	19.3	18.4	4.6	4.6	0.8	6.2	6.7	6.7	5.4	1.4	10.7	9.4

2

Table 4.1-2   Mean Normalized Gross Error Summary for Ozone

Monitoring Network	Pollutant	36-km Domain					12-km Domain					4-km Domain				
		Annual	Winter	Spring	Summer	Fall	Annual	Winter	Spring	Summer	Fall	Annual	Winter	Spring	Summer	Fall
AQS (Hourly)	1-hour O$_3$ (60 ppb threshold)	15.5	36.3	12.0	15.9	18.4	13.8	32.0	11.6	14.1	14.3	15.0	34.7	11.9	10.9	11.2
	1-hour O$_3$ (no threshold)	156.4	302.1	92.9	63.2	207.8	122.3	249.1	69.0	58.2	145.9	87.2	164.3	63.0	49.0	107.1
	Daily Max 1-hour O$_3$ (60 ppb threshold)	11.9	19.0	8.3	12.6	15.0	10.6	20.3	8.5	11.2	11.8	10.5	20.5	8.1	10.4	12.7
	Daily Max 1-hour O$_3$ (no threshold)	22.9	33.4	15.8	20.6	23.8	19.6	28.7	14.0	17.7	19.6	19.1	41.5	10.7	14.6	16.5
	8-hour O$_3$ (60 ppb threshold)	31.0	47.7	29.0	30.4	35.5	26.3	40.4	24.1	26.2	29.3	23.2	44.2	20.4	16.4	19.7
	8-hour O$_3$ (no threshold)	120.3	275.1	64.3	49.9	127.5	100.5	222.9	56.1	47.1	105.1	96.2	243.6	67.1	42.6	88.0
	Daily Max 8-hour O$_3$ (60 ppb threshold)	10.9	18.6	8.2	11.2	14.4	10.1	22.3	8.8	10.3	11.2	10.1	22.4	8.6	8.5	9.3
	Daily Max 8-hour O$_3$ (no threshold)	27.8	47.8	16.8	21.9	28.7	22.9	38.0	14.5	18.5	23.5	21.9	54.0	10.6	14.3	19.3
CASTNET (Hourly)	1-hour O$_3$ (60 ppb threshold)	15.4	15.5	13.6	16.6	16.8	13.0	16.5	12.5	13.5	11.7	10.3	13.8	11.3	9.1	10.2
	1-hour O$_3$ (no threshold)	55.1	39.1	40.0	73.7	67.3	16.3	14.2	12.5	21.4	16.8	14.1	13.5	10.9	16.6	15.3
	Daily Max 1-hour O$_3$ (60 ppb threshold)	10.4	10.0	8.4	12.4	10.5	10.2	9.5	8.9	11.1	11.5	9.7	4.5	8.6	10.2	17.8
	Daily Max 1-hour O$_3$ (no threshold)	19.0	17.3	15.1	22.1	21.4	12.0	11.1	9.9	14.6	12.2	11.8	10.0	9.4	15.1	12.6
	8-hour O$_3$ (60 ppb threshold)	25.1	11.3	23.8	24.2	29.7	16.4	12.5	15.1	17.6	15.0	11.5	NA	13.3	9.7	3.5
	8-hour O$_3$ (no threshold)	61.0	43.9	42.8	81.1	76.3	17.0	14.2	13.0	22.7	17.8	14.1	12.7	11.2	17.1	15.4
	Daily Max 8-hour O$_3$ (60 ppb threshold)	10.2	8.3	8.4	11.9	10.7	9.4	10.0	8.7	10.2	8.9	8.7	NA	8.3	9.0	11.6
	Daily Max 8-hour O$_3$ (no threshold)	19.6	17.4	14.7	23.6	22.6	11.0	10.6	8.4	13.6	11.3	10.8	9.6	8.3	13.5	11.9

1

Table 4.1-3   Normalized Mean Bias Summary for Ozone

Monitoring Network	Pollutant	36-km Domain					12-km Domain					4-km Domain				
		Annual	Winter	Spring	Summer	Fall	Annual	Winter	Spring	Summer	Fall	Annual	Winter	Spring	Summer	Fall
AQS (Hourly)	1-hour O$_3$ (60 ppb threshold)	-7.4	-32.1	-8.4	-7.1	-4.1	-7.8	-31.5	-9.3	-7.2	-2.7	-9.4	-32.3	-10.1	-1.9	5.5
	1-hour O$_3$ (no threshold)	17.3	28.0	12.1	13.3	22.6	15.4	23.0	9.8	12.7	21.2	15.8	16.5	7.9	17.0	23.9
	Daily Max 1-hour O$_3$ (60 ppb threshold)	0.0	-11.1	-3.2	0.3	4.5	-1.7	-19.5	-5.0	-0.8	2.7	-0.2	-15.4	-4.6	2.7	9.1
	Daily Max 1-hour O$_3$ (no threshold)	11.5	17.6	8.2	9.2	14.4	8.4	13.1	5.4	6.8	11.0	9.5	16.8	3.5	8.7	13.3
	8-hour O$_3$ (60 ppb threshold)	-29.4	-46.6	-28.7	-28.4	-32.7	-24.8	-40.6	-23.9	-24.2	-26.7	-22.9	-43.1	-20.7	-14.0	-18.8
	8-hour O$_3$ (no threshold)	12.1	22.6	7.7	8.4	16.3	12.0	19.9	6.9	9.4	17.0	15.2	18.2	7.1	16.0	22.6
	Daily Max 8-hour O$_3$ (60 ppb threshold)	-2.5	-13.4	-5.7	-1.5	0.6	-4.3	-22.4	-7.4	-3.2	0.3	-4.6	-20.3	-7.8	0.8	4.2
	Daily Max 8-hour O$_3$ (no threshold)	13.7	22.4	8.9	11.5	17.0	9.6	15.8	5.5	7.9	12.7	9.8	15.6	3.3	9.4	14.7
CASTNET (Hourly)	1-hour O$_3$ (60 ppb threshold)	-8.1	-14.4	-9.3	-6.0	-9.7	-9.1	-16.1	-11.4	-8.3	-2.9	-5.0	-11.3	-10.1	0.3	7.7
	1-hour O$_3$ (no threshold)	11.9	3.4	8.7	18.9	15.9	3.6	2.1	0.0	6.6	5.8	6.4	4.6	1.3	10.7	9.5
	Daily Max 1-hour O$_3$ (60 ppb threshold)	-1.5	-9.5	-2.7	0.2	-2.6	-3.7	-9.5	-6.1	-2.7	1.7	-0.7	-4.5	-6.2	4.0	11.9
	Daily Max 1-hour O$_3$ (no threshold)	10.4	8.4	7.8	13.2	12.0	4.3	4.9	0.9	4.9	7.1	7.1	5.3	1.1	11.8	10.4
	8-hour O$_3$ (60 ppb threshold)	-22.3	-11.3	-22.5	-19.9	-27.3	-13.3	-12.5	-14.2	-13.2	-9.4	-8.2	NA	-12.7	-3.2	0.3
	8-hour O$_3$ (no threshold)	11.9	3.6	8.7	18.9	15.8	3.6	2.2	0.0	6.6	5.6	6.4	4.7	1.4	10.5	9.2
	Daily Max 8-hour O$_3$ (60 ppb threshold)	-3.1	-8.4	-5.1	-0.5	-4.3	-5.8	-9.9	-7.9	-5.2	0.5	-3.0	NA	-7.7	1.9	11.7
	Daily Max 8-hour O$_3$ (no threshold)	10.4	6.6	7.0	15.1	12.1	3.3	3.9	0.0	4.1	5.9	6.0	4.7	0.7	9.9	9.3

Table 4.1-4   Normalized Mean Error Summary for Ozone

Monitoring Network	Pollutant	36-km Domain					12-km Domain					4-km Domain				
		Annual	Winter	Spring	Summer	Fall	Annual	Winter	Spring	Summer	Fall	Annual	Winter	Spring	Summer	Fall
AQS (Hourly)	1-hour O_3 (60 ppb threshold)	15.8	36.6	12.1	16.1	18.4	14.1	32.9	11.8	14.4	14.4	15.9	35.2	12.5	11.0	11.2
	1-hour O_3 (no threshold)	33.8	49.7	26.5	29.4	39.5	30.3	43.5	24.0	26.8	34.5	27.4	39.1	20.4	25.7	31.3
	Daily Max 1-hour O_3 (60 ppb threshold)	12.1	19.6	8.5	12.8	15.1	10.9	21.8	8.8	11.4	11.9	10.9	21.2	8.5	10.5	12.5
	Daily Max 1-hour O_3 (no threshold)	17.8	23.7	13.5	17.5	19.1	15.3	20.7	12.0	15.1	15.8	15.0	25.9	10.1	13.9	15.3
	8-hour O_3 (60 ppb threshold)	31.8	49.4	29.4	31.2	35.9	27.0	42.2	24.4	27.0	29.9	24.8	45.6	21.4	16.6	19.7
	8-hour O_3 (no threshold)	39.2	52.0	32.0	36.3	44.7	35.5	45.9	29.5	33.2	39.9	30.9	41.3	23.8	29.5	35.9
	Daily Max 8-hour O_3 (60 ppb threshold)	11.1	19.3	8.3	11.4	14.5	10.4	24.0	9.0	10.5	11.3	10.8	23.6	9.1	8.5	9.3
	Daily Max 8-hour O_3 (no threshold)	19.3	29.0	13.7	18.0	21.6	16.0	23.7	11.9	15.0	17.2	15.1	26.6	9.8	13.5	16.6
CASTNET (Hourly)	1-hour O_3 (60 ppb threshold)	15.5	15.5	13.6	16.7	16.8	13.3	16.6	12.7	13.9	11.8	10.4	13.8	11.4	9.1	10.2
	1-hour O_3 (no threshold)	27.6	23.3	23.4	33.0	31.2	14.6	13.1	11.9	18.0	15.0	13.1	12.1	10.7	15.3	14.2
	Daily Max 1-hour O_3 (60 ppb threshold)	10.6	10.1	8.5	12.6	10.7	10.6	9.6	9.3	11.5	11.6	9.9	4.5	8.8	10.2	17.8
	Daily Max 1-hour O_3 (no threshold)	16.1	14.7	13.1	19.3	17.0	11.7	10.6	9.8	14.0	11.8	11.5	9.3	9.3	14.6	12.6
	8-hour O_3 (60 ppb threshold)	25.3	11.3	23.9	24.6	29.8	16.8	12.5	15.3	18.3	15.2	11.7	NA	13.4	9.8	3.4
	8-hour O_3 (no threshold)	32.6	25.0	28.0	40.4	36.7	15.6	13.1	12.6	19.9	16.2	13.3	11.6	11.0	15.8	14.6
	Daily Max 8-hour O_3 (60 ppb threshold)	10.4	8.4	8.5	12.1	10.9	9.7	9.9	8.9	10.6	8.9	8.7	NA	8.4	9.0	11.7
	Daily Max 8-hour O_3 (no threshold)	16.3	14.6	12.7	20.3	17.6	10.6	10.1	8.4	12.8	10.8	10.5	8.9	8.2	13.1	11.8
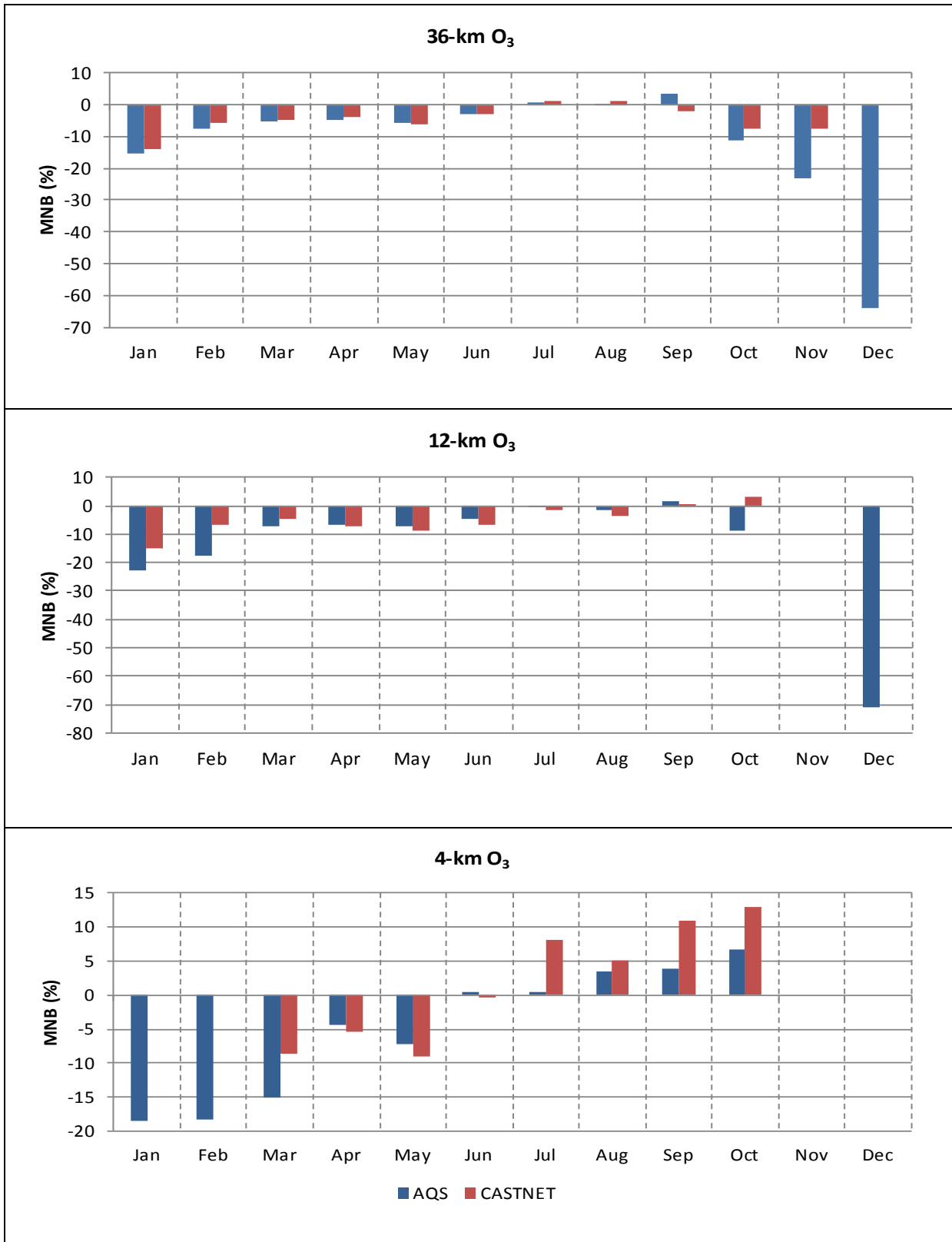
Figure 4.1-1   Monthly Mean Normalized Bias for Ozone
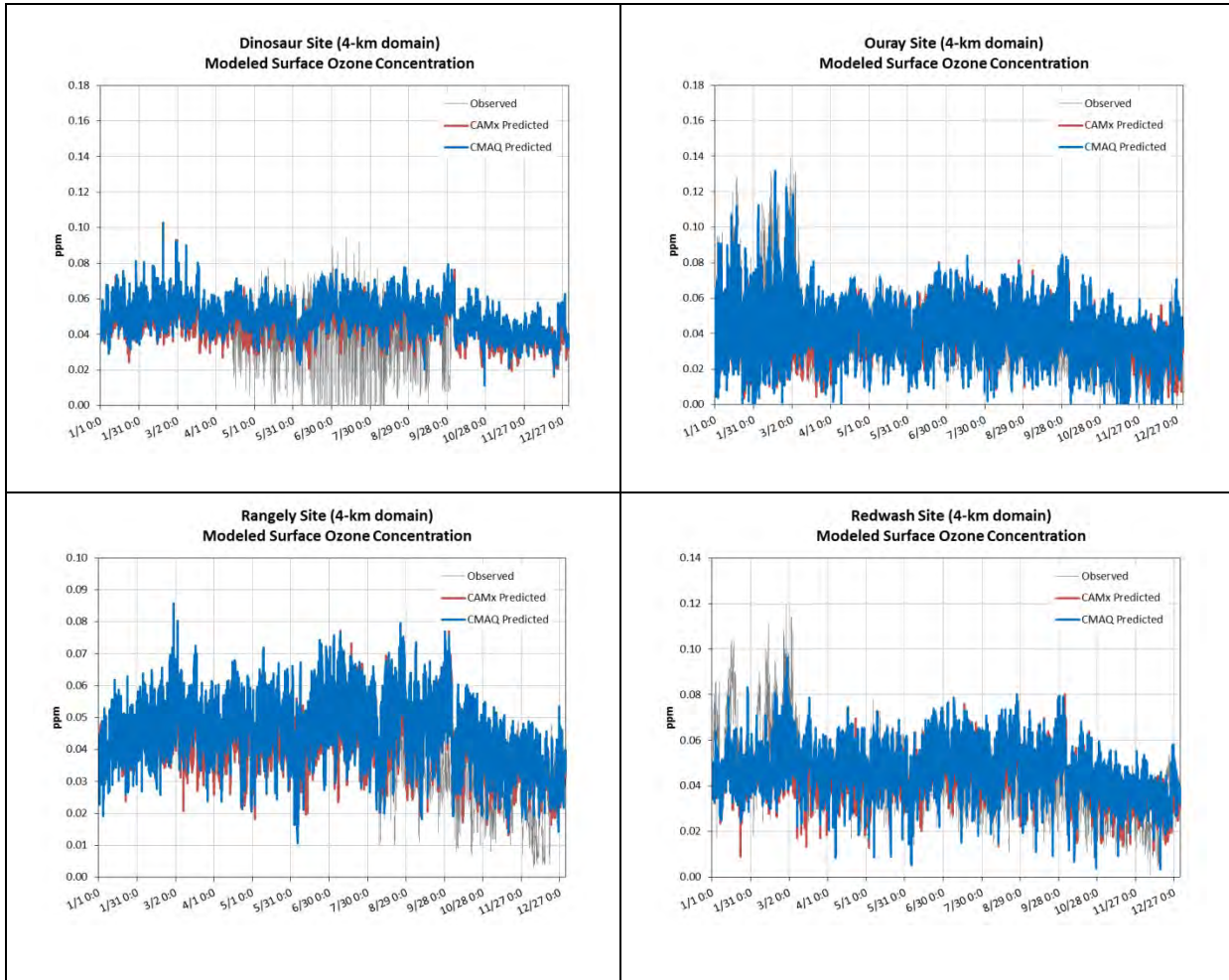
Figure 4.1-2   Annual Time Series for Ozone at Selected AQS Monitoring Sites
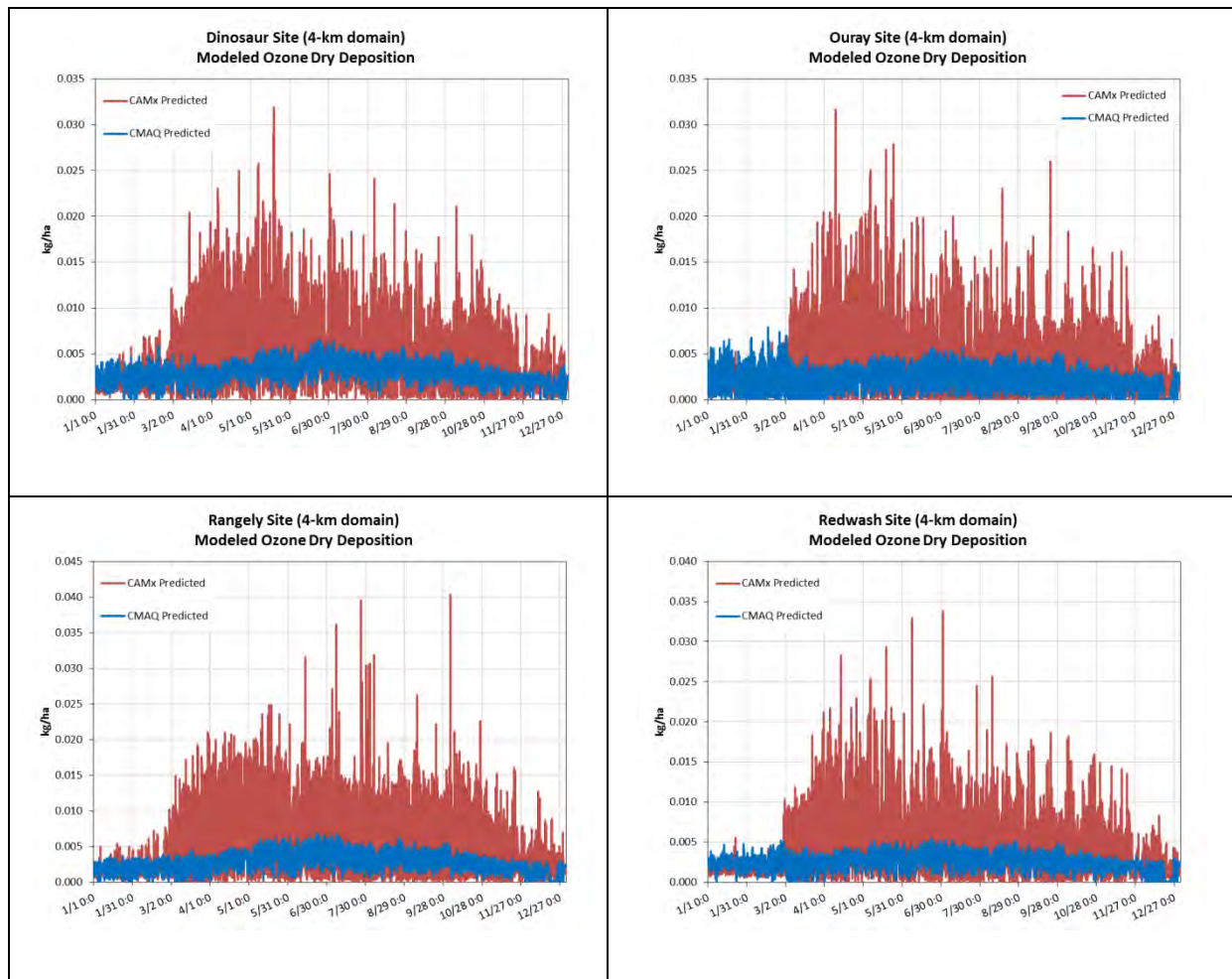
Figure 4.1-3   Annual Time Series for Ozone Dry Deposition at Selected AQS Monitoring Sites

4.1.2   Winter Ozone Model Performance

As described in **Chapter 1**, ozone model performance in the Uinta Basin was reviewed for four periods of interest in 2010. POI 1 and POI 2 occur in the winter and correspond with the periods of January 8 to 23, 2010 and February 21 to March 8, 2010, respectively. These two periods are analyzed in extensive detail in the following sections to evaluate the winter ozone model performance. In addition, these two periods in 2010 are compared with similar events that occurred in winter of 2011 when more extensive monitoring data was available in the Uinta Basin.

4.1.2.1   Conceptual Understanding of Winter Ozone Formation

A conceptual understanding of winter ozone formation has been developed based on field studies and observations of high ozone concentrations in southwestern Wyoming (ENVIRON 2010). The key environmental characteristics of ozone episodes in southwestern Wyoming are understood to be:

- Increased albedo due to extensive snow cover;

- Strong and persistent surface-based temperature inversion;

- Diurnal wind recirculation patterns that keep the ozone precursors in the airshed;

- Lack of ozone transport from upwind sources; and

- High concentrations of precursor emissions from local oil and gas development.

Recent ozone events during winter in the Uinta Basin have had many of the same characteristics as southwestern Wyoming, including extensive snow cover and strong temperature inversions (EDL 2011).

Previous reports and studies investigate aspects of winter ozone formation in the Uinta Basin. Meteorological characteristics that are important to winter ozone formation (i.e., snow cover, inversions, and wind direction) were analyzed for winter 2010 and presented in the ARMS Meteorological Model Performance Evaluation Report (AECOM and STI 2013). Model sensitivity tests, presented in **Appendix A** of this report, support the lack of ozone transport from upwind sources. The estimated emissions from all source sectors, with a focus on the oil and gas industry, are presented in the Emissions Inventory Technical Support Document (AECOM 2013). In the following sections, the winter ozone air quality model performance is evaluated and analyzes focus on the key characteristics described above.

4.1.2.2   Snow Cover

Snow cover was examined during the two winter POIs to verify that snow was present in the Uinta Basin. Snow cover fields used for the model simulation are shown in **Figure 4.1-4** and **4.1-5** for POI 1 and POI 2, respectively. As shown, the snow cover is uniform throughout the Uinta Basin study area during both winter POIs. During POI 1, the snow field covers most of the State of Utah, with a small amount melting at the end of the POI in the southwestern portion of the state. During POI 2, the snow cover field over Utah is more varied and melting occurs over areas in the western part of the state throughout the POI. This pattern is generally consistent with actual snow cover conditions during these periods (AECOM and STI 2013).

4.1.2.3   Winter Ozone Time Series Analyses

Surface Ozone

Figures 4.1-6 and **4.1-7** present time series plots of hourly ozone concentrations at monitoring locations in the Uinta Basin during POI 1 and POI 2. The plots compare hourly average ozone concentrations at four AQS monitoring sites with model-predicted ozone concentrations from the grid cells that contain the monitors. The monitoring sites selected for analysis of ozone model performance for the POIs include Dinosaur (AQS monitor 49-047-1002), Ouray (AQS monitor 49-047-2003), Rangely (AQS monitor 08-103-0006), and Redwash (AQS monitor 49-047-2002). Note that observations were not available in the winter POIs for the Dinosaur and Rangely sites. These monitoring locations are shown in **Figure 3-1** relative to the Uinta Basin study area and model domains. The model values in each time series are shown in red (CAMx) and blue (CMAQ), while the monitor values are shown in grey. The CAMx results are discussed in the model inter-comparison presented below, while the CMAQ results are summarized in more detail here.

Unlike many areas in the U.S., ozone concentrations in the Uinta Basin are highest during the winter months, especially January through March, when cold-pool stagnation events produce conditions that are conducive to photochemical ozone enhancement. This wintertime ozone enhancement is most pronounced in both the observations and model results at Ouray and Redwash, but is also apparent in the model results at Dinosaur and Rangely during POI 2.

In both POI 1 and POI 2 at the Ouray and Redwash monitoring sites, CMAQ captured much of the observed ozone enhancement (see **Figure 4.1-6** and **Figure 4.1-7**). Although CMAQ underestimated some of the highest ozone concentrations observed in Uinta Basin, the model consistently predicted peak ozone concentrations in excess of 75 ppb. Notably, the model performed better at Ouray than at Redwash during the winter POIs.

CMAQ predicted a more rapid drop from daytime peak ozone concentrations in winter compared to observations. This is further supported by an analysis of the diurnal patterns of ozone concentrations shown in **Figure 4.1-8** for each monitoring site. To generate the information shown in **Figure 4.1-8**, modeled hourly average surface ozone concentrations were selected from each grid cells that contains a monitor for the periods with elevated ozone during POI 1 and POI 2. The values were grouped by hour of the day, local time, and averaged for each monitoring site. When compared with monitored values at Ouray and Redwash that were processed the same way, the modeled surface concentrations have several important differences relative to the monitored diurnal patterns during winter episodes:

1. The modeled concentrations during nighttime hours are substantially lower than measured concentrations.
2. Modeled ozone production occurs earlier in the day and ramps up much more rapidly than measurements.
3. The modeled peak concentration occurs earlier in the day than measurements, this is perhaps due to the premature initiation of modeled ozone production.
4. The modeled peak declines much more rapidly than measurements.

These differences between model predictions and measurements could be attributed to precursor concentrations either at the surface (explored in the following section) or in the residual layer which is affected by the timing of the breakup of the inversion (which is explored in the vertical spatial analyses in **Section 4.1.2.4**). Additionally, the diurnal patterns of ozone removal pathways such as destruction or deposition also are analyzed in the following sections.

Surface NO$_x$ and VOC

Figures 4.1-9 and **4.1-10** show time series plots of model-predicted hourly NO$_x$, VOC, and ozone concentrations during the two winter POIs at the Uinta Basin monitoring sites. **Figure 4.1-9** illustrates a comparison of ozone concentrations with NO and NO$_2$ concentrations, while **Figure 4.1-10** illustrates a comparison of VOC concentrations with ozone and NO$_x$ concentrations. Note that a comprehensive assessment of modeled NOx performance is presented in **Section 4.3.1**. The discussion in this section is focused on the relationship between surface ozone precursors and modeled ozone at Ouray and Redwash sites, since observations were not available in the winter POI for the Dinosaur and Rangely sites. Also, model performance was typically better at Ouray and Redwash at other times of the year.

Time series plots in **Figure 4.1-9** demonstrate that NO and NO$_2$ concentrations are predicted to be about twice as high at the Ouray site compared to at the Redwash site. At Ouray, NO and NO$_2$ concentrations average about 5 and 10 ppb, respectively, and reach peak concentrations up to about 15 ppb and 40 ppb, respectively. At both sites, NO concentrations typically rise as NO$_2$ concentrations drop off, and titration of ozone by NO$_2$ is often apparent with ozone concentrations tending to reach a minimum as NO$_2$ concentrations peak. The range of NO and NO$_2$ concentrations is greater at the Ouray site than at the Redwash site. **Figure 4.1-10** shows that VOC concentrations are also about twice as high at Ouray (ranging from about 200 to 2000 pbb) compared to at Redwash (ranging from about 100 to 500 ppb). Similar to NO and NO$_2$, the range of VOC concentrations at Ouray is significantly larger than at Redwash. The results in **Figure 4.1-10** indicate that ozone formation is NO$_x$-limited at both sites.

The diurnal patterns of NO, NO$_2$, and VOC concentrations during periods with elevated ozone are shown in **Figure 4.1-11** for each monitoring site. To generate the information shown in **Figure 4.1-11**, modeled hourly average surface concentrations were selected from each grid cells that contains a monitor for the periods with elevated ozone during POI 1 and POI 2. The values were grouped by hour of the day, local time, and averaged for each monitoring site. Similar to the time series, NO concentrations typically rise as NO$_2$ concentrations drop off and the VOC and NO$_2$ concentrations tend

to track each other temporally. Also evident in **Figure 4.1-11** is the modeled minimum NO_2 and VOC concentrations which tend to occur in the afternoon at all sites, except for VOC at Dinosaur.

Ozone Deposition

To enhance the analysis of ozone performance, an assessment of ozone removal via a deposition pathway is conducted based on time series and spatial plots of CMAQ ozone deposition rates. Since no ozone deposition observations are available, information is presented to more fully understand model performance and cannot be evaluated for accuracy. While total ozone deposition values are presented and discussed, ozone deposition is exclusively due to dry deposition processes.

Figure 4.1-12 and **Figure 4.1-13** show time series analyses of modeled ozone deposition POI 1 and POI 2 at monitors in the Uinta Basin. All of the time series plots display CMAQ deposition results in blue, and CAMx results in red. During January and February, CMAQ tends to predict higher dry deposition rates throughout the diurnal cycle than CAMx. Dry deposition rates are relatively consistent across the Uinta Basin in CMAQ, while intra-site variability is more significant in CAMx.

The diurnal patterns of ozone dry deposition during periods with elevated ozone are shown in **Figure 4.1-14** for each monitoring site. To generate the information shown in **Figure 4.1-14**, modeled hourly average dry deposition values were selected from each grid cells that contains a monitor for the periods with elevated ozone during POI 1 and POI 2. The values were grouped by hour of the day, local time, and averaged for each monitoring site. Diurnal cycles in ozone dry deposition peak in the early afternoon at all sites, corresponding to diurnal cycles in both ozone concentration and ozone dry deposition velocity.

4.1.2.4   Winter Ozone Spatial Analyses

Ozone Spatial Analyses

Figure 4.1-15 shows contour plots of the daily maximum surface 1-hour ozone concentrations predicted by CMAQ in the 4-km domain for selected days in the POI 1. Monitored daily maximum 1-hour ozone concentrations from the AQS network are shown in the figure as circles. Throughout POI 1, there is reasonable agreement between modeled spatial patterns and observations in the 4-km domain, although the model tends to over-predict peak concentrations in the Salt Lake City area.

Figure 4.1-16 shows contour plots of the ozone concentrations predicted by CMAQ in the Uinta Basin study area at six different vertical layers at 4:00 pm MST on January 17, 2010 during POI 1. The vertical layers selected for analysis are layers 1, 3, 5, 8, 12, and 15, which correspond to heights of 20, 60, 121, 326, 662, and 1009 m above ground level, respectively, as shown in **Table 2-3**. Similarly, **Figure 4.1-17** shows data for 4:00 pm MST on February 28, 2010 during POI 2. The monitoring station locations are shown as black circles. Measurements above the surface are not available for comparison.

On January 17, 2010, the peak ozone concentration in the Uinta Basin is fairly similar within the lower layers 1 through 8; however, the spatial extent of the maximum decreases with altitude. There is a substantial decrease in the ozone concentrations above layer 8. The pattern is similar on February 28, 2010, except that the spatial extent of the elevated concentrations is much more widespread, particularly throughout the lower layers.

Ozone Vertical Profiles

Figure 4.1-18 shows modeled ozone vertical profiles at Redwash during January13 and 17, 2010 and February 25 and 28, 2010. These days were selected for analysis based on the models ability to reproduce and not reproduce measured surface concentrations as shown in **Figures 4.1-6** and **4.1-7**. Specifically, on January 13, 2010 the model is able to reproduce concentrations similar to

measurements at Redwash, while on January 17, 2010 the model significantly underpredicts concentrations relative to measurements. Similarly, on February 25, 2010 the model significantly underpredicts concentrations at Rewash, while on February 28, 2010 the model is able to reproduce measured concentrations.

Two plots of ozone vertical profile are shown for each day: the plot on the left shows the ozone concentrations throughout the vertical depth of the modeled atmosphere (i.e., layers 1 through 33); the plot on the right shows ozone concentrations within the lower layers of the modeled atmosphere (i.e., layers 1 through 14). Each plot contains an ozone profile for four different hours of the day corresponding to 6:00 am, 9:00 am, 1:00 pm, and 4:00 pm local time to enable an understanding of the modeled change in vertical ozone concentrations throughout the day.

Similarly, **Figure 4.1-19** shows the modeled ozone vertical profiles at Ouray for the same days analyzed for Redwash. On January 13 the model is able to reproduce concentrations similar to measurements at Ouray, while on January 17, 2010 the model slightly underpredicts concentrations relative to measurements. Similarly, on February 25 the model is able to reproduce concentrations similar to measurements at Ouray, while on February 28, 2010 the model slightly underpredicts concentrations relative to measurements. It is important to remember that the model generally performed better at Ouray than at Redwash.

In general, on days when the model performed better, there is a large separation between the initial morning concentrations at 6:00 and 9:00am and the afternoon concentrations at 1:00 and 4:00pm. This is perhaps more related to the model's tendency to underpredict the morning concentrations (as shown in **Figure 4.1-8**) than an indication of actual diurnal differences. An important commonality between all days with good model performance at Ouray and Redwash is the presence of a strong afternoon inversion with a boundary layer height of approximately 200 to 300 m above ground level, which corresponds with model layers 7 or 8.

NO_x and VOC Spatial Analyses

Figures 4.1-20 and **4.1-21** shows contour plots of the NO_x concentrations predicted by CMAQ in the Uinta Basin study area at six different vertical layers at 4:00 pm MST on January 17, 2010 (during POI 1) and 4:00 pm MST on February 28, 2010 (during POI 2), respectively. The vertical layers selected for analysis are identical to those selected for the spatial ozone plots above. Similarly, **Figures 4.1-22** and **4.1-23** shows contour plots of the total VOC concentrations predicted by on the same day, time, and vertical layers as the NO_x plots. The monitoring station locations are shown as black circles. Measurements are not available for comparison.

On January 17, 2010, the peak NO_x and VOC concentrations in the Uinta Basin at the surface are located in the vicinity of the Ouray monitor. Elevated NO_x concentrations also are evident downwind of the Ouray monitor, corresponding with the location of minimum ozone concentrations in **Figure 4.1-16**. Presumably, the location of the minimum ozone concentration is attributable to titration by fresh NO emissions downwind of a power plant. The spatial pattern of NO_x and VOC concentrations is fairly similar with increasing altitude in layers 1 through 5. There is a substantial decrease in the NO_x and VOC concentrations in most areas within the Uinta Basin study area at layer 8 and above, except for a peak in NO_x concentrations in layer 8 near a power plant.

The event on February 28, 2010 is quite different from January 17, 2010 in that the NO_x and VOC concentrations are substantially lower even though the modeled ozone concentrations are higher and inversion height is similar on the two days. Interestingly, the spatial ozone plots in **Figure 4.1-17** do not have a minimum concentration evident in the vicinity of the power plant on February 28, 2010, further supporting the premise that ozone concentrations are NO_x-limited during this period.

Ozone Deposition

Figure 4.1-24 shows spatial plots of daily cumulative ozone deposition from the CMAQ 4-km domain for POI 1 (January 8 through 23, 2010). During POI 1, the total ozone deposition rate is generally less than 80 grams per hectare per day (g/ha/day) throughout the 4-km domain, but occasionally higher rates occur in the mountains surrounding the Uinta Basin. Throughout the POI, the deposition rate peaks in the Uinta Basin study area during periods with elevated ozone concentrations. However, in general, the spatial variability in the deposition rates is fairly low presumably due to the consistent level of snow cover throughout the 4-km domain in winter (shown in **Figure 4.1-5**).

4.1.2.5   Comparison to 2011 Monitoring Data

During the winter of 2011 (January through March 2011), more extensive monitoring was conducted in the Uinta Basin than during winter 2010. The full analysis and monitoring records from the Uinta Basin 2011 winter ozone study is available in the "Final Report: Uinta Basin Ozone and Air Quality Study" (EDL 2011). For the purpose of evaluating 2010 model performance, winter 2011 monitoring data are compared to winter 2010 monitoring and modeling results using time series, diurnal plots, spatial plots, and vertical plots.

Comparison of Conditions in 2010 to 2011

Before comparing the 2010 model results to measurements collected in 2011it is important to understand the differences in the winter conditions between 2010 and 2011. As shown in **Table 4.1-5**, the average ozone concentrations were higher in 2010 than in 2011 both during the full year and the January-March period. However, the highest and second highest measured 1-hour average concentrations were higher in 2011 than in 2010 at all monitoring sites, which indicates that winter ozone events were more intense in 2011 than in 2010. This finding is further supported by the Ouray and Redwash time series shown in **Figure 4.1-25**. In general, when there is not an ozone episode, the 2010 values are higher than the 2011. When there is an ozone episode, the 2011 values are well above the 2010 values. This is especially true during the mid-February event in 2011 when concentrations peak around 140 ppb at Redwash and 149 ppb at Ouray. In contrast, during winter 2010 the peak values are approximately 120 ppb at Redwash and 139 ppb at Ouray.

Comparison of Diurnal Concentrations to 2011

The average hourly diurnal ozone profile during periods with elevated ozone in 2010 (POI1 and POI2) are compared to the diurnal ozone profile from 2011 (EDL 2011) for each of the four monitoring sites. To generate the diurnal profiles, modeled hourly average surface ozone concentrations were selected from each grid cells that contains a monitor for the periods with elevated ozone during POI 1 and POI 2. The values were grouped by hour of the day, local time, and averaged for each monitoring site. This information is slightly different than what is presented for 2011 diurnal profiles. The 2011 diurnal profiles (EDL 2011) show two different periods: February 2-6, 2011 and February 12-16, 2011. These two periods were selected to present results without elevated ozone and with elevated ozone, respectively. It is expected that the diurnal profiles for the two winter seasons have different absolute concentrations due to the differences in measured ozone concentration maximums as described previously. Therefore, the purpose of the analyses is not to evaluate the 2010 models' accuracy relative to the absolute concentrations measured during the winter of 2011, rather the intent of these analyses is to compare the timing of the ozone diurnal pattern and relative differences in concentrations throughout a day.

Figure 4.1-26 comparisons the diurnal ozone profiles from 2011 to 2010 for all four monitoring sites. In general, the findings presented in **Section 4.1.2.3** are consistent with measurements collected in 2010 and 2011. Specifically, modeled diurnal profiles tend to have lower nighttime concentrations, initiate ozone production earlier in the day, ozone concentrations peak earlier in the day, and decline more rapidly than measurements suggest. Notably, these findings are consistent both with periods of

elevated ozone (February 12-16, 2011) and periods without elevated ozone (February 2-6, 2011), perhaps with the exception that the modeled nighttime concentrations are not lower than measurements during periods without elevated ozone.

At Ouray, both the model and measurements show that this site has the overall highest concentrations of the four sites analyzed, while the Rangely site has the lowest concentrations. The modeled diurnal profiles at Rangely tend to have shorter durations of the higher ozone concentrations than other stations, which is contrary to 2011 measurements. Importantly, at Dinosaur the measurements in 2011 indicate ozone concentrations are similar to levels observed at Ouray and Redwash during ozone events, but the 2010 model predictions are much lower at Dinosaur than Ouray or Redwash. At Redwash, the 2010 modeled and measured diurnal profiles are flatter with a smaller difference between maximum and minimum values in comparison to measurements at Redwash in 2011 and in comparison to the other stations.

Comparison of the Modeled Spatial Concentrations to 2011

In general, the spatial extent of 2010 modeled ozone concentrations (**Figures 4.1-16 and 4.1-17**) show elevated concentrations occur in the vicinity of the oil and gas activities rather than the more uniformly distributed concentrations observed in 2011 (EDL 2011). This difference is perhaps due to differences in the actual meteorological conditions between the events or the spatial interpolation methods used on 2011 measurement data to generate the estimated spatial pattern. Regardless of these differences, the model appears to under estimate concentrations in the northern portion of the basin relative to 2011 measurements.

Comparison of Vertical Profiles to 2011

Figures 4.1-18 and 4.1-19 show the CMAQ-modeled vertical ozone at Redwash and Ouray sites, respectively. At both Redwash and Ouray sites, the ozone concentrations tend to increase with altitude in the morning. While in the afternoon, when surface temperature increases, ozone concentrations tend to be relatively constant at levels of below model layer 5 (~120m), indicating a well-mixed environment within the PBL. The difference between morning and afternoon vertical profiles is similar to vertical ozone measurements collected in 2011 at Redwash (EDL 2011).

There are some potentially important differences in the modeled 2010 vertical profiles versus 2011 measurements. Specifically, the modeled morning concentrations are substantially lower than measurements. In addition, morning measurements show a decline in concentrations with altitude, while the model shows both increases and decreases with altitude, depending on the day.
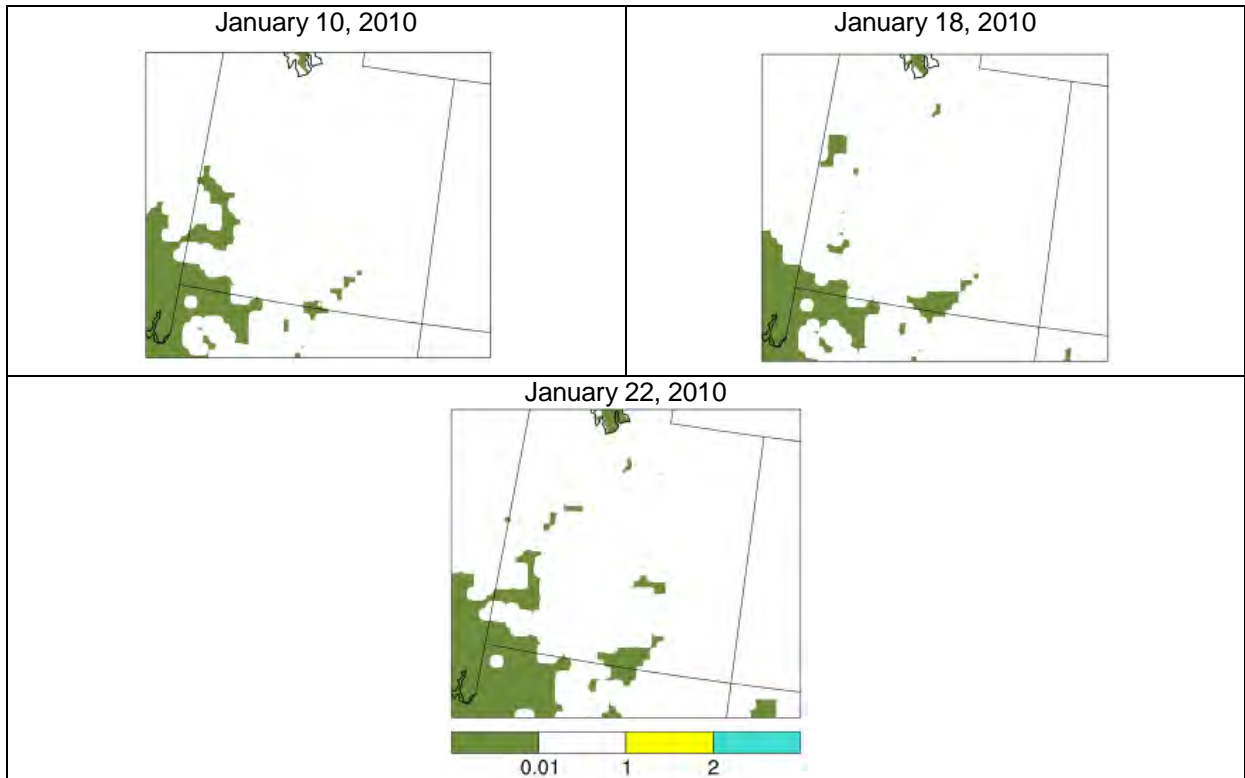
Figure 4.1-4   4-km Snow Cover Plots during January 8 to January 23, 2010

February 23, 2010 | February 27, 2010
March 3, 2010 | March 7, 2010
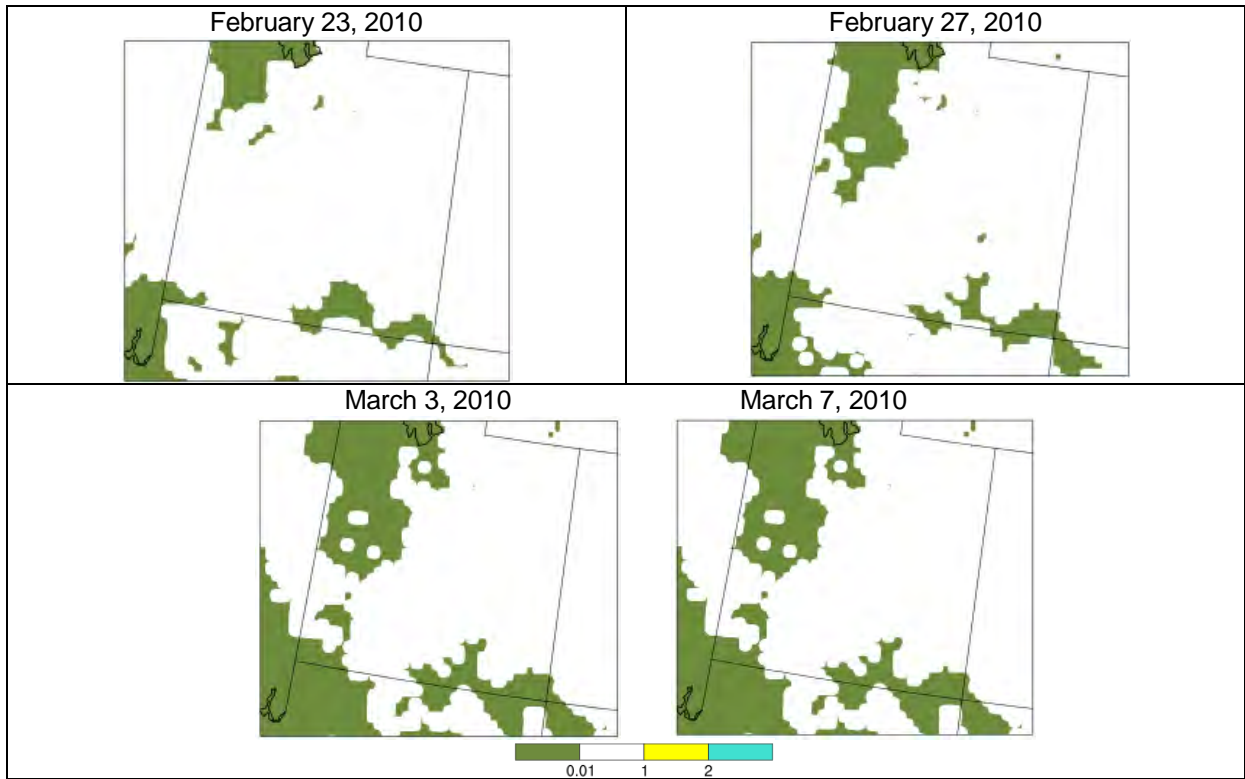
Figure 4.1-5   4-km Snow Cover Plots during February 21 to March 8, 2010
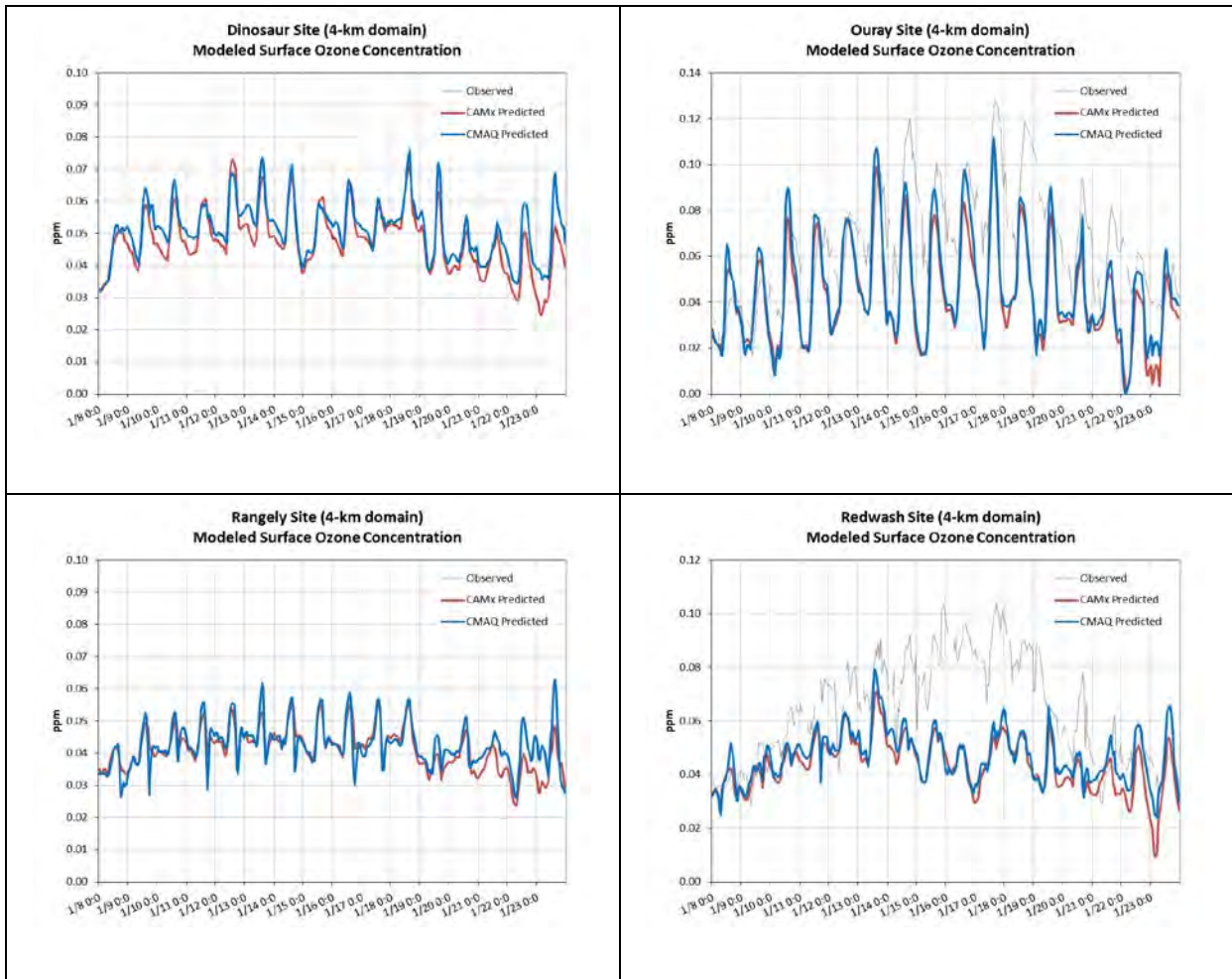
Figure 4.1-6   Time Series for Ozone at Selected AQS Monitoring Sites during January 8 to January 23, 2010
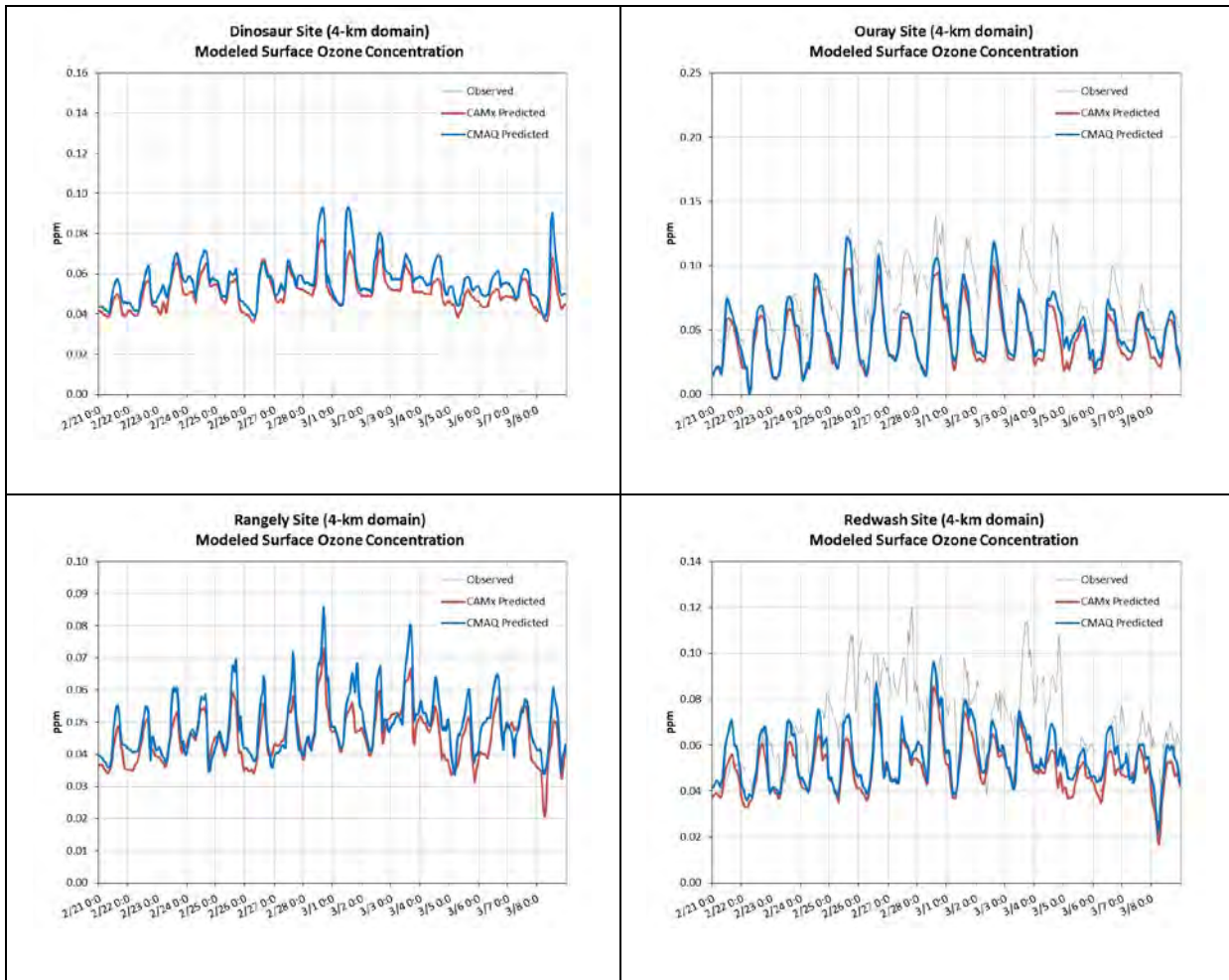
Figure 4.1-7   Time Series for Ozone at Selected AQS Monitoring Sites during February 21 to March 8, 2010
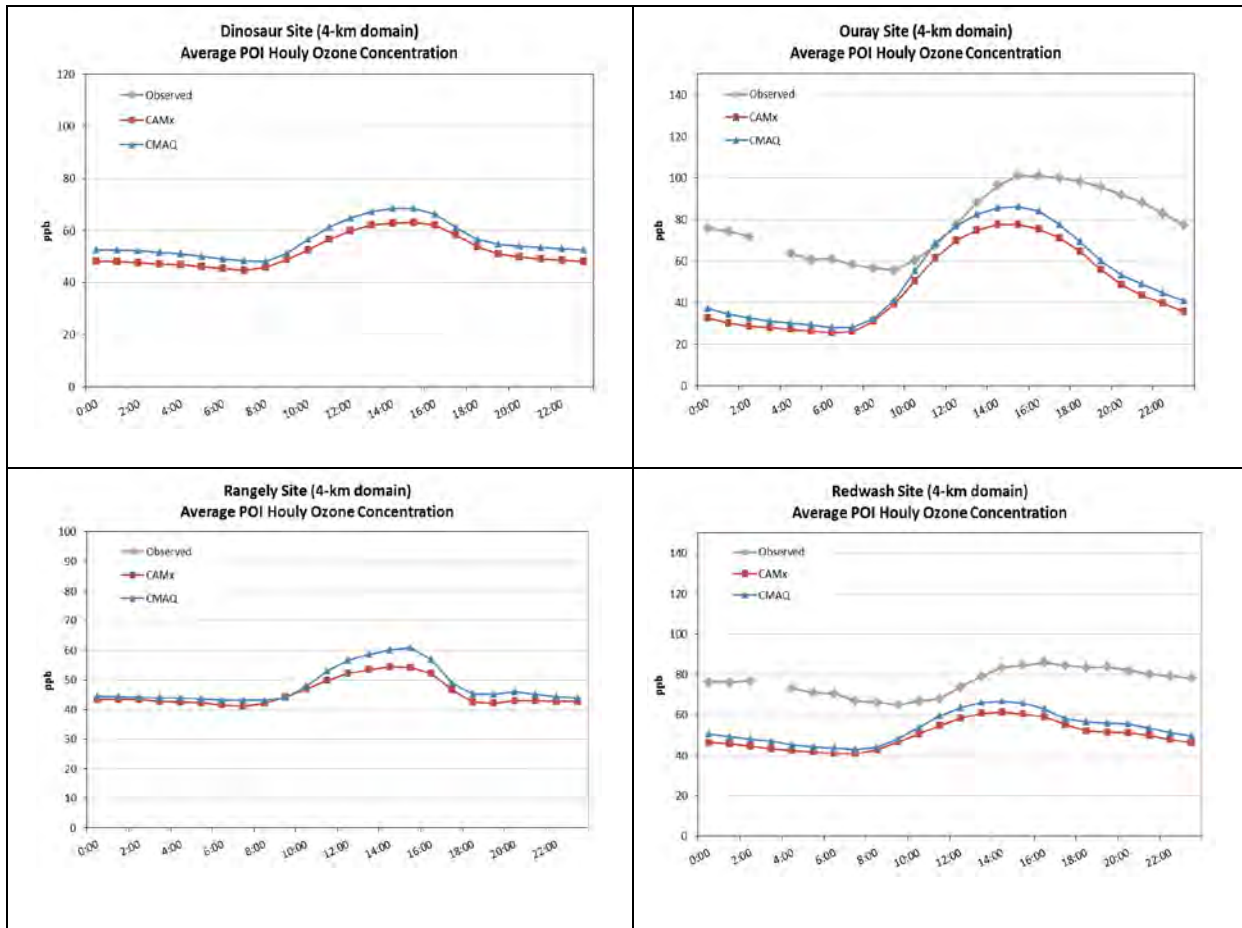
Figure 4.1-8   Hourly Average Diurnal Profile for Ozone at Selected AQS Monitoring Sites during January 8 to January 23, 2010 and February 21 to March 8, 2010
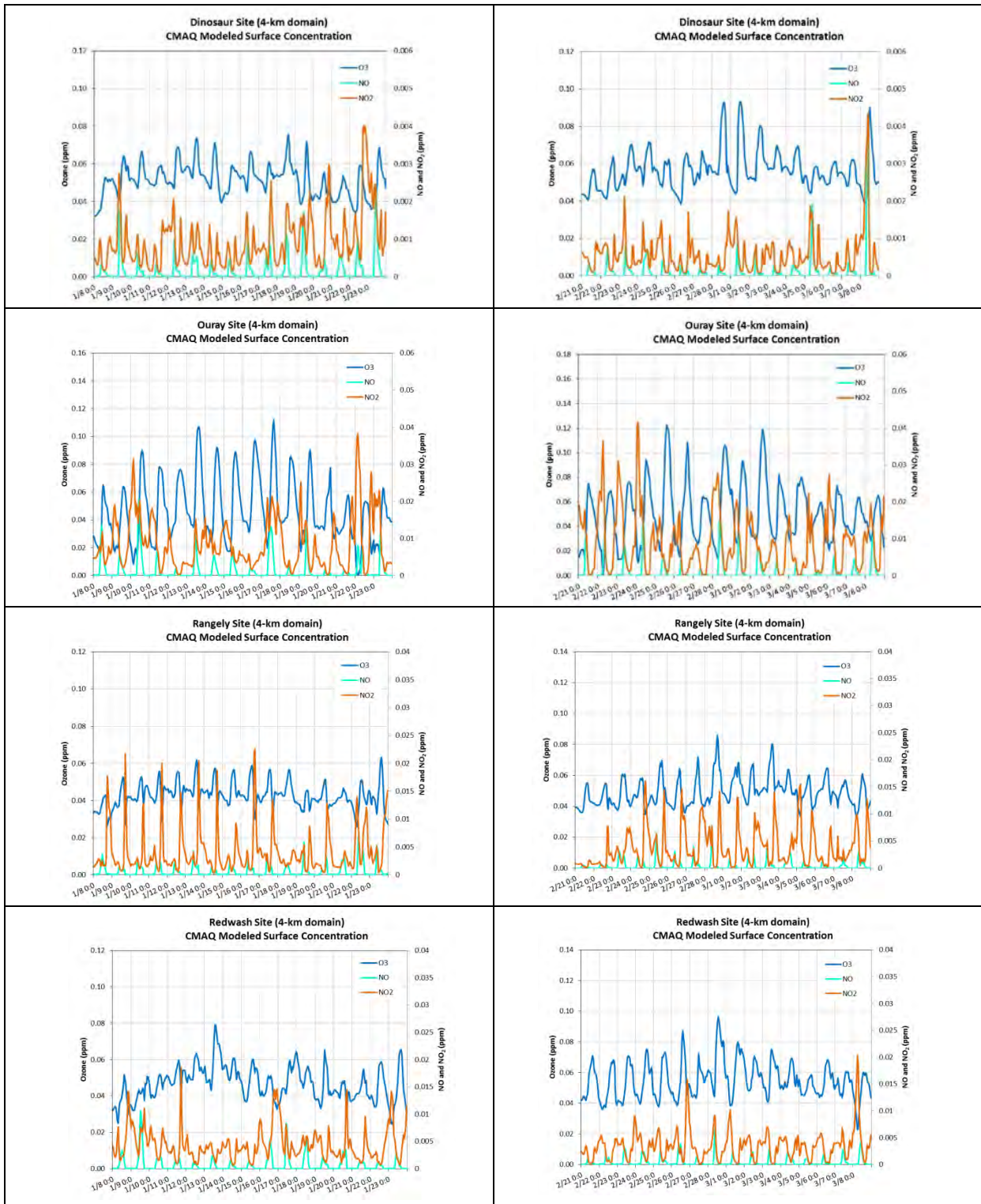
Figure 4.1-9   Winter Time Series for CMAQ-Modeled Ozone, NO, and NO₂ at Selected AQS Monitoring Sites
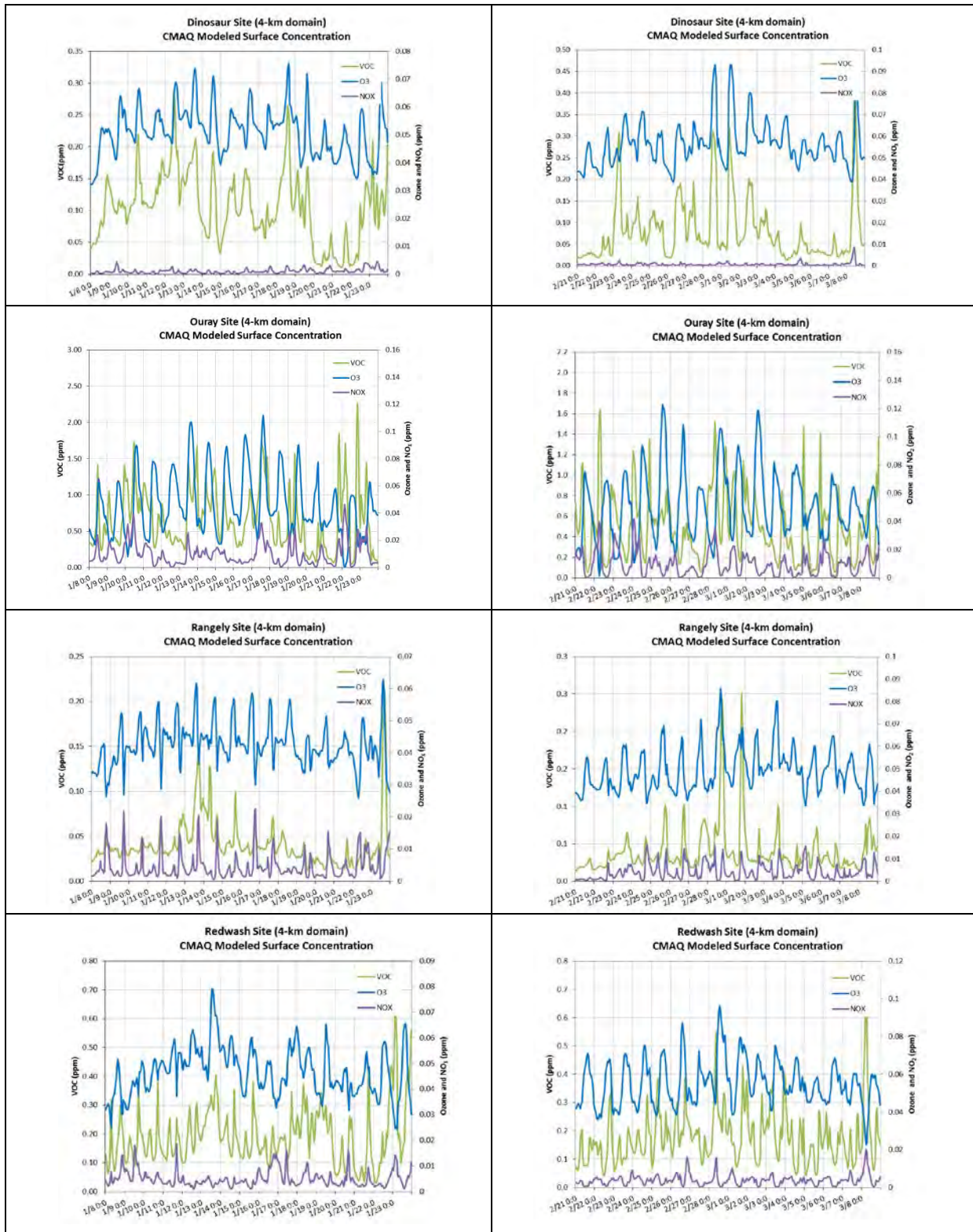
Figure 4.1-10   Winter Time Series for CMAQ-Modeled Ozone, NO$_X$, and VOC at Selected AQS Monitoring Sites
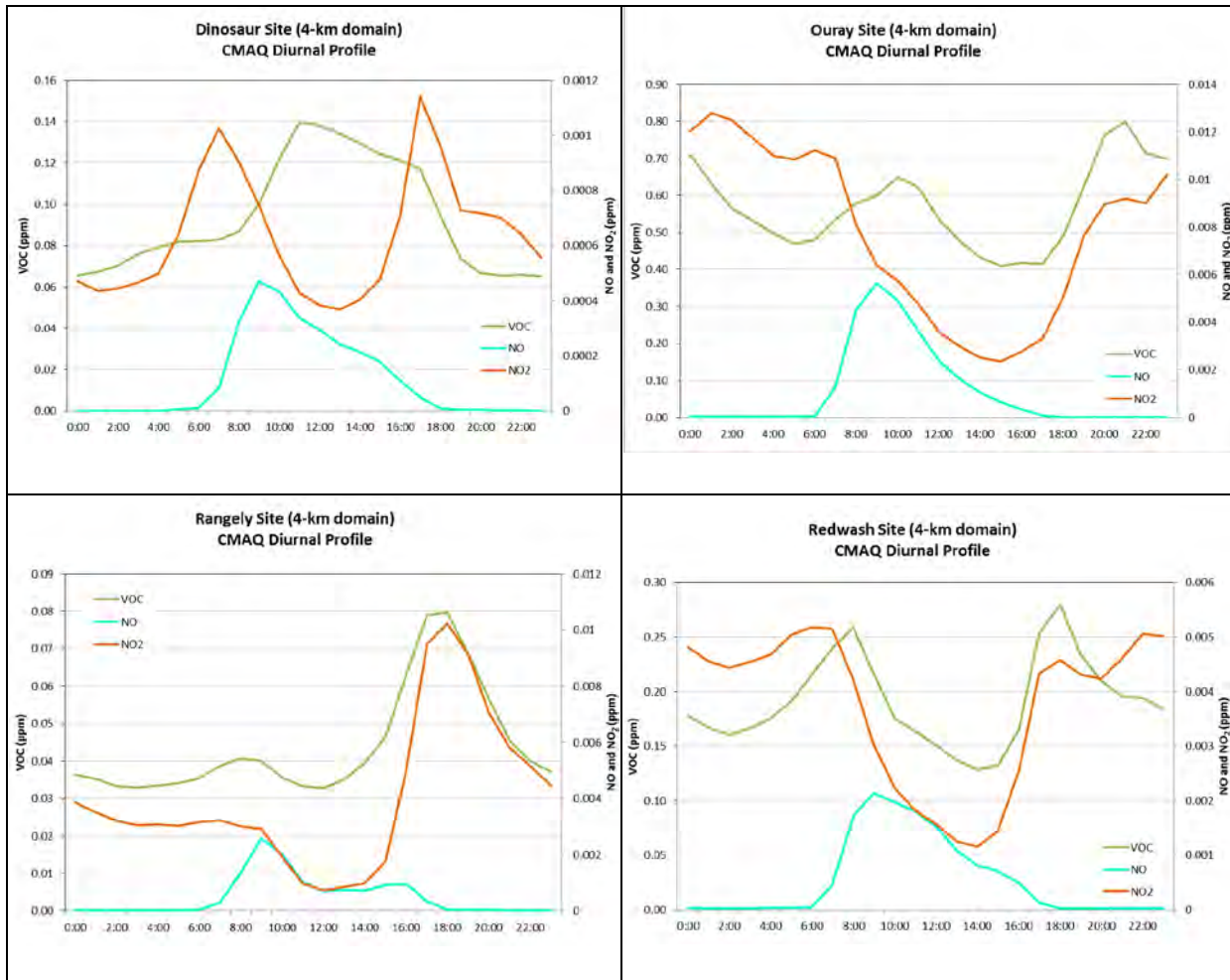
Figure 4.1-11 Winter Hourly Average Diurnal Profiles for CMAQ-Modeled NO, NO$_2$, and VOC at Selected AQS Monitoring Sites
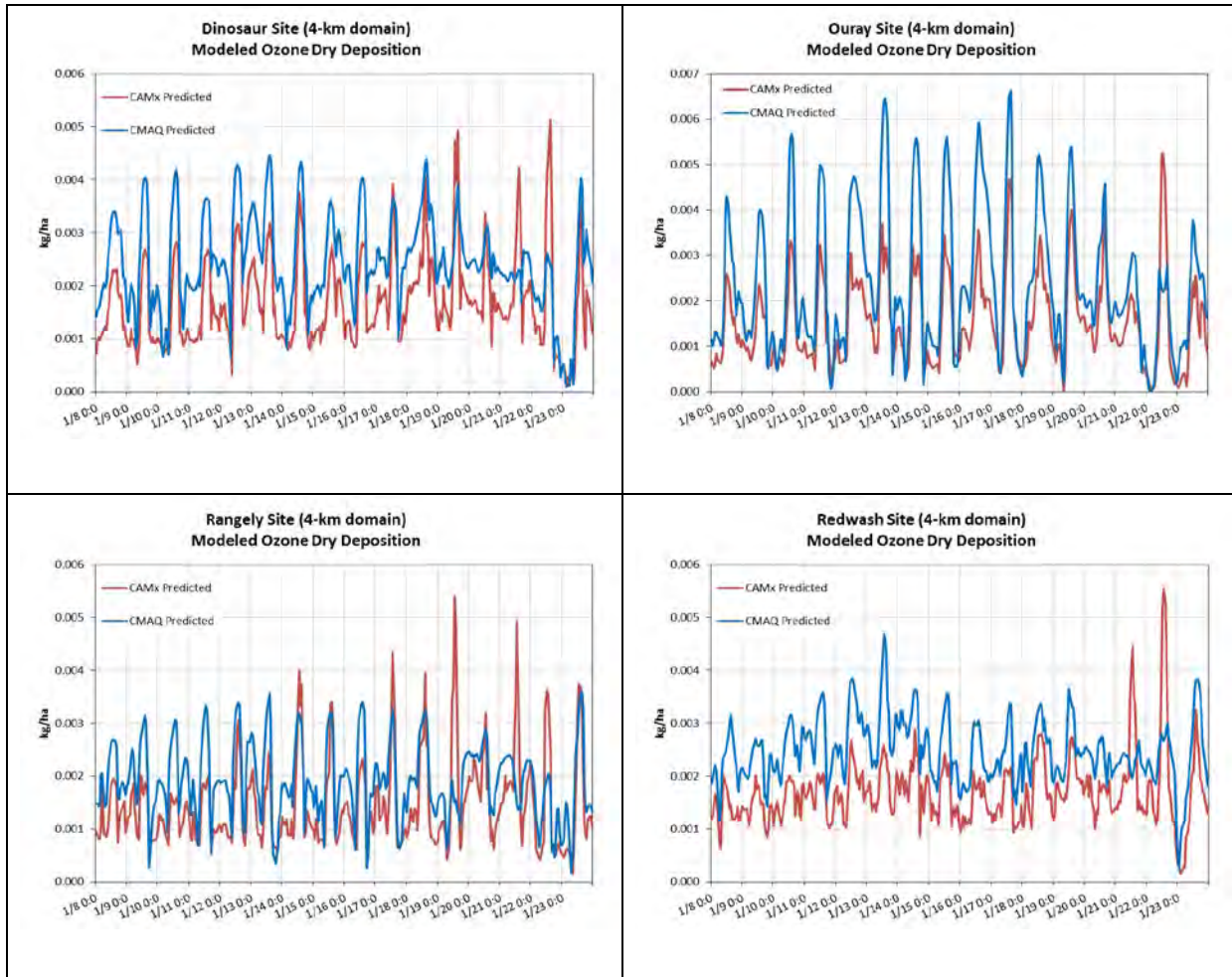
Figure 4.1-12   Time Series for Ozone Dry Deposition at Selected AQS Monitoring Sites during January 8 to January 23, 2010
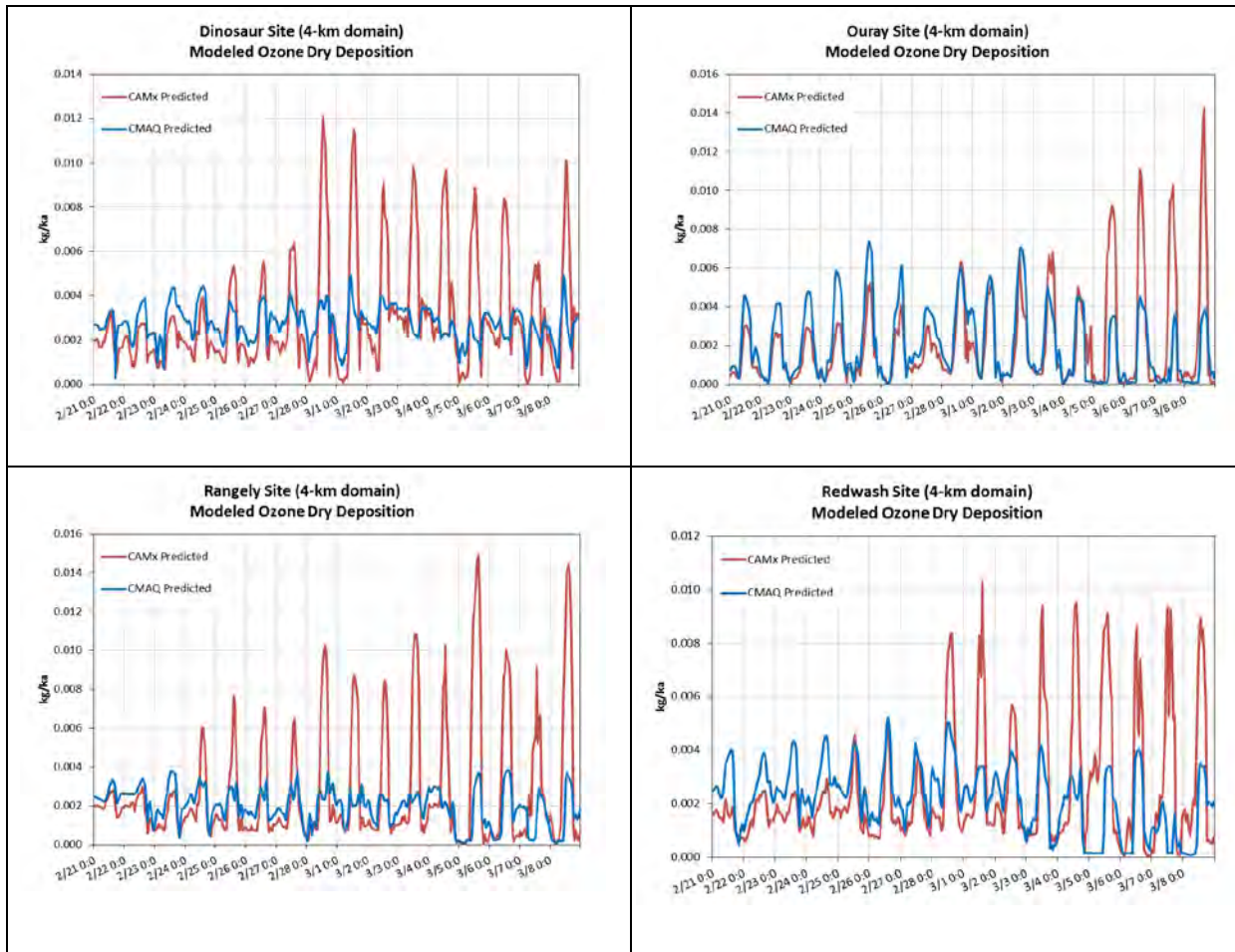
Figure 4.1-13 Time Series for Ozone Dry Deposition at Selected AQS Monitoring Sites during February 21 to March 8, 2010
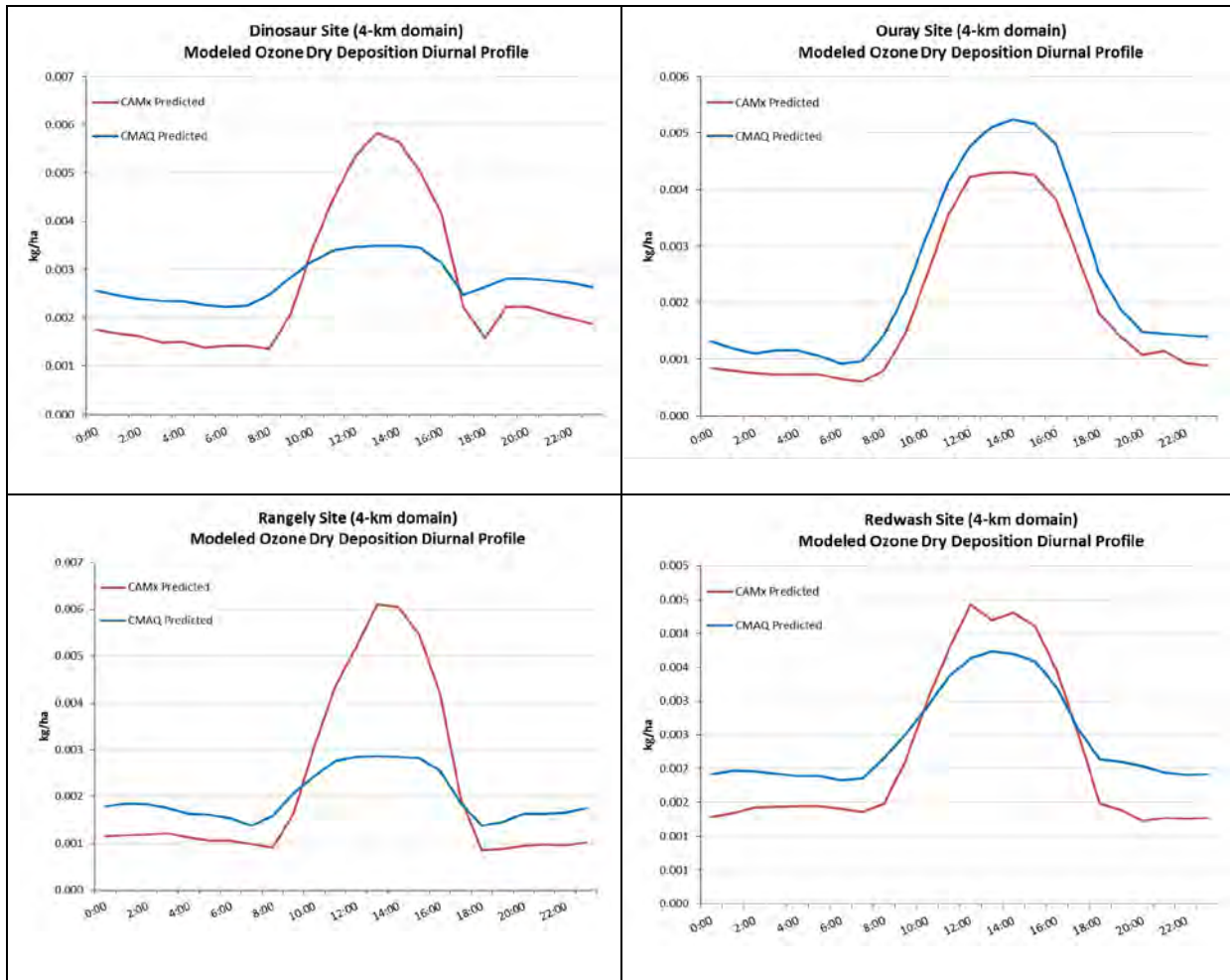
Figure 4.1-14   Winter Hourly Average Diurnal Profiles for Ozone Dry Deposition at Selected AQS Monitoring Sites
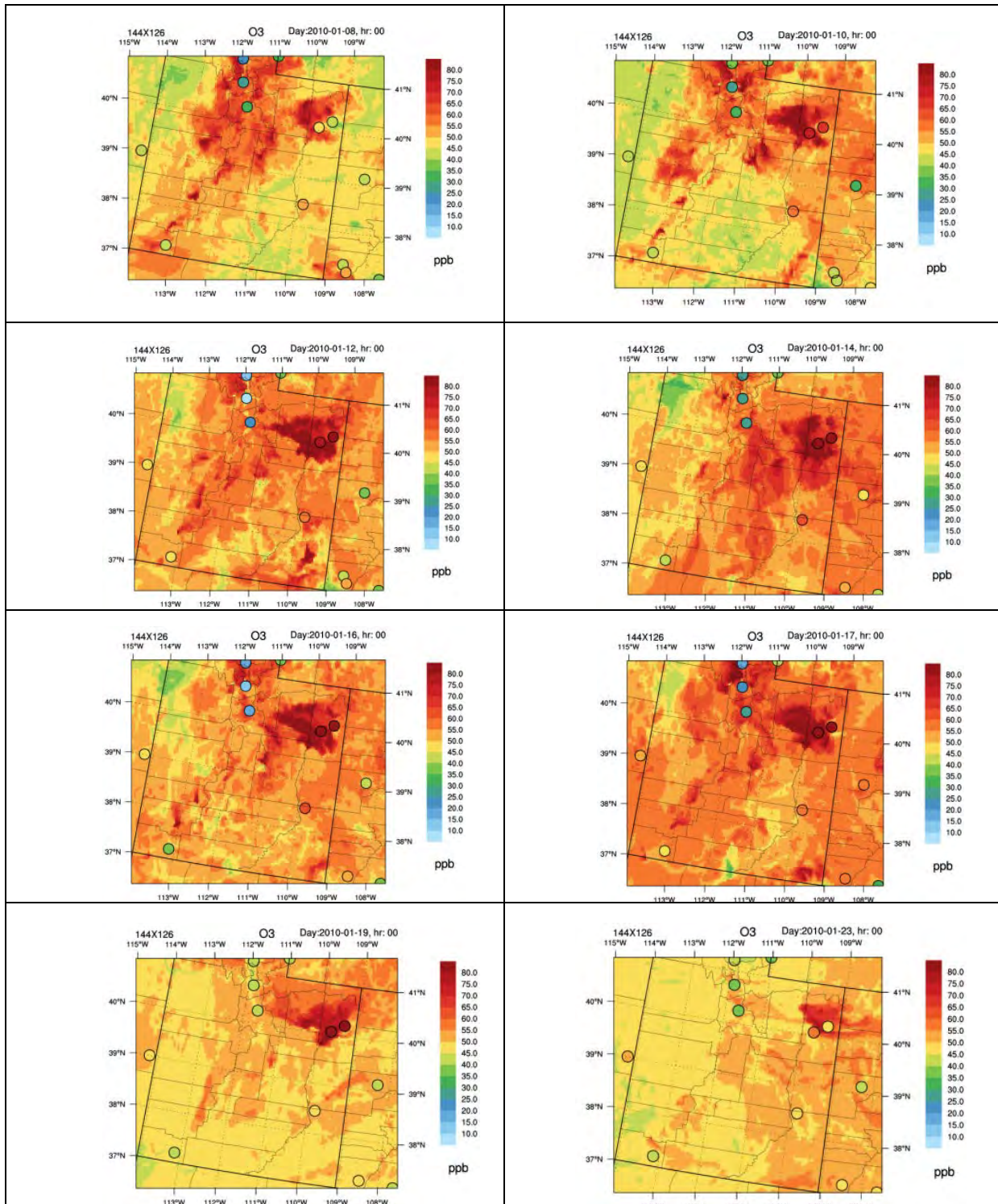
Figure 4.1-15   4-km Spatial Plots for Ozone during January 8 to January 23, 2010
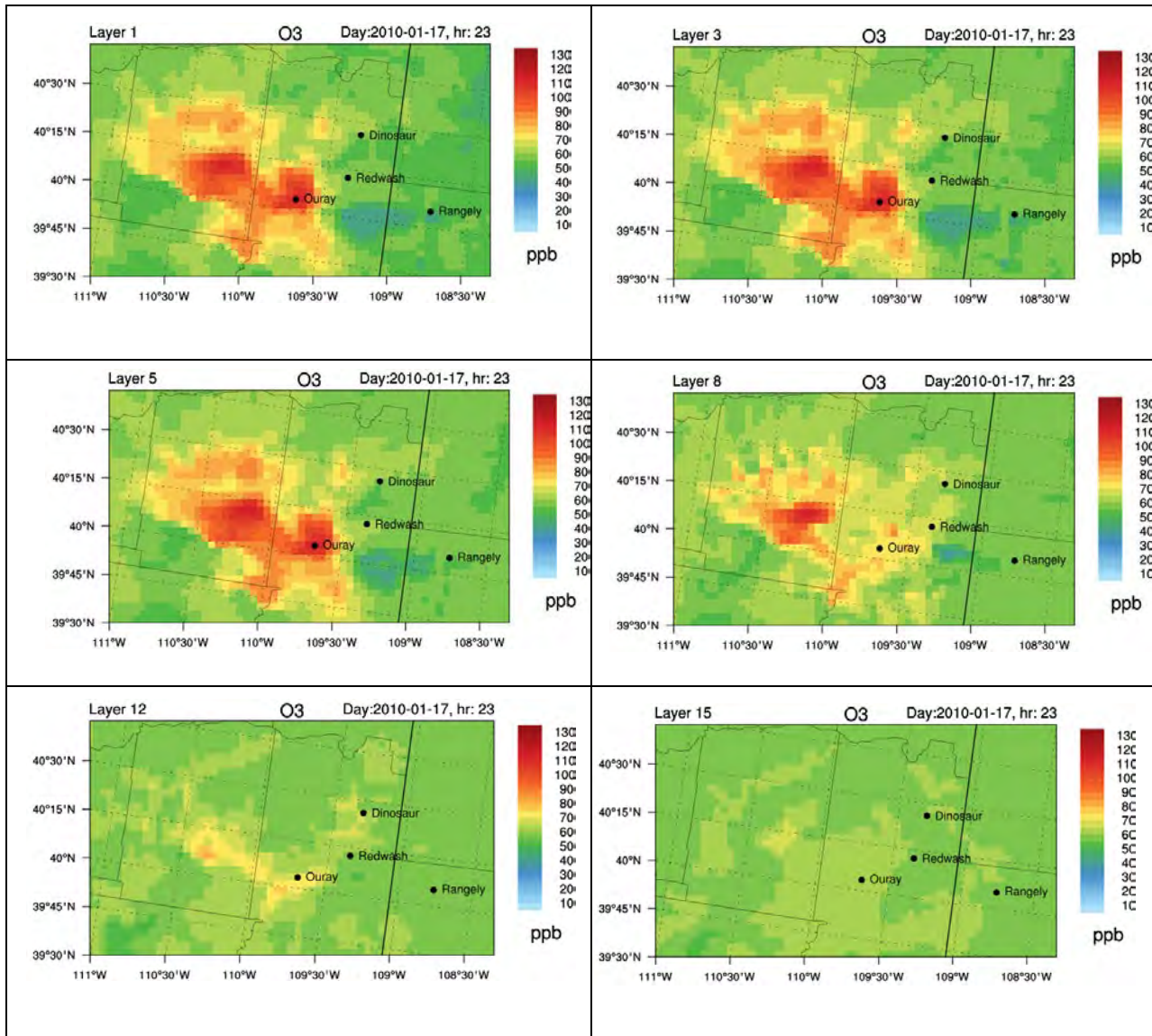
Figure 4.1-16   Spatial Plots of Ozone in the Uinta Basin on January 17, 2010 at Selected Vertical Levels
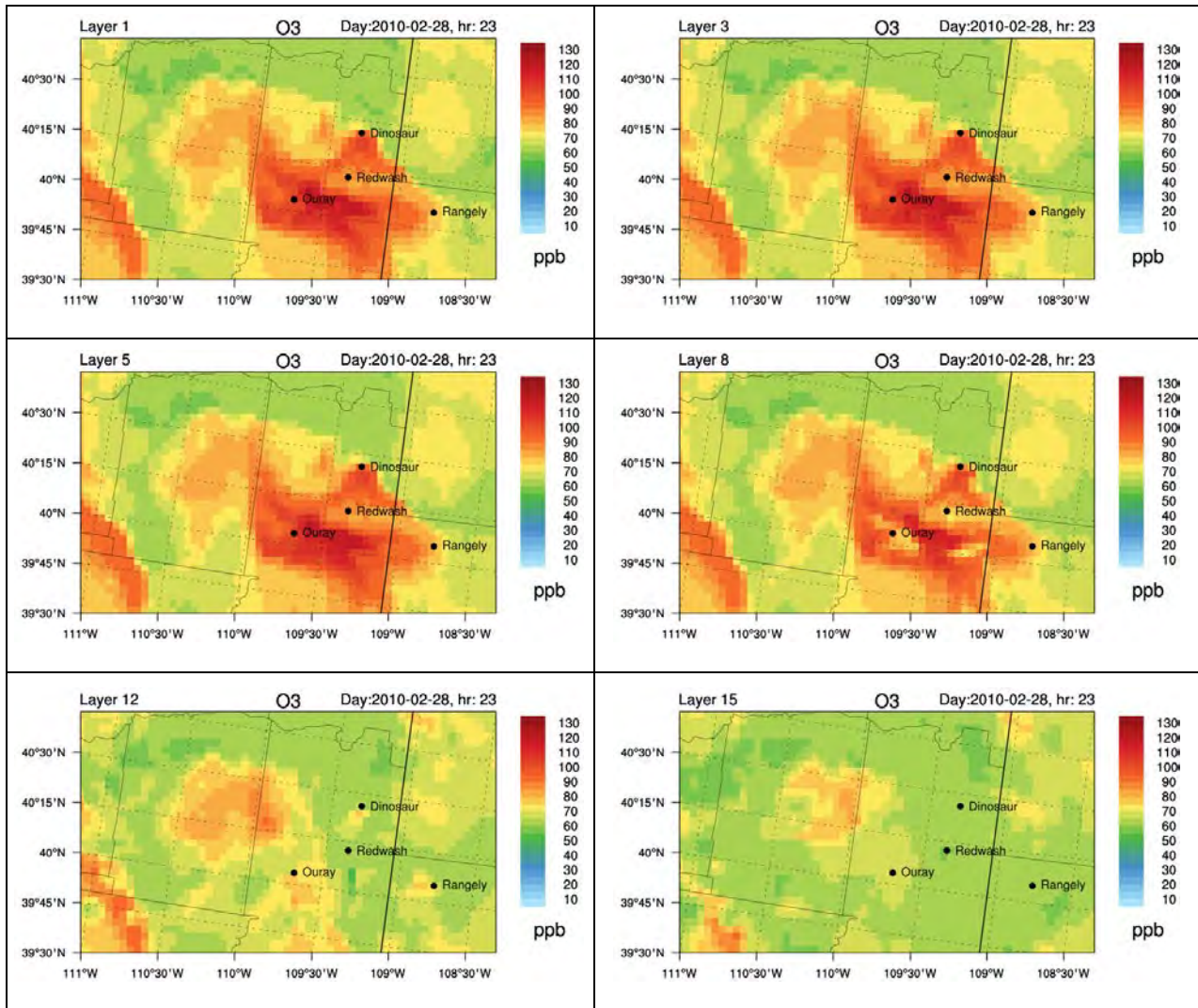
Figure 4.1-17   Spatial Plots of Ozone in the Uinta Basin on February 28, 2010 for Selected Vertical Layers

Date	Profiles below 12,000m	Profiles below 900 m (zoomed-in)
Jan. 13		
Jan. 17		
Feb. 25		
Feb 28		
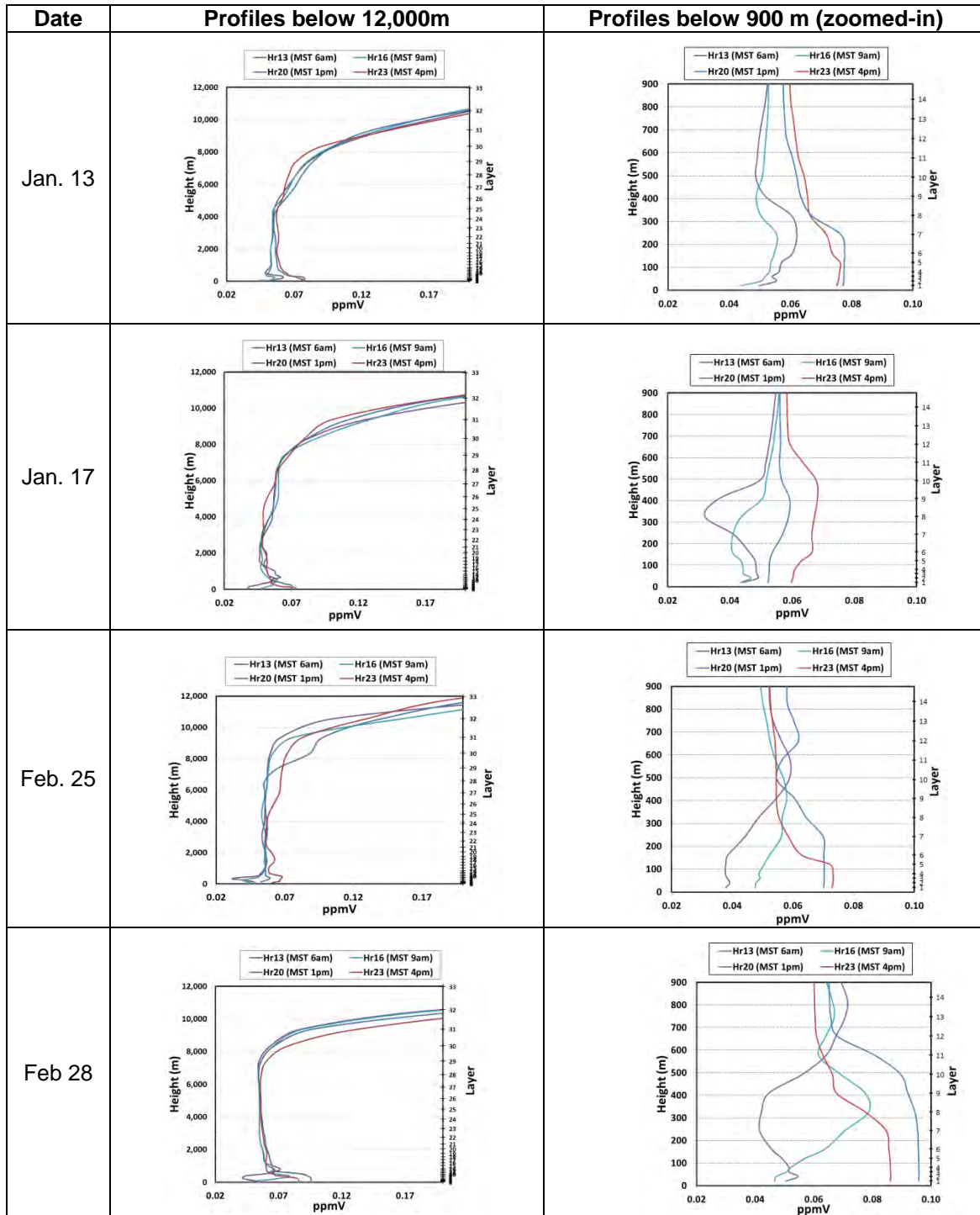
Figure 4.1-18   Ozone vertical profiles at Redwash

Date	Profiles below 12,000m	Profiles below 900 m (zoomed-in)
Jan. 13		
Jan. 17		
Feb. 25		
Feb 28		
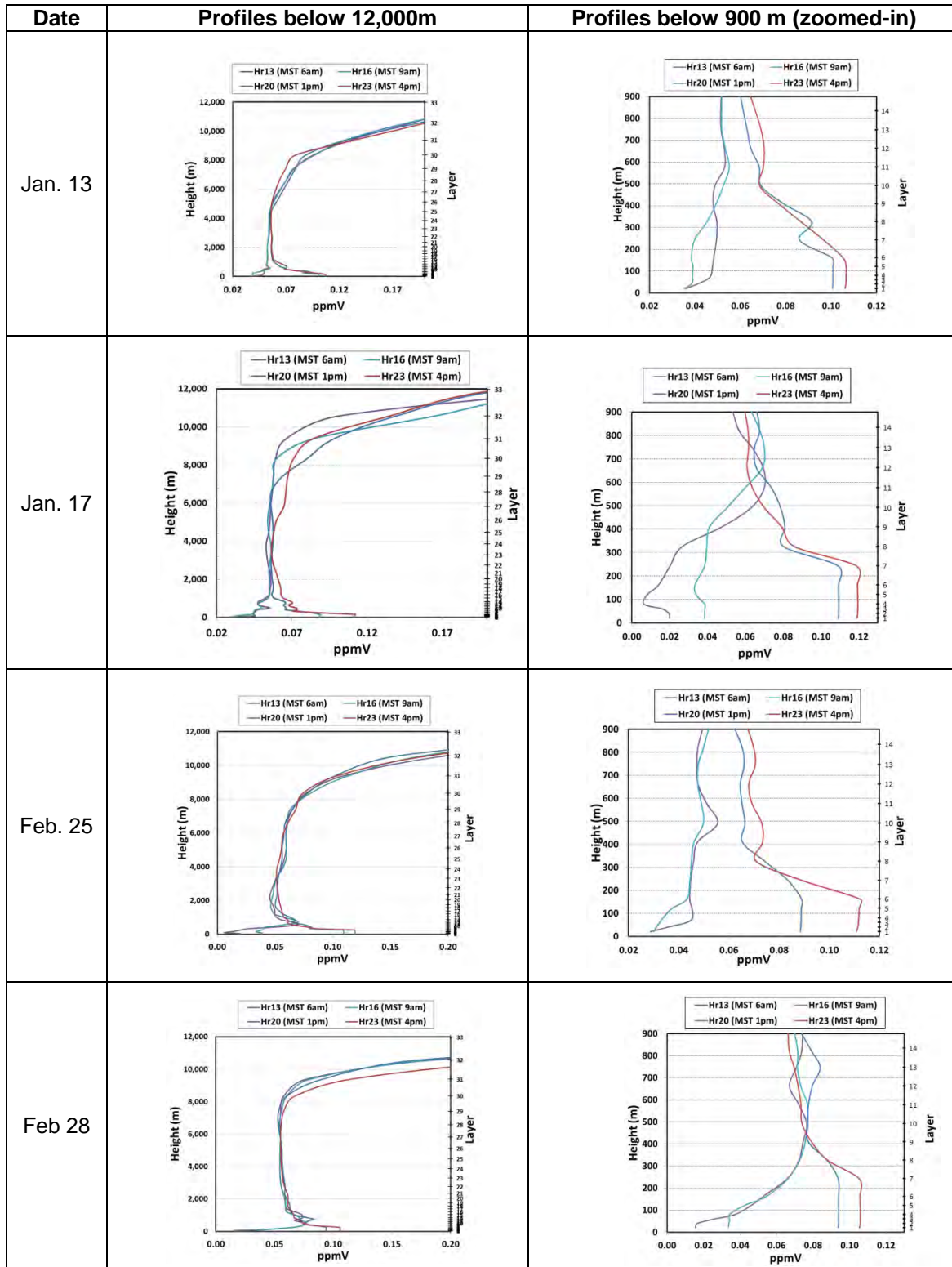
Figure 4.1-19   Ozone vertical profiles at Ouray
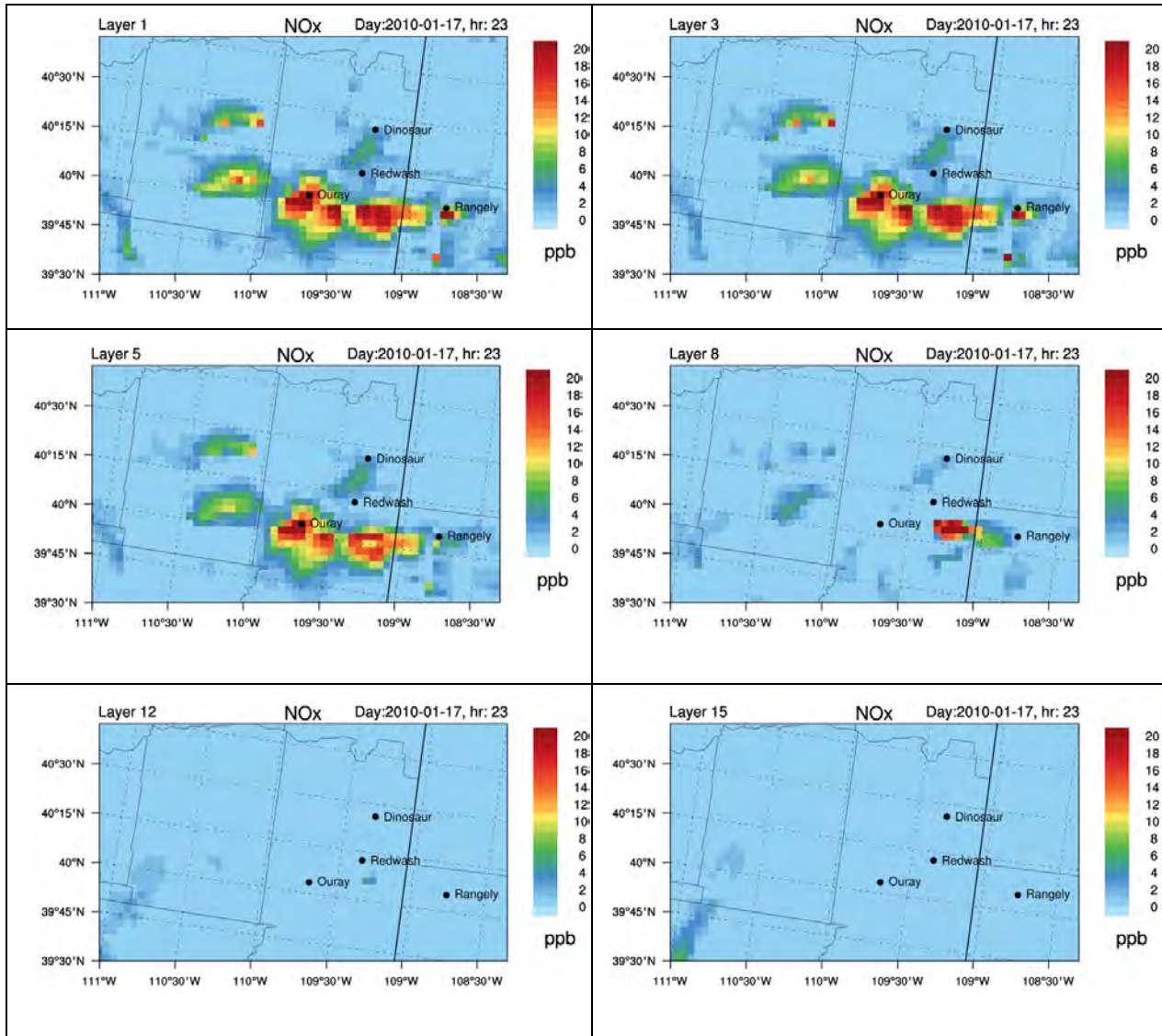
Figure 4.1-20   Spatial Plots of NOx on January 17, 2010 for Selected Vertical Layers
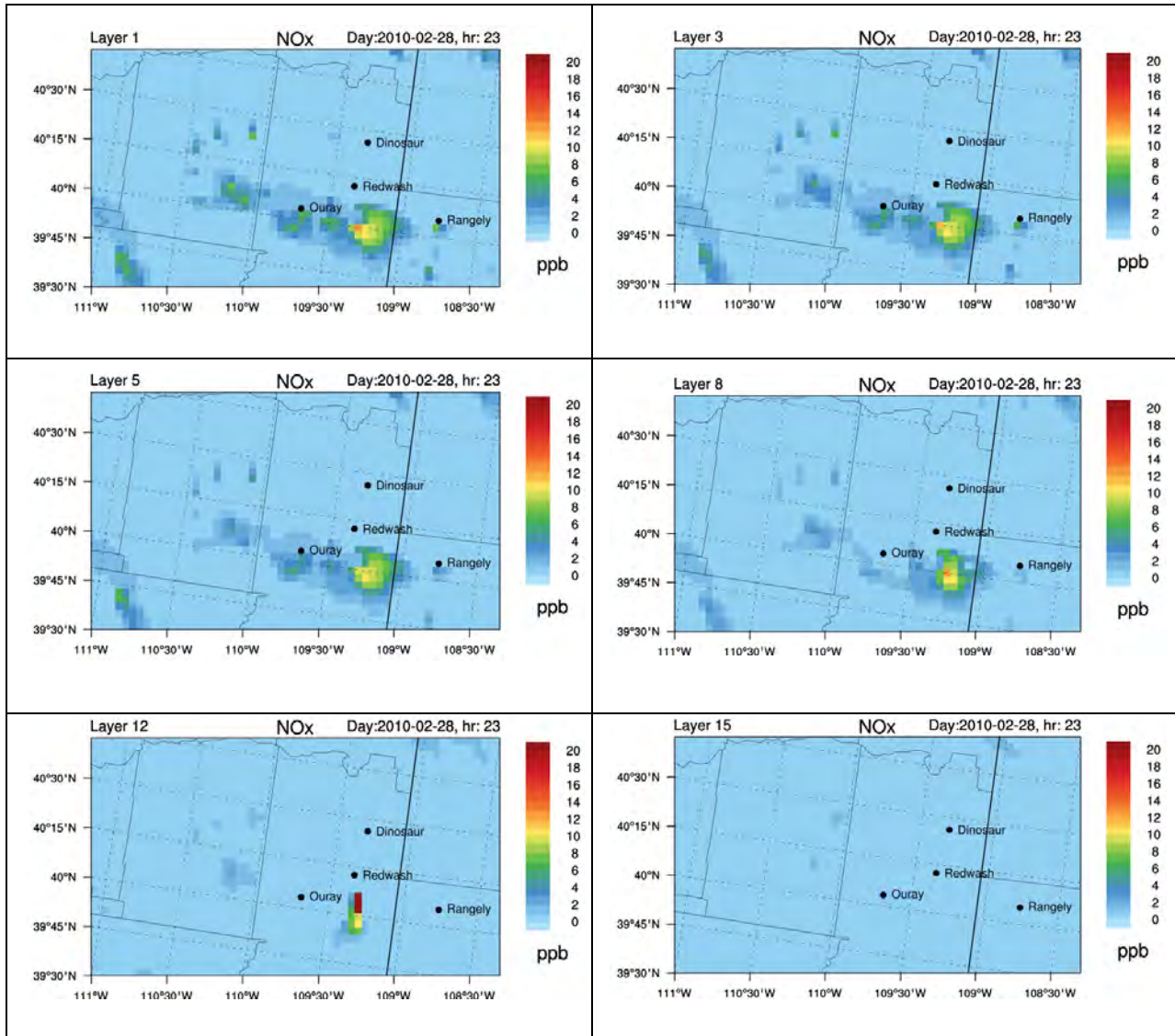
Figure 4.1-21   Spatial Plots of NOx on Feb 28, 2010 for Selected Vertical Layers
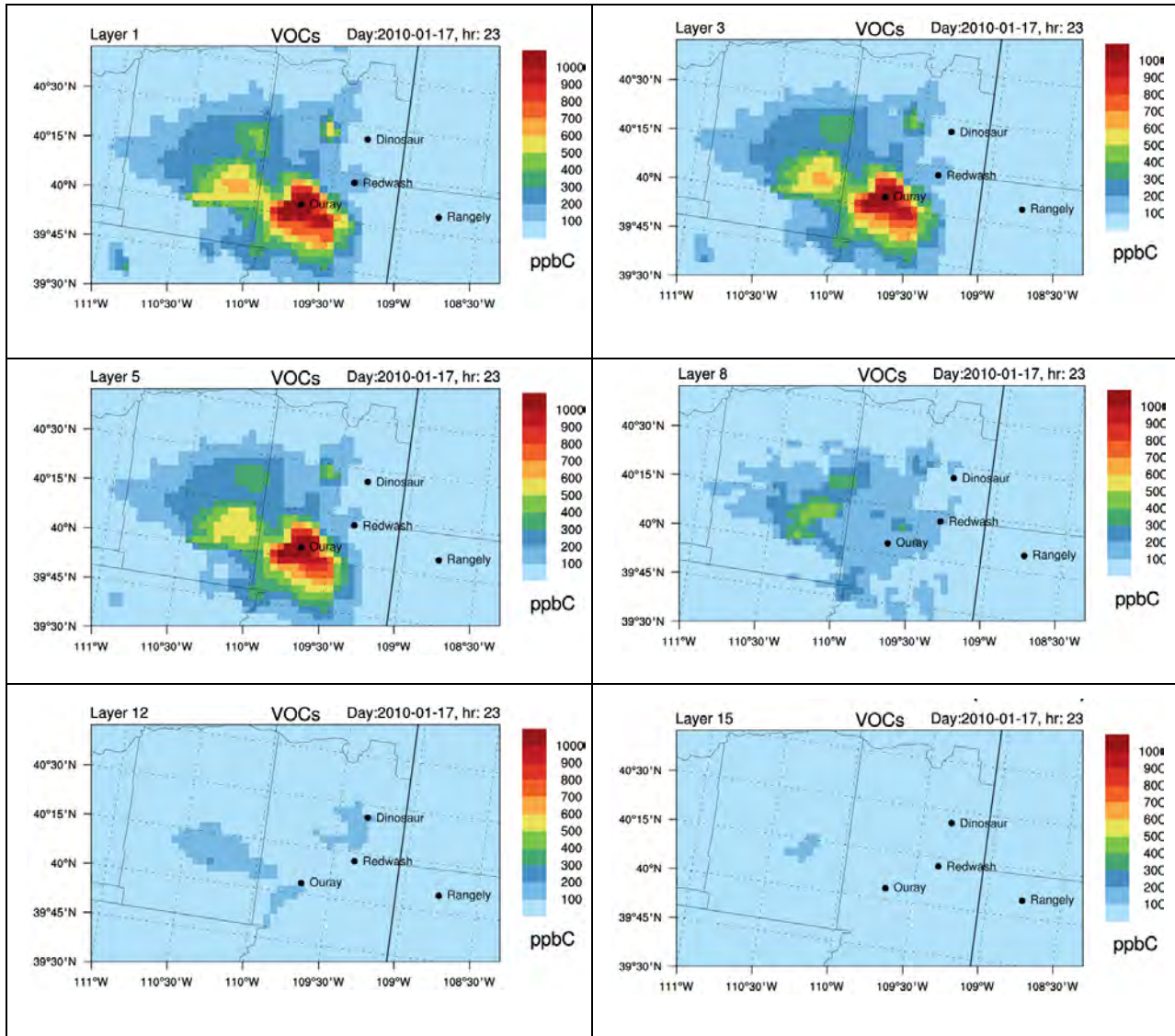
Figure 4.1-22   Spatial Plots of VOC on January 17, 2010 for Selected Vertical Layers
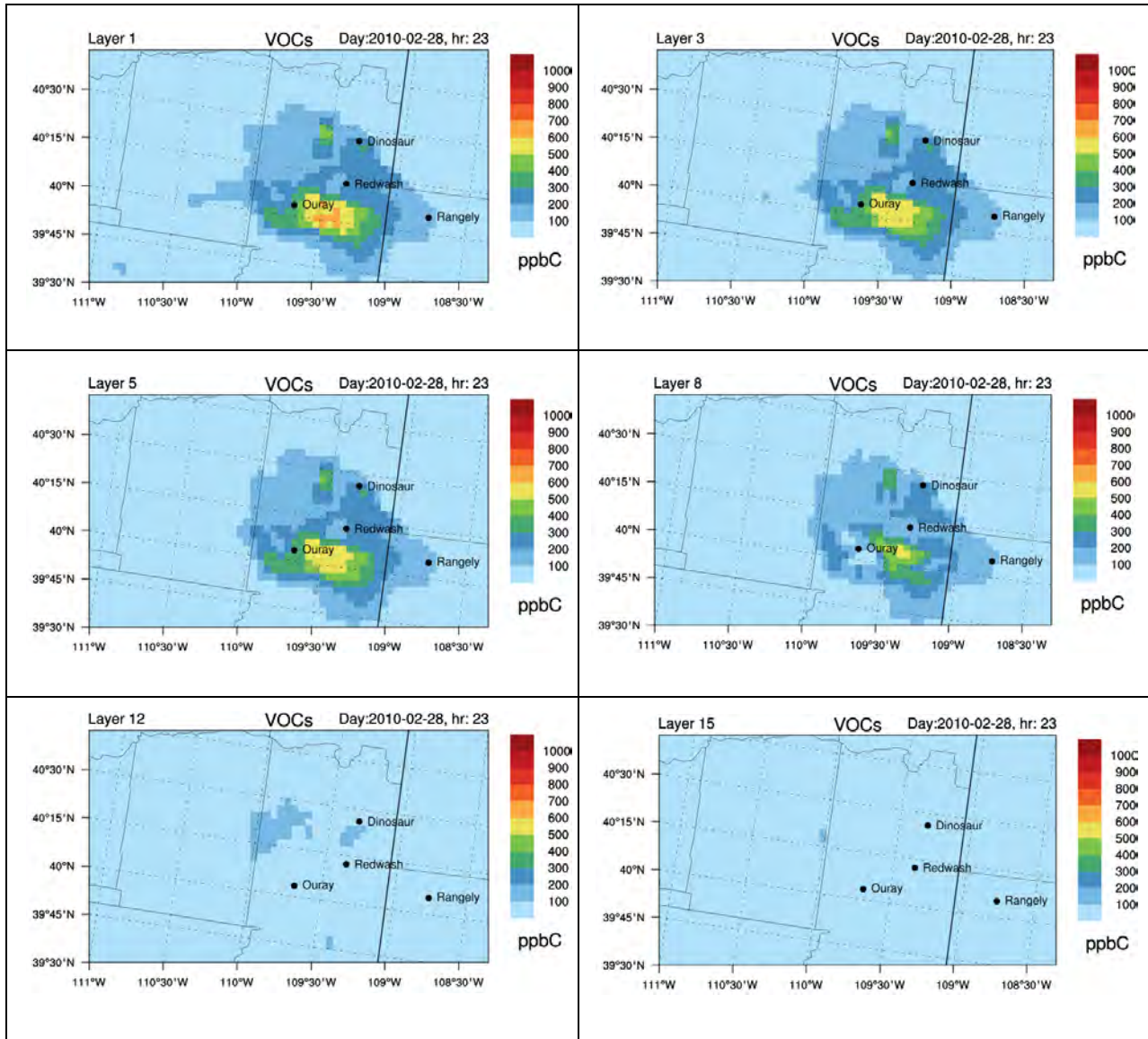
Figure 4.1-23   Spatial Plots of VOC on Feb 28, 2010 for Selected Vertical Layers
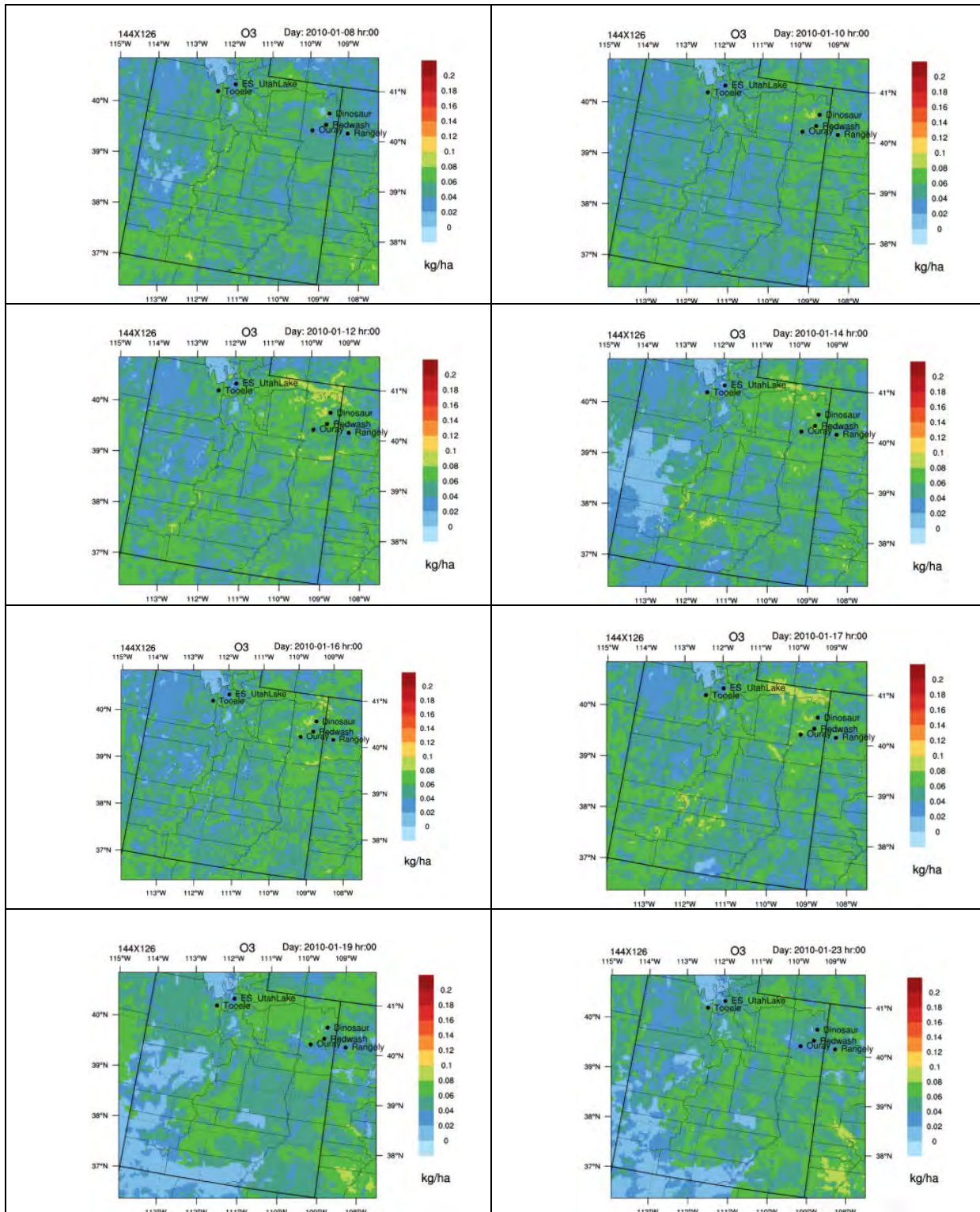
Figure 4.1-24   4-km Spatial Plots for Total Ozone Deposition during January 8 to January 23, 2010

Table 4.1-5   Comparison Between 2010 and 2011 Monitored Ozone Concentrations in the Uinta Basin

Monitor	Year	Average		1st Highest Maximum		2nd Highest Maximum	
		Annual	January-March	Annual	January-March	Annual	January-March
Dinosaur	2010	42	n/a	95	n/a	92	n/a
	2011	37	43	112	112	112	112
Ouray	2010	45	61	139	139	134	134
	2011	42	53	149	149	147	147
Rangely	2010	33	n/a	70	n/a	69	n/a
	2011	39	42	94	94	93	93
Redwash	2010	46	59	120	120	114	114
	2011	44	53	140	140	136	136
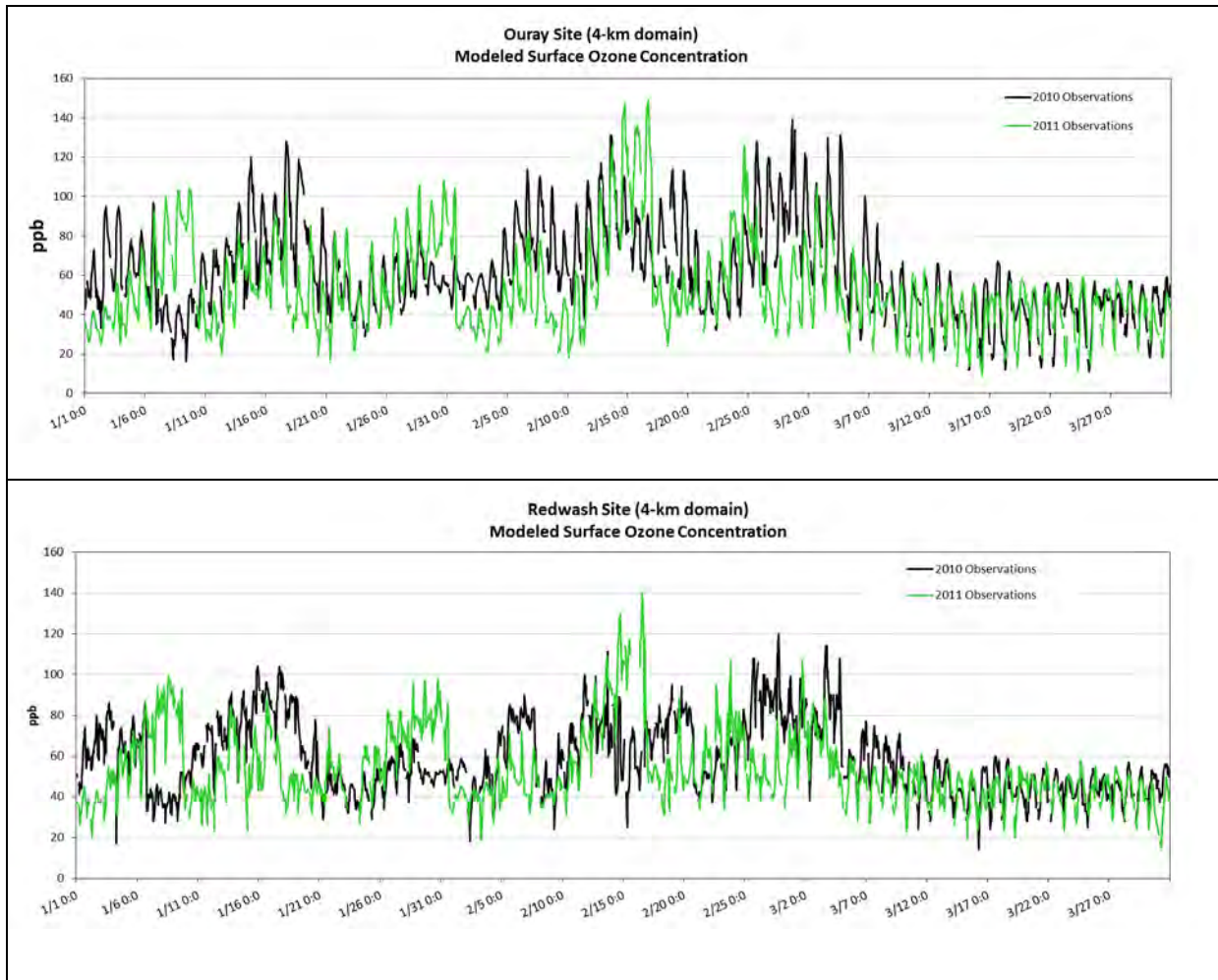
Figure 4.1-25   Comparison of 2010 and 2011 Monitored Ozone Concentrations
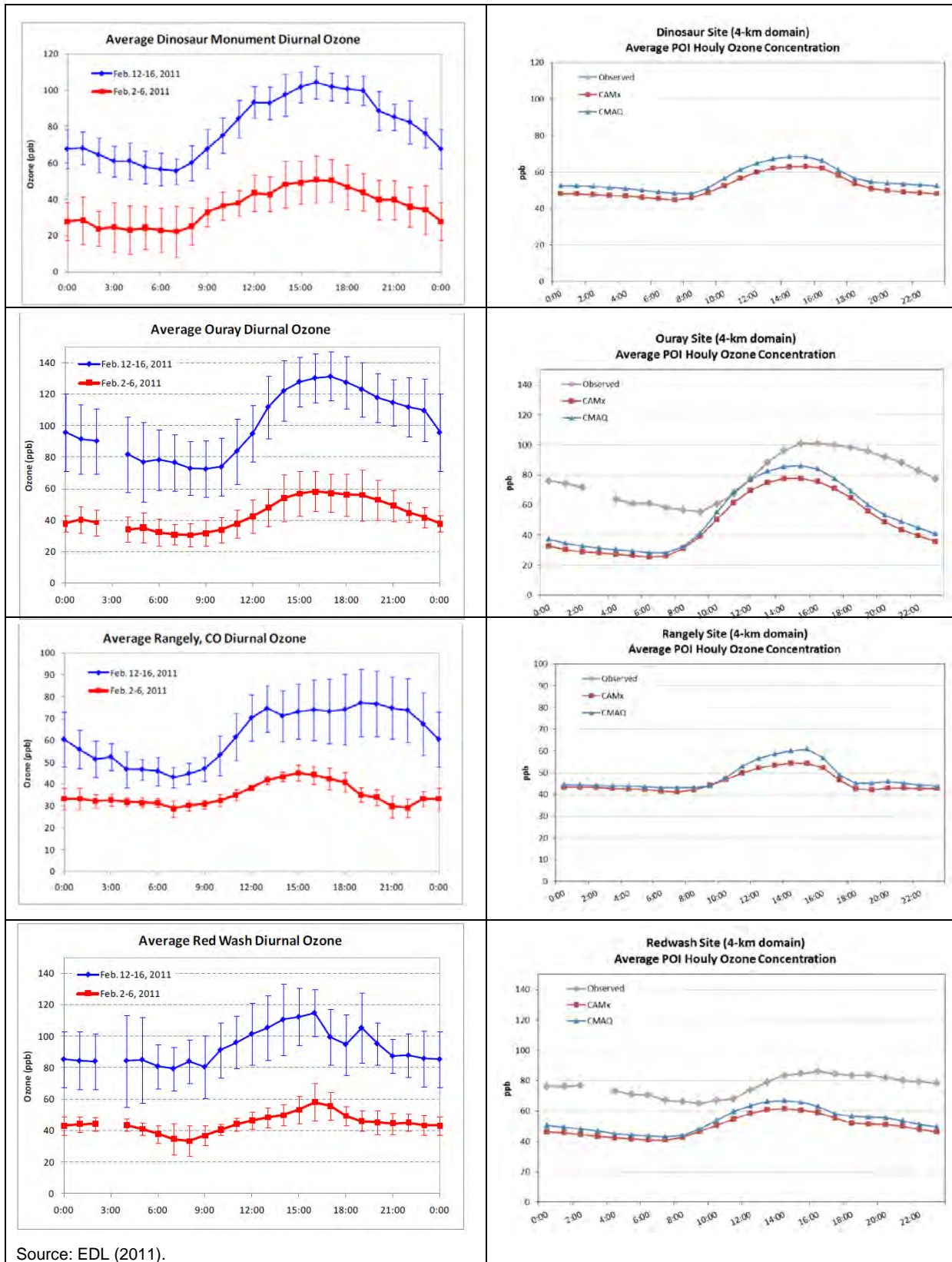
Figure 4.1-26   Hourly Average Ozone Diurnal Profile in 2010 and 2011

Source: EDL (2011).

4.1.3   Summer Ozone Model Performance

As described in Chapter 1, ozone model performance in the Uinta Basin was reviewed for four periods of interest in 2010. POI 3 and POI 4 occur in the summer and early fall and correspond with the periods of August 19 to 29, 2010 and September 27 to October 5, 2010, respectively. These two periods are analyzed in detail in the following sections to evaluate the summer ozone model performance.

4.1.3.1   Summer Ozone Time Series Analyses

Surface Ozone

Figures 4.1-27 and **4.1-28** present time series plots of hourly ozone concentrations at monitoring locations in the Uinta Basin during POI 3 and POI 4. The plots compare hourly average ozone concentrations at four AQS monitoring sites with model-predicted ozone concentrations from the grid cells that contain the monitors. These monitoring locations are shown in **Figure 3-1** relative to the Uinta Basin study area and model domains. The model values in each time series are shown in red (CAMx) and blue (CMAQ), while the monitor values are shown in grey. The CAMx results are discussed in the model inter-comparison presented below, while the CMAQ results are summarized in more detail here.

In both POI 3 and POI 4, the models systematically overestimate the lowest observed concentrations (in the range of about 0 to 30 ppb) at the Uinta Basin monitoring sites. While the model tends to overestimate the peak concentrations at the Dinosaur and Rangely sites, it generally reproduces the peak concentrations at the Ouray and Redwash sites well.

Ozone Deposition

While total ozone deposition values are presented and discussed, ozone deposition is exclusively due to dry deposition processes. **Figure 4.1-29** and **Figure 4.1-30** show time series analyses of modeled ozone deposition during POI 3 and POI 4 at monitors in the Uinta Basin. All of the time series plots display CMAQ deposition results in blue, and CAMx results in red.

Diurnal cycles in ozone dry deposition are apparent in both models, corresponding to diurnal cycles in both ozone concentration and in ozone dry deposition velocity. During both POI 3 and POI 4, CAMx shows a stronger diurnal cycle compared to CMAQ, with higher daytime peaks and lower nighttime minimums. Dry deposition rates are relatively consistent across the Uinta Basin in CAMQ, while intra-site variability is more significant in CAMx.

4.1.3.2   Summer Ozone Spatial Analyses

Surface Ozone

The spatial performance for modeled surface ozone was reviewed for POI 3. **Figure 4.1-31** shows contour plots of the daily maximum 1-hour ozone concentrations predicted by CMAQ in the 4-km domain for selected days in the POI 3. Monitored daily maximum 1-hour ozone concentrations from the AQS network are shown in the figure as circles. As discussed for the summer period time series analysis, peak ozone concentrations tend to be over-estimated by CMAQ at the Dinosaur and Rangely monitor sites, but reproduced relatively well at the Ouray and Redwash sites.

Ozone Deposition

Figure 4.1-32 shows spatial plots of daily cumulative ozone deposition from the CMAQ 4-km domain for POI 3 (August 19 to 29, 2010). During POI 3, total ozone deposition rates are larger than in POI 1 (shown in **Figure 4.1-24**), with deposition rates exceeding 100 g/ha/day throughout the 4-km domain, and exceeding 200 g/ha/day in the large mountain ranges of Utah and eastern Colorado. There is more spatial variability in total ozone deposition during the summer than winter, likely due to the

variability of land use types in the summer compared to the predominance of snow throughout the 4-km domain in winter.

4.1.4   Summary of Model Performance for Ozone

In general, CMAQ model performance for ozone meets the USEPA-recommended performance goals.

- Model results for ozone show good performance for all modeling domains, monitoring networks and seasons on a domain-wide basis, as supported by the MNB and MNGE model performance statistics for daily maximum 1-hour and daily maximum 8-hour average ozone with a 60 ppb threshold, which are well within the USEPA-recommended performance goals.
- When the 60 ppb concentration threshold is applied to observations, the model generally under-predicts daily maximum 8-hour ozone concentrations, except during the summer and fall on the 4-km domain.
- Modeled ozone time series at Uinta Basin sites tend to follow the seasonal trends in observations; however, the model consistently over-predicts ozone concentrations when observed values are low (in the range of 0 to 30 ppb).
- The model is generally able to reproduce elevated ozone concentrations during winter. Some key differences between measured and modeled concentrations include modeled daily peak ozone concentrations occur earlier and decline more rapidly than measurements. Although limited data is available for comparison with the 2010 model results, modeled vertical ozone concentrations and spatial extent of surface maximums are generally consistent with observations during other years.
- Evaluation of time series and spatial plots of ozone concentrations during the POIs indicate that the model captures moderate ozone concentrations, but tends to under-predict ozone peaks in winter and over-predict ozone peaks in summer.
- Spatially, there is substantial variation in the model results within the 4-km domain and Uinta Basin. The 4-km model concentrations have good spatial agreement with observations during the periods analyzed, with the exception of over-predictions in the Salt Lake City area during winter. In the Uinta Basin, the model spatial agreement with observations is generally adequate although it tends to under-prediction concentrations in some areas. Within the Uinta Basin, the model performs best at the Ouray monitor.

4.1.5   Comparison of CMAQ and CAMx Results

This section presents a summary of key similarities and differences between the CMAQ and CAMx models related to ozone model performance. Statistical results, spatial plots, and time series analyses from both models were examined understand how the models performed relative to EPA performance benchmarks, and to each other. Findings from this inter-comparison were used to provide context for the overall conclusions developed in **Chapter 5**, and to provide supporting evidence for the final model recommendations for the ARMS Modeling Project.

Figure 4.1-33 presents a comparison of monthly MNB statistics for all three CMAQ and CAMx modeling domains for the AQS and CASTNET monitoring networks. Both models perform well for ozone on a domain-wide basis. For all months except December, the MNB for ozone is within the recommended benchmark of ± 35% on all domains and all monitoring networks for both models. Both CMAQ and CAMx under-predict ozone concentrations during the winter months. During the summer months in the 4-km domain, CMAQ tends to over-predict ozone concentrations, while CAMx slightly under-predicts ozone concentrations. The biases in CMAQ are generally smaller in magnitude than the CAMx biases, except during the summer months in the 4-km domain.

In the Uinta Basin, both models produce elevated ozone concentrations during the winter months (shown in **Figures 4.1-6** and **4.1-7**). The spatial plots of ozone concentrations from both models on the 4-km on January 17 at 2000 UTC (during POI 1), shown in **Figure 1.4-34**, illustrate the ozone

enhancement in the Uinta Basin. The spatial plots also show how both models produce similar ozone spatial patterns throughout the 4-km domain. However, CMAQ produces higher ozone concentrations than CAMx in the Uinta Basin, and throughout the 4-km domain. This general trend is also seen during the summer, as illustrated by the spatial plots in **Figure 1.4-35**.

The time series analyses presented in **Figures 4.1-6, 4.1-7, 4.1-27**, and **4.1-28** compare ozone concentrations predicted by both models with ozone observations at the Uinta Basin monitoring sites during the 4 POI events. Although both models under-predict peak ozone concentrations on some days during wintertime ozone episodes in the Uinta Basin, CMAQ predicts higher winter ozone concentrations than CAMx, and CMAQ reproduces the observed maximum concentrations better than CAMx. However, both models fail to capture observed ozone enhancement in the Uinta Basin on some days, and neither model reproduces the peak observed ozone concentration during the winter episodes. Also, modeled ozone concentrations fall off from their daytime peaks more quickly than observed during the winter in both models. CAMx tends to have higher ozone dry deposition rates than CMAQ, as shown in **Figure 4.1-14**, despite the fact that the CAMx ozone concentrations are generally lower than CMAQ for the periods included in the analysis.

During the summer, both models perform similarly in the Uinta Basin, with both CMAQ and CAMx over-predicting peak daytime ozone concentrations. Throughout the year, both models perform better at Ouray than at Redwash.
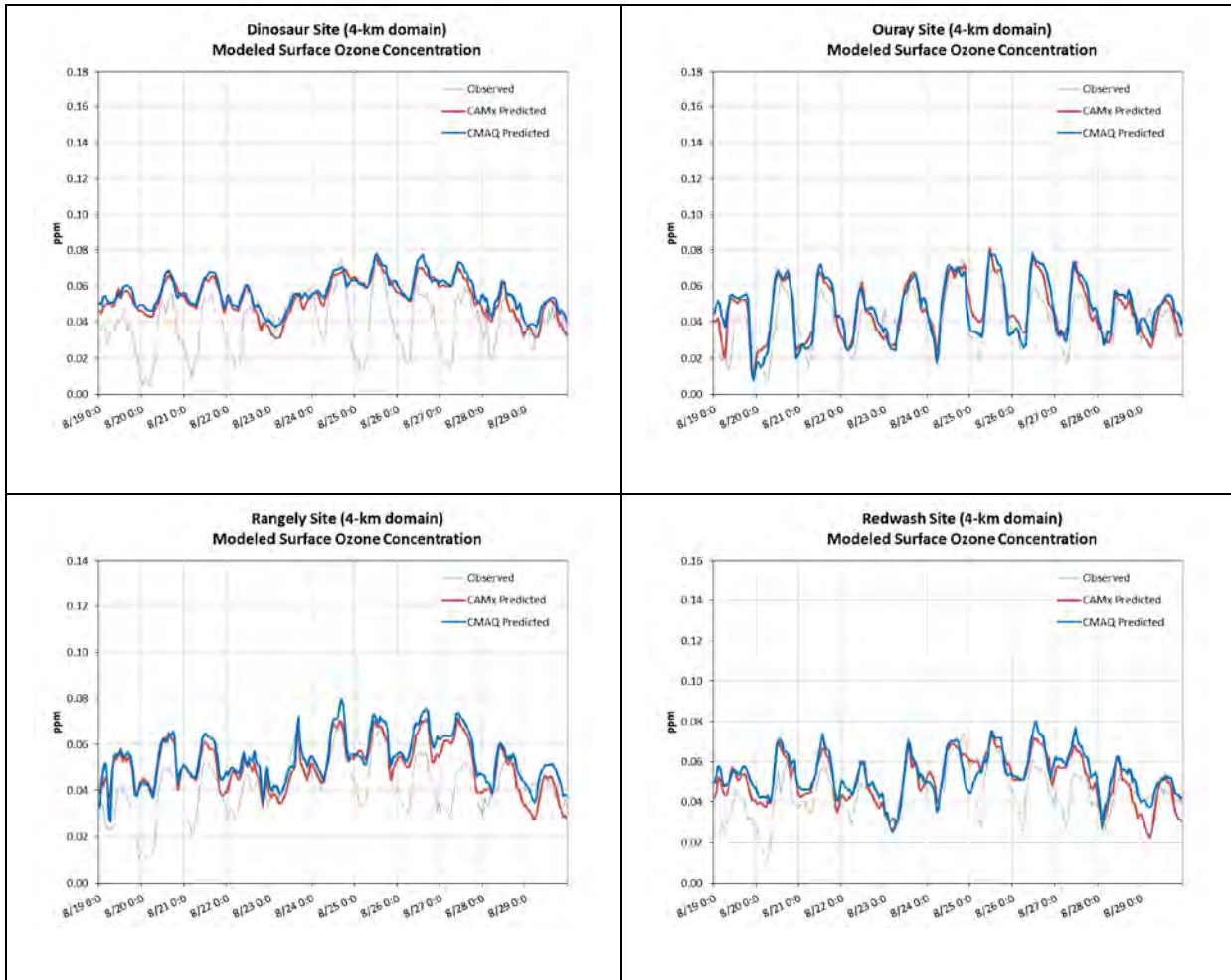
Figure 4.1-27   Time Series for Ozone at Selected AQS Monitoring Sites during August 19 to August 29, 2010
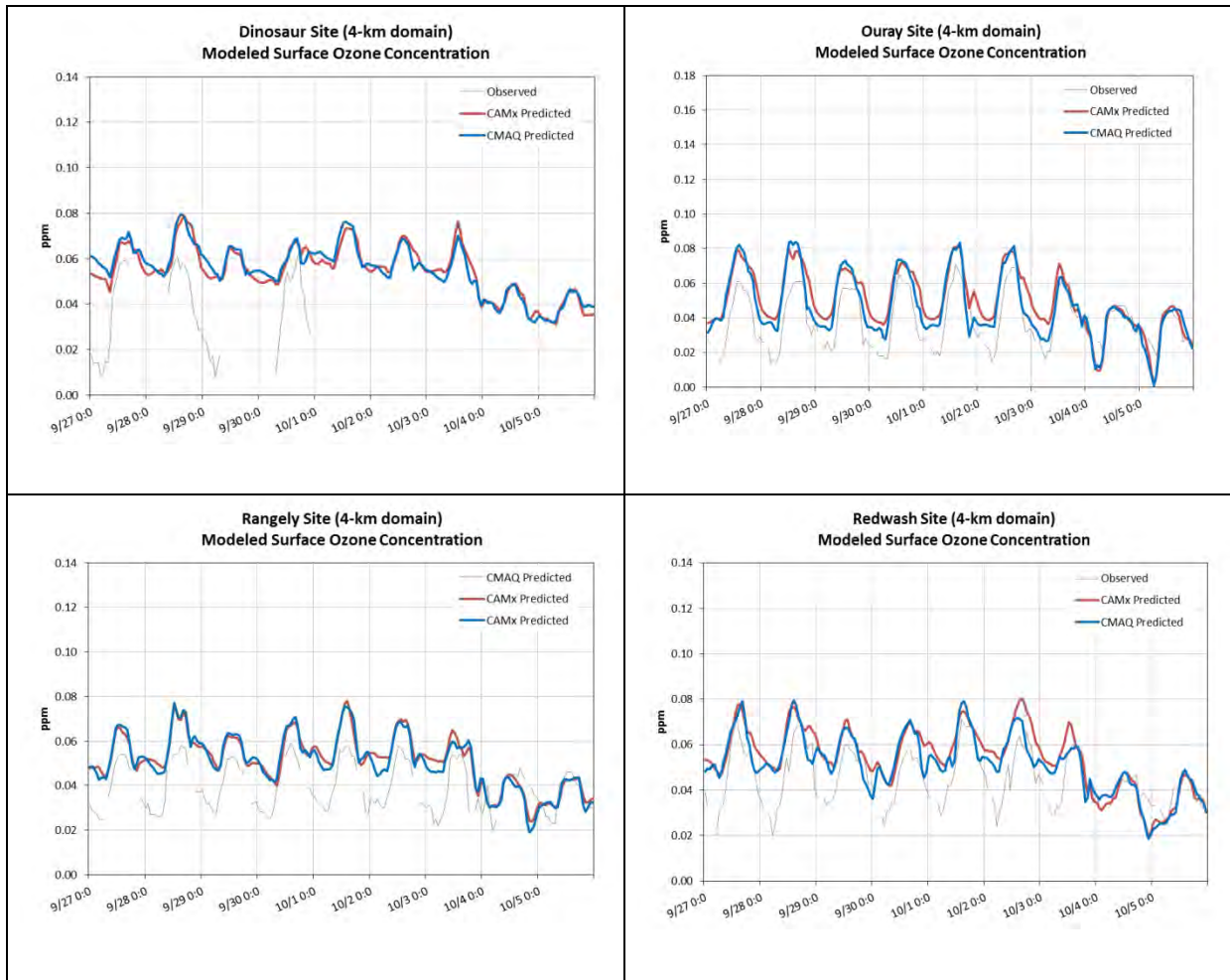
Figure 4.1-28   Time Series for Ozone at Selected AQS Monitoring Sites during September 27 to October 5, 2010
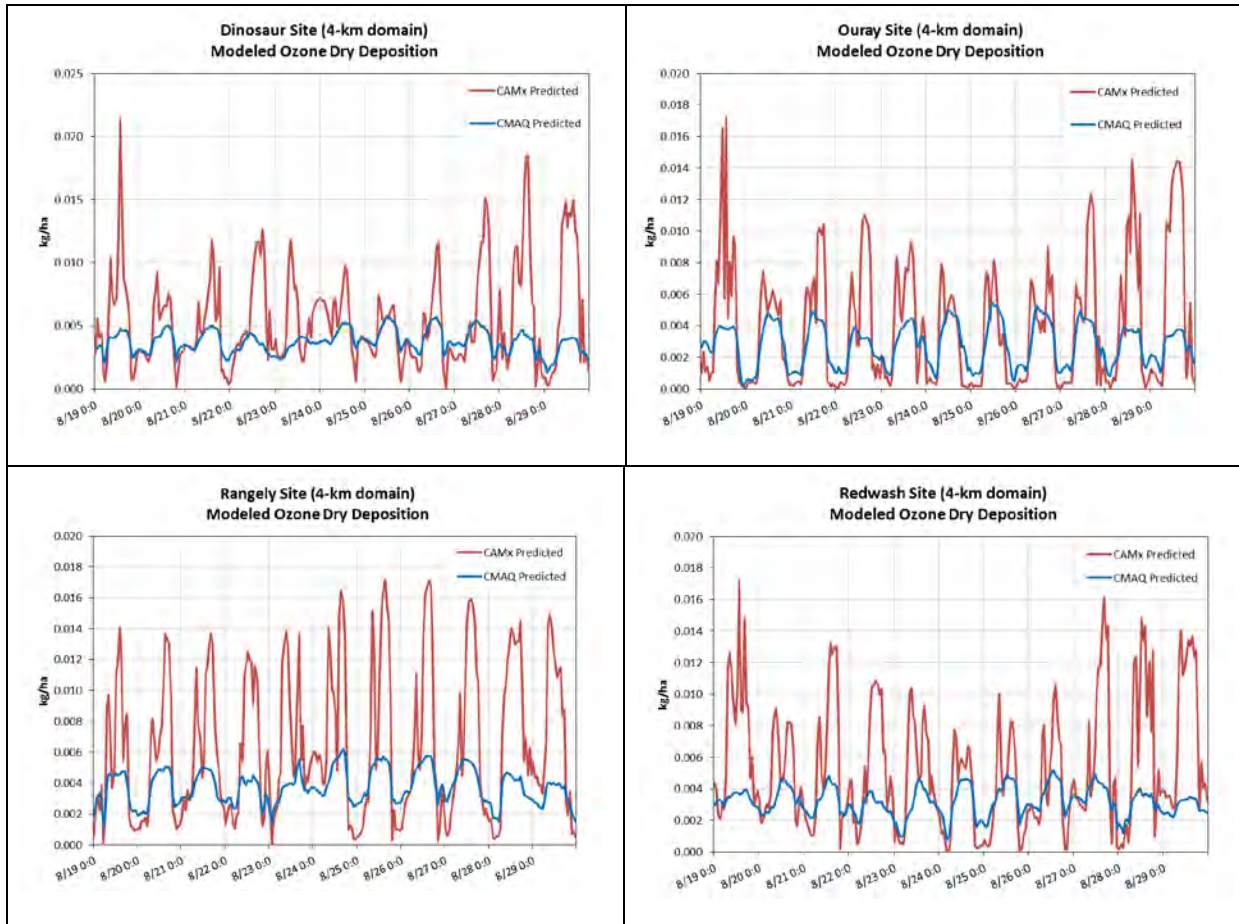
Figure 4.1-29   Time Series for Ozone Dry Deposition at Selected AQS Monitoring Sites during August 19 to August 29, 2010
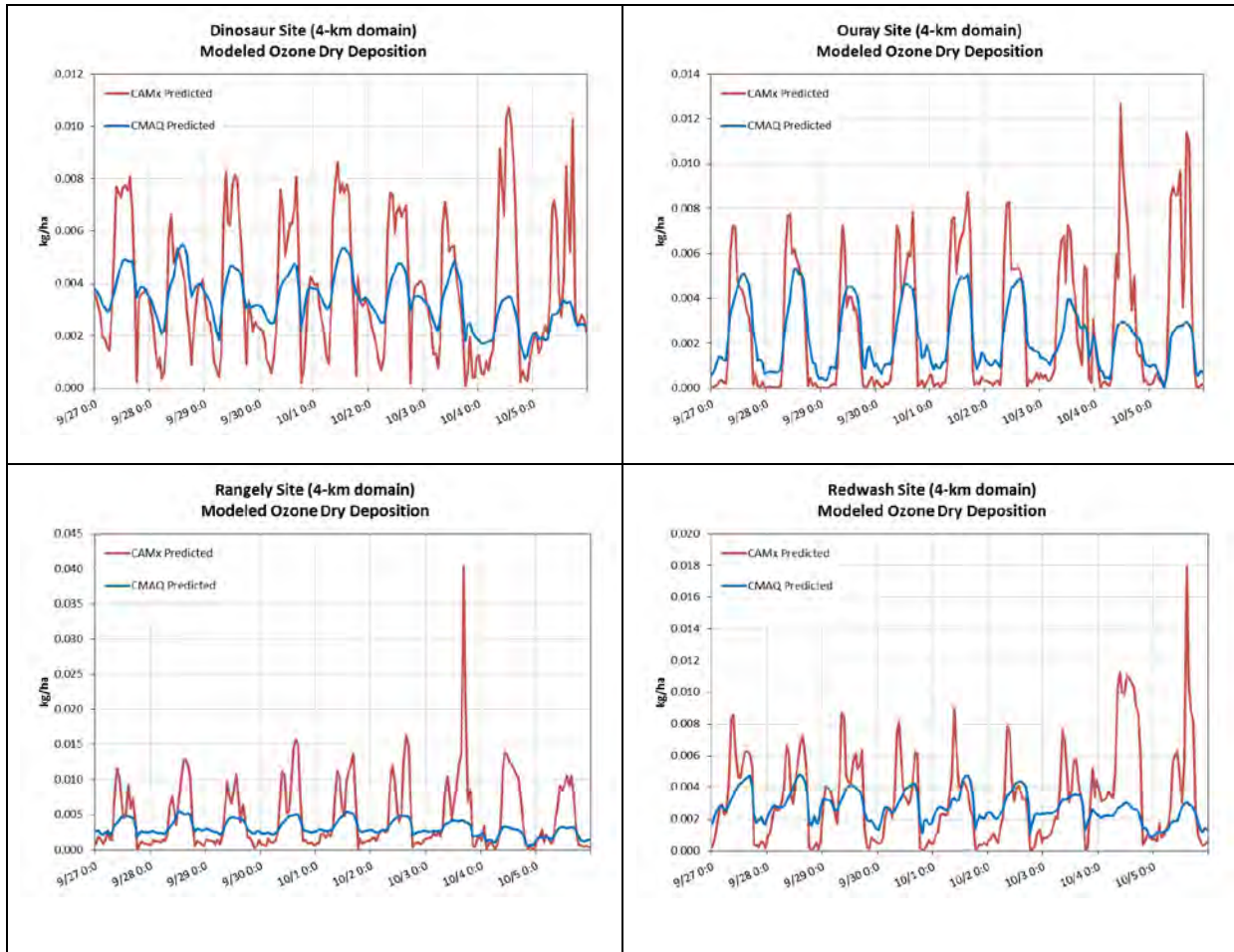
Figure 4.1-30   Time Series for Ozone Dry Deposition at Selected AQS Monitoring Sites during September 27 to October 5, 2010
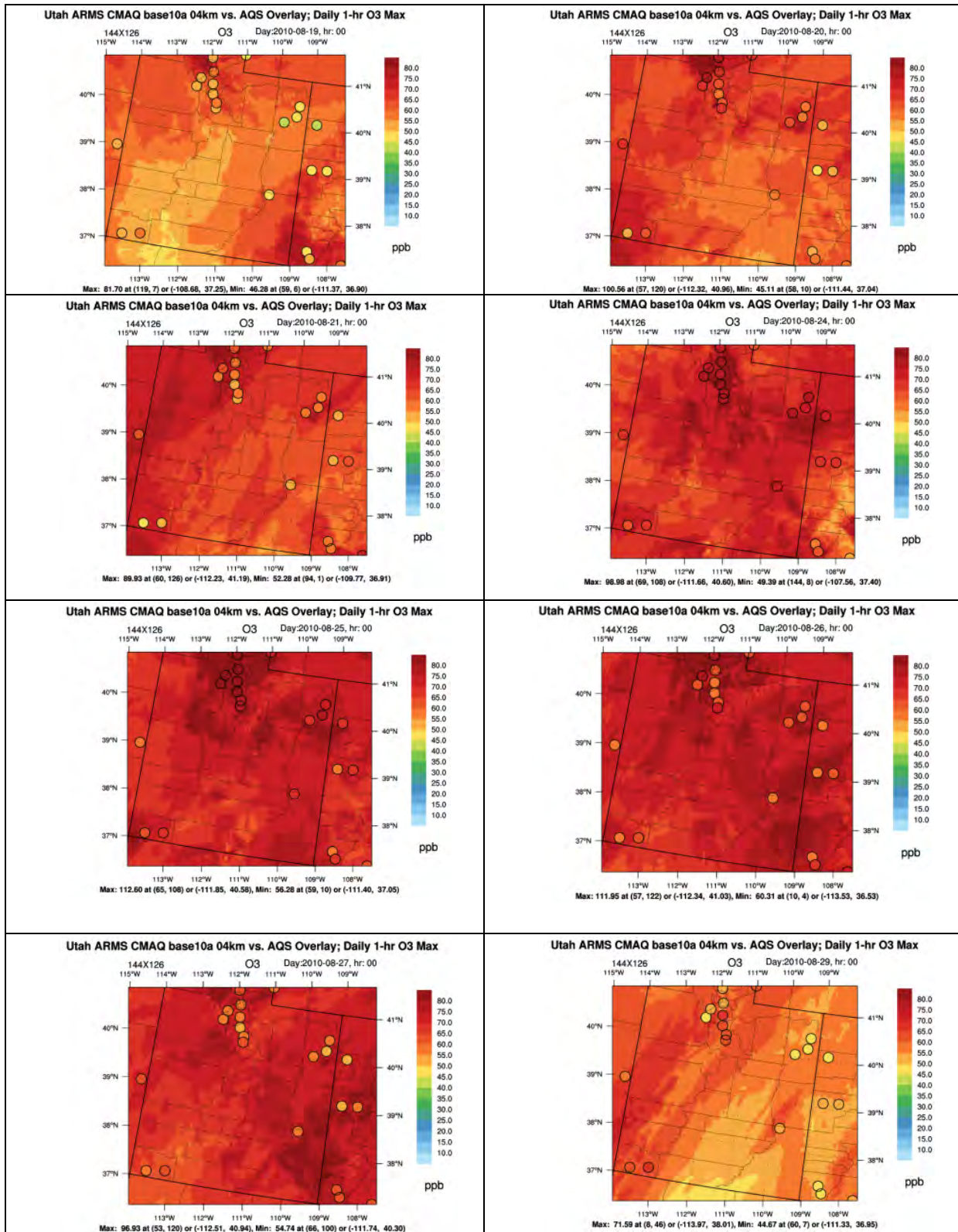
Figure 4.1-31   4-km Spatial Plots for Ozone during August 19 to August 29, 2010
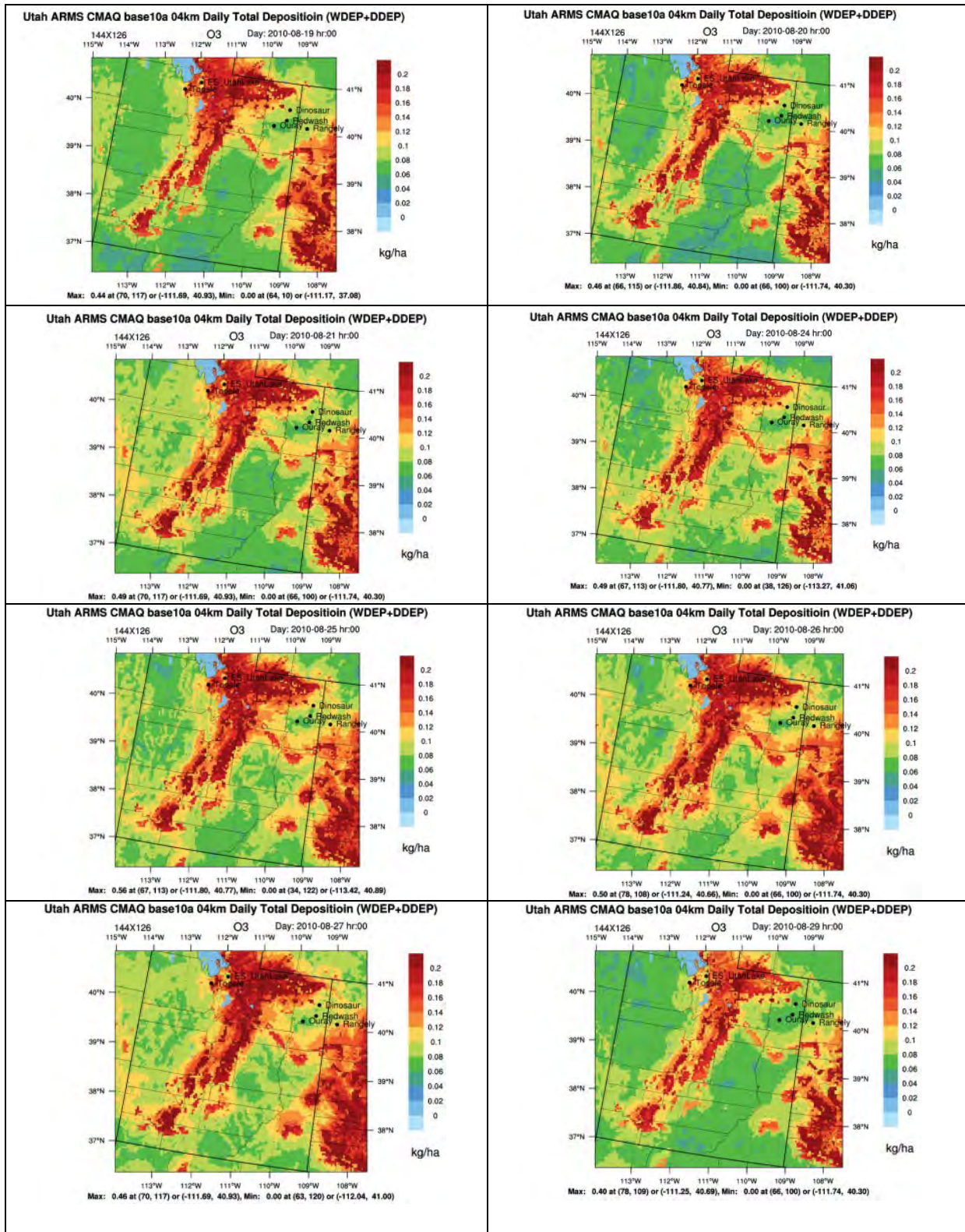
Figure 4.1-32   4-km Spatial Plots for Total Ozone Deposition during August 19 to August 29, 2010
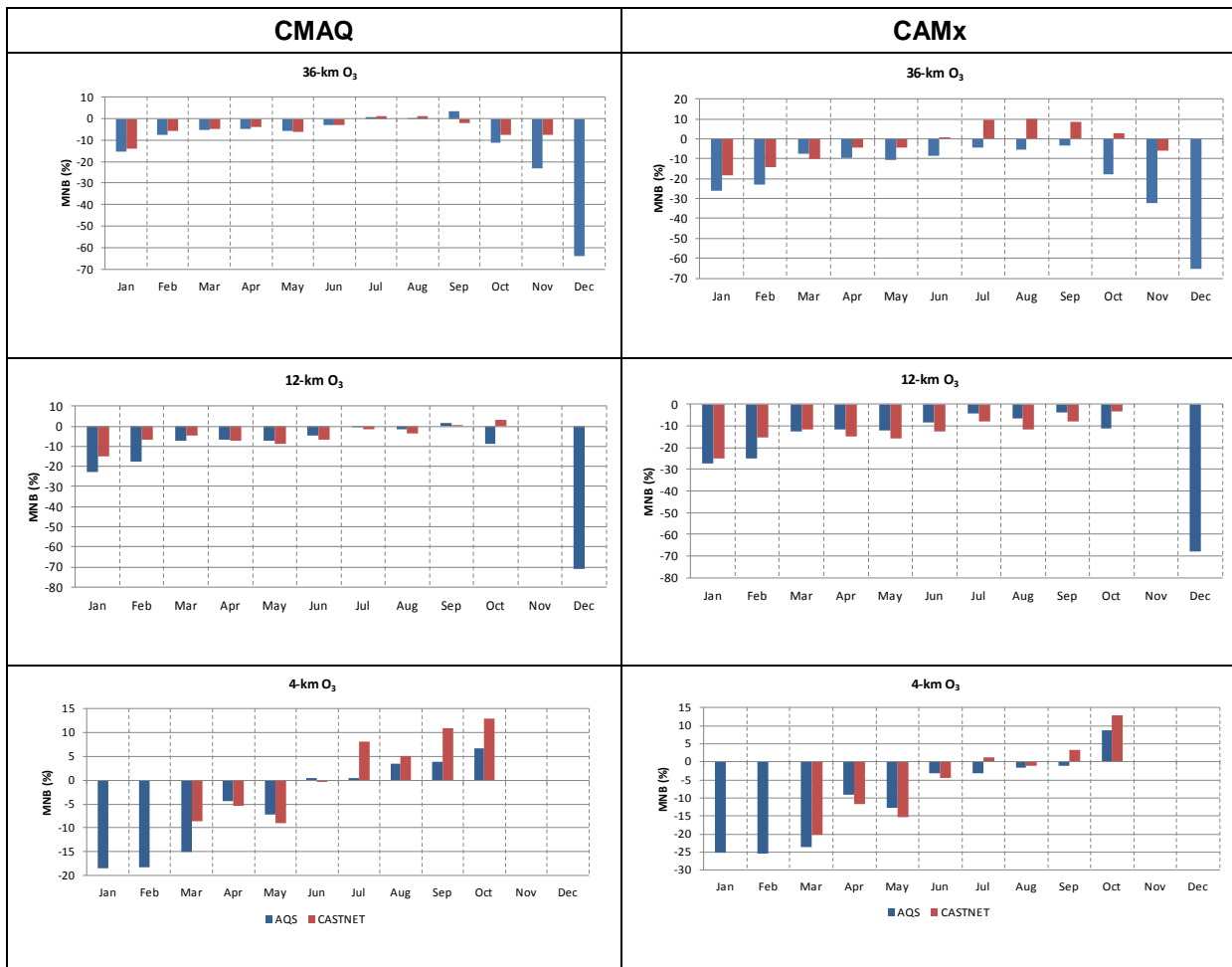
Figure 4.1-33   Monthly Mean Normalized Bias for Ozone for CMAQ and CAMx
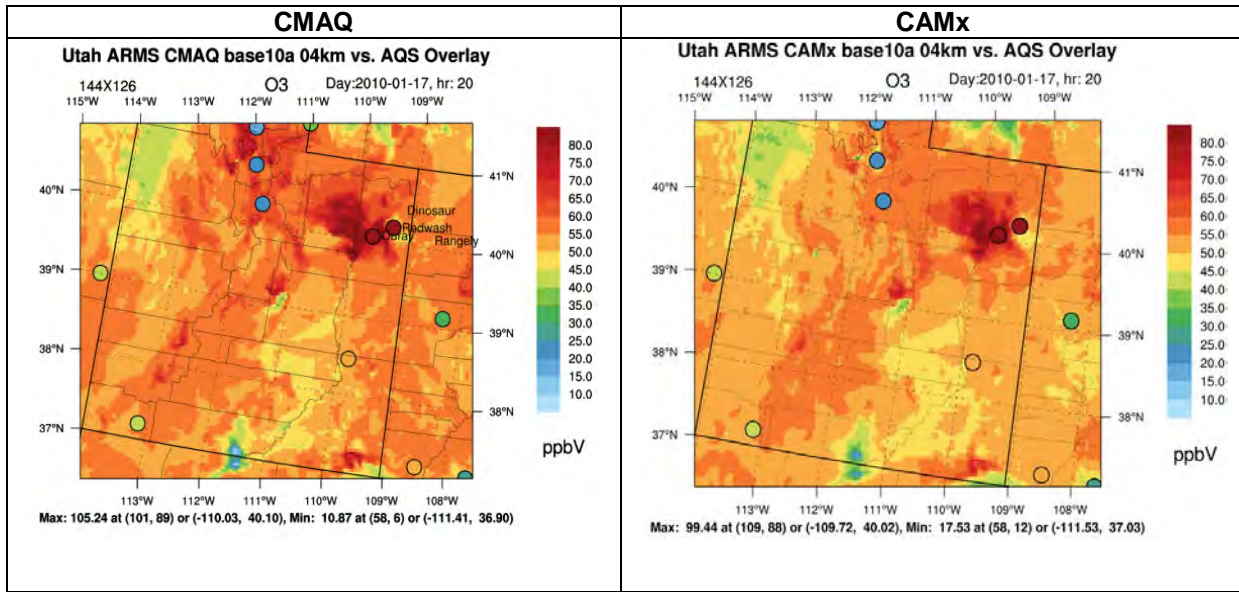
Figure 4.1-34   4-km Spatial Plots for Ozone on January 17, 2010 for CMAQ and CAMx
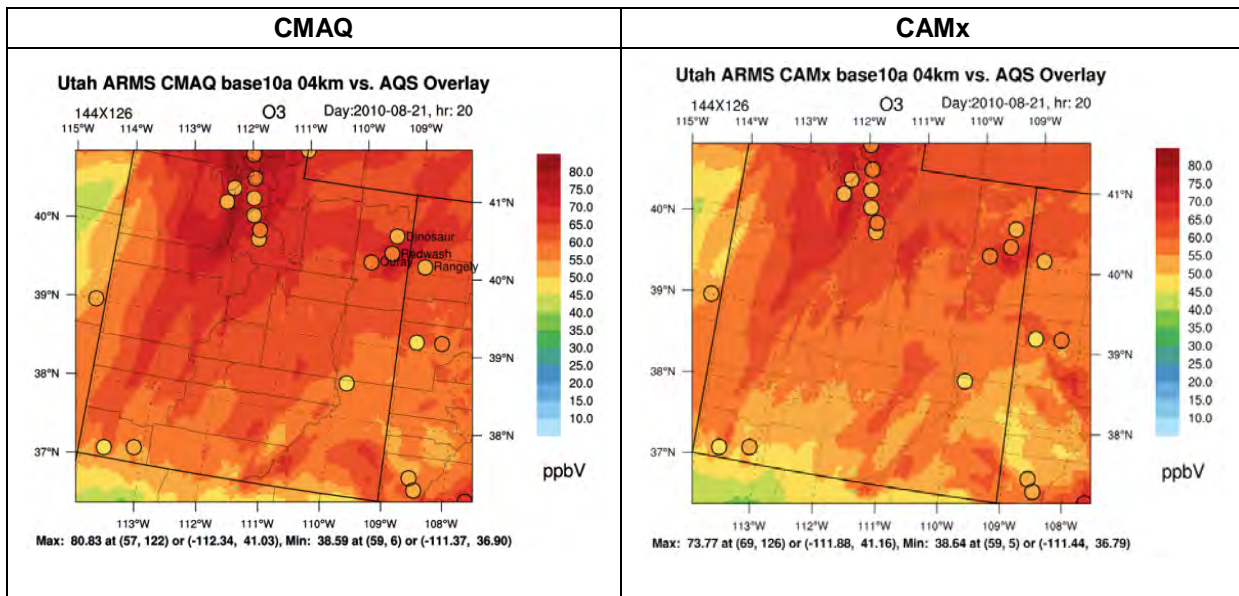
Figure 4.1-35   4-km Spatial Plots for Ozone on August 21, 2010 for CMAQ and CAMx

4.2   Particulate Matter

The model-predicted concentrations of particle-phase chemical species and total PM ($PM_{2.5}$ and PM_{10}) were compared to monitored values. Model performance was evaluated in detail for each of the individual chemical species that make up total PM, including SO_4, NO_3, NH_4, OC mass, EC mass, fine soil dust (SOIL), and CM. All species except CM are part of the $PM_{2.5}$ size range. Following the detailed analysis of the PM composition, the $PM_{2.5}$ model performance was evaluated by summing the individual species together (less CM) to estimate total $PM_{2.5}$ mass concentration. Total $PM_{2.5}$ mass concentration was then summed with CM to estimate and evaluate the model performance for total PM_{10} mass concentration.

The MPE for PM provides the following analyses for each individual pollutant, as well as total $PM_{2.5}$ and PM_{10} mass concentrations:

- Tables of annual and seasonal statistical metrics summaries by monitoring network and modeling domain;

- Bar charts of monthly mean fractional bias (MFB) by monitoring network and modeling domain;

- Bugle plots of monthly MFB and mean fractional gross error (MFGE) relative to USEPA (2007) goals and criteria for PM;

- Time series plots for selected monitoring stations within or near the Uinta Basin Project area; and

- Spatial plots for the selected POI.

Bugle plots are developed specifically for PM model performance assessment; therefore, bugle plots are only presented in this section for PM evaluation. Similar to the ozone assessment, the model performance evaluation focuses on CMAQ results and presents a comparison relative to CAMx when results are notably different. CAMx model performance results are presented in **Appendix B**.

4.2.1   PM Composition

4.2.1.1 Sulfate

Statistical Analyses for the CMAQ 36-km, 12-km, and 4-km Domains

Annual and seasonal SO_4 statistical summaries are presented in **Table 4.2-1** for each monitoring network and modeling domain. Note that the number of monitors with valid data used to calculate the statistical summaries is provided in **Table 3-2**. A more detailed assessment of the MFB is presented for each month in **Figure 4.2 1**.

In general, the model performed well for SO_4 across most monitoring networks and all modeling domains. The annual average model predictions are fairly consistent with observed annual average concentrations, as shown in **Table 4.2-1**. In the 36- and 12-km domains (**Figure 4.2-1**), the model tends to over-predict SO_4 concentrations relative to observations, particularly during winter months with a slight under-prediction during summer. For the 4-km domain, the model is consistently over-predicting during November and December for all monitoring networks and under-predicting during the summer months for all monitoring networks.

The monthly mean MFB and MFGE are presented in **Figure 4.2-2** with the USEPA-recommended goals and performance criteria (2007). As shown in **Figure 4.2-2**, the monthly mean MFB and MFGE for SO_4 are well within the USEPA-recommended performance goals for all monitoring networks and modeling domains.

Time Series Analyses

Time series plots of the SO_4 and SO_2 concentrations are shown in **Figure 4.2-3** for the Canyonlands NP CASTNet site. Time series plots of the SO_4 concentrations are shown in **Figure 4.2-4** for the Canyonlands NP IMPROVE site. These two sites were selected for analysis based on several factors, including monitoring network, location within the 4-km domain, and sample averaging time. CASTNet monitors collect gas-phase precursors, such as SO_2, which are useful during the assessment of particulate composition like SO_4, which is formed via oxidation reactions in the atmosphere. IMPROVE monitors collect PM species, such as SO_4, that influence the visibility conditions in remote areas of scenic interest.

The time series plots (**Figure 4.2-3**) present the weekly average CMAQ and CAMx model-predicted particulate SO_4 (left series) and gaseous SO_2 (right series) concentrations for the grid cells that contain the CASTNet monitor. CAMx was not modeled with SO_2 therefore those values are missing from the time series. These model values were compared with the monitored weekly average SO_4 and SO_2 concentrations at the CASTNet site in Canyonlands NP, Utah. **Figure 4.2-4** displays the time series plots of the daily average model-predicted SO_4 concentrations for the model grid cells that also contain the IMPROVE monitor, Canyonlands NP, Utah. For both monitors, time series are presented for the full year, as well as POI 1 (January 8 to January 23, 2010), and POI 4 (September 27 to October 5, 2010).

In 2010, both monitor sites record peak SO_4 concentrations in early spring, with smaller peaks throughout the summer and fall. The lowest SO_4 concentrations occur in the early winter. The models results generally follow these seasonal trends and the episodic peaks in the monitored SO_4 concentrations, except for the CAMx modeled event in mid-March that was not observed in the monitoring record. With the exception of this event, the model results show lower concentrations during the early winter and higher concentrations during the spring, similar to the monitoring record.

CMAQ Spatial Analyses

The SO_4 spatial performance is reviewed for POI 1 (January 8 to January 23, 2010) and POI 4 (September 27 to October 5, 2010). **Figure 4.2-4** shows the daily average 4-km modeling results for January 8 to January 23, 2010. When available, monitored 24-hour average SO_4 concentrations from the IMPROVE networks are shown in the figure as circles. Throughout POI 1, the model generally reproduced a spatial pattern consistent with the observations, except the model over-estimated the peak SO_4 concentrations on January 14 and under-estimated the peak on January 17, which is supported by the time series shown in **Figure 4.2-4**.

Figure 4.2-6 shows the daily average 4-km modeling results for POI 4 (September 27 to October 5, 2010). For POI 4, contributions from wildfires can be observed in the central portion of the 4-km domain, most notable on September 29. By the end of September two large fires, the Coffee Pot and the Twitchell Canyon, were burning in Utah (National Oceanic and Atmospheric Administration-National Climate Data Center [NOAA-NCDC] 2013; NASA 2013). The most likely source of higher SO_4 concentration during this period is the Twitchell Canyon Fire located in central Utah; this fire was ignited by lighting on July 20th and rapidly grew out of control. The fire was only 30 percent contained by October 1st with emissions impacting southern Utah, northern Arizona and southern Nevada (The Smog Blog 2013). In the beginning of POI 4, model seems to partially capture the plume at eastern sites. Throughout the POI, the model transport of wildfire emissions can be seen by spreading of the SO_4 concentrations. However, the model appears to over-estimates the magentude of the SO_4 concentrations relative to most IMPROVE monitoring stations. The fire emissions are typically speciated using a speciation profile with a higher than expected SO_4 percentage. This SO_4 biased speciation profile can result in model greatly over-estimating SO_4 concentrations related to wildfire influences, as seen during this POI. By October 5, the modeled SO_4 concentrations are consistent with observations.

<u>Summary of Model Performance for SO$_4$</u>

In general, the model appears to perform well for SO$_4$; however, it tends to over-predict concentrations in winter at most locations.

- The model tends to be under-predicted in the summer and over-predicted for the rest of year for the 12-km and 36-km domains across most monitoring networks.
- For the 4-km domain, there are consistent model over-predictions in November and December for all monitoring networks and an under-prediction during summer months for all monitoring networks.

- The model performance for SO$_4$ is well within the USEPA-established performance goals and criteria (USEPA 2007) for all months, monitoring networks, and modeling domains.

- The model tends to reproduce the seasonal patterns and episodic peaks at key monitoring stations in the 4-km domain; however, the model tends to systematically over-predict the concentrations during wintertime and wild fire events.

- Spatial gradients of SO$_4$ during the POIs tend to be consistent with observations, except during wildfire events.

<u>Comparison of CMAQ and CAMx Results</u>

The complete set of CAMx MPE tables, bar charts, and spatial plots is found in **Appendix B**. For the 36- and 12-km domains, CMAQ under-predicts SO$_4$ concentrations during the summer and over-predicts sulfate concentrations the rest of the year, while CAMx over-predicts SO$_4$ for the entire year. For the 4-km domain, CMAQ does not demonstrate a consistent seasonal bias across all networks, while CAMx has small MFB biases during the summer and larger values the rest of the year. Both models over-predict SO$_4$ concentrations during the winter months, except in the CMAQ 4-km domain, where both positive and negative biases occur depending on month and network. On an annual basis, the biases are larger in CAMx than in CMAQ for all domains. The model performance of SO$_4$ from both models is within the USEPA-recommended performance criteria throughout the year for all networks and domains.

Table 4.2-1   Model Performance Statistical Summary for Sulfate

Monitoring Network	Statistic (%)/ Concentration (µg/m³)	36-km Domain					12-km Domain					4-km Domain				
		Annual	Winter	Spring	Summer	Fall	Annual	Winter	Spring	Summer	Fall	Annual	Winter	Spring	Summer	Fall
CASTNET (Weekly)	MFB	12	7	20	-3	27	6	31	-10	-14	20	-1	18	-21	-16	15
	MFGE	33	37	33	27	36	31	42	24	26	33	29	34	29	23	33
	MNB	29	27	45	7	42	21	64	-6	-9	40	6	29	-16	-12	26
	MNGE	46	52	56	31	49	41	74	22	24	51	31	42	25	20	41
	NMB	10	3	31	0	11	-1	29	-11	-16	14	-6	9	-20	-12	11
	NME	35	35	41	24	46	29	45	23	26	32	26	31	27	20	32
	R²	0.064	0.588	0.640	0.620	0.014	0.477	0.553	0.300	0.497	0.460	0.392	0.663	0.050	0.453	0.326
	Observed Mean Concentration (µg/m³)	2.01	1.70	1.83	2.62	1.80	0.54	0.31	0.66	0.68	0.47	0.55	0.39	0.67	0.63	0.47
	Predicted Mean Concentration (µg/m³)	2.20	1.75	2.41	2.61	2.00	0.53	0.39	0.59	0.57	0.54	0.52	0.43	0.54	0.55	0.52
IMPROVE (Daily)	MFB	19	26	19	0	32	11	33	3	-14	22	9	17	3	-8	22
	MFGE	47	57	42	40	49	42	56	33	35	43	37	48	28	29	43
	MNB	64	97	45	50	67	44	71	19	40	46	23	43	11	-2	43
	MNGE	85	120	63	81	81	68	89	43	78	63	46	66	32	29	59
	NMB	18	13	30	1	33	5	38	0	-17	19	7	12	5	-5	24
	NME	48	53	52	39	53	41	66	33	34	45	37	49	30	28	48
	R²	0.572	0.497	0.552	0.643	0.642	0.358	0.384	0.386	0.393	0.327	0.369	0.409	0.349	0.363	0.240
	Observed Mean Concentration (µg/m³)	1.17	0.94	1.19	1.52	1.01	0.54	0.33	0.59	0.72	0.52	0.47	0.34	0.50	0.61	0.44
	Predicted Mean Concentration (µg/m³)	1.38	1.06	1.55	1.53	1.34	0.57	0.45	0.59	0.60	0.61	0.51	0.38	0.52	0.58	0.54

Table 4.2-1   Model Performance Statistical Summary for Sulfate

Monitoring Network	Statistic (%)/ Concentration (µg/m³)	36-km Domain					12-km Domain					4-km Domain				
		Annual	Winter	Spring	Summer	Fall	Annual	Winter	Spring	Summer	Fall	Annual	Winter	Spring	Summer	Fall
STN (Daily)	MFB	4	15	6	-18	15	12	31	10	-12	19	-8	-19	-4	-26	13
	MFGE	47	57	42	43	46	47	62	38	48	44	38	60	31	29	31
	MNB	36	60	48	-1	38	50	100	47	14	41	8	17	5	-20	24
	MNGE	68	91	76	45	61	77	121	69	59	62	43	74	33	24	39
	NMB	4	14	13	-19	16	-1	27	1	-23	8	-14	-27	-6	-23	12
	NME	50	61	49	40	51	48	71	38	46	46	40	61	28	26	32
	R^2	0.348	0.373	0.388	0.363	0.380	0.289	0.084	0.408	0.335	0.379	0.074	0.007	0.280	0.285	0.250
	Observed Mean Concentration (µg/m³)	1.25	1.16	1.20	1.55	1.08	0.99	0.72	0.90	1.39	0.92	0.75	1.08	0.68	0.71	0.52
	Predicted Mean Concentration (µg/m³)	1.30	1.33	1.36	1.26	1.25	0.97	0.92	0.92	1.07	0.99	0.64	0.79	0.64	0.55	0.58
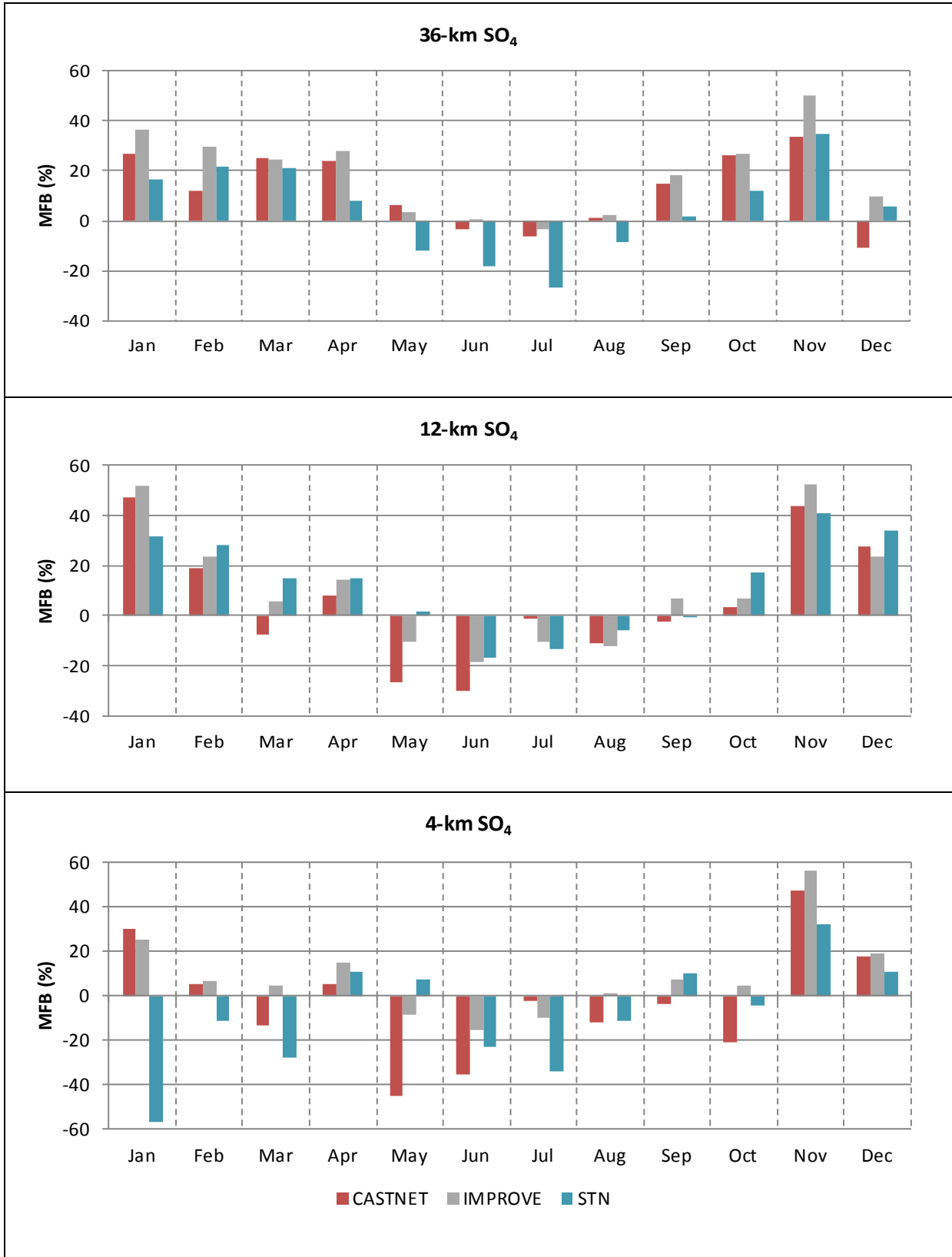
Figure 4.2-1   Monthly Mean Fractional Bias for Sulfate
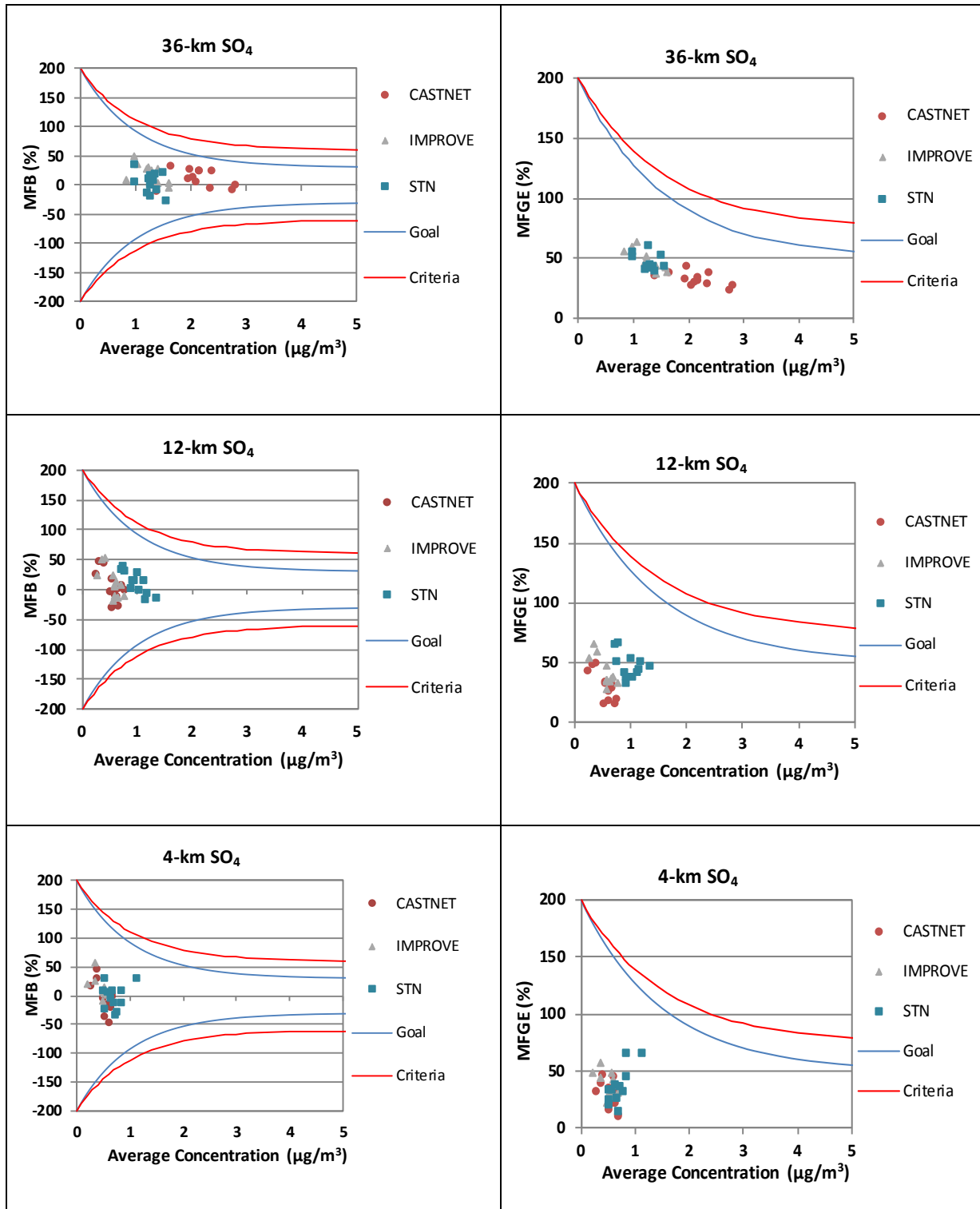
Note: Goals and criteria based on Boylan and Russell (2006) and accepted by USEPA (2007).

Figure 4.2-2   Bugle Plots of Sulfate Monthly Mean Fractional Bias and Mean Fractional Gross Error
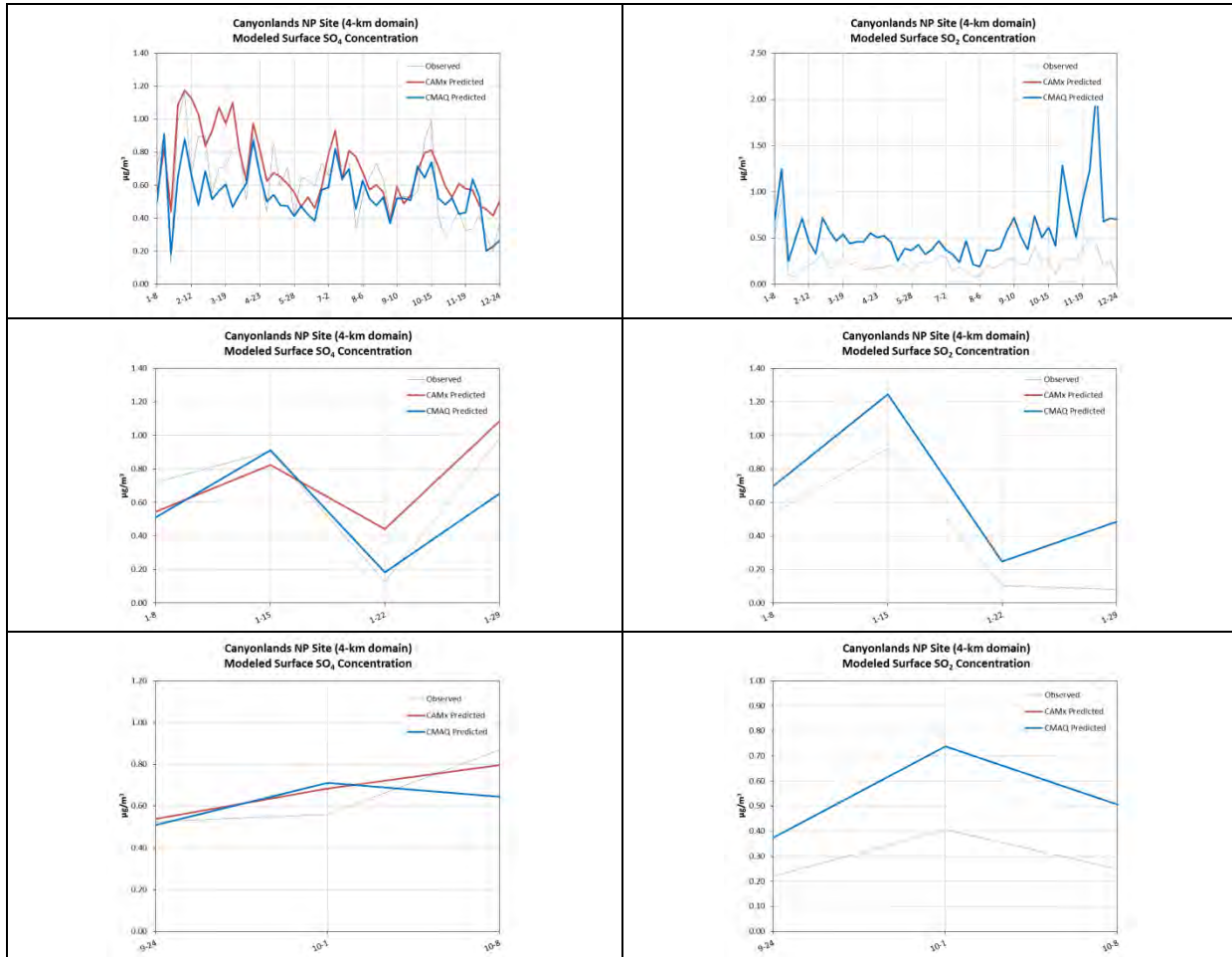
Figure 4.2-3   Time Series for Sulfate and Sulfur Dioxide at the Canyonlands National Park CASTNET Site (CAN407)
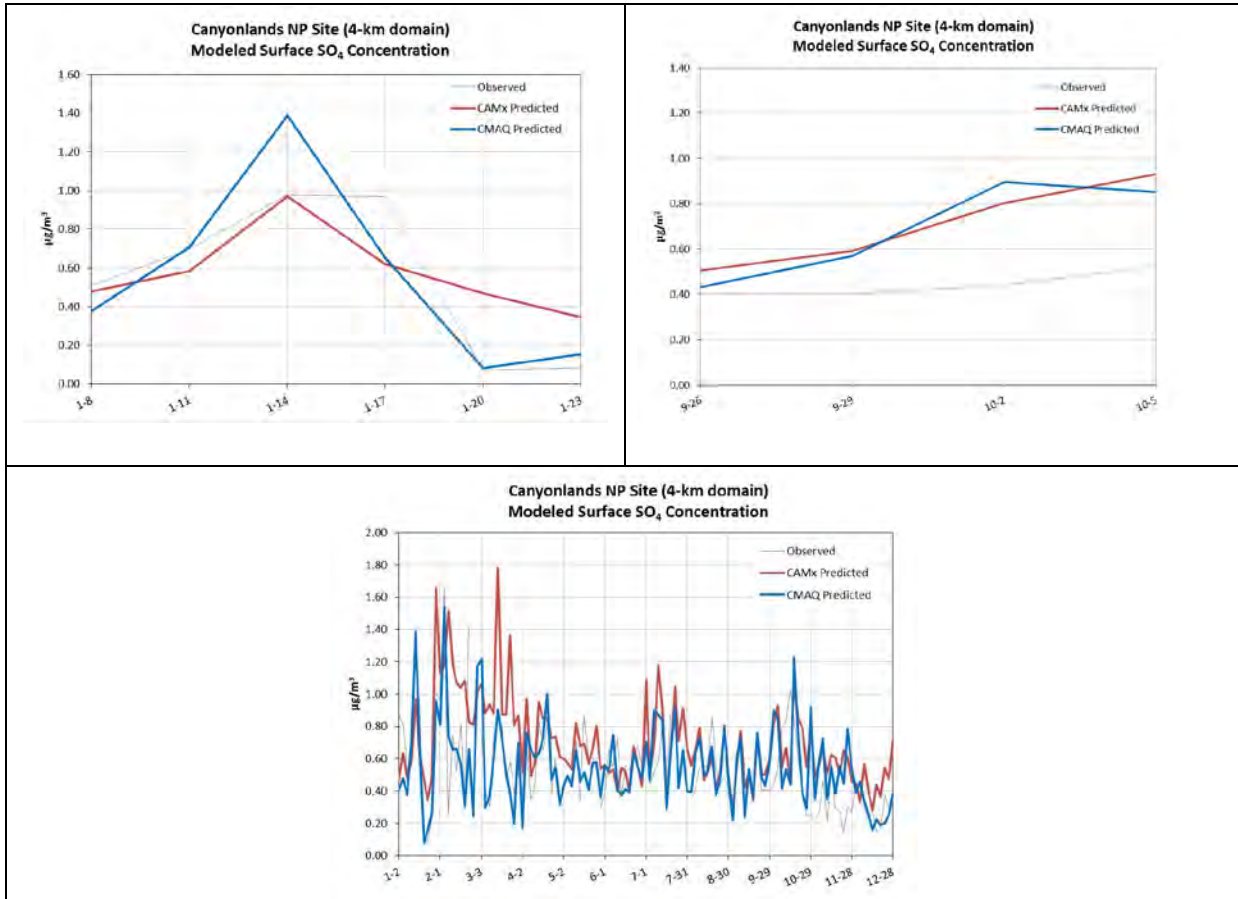
Figure 4.2-4   Time Series for Sulfate at the Canyonlands National Park IMPROVE Site (CANY1)
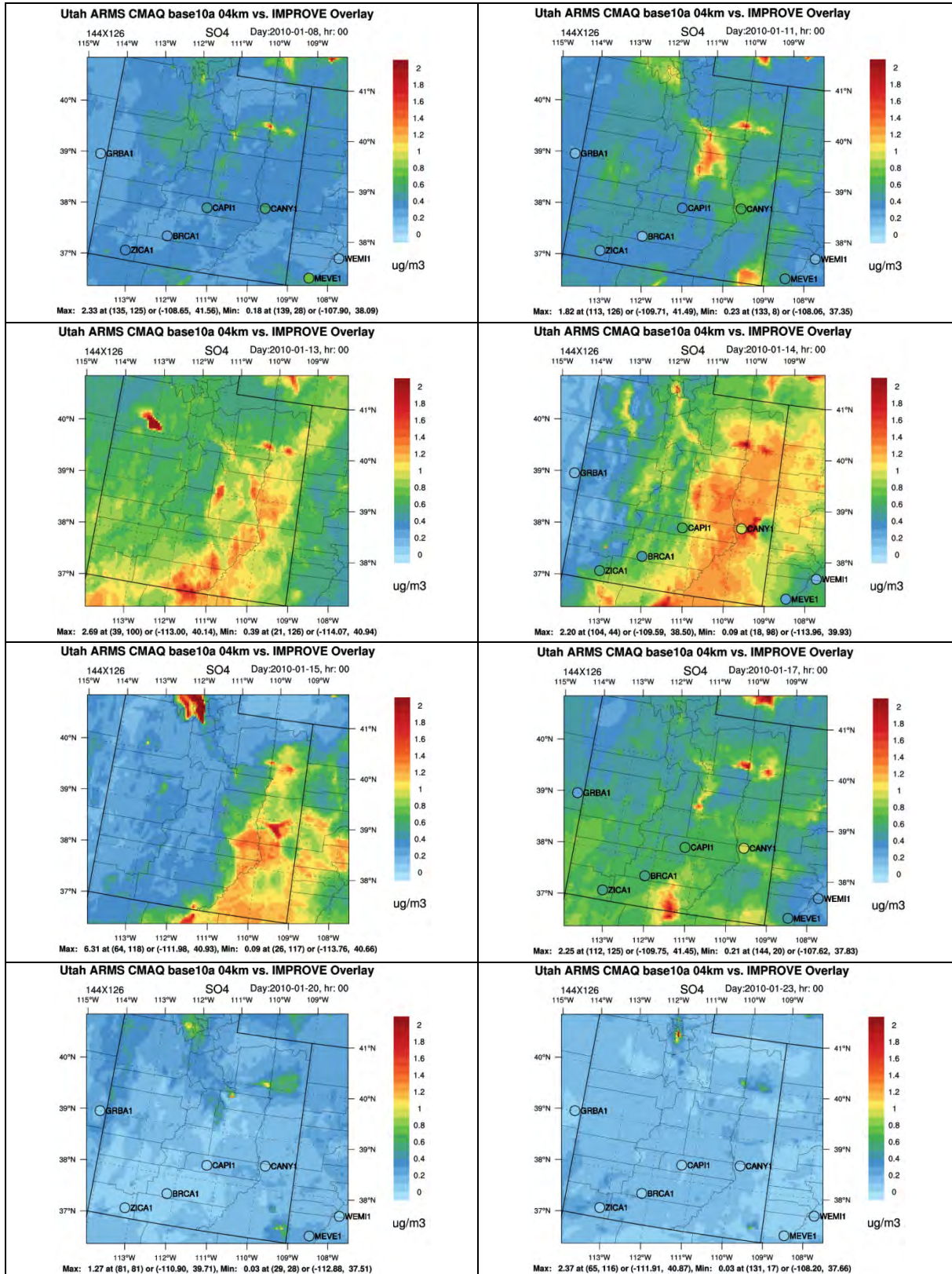
Figure 4.2-5   4-km Spatial Plots for Sulfate during January 8 to January 23, 2010
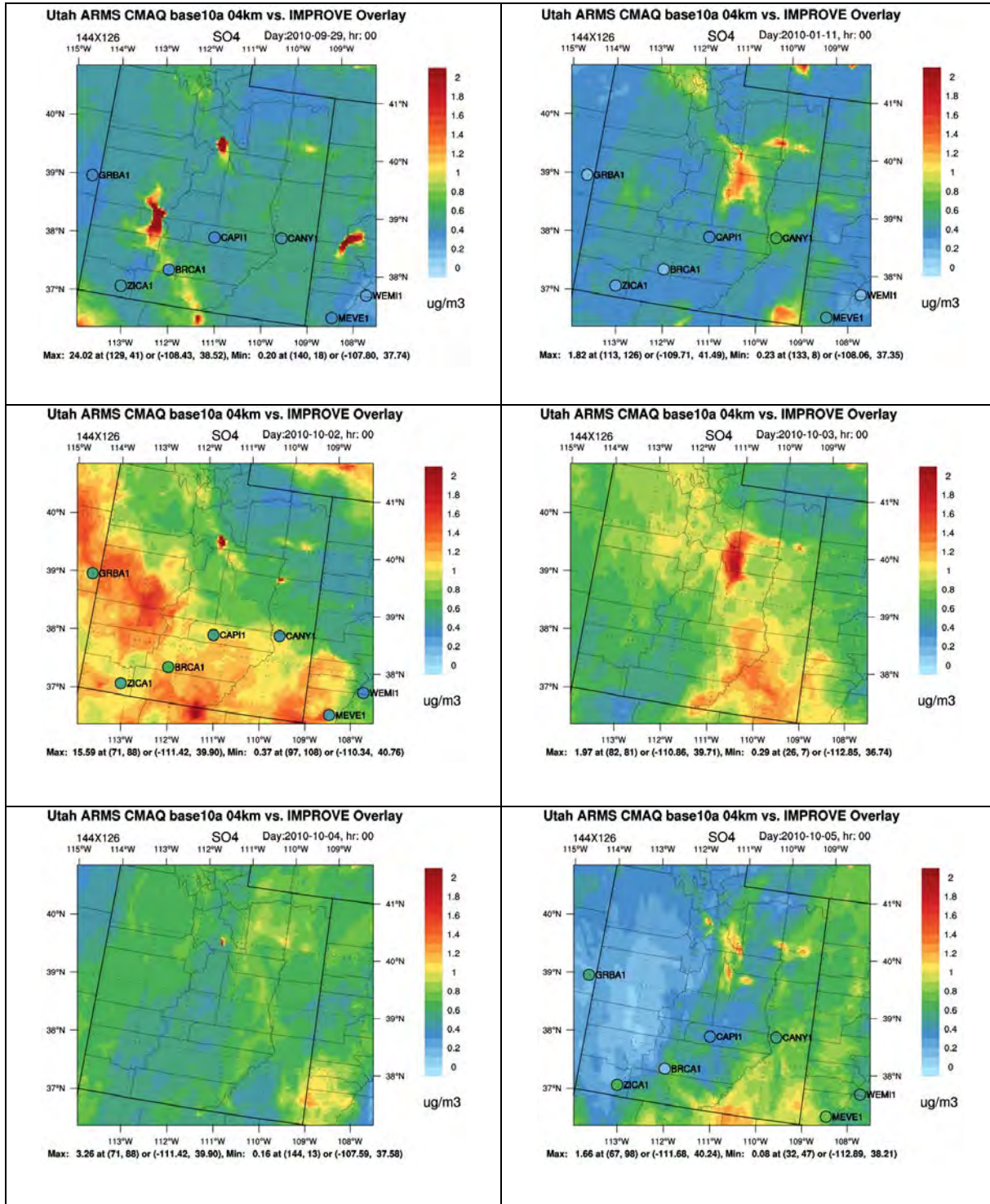
Figure 4.2-6   4-km Spatial Plots for Sulfate during September 27 to October 5, 2010

4.2.1.2 Nitrate

<u>**Statistical Analyses for the CMAQ 36-km, 12-km, and 4-km Domains**</u>

Annual and seasonal NO_3 statistical summaries are presented in **Table 4.2-2** for each monitoring network and modeling domain. Note that the number of monitors with valid data used to calculate the statistical summaries is provided in **Table 3-2**. A more detailed assessment of the MFB is presented for each month in **Figure 4.2-7**. The monthly MFB and MFGE are presented in **Figure 4.2-8** with the USEPA-recommended goals and performance criteria (USEPA 2007). In addition to assessing particulate nitrate, an analysis of the total nitrate in both gaseous and particulate forms is presented in **Table 4.2-3**. Total NO_3 is assessed relative to measurements from the CASTNet network by summing particulate NO_3 and gas-phase nitric acid (HNO_3) compounds. This is done to better understand the model performance for total NO_3, independent of the model's partitioning between gas and particle phases.

In general, the model tends to under-predict particulate NO_3 across all monitoring networks and modeling domains during the summer and surrounding months. For the most part, the model is positively biased in the winter and negatively biased during the other seasons. As shown in **Figure 4.2-7**, the model tends to under-predict particulate NO_3 concentrations relative to observations from April through October. The MFB tend to be fairly similar for a given month and modeling domain for the CASTNet and IMPROVE networks. The STN network's MFB is similar to the other networks during summer months for all domains. However, during the winter months the MFB for STN is negative while the other networks are positive. This difference could be due to the majority of STN monitoring stations being located in urban areas, whereas the monitoring stations for IMPROVE and CASTnet are located in more rural settings. The similarities of the CASTNet and IMPROVE biases suggest that the model biases are fairly accurate with respect to monitored concentrations of particulate NO_3 in non-urban environments. The largest biases tend to occur the summer for all networks and domains with the smallest biases occurring in spring.

There are several possible explanations for the NO_3 model performance. While particulate NO_3 tends to be under-predicted (negative MFB) in summer months, gaseous HNO_3 is over-predicted (positive MFB), throughout all modeling domains and seasons analyzed. This indicates the model favors the partitioning of nitrate into the gas-phase more than the particulate phase during the summer months. For the winter, both gaseous HNO_3 and particulate NO_3 are over-predicted by the model.

Importantly, the total NO_3 measured by the CASTNet network shown in **Table 4.2-3** has a large positive bias independent of modeling domain and season, although the bias tends to be smallest during summer. This indicates that the model-predicted total NO_3 is greater than measurements, regardless of whether the NO_3 is in particulate- or gas-phase. Importantly, it is worth considering that particulate NO_3 measurements can have notable uncertainties, due to volatilization, particularly during periods of low concentrations.

As shown in **Figure 4.2-8**, the monthly MFB and MFGE for particulate NO_3 are within the USEPA-recommended performance criteria for all monitoring networks in the 4-km domain, although a few months exceed the recommended goals. The 36-km and 12-km domain monthly MFB and MFGE meet the USEPA performance criteria, with the exception of a few months relative to the STN network and a single month relative to the CASTNet monitor.

Time Series Analyses

For the assessment of model trends, the same CASTNet and IMPROVE sites and POIs selected for SO_4 are used to assess NO_3 for similar reasons of network averaging periods and type of data collected. In addition to measuring particulate NO_3, CASTNet monitors HNO_3, a species which is useful to consider when assessing the concentrations of total NO_3 that readily partitions between gas- and particle-phase. **Figure 4.2-9** presents the time series plots for particulate NO_3 (left series), gaseous HNO_3 (middle series), and total NO_3 (right series) concentrations at Canyonlands NP. **Figure 4.2-10** shows the time series of particulate NO_3 for the IMPOVE Canyonlands NP monitoring site. The time series plots present the weekly (CASTNet) or daily (IMPROVE) average model-predicted NO_3 concentrations for the grid cells that also contain the monitors. These model values are compared to the monitored weekly or daily average NO_3 concentrations.

As shown in **Figure 4.2-9**, particulate NO_3 observed concentrations peak in the spring and winter, corresponding with lower temperatures and higher relative humidity values. While gaseous HNO_3 concentrations have sustained higher concentrations during the summer months, at Canyonlands there are several episodes of high HNO_3 during winter months. The total NO_3 concentrations follow a season pattern that is fairly flat, with the exception of higher episodes during winter months.

In general, the model does reproduce the expected seasonal trends observed in the monitoring record for NO_3. The model tends to over-predict particulate NO_3 at both monitoring stations during the winter (shown in **Figure 4.2-9** and **4.2-10**), while during summer the model tends to under-predict particulate NO_3. Overall, the models tend to over-predict total NO_3 (the sum of particulate NO_3 and gaseous HNO_3) throughout the year. The elevated concentrations of total NO_3 at the CASTNet station during POI 1 (**Figure 4.2-9,** top row) was fairly accurately captured by the models; however, both models partitioned the NO_3 into the particle phase while the monitoring data suggest that it was in the gas phase as HNO_3. The opposite occurred during POI 4 (**Figure 4.2-9,** middle row), whereby the model partitioned more of the NO_3 into the gas phase than measurement data suggest. The model generally reproduces the timing of most events; however, it generally does not capture the magnitude of the maximum and minimum concentrations nor the partitioning between gas and particle phase.

CMAQ Spatial Analyses

The particulate NO_3 spatial performance was reviewed for POI 1 (January 8 to January 23, 2010) and POI 4 (September 27 to October 5, 2010). When available, monitored 24-hour average NO_3 concentrations from the IMPROVE networks are shown in the figure as circles. **Figure 4.2-11** shows the daily average 4-km modeling results for January 8 to January 23, 2010. During this time period the meteorological conditions are fairly stagnant leading to build up of NO_3 concentrations. At the beginning of POI 1, the model over-predicts the NO_3 observed concentrations throughout the State of Utah. As the event proceeds, the modeled concentrations increase throughout the state. Starting January 19, the model concentrations decrease and at the conclusion of the POI the modeled concentrations are consistent with observations. Although modeled concentrations in the Uinta Basin study area remain elevated in the model, which cannot be evaluated due to a lack of monitoring data in this area.

Throughout the POI, the model shows elevated concentrations of NO_3 over the majority of the state of Utah. To understand the potential source of this discrepancy, the modeled annual NH_3 emissions were reviewed and the emissions were higher in the State of Utah than surrounding states (AECOM 2013). The stagnate conditions combined with higher amounts of available NH_3 during this POI led to higher concentrations of particulate NO_3 within Utah than the surrounding areas. However, given that the total nitrate concentrations are over-predicted by the model in the 4-km domain (shown in **Table 4.2-3**), the over-prediction of particulate NO_3 is not necessarily attributable exclusively to NH_3 availability, rather it could be due to excess NO_x emissions or excess conversion of NO_x to NO_3.

Figure 4.2-12 shows the daily average 4-km modeling results for POI 4 (September 27 to October 5), 2010. While monitored concentrations are very spatially uniform at monitors in the southern portion of the state, the model shows quite a bit of spatial variability in unmonitored locations. While the model may under- or over-estimate concentrations relative to individual monitors throughout this period, in general the modeled concentrations are consistent with observations.

Summary of Model Performance for NO$_3$

In general, the model performs adequately for particulate NO$_3$; however, it tends to under-predict concentrations during the summer and over-predict concentrations during the winter.

- For the IMPROVE and CASTNet networks, the model tends to under-predict particulate NO$_3$ concentrations from April to October and over-predict concentrations throughout the rest of the year.
- Relative to the STN network, the model under-predicts concentrations almost year-round for all domains.
- For gas-phase HNO$_3$, the model over-predicts concentrations for all domains with the smallest biases and errors in the summer and the largest biases and errors in the winter or fall.
- The model for total nitrate (the combined mass of nitric acid and particulate NO$_3$) shows failrly consistent over-predictions throughout the year for all modeling domains.
- Monthly MFB and MFGE are within USEPA performance criteria for all networks and all domains, with the exception of a few months relative to the STN network and one month relative to the CASTNet network.
- The model mostly reproduces the timing of the NO$_3$ events; however, it over-estimates the total NO$_3$ and is not able to accurately reproduce the partitioning between gas and particle phase.

Comparison of CMAQ and CAMx Results

The complete set of the CAMx MPE tables, bar charts, and spatial plots is found in **Appendix B**. Both the CMAQ and CAMx models consistently under-predict particulate NO$_3$ concentrations from April to October for all domains. Both models over-predict nitrate concentrations for some months and networks from November to February. For both models, nitrate predictions are within USEPA performance criteria for all domains, except for the STN network during the summer months. Interestingly, as shown in **Figure 4.2-9** and **4.2-10**, the CAMx particulate NO$_3$ concentrations are close to zero during POI 4 at Cayonlands. It is speculated that the CAMx model may be ammonia limited during this period, as there is HNO$_3$ available, and the ammonium time series closely resembles the sulfate time series.

Table 4.2-2   Model Performance Statistical Summary for Nitrate

Monitoring Network	Statistic (%)/ Concentration (µg/m³)	36-km Domain					12-km Domain					4-km Domain				
		Annual	Winter	Spring	Summer	Fall	Annual	Winter	Spring	Summer	Fall	Annual	Winter	Spring	Summer	Fall
CASTNET (Weekly)	MFB	-4	57	15	-70	-8	-25	85	-34	-137	2	-35	79	-32	-168	-10
	MFGE	90	84	83	107	84	109	119	75	138	103	113	99	80	168	98
	MNB	115	320	106	-9	76	166	626	2	-78	196	93	299	10	-91	148
	MNGE	172	338	149	94	132	246	647	73	78	256	178	313	81	91	215
	NMB	45	62	85	-41	17	2	172	-31	-85	34	80	274	2	-92	97
	NME	91	80	123	88	85	110	228	67	85	130	158	282	76	92	168
	R²	0.245	0.705	0.617	0.004	0.032	0.049	0.215	0.193	0.209	0.009	0.492	0.768	0.012	0.005	0.010
	Observed Mean Concentration (µg/m³)	0.82	1.55	0.77	0.34	0.73	0.30	0.23	0.47	0.29	0.21	0.23	0.30	0.31	0.20	0.15
	Predicted Mean Concentration (µg/m³)	1.20	2.51	1.42	0.20	0.85	0.31	0.62	0.32	0.04	0.28	0.42	1.14	0.31	0.02	0.30
IMPROVE (Daily)	MFB	-29	35	-15	-111	-21	-34	41	-27	-132	-11	12	93	25	-122	53
	MFGE	114	105	101	135	114	120	118	94	145	123	120	130	97	134	125
	MNB	183	510	108	-35	181	272	827	57	-60	323	402	977	156	-57	581
	MNGE	264	551	176	101	258	359	872	130	91	400	465	997	199	88	624
	NMB	70	78	93	-39	75	32	142	-1	-74	65	193	289	127	-59	417
	NME	125	117	143	96	143	127	194	87	86	166	239	299	169	86	454
	R²	0.460	0.470	0.477	0.070	0.259	0.133	0.202	0.206	0.242	0.045	0.358	0.429	0.246	0.081	0.103
	Observed Mean Concentration (µg/m³)	0.46	0.91	0.45	0.19	0.30	0.23	0.24	0.31	0.18	0.16	0.16	0.26	0.18	0.11	0.08
	Predicted Mean Concentration (µg/m³)	0.78	1.62	0.87	0.11	0.53	0.30	0.58	0.31	0.05	0.27	0.46	1.02	0.40	0.04	0.41

Table 4.2-2   Model Performance Statistical Summary for Nitrate

Monitoring Network	Statistic (%)/ Concentration (µg/m^3)	36-km Domain					12-km Domain					4-km Domain				
		Annual	Winter	Spring	Summer	Fall	Annual	Winter	Spring	Summer	Fall	Annual	Winter	Spring	Summer	Fall
STN (Daily)	MFB	-78	-53	-51	-136	-71	-77	-44	-42	-144	-77	-10	-23	16	-70	23
	MFGE	112	94	95	146	113	100	76	79	144	101	59	52	42	80	67
	MNB	-13	7	9	-66	-4	-24	20	-9	-80	-26	21	-6	34	-42	86
	MNGE	95	95	97	88	101	81	97	69	80	79	69	48	54	55	116
	NMB	-38	-29	-18	-83	-47	-57	-43	-41	-91	-63	-19	-33	35	-44	30
	NME	79	73	76	89	87	71	60	67	91	76	49	48	49	57	57
	R2	0.237	0.172	0.421	0.293	0.072	0.232	0.262	0.192	0.432	0.119	0.540	0.292	0.838	0.028	0.710
	Observed Mean Concentration (µg/m3)	1.82	3.61	1.39	1.06	1.35	2.21	3.81	1.62	1.91	1.66	2.78	8.37	1.24	0.29	0.96
	Predicted Mean Concentration (µg/m3)	1.13	2.56	1.14	0.18	0.71	0.95	2.16	0.96	0.17	0.61	2.25	5.62	1.68	0.16	1.25

Table 4.2-3   Model Performance Statistical Summary for Nitric Acid and Total Nitrate for CASTNet Monitors

Chemical Compound	Statistic (percent) /b_{ext}	36-km Domain					12-km Domain					4-km Domain				
		Annual	Winter	Spring	Summer	Fall	Annual	Winter	Spring	Summer	Fall	Annual	Winter	Spring	Summer	Fall
HNO$_3$ (gas)	MFB	29	41	21	11	46	57	59	57	46	69	57	21	73	59	74
	MFGE	50	63	44	40	56	68	87	61	53	74	82	108	81	59	85
	MNB	72	109	52	34	103	133	195	113	80	155	139	137	168	93	166
	MNGE	89	125	70	57	111	140	213	117	86	159	154	190	174	93	174
	NMB	19	51	14	6	15	62	79	52	41	93	81	15	108	85	121
	NME	56	71	42	42	73	75	123	64	49	98	111	117	120	85	130
	R^2	0.012	0.439	0.459	0.160	0.004	0.649	0.141	0.654	0.833	0.745	0.180	0.016	0.259	0.458	0.654
	Reconstructed Mean	0.91	0.78	0.88	0.99	0.96	0.57	0.38	0.46	0.88	0.52	0.54	0.61	0.32	0.69	0.52
	Model-predicted Mean	1.08	1.19	1.00	1.05	1.11	0.92	0.69	0.70	1.23	1.00	0.98	0.71	0.66	1.28	1.15
Total NO$_3$	MFB	26	55	25	-5	36	46	84	24	19	64	56	79	39	34	73
	MFGE	49	61	46	39	51	55	86	37	36	67	57	80	39	36	73
	MNB	59	117	50	7	74	102	212	40	33	141	95	154	54	46	129
	MNGE	77	122	66	41	86	110	214	51	47	144	96	155	55	48	129
	NMB	40	58	48	-1	45	41	113	14	9	74	80	102	56	46	113
	NME	57	64	64	37	59	58	119	40	31	80	82	108	56	47	113
	R^2	0.719	0.787	0.686	0.534	0.629	0.605	0.604	0.640	0.849	0.648	0.619	0.680	0.588	0.448	0.791
	Reconstructed Mean	1.61	2.34	1.61	1.25	1.34	0.86	0.61	0.87	1.16	0.73	0.77	0.91	0.62	0.87	0.68
	Model-predicted Mean	2.26	3.71	2.38	1.24	1.95	1.21	1.30	1.00	1.27	1.27	1.38	1.83	0.97	1.27	1.44
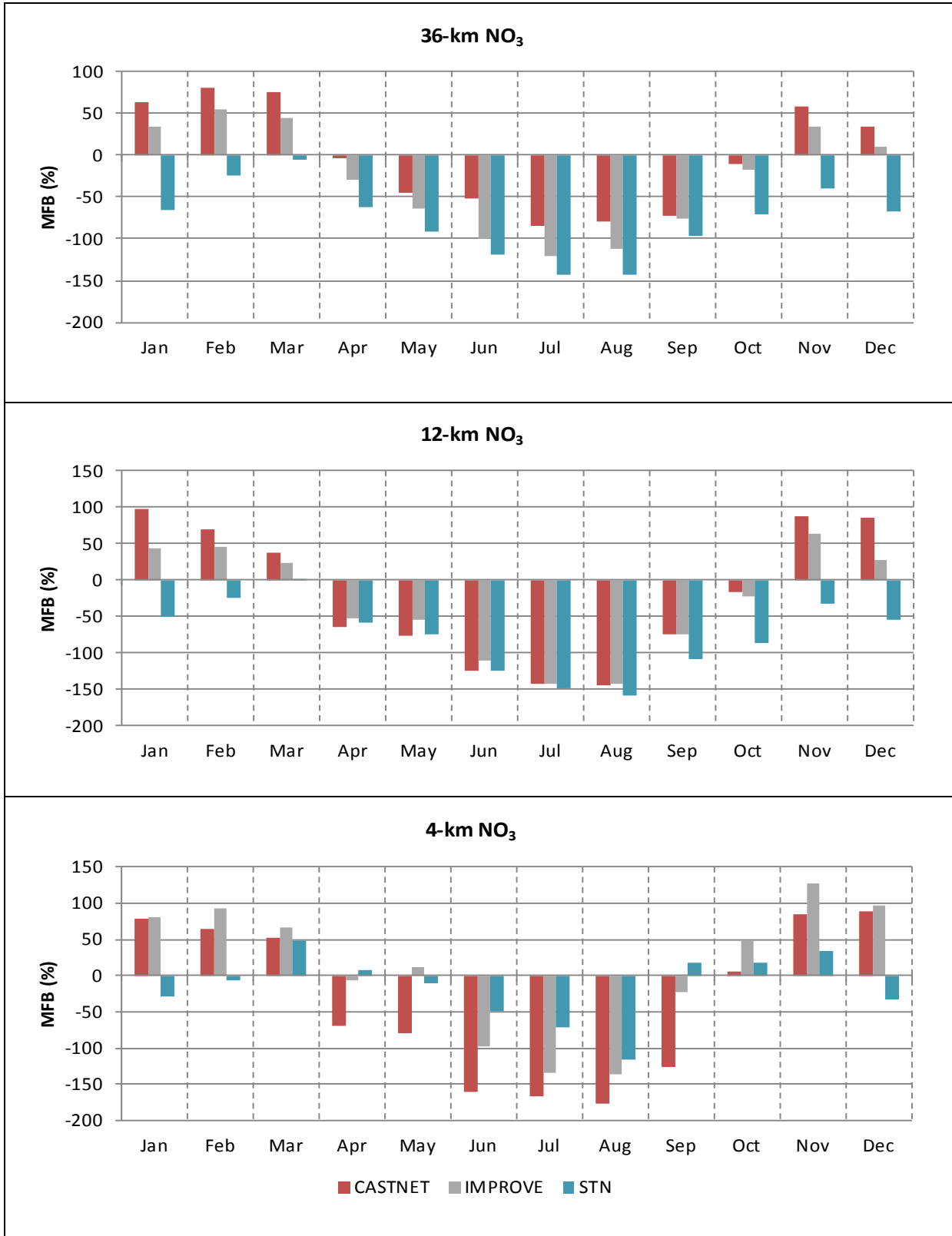
Figure 4.2-7   Monthly Mean Fractional Bias for Nitrate
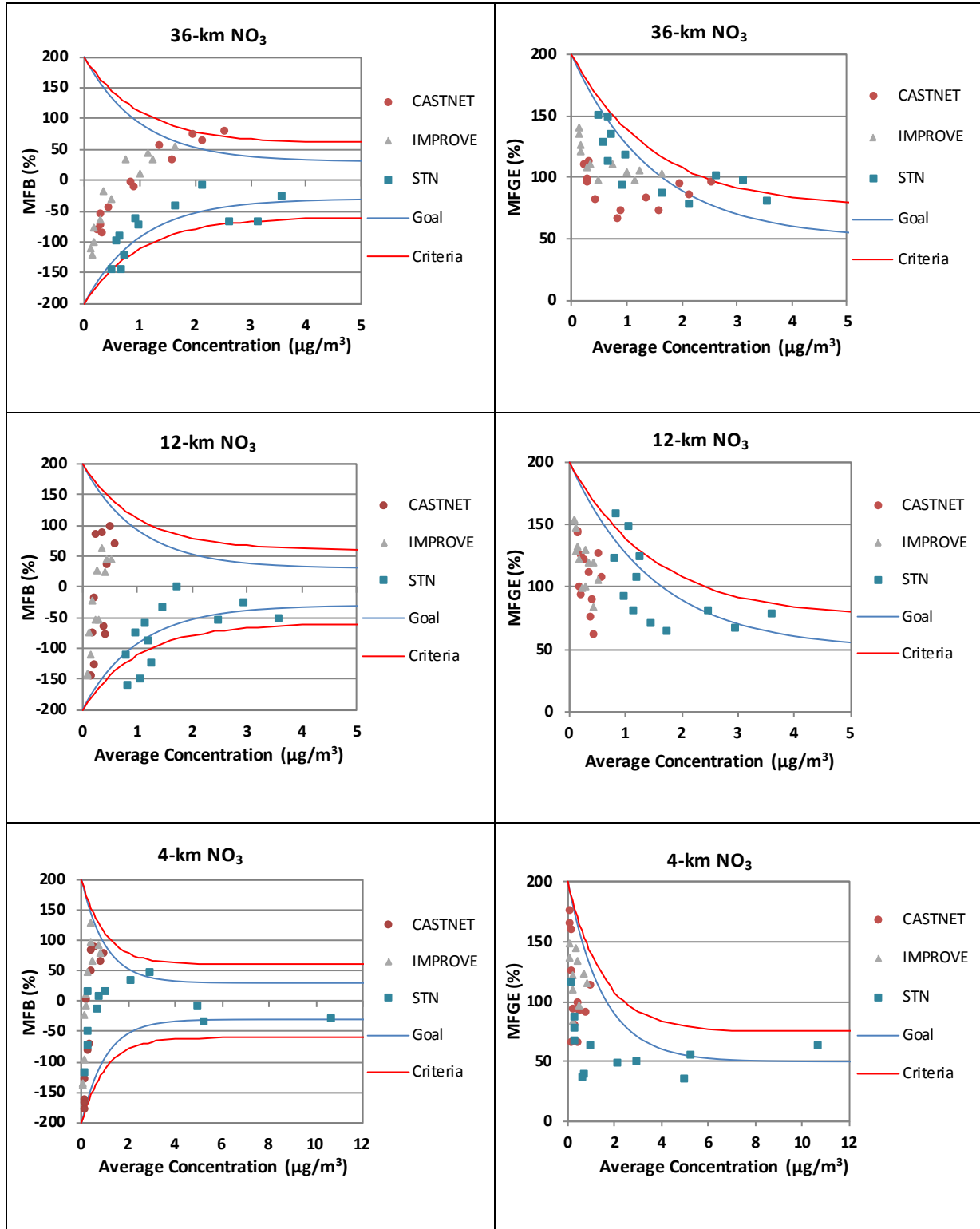
Note: Goals and criteria based on Boylan and Russell (2006) and accepted by USEPA (2007).

Figure 4.2-8   Bugle Plots of Nitrate Monthly Mean Fractional Bias and Mean Fractional Gross Error
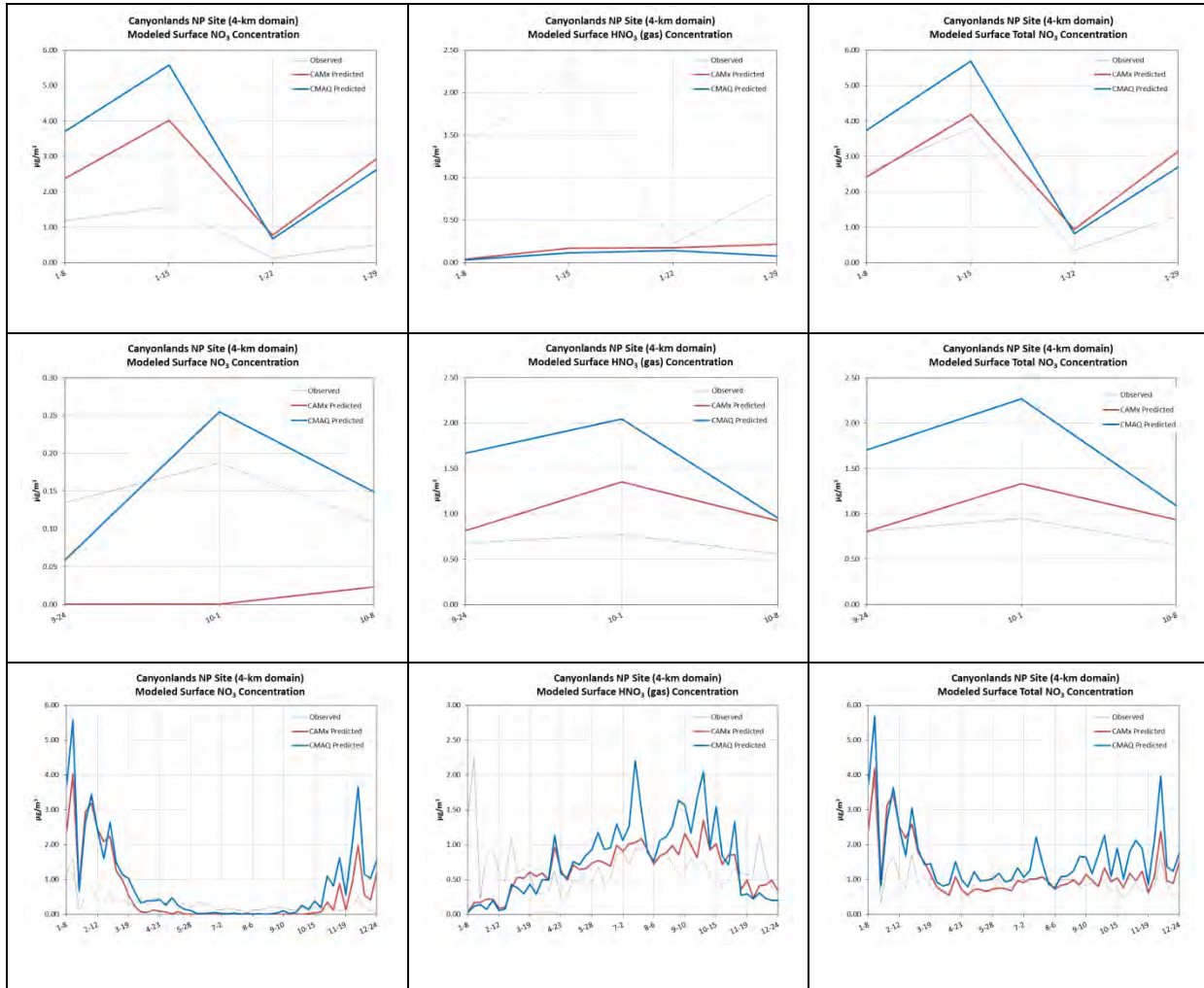
Figure 4.2-9   Time Series for Nitrate, Nitric Acid, and Total Nitrate at the Canyonlands National Park CASTNET Site (CAN407)
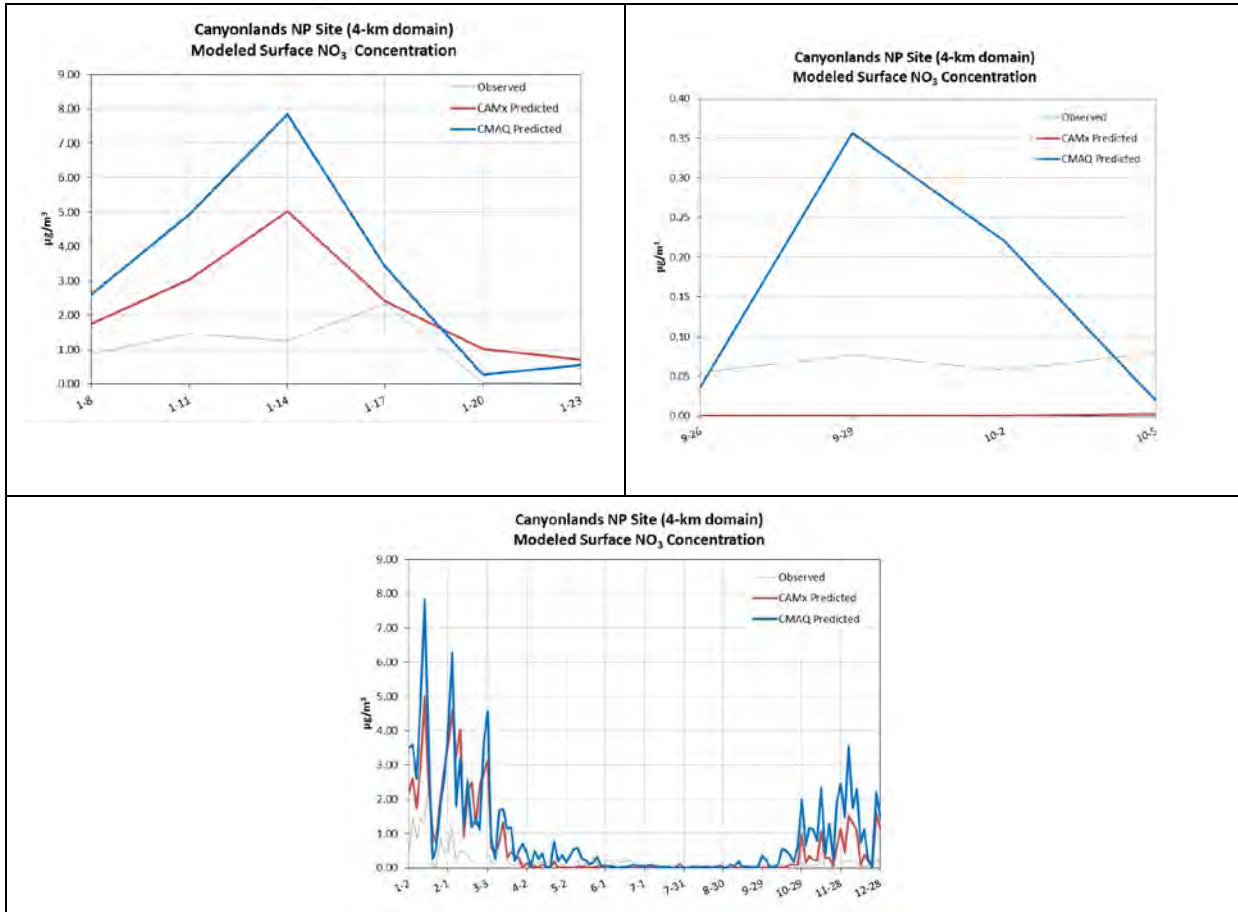
Figure 4.2-10   Time Series for Nitrate at the Canyonlands National Park IMPROVE Site (CANY1)
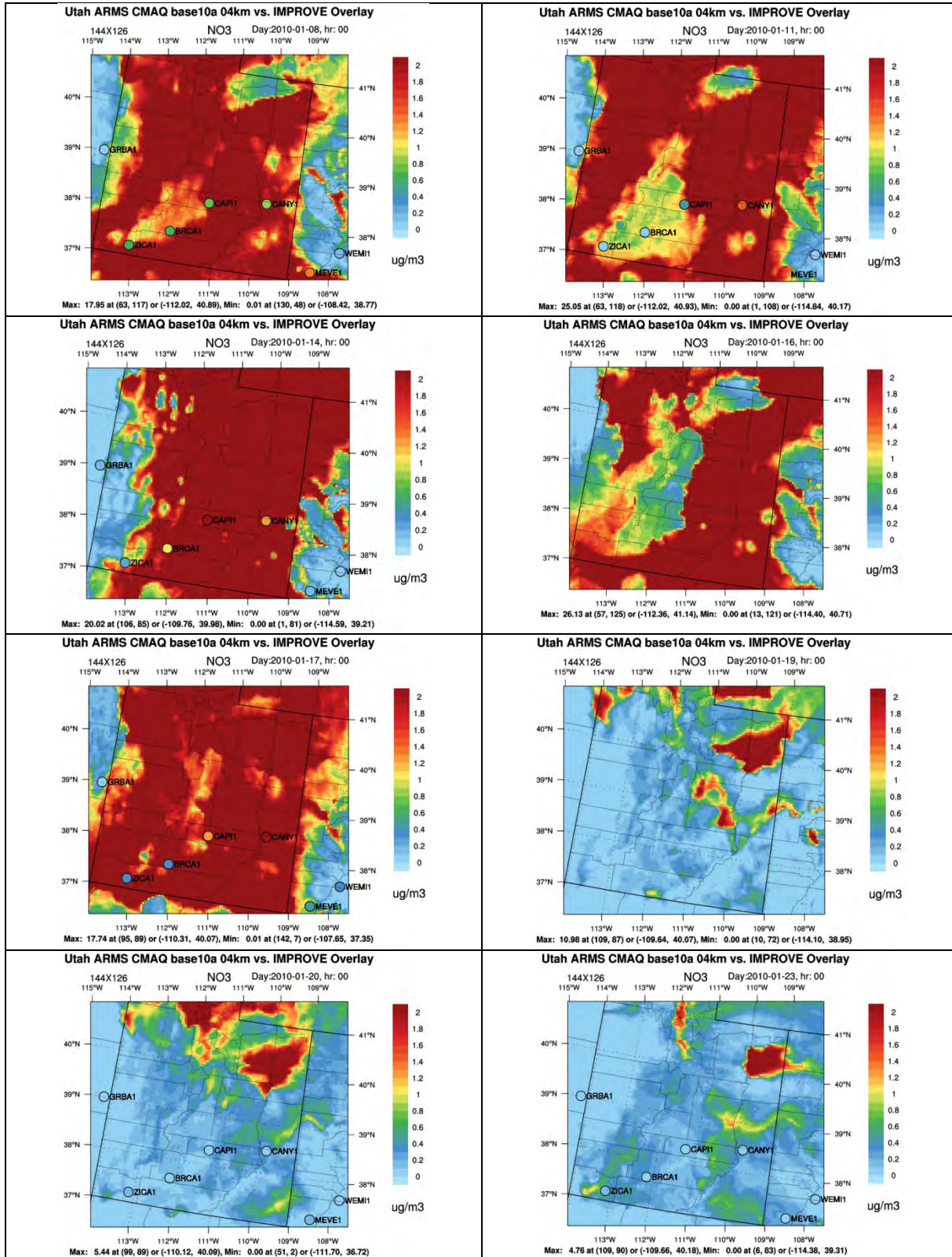
Figure 4.2-11   4-km Spatial Plots for Nitrate during January 8 to January 23, 2010
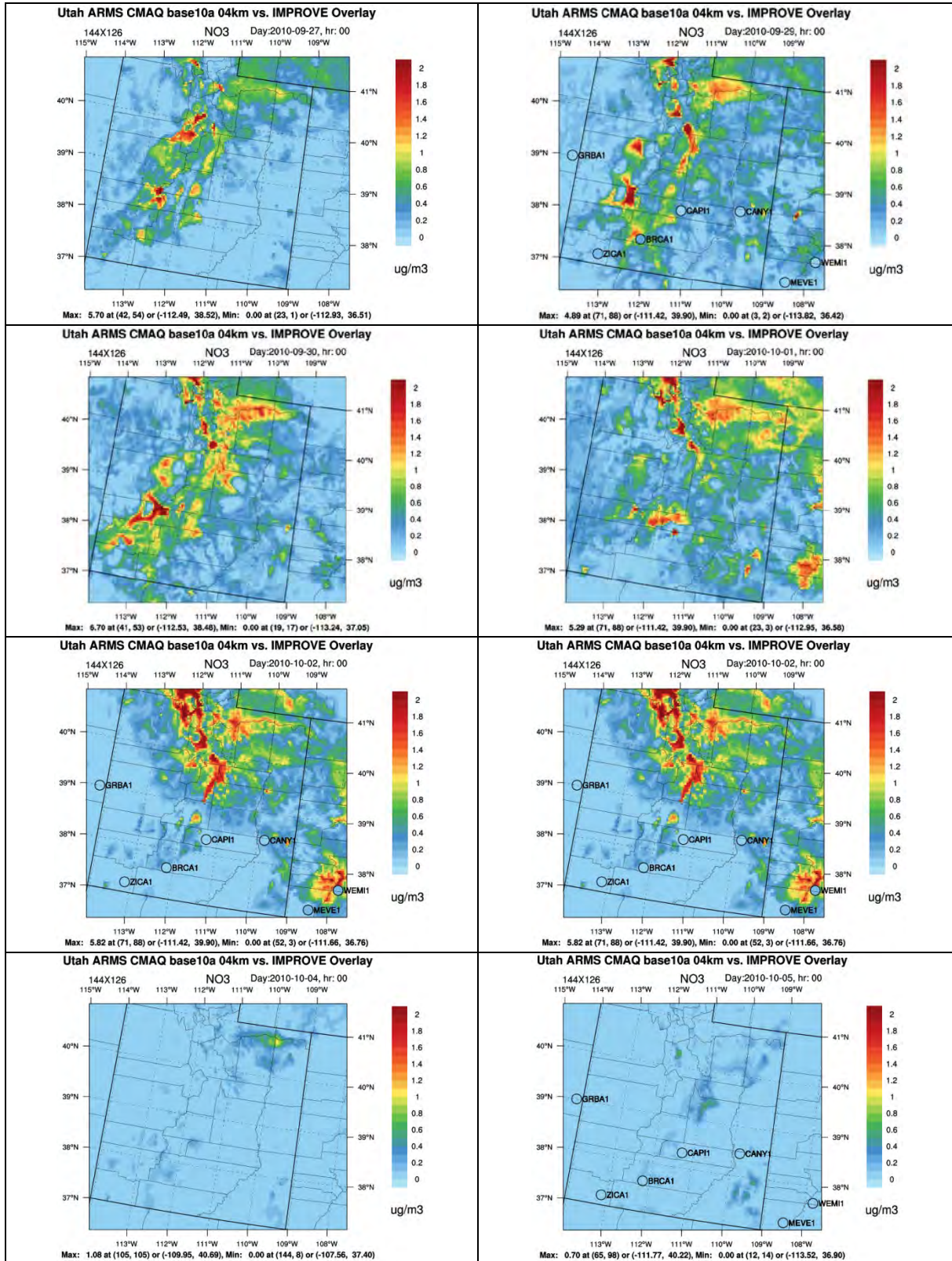
Figure 4.2-12   4-km Spatial Plots for Nitrate during September 27 to October 5, 2010

4.2.1.3 Ammonium

Statistical Analyses for the CMAQ 36-km, 12-km, and 4-km Domains

Annual and seasonal NH_4 statistical summaries are presented in **Table 4.2-4** for each monitoring network and modeling domain. Note that the number of monitors with valid data used to calculate the statistical summaries is provided in **Table 3-2**. A more detailed assessment of the MFB is presented for each month in **Figure 4.2-13**. The monthly MFB and MFGE are presented in **Figure 4.2-14** with the USEPA-recommended goals and performance criteria (USEPA 2007).

In general, the model shows good performance predicting annual NH_4 concentrations across all monitoring networks and modeling domains. As shown in **Table 4.2-4**, model-predicted values are similar to observed concentrations during summer, with small over- or under-predictions by modeling network and domain. For the remaining seasons in the 36- and 12-km domains, the MFB exhibits positive biases, particularly in winter relative to all monitoring networks. In the 4-km domain, the model over-predicts NH_4 concentrations during all seasons, except summer, for CASTNet and IMPROVE while relative to the STN network, the model over-predicts NH_4 concentrations for all season, except winter.

While the annual average model predictions are fairly consistent with observed annual average concentrations, the seasonal trends in model performance are similar to SO_4 whereby positive biases occur in the winter and lower positive or negative biases occur in the summer (depending on the monitoring network). This similarity is most notable with the monthly biases in the 36- and 12-km domains (**Figure 4.2-1** and **Figure 4.2-13**). Typically, the NH_4 concentrations are closely associated with the availability of SO_4 and NO_3. In general, the NH_4 model performance closely resembles the SO_4 performance more than the NO_3 performance.

In addition, the differences by network may be an indication of how difficult it is to obtain accurate measurements of NH_4, rather than an indication of real differences in model performance. It is important to note that the IMPROVE-reported NH_4 concentrations are not based on measured concentrations; rather, the values are calculated based on the assumption that the particulate SO_4 and NO_3 are fully neutralized and bonded with NH_4. Therefore, the NH_4 model performance relative to the IMPROVE network is more an indication of the combined model performance for particulate NO_3 and SO_4.

As shown in **Figure 4.2-14**, the monthly fractional MFB and MFGE for NH_4 are within the USEPA-recommended performance goals for all networks and model domains, with the exception of a single month relative to the STN network.

Time Series Analyses

Time series plots of the NH_4 concentrations for the full year, January 8 to January 23, 2010, and September 27 to October 5, 2010 are shown in **Figure 4.2-15** for the Canyonlands NP IMPROVE and CASTNet sites. Similar to the previous time series, the plots display the daily average model-predicted NH_4 concentrations for the CMAQ and CAMx grid cells that contain the monitor. The observations show NH_4 concentration peaks during the early part of the year with lower concentrations and smaller peaks during the rest of the year. In general, the models over-predict the NH_4 concentrations during the winter months and show good performance during the summer months. Similar to the temporal pattern for particulate NO_3, the models over-estimate the magnitude of the winter observed peaks, but tend to capture the general seasonal pattern found in the observations.

CMAQ Spatial Analyses

The NH_4 spatial performance was reviewed for POI 1 (January 8 to January 23, 2010 shown in **Figure 4.2-716**) and POI 4 (September 27 to October 5, 2010 shown in **Figure 4.2-17**). When available, monitored 24-hour average NH_4 concentrations from the IMPROVE networks are shown in the figure

as circles. **Figure 4.2-16** shows the daily average 4-km modeling results for January 8 to January 23, 2010. During the beginning of this POI, the model tends to over-estimate the NH_4 concentrations relative to the observations. Similar to SO_4 and NO_3, the model tends to over-predict the NH_4 concentrations during this POI. As discussed with NO_3, the model's over-prediction could be the result of stagnate weather conditions and higher concentrations of NH_4 in Utah due to the emission inventory used. However, the spatial extent of the over-predictions of NH_4 concentrations is not as expansive as seen in the NO_3 spatial plots (**Figure 4.2-11**) likely due to preferential bonding with SO_4. By the end of POI 1, the modeled NH_4 concentrations are similar to observations.

Figure 4.2-17 shows the daily average 4-km modeling results for September 27 to October 5, 2010. Overall, the model slightly over-predicts the NH_4 concentrations relative to observations. The wildfires seen in the SO_4 spatial plots (**Figure 4.2-5**) also are seen in the NH_4 spatial plots. Although, the magnitude of the model predicted NH_4 concentrations and extent of the wildfire plumes are not as widespread as shown in the SO_4 spatial plots. By the end of the POI, the observations sites are still reporting higher NH_4 concentrations compared to what the model is producing.

Summary of Model Performance for NH_4

In general, the model performs adequately for particulate NH_4; however, it tends to over-predict concentrations in most locations, particularly during the winter.

- Annual model predictions are fairly similar to observed concentrations for all monitoring networks and modeling domains. Seasonally, the model tends to over-predict in winter and shows a small positive or slightly negative bias in summer.

- The model performance for NH_4 is within the USEPA-established performance goals (USEPA 2007) for all months, monitoring networks, and modeling domains.

- Spatial gradients of particulate NH_4 during the POI tend to be consistent with SO_4 and NO_3.

Comparison of CMAQ and CAMx Results

The complete set of the CAMx MPE tables, bar charts, and spatial plots is found in **Appendix B**. Both models generally over-predict NH_4 concentrations during the winter and under-predict NH_4 concentrations during the summer. The smallest biases tend to occur during the summer months for all networks and domains. The biggest differences in NH_4 performance between CMAQ and CAMx occur during the summer months. The nature of these differences varies depending on domain and network. For both models, ammonium predictions are within USEPA performance criteria for all networks and domains, and overall ammonium model performance is similar for both models.

Table 4.2-4   Model Performance Statistical Summary for Ammonium

Monitoring Network	Statistic (%)/ Concentration ($\mu g/m^3$)	36-km Domain					12-km Domain					4-km Domain				
		Annual	Winter	Spring	Summer	Fall	Annual	Winter	Spring	Summer	Fall	Annual	Winter	Spring	Summer	Fall
CASTNET (Weekly)	MFB	31	41	46	-2	42	24	67	17	-17	35	23	73	14	-22	33
	MFGE	46	52	52	30	51	43	75	31	25	47	45	74	32	26	51
	MNB	64	92	88	7	78	59	164	28	-13	79	64	169	26	-18	97
	MNGE	76	101	93	32	85	76	170	40	22	89	82	170	41	22	112
	NMB	35	39	80	0	33	28	113	18	-16	41	45	157	21	-18	50
	NME	54	50	84	30	67	50	126	34	23	55	65	158	38	22	70
	R^2	0.084	0.749	0.705	0.356	0.015	0.178	0.405	0.371	0.570	0.064	0.344	0.755	0.147	0.551	0.000
	Observed Mean Concentration ($\mu g/m^3$)	0.78	0.94	0.66	0.84	0.67	0.21	0.15	0.23	0.24	0.19	0.20	0.19	0.21	0.23	0.17
	Predicted Mean Concentration ($\mu g/m^3$)	1.04	1.30	1.20	0.84	0.88	0.26	0.32	0.27	0.20	0.26	0.29	0.48	0.25	0.18	0.26
IMPROVE (Daily)	MFB	7	32	5	-26	18	2	40	-12	-35	18	17	59	6	-29	35
	MFGE	54	65	49	49	53	53	72	43	48	51	54	82	41	39	56
	MNB	60	115	34	41	55	45	122	12	-2	57	63	161	22	-20	95
	MNGE	94	138	67	95	80	83	144	53	59	82	91	176	50	33	112
	NMB	15	35	28	-22	23	2	73	-12	-35	17	35	115	16	-23	61
	NME	57	66	64	42	57	56	101	43	43	58	68	127	47	33	83
	R^2	0.470	0.575	0.447	0.552	0.479	0.182	0.354	0.307	0.381	0.113	0.251	0.553	0.248	0.314	0.021
	Observed Mean Concentration ($\mu g/m^3$)	0.57	0.61	0.57	0.62	0.46	0.27	0.19	0.31	0.32	0.24	0.22	0.20	0.24	0.26	0.18
	Predicted Mean Concentration ($\mu g/m^3$)	0.65	0.82	0.73	0.49	0.57	0.27	0.33	0.27	0.21	0.28	0.30	0.42	0.27	0.20	0.30

Table 4.2-4   Model Performance Statistical Summary for Ammonium

Monitoring Network	Statistic (%)/ Concentration (µg/m³)	36-km Domain					12-km Domain					4-km Domain				
		Annual	Winter	Spring	Summer	Fall	Annual	Winter	Spring	Summer	Fall	Annual	Winter	Spring	Summer	Fall
STN (Daily)	MFB	17	11	27	-1	31	15	21	28	-12	22	30	-12	50	20	56
	MFGE	68	75	64	61	72	65	73	61	63	63	52	55	57	30	62
	MNB	169	81	319	74	186	100	239	75	19	83	73	29	103	31	116
	MNGE	205	125	347	118	215	135	276	100	69	112	90	77	109	40	122
	NMB	-1	-9	25	-21	9	-23	-18	-1	-52	-18	-11	-33	57	20	56
	NME	71	68	74	64	83	65	65	61	68	64	52	50	62	32	66
	R^2	0.245	0.224	0.376	0.156	0.070	0.229	0.220	0.279	0.257	0.229	0.553	0.319	0.823	0.324	0.687
	Observed Mean Concentration (µg/m³)	0.77	1.35	0.63	0.58	0.57	0.83	1.26	0.60	0.85	0.64	1.01	2.92	0.45	0.20	0.37
	Predicted Mean Concentration (µg/m³)	0.77	1.22	0.79	0.46	0.63	0.63	1.04	0.59	0.41	0.53	0.89	1.95	0.71	0.24	0.58

Figure 4.2-13   Monthly Mean Fractional Bias for Ammonium

Note: Goals and criteria based on Boylan and Russell (2006) and accepted by USEPA (2007).

Figure 4.2-14   Bugle Plots of Ammonium Monthly Mean Fractional Bias and Mean Fractional Gross Error

Figure 4.2-15   Time Series for Ammonium at the Canyonlands National Park IMPROVE Site (CANY1) and CASTNET Site (CAN407)
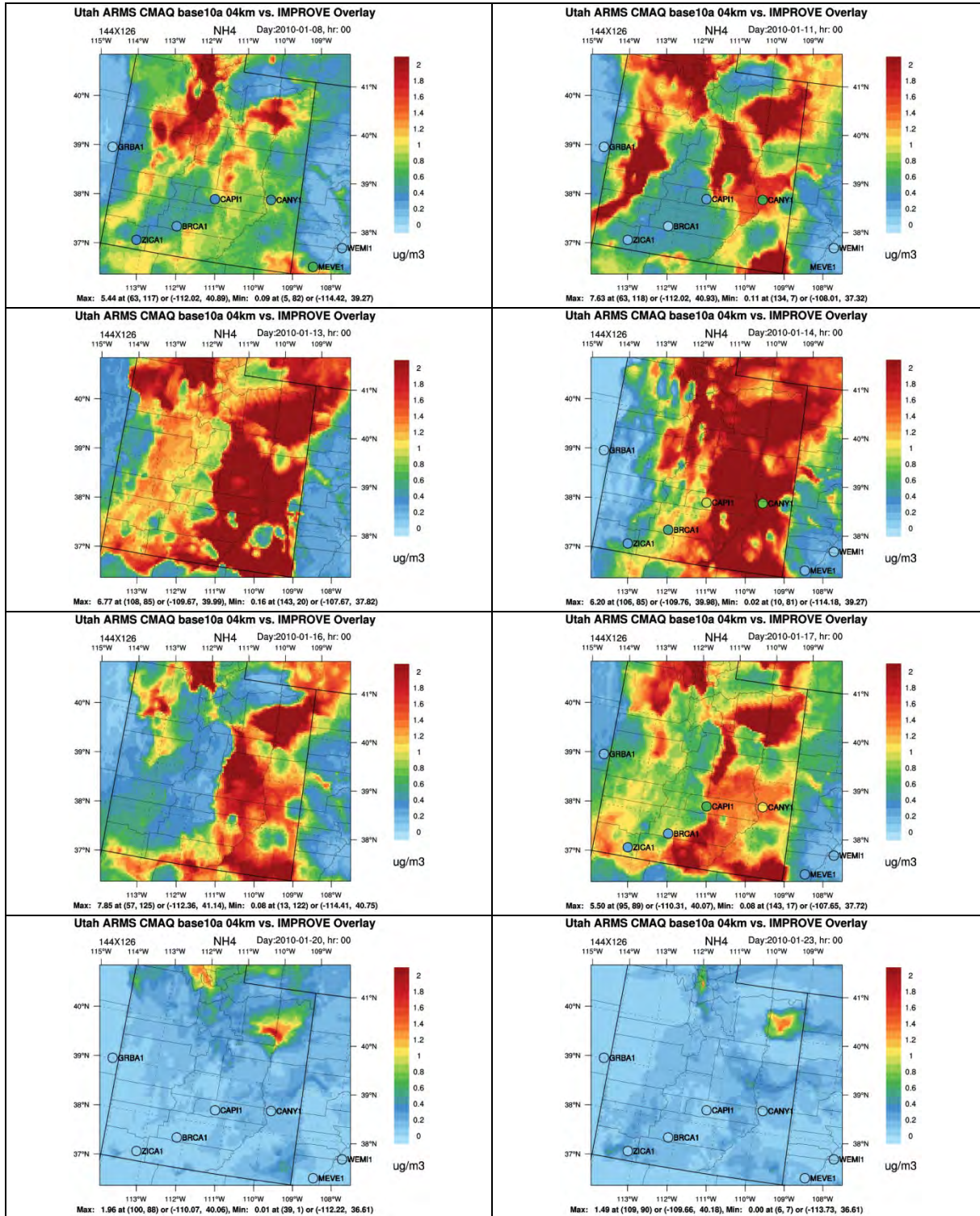
Figure 4.2-16   4-km Spatial Plots for Ammonium during January 8 to January 23, 2010
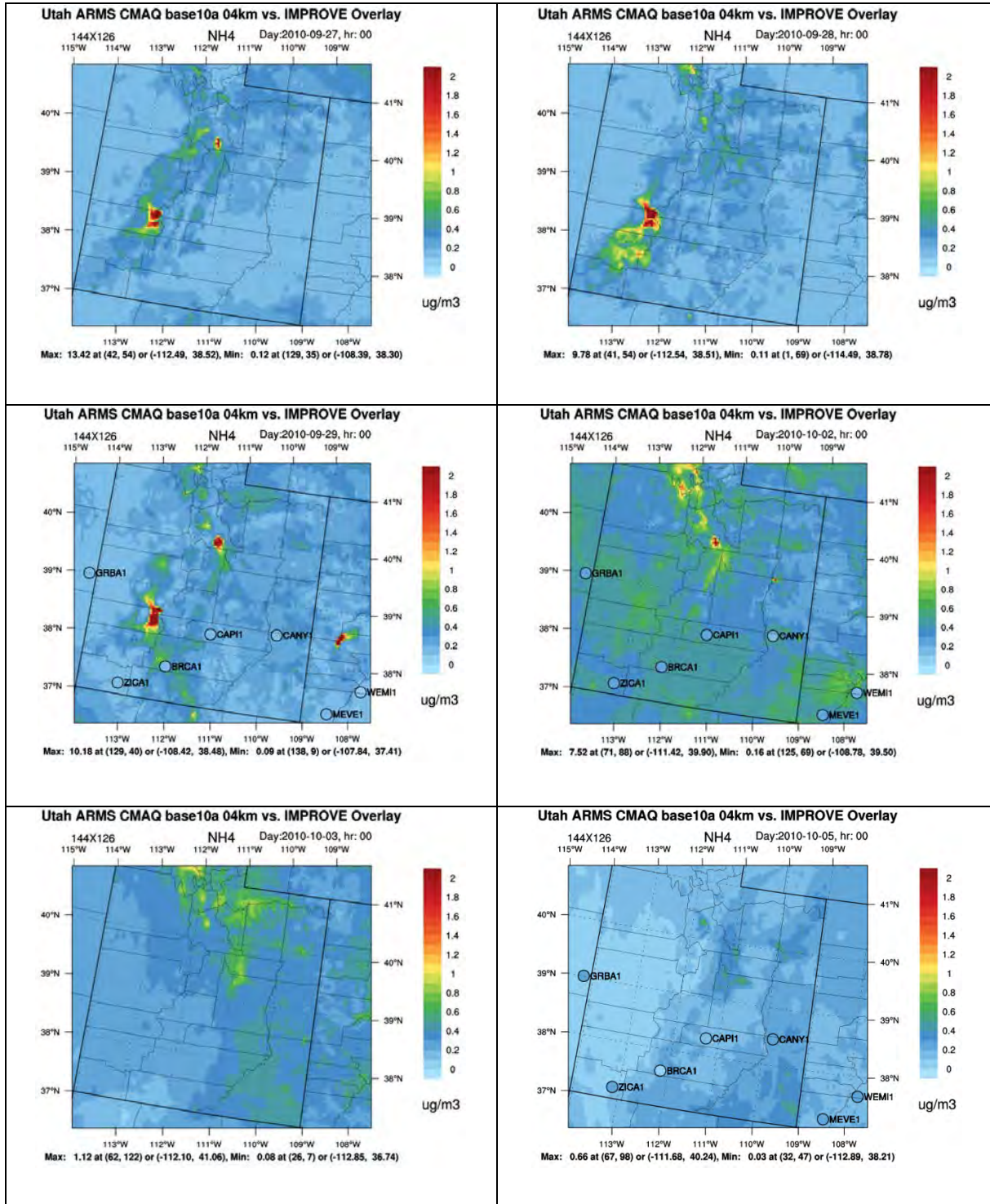
Figure 4.2-17   4-km Spatial Plots for Ammonium during September 27 to October 5, 2010

4.2.1.4 Organic Carbon

Statistical Analyses for the CMAQ 36-km, 12-km, and 4-km Domains

Annual and seasonal OC statistical summaries are presented in **Table 4.2-5**for each monitoring network and modeling domain. Note that the number of monitors with valid data used to calculate the statistical summaries is provided in **Table 3-2**. A more detailed assessment of the MFB is presented for each month in **Figure 4.2-18**. The monthly MFB and MFGE are presented in **Figure 4.2-19** with the USEPA-recommended goals and performance criteria (USEPA 2007).

In general, the model tends to under-predict OC concentrations relative to the measurements at IMPROVE sites in all three domains. The 12- and 4-km domains OC performance relative to the STN network is notably different than for the IMPROVE network. The model under-predicts the STN concentrations in the 36-km domain like the IMPROVE network but tends to over-predict concentrations in the 12- and 4-km domains. Largest biases and errors for IMPROVE tend to occur in the summer for all domains and are smallest in the winter and spring. For STN, the smallest biases and errors tend to occur in the summer for the 12- and 4-km domains and in the spring in the 36-km domain.

Notably, there are substantial differences in the monthly performance relative to the STN network between the 36-km domain and the 12- and 4-km domains (**Error! Reference source not found.**), while the overall monthly trends for the IMPROVE network are similar between all model domains. This may be important to consider in the context of the monitoring network objectives and siting criteria: the IMPROVE network is designed for assessing visibility impairment at remote areas of scenic interest, while the STN network is designed for assessing human exposure in urban areas. The fact that the model performance relative to IMPROVE monitors is relatively consistent independent of model domain indicates that the model is performing similarly in rural and remote areas. On the other hand, the fact that the model performance in the 36-km domain tends to have a larger bias relative to the STN network may indicate that urban sources of OC emissions (e.g., mobile sources) are not as well characterized as they are in the 12-km and 4-km domains. In addition as shown in **Table 3-2**, there are considerably less STN monitoring sites than IMPROVE monitoring sites in the 12- and 4-km domains making it difficult to draw conclusions of the overall model performance in either 12- or 4-km domains relative to the STN network.

Despite the systematic under-predictions, the MFB and MFGE for OC is within the USEPA recommended goals (2007) for almost all months and domains, and is always within the USEPA criteria as shown in **Figure 4.2-19**.

Time Series Analyses

Time series plots of the OC concentrations for the full year, January 8 to January 23, 2010, and September 27 to October 5, 2010 are shown in **Figure 4.2-20** for the Canyonlands NP IMPROVE site. Like with the previous PM species, the time series plots display the daily average model-predicted OC concentrations for the CMAQ and CAMx grid cells that also contain the IMPROVE monitor. In general, the observed OC concentrations have larger peaks in late summer and early fall coincident with wild fire activity and smaller peaks throughout the year. The CMAQ and CAMx modeled OC concentrations tend to under-predict the OC concentration throughout the year. During POI 1, the modeled OC concentrations are slightly elevated during monitored peak concentrations, but the magnitude is under-predicted. On September 29, the models predict an OC maximum that correspond with observed peak, however, the models under-predict the magnitude of that peak.

CMAQ Spatial Analyses

The OC spatial performance was reviewed for POI 1 (January 8 to January 23, 2010) and POI 4 (September 27 to October 5, 2010). The daily average 4-km OC concentrations are shown in **Figures 4.2-21** and **22** for the two POIs. When available, monitored 24-hour average OC concentrations from

the IMPROVE networks are shown in the figure as circles. In general for the first POI (**Figure 4.2-21**), the model-predicted OC concentrations are similar to the observed OC throughout the time period. For the second POI (**Figure 4.2-22**), the model tends to over-predict OC concentrations compared to observations. This over-prediction is likely due to model transport of the Coffee Pot and Twitchell Canyon wildfires emissions. The model processing and tendency to over-predict the wildfires emissions intensity and transport has been identified in spatial plots of other PM species. By the end of POI 4 (October 5), without the presence of the wildfires, the model-predicted OC concentrations are consistent with the observed OC.

Summary of Model Performance for Organic Carbon

In general, the model performs adequately for particulate OC, with notable differences between rural and urban areas.

- The model consistently under-predicts OC concentrations relative to the IMPROVE network for all domains with the largest biases and errors occurring in the summer for all domains and the smallest biases and errors occurring in the spring.
- For the STN network, the model OC concentrations are over-predicted in the 12- and 4-km domains with the smallest biases and errors in the summer, while the concentrations are systematically under-predicted in the 36-km domain.
- The monthly MFB and MFGE are within the USEPA-recommended performance criteria for all networks and model domains
- The largest discrepancies between observations and model spatial gradients of OC are observed during the POI when wildfires occur. In the absence of wildfires, the model spatial gradients are similar to the observed OC concentrations from the IMPROVE network.

Comparison of CMAQ and CAMx Results

The complete set of the CAMx MPE tables, bar charts, and spatial plots is found in **Appendix B**. Both models consistently under-predict OC concentrations in all domains at IMPROVE sites, with larger biases in CMAQ than in CAMx. For CMAQ, biases at the IMPROVE sites are larger in the summer, whereas in CAMx, biases at IMPROVE sites show a less prominent seasonal trend. For the 12- and 4-km domains, biases at the STN sites are larger in CAMx than in CMAQ throughout the year. CAMx tends to over-predict OC concentrations throughout the year at the STN sites in the 12-km and 4-km domains. OC predictions are within USEPA performance criteria for all domains and all networks for both models, except for the STN network in the CAMx 4-km domain during the fall and winter.

Table 4.2-5   Model Performance Statistical Summary for Organic Carbon

Monitoring Network	Statistic (%)/ Concentration (µg/m³)	36-km Domain					12-km Domain					4-km Domain				
		Annual	Winter	Spring	Summer	Fall	Annual	Winter	Spring	Summer	Fall	Annual	Winter	Spring	Summer	Fall
IMPROVE (Daily)	MFB	-49	-29	-39	-75	-51	-70	-56	-59	-99	-68	-67	-63	-44	-89	-71
	MFGE	72	67	64	87	70	84	82	70	102	83	75	75	56	90	79
	MNB	1	50	-2	-34	-3	-20	27	-29	-57	-16	-38	-35	-25	-58	-34
	MNGE	82	115	70	71	78	81	115	59	69	83	57	55	47	59	66
	NMB	-39	-32	-26	-52	-40	-58	-52	-54	-67	-57	-59	-48	-42	-64	-68
	NME	59	56	61	61	56	66	67	62	69	67	62	57	47	64	69
	R^2	0.120	0.239	0.069	0.211	0.146	0.052	0.156	0.010	0.200	0.055	0.038	0.082	0.171	0.064	0.033
	Observed Mean Concentration (µg/m³)	1.26	1.02	1.09	1.57	1.34	0.80	0.70	0.62	1.00	0.90	0.59	0.42	0.36	0.72	0.85
	Predicted Mean Concentration (µg/m³)	0.77	0.70	0.81	0.75	0.81	0.33	0.34	0.28	0.32	0.39	0.24	0.22	0.21	0.26	0.28
STN (Daily)	MFB	-55	-62	-51	-54	-56	4	4	17	-8	3	30	35	32	8	40
	MFGE	70	74	64	72	69	38	48	37	29	37	36	43	39	18	41
	MNB	-31	-36	-30	-28	-33	19	28	34	-1	16	44	54	49	10	56
	MNGE	54	53	50	59	53	45	60	51	29	43	49	60	55	19	57
	NMB	-40	-46	-34	-37	-40	6	4	24	-4	5	33	30	43	8	49
	NME	55	56	50	56	56	42	49	45	29	43	43	45	52	19	52
	R^2	0.135	0.121	0.259	0.067	0.070	0.226	0.102	0.234	0.339	0.085	0.621	0.517	0.342	0.513	0.536
	Observed Mean Concentration (µg/m³)	2.24	3.03	1.78	1.86	2.34	2.23	3.29	1.56	1.88	2.29	1.90	3.13	1.21	1.49	1.74
	Predicted Mean Concentration (µg/m³)	1.34	1.64	1.18	1.18	1.40	2.36	3.42	1.93	1.81	2.41	2.53	4.06	1.74	1.62	2.61

36-km OC

12-km OC
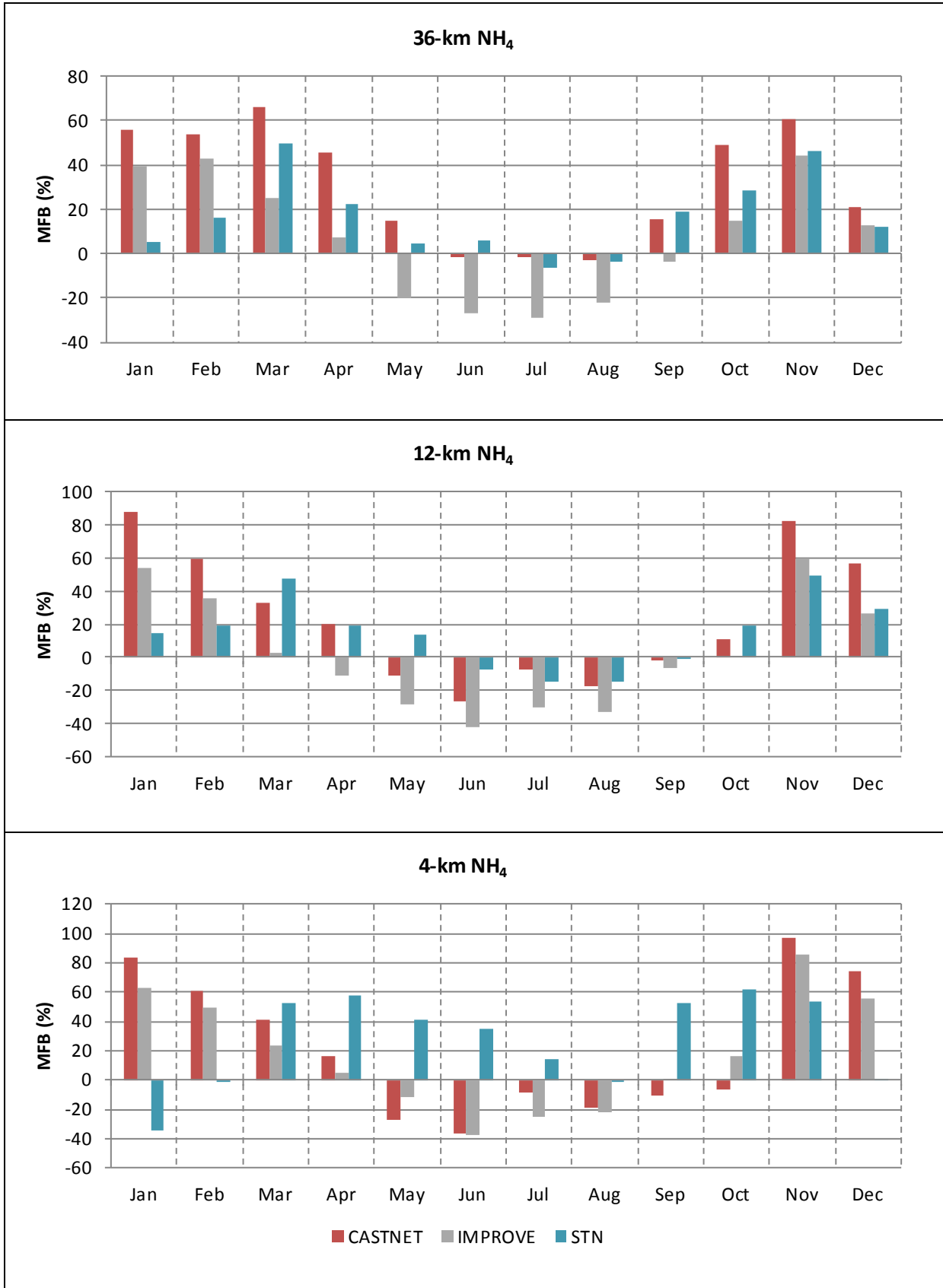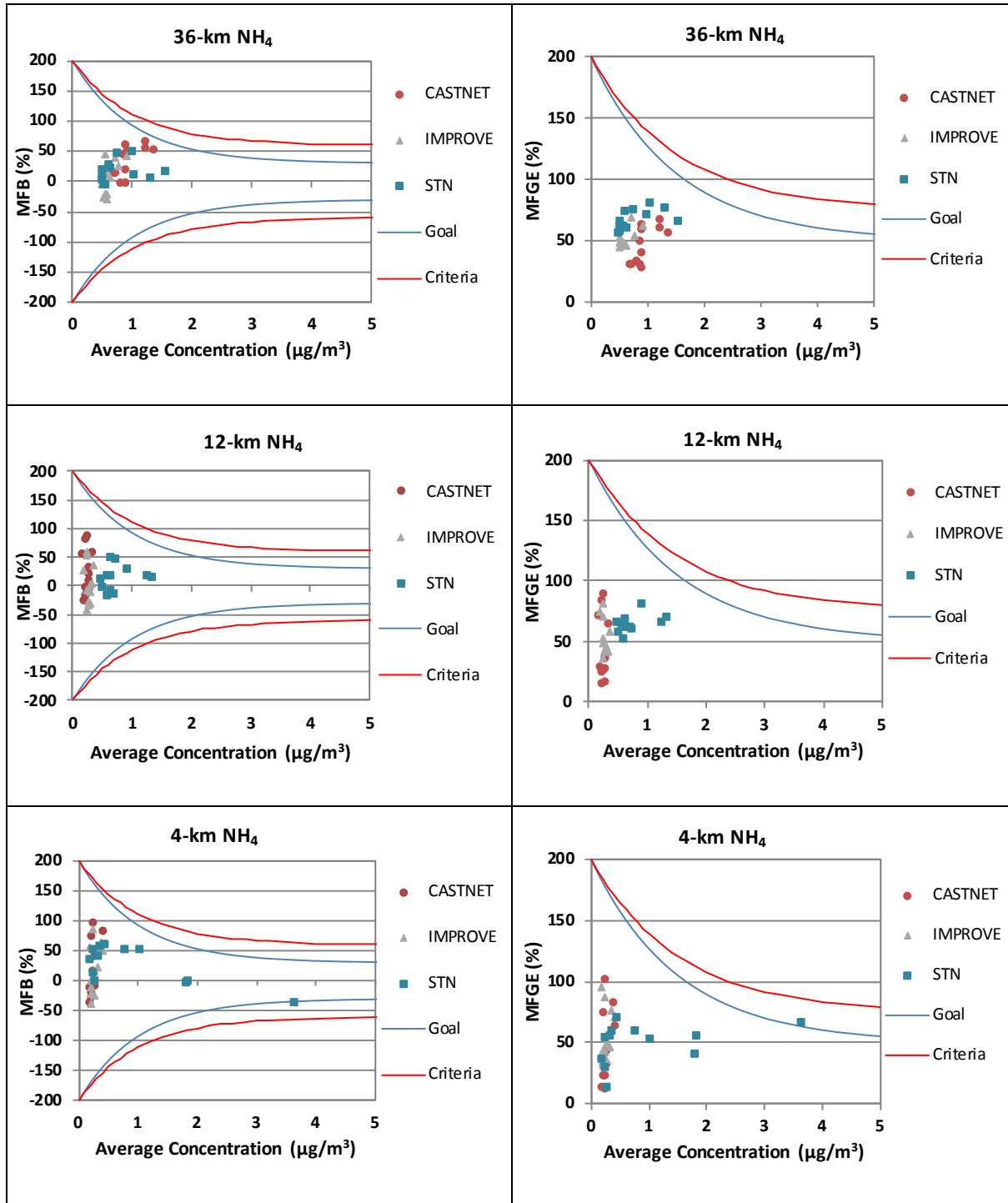
4-km OC

■ IMPROVE ■ STN
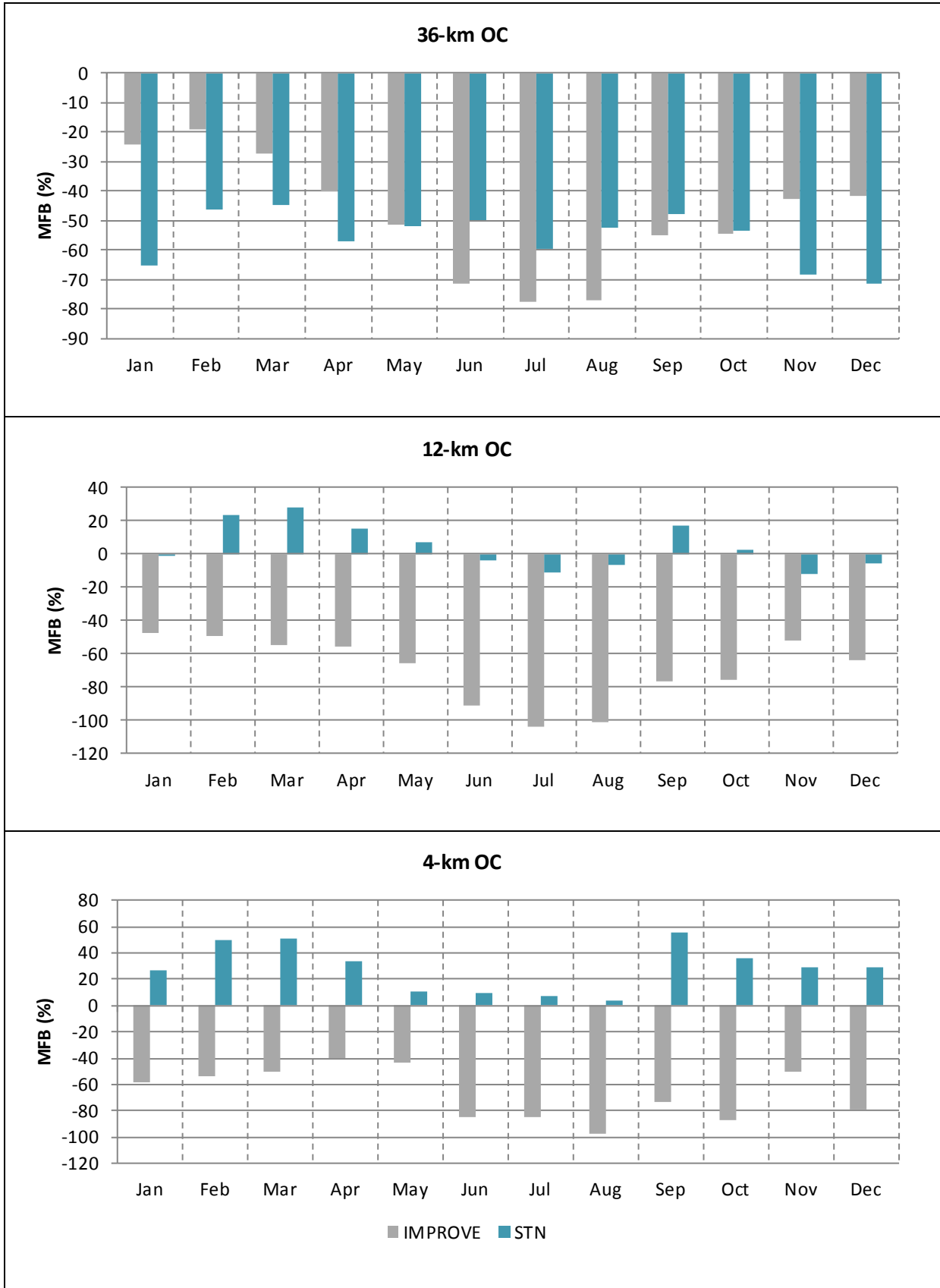
Figure 4.2-18   Monthly Mean Fractional Bias for Organic Carbon
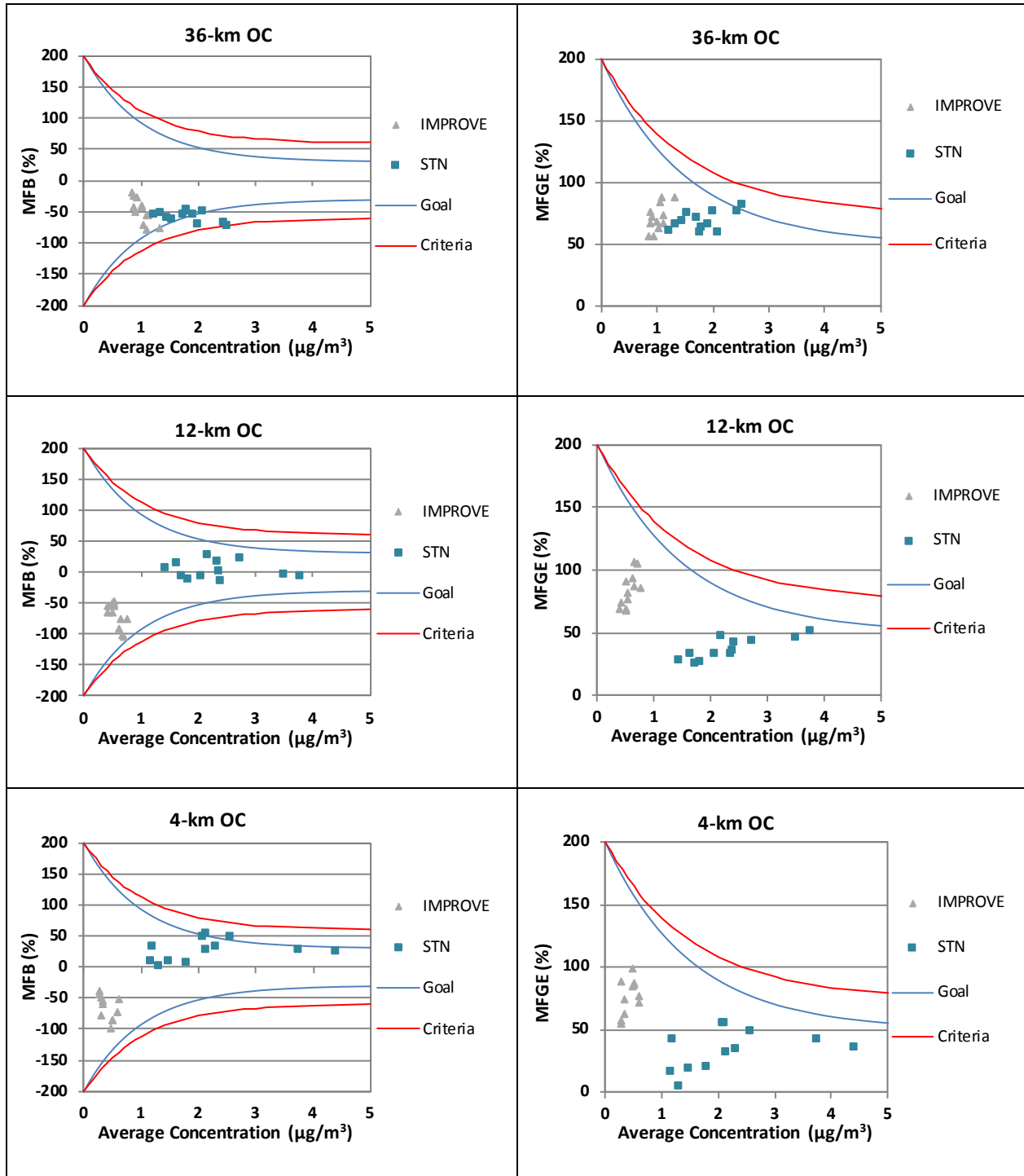
Note: Goals and criteria based on Boylan and Russell (2006) and accepted by USEPA (2007).

Figure 4.2-19   Bugle Plots of Organic Carbon Monthly Mean Fractional Bias and Mean Fractional Gross Error
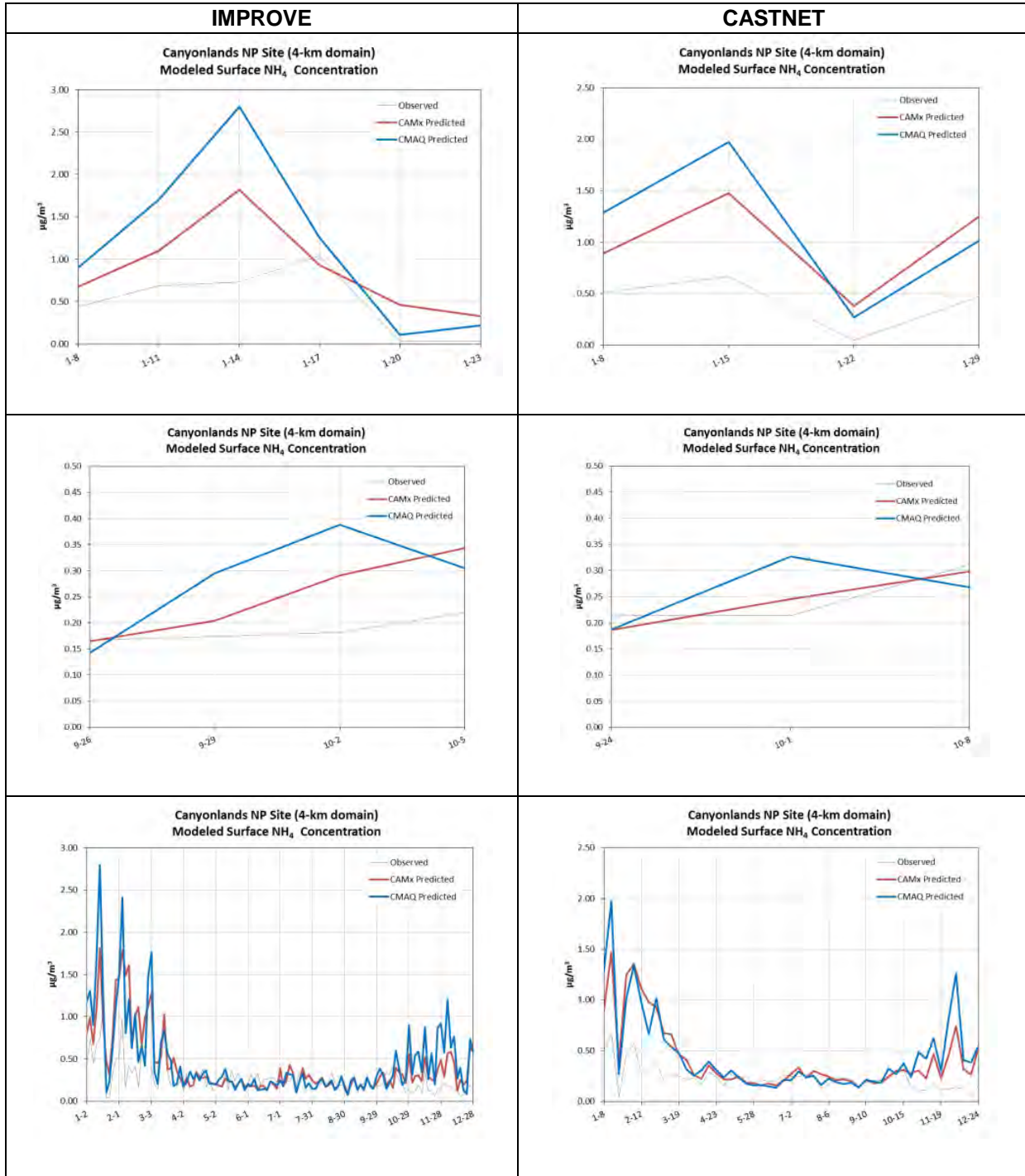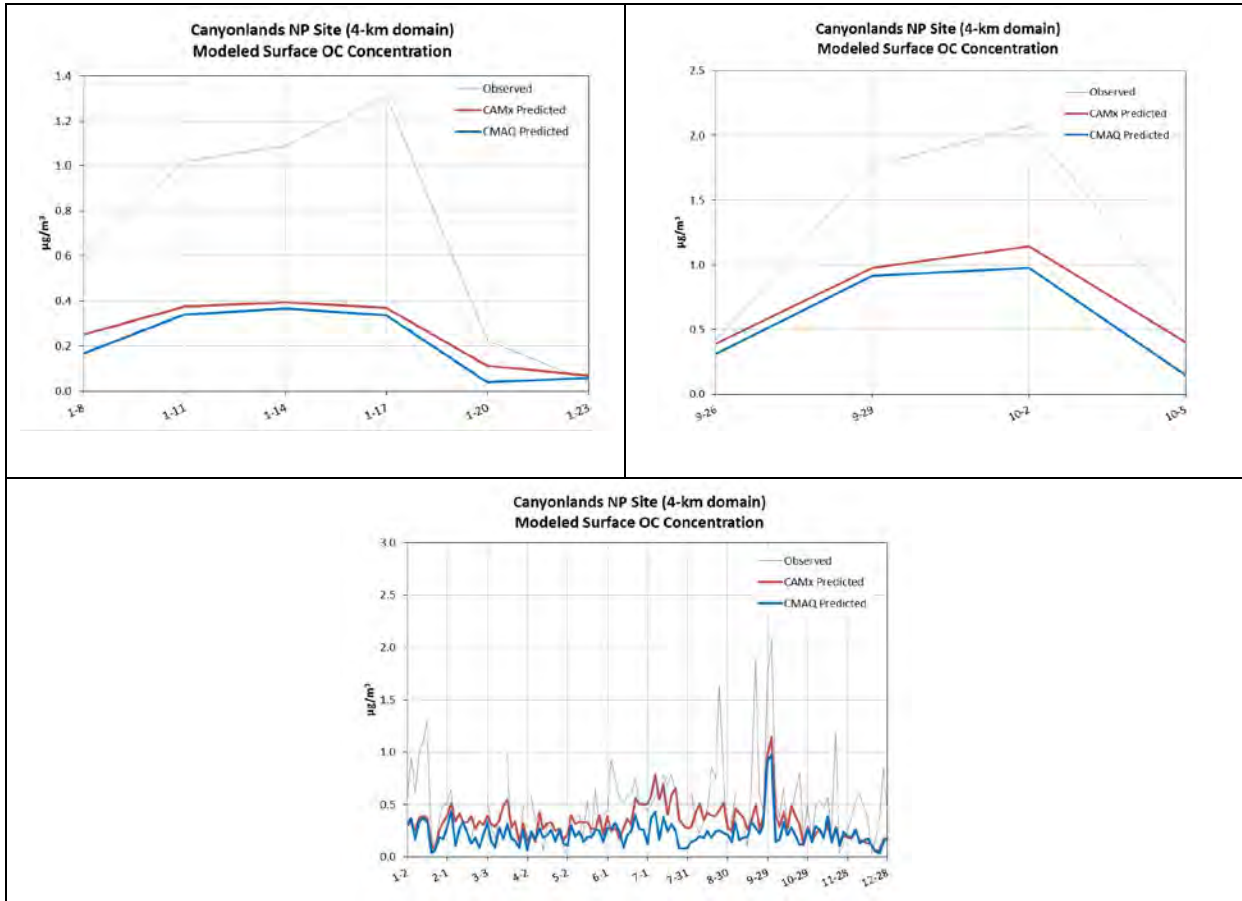
Figure 4.2-20   Time Series for Organic Carbon at the Canyonlands National Park IMPROVE Site (CANY1)
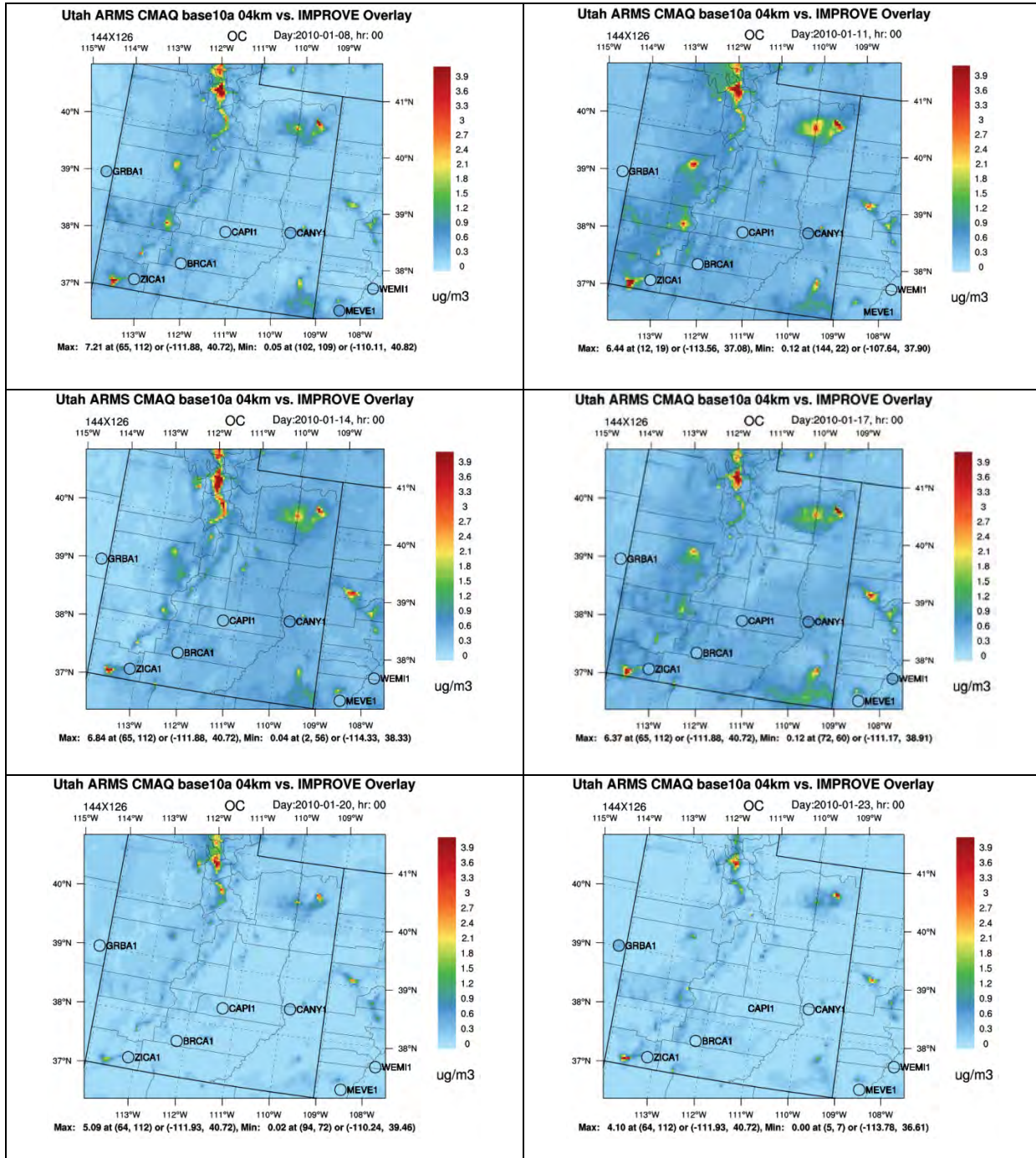
Figure 4.2-21   4-km Spatial Plots for Organic Carbon during January 8 to January 23, 2010

Figure 4.2-22   4-km Spatial Plots for Organic Carbon during September 27 to October 5, 2010

4.2.1.5 Elemental Carbon

Statistical Analyses for the CMAQ 36-km, 12-km, and 4-km Domains

Annual and seasonal EC statistical summaries are presented in **Table 4.2-6** for each monitoring network and modeling domain. Note that the number of monitors with valid data used to calculate the statistical summaries is provided in **Table 3-2**. A more detailed assessment of the MFB is presented for each month in **Figure 4.2-23**. The monthly MFB and MFGE are presented in **Figure 4.2-24** with the USEPA-recommended goals and performance criteria (USEPA 2007).

In general, the model tends to under-predict EC concentrations relative to the IMPROVE network and over-predict relative to the STN network. For the IMPROVE network, the model does an adequate job of representing the EC concentrations as a majority of the time periods have low bias and error. The model has the largest under-predictions during summer characterized by a higher negative MFB. For the STN network, the model over-predicts in all domains with the smallest biases and errors in the fall. For all time periods, the model tends to have the best performance in the 36-km domain which degrades when refining the grid resolution to 12- and 4-km domains. In the 4-km domain, the model shows large positive MFB values relative to the STN network, which could be attributed to having only one STN monitoring station in the 4-km (**Table 3-2**).

As shown in **Figure 4.2-24**, the monthly MFB and MFGE for EC are within the USEPA-recommended performance criteria for all model domains and networks, except for four months relative to the STN network in the 4-km domain.

Time Series Analyses

Time series plots of the EC concentrations for the full year, January 8 to January 23, 2010, and September 27 to October 5, 2010 are shown in **Figure 4.2-24** for the Canyonlands NP IMPROVE site. Similar to previous time series, the plots display the daily average model-predicted EC concentrations for the CMAQ and CAMx grid cells that also contain the IMPROVE monitor. In general, the observed EC concentrations have larger peaks in late summer coincident with wild fires, as well as peaks in early winter, and smaller concentrations throughout the year. The CMAQ and CAMx modeled EC concentrations tend to under-predict the EC concentrations during episodic peaks; however, the rest of the year concentrations are similar to monitored values. Similar to OC, the models predict an EC peak during both POI1 and POI 4 which corresponds with the timing of the observed peak concentrations. However, the models under-predict the magnitude of monitored events.

CMAQ Spatial Analyses

The daily average 4-km EC concentrations are shown for POI 1 (January 8 to January 23, 2010 shown in **Figure 4.2-26**) and POI 4 (September 27 to October 5, 2010 shown in **Figure 4.2-17**). When available, monitored 24-hour average EC concentrations from the IMPROVE networks are shown in the figure as circles. In general the model-predicted spatial gradients of EC concentrations are similar to the observed EC spatial patterns throughout both POIs. For both POIs, the areas of larger EC concentrations are located in areas without monitoring sites making it difficult to assess the accuracy of the modeled spatial variability. During POI 4, an elevated region of EC concentrations is found in central Utah corresponding to the wildfires seen in other PM species spatial plots, both modeled and monitored EC are higher in this area.

Summary of Model Performance for Elemental Carbon

In general, the model tends to under-predict EC concentrations relative to the IMPROVE network and over-predict relative to the STN network.

- For IMPROVE, the model tends to under-predict EC concentrations independent of season in the 12-km and 4-km domains; however, in the 36-km domain EC concentrations are over-predicted in the winter and under-predicted in the summer.
- Relative to the STN network, the model tends to over-predict EC concentrations independent of domain and season.
- The monthly MFB and MFGE are within the USEPA-recommended performance goals for all networks and model domains except for four months relative to the STN network in the 4-km domain.
- During the POIs, the model-predicted EC concentrations peak with observations, but the magnitude is under-predicted.

Comparison of CMAQ and CAMx Results

The complete set of the CAMx MPE tables, bar charts, and spatial plots is found in **Appendix B**. Both models consistently over-predict EC concentrations in all domains relative to the STN network, with larger biases in CAMx than in CMAQ throughout the year. For the IMPROVE network, the models slightly under-predict the EC concentrations, but overall do an adequate job of representing the EC concentrations within the majority of the time periods. EC predictions fall within USEPA performance criteria for all networks in the 36-km and 12-km domains for both models. In the 4-km domain for STN network, predictions consistently fall outside the performance criteria in CAMx, and for some months in CMAQ.

Table 4.2-6   Model Performance Statistical Summary for Elemental Carbon

| Monitoring Network	Statistic (%)/ Concentration (µg/m³)	36-km Domain					12-km Domain					4-km Domain				
		Annual	Winter	Spring	Summer	Fall	Annual	Winter	Spring	Summer	Fall	Annual	Winter	Spring	Summer	Fall
IMPROVE (Daily)	MFB	5	29	12	-17	-4	-23	-11	-10	-46	-29	-15	-17	10	-34	-22
	MFGE	63	73	59	62	57	65	77	55	67	61	56	72	47	54	51
	MNB	93	162	85	54	55	22	57	41	-18	7	36	44	109	-11	-1
	MNGE	133	193	118	110	98	83	116	88	59	70	86	104	137	51	52
	NMB	29	42	51	10	11	-1	19	7	-18	-12	-25	-19	4	-36	-35
	NME	77	82	95	70	63	76	90	80	65	68	51	62	44	48	50
	R²	0.188	0.480	0.137	0.200	0.332	0.354	0.560	0.091	0.246	0.323	0.058	0.103	0.221	0.017	0.055
	Observed Mean Concentration (µg/m³)	0.19	0.20	0.18	0.18	0.21	0.11	0.13	0.09	0.11	0.13	0.07	0.07	0.04	0.08	0.09
	Predicted Mean Concentration (µg/m³)	0.24	0.28	0.27	0.20	0.23	0.11	0.16	0.10	0.09	0.12	0.05	0.05	0.05	0.05	0.06
STN (Daily)	MFB	18	16	26	25	3	75	69	88	85	58	112	115	118	114	102
	MFGE	70	79	68	70	65	80	78	89	86	68	112	115	118	114	102
	MNB	88	104	95	103	52	173	175	211	186	122	298	319	347	291	231
	MNGE	125	146	124	135	94	177	182	212	187	130	298	319	347	291	231
	NMB	35	26	65	68	12	118	110	168	157	81	252	255	299	273	207
	NME	88	85	100	106	74	126	119	170	158	93	252	255	299	273	207
	R²	0.118	0.105	0.124	0.099	0.066	0.424	0.299	0.311	0.444	0.409	0.615	0.330	0.403	0.408	0.702
	Observed Mean Concentration (µg/m³)	0.46	0.68	0.31	0.29	0.57	0.57	0.92	0.36	0.36	0.67	0.50	0.85	0.31	0.29	0.53
	Predicted Mean Concentration (µg/m³)	0.62	0.86	0.51	0.49	0.64	1.25	1.94	0.97	0.93	1.22	1.76	3.03	1.23	1.08	1.63
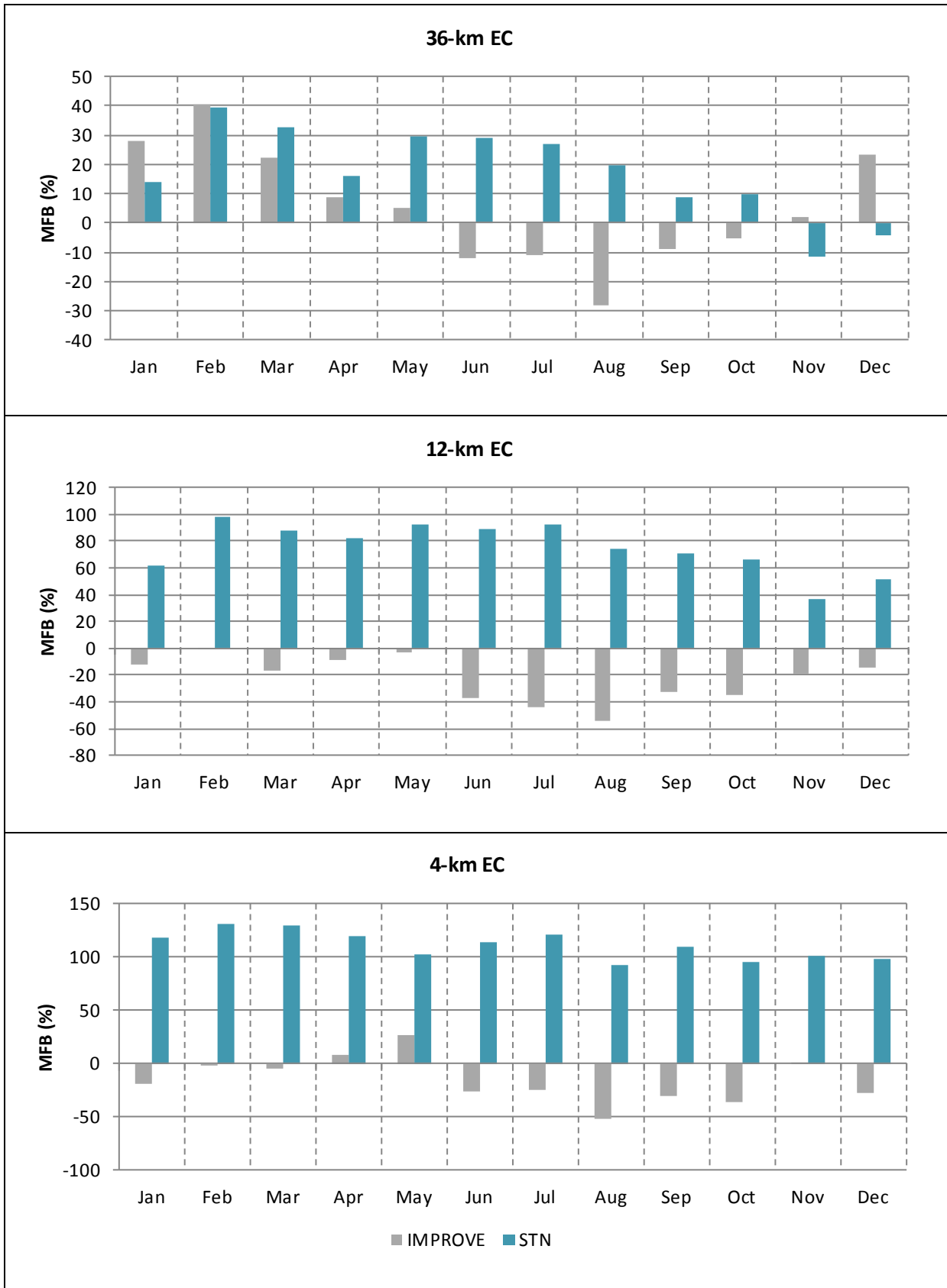
Figure 4.2-23 Monthly Mean Fractional Bias for Elemental Carbon
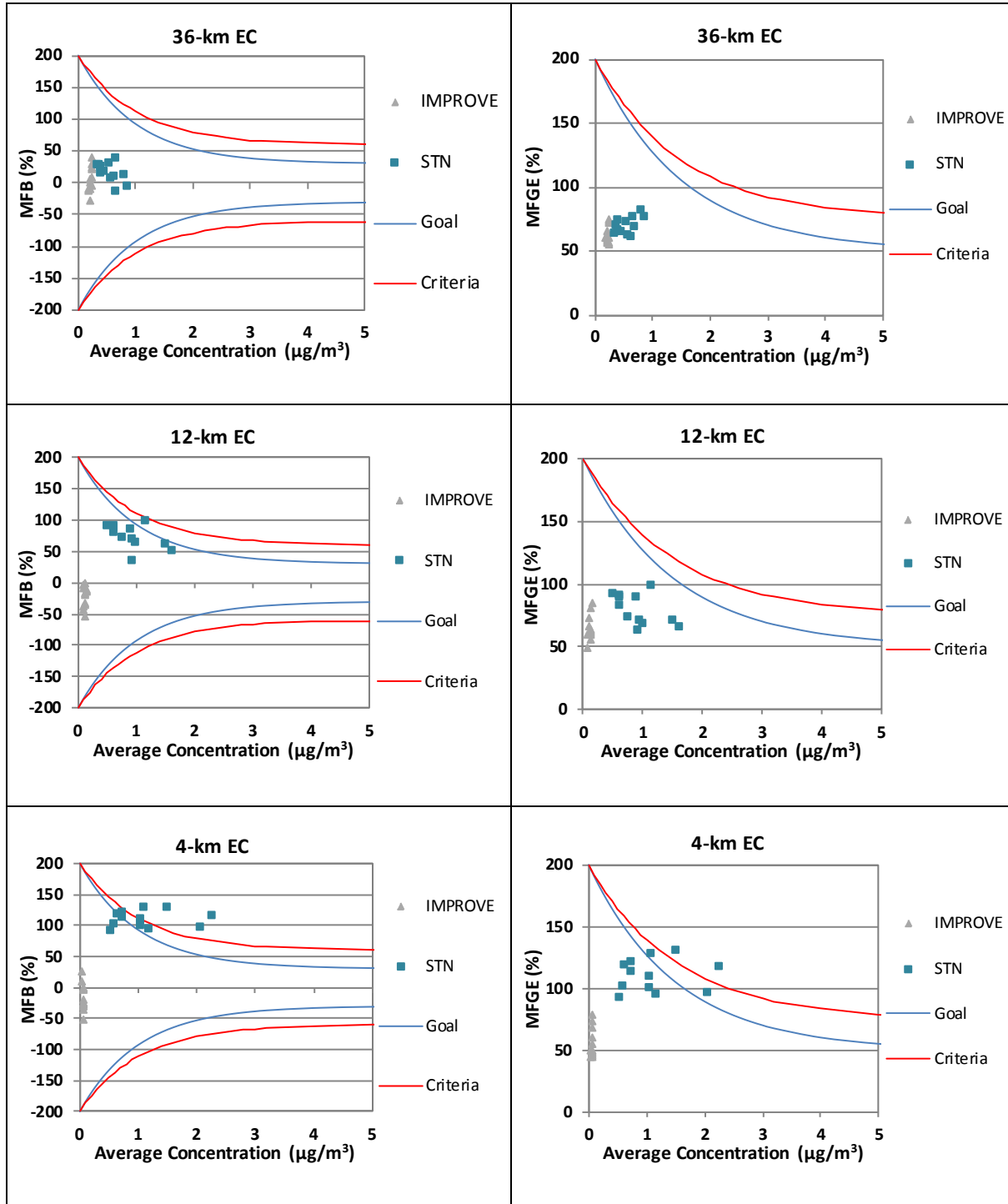
Note: Goals and criteria based on Boylan and Russell (2006) and accepted by USEPA (2007).

Figure 4.2-24   Bugle Plots of Elemental Carbon Monthly Mean Fractional Bias and Mean Fractional Gross Error
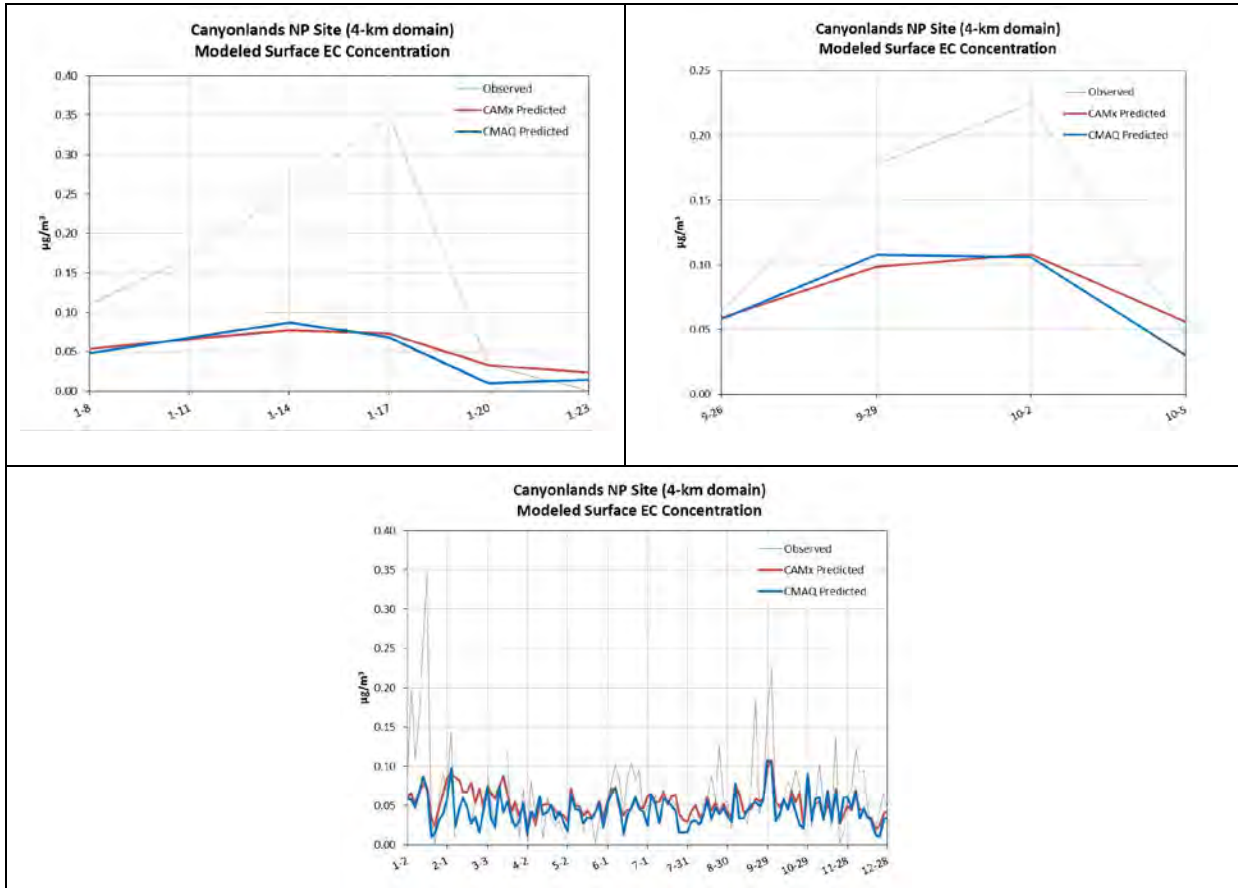
**Figure 4.2-25   Time Series for Elemental Carbon at the Canyonlands National Park IMPROVE Site (CANY1)**
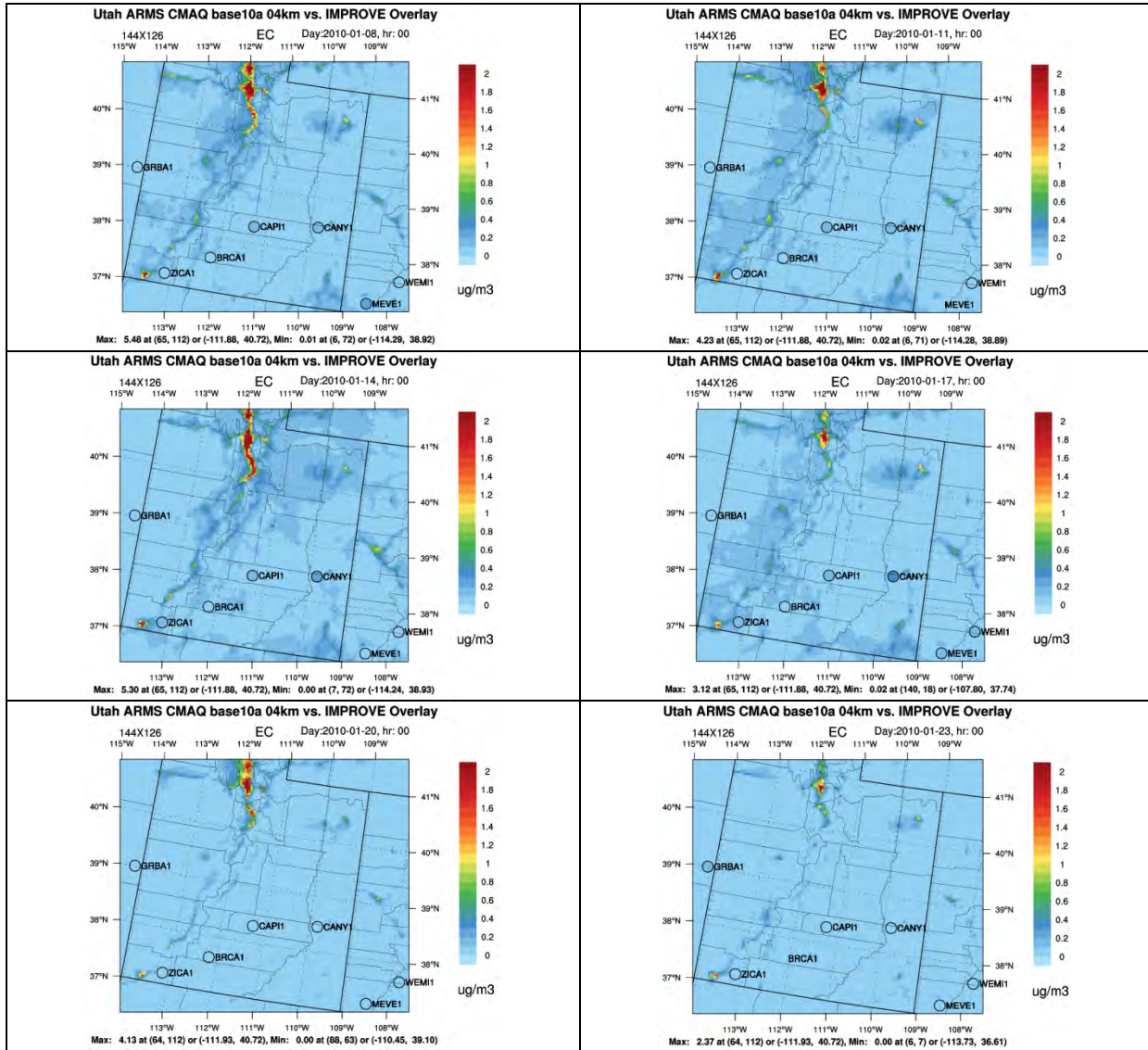
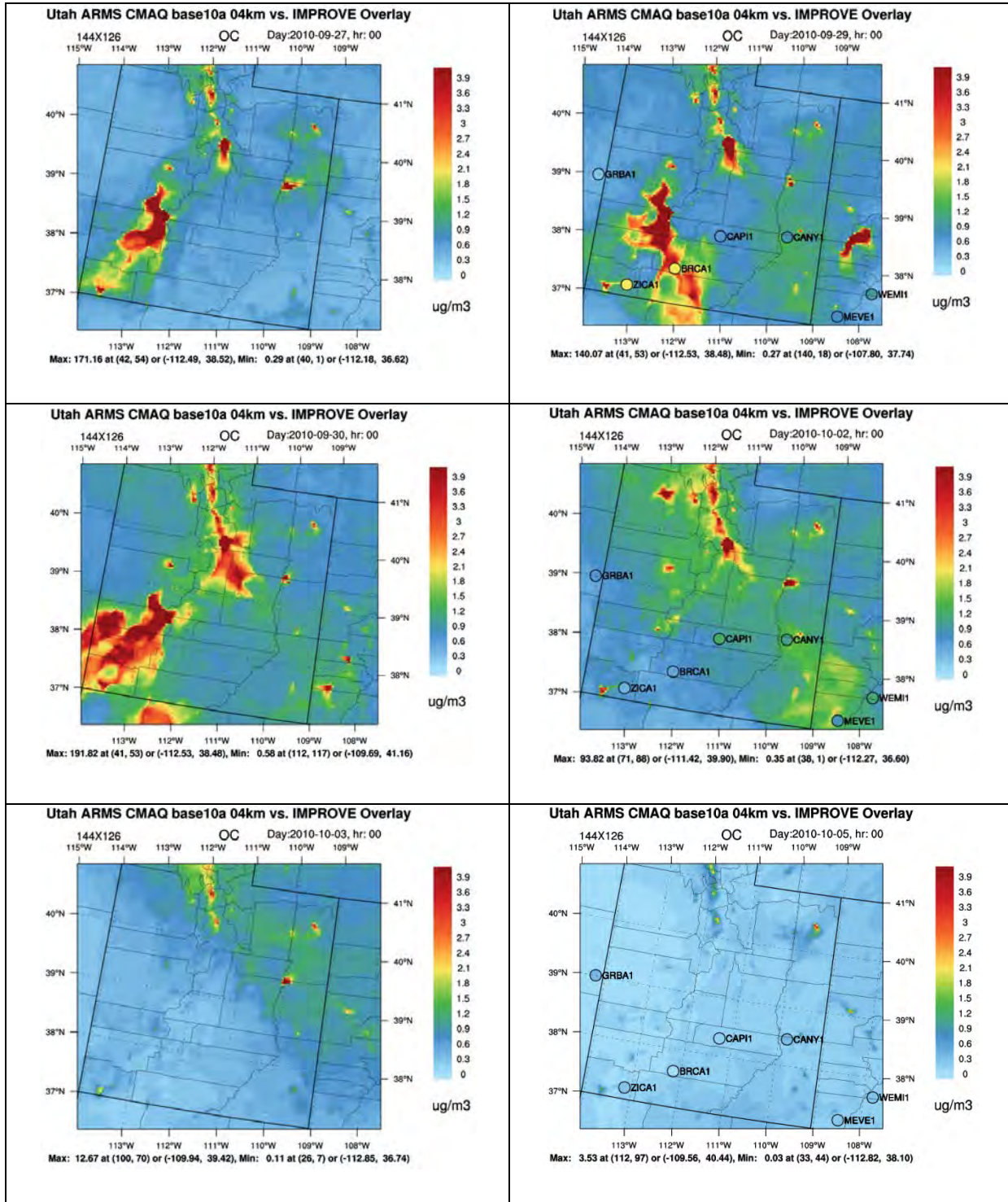**Figure 4.2-26   4-km Spatial Plots for Elemental Carbon during January 8 to January 23, 2010**
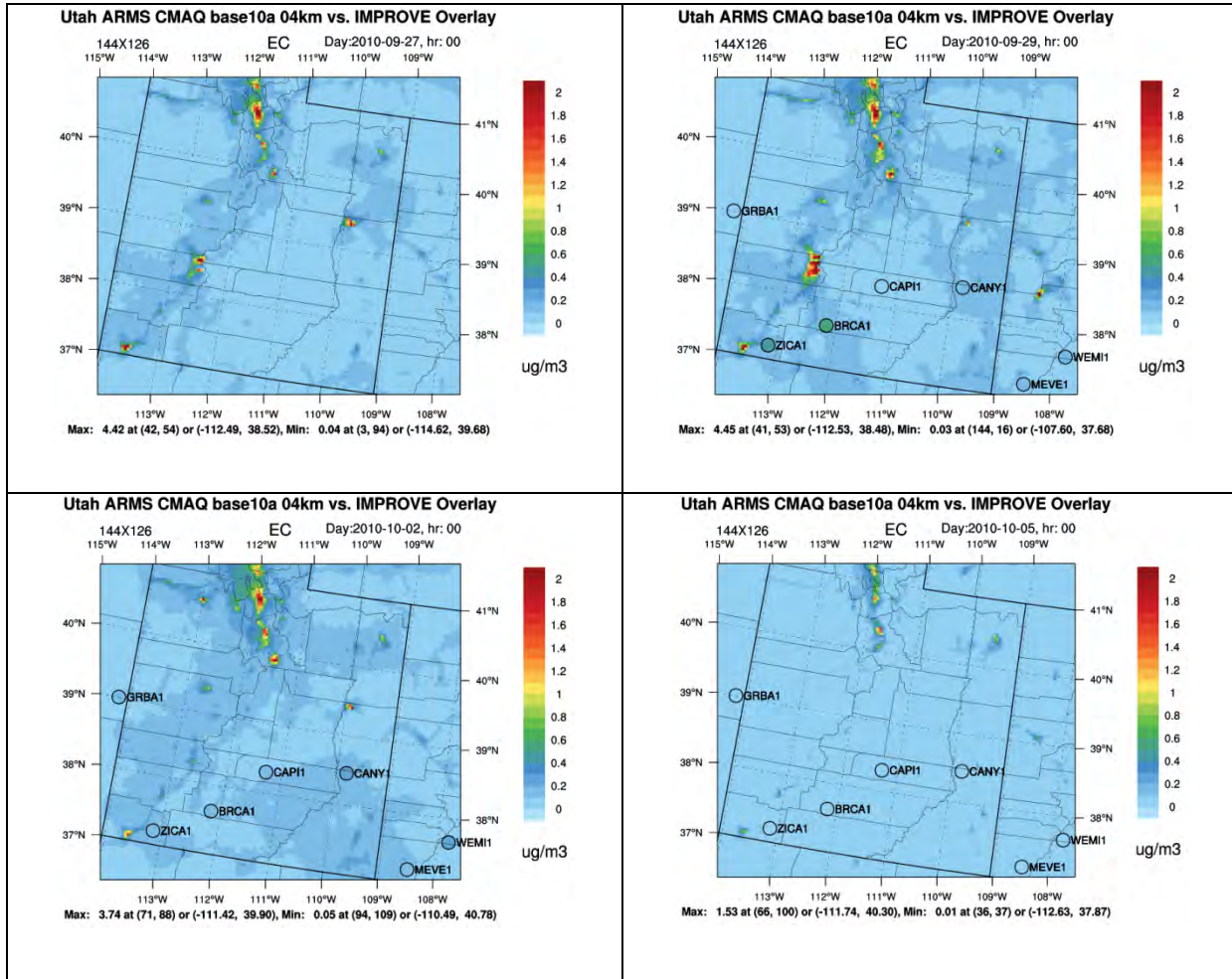
Figure 4.2-27   4-km Spatial Plots for Elemental Carbon during September 27 to October 5, 2010

4.2.1.6 Fine Soil

Statistical Analyses for the CMAQ 36-km, 12-km, and 4-km Domains

Annual and seasonal SOIL statistical summaries are presented in **Table 4.2-7** for each monitoring network and modeling domain. Note that the number of monitors with valid data used to calculate the statistical summaries is provided in **Table 3-2**. A more detailed assessment of the MFB is presented for each month in **Figure 4.2-28**. The monthly MFB and MFGE are presented in **Figure 4.2-29** with the USEPA-recommended goals and performance criteria (USEPA 2007).

In general, the model tends to over-predict SOIL concentrations in the winter for all networks and modeling domains (**Table 4.2-7**). For the STN network, the model generally over-predicts for all domains and all seasons with the smallest biases and errors in the summer and the largest biases and errors in the winter. However for the IMPROVE network, the model shows negative biases in the summer months with positive biases in the winter for the 12- and 4-km domain. The smallest biases and errors occur during spring and fall for the IMPROVE network. The model predictions of SOIL concentrations are notably different for the two networks in the summer for the 12- and 4-km domain. Since IMPROVE stations are typically located in rural environments, it can be inferred that the model under-predicts SOIL concentrations at rural locations in the summer. Due to the fact there is a single STN station in the 4-km domain, the model performance relative to the STN network is not applicable to the entire 4-km domain.

As shown in **Figure 4.2-29**, the monthly MFB and MFGE for SOIL are within the USEPA-recommended performance criteria for the IMPROVE network for each domain. For the STN network, the monthly MFB and MFGE generally are within the performance criteria for the 36-km domain, except for a few months. However, the monthly MFB and MFGE for STN in the 12- and 4-km are not within the USEPA-recommended performance criteria for a majority of the year, generally when the concentrations are higher. The model MFB and MFGE exceedance of the USEPA performance criteria relative to the STN network indicates that the model is over-predicting the maximum values in urban areas and the model is not reproducing the timing of peak concentrations in urban areas.

Time Series Analyses

Time series plots of the SOIL concentrations for the full year, January 8 to January 23, 2010, and September 27 to October 5, 2010 are shown in **Figure 4.2-30** for the Canyonlands NP IMPROVE site. Similar to previous time series, the plots display the daily average model-predicted SOIL concentrations for the CMAQ and CAMx grid cells that also contain the IMPROVE monitor. Due to their relationship, the time series of CM is also displayed in **Figure 4.2-30** for comparison to the SOIL concentrations. According the observations, there are several episodes of elevated SOIL and CM concentrations in the spring. During the spring, but particularly in April and May, a series of spring frontal systems affected the Southwestern US. These fronts increased the possibility of windblown dust events and affected large areas of the southwest region (USGS 2013). These windblow dust events would result in higher SOIL and CM concentrations, which are seen in the observations. However, the models do not reproduce any of the magnitude of these events in either SOIL or CM concentration patterns. For the rest of the year, the model SOIL concentrations generally correspond to the observed concentrations.

CMAQ Spatial Analyses

The SOIL spatial performance was reviewed for POI 1 (January 8 to January 23, 2010 shown in **Figure 4.2-31**) and POI 4 (September 27 to October 5, 2010 shown in **Figure 4.2-32**). When available, monitored 24-hour average SOIL concentrations are shown as circles. If the POIs have elevated concentrations of SOIL due to windblown dust events, the spatial patterns for CM are expected to be similar to SOIL; therefore, these two species are plotted together. In general, the model is in reasonable agreement with monitored concentrations during the POI 1. Throughout the POI, elevated

concentrations of SOIL are evident in isolated regions without monitors. Since these events do not appear to spreading or transporting the SOIL concentrations to other areas, it is likely they are the result of local emissions couples with accumulation during stagnate weather conditions. Due to the limited number of monitor sites in the modeling domain, it is difficult to verify the spatial patterns of the elevated concentrations. POI 4 (**Figure 4.2-32**) is very different than POI 1 due to the presence of wildfires. In general, the model is over-predicting the SOIL concentrations relative to the monitor sites. On September 29th, the fire plume is evident in the spatial plots and concentrations exceed monitored values. By the end of the POI, the model predicted SOIL concentrations are consistent with observations.

Summary of Model Performance for Fine Soil

In general, the model over-predicts SOIL concentrations in most locations, particularly during the winter.

- Generally for the STN network, the model over-predicted SOIL concentrations in all domains with the smallest biases and errors occurring in the summer and the largest biases and errors in the winter
- Relative to the IMPROVE network, the model tends to under-predict SOIL in the summer and over-predict it in the winter for the 12- and 4-km domains.
- The model performance for SOIL for monthly MFB and MFGE are within the USEPA-recommended performance goals for IMPROVE and typically exceed the USEPA-recommended performance criteria relative to the STN network.
- POI 1 tends to reproduce observed spatial patterns for SOIL in the vicinity of monitor sites; however, the domain-wide analysis of spatial coverage is limited due to the number of monitor sites available. In POI 4, with the presence of fire, the model over-predicts the wildfire SOIL concentrations impacts relative to observations.

Comparison of CMAQ and CAMx Results

The complete set of the CAMx MPE tables, bar charts, and spatial plots is found in **Appendix B**. For both networks, SOIL biases are generally smaller in CMAQ than in CAMx throughout the year. Seasonal bias trends are similar in both models. For both models, SOIL predictions consistently fall outside USEPA performance criteria in all domains relative to STN and fall within performance criteria for all domains relative to IMPROVE.

Table 4.2-7   Model Performance Statistical Summary for Fine Soil

| Monitoring Network	Statistic (%)/ Concentration ($\mu g/m^3$)	36-km Domain					12-km Domain					4-km Domain				
		Annual	Winter	Spring	Summer	Fall	Annual	Winter	Spring	Summer	Fall	Annual	Winter	Spring	Summer	Fall
IMPROVE (Daily)	MFB	46	102	30	-2	57	-19	40	-33	-74	-9	-28	35	-51	-88	-9
	MFGE	89	116	73	78	89	73	77	63	84	67	73	72	70	89	61
	MNB	317	656	168	172	292	51	156	-1	9	41	20	144	-26	-57	27
	MNGE	347	666	199	225	314	113	181	65	112	93	87	169	55	59	77
	NMB	50	272	27	-13	74	-37	91	-48	-62	-24	-58	43	-69	-70	-21
	NME	124	312	100	84	132	72	133	65	69	70	72	88	75	70	57
	R^2	0.014	0.040	0.005	0.029	0.048	0.035	0.440	0.027	0.023	0.023	0.087	0.121	0.051	0.091	0.076
	Observed Mean Concentration ($\mu g/m^3$)	0.71	0.32	1.01	0.92	0.58	0.83	0.24	1.40	0.97	0.64	0.91	0.17	1.97	1.00	0.45
	Predicted Mean Concentration ($\mu g/m^3$)	1.07	1.17	1.27	0.80	1.02	0.52	0.46	0.73	0.37	0.49	0.38	0.25	0.60	0.30	0.35
STN (Daily)	MFB	77	118	76	39	77	104	142	101	74	100	101	148	79	41	122
	MFGE	97	125	91	78	95	111	143	107	88	106	111	148	99	64	123
	MNB	1245	718	3592	166	326	494	909	390	229	481	400	764	216	98	460
	MNGE	1259	723	3604	193	339	499	909	394	239	486	407	764	229	115	461
	NMB	123	382	108	35	105	204	516	160	107	167	138	541	17	22	292
	NME	172	398	151	100	160	231	520	200	138	192	196	541	123	66	295
	R^2	0.006	0.027	0.016	0.040	0.003	0.001	0.137	0.000	0.000	0.043	0.001	0.257	0.009	0.104	0.169
	Observed Mean Concentration ($\mu g/m^3$)	0.95	0.56	1.02	1.16	1.03	0.94	0.64	1.00	1.02	1.06	1.11	0.60	1.75	1.42	0.71
	Predicted Mean Concentration ($\mu g/m^3$)	2.12	2.70	2.11	1.57	2.13	2.85	3.92	2.61	2.11	2.82	2.64	3.82	2.06	1.73	2.78
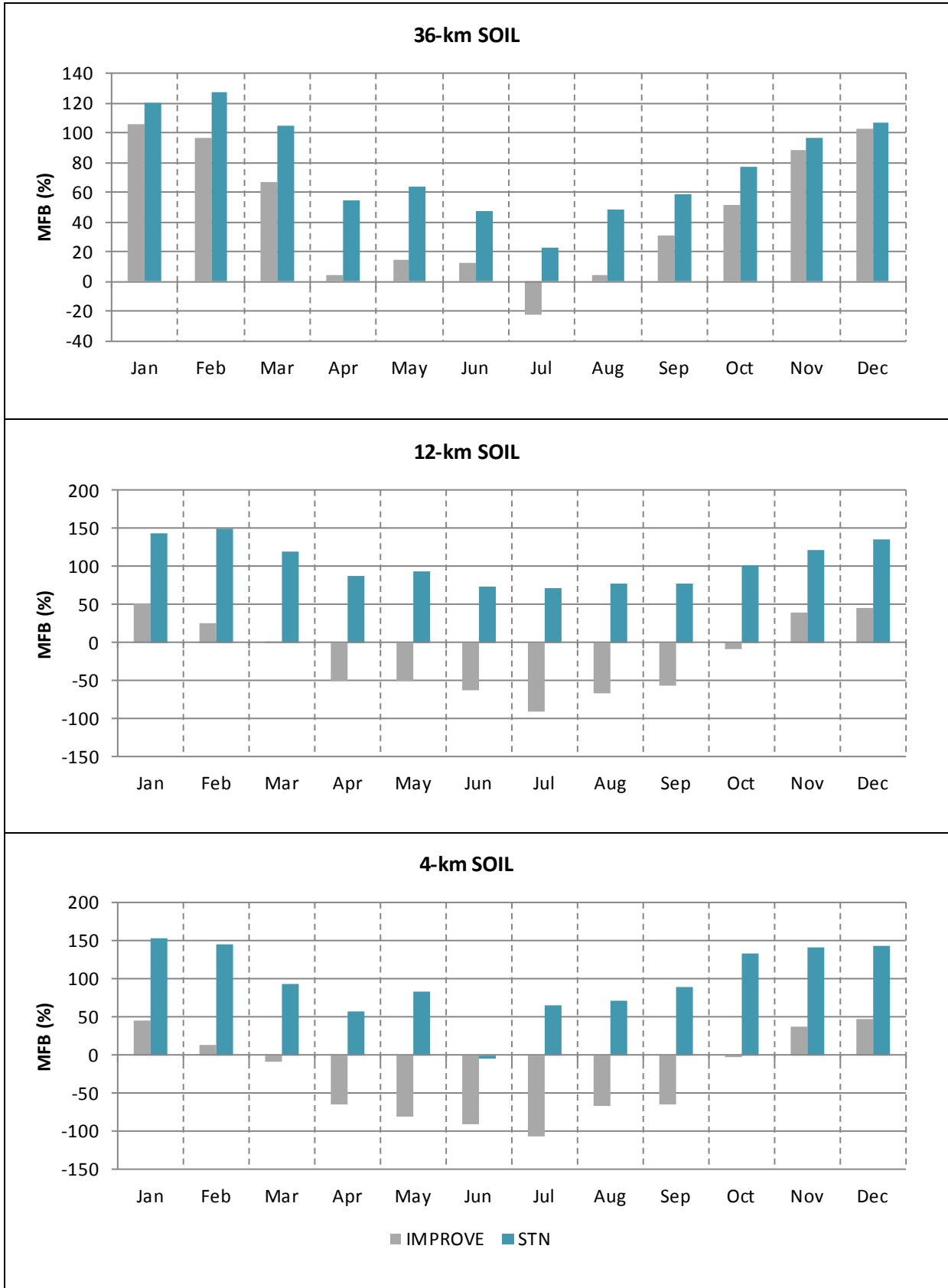
Figure 4.2-28   Monthly Mean Fractional Bias for Fine Soil
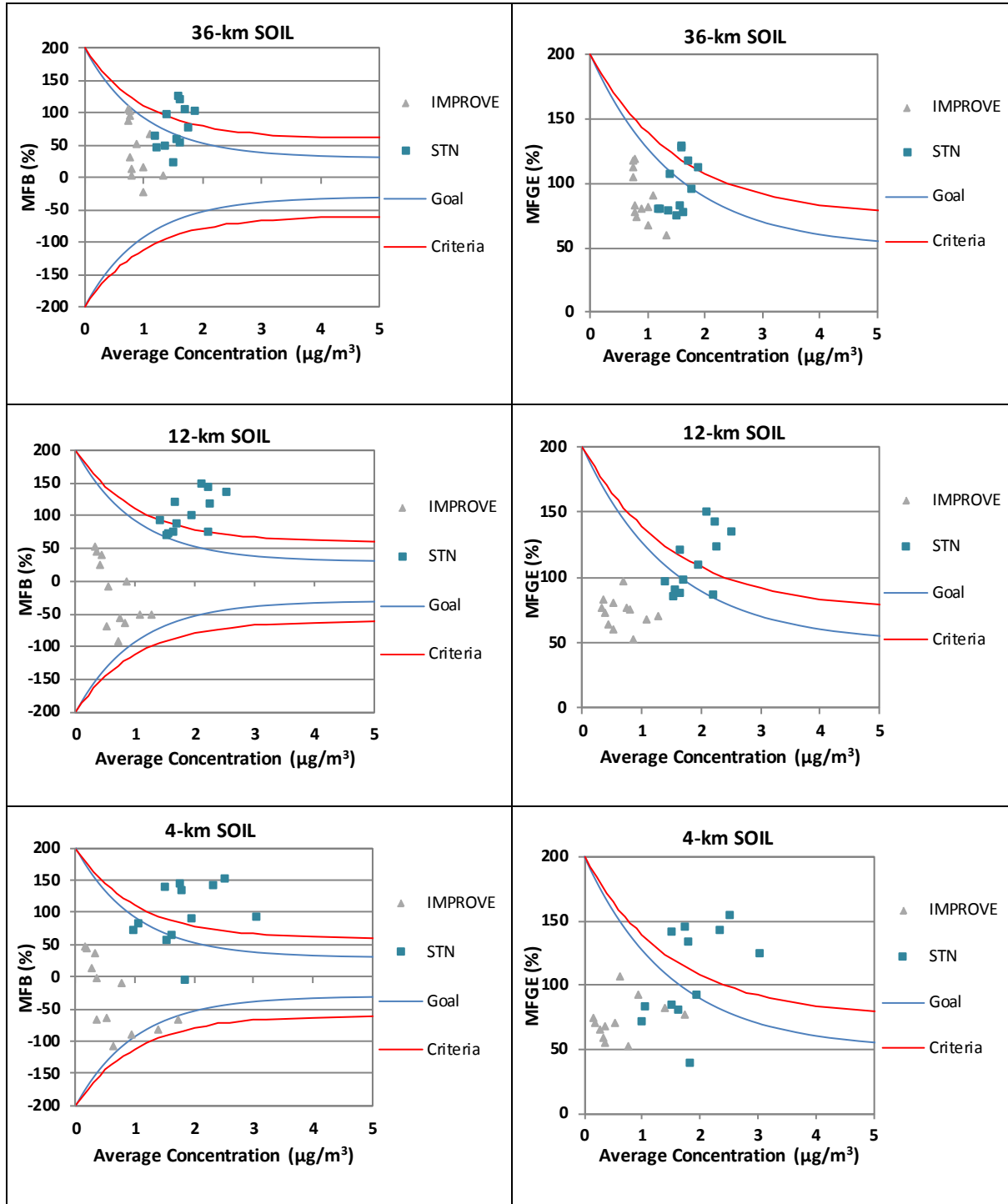
Note: Goals and criteria based on Boylan and Russell (2006) and accepted by USEPA (2007).

Figure 4.2-29   Bugle Plots of Fine Soil Monthly Mean Fractional Bias and Mean Fractional Gross Error
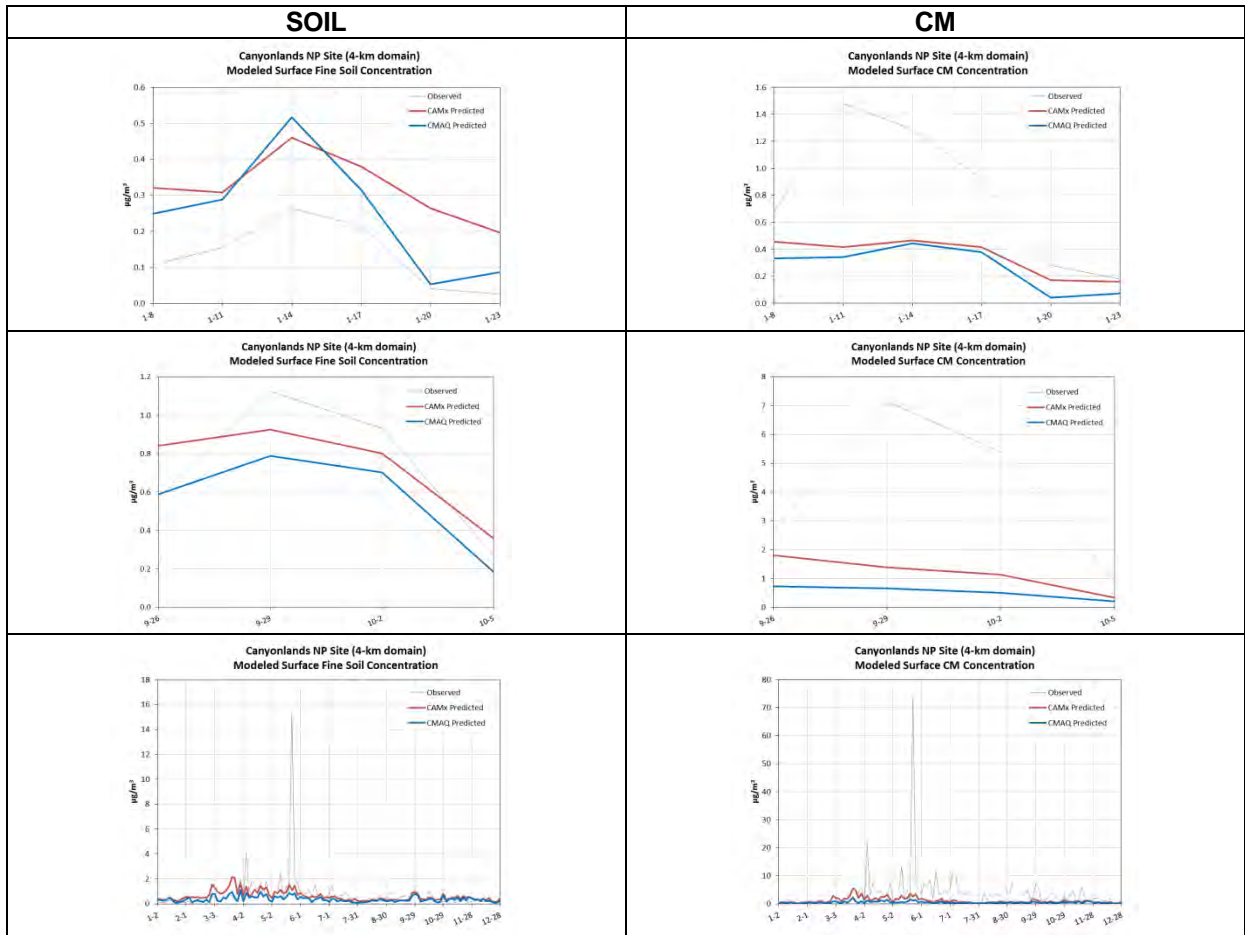
**Figure 4.2-30   Time Series for Fine Soil and Coarse Mass at the Canyonlands National Park IMPROVE Site (CANY1)**

SOIL	CM

Utah ARMS CMAQ base10a 04km vs. IMPROVE Overlay
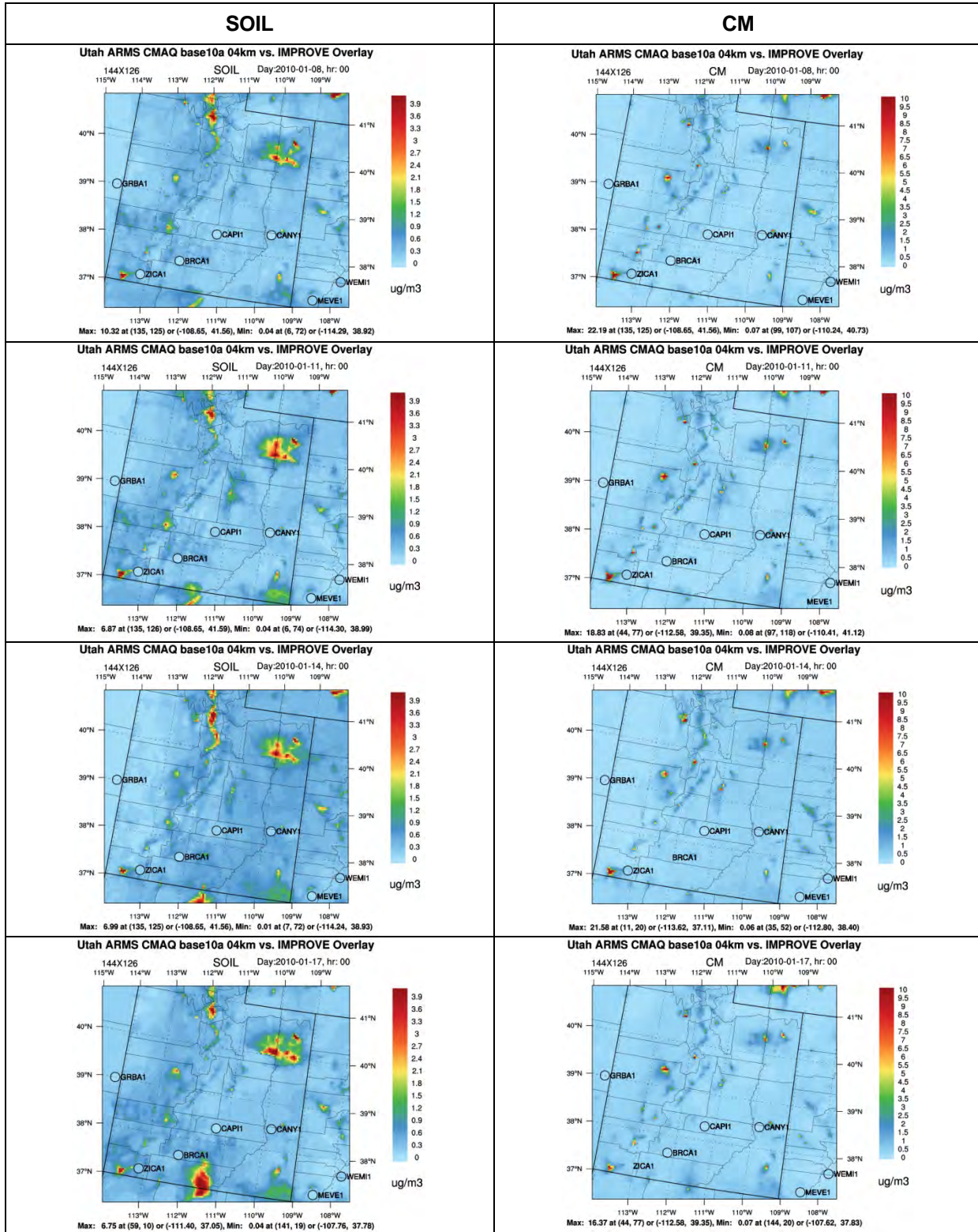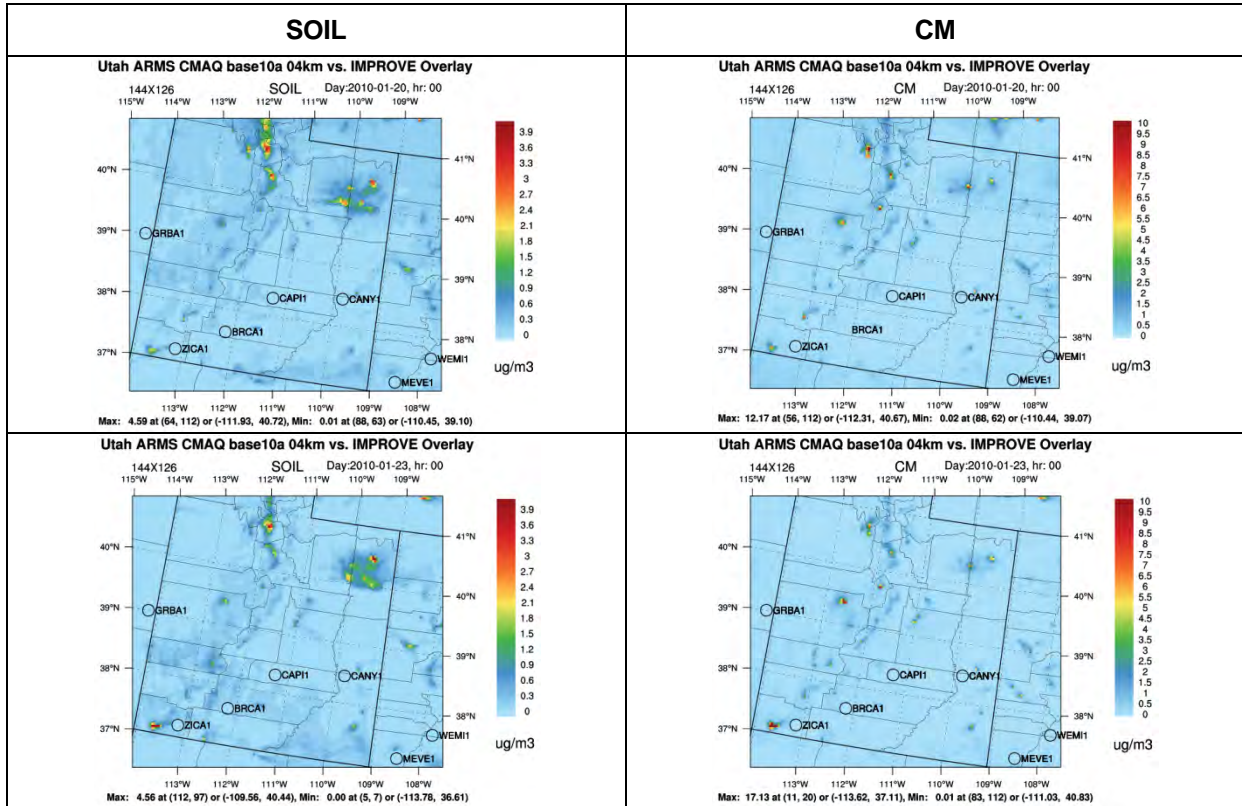
Figure 4.2-31   4-km Spatial Plots for Fine Soil and Coarse Mass during January 8 to January 23, 2010
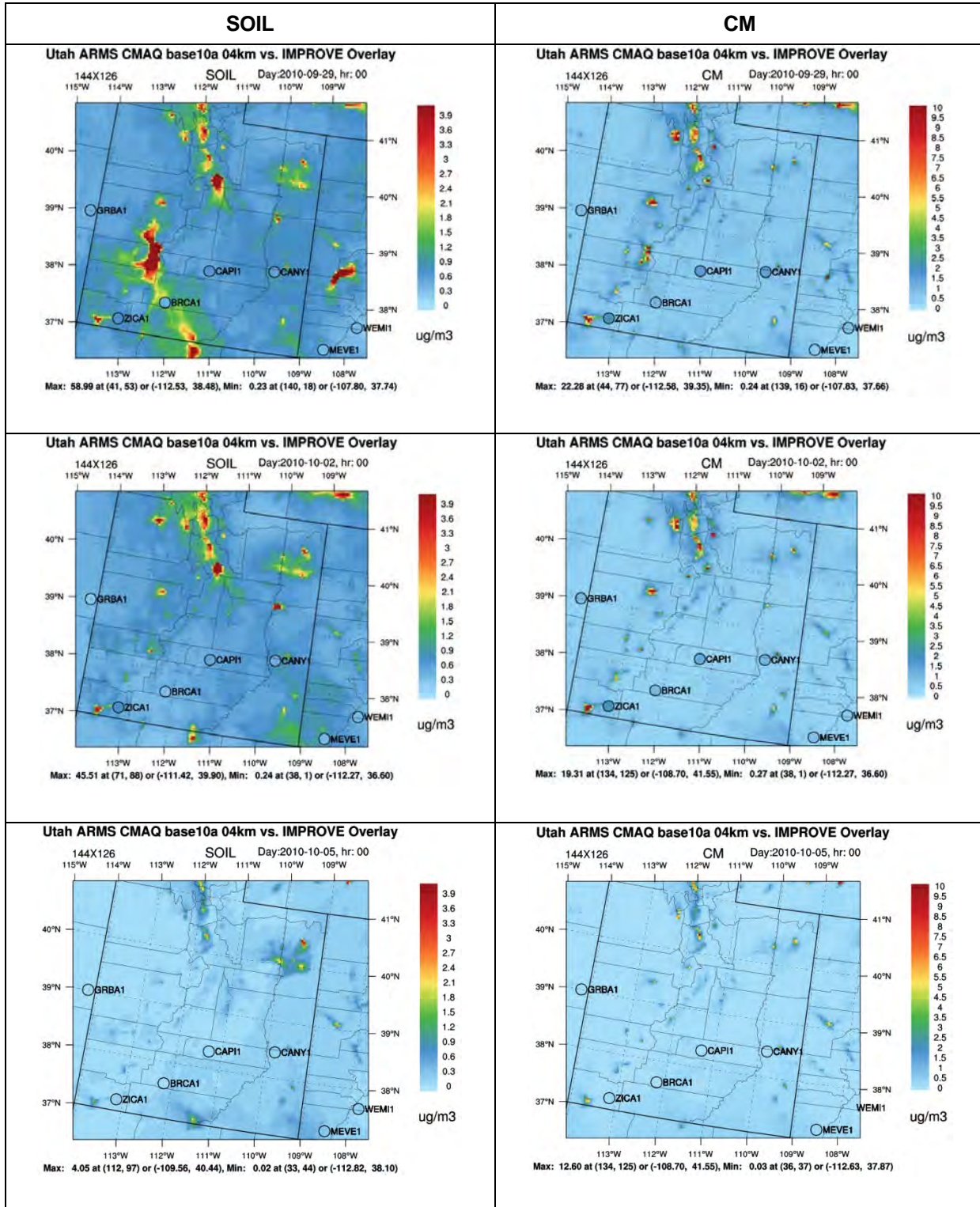
Figure 4.2-32   4-km Spatial Plots for Fine Soil and Coarse Mass during September 27 to October 5, 2010

4.2.1.7 Coarse Mass

Statistical Analyses for the CMAQ 36-km, 12-km, and 4-km Domains

Annual and seasonal CM statistical summaries are presented in **Table 4.2-8** relative to the IMPROVE network for each modeling domain. Note that the number of monitors with valid data used to calculate the statistical summaries is provided in **Table 3-2**. A more detailed assessment of the MFB is presented for each month in **Figure 4.2-33**. The monthly MFB and MFGE are presented in **Figure 4.2-34** with the USEPA-recommended goals and performance criteria (USEPA 2007).

In general, the model systematically under-predicts CM concentrations in all three modeling domains. The model is more similar to observations (has a smaller MFB) during winter than during the rest of the year. The model's tendency to under-predict CM during winter is likely is due to an under-prediction of the portion of PM that is in the larger size range (as supported by the over-prediction of file soil in winter relative to all networks and all model domains). However, during other times of the year, the under-prediction of CM corresponding with under-predictions of fine SOIL is likely attributable to an under-estimate of dust emissions.

As shown in **Figure 4.2-34**, the monthly MFB and MFGE for CM exceed the USEPA-recommended performance criteria for periods with higher concentrations for all modeling domains.

Time Series Analyses

Time series plots of the daily average model-predicted and observed CM concentrations for the full year, January 8 to January 23, 2010, and September 27 to October 5, 2010 are shown in **Figure 4.2-30** for the Canyonlands NP IMPROVE site alongside the SOIL concentrations. As was seen with the SOIL concentration observations, there are periods with elevated CM concentrations in the spring. During this time of year there were several windblown dust events that models strongly under-predicted. The models show small peaks around the time of the events but do not capture the magnitude or intensity of the observed CM concentrations. Even during fall and winter the observations are showing smaller peaks of CM concentrations that model is not reproducing.

CMAQ Spatial Analyses

The CM spatial performance was reviewed for POI 1 (January 8 to January 23, 2010 shown in **Figure 4.2-31**) and POI 4 (September 27 to October 5, 2010 shown in **Figure 4.2-32**). When available, monitored 24-hour average CM concentrations are shown as circles. If the POIs have elevated concentrations of SOIL due to windblown dust events, the spatial patterns for CM are expected to be similar to SOIL; therefore, these two species are plotted together. SOIL concentrations are shown on the left and CM is shown on the right. In general, the model is in agreement with monitored concentrations during the POI 1. Both the model and observation sites show low concentrations of CM. For POI 4, the model predicted CM concentrations are lower than the monitored concentrations. In general, the monitor sites are not located in areas that the model predicts higher CM concentrations making it difficult to assess the model's performance. It appears that the higher CM concentrations predicted by the model correspond to wildfire locations and urban areas.

Summary of Model Performance for CM

In general, the model under-predicts CM concentrations for all modeling domains, particularly during spring and summer.

- Annual model predictions under-predict CM relative to observed concentrations in all three modeling domains. Seasonally, the model bias is lowest in the winter, and the highest in spring and summer.

- The model performance for CM exceeds the USEPA-established performance criteria (USEPA 2007) for periods with higher concentrations for all modeling domains.

- Throughout the year at the Canyonlands NP IMPROVE site, the model generally under-predicts the magnitude of the CM concentrations.

- It is difficult to verify the spatial gradients of CM during the two selected POIs based on location of monitor sites; however, the modeled spatial gradient corresponds with available observations during the selected POIs.

Comparison of CMAQ and CAMx Results

The complete set of the CAMx MPE tables, bar charts, and spatial plots is found in **Appendix B**. Both models generally under-predict CM concentrations in all domains, except during March in CAMx. In general, biases are larger in CMAQ than in CAMx in all domains, especially during the spring where they are substantially larger in CMAQ than in CAMx. CM predictions consistently fall outside of the USEPA performance criteria in all domains for both models.

Table 4.2-8   Model Performance Statistical Summary for Coarse Mass

| Monitoring Network	Statistic (%)/ Concentration (µg/m³)	36-km Domain					12-km Domain					4-km Domain				
		Annual	Winter	Spring	Summer	Fall	Annual	Winter	Spring	Summer	Fall	Annual	Winter	Spring	Summer	Fall
IMPROVE (Daily)	MFB	-75	-25	-71	-118	-84	-98	-48	-87	-151	-105	-115	-74	-107	-164	-119
	MFGE	103	84	95	127	105	113	86	99	151	116	122	93	113	164	122
	MNB	21	115	29	-60	-17	-34	36	-47	-84	-42	-58	-12	-62	-90	-68
	MNGE	129	185	132	83	97	92	121	68	85	89	81	94	70	90	73
	NMB	-62	-29	-60	-74	-66	-75	-34	-73	-87	-76	-86	-64	-86	-92	-84
	NME	78	76	76	81	77	80	65	77	87	79	87	70	88	92	85
	R^2	0.036	0.116	0.021	0.026	0.065	0.082	0.526	0.032	0.175	0.130	0.033	0.134	0.008	0.102	0.001
	Observed Mean Concentration (µg/m³)	4.87	2.62	5.20	6.05	5.39	4.02	1.52	4.82	5.48	4.03	3.67	0.78	6.20	4.74	2.91
	Predicted Mean Concentration (µg/m³)	1.84	1.87	2.08	1.55	1.81	1.00	1.00	1.30	0.72	0.95	0.50	0.28	0.85	0.39	0.47
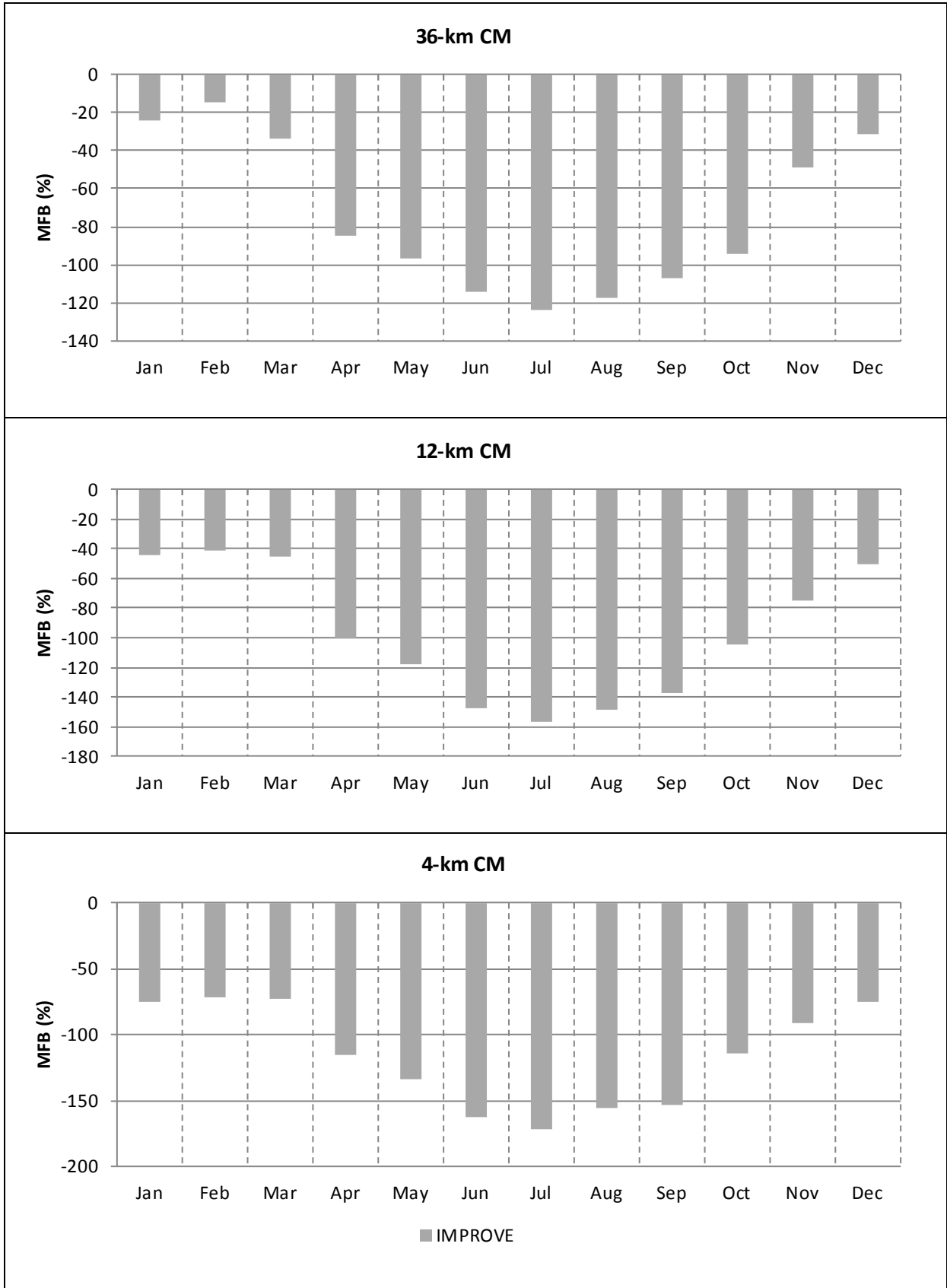
**Figure 4.2-33   Monthly Mean Fractional Bias for Coarse Mass**
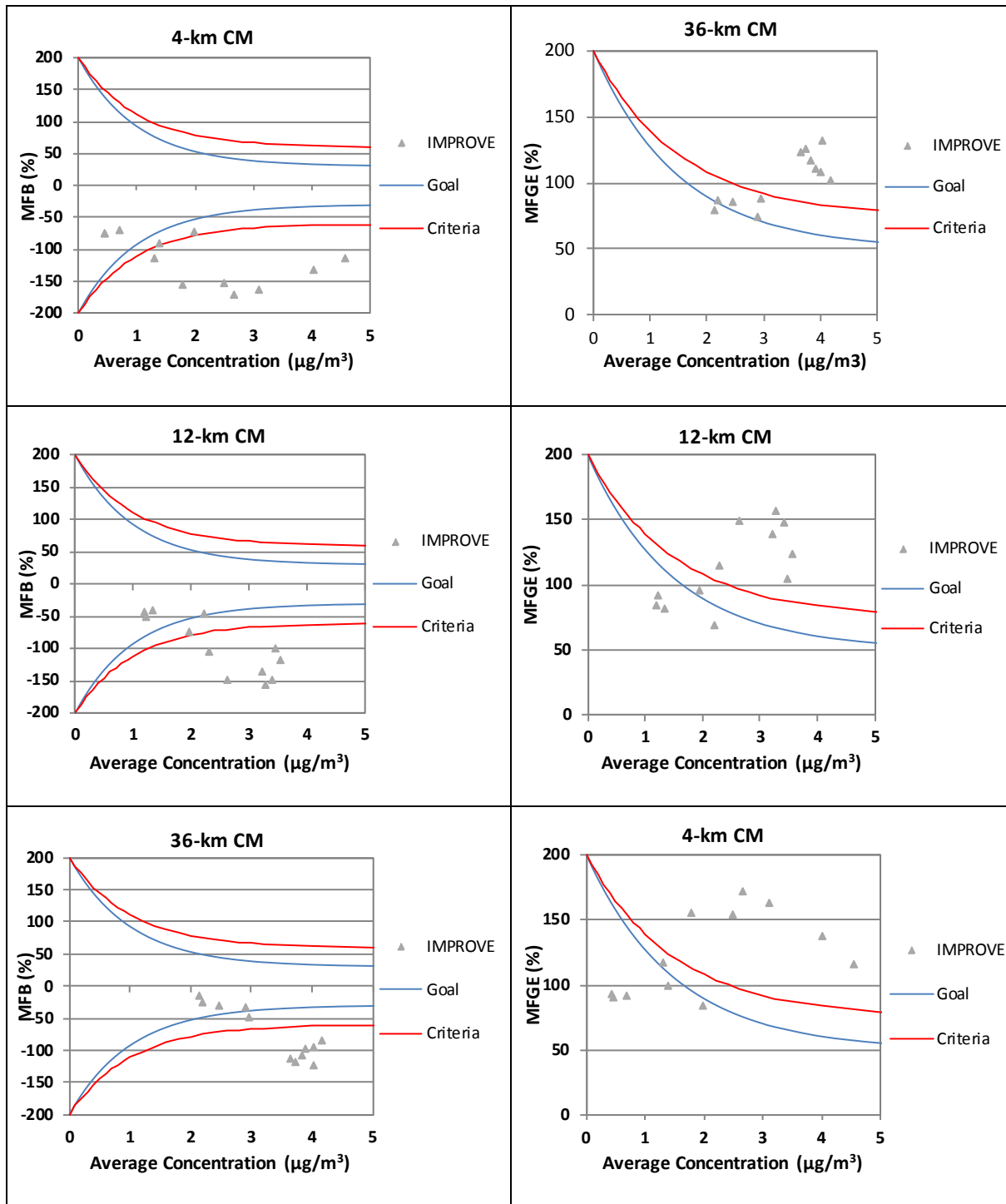
Note: Goals and criteria based on Boylan and Russell (2006) and accepted by USEPA (2007).

Figure 4.2-34   Bugle Plots of Coarse Mass Monthly Mean Fractional Bias and Mean Fractional Gross Error

4.2.2 Total PM$_{2.5}$

Statistical Analyses for the CMAQ 36-km, 12-km, and 4-km Domains

Annual and seasonal total PM$_{2.5}$ statistical summaries are presented in **Table 4.2-9** for the daily measurements and in **Table 4.2-10** for the hourly measurements for each monitoring network and modeling domain. Note that the number of monitors with valid data used to calculate the statistical summaries is provided in **Table 3-2**. A more detailed assessment of the MFB for daily measurements is presented for each month in **Figure 4.2-35**. The monthly MFB and MFGE relative to daily measurements are presented in **Figure 4.2-36** with the USEPA-recommended goals and performance criteria (USEPA 2007). Likewise, the same information is presented for the hourly measurements in **Figure 4.2-37** and **Figure 4.2-38**.

For the majority of the time periods and networks, the model tends to under-predict total PM$_{2.5}$ independent of the modeling domain. The maximum biases and errors occur in the summer for most networks and domains. Relative to the IMPROVE and STN networks the model tends to over-predict total PM$_{2.5}$ during the winter. Similar seasonal performance occurs between daily and hourly measurements as shown by comparing **Figures 4.2-35** and **4.2-39**.

The monthly MFB and MFGE of the daily total PM$_{2.5}$ are mostly within the USEPA-recommended performance criteria for almost all months and networks, as shown in **Figures 4.2-36** and **Figure 4.2-38**. For STN and AQS, a few months with lower concentrations exceed the USEPA-recommended criteria for MFB. While a majority of the months are within the USEPA criteria for MFGE relative to daily measurements, a majority of the months exceed the criteria for the 36-km and 12-km domains relative to hourly measurements.

Time Series Analyses

Figures 4.2-39 through **4.2-41** present time series plots for POI 1 (January 8 to January 23, 2010), POI 4 (September 27 to October 5, 2010) and the annual period, respectively, comparing daily PM$_{2.5}$ observations to model results at selected sites within the Uinta Basin study area. The figure presents the hourly average model-predicted PM$_{2.5}$ concentrations for the grid cells that contain the AQS monitors. Four AQS sites were selected for this analysis based on their location within the Uinta Basin study area. These sites are Dinosaur, UT (AQS monitoring site 49_047_1002), Ouray, Utah (AQS monitoring site 49_047_2003), Redwash, Utah (AQS monitoring site 49_047_2002), and Rangely, CO (AQS monitoring site 08_103_0006). Note that observations are missing for some of the stations during select POIs.

The model tends to under-predict the average PM$_{2.5}$ concentrations at all stations relative to observations, especially during elevated events and the summer season. Most sites show elevated events in the spring and summer, which both CMAQ and CAMx under-predict. These events are likely due to windblown dust as was shown in the SOIL time series. The PM$_{2.5}$ concentration maximums in the fall and winter reflect the prevalent stagnant conditions that lead to accumulation of particulates in the Uinta Basin. The highest model predicted PM$_{2.5}$ concentration values are found in the winter months with lower values in the summer months. The observations generally follow this pattern with the exception of the elevated events. Neither model tends to capture these events well, although CMAQ is slightly more accurate, predicting higher PM$_{2.5}$ concentrations during these events.

CMAQ Spatial Analyses

The total PM$_{2.5}$ spatial performance was reviewed for two POIs: POI 1 (January 8 to January 23, 2010); and POI 4 (September 27 to October 5, 2010). Daily average total concentrations of total PM$_{2.5}$ and total PM$_{10}$ in the 4-km domain are shown in **Figure 4.2-42** and **Figure 4.2-43**. The spatial patterns for total PM$_{2.5}$ are expected to be similar to total PM$_{10}$ if the POIs have elevated concentrations due to windblown dust events. Total PM$_{2.5}$ concentrations are shown on the left and total PM$_{10}$ concentrations

are shown on the right. Monitored 24-hour average concentrations from the IMPROVE network are shown in the figures as circles.

In general, the model over-predicts the magnitude of the PM$_{2.5}$ concentrations. During the POI 1, the monitoring stations show much lower PM$_{2.5}$ concentrations relative to the model. This over-prediction is likely related to model over-estimating the impact of the stagnant weather conditions on the PM$_{2.5}$ concentrations. By the end of the POI, the high PM$_{2.5}$ concentrations clear out leaving only a few areas with elevated PM$_{2.5}$ concentrations. However, due to the location of the monitors it is difficult to assess the model's ability to predict the conditions. Throughout POI 1, all monitors show similar concentrations (i.e., there isn't a noticeable spatial gradient or pattern), which is not consistent with the model. The model predicts a large spatial variability both within the domain during a given day, as well as throughout the POI event.

During the POI 4, the model predicted higher concentrations than observations suggest. The modeled wildfire plumes show impacts at Bryce NP that are higher than observed concentrations. At the remaining stations, the spatial pattern from the model is similar to the observed values. The model spatial coverage compares well with the observations both in magnitude and location of impacts at the end of the POI.

Summary of Model Performance for Total PM$_{2.5}$

In general, the model under-predicted total PM$_{2.5}$ concentrations in most locations and seasons.

- The model generally under-predicts AQS PM$_{2.5}$ concentrations (hourly and daily) for all domains and seasons with the largest biases occurring in the summer.

- For IMPROVE and STN networks, the model tends to over-predict total PM$_{2.5}$ only during the winter.

- The monthly MFB and MFGE of the daily total PM$_{2.5}$ are mostly within the USEPA-recommended performance criteria for almost all months and networks, but exceed the criteria for the MFGE relative to hourly measurements.

- The model spatial gradients of total PM$_{2.5}$ during the two selected POIs tend to over-predict the PM$_{2.5}$ concentrations during events. While monitors suggest limited spatial variability, the model predicts a large spatial variability both within the domain during a given day, as well as during a series of days.

Comparison of CMAQ and CAMx Results

The complete set of the CAMx MPE tables, bar charts, and spatial plots is found in **Appendix B**. Both CMAQ and CAMx tend to under-predict PM$_{2.5}$ concentrations during the summer months for all domains, regardless of monitoring network. However, summer PM$_{2.5}$ biases were smaller in CAMx than in CMAQ. With respect to hourly measurements, both models under-predicted PM$_{2.5}$ concentrations throughout the year in all domains with larger errors in summer than winter. These errors were generally smaller than CAMx than in CMAQ. With respect to daily measurements, both models tend to over-predict PM$_{2.5}$ concentrations during the winter months. For CMAQ, performance was better in the winter than in the summer, whereas the reverse was generally true for CAMx. PM$_{2.5}$ performance for both models is within the USEPA-recommended performance criteria for almost all months and networks. Performance criteria are not met for all domains in CMAQ during the summer months or for the 4-km domain in CAMx during the winter months.

Figure 4.2-44 shows the spatial distribution of daily average concentrations of total PM$_{2.5}$ for CMAQ (left) and CAMx (right) on January 12, 2010 during the first POI. For this figure, the monitored 24-hour average concentrations from the AQS network are shown in the figures as circles. As shown in **Figure 4.2-44**, predicted PM$_{2.5}$ concentrations are significantly higher in CMAQ than in CAMx. This difference is also seen throughout the wintertime for PM$_{2.5}$ episodes in the Uinta Basin. During these events, the

CMAQ concentrations are typically closer to the observations than CAMx. However, both models generally under-predict $PM_{2.5}$ concentrations in the Uinta Basin throughout the year. During the summer, both models under-predict $PM_{2.5}$ concentrations across the 4-km domain. In general, neither model captures the fire-induced elevated $PM_{2.5}$ concentrations in August or the occasional elevated $PM_{2.5}$ events in the Salt Lake City area or in the Uinta Basin seen throughout the year. Both models produce similar spatial patterns for $PM_{2.5}$ in the 4-km domain during the wintertime $PM_{2.5}$ events and during the summer months.

Table 4.2-9   Model Performance Statistical Summary for Total PM$_{2.5}$ (Daily)

Monitoring Network	Statistic (%)/ Concentration (µg/m^3)	36-km Domain					12-km Domain					4-km Domain				
		Annual	Winter	Spring	Summer	Fall	Annual	Winter	Spring	Summer	Fall	Annual	Winter	Spring	Summer	Fall
AQS (Daily)	MFB	-53	-46	-41	-75	-48	-24	-12	-13	-54	-16	-21	-18	-6	-58	-3
	MFGE	67	73	56	78	61	53	60	46	61	46	50	51	44	62	42
	MNB	-29	-12	-23	-50	-28	-2	22	5	-36	1	-4	2	9	-40	11
	MNGE	53	66	46	54	49	53	72	49	46	48	47	52	45	45	46
	NMB	-42	-42	-33	-53	-38	-20	-18	-11	-41	-12	-24	-29	-13	-47	3
	NME	54	59	47	55	51	49	56	46	48	43	47	45	50	50	41
	R^2	0.214	0.165	0.176	0.292	0.179	0.232	0.190	0.151	0.230	0.241	0.381	0.415	0.044	0.026	0.374
	Observed Mean Concentration (µg/m^3)	8.55	12.00	6.77	7.77	7.79	7.86	11.25	6.29	7.23	6.80	8.85	16.46	6.36	6.87	6.13
	Predicted Mean Concentration (µg/m^3)	4.99	7.01	4.56	3.64	4.80	6.26	9.18	5.61	4.23	5.96	6.71	11.61	5.51	3.67	6.31
IMPROVE (Daily)	MFB	-6	29	-2	-48	-3	-29	14	-29	-77	-23	-22	32	-28	-76	-15
	MFGE	53	59	47	61	47	59	57	48	79	52	60	64	50	76	52
	MNB	25	87	24	-25	18	-2	55	-12	-50	-1	6	80	-10	-53	12
	MNGE	68	108	60	52	56	60	86	45	57	54	65	103	47	53	61
	NMB	4	40	18	-33	4	-28	33	-29	-56	-25	-26	64	-38	-56	-20
	NME	54	67	60	46	48	54	68	46	57	49	58	83	55	56	51
	R^2	0.325	0.508	0.267	0.389	0.423	0.177	0.468	0.133	0.273	0.092	0.016	0.522	0.018	0.125	0.006
	Observed Mean Concentration (µg/m^3)	4.71	4.03	4.64	5.75	4.31	2.90	1.74	3.21	3.73	2.88	2.58	1.39	3.26	3.23	2.39
	Predicted Mean Concentration (µg/m^3)	4.90	5.64	5.49	3.87	4.49	2.10	2.32	2.28	1.64	2.15	1.91	2.29	2.03	1.42	1.91

Table 4.2-9   Model Performance Statistical Summary for Total PM$_{2.5}$ (Daily)

Monitoring Network	Statistic (%)/ Concentration (µg/m^3)	36-km Domain					12-km Domain					4-km Domain				
		Annual	Winter	Spring	Summer	Fall	Annual	Winter	Spring	Summer	Fall	Annual	Winter	Spring	Summer	Fall
STN (Daily)	MFB	-39	-32	-32	-59	-32	-4	9	4	-30	1	16	19	16	-28	47
	MFGE	61	61	57	69	55	43	51	42	43	37	43	45	41	36	50
	MNB	-17	-8	-7	-37	-15	12	31	22	-18	13	35	42	32	-20	71
	MNGE	52	55	55	52	48	48	62	51	37	41	55	62	50	28	74
	NMB	-28	-22	-20	-45	-26	-8	1	0	-31	-4	6	0	6	-30	59
	NME	52	54	50	53	51	43	49	44	40	38	47	41	56	36	63
	R^2	0.171	0.123	0.262	0.133	0.080	0.202	0.141	0.113	0.229	0.192	0.418	0.380	0.027	0.024	0.581
	Observed Mean Concentration (µg/m^3)	10.07	13.29	8.81	9.17	9.24	9.83	13.34	8.04	9.41	8.93	10.21	19.33	7.59	7.74	5.91
	Predicted Mean Concentration (µg/m^3)	7.30	10.38	7.06	5.08	6.81	9.06	13.54	8.00	6.53	8.56	10.80	19.27	8.06	5.43	9.39

Table 4.2-10   Model Performance Statistical Summary for Total PM$_{2.5}$ (Hourly)

Monitoring Network	Statistic (%)/ Concentration (µg/m^3)	36-km Domain					12-km Domain					4-km Domain				
		Annual	Winter	Spring	Summer	Fall	Annual	Winter	Spring	Summer	Fall	Annual	Winter	Spring	Summer	Fall
AQS (Hourly)	MFB	-52	-40	-48	-73	-45	-37	-21	-32	-63	-30	-48	-21	-42	-90	-35
	MFGE	91	94	85	98	86	87	90	82	95	83	82	74	75	100	78
	MNB	2271	3166	2421	1763	1840	2454	3657	2674	1663	1984	2	32	8	-36	8
	MNGE	2372	3250	2508	1872	1927	2543	3729	2750	1765	2059	88	96	86	86	87
	NMB	-51	-45	-48	-62	-49	-40	-30	-37	-57	-35	-39	-26	-40	-66	-30
	NME	71	73	68	72	69	71	74	69	72	69	64	60	65	72	63
	R^2	0.072	0.070	0.041	0.100	0.081	0.067	0.075	0.033	0.072	0.073	0.116	0.237	0.014	0.011	0.077
	Observed Mean Concentration (µg/m^3)	9.00	10.61	7.90	8.96	8.64	8.55	10.41	7.50	8.55	7.90	8.41	12.80	7.78	7.64	5.94
	Predicted Mean Concentration (µg/m^3)	4.40	5.80	4.12	3.39	4.44	5.16	7.32	4.73	3.72	5.14	5.11	9.49	4.65	2.60	4.18
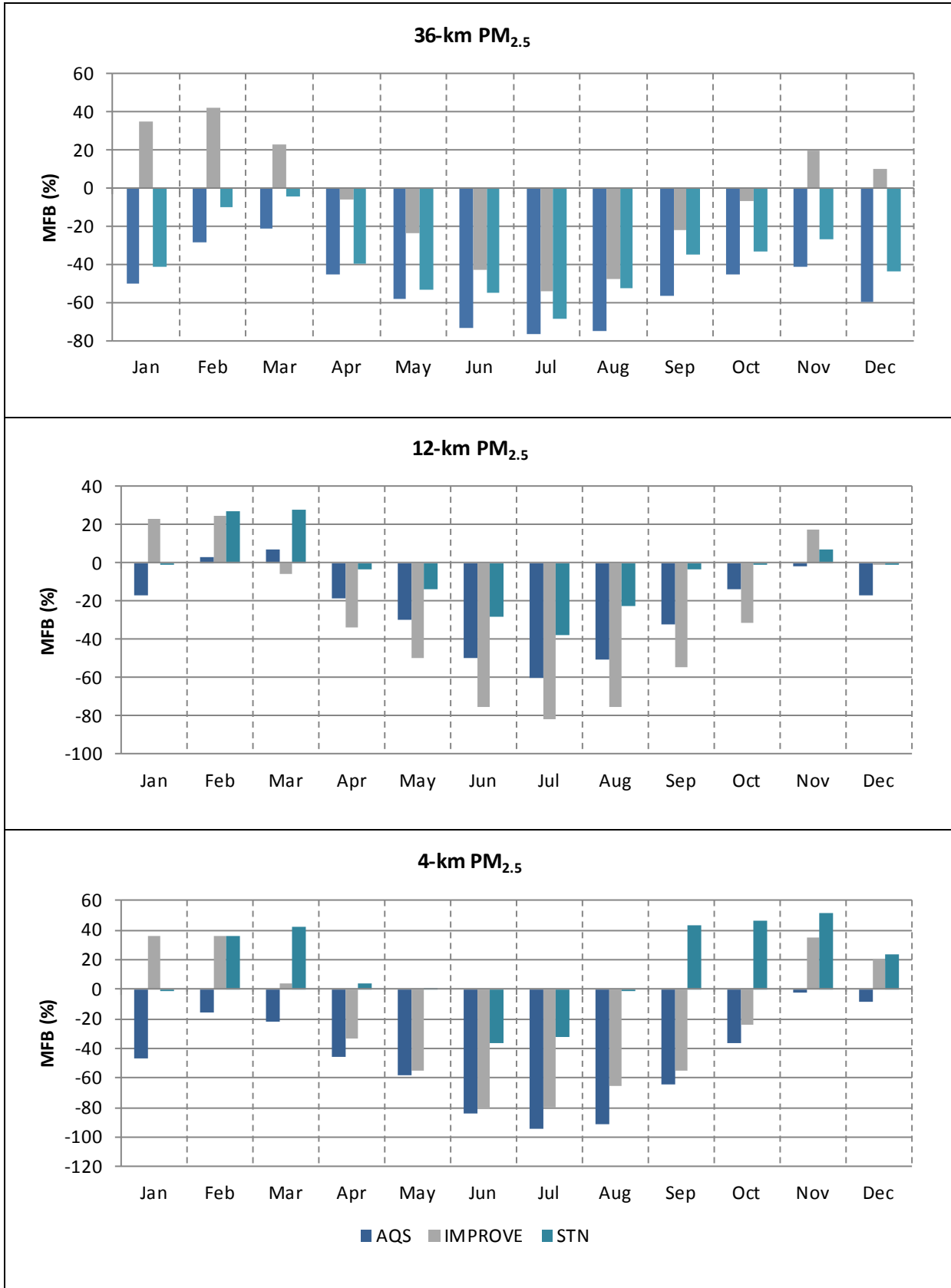
Figure 4.2-35   Monthly Mean Fractional Bias for Total PM$_{2.5}$ (Daily)
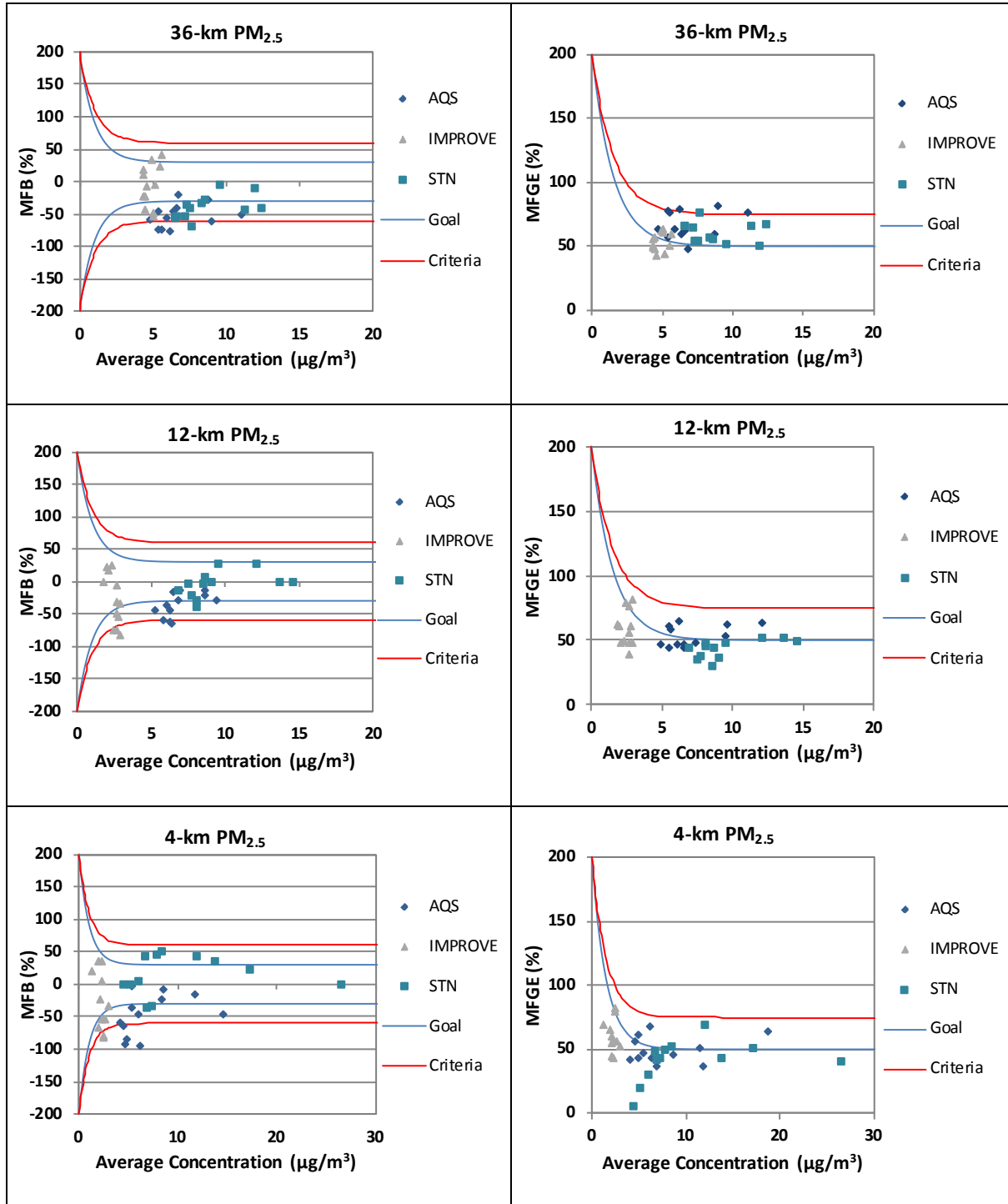
Note: Goals and criteria based on Boylan and Russell (2006) and accepted by USEPA (2007).

Figure 4.2-36 Bugle Plots of Total PM$_{2.5}$ (Daily) Monthly Mean Fractional Bias and Mean Fractional Gross Error
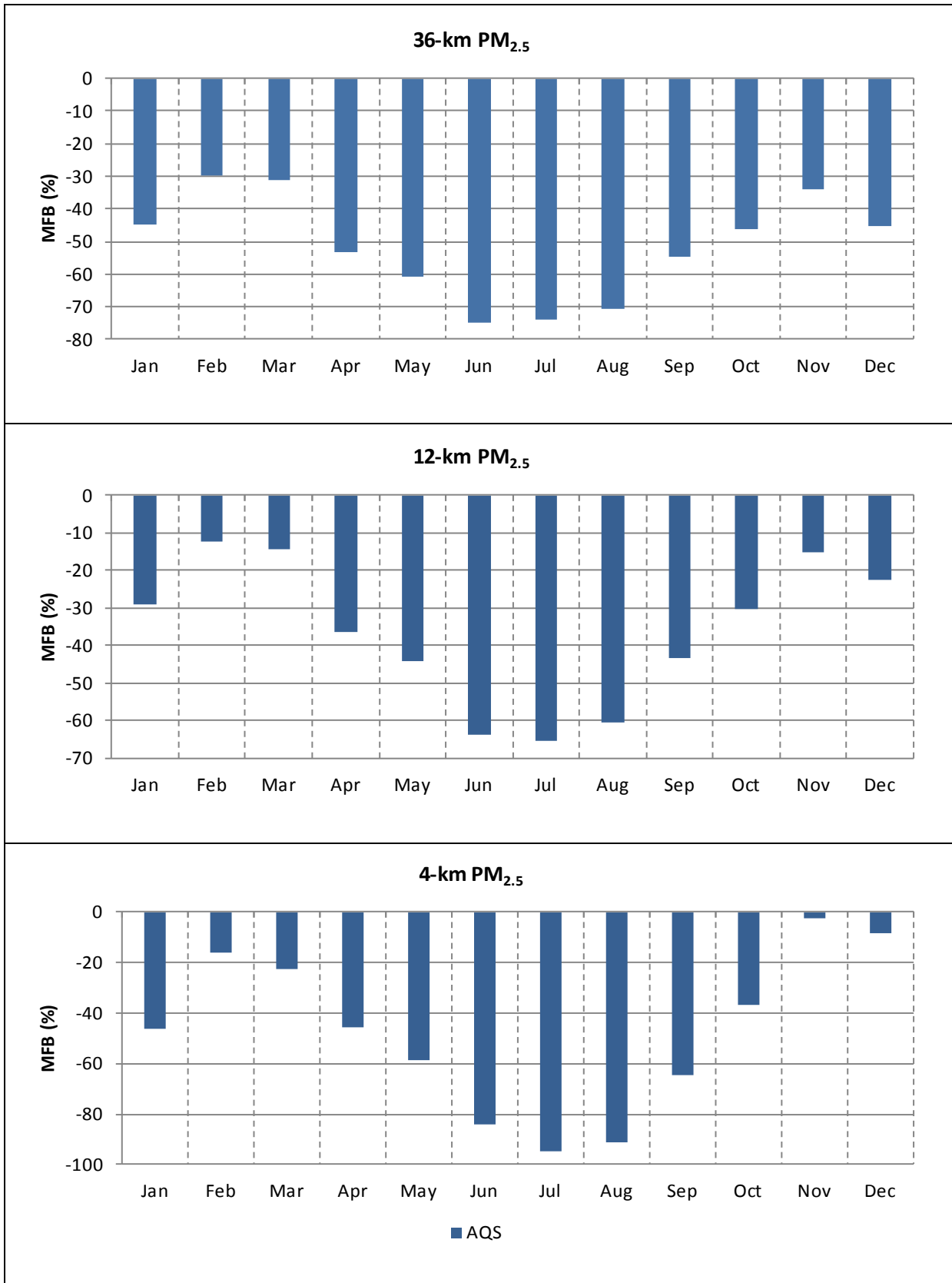
Figure 4.2-37   Monthly Mean Fractional Bias for Total PM$_{2.5}$ (Hourly)
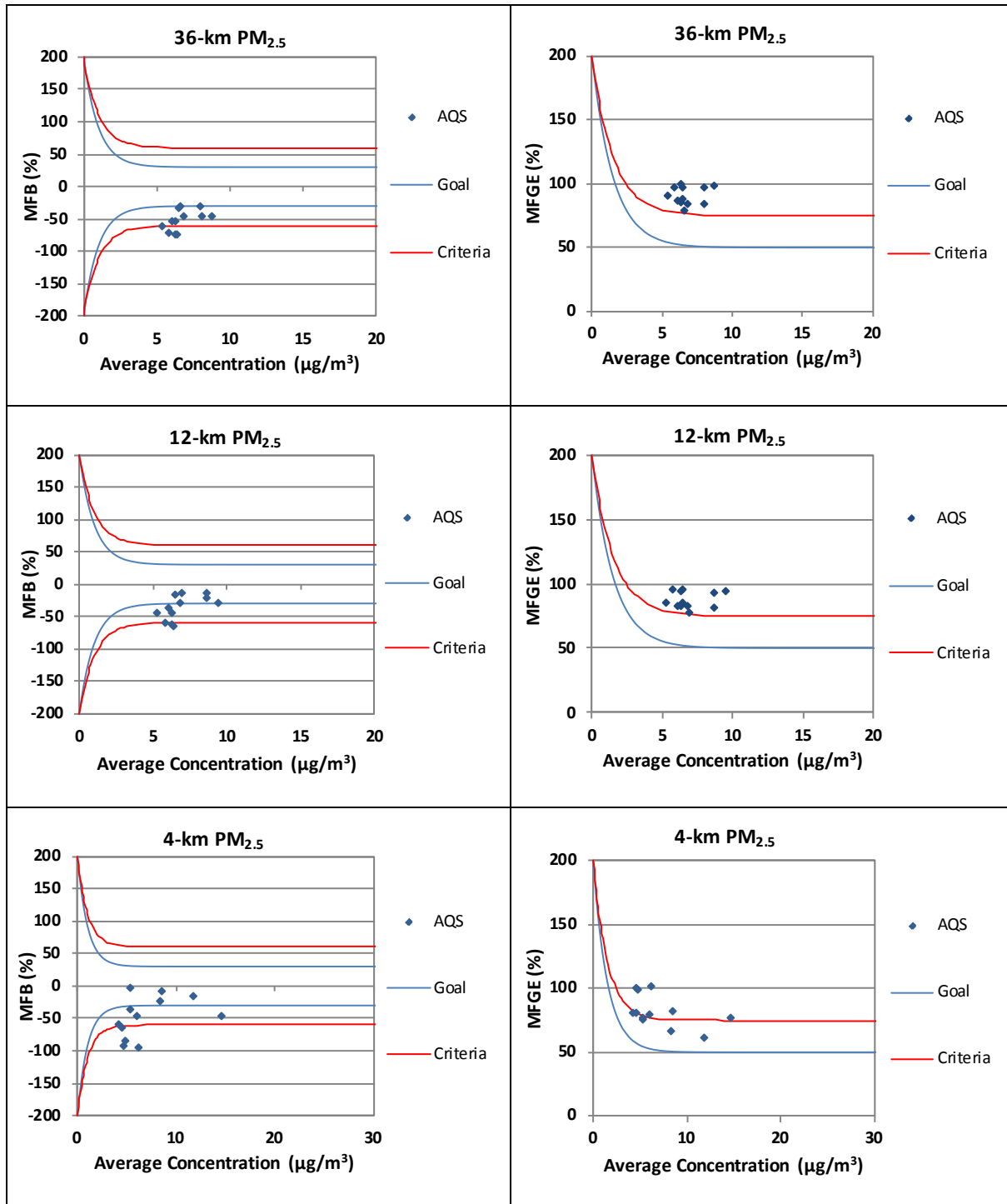
Note: Goals and criteria based on Boylan and Russell (2006) and accepted by USEPA (2007).

Figure 4.2-38   Bugle Plots of Total PM$_{2.5}$ (Hourly) Monthly Mean Fractional Bias and Mean Fractional Gross Error
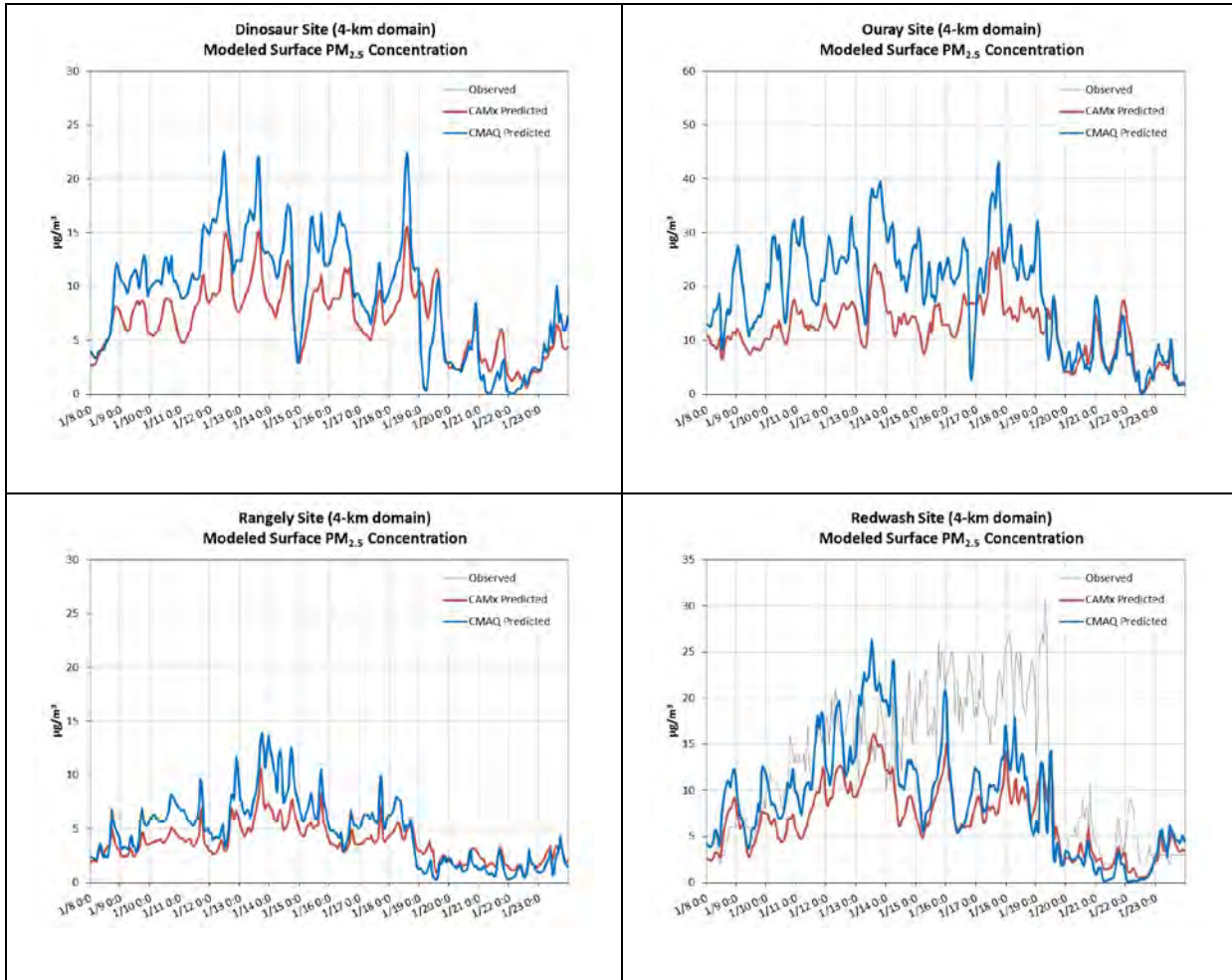
Figure 4.2-39   Time Series for PM$_{2.5}$ at Selected AQS Monitoring Sites from January 8 to January 23, 2010
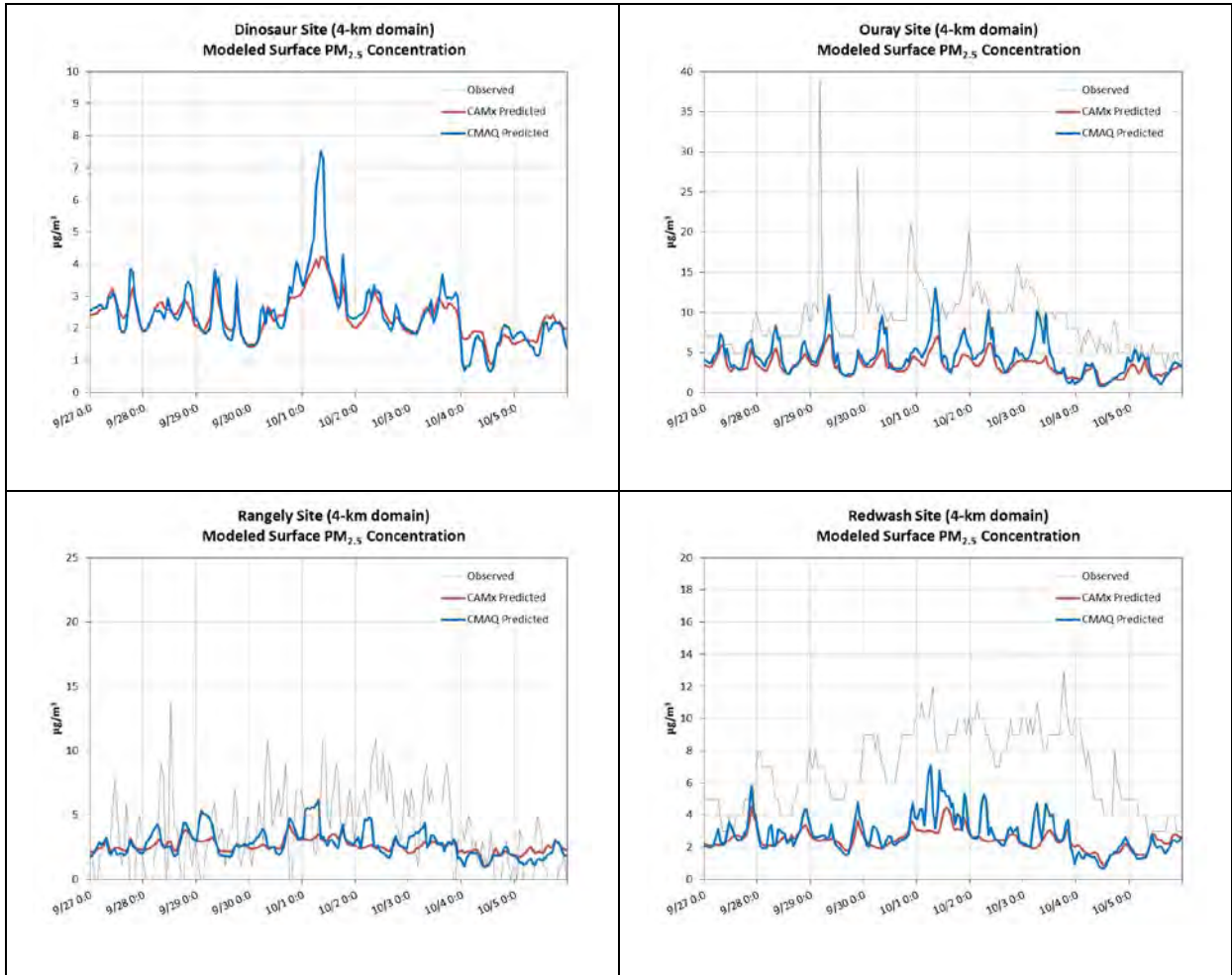
Figure 4.2-40   Time Series for PM$_{2.5}$ at Selected AQS Monitoring Sites from September 27 to October 5, 2010
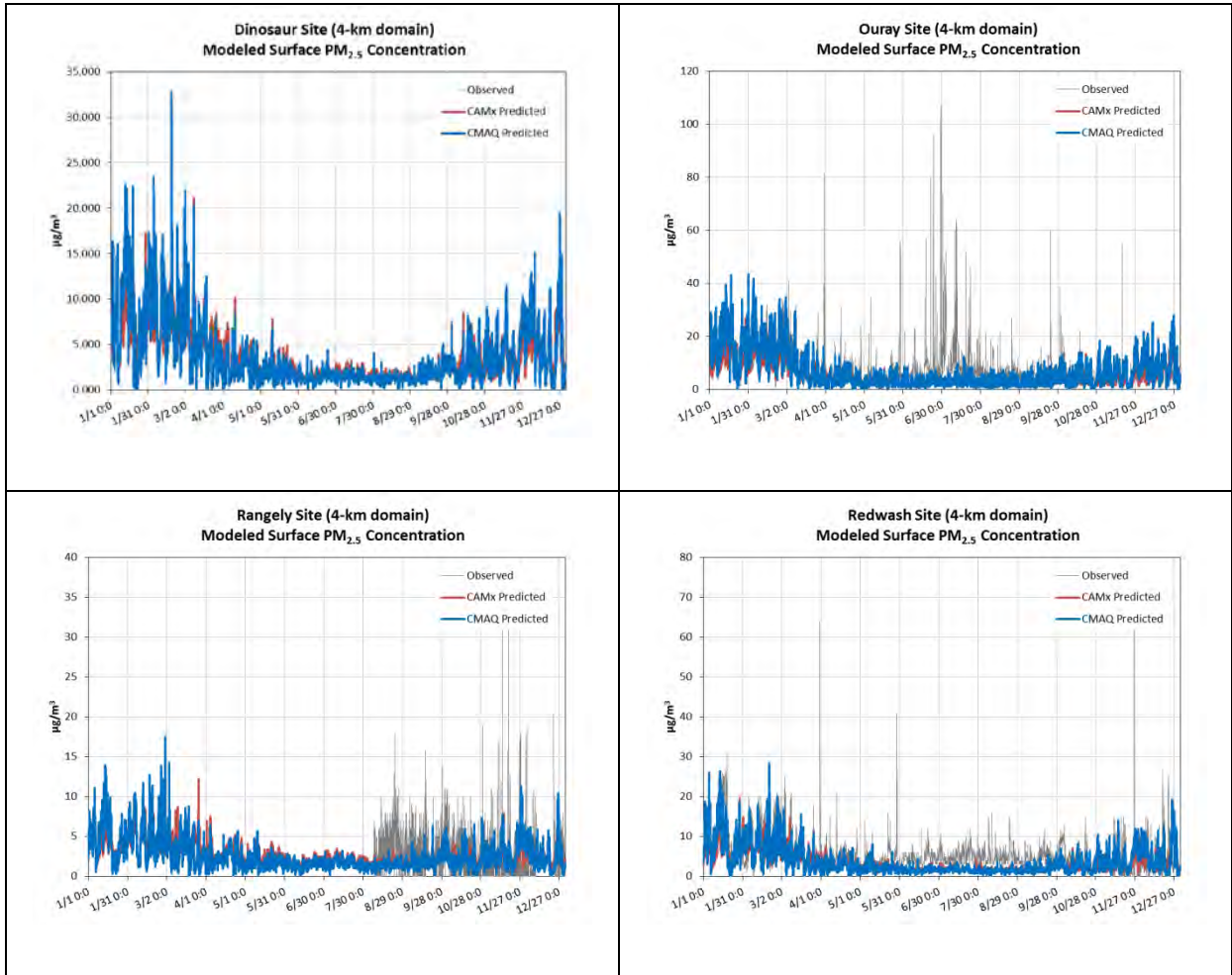
Figure 4.2-41   Annual Time Series for PM$_{2.5}$ at Selected AQS Monitoring Sites

PM~2.5~	PM~10~
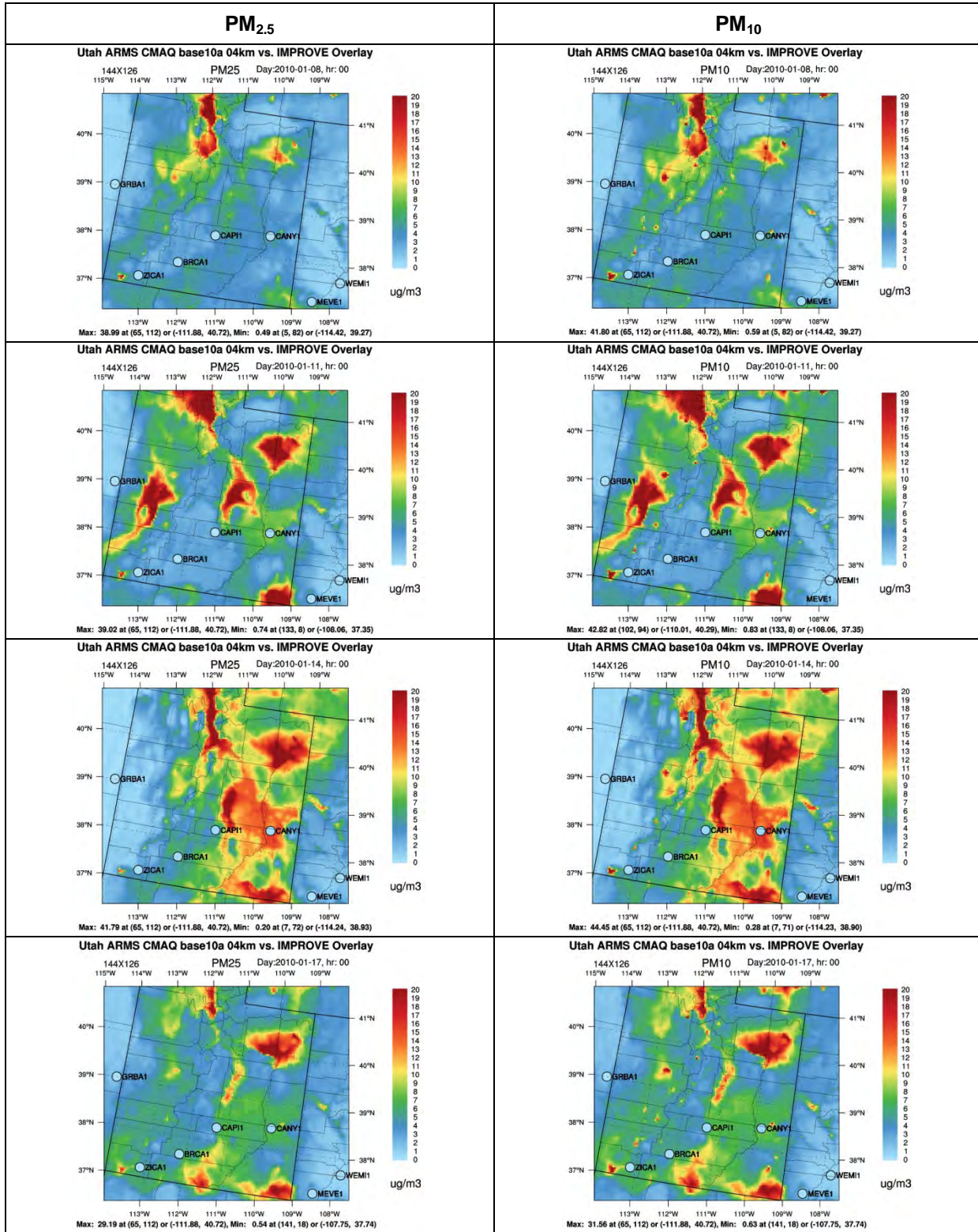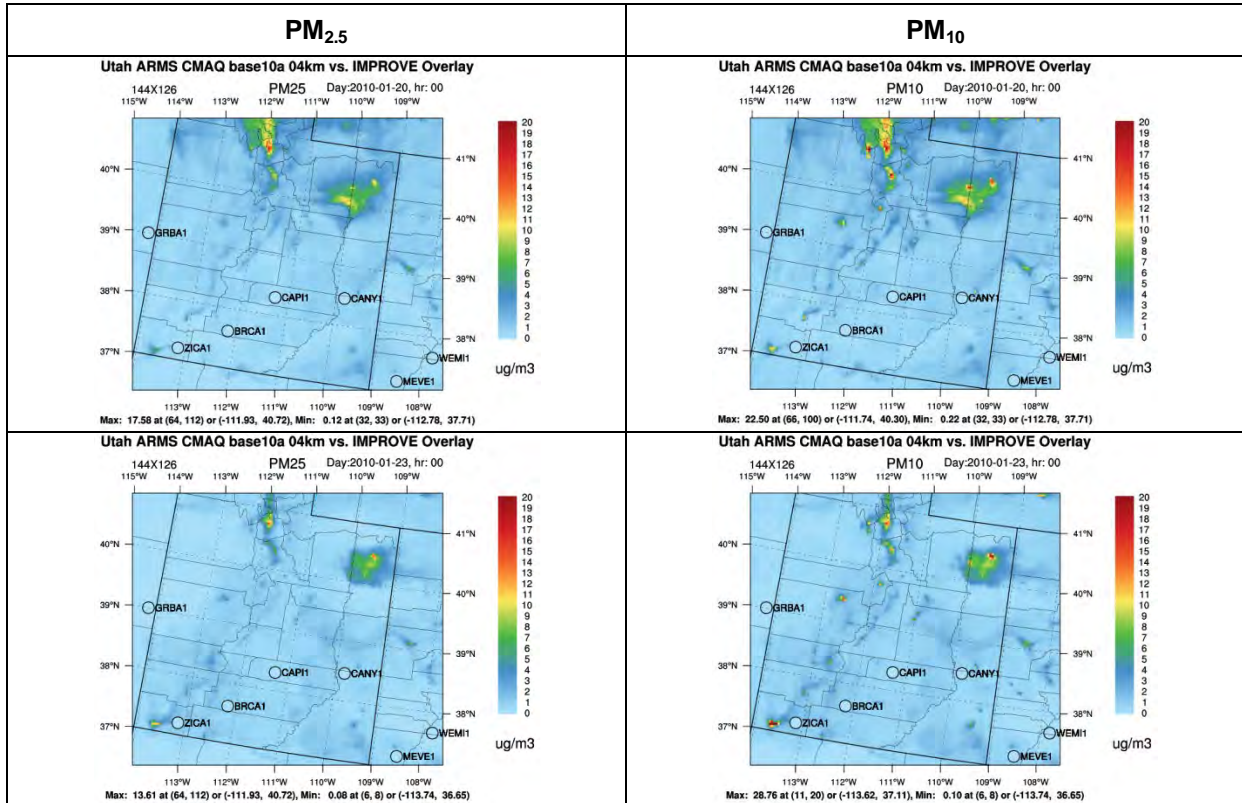
Figure 4.2-42   4-km Spatial Plots for Total PM₂.₅ and PM₁₀ during January 8 to January 23, 2010
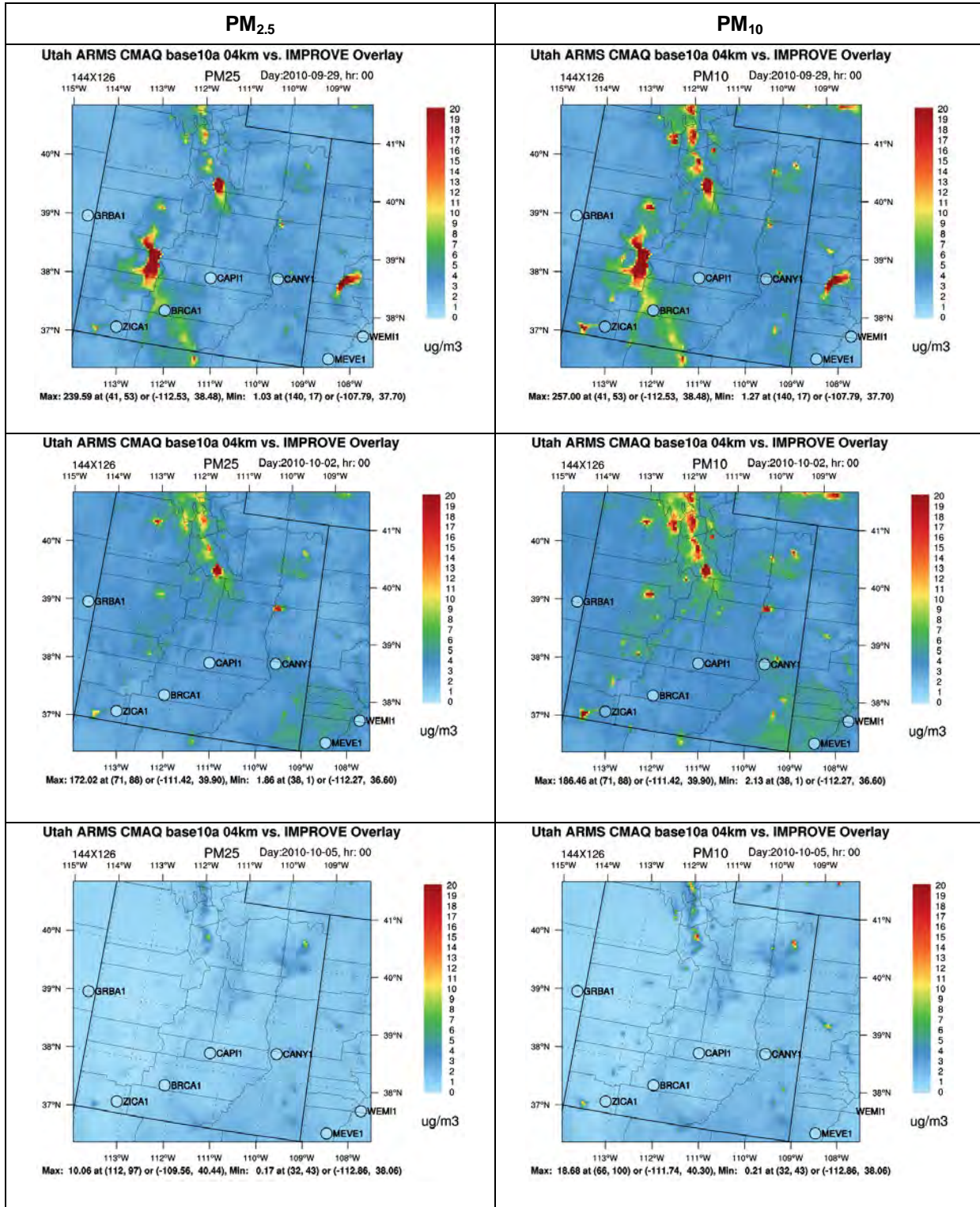
Figure 4.2-43   4-km Spatial Plots for Total PM$_{2.5}$ and PM$_{10}$ during September 27 to October 5, 2010
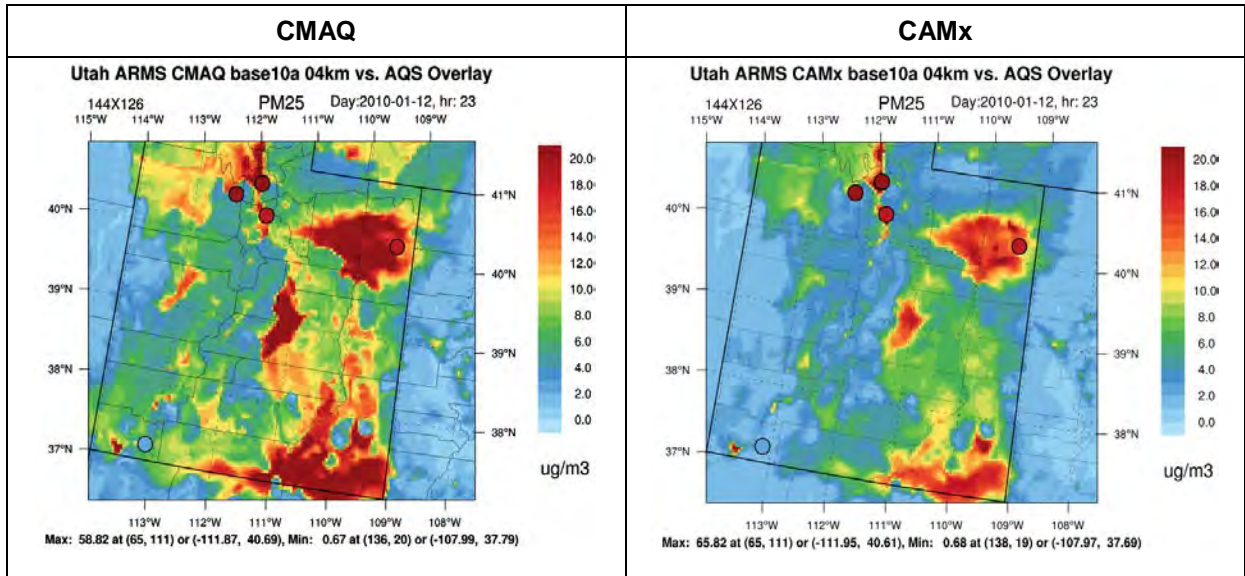
Figure 4.2-44   4-km Spatial Plots for Total PM$_{2.5}$ on January 12, 2010 at 2300 UTC for CMAQ (left) and CAMx (right)

4.2.3   Total PM$_{10}$

Statistical Analyses for the CMAQ 36-km, 12-km, and 4-km Domains

Annual and seasonal total PM$_{10}$ statistical summaries are presented in **Table 4.2-11** for the IMPROVE and APS daily measurements and **Table 4.2-12** for the AQS hourly measurements for all domains. Note that the number of monitors with valid data used to calculate the statistical summaries is provided in **Table 3-2**. A more detailed assessment of the MFB relative to daily measurements is presented for each month in **Figure 4.2-45**. The monthly fractional MFB and MFGE are presented in **Figure 4.2-46** relative to daily measurements with the USEPA-recommended goals and performance criteria (USEPA 2007).

In general, the model has a strong negative bias with respect to the AQS (daily and hourly), independent of season and domain. For IMPROVE, with the exception of winter, the model under-predicts the total PM$_{10}$ concentrations. The model performance is most accurate (smallest negative or positive bias) in winter, independent of domain, relative to all networks. In rural and remote areas, such as the IMPROVE network, the model has better performance for total PM$_{10}$.

The monthly MFB and MFGE for total PM$_{10}$ often exceed the USEPA-recommended performance criteria for all domains, as shown in **Figure 4.2-46**.

Time Series Analyses

Time series plots of the daily average model-predicted and observed PM$_{10}$ concentrations for the full year, January 8 to January 23, 2010, and September 27 to October 5, 2010 are shown in **Figure 4.2-47** for the Canyonlands NP IMPROVE site. As shown in **Figure 4.2-47**, the model tends to under-predict the PM$_{10}$ concentrations throughout the year. As was seen with the CM concentrations, there are several episodes of elevated PM$_{10}$ concentrations in the spring when there were several windblown dust events that the models strongly under-predicted. The model under-prediction of CM is likely the primary reason that the model is not performing as well for PM$_{10}$ as it did for PM$_{2.5}$.During the winter POI 1, however, the models over-predict the elevated concentrations.

CMAQ Spatial Analyses

The total PM$_{10}$ spatial performance was reviewed for two POIs: January 8 to January 23, 2010; and September 27 to October 5, 2010. Daily average total concentrations of total PM$_{2.5}$ and total PM$_{10}$ in the 4-km domain are shown in **Figure 4.2-42** and **Figure 4.2-43**. Total PM$_{2.5}$ concentrations are shown on the left and total PM$_{10}$ concentrations are shown on the right. In general, the spatial patterns and intensity of the PM$_{10}$ concentrations are very similar to the PM$_{2.5}$ spatial distribution. At the beginning of both POIs, the model over-estimates the magnitude of the events relative to the observations stations. By the end of the POIs, the model PM$_{10}$ concentrations correspond to observed values. The similarities of the PM$_{10}$ and PM$_{2.5}$ spatial pattern are likely due to the model under-prediction of CM, while the difference in the plots can be attributed the areas of higher CM concentrations (shown in **Figure 4.2-31** and **Figure 4.2-32**).

Summary of Model Performance for Total PM$_{10}$

In general, the model under-predicts total PM$_{10}$ concentrations.

- The model predictions of total PM$_{10}$ are under-predicted relative to observed concentrations for all modeling domains, time periods, and most monitoring networks except during the winter for IMPROVE. Seasonally, the model tends to be the most accurate in winter.

- The model performance for total PM$_{10}$ exceeds the USEPA-established performance criteria (UESPA 2007) for most months and modeling domains, except for some months relative to the IMPROVE network.

- The model tends to under-predict the PM_{10} concentrations throughout the year with the magnitudes of the model values being much lower than observations, which likely is a result of under-predicted CM.

- Spatial gradients of total PM_{10} and $PM_{2.5}$ are very similar indicting the model is under-predicting CM concentrations.

Comparison of CMAQ and CAMx Results

The complete set of the CAMx MPE tables, bar charts, and spatial plots is found in **Appendix B**. Both CMAQ and CAMx tend to under-predict PM_{10} concentrations for most months for all domains, regardless of monitoring network. During the winter months, both models over-predict PM_{10} concentrations relative to the IMPROVE network. In general for the summer months, the PM_{10} biases are smaller in CAMx than in CMAQ. With respect to hourly measurements, both models under-predicted $PM_{2.5}$ concentrations throughout the year in all domains with largest errors in spring. For both models, the performance is better in the winter than in the summer. PM_{10} performance for both models exceeds the USEPA-recommended performance criteria for most months and networks with CAMx having more months within the USEPA-recommend performance criteria than CMAQ.

Table 4.2-11   Model Performance Statistical Summary for Total PM$_{10}$ (Daily)

Monitoring Network	Statistic (%)/ Concentration (µg/m^3)	36-km Domain					12-km Domain					4-km Domain				
		Annual	Winter	Spring	Summer	Fall	Annual	Winter	Spring	Summer	Fall	Annual	Winter	Spring	Summer	Fall
AQS (Daily)	MFB	-101	-69	-97	-134	-102	-87	-57	-83	-120	-88	-88	-61	-88	-120	-85
	MFGE	108	89	102	134	108	100	84	95	122	98	96	77	94	121	92
	MNB	-57	-32	-58	-78	-60	-46	-17	-46	-70	-49	-53	-35	-53	-72	-51
	MNGE	70	68	65	79	69	69	73	65	74	67	64	59	62	73	62
	NMB	-71	-54	-74	-81	-71	-62	-41	-67	-75	-61	-67	-55	-75	-78	-62
	NME	74	65	76	81	73	71	65	74	76	68	70	59	77	78	65
	R^2	0.015	0.069	0.001	0.062	0.034	0.014	0.121	0.000	0.036	0.067	0.045	0.424	0.000	0.006	0.109
	Observed Mean Concentration (µg/m^3)	20.79	17.98	22.55	22.28	20.35	20.34	17.35	21.90	22.21	19.72	23.16	25.01	26.04	21.34	20.29
	Predicted Mean Concentration (µg/m^3)	6.05	8.21	5.89	4.24	5.99	7.63	10.28	7.18	5.56	7.62	7.59	11.38	6.52	4.73	7.76
IMPROVE (Daily)	MFB	-32	14	-27	-76	-36	-58	-3	-55	-113	-60	-57	5	-61	-118	-57
	MFGE	65	56	58	85	62	78	57	67	114	73	80	55	74	118	76
	MNB	5	65	-2	-35	-9	-23	40	-32	-67	-32	-22	38	-35	-73	-20
	MNGE	71	95	57	70	58	66	82	51	75	58	66	73	54	73	69
	NMB	-28	16	-21	-53	-33	-54	6	-53	-74	-54	-60	21	-67	-77	-55
	NME	58	59	58	60	54	64	52	60	74	61	70	55	73	77	64
	R^2	0.138	0.385	0.085	0.156	0.208	0.121	0.679	0.060	0.229	0.147	0.008	0.461	0.007	0.131	0.003
	Observed Mean Concentration (µg/m^3)	9.48	6.45	9.74	11.92	9.65	6.82	3.07	7.88	9.39	6.86	6.09	2.14	9.08	7.83	5.27
	Predicted Mean Concentration (µg/m^3)	6.85	7.49	7.70	5.66	6.42	3.14	3.27	3.68	2.42	3.18	2.46	2.59	2.95	1.83	2.39

Table 4.2-12   Model Performance Statistical Summary for Total PM$_{10}$ (Hourly)

Monitoring Network	Statistic (%)/ Concentration (μg/m^3)	36-km Domain					12-km Domain					4-km Domain				
		Annual	Winter	Spring	Summer	Fall	Annual	Winter	Spring	Summer	Fall	Annual	Winter	Spring	Summer	Fall
AQS (Hourly)	MFB	-94	-59	-91	-127	-97	-79	-36	-75	-118	-85	-127	NA	-134	-76	-112
	MFGE	113	97	108	133	113	108	94	102	127	109	127	NA	134	90	117
	MNB	-26	36	-24	-71	-44	5	99	-2	-61	-15	-76	NA	-77	-34	-65
	MNGE	98	132	96	80	83	118	181	107	82	103	76	NA	80	73	74
	NMB	-68	-46	-69	-81	-72	-51	-6	-54	-74	-60	-79	NA	-82	-64	-80
	NME	80	77	79	83	79	84	94	82	82	82	79	NA	82	67	81
	R^2	0.008	0.014	0.001	0.008	0.014	0.007	0.047	0.001	0.004	0.010	0.006	NA	0.011	0.328	0.014
	Observed Mean Concentration (μg/m^3)	22.51	19.05	22.84	24.24	23.93	21.87	18.01	21.94	23.99	23.26	27.16	NA	23.12	20.54	23.32
	Predicted Mean Concentration (μg/m^3)	7.20	10.30	7.08	4.62	6.78	10.62	16.89	9.99	6.18	9.38	5.83	NA	4.20	7.41	4.60
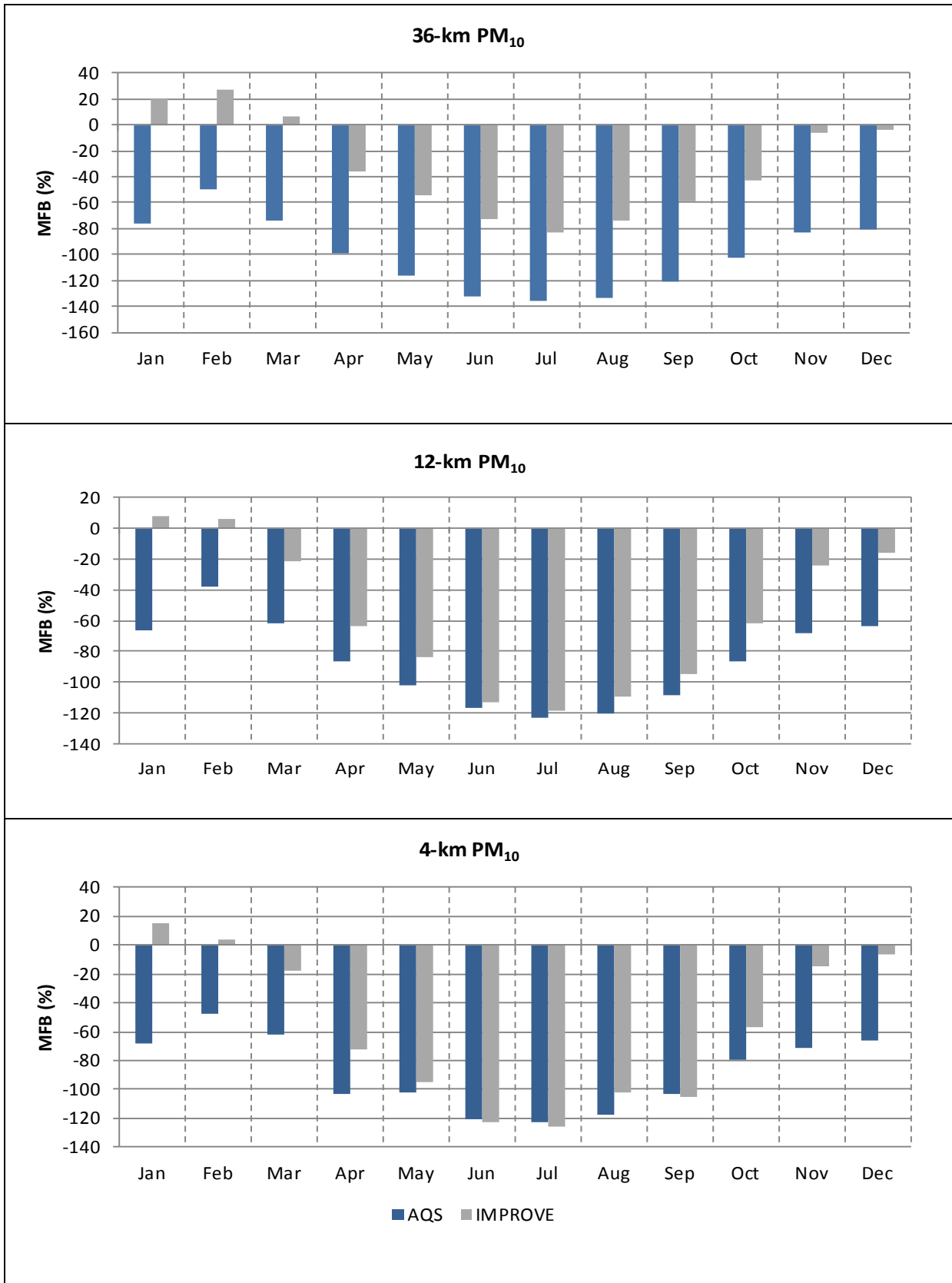
Figure 4.2-45   Monthly Mean Fractional Bias for Total PM$_{10}$ (Daily)
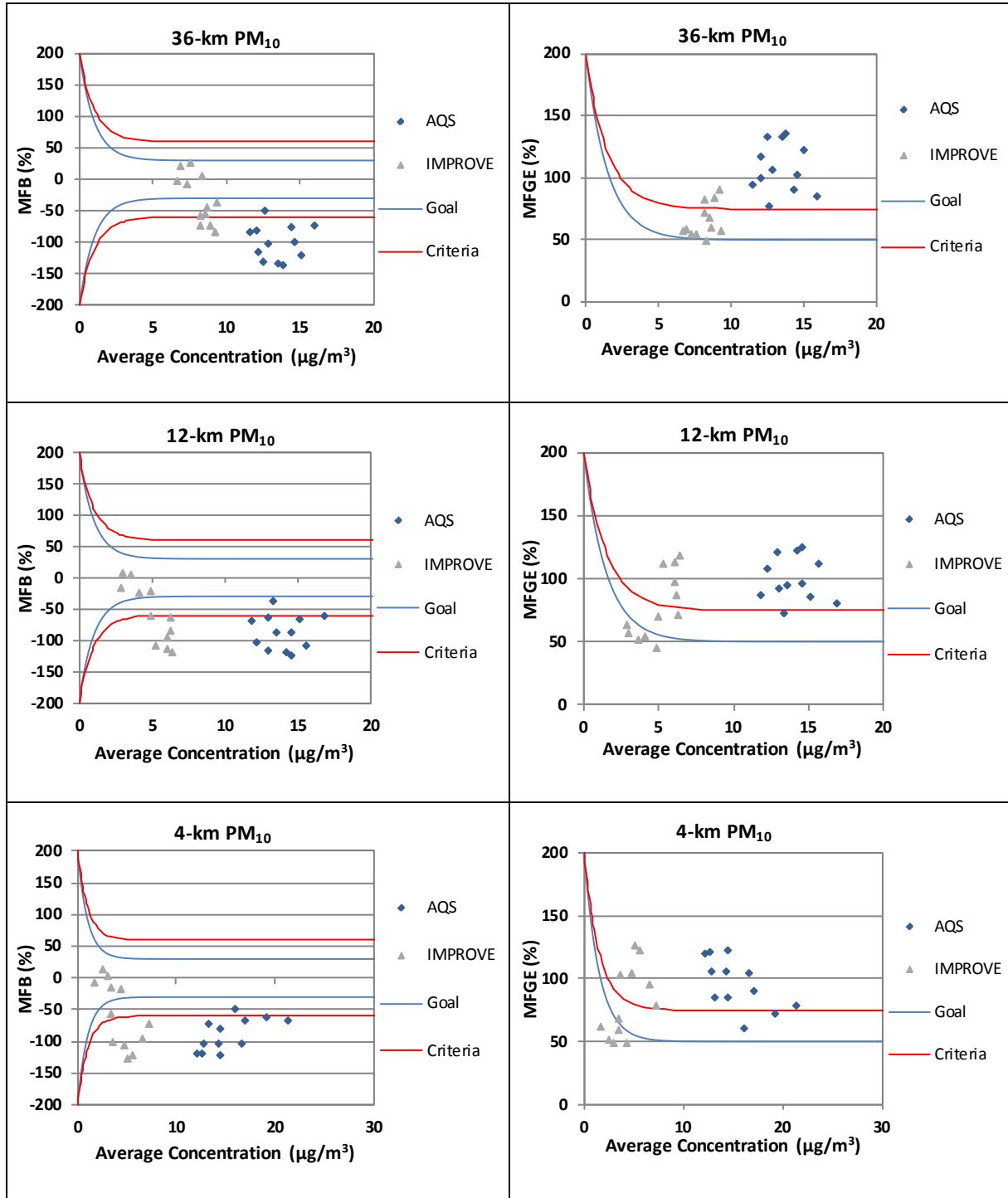
Note: Goals and criteria based on Boylan and Russell (2006) and accepted by USEPA (2007).

Figure 4.2-46   Bugle Plots of PM₁₀ (Daily) Monthly Mean Fractional Bias and Mean Fractional Gross Error
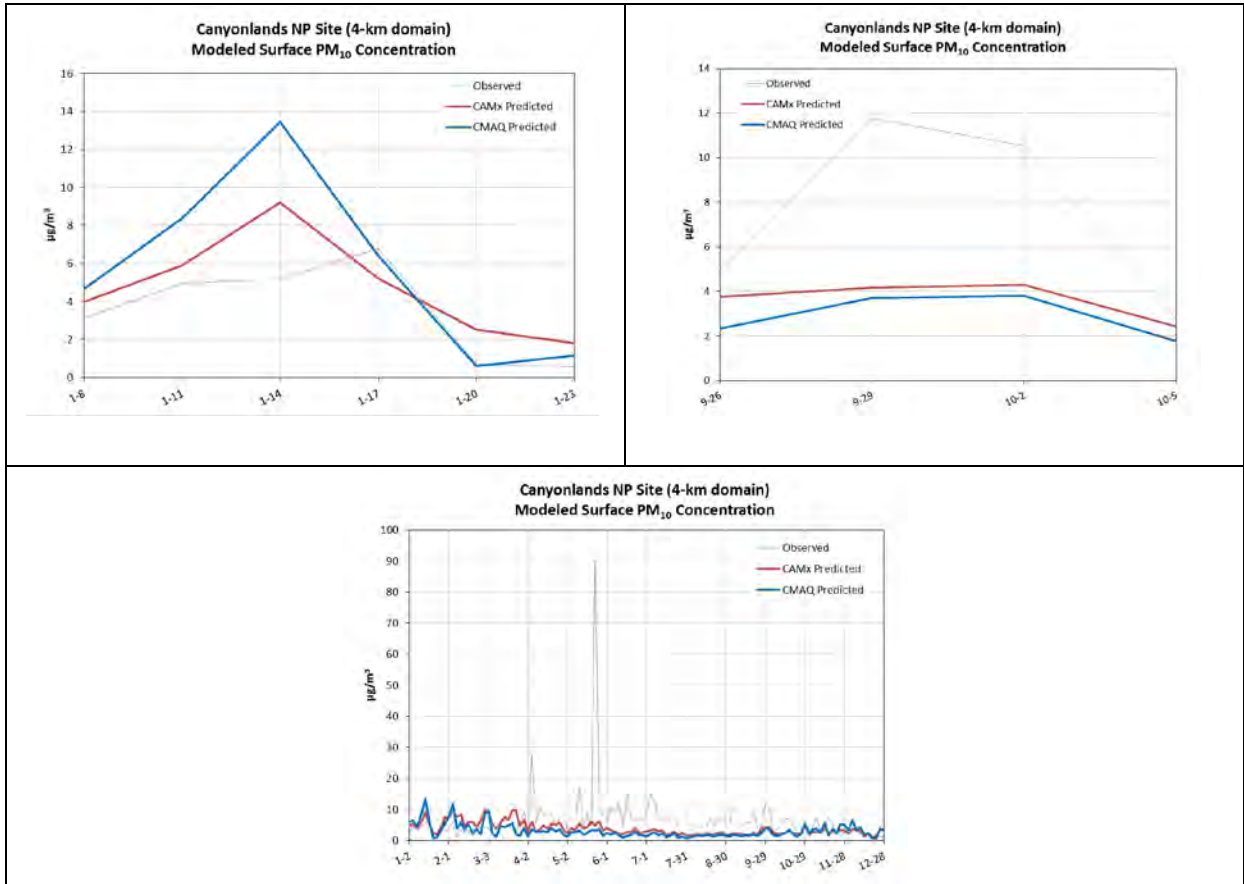
Figure 4.2-47   Time Series for PM$_{10}$ at the Canyonlands National Park IMPROVE Site (CANY1)

4.3   Other Gaseous Pollutants

4.3.1   Nitrogen Oxides

This section presents statistical and graphical results of the CMAQ model performance evaluation for nitrogen oxides. The full set of hourly NO_x model results was used to qualitatively assess model performance when evaluating time series and spatial performance.

4.3.1.1   Statistical Analyses for the 36-km, 12-km, and 4-km Domains

Various annual and seasonal model performance statistics for NO_x are shown in **Table 4.3-1** for the AQS monitoring network and each modeling domain. Mean observed and predicted NO_x concentrations are also shown in the table. Considering the NMB values displayed graphically in **Figure 4.3-1**, model performance is better in the 12-km and 4-km domains than in the 36-km domain. The figure also shows that the model under-predicts observed NO_x concentrations throughout the year in the 36-km domain. In the 12-km domain, the model under-predicts NO_x in all months except June and July. In the 4-km domain, the model under-predicts NO_x in the winter and fall, but over-predicts NO_x in the spring and summer. Some of the largest biases, in magnitude, in the 4-km domain occurred from April through July.

4.3.1.2   Time Series Analyses

Figure 4.3-2 to **Figure 4.3-6** present time series plots of hourly NO_x concentrations at selected sites in the Uinta Basin. The plots compare hourly average NO_x concentrations at four AQS monitoring sites with model-predicted NO_x concentrations for the model grid cells that contain those AQS monitors. As described in **Chapter 1**, NO_x model performance in the Uinta Basin was reviewed for four periods of interest (POI) in 2010. The monitoring sites selected for analysis include Dinosaur (AQS monitor 49-047-1002), Ouray (AQS monitor 49-047-2003), Rangely (AQS monitor 08-103-0006), and Redwash (AQS monitor 49-047-2002), all of which are shown in **Figure 3-1** relative to the Uinta Basin study area and model domains. The model-predicted values in each time series are shown in red (CAMx) and blue (CMAQ), while the monitored values are shown in grey. Ambient NO_x data were not available at Dinosaur throughout the year or at Rangely during the winter POIs. The CAMx model results are discussed briefly in the model inter-comparison presented below, while only the CMAQ results are summarized here.

During POI 1 (shown in **Figure 4.3-2**), observed NO_x concentrations at Ouray and Redwash generally ranged between 15 and 40 ppb, with lower concentrations observed after January 21 as the ozone episode was ending. CMAQ generally under-predicted NO_x concentrations at both Ouray and Redwash, although modeled NO_x concentrations were typically higher and therefore closer to observations at Ouray than at Redwash. On January 17 at Ouray, when ozone concentrations peaked above 120 ppb, the model performed particularly well for NO_x. At Redwash, although ozone concentrations on January 17 also exceeded 100 ppb, the model performed poorly with respect to both NO_x and ozone.

During POI 2 (shown in **Figure 4.3-3**), observed NO_x concentrations at Ouray and Redwash ranged from 10 to 20 ppb, with occasional spikes above 20 ppb. As was the case for POI 1, during POI 2 NO_x model performance was better at Ouray than at Redwash. The model still consistently under-predicted NO_x concentrations at Redwash, but the model performed reasonably well at Ouray with peak daily NO_x concentrations often in the 10 to 20 ppb range. Coincidently, there were many days in POI 2 when both modeled and observed ozone concentrations exceeded 100 ppb at Ouray. However, on March 3 and 4, CMAQ under-predicted NO_x concentrations at Ouray, while significantly under-predicting enhanced ozone concentrations.

During both POI 3 and 4 (shown in **Figures 4.3-4** and **4.3-5**, respectively), CMAQ generally over-predicted peak nighttime NO_x concentrations at Ouray, and under-predicted peak nighttime NO_x

concentrations at Redwash. During the afternoon hours, the model performed well at all Uinta Basin sites, as both modeled and observed NO_x concentrations were generally below 5 ppb.

4.3.1.3   Spatial Analyses

The spatial performance of modeled NO_x was reviewed for POI 1 and 3. **Figure 4.3-7** shows contour plots of 1-hour NO_x concentrations predicted by CMAQ at 21:00 UTC (14:00 MST) for the 4-km domain during POI 1. Corresponding monitored concentrations from the AQS network are shown in the figure as filled circles. The plots show enhanced NO_x concentrations in the Salt Lake City urban area, the Uinta Basin, and the Four Corners region. The observed spatial extent of the enhanced NO_x concentrations in Salt Lake City and Uinta Basin tends to be larger than predicted by the model, suggesting the emissions sources in these regions might not be spatially allocated correctly. The plots also show the model's tendency to under-predict NO_x concentrations in the Uinta Basin study area. **Figure 4.3-8** shows similar spatial plots for selected days during POI 3 at 21:00 UTC (15:00 MDT). Consistent with the low predicted and observed afternoon NO_x concentrations shown by the Uinta Basin time series analyses, these summertime spatial plots show that the model performed well in afternoon during this POI.

4.3.1.4   Summary of CMAQ Model Performance for Nitrogen Oxides

In general, the CMAQ model performs reasonably well for NO_x. Performance tends to be better on the 12-km and 4-km domains, compared to the 36-km domain.

- Model results for NO_x show reasonable performance for all modeling domains, monitoring networks and seasons on a domain-wide basis.
- On the 4-km domain, the model under-predicts NO_x in the winter and fall and over-predicts NO_x in the spring and summer.
- Model bias tends to be smaller in summer and larger in winter on the 36-km and 12-km domains, while bias tends to be larger in late spring and early summer on the 4-km domain.
- In the Uinta Basin during winter, the model consistently under-predicts NO_x concentrations although performance is better at the Ouray site than at Redwash. During summer, the model generally over-predicts peak nighttime NO_x concentrations at Ouray, under-predicts peak nighttime NO_x concentrations at Redwash, and performs well in the afternoon at both sites.
- During winter the spatial extent of model-predicted elevated NOx concentrations are not as wide-spread as suggested by observations, but good spatial agreement with afternoon observations is apparent in summer when NO_x concentrations are low.

4.3.1.5   Comparison of CMAQ and CAMx Results

Figure 4.3-9 presents a comparison of monthly NMB statistics for all three CMAQ and CAMx modeling domains for the AQS monitoring network. Both models perform reasonably well for NO_x on a domain-wide basis. They under-predict NO_x concentrations throughout the year in the 36-km domain, while they typically under-predict NO_x concentrations during the fall and winter months, and over-predict NO_x in during the summer months in the 12-km and 4-km domains. Biases are somewhat larger in CMAQ than in CAMx throughout the year in the 36-km domain, as well as in the 12-km domain for all seasons except summer. In the 4-km domain, CMAQ tends to over-predict NO_x concentrations to a lesser extent than CAMx during the spring and summer months, while the magnitude of biases in CMAQ predictions is somewhat larger than in CAMx for fall and winter. The largest model biases in NO_x concentrations are in the CAMx 4-km domain from April through July.

Table 4.3-1   Model Performance Statistical Summary for Nitrogen Oxides

Monitoring Network	Statistics (percent)/ Concentration (parts per million [ppm])	36-km Domain					12-km Domain					4-km Domain				
		Annual	Winter	Spring	Summer	Fall	Annual	Winter	Spring	Summer	Fall	Annual	Winter	Spring	Summer	Fall
AQS (Hourly)	MFB	-25	-25	-26	-21	-28	-2	-23	6	8	0	7	-19	22	15	7
	MFGE	91	85	95	92	92	95	94	98	94	95	83	82	87	82	80
	MNB	24	25	14	31	25	28	20	27	31	37	83	70	101	77	86
	MNGE	103	98	97	110	106	100	100	98	96	107	136	136	148	125	137
	NMB	-33	-40	-31	-17	-34	-23	-36	-12	1	-22	-10	-27	15	31	-14
	NME	76	72	77	79	78	74	72	75	75	74	80	74	93	95	75
	R^2	0.165	0.183	0.150	0.143	0.122	0.230	0.210	0.224	0.246	0.203	0.191	0.129	0.136	0.183	0.232
	Observed Mean Concentration (ppm)	0.013	0.020	0.010	0.007	0.014	0.014	0.024	0.009	0.008	0.014	0.015	0.032	0.011	0.007	0.013
	Predicted Mean Concentration (ppm)	0.008	0.012	0.007	0.006	0.009	0.010	0.016	0.008	0.008	0.011	0.014	0.023	0.012	0.009	0.011

1

2
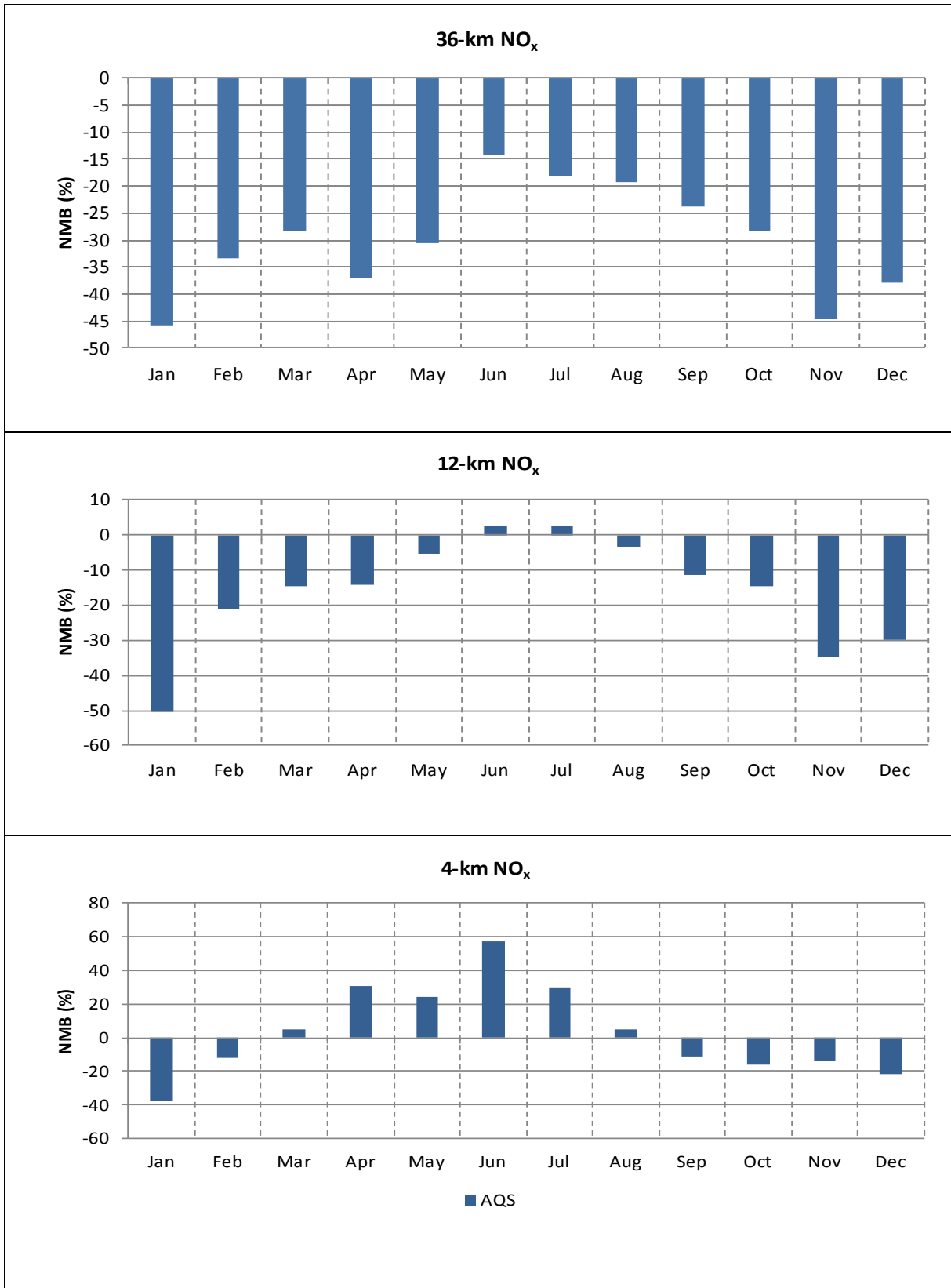
Figure 4.3-1   Monthly Normalized Mean Bias for Nitrogen Oxides
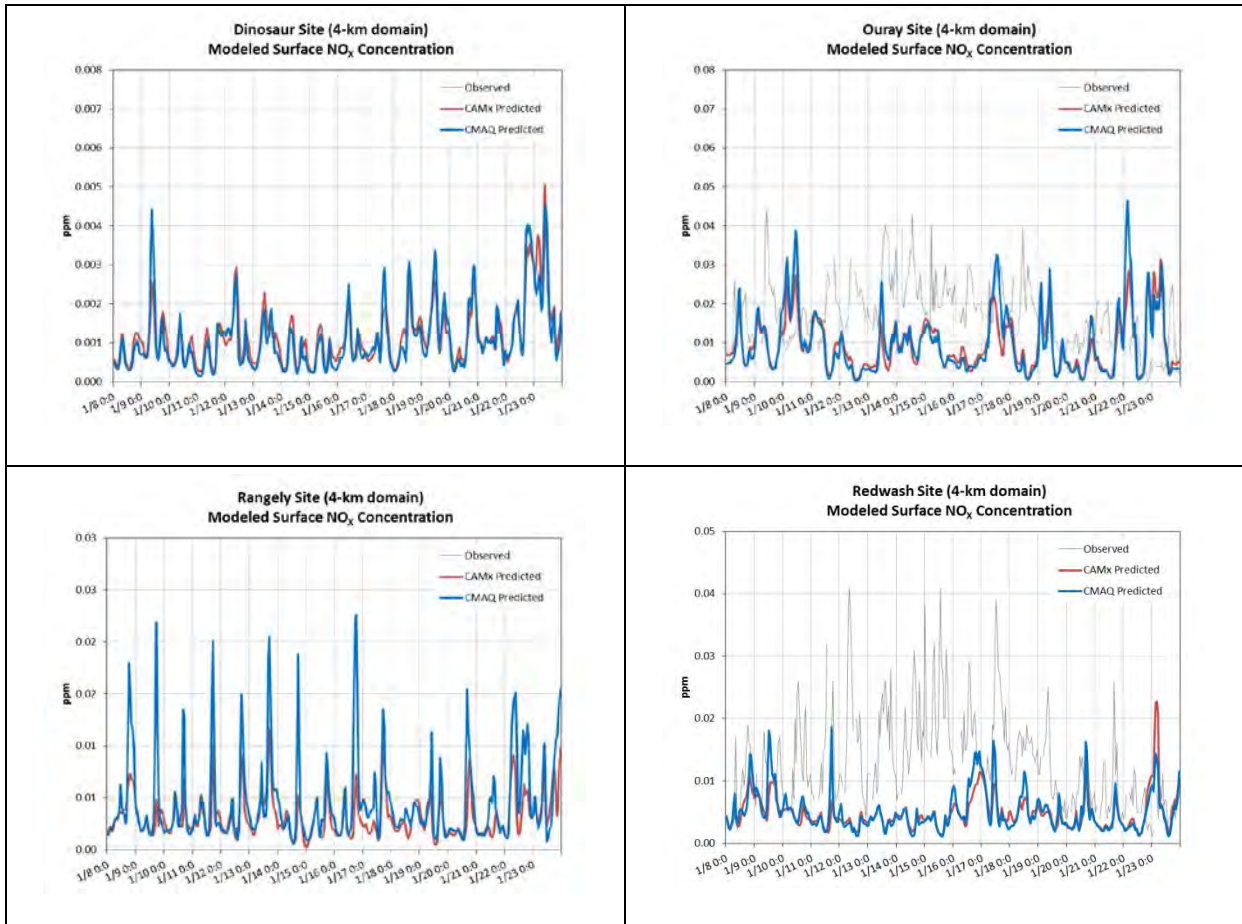
Figure 4.3-2   Time Series for Nitrogen Oxides at Selected AQS Sites from January 8 to January 23, 2010
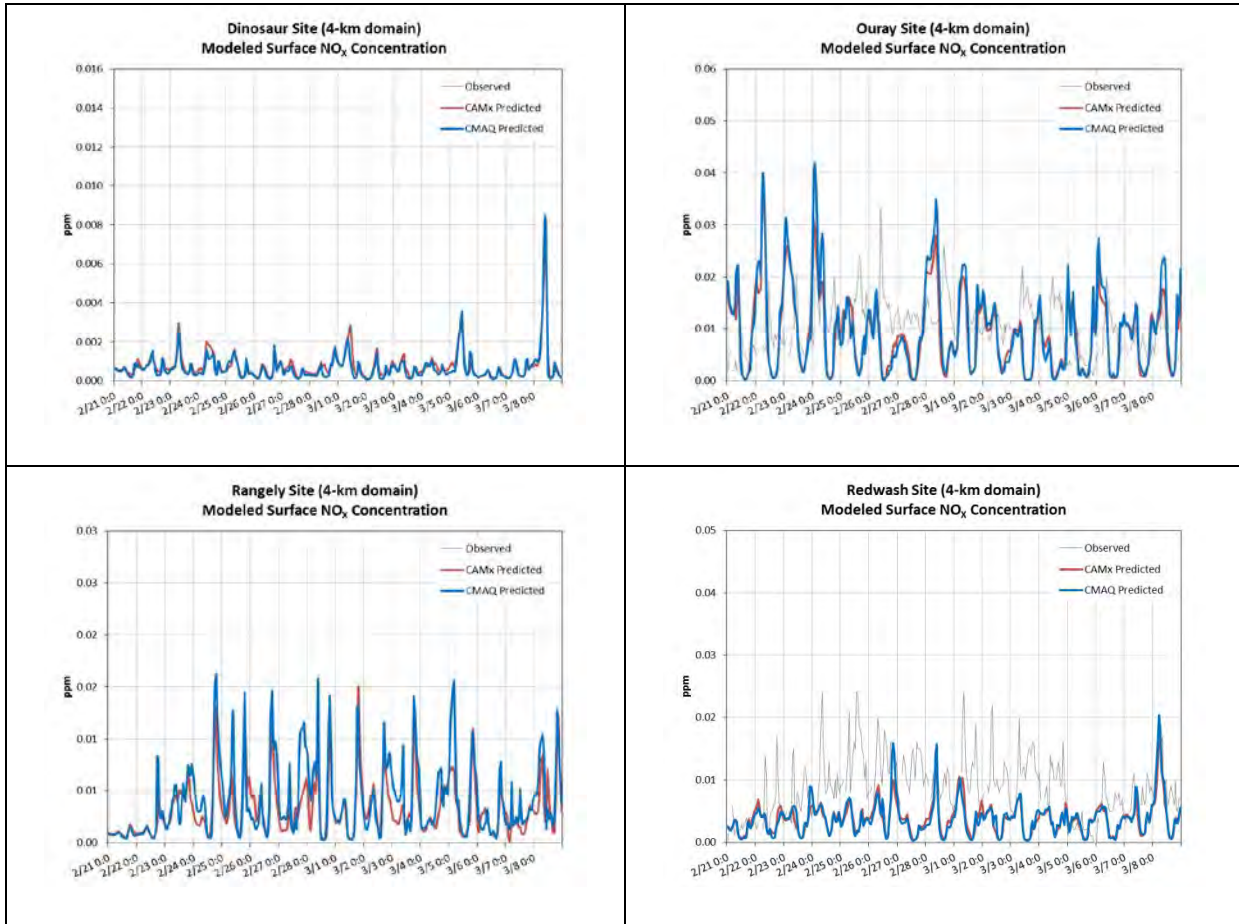
Figure 4.3-3   Time Series for Nitrogen Oxides at Selected AQS Sites from February 21 to March 8, 2010
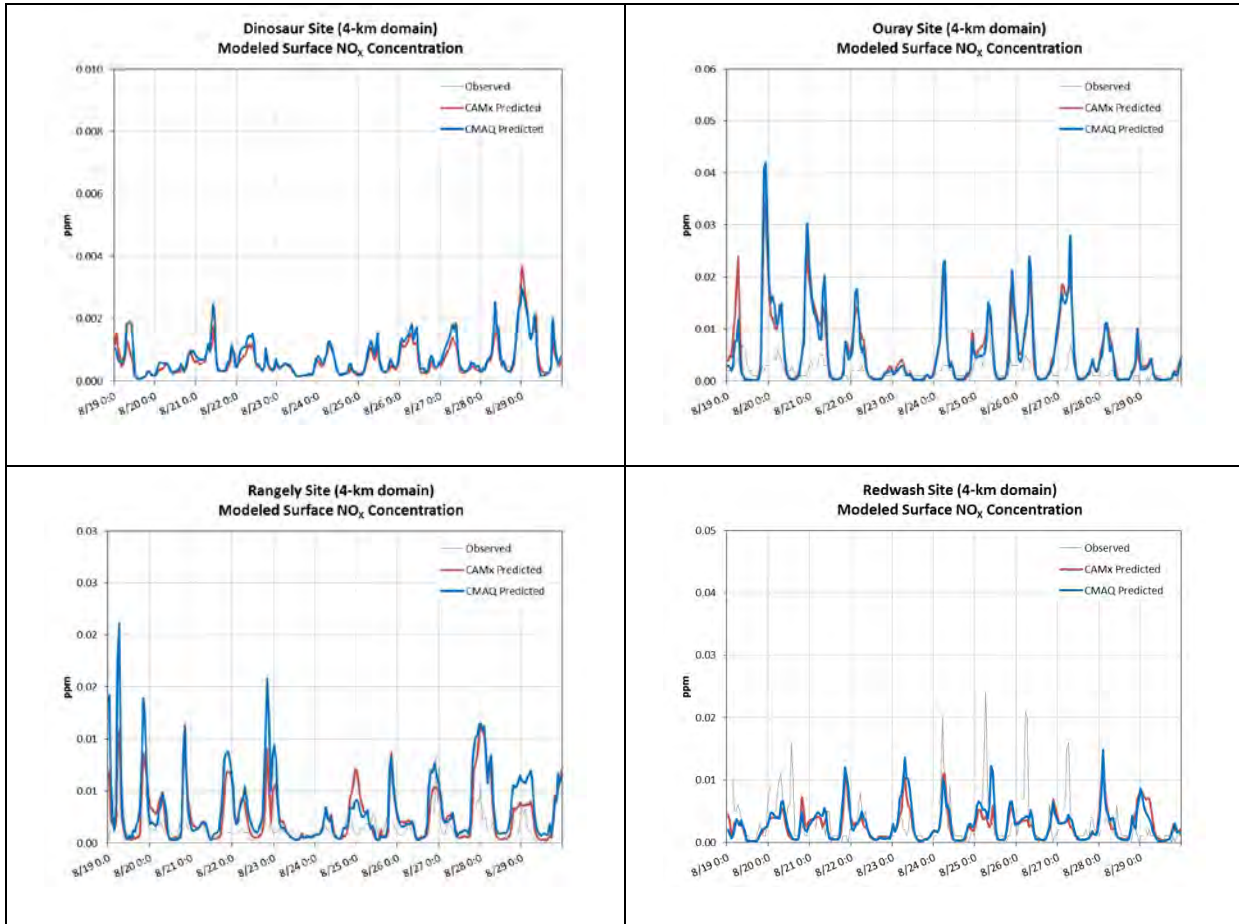
Figure 4.3-4   Time Series for Nitrogen Oxides at Selected AQS Sites from August 19 to August 29, 2010
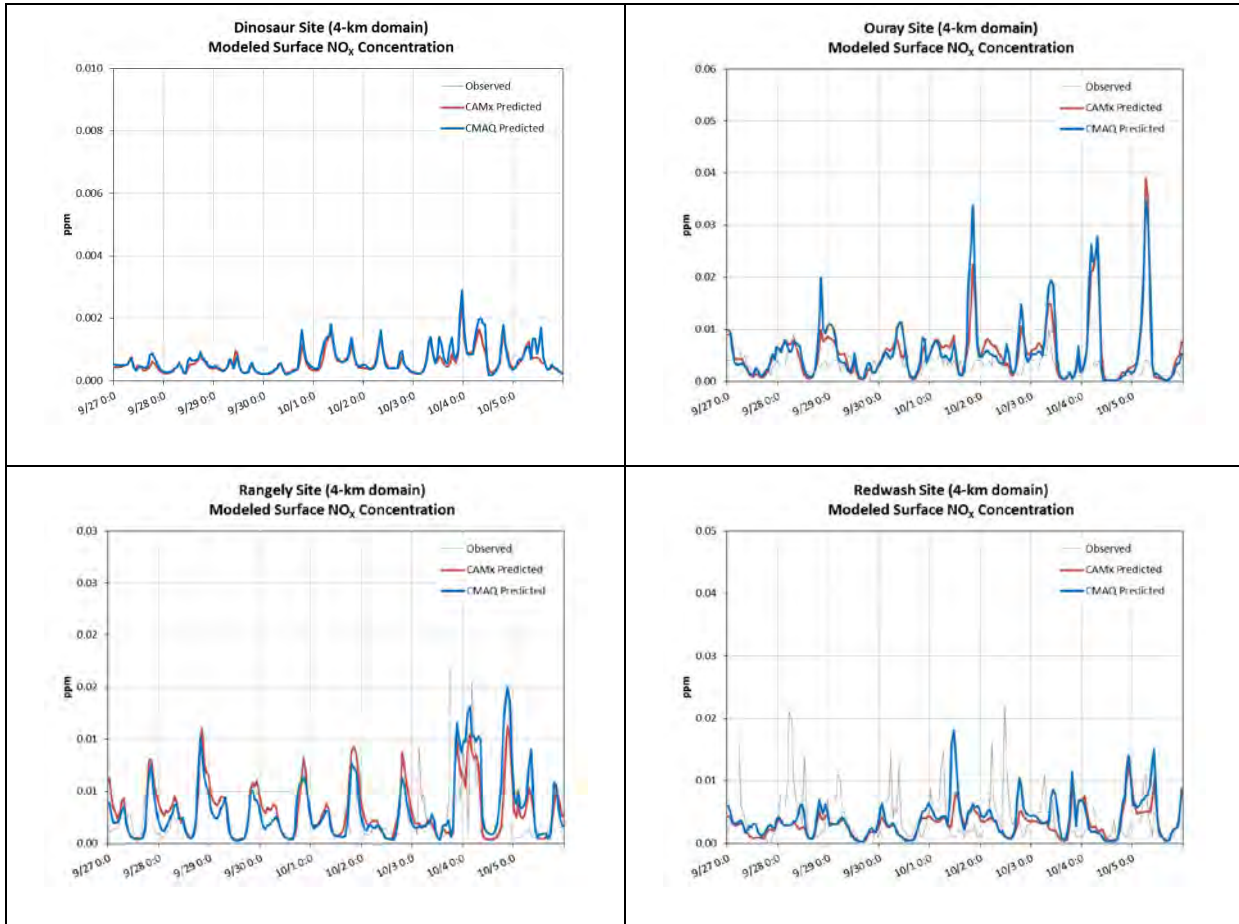
Figure 4.3-5   Time Series for Nitrogen Oxides at Selected AQS Sites from September 27 to October 5, 2010
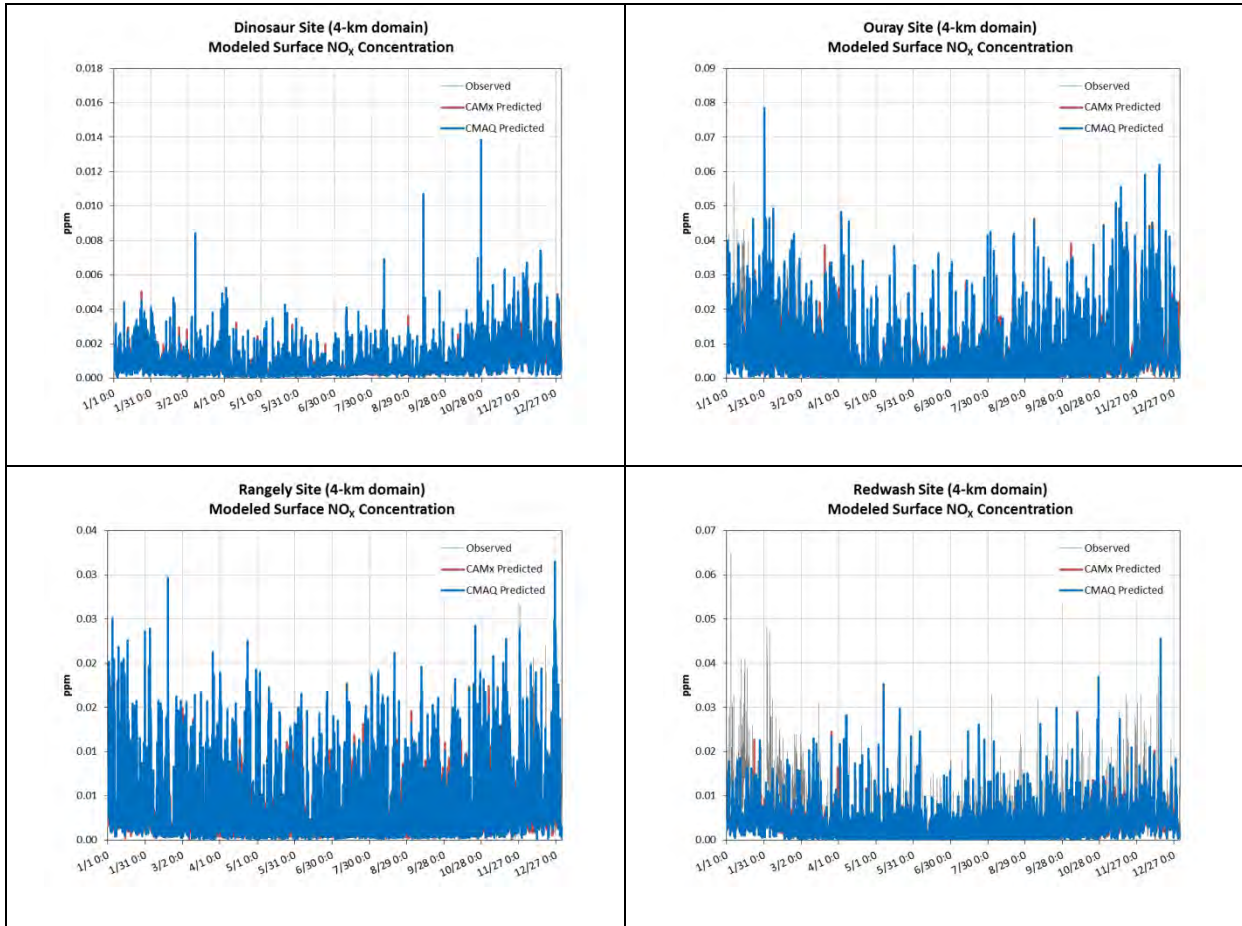
Figure 4.3-6   Annual Time Series for Nitrogen Oxides at Selected AQS Sites

Figure 4.3-7   4-km Spatial Plots for Nitrogen Oxides during January 8 to January 23, 2010
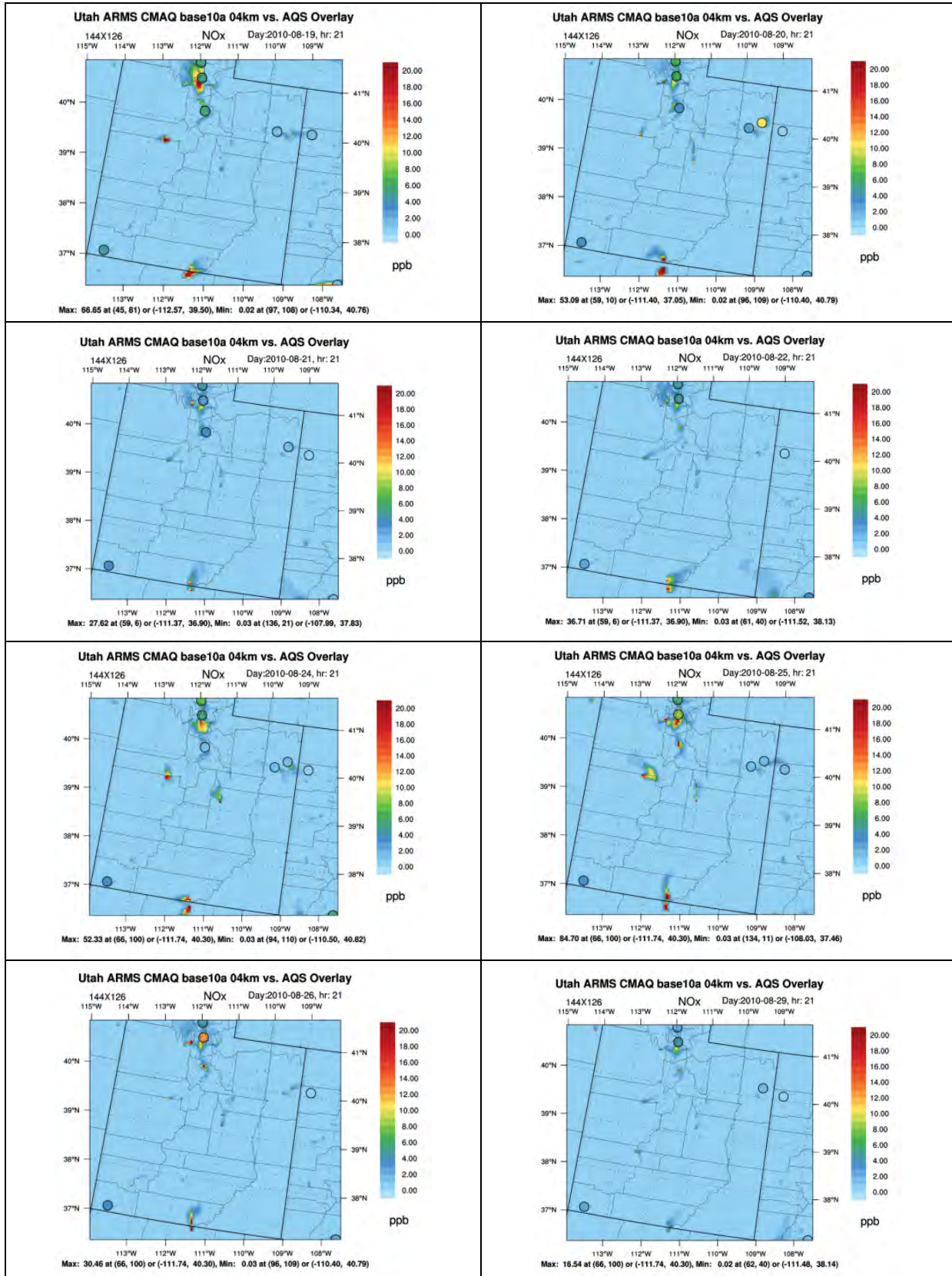
Figure 4.3-8   4-km Spatial Plots for Nitrogen Oxides during August 19 to August 29, 2010
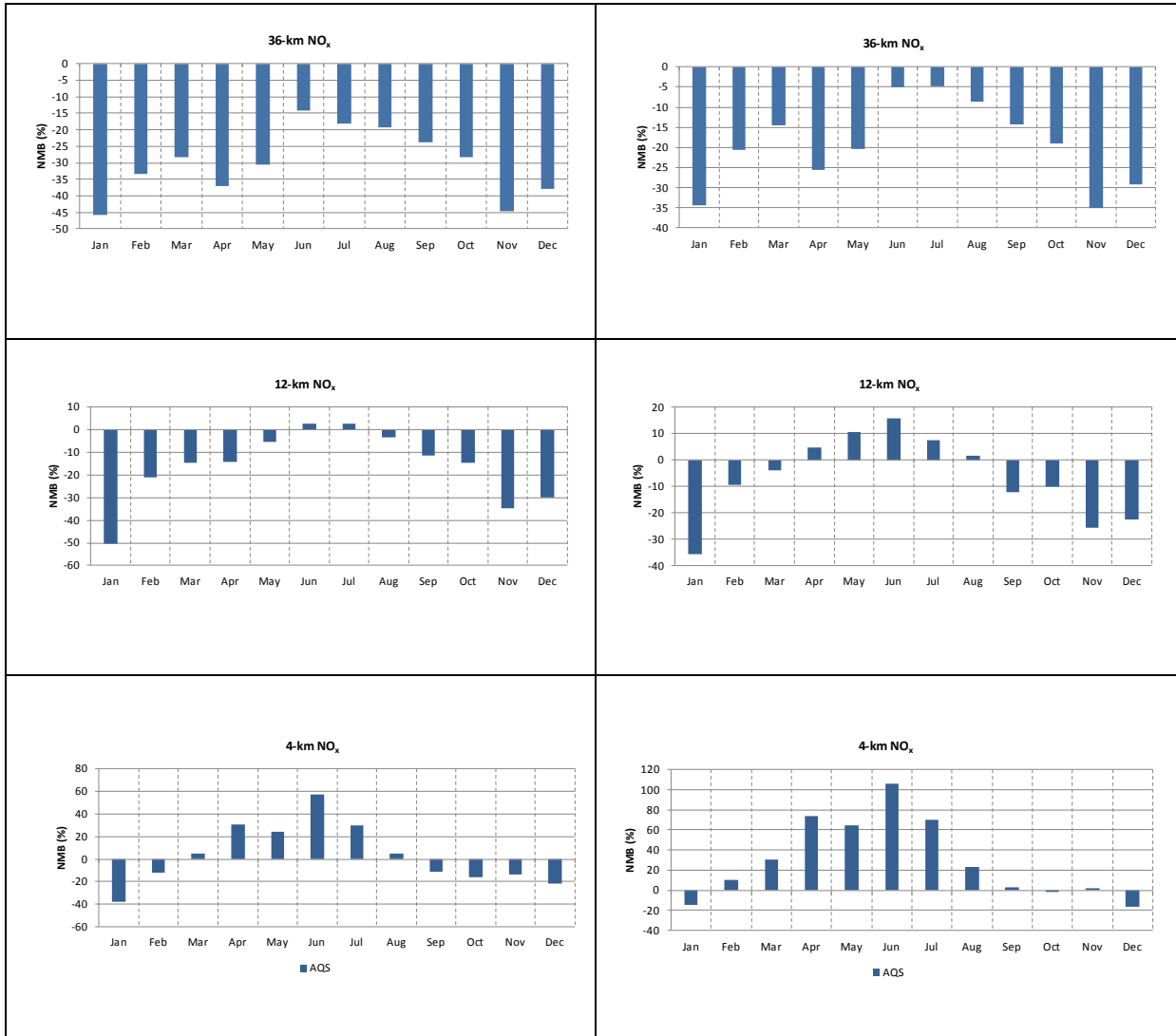
Figure 4.3-9 Monthly Normalized Mean Bias for Nitrogen Oxides for CMAQ (left) and CAMx (right)

4.3.2   Carbon Monoxide

The following sections present an analysis of the model performance for CO using statistical, time series, and spatial analyses.

4.3.2.1   Statistical Analyses for the 36-km, 12-km, and 4-km Domains

Annual and seasonal CO statistical summaries are presented in **Table 4.3-2** relative to the AQS network for each modeling domain. A more detailed assessment of the NMB is presented for each month in **Figure 4.3-10**.

In general, the model tends to under-predict CO throughout the year for the 36-km, 12-km, and 4-km modeling domains. For all modeling domains, the NMB is smaller in the summer than other seasons; however, the MNGE is larger in the summer than during other seasons. The NME remains relatively constant throughout the year, being only slightly smaller in the spring.

It is important to note that the statistics for the 4-km domain were calculated relative to unevenly distributed AQS monitors. These monitors include a densely located group in the Salt Lake City area, a monitor in Grand Junction, Colorado, and a monitor near Ignacio, Colorado on the edge of the 4-km domain. The model performance for CO in the study area may not be adequately represented by these monitors. However, it also is important to note that the model performance for CO has no effect on the photochemistry and resulting performance of other pollutants.

4.3.2.2   Time Series Analyses

Time series comparing hourly CO observations recorded at the Grand Junction, Colorado monitoring station (08-077-0018) to model results are shown in **Figure 4.3-11**. The figure presents the hourly average model-predicted CO concentrations for the grid cell that contains the AQS monitor for annual and POI time series. The model values are shown in red and blue for the 4-km results. The monitored hourly average CO concentrations are shown in gray.

In general, the model under-predicts CO concentrations for most of the year in the 4-km domain. Observations suggest a seasonal pattern for CO levels with elevated CO concentrations during the fall and winter and smaller concentrations in the spring and summer. Throughout the year, the magnitude of the modeled concentrations is lower than observations though the model captures some seasonal variation. Modeled CO also suggests two daily peaks in CO concentrations though this is not consistently observed in observations.

4.3.2.3   Spatial Analyses

The CO spatial performance is reviewed for two POIs: January 8 to January 23, 2010 and August 19 to August 29, 2010. **Figure 4.3-12** shows the modeled 1-hour average CO concentration at hour 21 (2 PM MST) for January 8, 11, 13, 15, 18, and 23. **Figure 4.3-13** shows the modeled 1-hour average CO concentration at hour 21 (3 PM MDT) for August 19, 21, 23, 25, 27, and 29. Monitored 1-hour average CO concentrations from the AQS network are shown in the figure as circles. Throughout both POIs in the 4-km domain, modeled concentrations indicate elevated levels of CO near the Salt Lake City area with relatively low levels throughout the rest of Utah and the 4-km domain. Though monitors are not available throughout the 4-km domain, the monitors near Salt Lake City, in the less urbanized Grand Junction, Colorado (AQS site 08-077-0018) and in the rural area near Ignacio, Colorado (AQS site 08-067-7001) all indicate a general under-prediction of CO by the model.

4.3.2.4   Summary of Model Performance for Carbon Monoxide

In general, the model tends to under-predict CO throughout the year for the 36-km, 12-km, and 4-km modeling domains.

- The NMB shows a general seasonal pattern for all modeling domains with the largest biases occurring in the winter and smallest in the summer.
- The modeled time series results for the Grand Junction AQS site tend to follow the seasonal trends in observations; however, the model under-predicts values by over 0.2 ppm, on average, throughout the year.
- Modeled spatial plots of CO concentrations over two POIs indicate elevated CO concentrations in the Salt Lake City area and relatively low concentrations throughout the rest of the 4-km domain. Sparsely located monitors, however, indicate a general under-prediction of CO by the model throughout the 4-km domain.

4.3.2.5 Comparison of CMAQ and CAMx Results

The complete set of the CAMx MPE tables, bar charts, and spatial plots is found in **Appendix B**. Both models under-predict CO concentrations throughout the year in all modeling domains. Biases in CO concentration predictions are larger in CMAQ than in CAMx throughout the year in all modeling domains. Both models have the largest biases and errors during the winter months.

Table 4.3-2   Model Performance Statistical Summary for Carbon Monoxide

Monitoring Network	Statistics (percent)/ Concentration (parts per million [ppm])	36-km Domain					12-km Domain					4-km Domain				
		Annual	Winter	Spring	Summer	Fall	Annual	Winter	Spring	Summer	Fall	Annual	Winter	Spring	Summer	Fall
AQS (Hourly)	MFB	-43	-59	-34	-32	-44	-27	-42	-16	-18	-30	-30	-48	-34	-4	-34
	MFGE	75	82	68	71	78	68	73	61	69	70	68	70	60	73	70
	MNB	-12	-27	-18	4	-6	-6	-22	-8	7	1	-9	-25	-17	18	-9
	MNGE	70	68	56	80	78	63	58	50	72	72	62	57	52	77	65
	NMB	-49	-58	-42	-39	-48	-37	-48	-26	-26	-36	-35	-39	-33	-19	-40
	NME	63	67	58	59	64	60	63	54	59	60	58	58	53	63	58
	R^2	0.066	0.050	0.047	0.033	0.079	0.092	0.074	0.086	0.036	0.115	0.124	0.065	0.069	0.024	0.097
	Observed Mean Concentration (ppm)	0.40	0.54	0.32	0.29	0.41	0.39	0.54	0.31	0.28	0.40	0.40	0.62	0.35	0.25	0.38
	Predicted Mean Concentration (ppm)	0.20	0.23	0.19	0.17	0.21	0.25	0.28	0.23	0.21	0.26	0.26	0.38	0.23	0.20	0.23
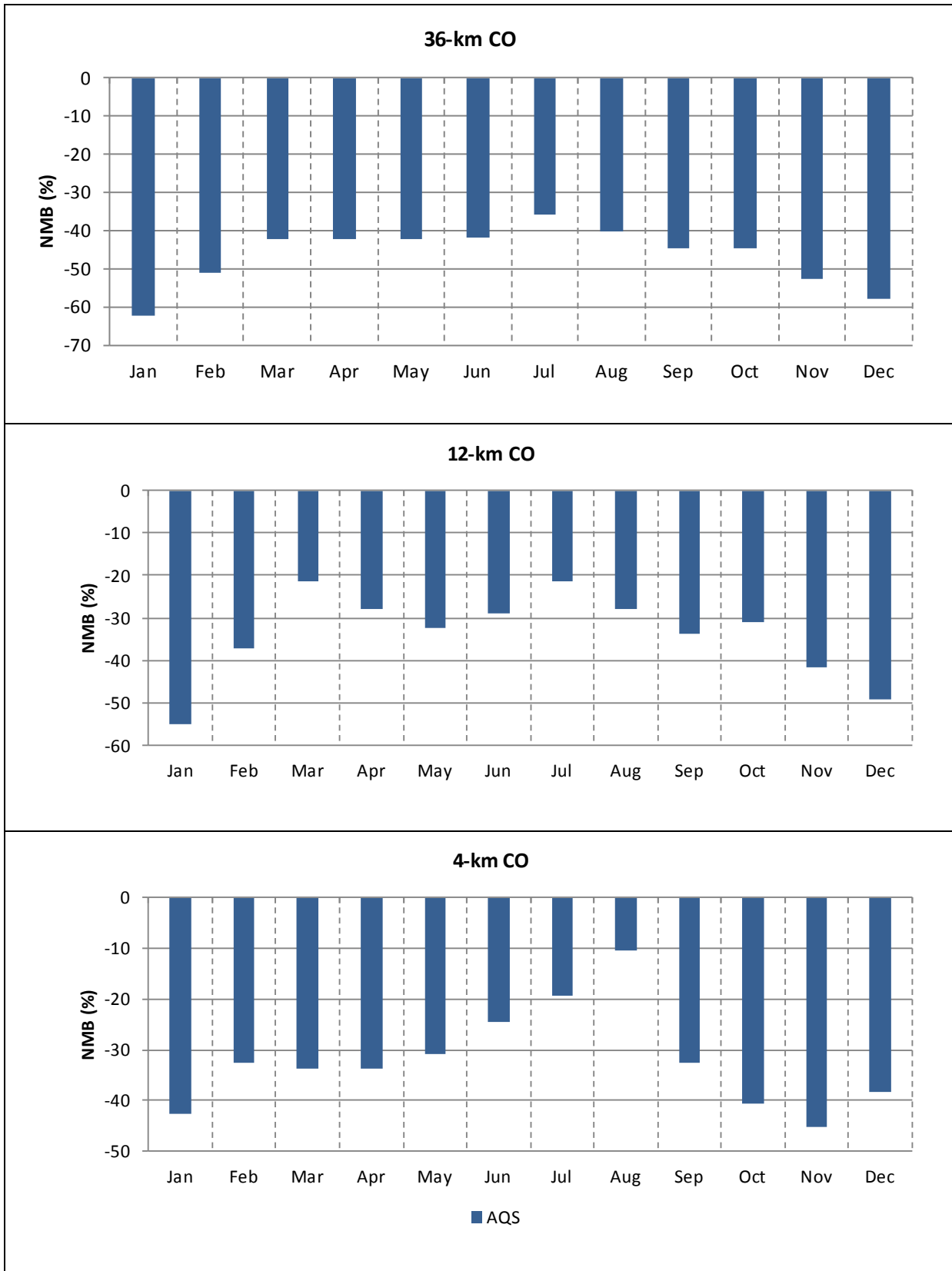
Figure 4.3-10   Monthly Normalized Mean Bias for Carbon Monoxide
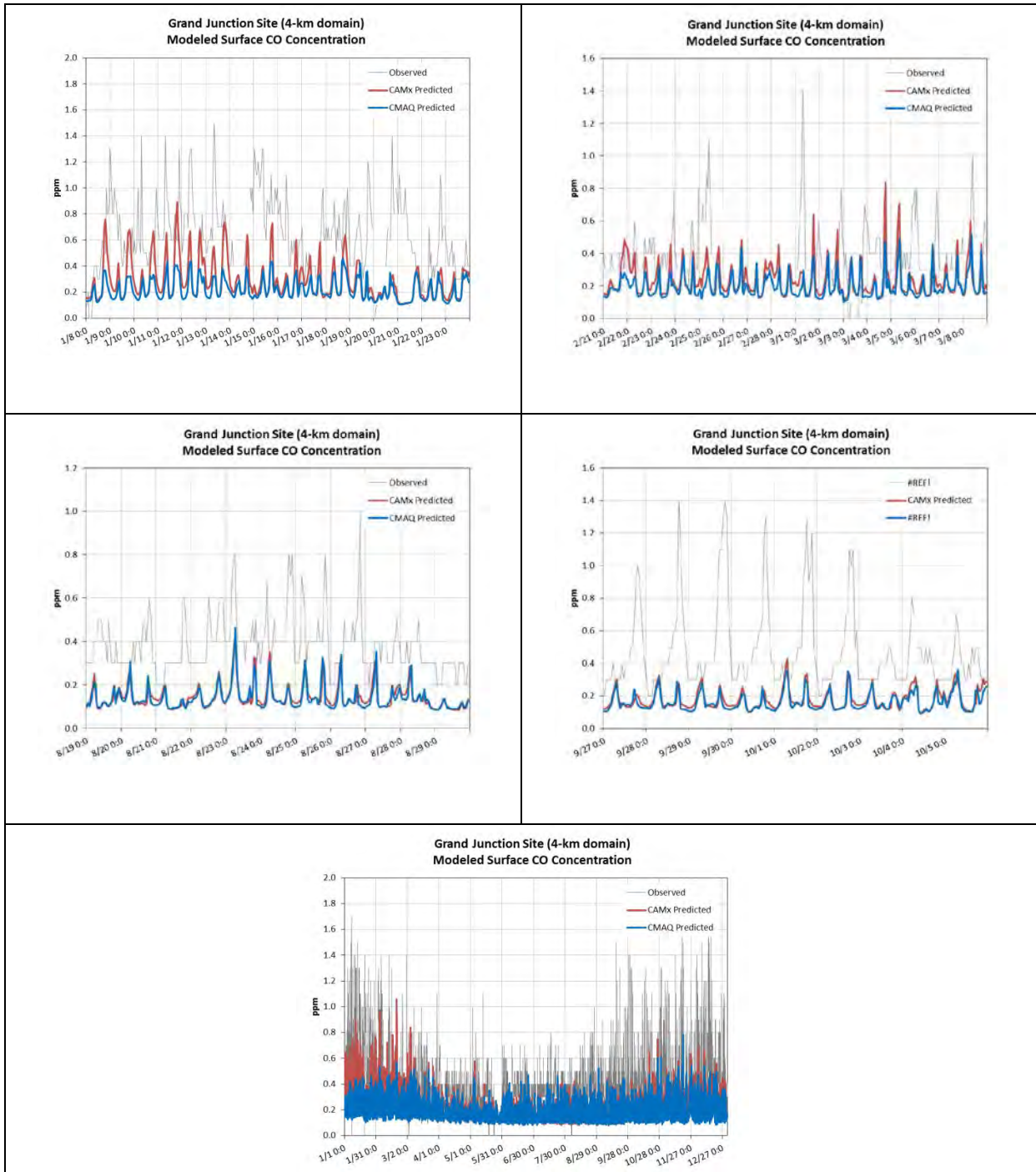
Figure 4.3-11   Time Series for Carbon Monoxide at the Grand Junction, Colorado AQS Site (08-077-0018)
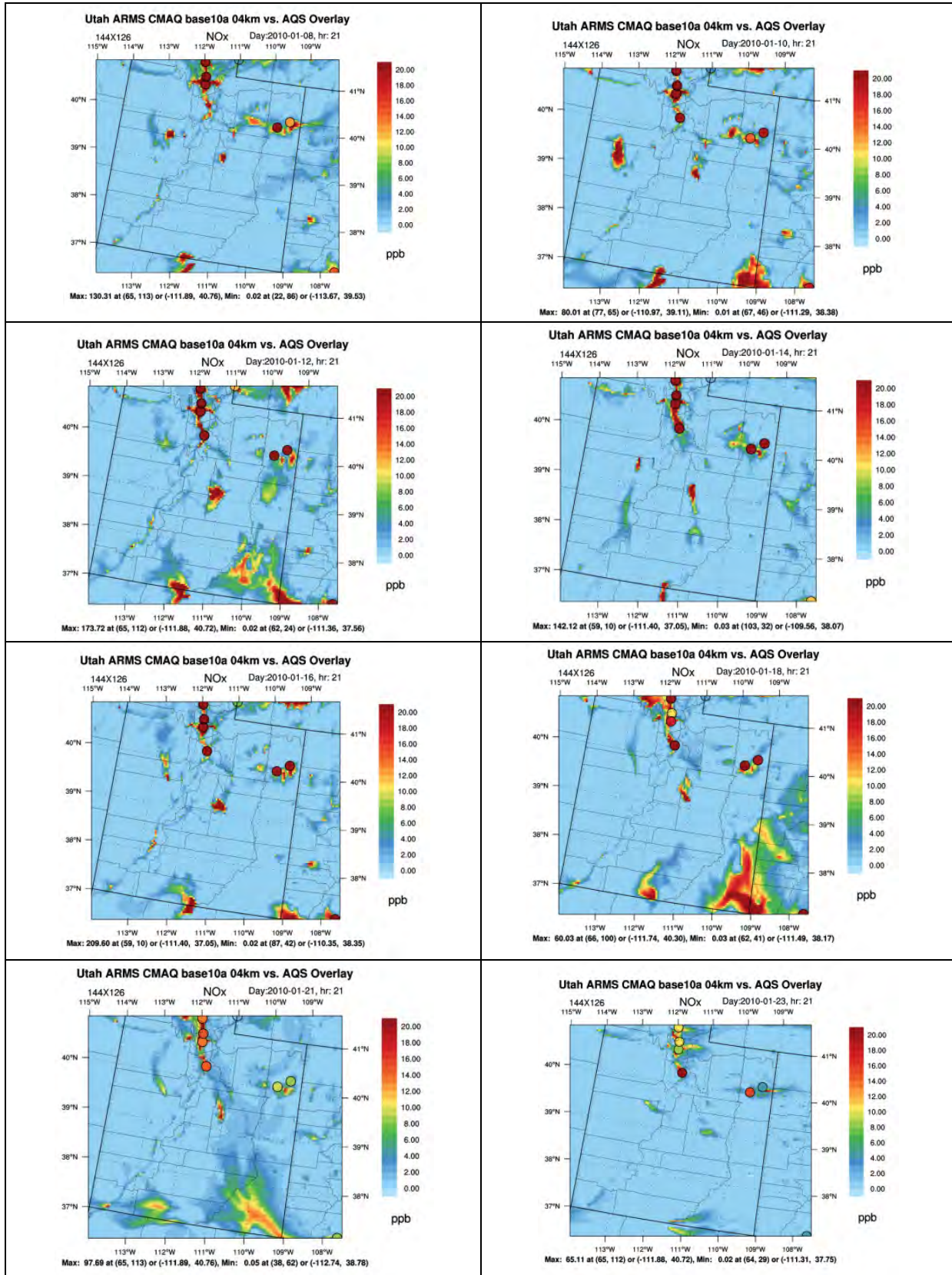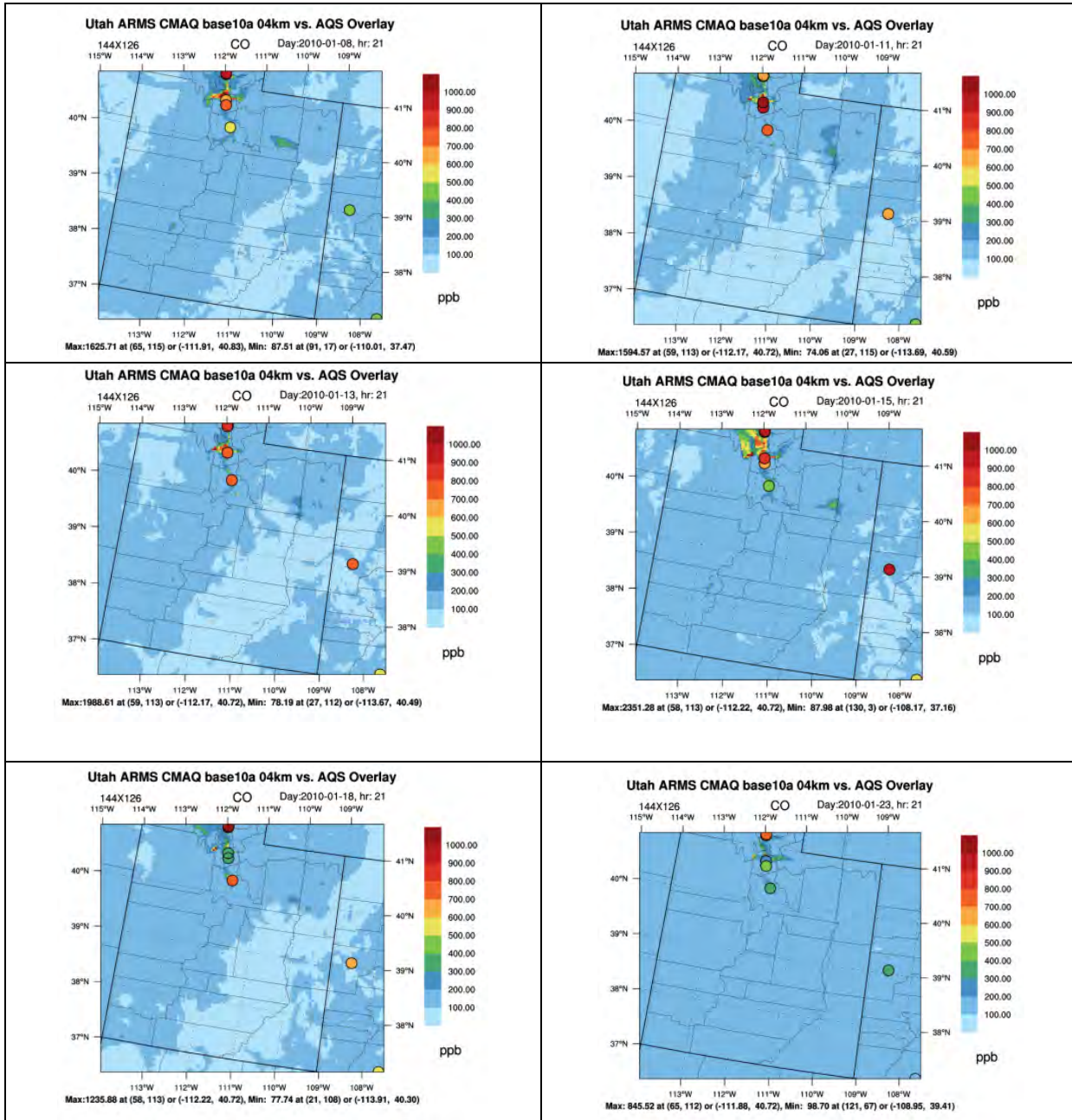
Figure 4.3-12   4-km Spatial Plots for Carbon Monoxide during January 8 to January 23, 2010
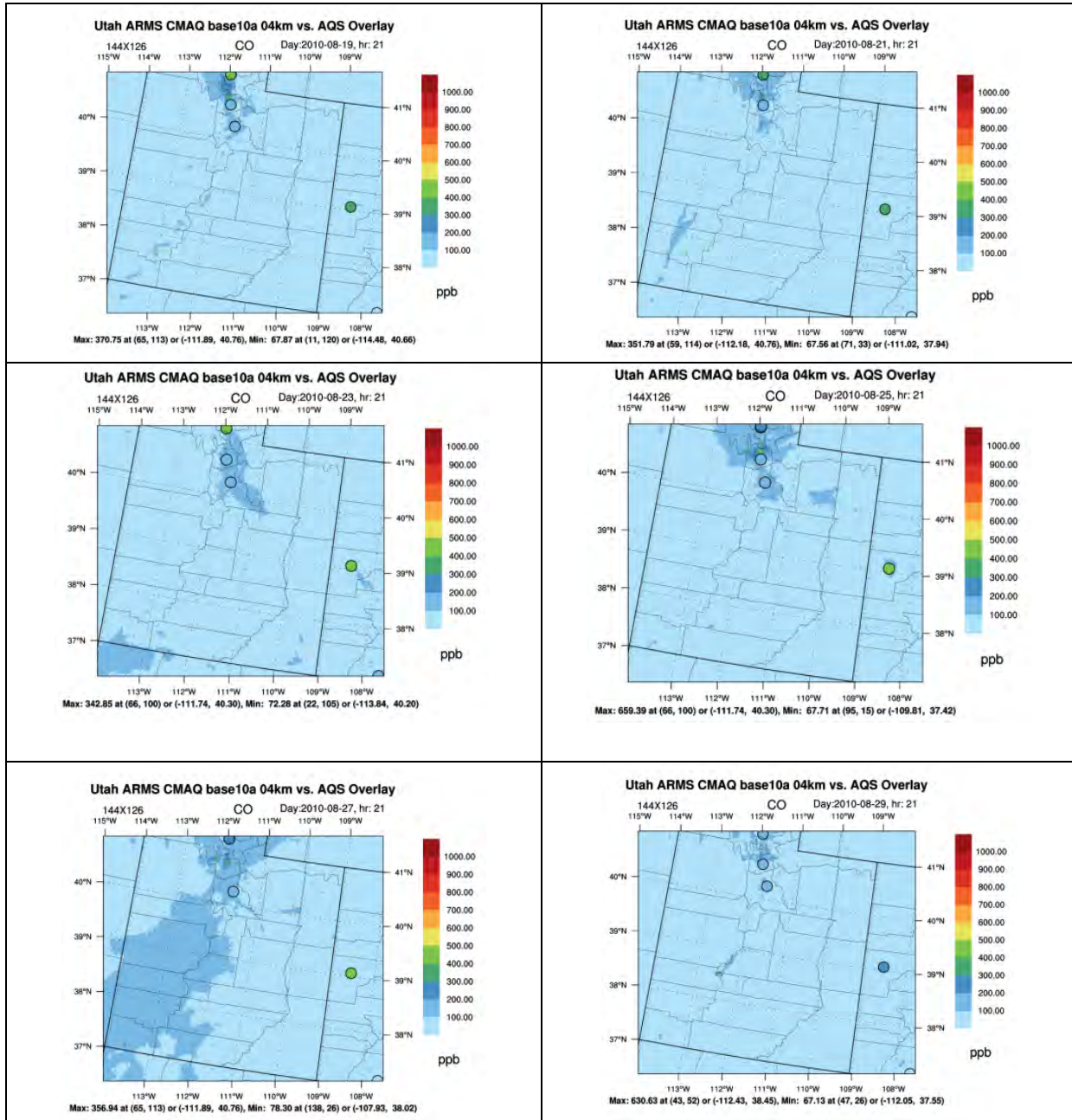
**Figure 4.3-13   4-km Spatial Plots for Carbon Monoxide during August 19 to August 29, 2010**

4.3.3 Sulfur Dioxide

The following sections present an analysis of the model performance for SO$_2$ using statistical, time series, and spatial analyses.

4.3.3.1 Statistical Analyses for the CMAQ 36-km, 12-km, and 4-km Domains

Annual and seasonal SO$_2$ statistical summaries are presented in **Table 4.3-3** for each monitoring network and modeling domain. A more detailed assessment of the NMB is presented for each month in **Figure 4.3-14**.

The SO$_2$ statistical results vary depending on the network. Large variability between networks is more an indication of different measurement techniques and network objectives than an indication of differing model performance. The 36-km domain NMB results suggest that the model over-predicts SO$_2$ concentrations in the winter while under-predicting concentrations throughout the rest of the year relative to the AQS network. The NMB is positive for the winter months for all modeling domains. In the 12-km domain, some seasonal variation in model performance also is observed relative to the AQS network, though no seasonal pattern is evident in the 4-km domain. Errors relative to the AQS network remain relatively constant throughout the year in each modeling domain with no seasonal pattern evident.

Model results for CASTNet, however, have large positive biases, indicating model over-prediction, throughout the year for all modeling domains. The NMB in **Figure 4.3-14** indicates some seasonal variability in the 12-km and 4-km domain model performance for CASTNET, larger biases occurring in the fall and winter and smaller in the spring and summer. The NMB for January, however, in the 12-km and 4-km domains has anomalously low values compared to most other months of the year. While the magnitudes of the CASTNet biases are much larger than AQS, the magnitudes of the errors are similar to AQS.

4.3.3.2 Time Series Analyses

Figure 4.3-15 presents annual and POI time series comparing hourly SO$_2$ observations to model results at a Salt Lake City monitor location (AQS site 49-035-0012). The figure presents the hourly average model-predicted SO$_2$ concentrations for the grid cells that contain the selected monitor site. Sulfur dioxide results were not selected for the output files when CAMx was run, therefore, only CMAQ model results are shown. The model values are shown in blue, and observations are shown in gray.

Based on the time series in **Figure 4.3-15**, the model does not systematically over-predict or under-predict SO$_2$ concentrations consistently during the year relative to this AQS monitor. There is no clear seasonal or diurnal SO$_2$ trend in the monitoring data or in modeled results, which indicates both the relatively short atmospheric lifetime of SO$_2$ as well as the proximity of this AQS monitor to urban SO$_2$ emissions sources. The annual time series displays several observed high SO$_2$ events throughout the year lasting only a few hours. The highest include 0.031 ppm measured on July 1 at 10 PM MDT, 0.031 ppm measured on Sept 22 at 2 AM MDT, and 0.027 ppm measured on Feb 22 at 10 AM MST. The model predicts significantly lower concentrations during these events, predicting 10% to 20% of observed concentrations.

4.3.3.3   CMAQ Spatial Analyses

The SO_2 spatial performance was reviewed for two of the same POIs selected for the time series analysis. **Figure 4.3-16** shows the modeled 1-hour average SO_2 concentrations at hour 21 (2 PM MST) for January 8, 2010 through January 23, 2010. **Figure 4.3-17** shows the modeled 1-hour average SO_2 concentrations at hour 21 (2 PM MST) for September 27, 2010 through October 5, 2010. Monitored 1-hour average SO_2 concentrations from the AQS network are shown in the figure as circles. All AQS SO_2 monitors in the 4-km domain are clustered in the Salt Lake City area and may not adequately assess conditions and model performance throughout the 4-km domain.

During the first POI, the model predicts an area of elevated SO_2 concentrations in the Salt Lake City area as well as several isolated hotspots that can been seen over multiple days throughout the 4-km domain. These distinct features likely exist because of stagnant conditions with very light winds during the beginning of the POI. Stronger winds are observed at many of these locations toward the end of the first POI. On January 8, eight distinct stagnant plumes of SO_2 concentrations can be identified that also are distinguishable to varying degrees throughout much of the POI. These plumes are thought to be attributable to the electric-generating unit (EGU) sources, including: Cameo Power Plant near Grand Junction, Colorado; Nucla Station near Nucla, Colorado; Navajo Generating Station in northern Arizona; Bonanza Power Plant near Bonanza, Utah; Carbon Power Plant near Helper, Utah; Hunter Power Plant near Castledale, Utah; Huntington Power Plant near Huntington, Utah; Intermountain Power Project near Delta, Utah; and Jim Bridger Power Plant in Rock Springs, Wyoming. There are no SO_2 monitoring stations, however, near these EGUs or the Uinta Basin study area available for comparison to model-predicted concentrations.

Many SO_2 features attributable to the EGU sources during the first POI can also be identified during the second POI, although to a lesser extent.

4.3.3.4   Summary of Model Performance for Sulfur Dioxide

In general, there is no trend of under-prediction or over-prediction of SO_2 concentrations relative to the AQS network, though the model significantly over-predicts SO_2 relative to CASTNET.

- The statistical model performance results vary depending on the network.

- AQS monitors in the Salt Lake City area may not adequately represent model performance throughout the 4-km domain and in the study area.

- The modeled spatial analysis indicated localized hotspots of SO_2 concentrations scattered throughout the 4-km domain that are likely attributable to plumes from electric generating units.

The modeled spatial analysis also indicates generally low SO_2 concentrations throughout the rest of the 4-km domain though relatively few monitoring station locations are available for comparison.

Table 4.3-3   Model Performance Statistical Summary for Sulfur Dioxide

Monitoring Network	Statistics (percent)/ Concentration (parts per million [ppm])	36-km Domain					12-km Domain					4-km Domain				
		Annual	Winter	Spring	Summer	Fall	Annual	Winter	Spring	Summer	Fall	Annual	Winter	Spring	Summer	Fall
AQS (Hourly)	MFB	40	39	31	37	52	28	31	19	25	35	-9	-22	-4	-4	-7
	MFGE	131	125	136	133	133	130	123	135	134	128	111	107	113	116	107
	MNB	78	72	31	106	104	59	91	26	57	61	14	25	12	14	5
	MNGE	164	148	130	196	185	148	167	127	153	144	98	110	96	99	86
	NMB	-1	24	-9	-15	-4	24	53	5	16	19	1	33	5	-10	-11
	NME	125	129	126	121	126	139	149	135	139	134	88	107	88	84	81
	R^2	0.006	0.024	0.006	0.002	0.006	0.003	0.013	0.000	0.001	0.003	0.104	0.173	0.117	0.101	0.093
	Observed Mean Concentration (ppm)	0.002	0.002	0.001	0.002	0.002	0.001	0.002	0.001	0.001	0.002	0.002	0.002	0.002	0.003	0.003
	Predicted Mean Concentration (ppm)	0.002	0.002	0.001	0.001	0.002	0.0018	0.0023	0.0014	0.0016	0.0019	0.0023	0.0025	0.0021	0.0023	0.0024
CASTNET (Weekly)	MFB	82	63	81	84	99	81	100	68	62	96	98	108	89	84	108
	MFGE	91	75	88	98	103	96	111	89	83	102	99	111	90	87	108
	MNB	253	185	220	279	320	235	362	169	148	267	308	523	213	213	305
	MNGE	260	194	225	289	323	245	370	182	162	271	309	526	214	215	305
	NMB	106	49	154	175	110	149	161	116	118	203	286	396	230	218	295
	NME	135	70	158	200	168	178	214	154	138	213	287	397	231	220	295
	R^2	0.029	0.571	0.521	0.078	0.007	0.062	0.028	0.028	0.224	0.240	0.309	0.107	0.557	0.269	0.603
	Observed Mean Concentration ($\mu g/m^3$)	1.563	2.508	1.207	0.895	1.770	0.255	0.269	0.240	0.250	0.258	0.201	0.216	0.178	0.188	0.233
	Predicted Mean Concentration ($\mu g/m^3$)	3.226	3.737	3.066	2.460	3.710	0.634	0.702	0.519	0.545	0.783	0.775	1.072	0.586	0.598	0.921

1

2
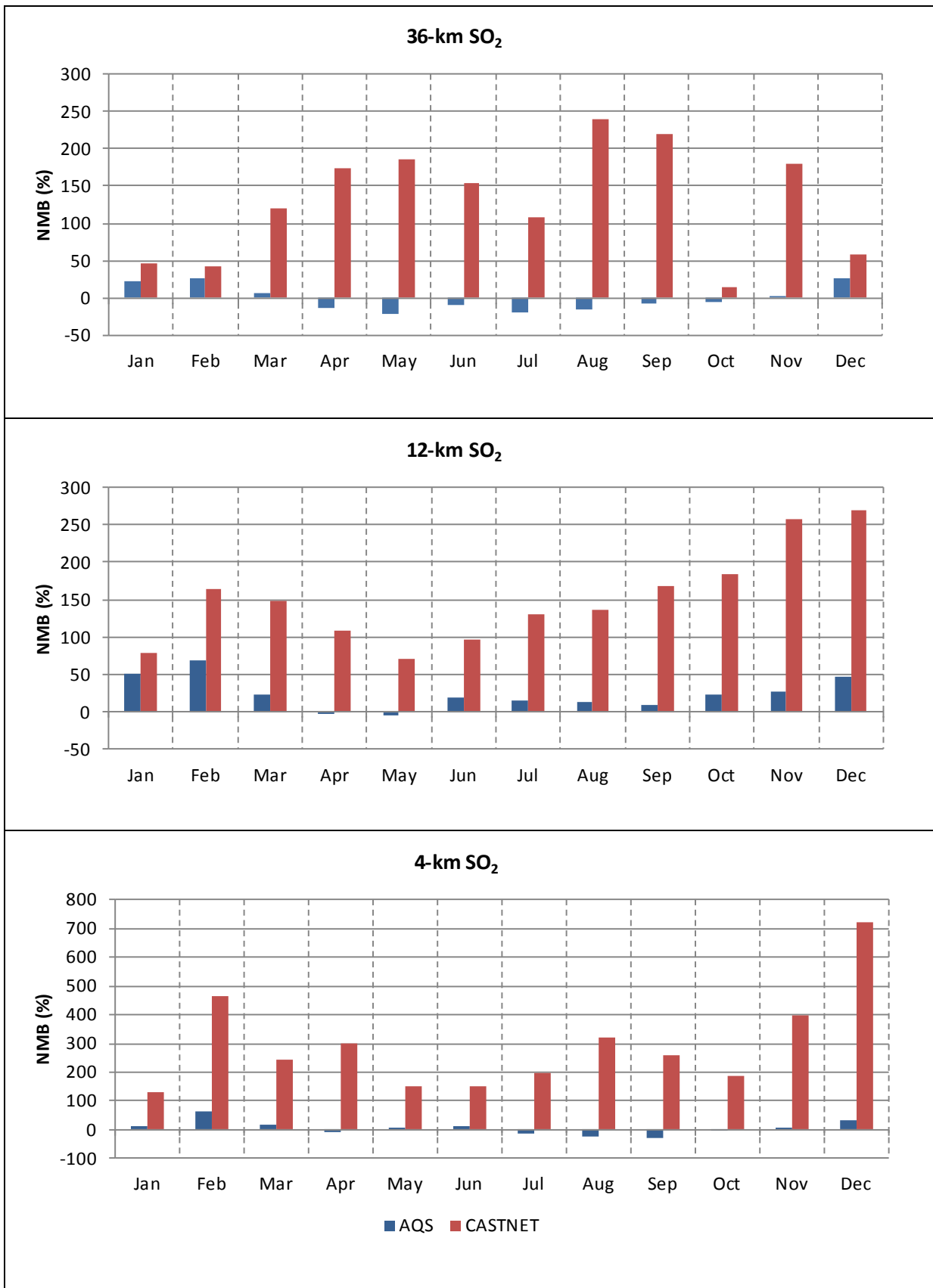
Figure 4.3-14   Monthly Normalized Mean Bias for Sulfur Dioxide
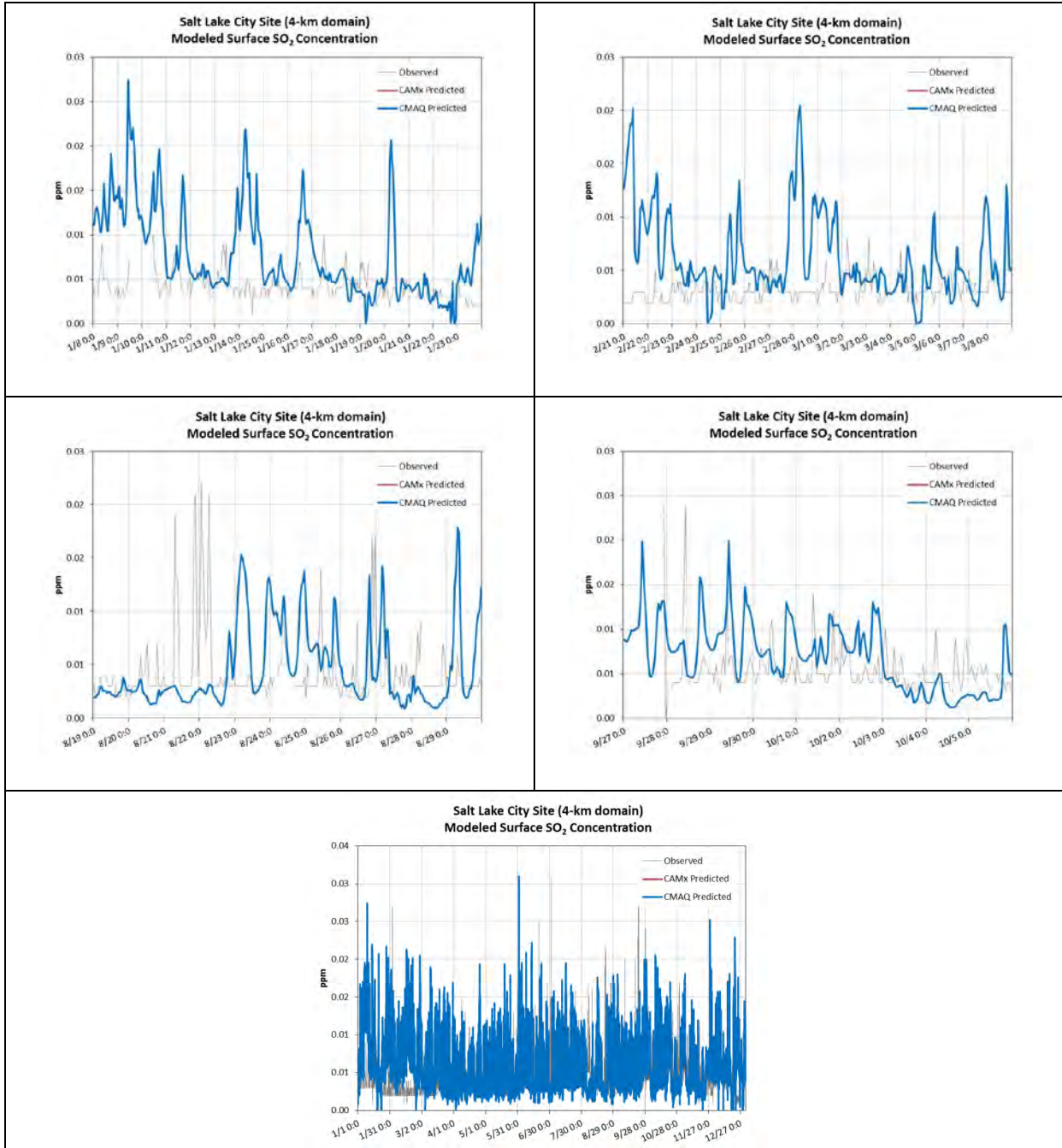
Figure 4.3-15   Time Series for Sulfur Dioxide at the Salt Lake City AQS Site (49-035-0012)
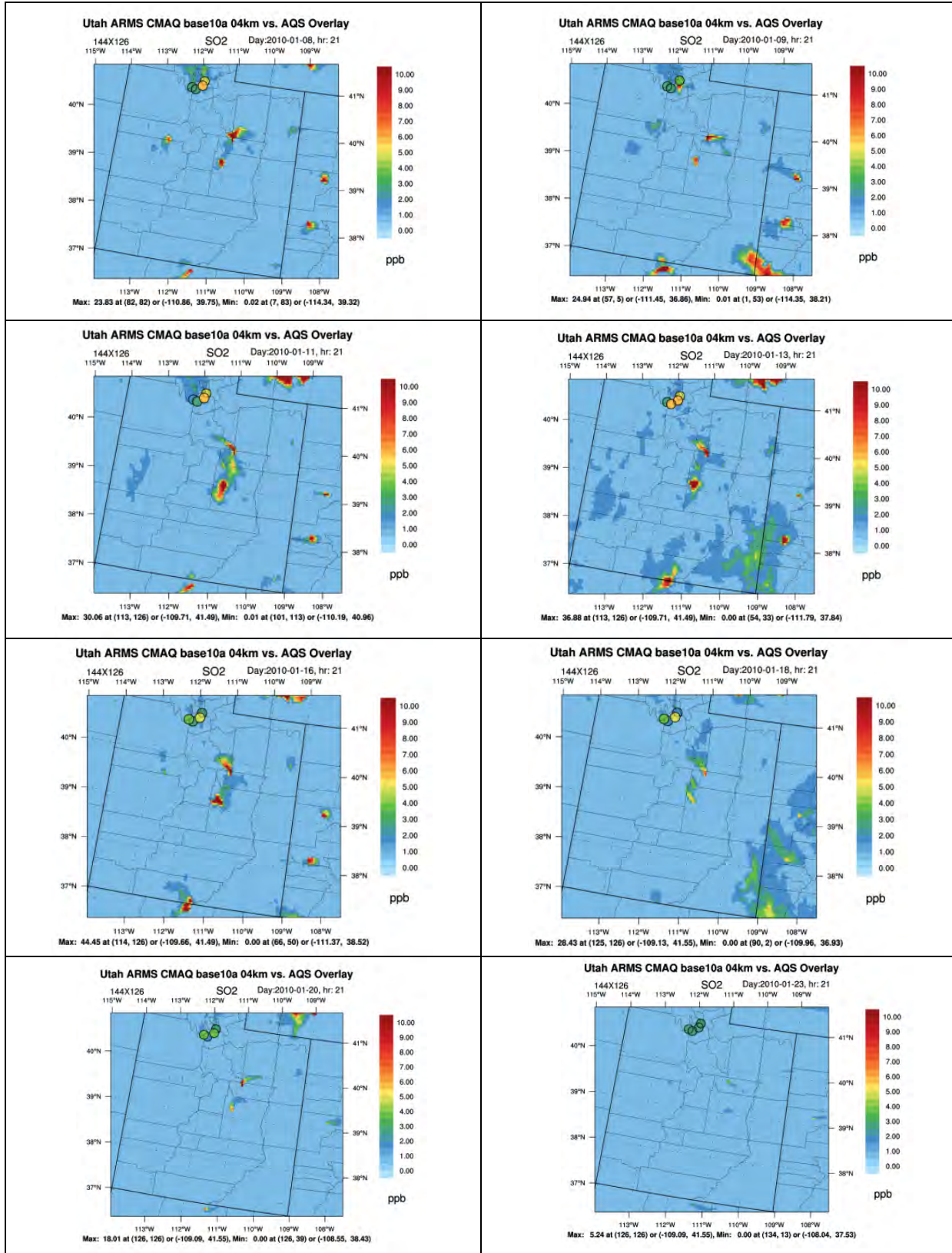
Figure 4.3-16   4-km Spatial Plots for Sulfur Dioxide during January 8 to January 23, 2010
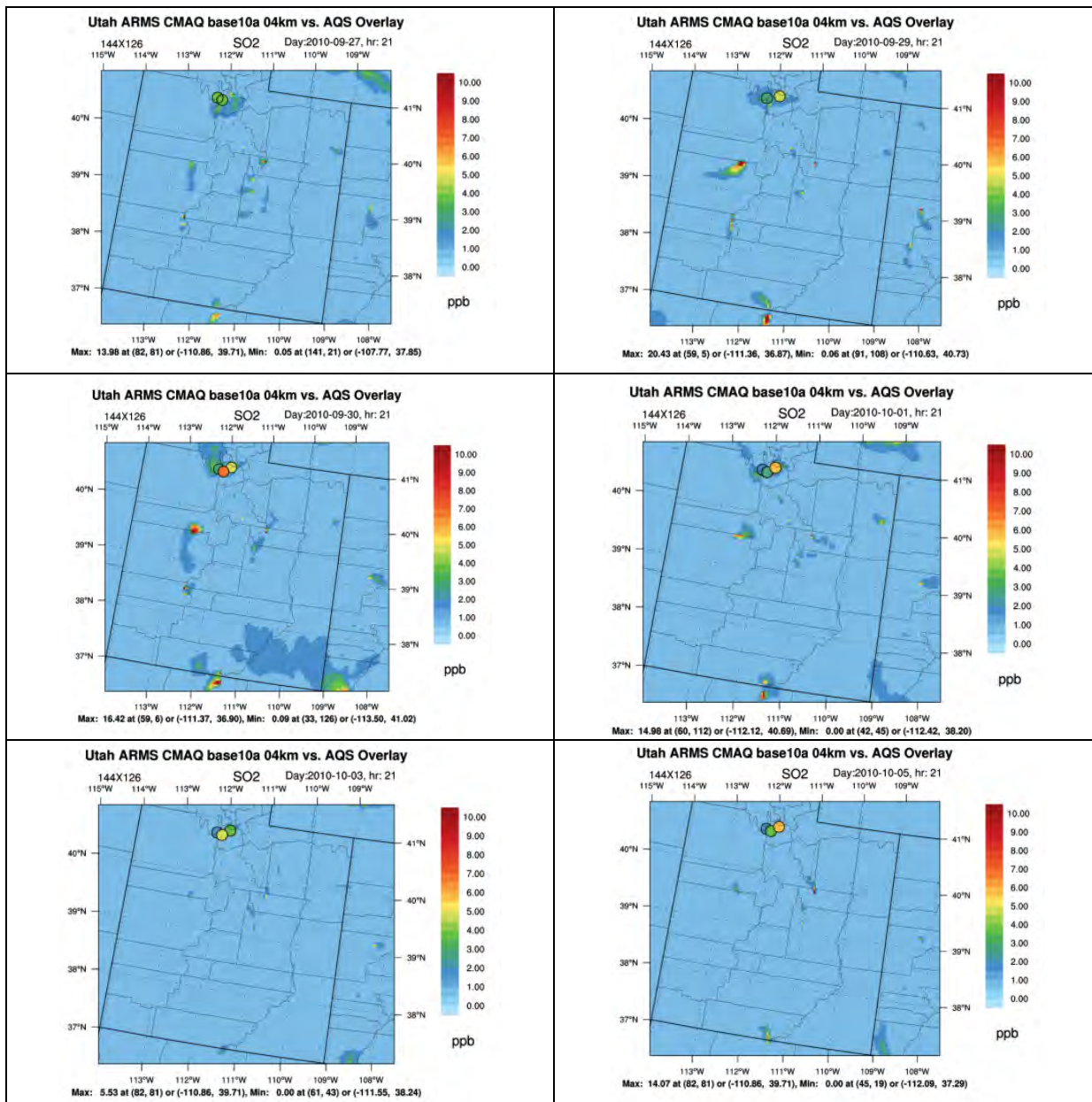
Figure 4.3-17   4-km Spatial Plots for Sulfur Dioxide during September 27 to October 5, 2010

4.4   Visibility

Particulate matter in the atmosphere contributes to visibility degradation by both scattering and absorption of visible light. The combined effect of scattered and absorbed light is called light extinction (b_{ext}). **Table 3-4** provides the equation used in the estimates of total b_{ext} presented in this section, which is based on the concentrations of various atmospheric pollutants as described by Hand and Malm 2006. This equation is applied to both model-predicted as well as measured pollutant concentrations. The estimated b_{ext} from measured pollutant concentrations is also known as the reconstructed b_{ext}. The following section presents an assessement of the model performance for visibility by comparing the model-predicted b_{ext} with the reconstructed b_{ext}.

The model performance for visibility presented in this section is based on comparison with reconstructed b_{ext} from the IMPROVE monitoring network. As part of the visibility MPE, the b_{ext} was compared for both the contribution from individual chemical compounds, as well as the total light extinction. The MPE for concentrations of the same individual compounds was already presented in **Section 4.2**, and the assessment of the model performance for visibility builds on the information presented previously. Note that the model performance for SS was not part of **Section 4.2** since it is generally not considered to be a species of concern in the Uinta Basin study area. However, SS was included in the calculation and evaluation of visibility for completeness.

The visibility model performance is only presented for 12-km and 4-km domain results following a series of analyses done for both the b_{ext} for individual pollutants and total b_{ext}:

- Tables of annual and seasonal statistical summaries by modeling domain;

- Bar charts of seasonal MFB and MFGE by modeling domain;

- Time series plots for selected monitoring stations within the 4km domain;

- Daily stacked bar charts for both modeled and reconstructed b_{ext} ; and

- Spatial plots for selected POIs.

4.4.1   Statistical Analyses for the 12-km and 4-km Domains

Annual and seasonal statistical summaries for total comparing light extinction b_{ext} for the 12- and 4-km model domains to the IMPROVE network are presented in **Table 4.4-1**. Note that the number of monitors with valid data used to calculate the statistical summaries is provided in **Table 3-2**. **Table 4.4-2** presents a comparison of the b_{ext} for each model-predicted PM chemical compound and the reconstructed b_{ext} as determined from the IMPROVE network concentrations data. The annual and seasonal b_{ext} MFB and b_{ext} MFGE for each chemical compound are shown in **Figures 4.4-1** and **4.4-2**, respectively, for both the 12- and 4-km domains.

In general, the model performs well for total b_{ext} for both the 12- and 4-km domains (**Table 4.4-1**). The predicted b_{ext} from annual-average model concentrations are fairly consistent with reconstructed annual-average visibility. Based on the mean extinction and MFB values, the model tends to slightly under-predict the extinction annually and for all seasons, except winter, meaning that the model tends to predict a smaller visibility impairment than observed in the monitoring data for most seasons except for winter. The largest under-prediction occurs during summer. The MFB values indicate that performance for the extinction predictions in the 4-km domain is generally better than the 12-km domain, with the exception of the winter b_{ext} which shows a larger over-prediction for the 4-km domain. The MFGE values are also generally smaller for the 4-km than the 12-km domain.

As shown in **Table 4.4-2** and **Figure 4.4-1**, the MFB in the b_{ext} due to SO_4 is slightly over-predicted in all seasons except summer. The b_{ext} due to NO_3 in the 12-km domain is under-predicted for all seasons except winter, while in the 4-km domain is over-predicted for all seasons except the summer. The b_{ext} due to OC and CM is under-predicted by the model for all seasons and domains. The b_{ext} due to EC is generally under-predicted by the model for all seasons and domains, except in the spring for 4-km domain. The b_{ext} due to SOIL is under-predicted by the model for all seasons and domains, except during the winter season. The b_{ext} due to SS is over-predicted for all seasons and domains. The largest under-predictions tend to occur during the summer for all components.

Table 4.4-2 and **Figure 4.4-2**, show that the b_{ext} MFGE are similar between the 12- and 4-km domains. The b_{ext} annual MFGE is largest for SS followed by CM, NO_3, OC, SOIL, EC and SO_4 in decreasing order. The largest MFGE for all seasons are consistently observed for SS, while for CM, NO_3, OC, and SOIL the largest MFGE are observed during the summer. In general, the smallest errors tend to occur during the spring for both domains. However for SS, is expected that the contributions to the extinction within the 4-km and the region of interest (Utah) are minimal given its inland location.

4.4.2 Time Series Analyses

4.4.2.1 Annual Time Series

Figure 4.4-3 shows annual time series plots that compare total model-predicted with reconstructed b_{ext} at available IMPROVE monitoring sites located within the 4-km domain. Model-predicted b_{ext} was calculated to match period of monitoring data in the grid cell that contains each IMPROVE monitor. CMAQ predicted b_{ext} values are shown in blue, CAMx in red and reconstructed b_{ext} in gray. The vertical scales are different on each of the time series plots in the figure.

The top and bottom panel of **Figure 4.4-3** show time series at sites located within Utah, in general both models produce very similar results and they track well with reconstructed b_{ext} values throughout the year, with a few exceptions when the reconstructed b_{ext} exceeds model-predicted values in October (Bryce Canyon NP, Zion NP) and May (Canyonlands NP). The middle panel presents time series at sites located in Nevada and Colorado, which show that model-predicted values are similar and track fairly well with reconstructed b_{ext}, except in November (Great Basin NP) and April and May (Mesa Verde NP, Weminuche WA). In general the average observed total extinction for all or most sites is close to 20 inverse megameters, with higher values during late winter at most sites in Utah. The models generally are able to reproduce this seasonal pattern and general magnitude for the predicted extinction.

4.4.2.2 Stacked Bar Charts

The total b_{ext} can be analyzed in more detail using stacked bar charts that depict the contribution to the total extinction by each of the PM chemical species. The stacked bar charts for Bryce Canyon NP UT (BRCA1), Canyonlands NP UT (CANY1), Capitol Reef NP UT(CAPI1), Great Basin NP NV (GRBA1), Mesa Verde NP CO (MEVE1), Weminuche WA CO (WEMI1), Zion NP UT (ZICA1) are presented in **Figures 4.4-4** to **4.4-10**, respectively. For each monitoring site, two stacked bar charts are presented together to provide a method that qualitatively compares the reconstructed b_{ext} with model-predicted extinction as a function of time. The top stacked bar chart displays the reconstructed b_{ext}, while the bottom chart shows the model-predictted b_{ext}. Each color in the stacked bar chart indicates the calculated b_{ext} from a single chemical compound. The b_{ext} is a function of speciated mass concentration, extinction effciency, and relative humidity at each monitoring site.

Most of the stacked bar chart figure shows that the contribution to the extinction from SO_4 is very similar in magnitude and temporal variation for both model and observations, while the model estimates overstates the contributions from NO_3 in the fall, winter and early spring. This is consistent with the model predicted concentrations of these species shown in **Section 4.2**. The figures also show that the observed extinction has a significant contribution from OC and CM, but in general the model is

not able to represent those species well. The stacked bar chart also illustrate that for model and reconstructed b_{ext}. the contribution from SS does not play an important role in visibility degradation.

The figures also illustrate single episodes that are difficult for the model to accurately capture. For instance for both Bryce Canyon NP (**Figure 4.4-4**) and Zion NP (**Figure 4.4-10**) observed extinction values show an event occurring in late September or early October when OC contributes a significant portion of the visibility degration for that day (and to a lesser extent CM and EC) indicative of smoke from a wildfire. During this period, two large fires were burning in Utah: the Coffee Pot and the Twitchell Canyon(NOAA-NCDC 2013; NASA 2013). The most likely source of smoke during this period is the Twitchell Canyon Fire located in central Utah; this fire was ignited by lighting on July 20th and rapidly grew out of control, it was only 30 percent contained by October 1st and a large area of quasi-stationary smoke produced by this fire affected southern Utah, northern Arizona and southern Nevada (The Smog Blog 2013). The model seems to partially capture this event at Bryce Canyon NP, but does not transport the plume as far as Zion NP.

Similarly, during the spring, but particularly in April and May, a series of spring frontal systems affected the Southwestern US increasing the windblown dust (USGS 2013). The large values for the extinction observed in Mesa Verde NP and Weminuche WA in Colorado during early April and Canyonlands NP in late May are indicative of windblown dust given that the major contributors to the extinction are CM and SOIL. The model is not able to reproduce these monitored dust events.

4.3.4   Summary of Model Performance for Visibility

In general, the model performs well for total b_{ext} for both the 12- and 4-km domains.

- The model-predicted, annual average total b_{ext} is fairly consistent with reconstructed annual average b_{ext}.

- Based on the mean extinction and MFB values, the model tends to over-predict b_{ext} for winter and under-predict it for all other seasons.

- The overall model performance for visibility is influenced by the contributions from individual PM species. The largest errors in the b_{ext} due to individual species are for SS, followed by CM, NO_3, OC, SOIL, EC and SO_4 in decreasing order. In general, the model:

    - Slightly over-predicts SO_4 in the 12-km and 4-km domains except during the summer

    - Under-predicts NO_3 in the 12-km domain except during the winter and over-predicts NO_3 in the 4-km domain except during the summer

    - Under-predicts OC, EC, CM, and total PM_{10} throughout the year;

    - Over-predicts SS throughout the year, but stacked bar charts show it does not significantly contribute to light extinction;

    - Under-predicts SOIL, except during the winter, for both domains

- Time series plots show very good agreement between model-predicted bext and reconstructed bext for all sites selected within the 4-km domain. The sites located in Utah show good agreement with the exception a few high events caused by fires or windblown dust.

- The model was not able to reproduce the maximum reconstructed b_{ext} values. Further analysis using stacked bar time series plots suggests that the reconstructed b_{ext} during major events is dominated by OC, which in the cases analyzed is an indicator of impacts from wildfire events and CM which is an indicator of windblown dust events. While the model predictions were not able to match the timing and magnitude of the observations during these fire and dust events, the impacts for the rest of the year were in general very similar. In general the contribution to the extinction from SO_4 is very similar in magnitude and temporal variation for both model and

observations, while the model estimates overstates the contributions from NO_3 in the fall, winter and early spring.

4.4.3   Comparison of CMAQ and CAMx Results

This section presents a brief inter-comparison of visibility results between CMAQ and CAMx. **Figure 4.4-11** shows the MFB seasonal bar charts for both CMAQ (left panel) and CAMx (right panel). The are noticeable differences between the seasonal performance for sulfate and nitrate. The nitrate b_{ext} values show a larger over-prediction during the winter and a smaller under-prediction during the summer by CMAQ relative to CAMx in the 4-km domain, also CAMx tends to under-predict nitrate during the spring and fall while CMAQ over-predicts. For sulfate the biases shown by CMAQ are of smaller magnitude than CAMx. While the SS bias are different between models, the contribution of SS to light extinction is not significant and very small values could lead to this type of differences in both models. The figure confirms that both models consistently under-predict CM, EC, and OC.

The MFB of total b_{ext} are also similar for both models with a positive over-prediction for all domains during the winter.

Figure 4.4-12 compares model-predicted light extinction stacked bar charts for CMAQ and CAMx for two IMPROVE sites within the 4-km domain: Bryce Canyon NP UT (BRCA1), and Great Basin NP NV (GRBA1). In general these two sites illustrate what it is observed at other monitoring locations. The figure illustrates that the contribution from sulfate during the first five months of the year is generally larger in CAMx than CMAQ. The contribution of nitrate to the total extinction shows a well defined seasonality with higher values in the winter for both models at Bryce, but CMAQ's contribution is generally higher than what is observed for CAMx. Also there is a wildfrire event observed in Bryce during the end of September that both models seem to reproduce equally. In general, the contribution of OC and CM from CAMx is slightly larger than CMAQ at both sites. At Great Basin NP, the models seem to produce similar results with the exception of a very large nitrate event that is not observed in CMAQ.

Table 4.4-1   Model Performance Statistical Summary for Total Light Extinction

Monitoring Network	Statistic (percent) /b_{ext}	12-km Domain					4-km Domain				
		Annual	Winter	Spring	Summer	Fall	Annual	Winter	Spring	Summer	Fall
IMPROVE (Daily)	MFB	-14	11	-15	-39	-12	-6	22	-9	-34	-3
	MFGE	30	28	25	40	27	29	32	24	34	26
	MNB	-7	21	-10	-31	-6	2	34	-4	-28	3
	MNGE	29	35	23	32	26	30	43	22	29	28
	NMB	-14	15	-16	-35	-15	-5	36	-15	-30	-9
	NME	32	38	27	35	30	34	45	30	30	33
	R^2	0.195	0.330	0.257	0.502	0.106	0.022	0.505	0.010	0.175	0.001
	Reconstructed Mean	22.12	19.38	22.84	24.01	22.18	19.30	17.36	20.52	19.97	19.35
	Model-predicted Mean	19.03	22.38	19.18	15.72	18.84	18.26	23.63	17.53	14.03	17.56

Table 4.4-2   Model Performance Statistical Summary for Individual Chemical Compound Light Extinction Coefficients

Chemical Compound	Statistic (percent) /b_{ext}	12-km Domain					4-km Domain				
		Annual	Winter	Spring	Summer	Fall	Annual	Winter	Spring	Summer	Fall
SO$_4$	MFB	11	34	3	-14	22	8	18	3	-10	21
	MFGE	42	57	34	36	44	38	49	29	30	43
	MNB	107	74	181	121	47	23	44	11	-3	42
	MNGE	132	91	205	160	65	47	68	32	29	59
	NMB	7	39	1	-18	22	8	11	5	-5	25
	NME	44	67	35	36	48	39	49	31	30	50
	R^2	0.342	0.343	0.460	0.481	0.287	0.363	0.420	0.380	0.452	0.216
	Reconstructed Mean	3.51	2.68	3.90	4.13	3.31	2.92	2.97	3.07	3.02	2.60
	Model-predicted Mean	3.77	3.72	3.95	3.38	4.03	3.16	3.31	3.21	2.86	3.26

Table 4.4-2   Model Performance Statistical Summary for Individual Chemical Compound Light Extinction Coefficients

Chemical Compound	Statistic (percent) /b_{ext}	12-km Domain					4-km Domain				
		Annual	Winter	Spring	Summer	Fall	Annual	Winter	Spring	Summer	Fall
NO$_3$	MFB	-33	43	-26	-135	-12	14	95	26	-122	55
	MFGE	122	122	96	147	123	122	131	98	135	126
	MNB	266	810	62	-62	293	430	1004	167	-56	627
	MNGE	355	858	135	92	370	493	1025	211	89	669
	NMB	52	165	2	-74	76	239	303	141	-59	487
	NME	143	221	89	86	174	275	313	181	88	522
	R^2	0.130	0.140	0.254	0.328	0.055	0.421	0.398	0.283	0.062	0.127
	Reconstructed Mean	1.59	2.01	2.16	1.04	1.09	1.15	2.38	1.15	0.52	0.49
	Model-predicted Mean	2.41	5.32	2.20	0.27	1.91	3.89	9.60	2.78	0.21	2.89
OC	MFB	-85	-64	-74	-115	-87	-86	-83	-64	-107	-92
	MFGE	99	95	87	118	98	92	90	74	110	97
	MNB	-38	-1	-42	-67	-42	-53	-51	-42	-68	-50
	MNGE	79	102	66	75	76	63	59	54	68	72
	NMB	-70	-65	-67	-75	-72	-71	-61	-55	-73	-80
	NME	75	75	74	76	74	73	64	57	74	80
	R^2	0.024	0.073	0.001	0.175	0.093	0.016	0.080	0.171	0.066	0.013
	Reconstructed Mean	3.36	3.06	2.62	3.89	3.92	2.40	1.59	1.33	2.76	4.02
	Model-predicted Mean	1.00	1.09	0.87	0.96	1.09	0.69	0.61	0.59	0.74	0.81
EC	MFB	-19	-6	-5	-39	-26	-15	-17	10	-34	-22
	MFGE	64	77	55	64	60	56	72	47	54	51
	MNB	33	68	71	-14	6	36	42	109	-11	-1
	MNGE	91	124	114	58	66	86	102	137	51	52
	NMB	1	21	10	-13	-12	-25	-21	4	-36	-35
	NME	75	89	80	65	67	51	62	44	48	50
	R^2	0.352	0.561	0.092	0.212	0.325	0.058	0.101	0.221	0.017	0.055
	Reconstructed Mean	1.13	1.26	0.87	1.10	1.29	0.70	0.68	0.44	0.81	0.87
	Model-predicted Mean	1.14	1.53	0.96	0.95	1.14	0.52	0.54	0.46	0.52	0.57

Table 4.4-2   Model Performance Statistical Summary for Individual Chemical Compound Light Extinction Coefficients

Chemical Compound	Statistic (percent) /b_{ext}	12-km Domain					4-km Domain				
		Annual	Winter	Spring	Summer	Fall	Annual	Winter	Spring	Summer	Fall
SOIL	MFB	-20	42	-33	-73	-11	-26	35	-49	-84	-8
	MFGE	73	77	63	84	68	72	72	68	85	62
	MNB	39	159	-2	-34	38	20	130	-25	-55	30
	MNGE	101	184	64	68	91	86	156	54	57	79
	NMB	-38	94	-48	-61	-28	-55	44	-66	-67	-21
	NME	72	135	65	69	69	69	88	72	67	58
	R^2	0.033	0.428	0.023	0.021	0.024	0.081	0.119	0.041	0.103	0.084
	Reconstructed Mean	0.84	0.24	1.42	0.99	0.67	0.83	0.17	1.75	0.91	0.44
	Model-predicted Mean	0.52	0.47	0.73	0.38	0.48	0.38	0.25	0.60	0.30	0.35
SS	MFB	141	157	144	111	153	154	161	163	122	170
	MFGE	164	174	158	153	172	169	172	169	155	181
	MNB	10218	10128	13442	4348	12814	11481	12855	13359	4232	15366
	MNGE	10233	10138	13451	4375	12826	11491	12862	13364	4254	15374
	NMB	109	181	131	-18	190	306	373	363	19	836
	NME	212	284	218	109	286	388	457	427	124	904
	R^2	0.060	0.066	0.151	0.158	0.182	0.012	0.010	0.025	0.240	0.009
	Reconstructed Mean	0.11	0.10	0.14	0.12	0.06	0.04	0.04	0.05	0.05	0.02
	Model-predicted Mean	0.22	0.27	0.33	0.10	0.18	0.17	0.20	0.24	0.06	0.16
CM	MFB	-92	-28	-86	-149	-106	-110	-67	-100	-160	-117
	MFGE	116	94	101	152	117	123	94	115	164	123
	MNB	-36	40	-49	-85	-44	-58	-14	-62	-90	-68
	MNGE	90	124	68	85	89	81	91	70	90	73
	NMB	-76	-31	-74	-87	-77	-86	-63	-86	-92	-84
	NME	81	69	78	87	80	88	71	88	92	85
	R^2	0.075	0.487	0.028	0.180	0.125	0.034	0.143	0.009	0.102	0.001
	Reconstructed Mean	2.39	0.82	2.96	3.31	2.44	2.17	0.45	3.63	2.81	1.74
	Model-predicted Mean	0.58	0.56	0.76	0.42	0.55	0.30	0.17	0.51	0.23	0.28
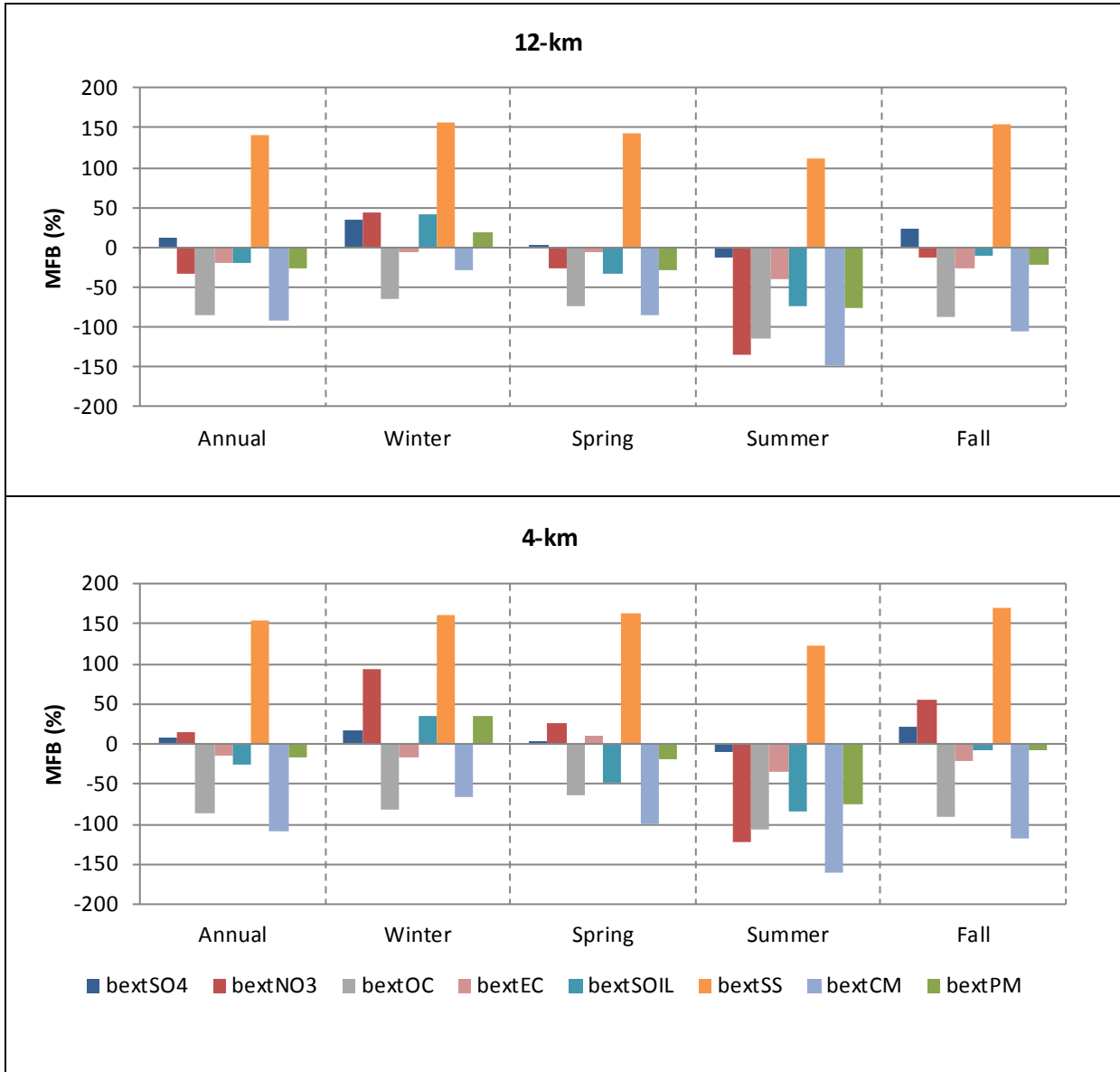
Figure 4.4-1   Mean Fractional Bias for Light Extinction Coefficients
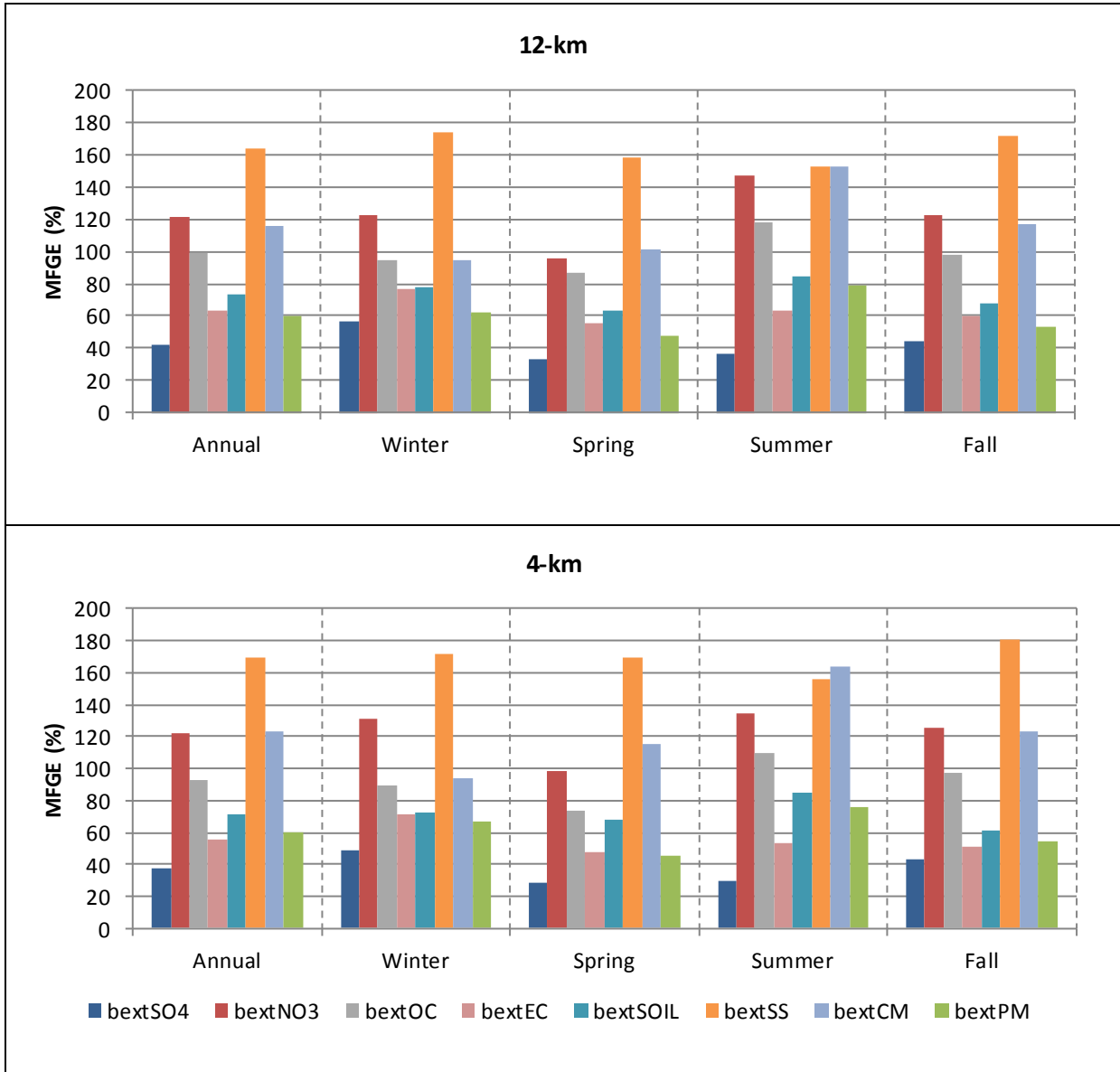
Figure 4.4-2   Mean Fractional Gross Error for Light Extinction Coefficients
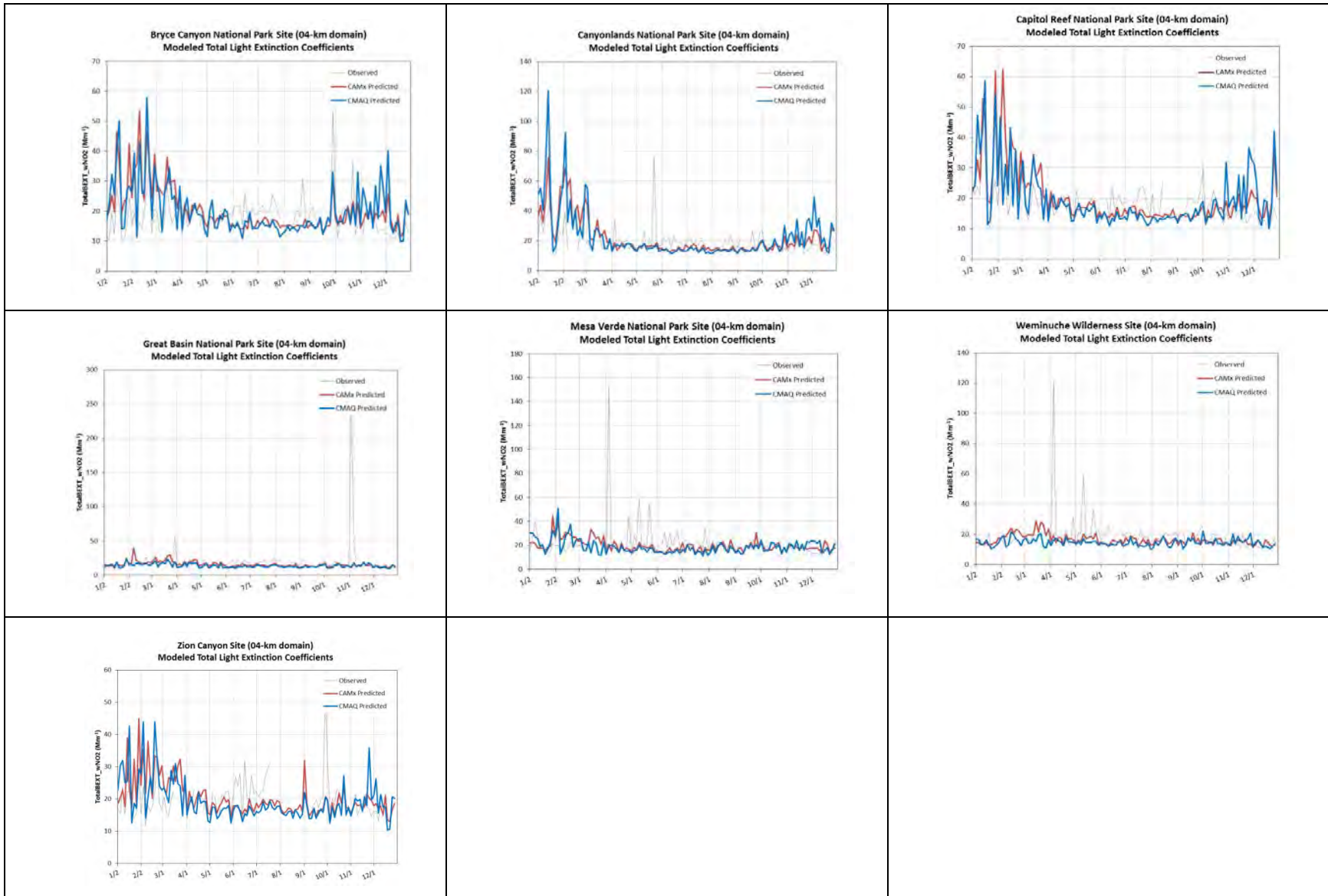
Figure 4.4-3   Annual Time Series for Light Extinction Coefficients at Selected IMPROVE Sites
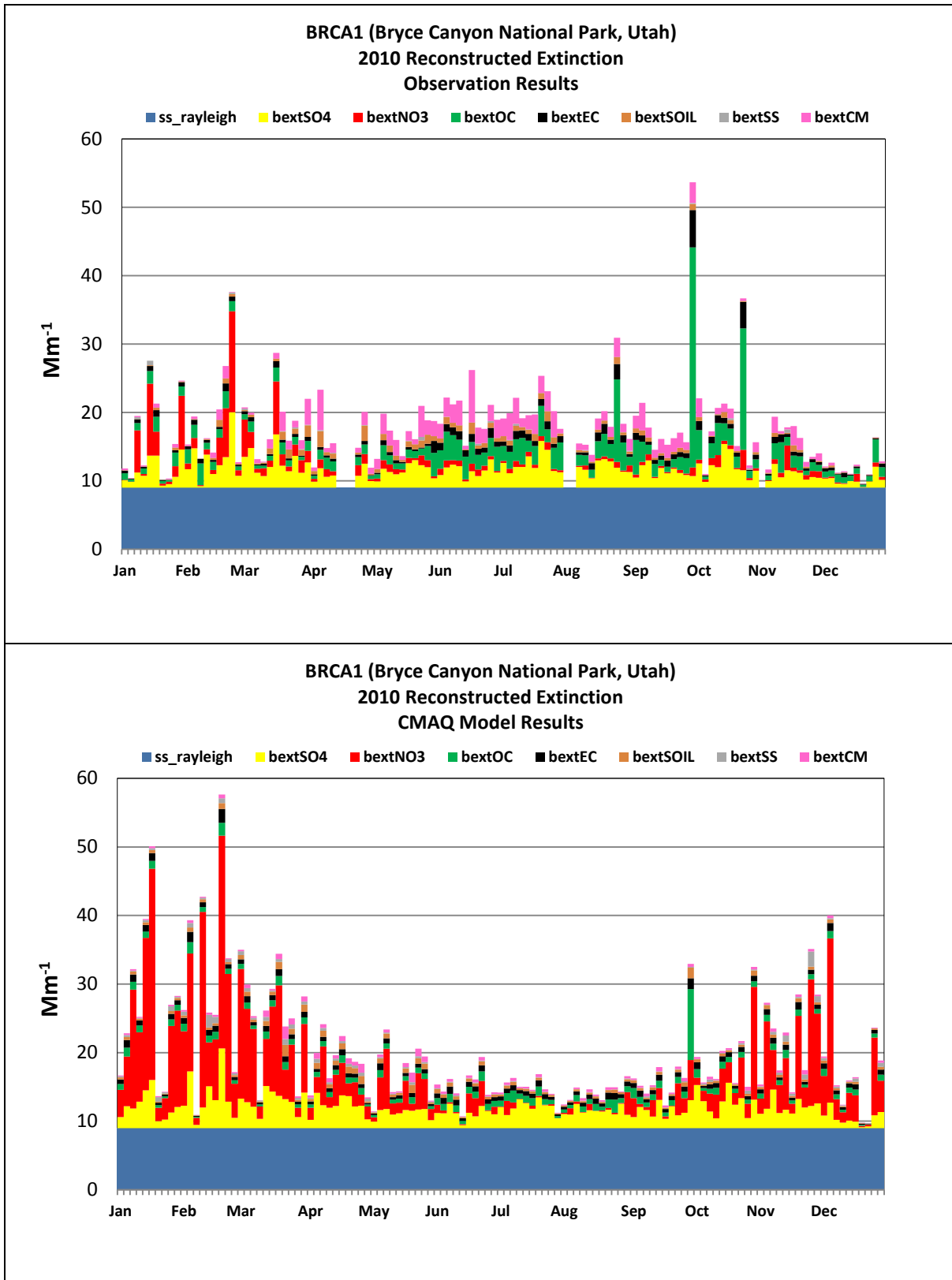
Figure 4.4-4   Reconstructed versus Model-predicted Light Extinction Coefficients at Bryce Canyon National Park, Utah
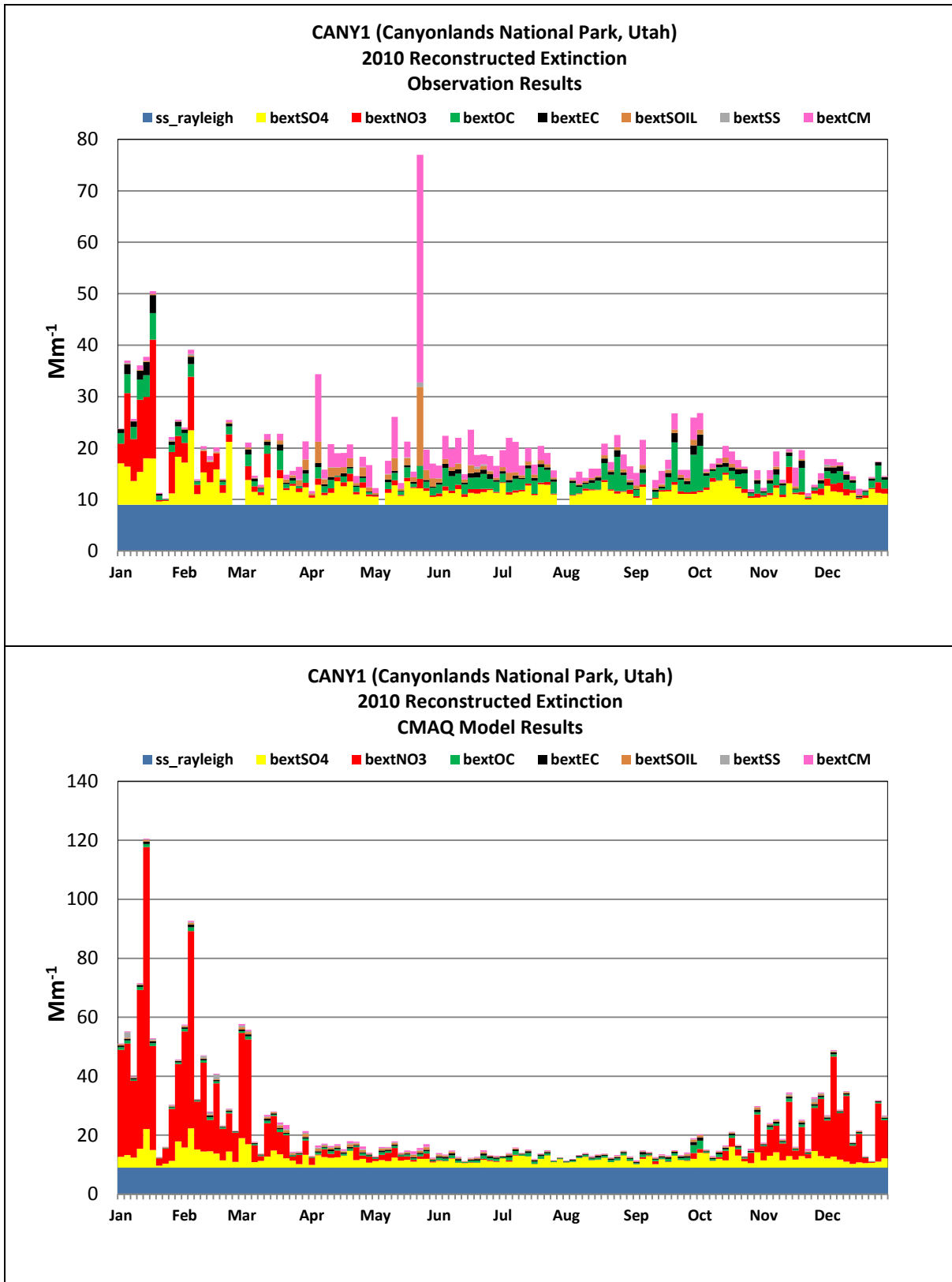
Figure 4.4-5   Reconstructed versus Model-predicted Light Extinction Coefficients at Canyonlands National Park, Utah

Figure 4.4-6   Reconstructed versus Model-predicted Light Extinction Coefficients at Capitol Reef National Park, Utah
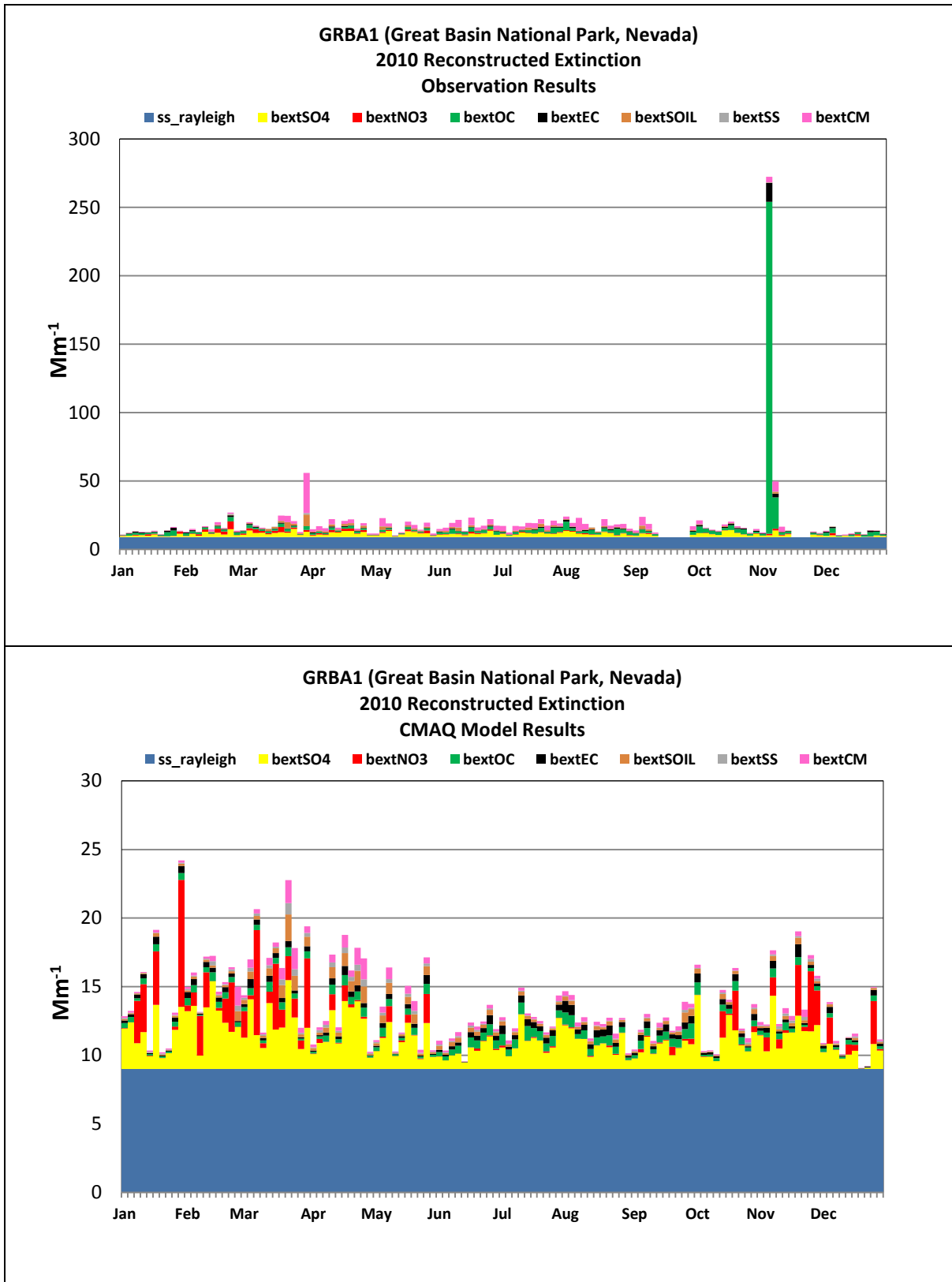
Figure 4.4-7   Reconstructed versus Model-predicted Light Extinction Coefficients at Great Basin National Park, Nevada
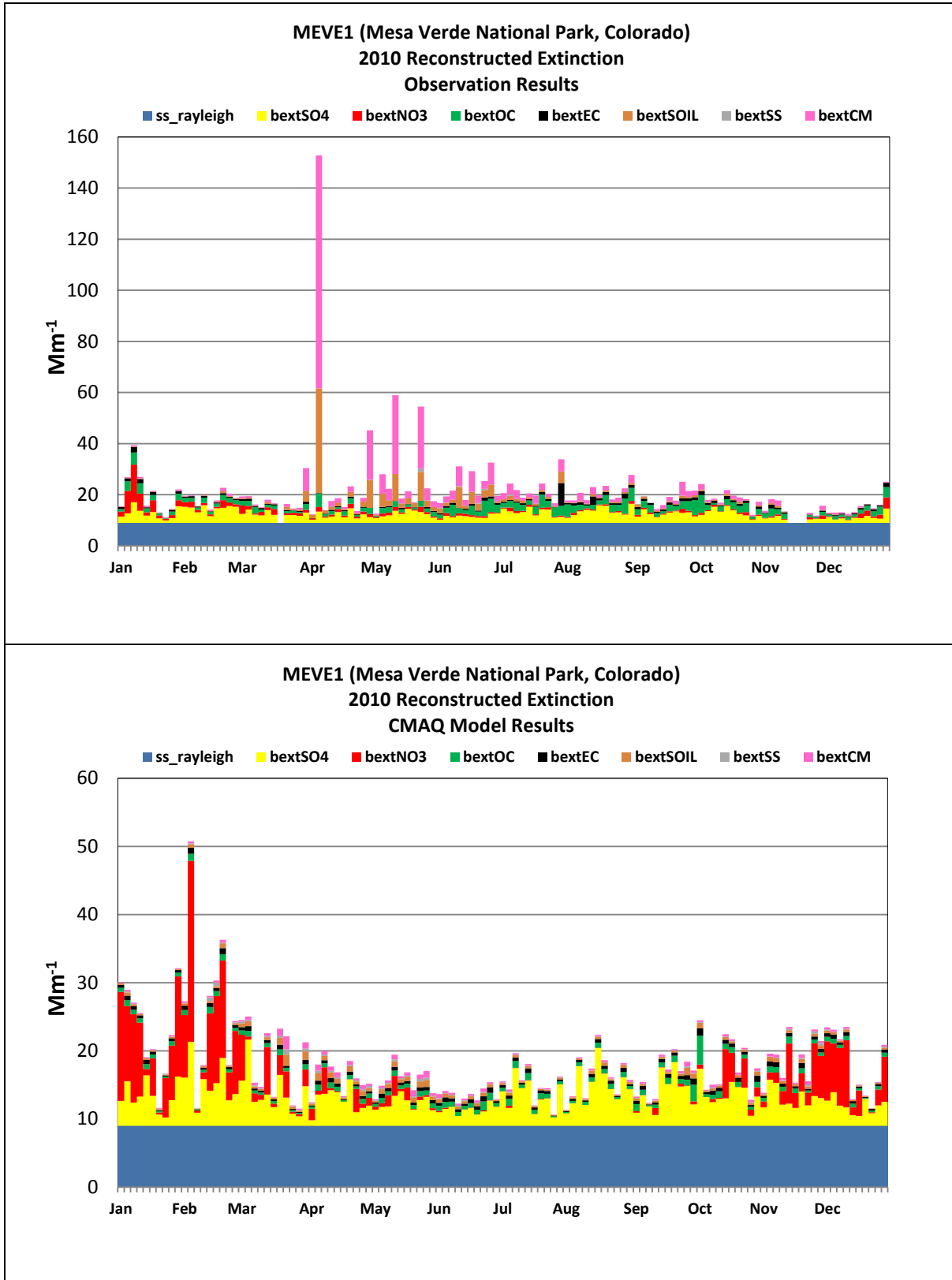
Figure 4.4-8   Reconstructed versus Model-predicted Light Extinction Coefficients at Mesa Verde National Park, Colorado
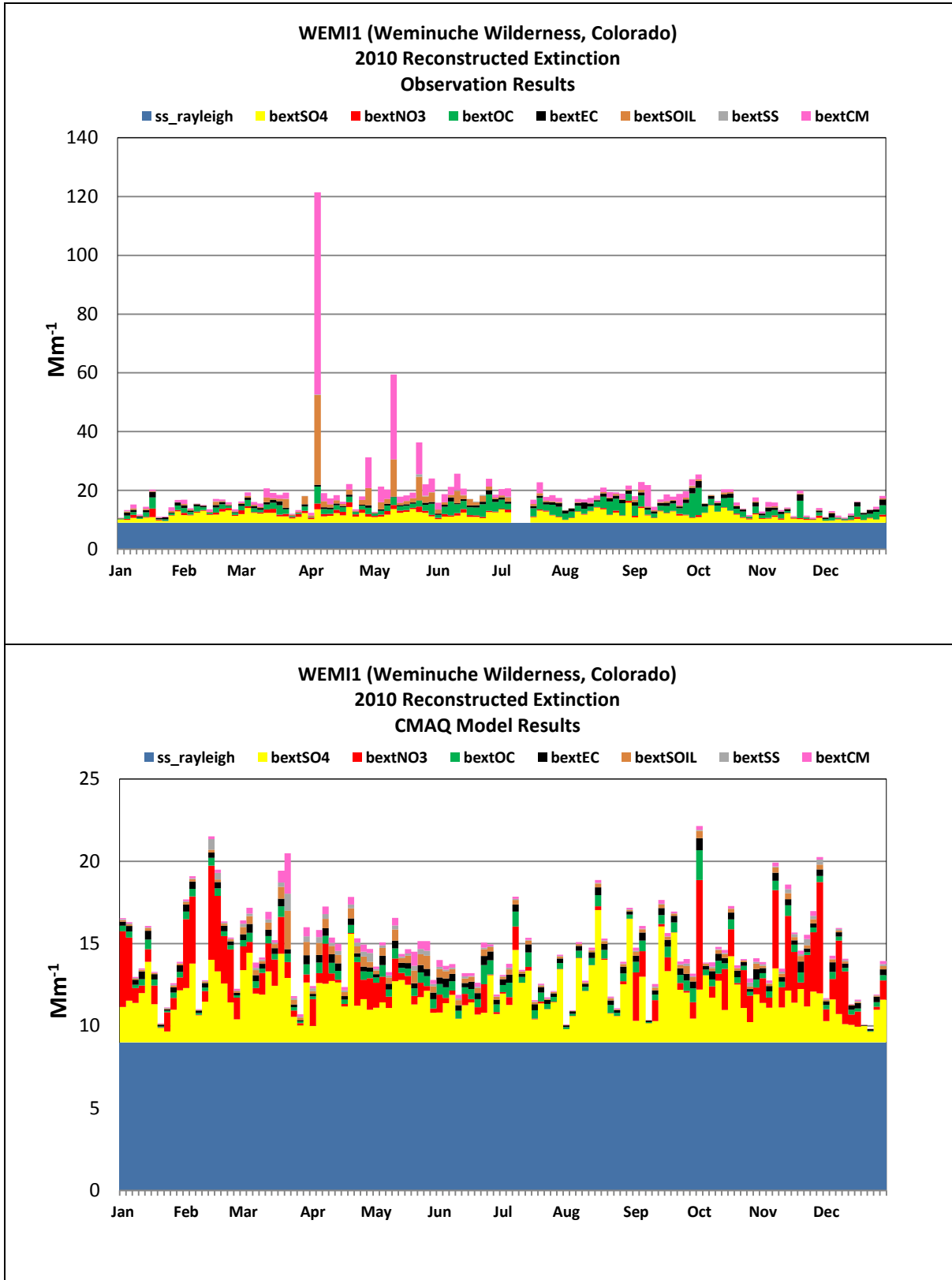
Figure 4.4-9   Reconstructed versus Model-predicted Light Extinction Coefficients at Weminuche Wilderness, Colorado
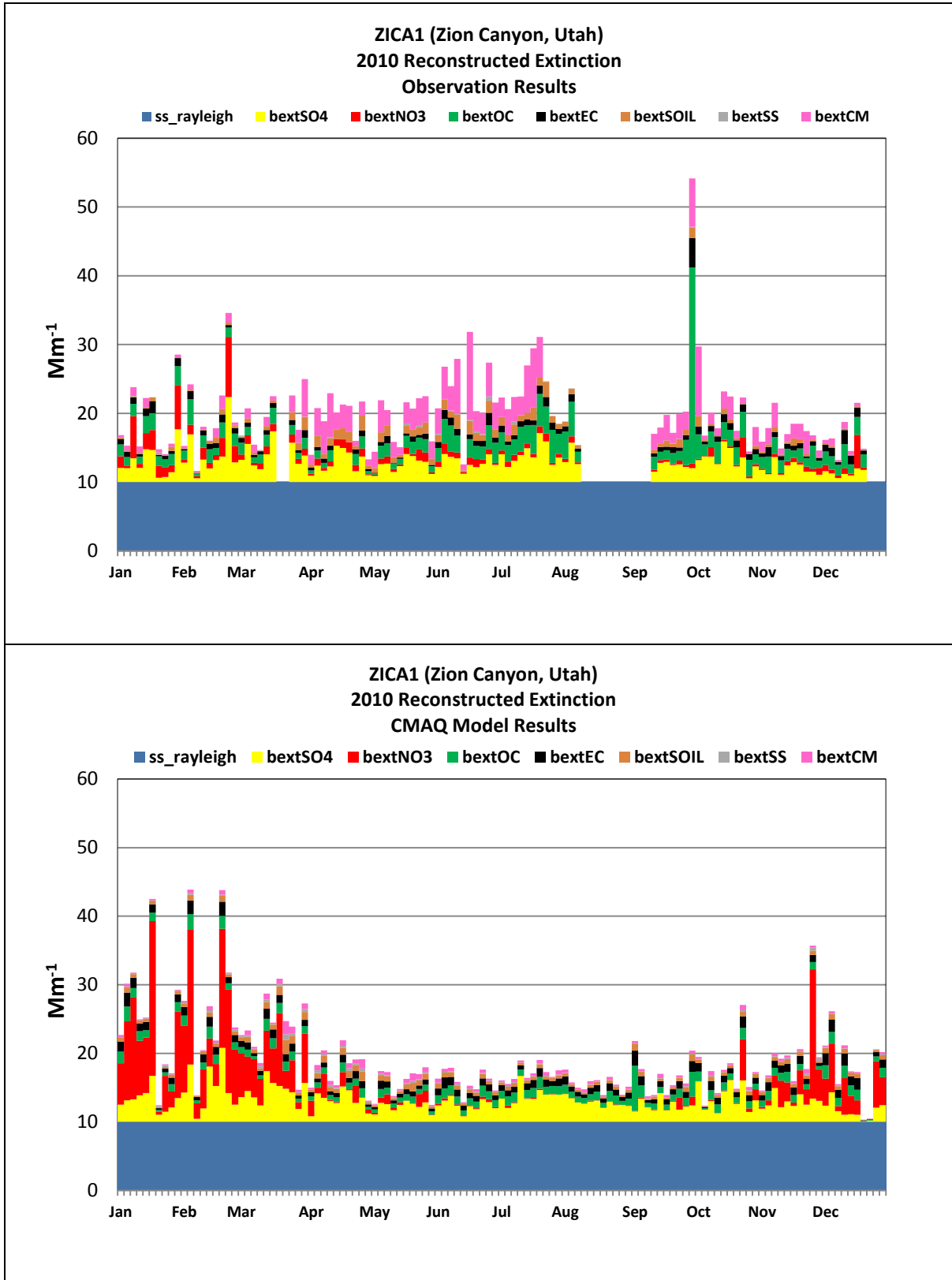
Figure 4.4-10 Reconstructed versus Model-predicted Light Extinction Coefficients at Zion Canyon, Utah
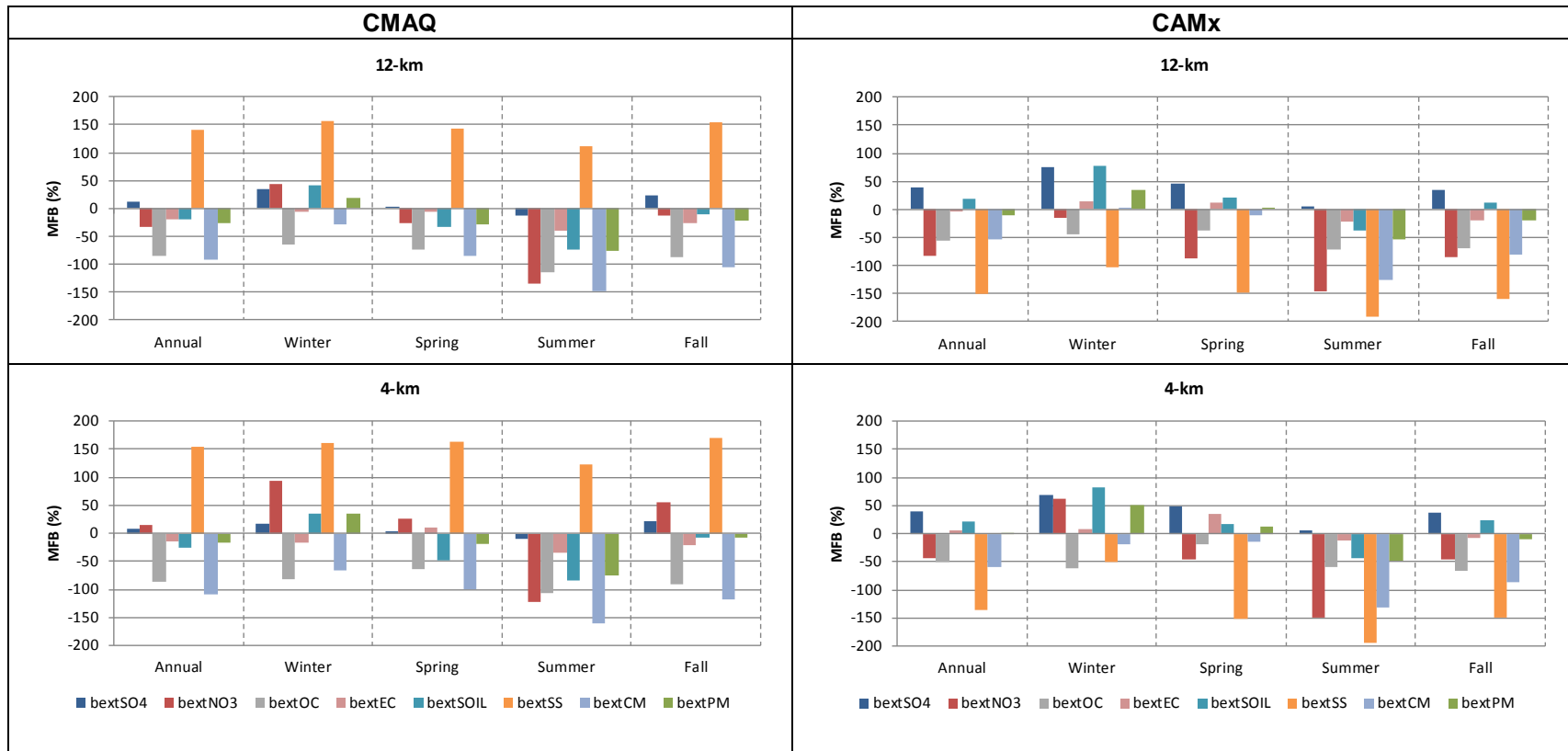
Figure 4.4-11   Mean Fractional Bias for Light Extinction Coefficients CMAQ (left) and CAMx (right)

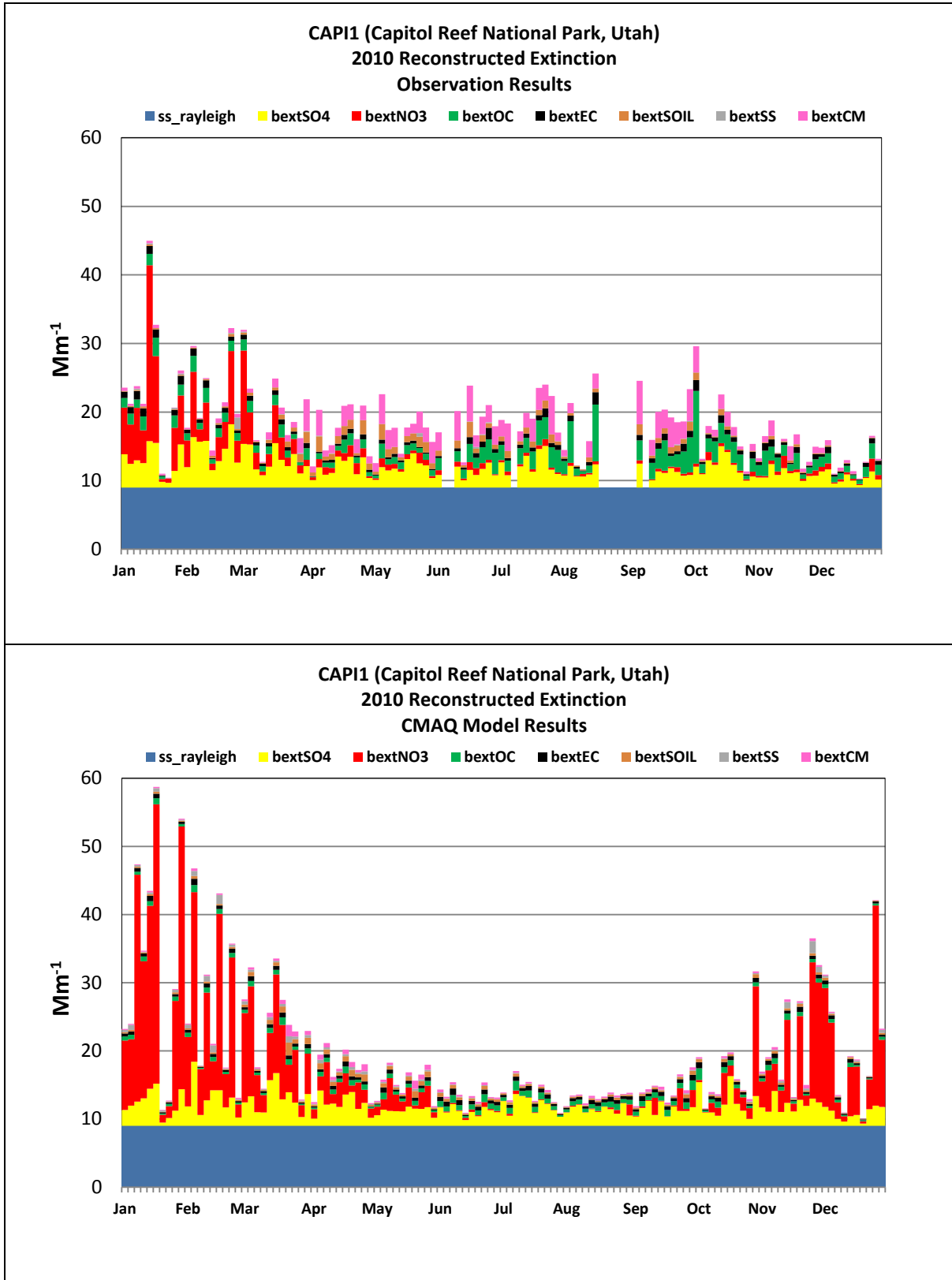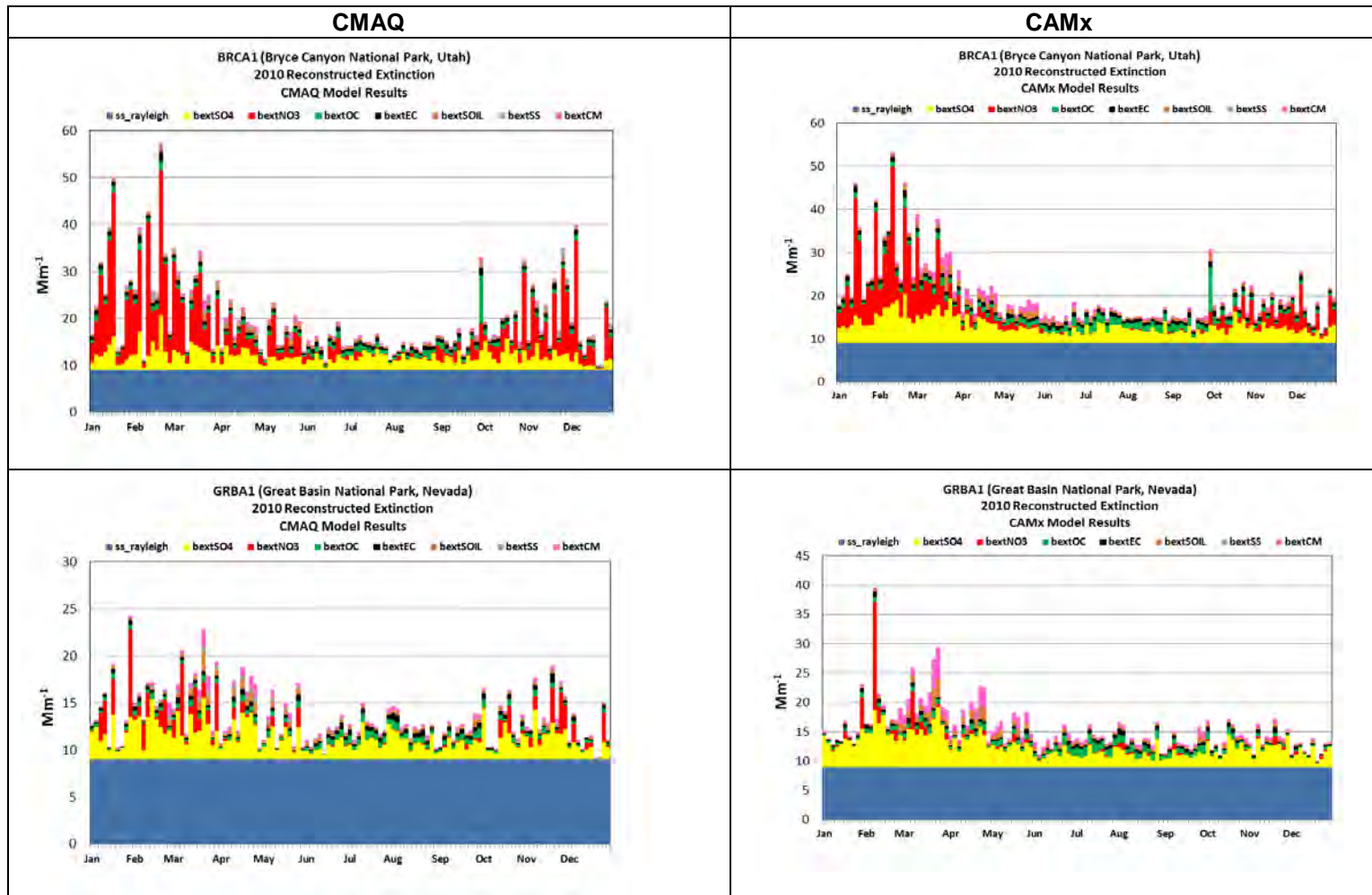**Figure 4.4-12   Model-predicted Light Extinction Coefficients at Bryce Canyon National Park, Utah and Great Basin National Park, Nevada. CMAQ (left) and CAMx (right)**

4.5   Deposition

In addition to airborne ambient concentrations, the model is able to predict sulfur- and nitrogen-containing compounds wet and dry deposition fluxes into the surface. However, reliable data availability limits the comparison to wet deposition fluxes measured by NADP monitors. Since there are no direct measured estimates of dry deposition fluxes, this model assessment focuses exclusively on the model's performance for wet deposition.

The model-predicted wet deposition fluxes were compared to measured fluxes at available NADP sites. The wet deposition of SO_4, NO_3, and NH_4 ions were examined for the 36-, 12-, and 4-km domains using the following assessment methods:

- Tables of annual and seasonal statistical summaries by modeling domain;

- Bar charts of monthly MFB by modeling domain;

- Time series plots for selected monitoring stations within the 4km domain

- Scatter plots of NADP measurements and model predicted values; and

- Spatial plots for total annual wet deposition in the 4-km domain.

4.5.1   Sulfate

Annual and seasonal performance statistics are presented in **Table 4.5-1** while monthly MFB bar charts are presented in **Figures 4.5-1** for SO_4 wet deposition for all three domains. Note that the number of monitors with valid data used to calculate the statistical summaries is provided in **Table 3-2**.

 In general, based on mean predicted and MFB values, the model tends to over-predict SO_4 wet deposition relative to observations throughout the year and for all domains. For the 36-km domain the over-prediction seems to be more pronounced during the summer, but this trend is not observed in the 12- or 4-km domains. For the both the 12- and 4-km domains, there are not seasonal trends observed with the MFB, except that during the fall and winter the model tends to under-predict SO_4 wet deposition, while for the rest of the year it mostly over-predicts deposition values. The MFB values in **Table 4.5-1** suggest that for the 12- and 4-km domain, spring is the season with slightly better performance since the MFB values are the lowest. However, during the summer the MFGE is lower and the coefficient of determination is higher relative to spring.

Annual time series compare weekly total SO_4 wet deposition at Bryce Canyon NP (UT99), Canyonlands NP (UT09), Green River (UT98), and Great Basin NP (NV05) NADP monitoring sites to modeled deposition rates in **Figure 4.5-2**. The time series for these sites generally show CMAQ deposition values are significantly higher than CAMx for most of the year. The comparison of CMAQ with available observations is remarkable, for instance the model is able to capture the correct magnitude and timing of a significant deposition event in late March and April at the Great Basin NP site. Other significant events are generally captured by the model although neither the exact timing nor the magnitudes are always correct, as shown for June-August and September-October at Bryce Canyon NP; July and August at Green River; September-October at Great Basin NP. There are also periods and locations where CMAQ seems to systematically over-predict SO_4 wet deposition, such as January and February at most sites and throughout the entire year at Canyonlands NP.

A scatter plot of SO_4 wet deposition is presented in **Figure 4.5-3**. In this figure, NADP measurements collected within the 4-km domain are compared with model-predicted SO_4 wet deposition. Overall, the model tends to over-predict wet deposition of SO_4 in the 4-km domain especially for values less than 0.2 kg/ha, but it under-predicts higher deposition values.

Figure 4.5-4 shows a spatial plot of the modeled annual SO_4 wet deposition overlaid with measured NADP concentrations (shown in circles) for the 4-km domain. Although there relatively few monitoring

sites in the 4-km and the distribution is uneven, the figure shows that the model captures the spatial variation well. The model has a tendency to over-predict the SO_4 wet deposition during this period, especially for sites near the southeast portion of the domain. In the central part of the domain the model over-prediction is not as significant.

Figure 4.5-5 provides a comparison between model simulated annual precipitation to the NADP spatially interpolated precipitation. In general the comparison for the 36-km model precipitation seems to show very similar patterns and is close in magnitude to the NADP spatially interpolated measurements. The figure also shows that the model spatial precipitation for the 4-km domain closely resembles the topographic features in the region like the Uinta Mountains, the Wasatch Range, the Pahvant Range and the Tushar Range. Generally in the area covered by the 4-km domain, the model predicts precipitation to be in the range of 0 to 60 cm for those areas in lower elevations like the Uinta Basin and the Great Basin Desert, while NADP values range between 0 to 50 cm. For higher elevations like the Uinta Mountains or the Wasatch Range, the model predicts values between 100 and up to 219 cm a year, while NADP values range between 90 up to 200 cm. The figure suggests that on an annual basis, the model is able to generally capture the spatial patterns as well as the magnitude of the observed precipitation; however there is some uncertainty about the actual timing in which the removal occurs and this could have an important effect on the actual wet deposition values observed for all ions.

4.5.2   Nitrate

Annual and seasonal performance statistics are presented in **Table 4.5-2** while monthly MFB bar charts are presented in **Figures 4.5-6** for NO_3 wet deposition for all three domains. In general, based on mean predicted and MFB values, the model tends to be relatively close to measured NO_3 wet deposition throughout the year and for all domains. For all the domains, the monthly bar charts show a tendency for modeled NO_3 wet deposition to be biased low during the fall, especially for the 4-km domain.

Annual time series that compare weekly total NO_3 wet deposition at Bryce Canyon NP (UT99), Canyonlands NP (UT09), Green River (UT98), and Great Basin NP (NV05) NADP monitoring sites are presented in **Figure 4.5-7**. The time series for these sites generally show CMAQ deposition values are significantly higher than CAMx for most of the year. Similar to sulfate wet deposition performance, the comparison of CMAQ with available observations is remarkable, for instance the model is able to capture the correct magnitude and timing of various deposition events. In contrast to sulfate depositions performance, CMAQ seems to systematically under-predict NO_3 wet deposition at the Green River site. A scatter plot of NO_3 wet deposition is presented in **Figure 4.5-8**. In this figure, NADP measurements collected within the 4-km domain are compared with model-predicted NO_3 wet deposition. Overall, the scatterplot shows that the model tends to mostly over-predict wet deposition of NO_3 in the 4-km domain.

Figure 4.5-9 shows a spatial plot of the modeled annual NO_3 wet deposition overlaid with measured NADP concentrations (shown in circles) of NO_3 wet deposition for the 4-km domain. The figure illustrates that on an annual basis the model tends to reproduce the spatial variability of wet deposition well relative to measurements, with a slight tendency to over-predict deposition. The spatial plot also shows that the NO_3 wet deposition closely mirrors the main topographic features in Utah.

4.5.3   Ammonium

Annual and seasonal performance statistics are presented in **Table 4.5-3** while monthly MFB bar charts are presented in **Figures 4.5-10** for NH_4 wet deposition for all three domains. In general, based on mean predicted and MFB values, the model tends to be relatively close to measured NH_4 wet deposition throughout the year and for all domains. Also, for the 4-km domain the model tends to over-predict NH_4 wet deposition during spring and summer, but under-predict deposition during the fall and

winter. However for the 36- and 12-km domains the bias shows a seasonal trend with larger over-predictions during the summer months.

Annual time series that compare weekly total NH$_4$ wet deposition at Bryce Canyon NP (UT99), Canyonlands NP (UT09), Green River (UT98), and Great Basin NP (NV05) NADP monitoring sites are presented in **Figure 4.5-11**. The time series for these sites generally show CMAQ deposition values are significantly higher than CAMx for most of the year. The comparison of CMAQ with available observations is very good, for instance the model is able to capture the correct magnitude and timing of some deposition events like the Spring event in Great Basin and the September-October event at Bryce Canyon NP. While other significant events are generally captured neither the exact timing nor the magnitudes are always correct: June-August at Bryce Canyon NP; July and August at Green River. A scatter plot of NH$_4$ wet deposition is presented in **Figure 4.5-12**. Overall, the scatterplot shows that the model does not have a distinct over- or under-prediction.

Figure 4.5-13 shows a spatial plot of the modeled annual NH$_4$ wet deposition overlaid with measured NADP values (shown in circles) of NH$_4$ wet deposition for the 4-km domain. The figure illustrates that on an annual basis, the model predicts NH$_4$ wet deposition adequately through the entire 4-km domain. The spatial plot also shows that the NH$_4$ wet deposition closely mirrors the main topographic features in Utah.

4.5.4   Summary of Model Performance for Deposition

- In general, the model tends to over-predict wet deposition of SO$_4$ and NH$_4$ for all three domains except in the fall and winter for the 12- and 4-km domains. NO$_3$ wet deposition does not show any particular seasonal trend for the bias.

- Annual time series for selected sites within the 4-km domain show CMAQ deposition values are significantly higher than CAMx for most of the year.

- Comparison of CMAQ with observations for SO$_4$, NH$_4$ and NO$_3$ wet deposition shows that the model is able to capture the correct magnitude and occasionally the timing of a significant number of deposition events.

- Annual precipitation was compared between model and NADP. The model spatial precipitation closely resembles the topographic features in the region like the Uinta Mountains, the Wasatch Range, the Pahvant Range and the Tushar Range. On an annual basis for the 4-km domain, the model is able to capture the spatial patterns as well as the magnitude of the observed precipitation.

4.5.5   Comparison of CMAQ and CAMx Results

This section presents a brief inter-comparison of deposition results between CMAQ and CAMx. **Figure 4.5-14** shows the sulfate wet deposition MFB seasonal bar charts for both CMAQ (left panel) and CAMx (right panel). This figure illustrates that for all domains CAMx systematically under-predicts sulfate wet deposition regardless of season, while CMAQ mostly over-predicts sulfate wet deposition for all domains except for the fall and winter in the 12- and 4-km domains. **Figure 4.5-15** shows scatterplots for the 4km that compare CMAQ and CAMx sulfate wet deposition with measured values. The figure supports the information shown in the MFB bar charts, but it shows that the CMAQ over-prediction mostly occurs in the range from 0 to 0.2 kg/ha while CAMx under-predicts in the range of 0 to 0.15 kg/ha.

Figure 4.5-16 shows the nitrate wet deposition MFB seasonal bar charts for both CMAQ (left panel) and CAMx (right panel). This figure illustrates that for all domains CAMx systematically under-predicts nitrate wet deposition regardless of season, while CMAQ has no distinguishable trend throughout the year for all domains except for the fall and winter in the 12- and 4-km domains in which it seems to under-predict nitrate wet deposition. **Figure 4.5-17** shows scatter plots for the 4-km that compare CMAQ and CAMx nitrate wet deposition with measured values. T The figure supports the information

shown in the MFB bar charts, but it shows that the CMAQ over-prediction mostly occurs in the range from 0 to 0.2 kg/ha while CAMx under-predicts in the range of 0 to 0.1 kg/ha.

Figure 4.5-18 shows the ammonium wet deposition MFB seasonal bar charts for both CMAQ (left panel) and CAMx (right panel). This figure illustrates that for all domains CAMx systematically under-predicts ammonium wet deposition regardless of season, while CMAQ has no distinguishable trend throughout the year for all domains except for the fall and winter in the 12- and 4-km domains in which it seems to under-predict ammonium wet deposition. **Figure 4.5-19** shows scatter plots for the 4-km that compare CMAQ and CAMx ammonium wet deposition with measured values. The figure supports the information shown in the MFB bar charts, but it shows that the CMAQ over-prediction mostly occurs in the range from 0 to 0.05 kg/ha while CAMx under-predicts over the full range of monitored values.

Table 4.5-1 Model Performance Statistical Summary for Sulfate Wet Deposition

Monitoring Network	Statistic (percent)/ Concentration (kilogram per hectare [kg/ha])	36-km Domain					12-km Domain					4-km Domain				
		Annual	Winter	Spring	Summer	Fall	Annual	Winter	Spring	Summer	Fall	Annual	Winter	Spring	Summer	Fall
NADP (Annual/ Seasonal)	MFB	32	26	34	46	18	20	20	33	53	-17	13	35	22	42	-35
	MFGE	84	92	77	84	82	105	118	97	93	101	115	133	122	94	103
	MNB	249	274	206	333	171	290	437	341	265	123	243	376	320	191	47
	MNGE	282	314	234	359	211	340	491	380	291	192	301	428	376	225	128
	NMB	53	49	44	64	42	45	66	17	101	7	123	274	149	132	3
	NME	95	90	84	106	87	122	138	111	145	89	175	302	203	175	77
	R^2	0.256	0.346	0.243	0.184	0.297	0.029	0.225	0.005	0.071	0.178	0.206	0.449	0.115	0.161	0.409
	Observed Mean Deposition (kg/ha)	0.16	0.10	0.18	0.23	0.13	0.07	0.04	0.11	0.08	0.05	0.05	0.03	0.04	0.09	0.06
	Predicted Mean Deposition (kg/ha)	0.24	0.14	0.26	0.38	0.18	0.10	0.07	0.12	0.16	0.06	0.11	0.12	0.10	0.20	0.06
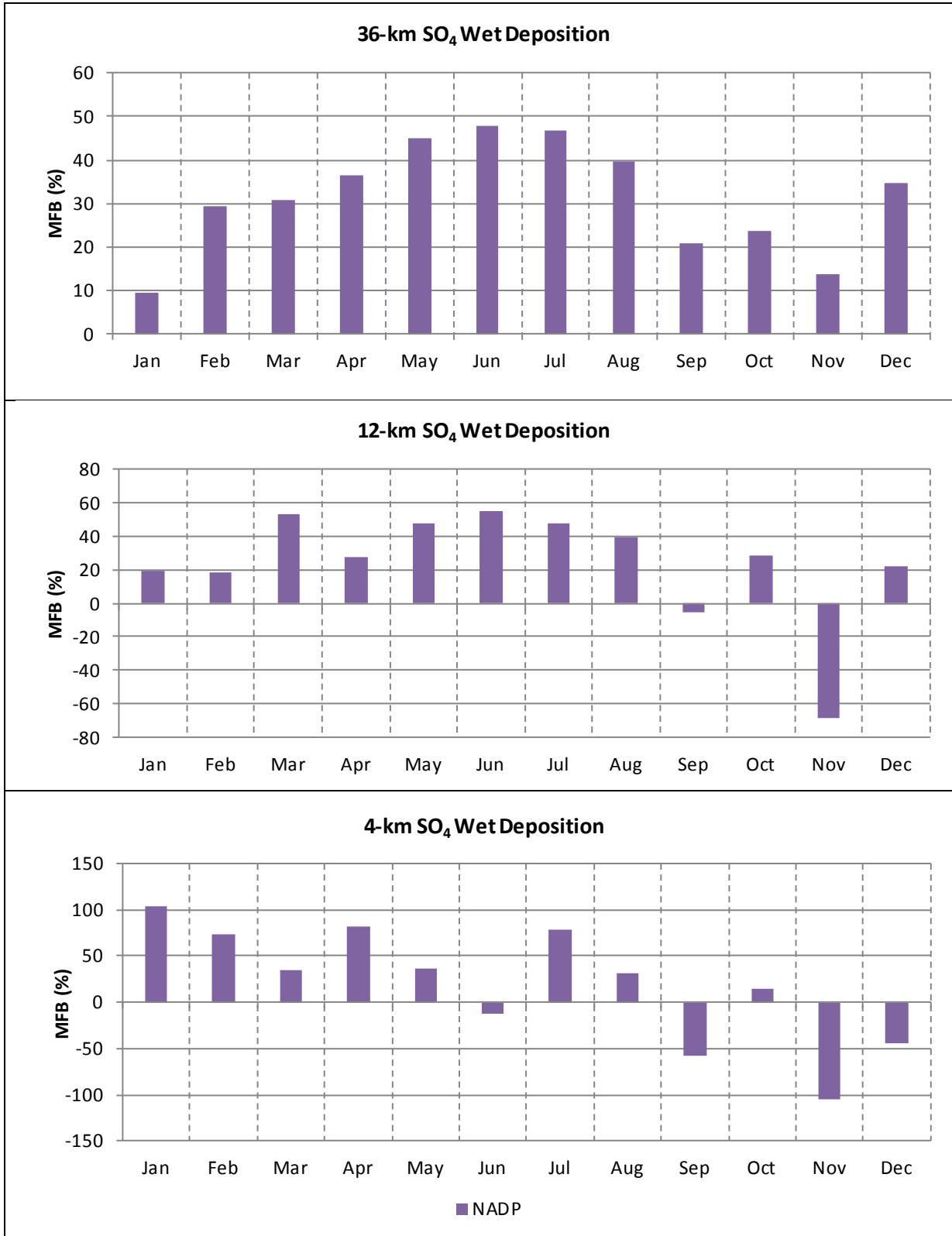
Figure 4.5-1   Monthly Mean Fractional Bias for Sulfate
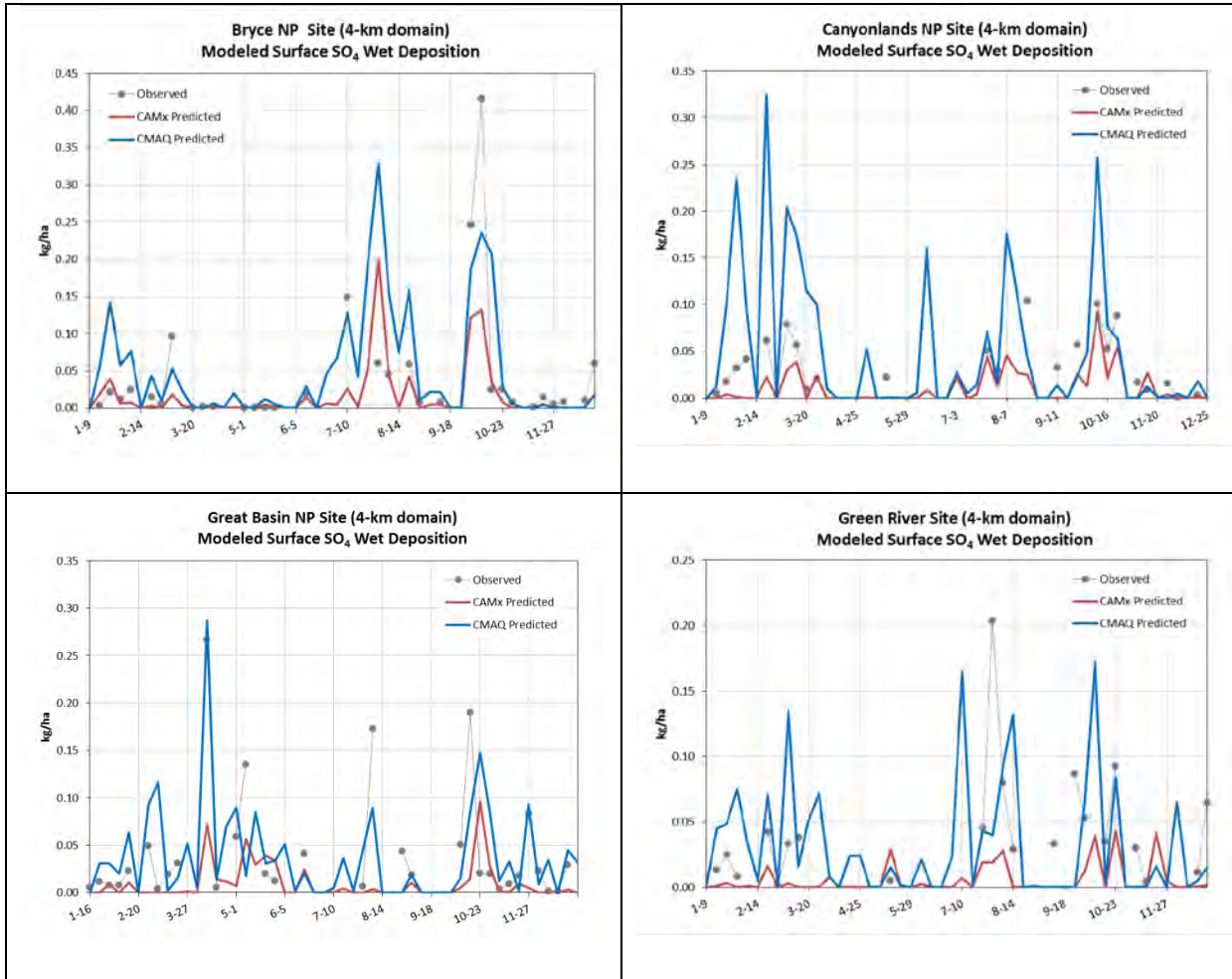
Figure 4.5-2   Annual Time Series for Sulfate at Selected NADP Sites
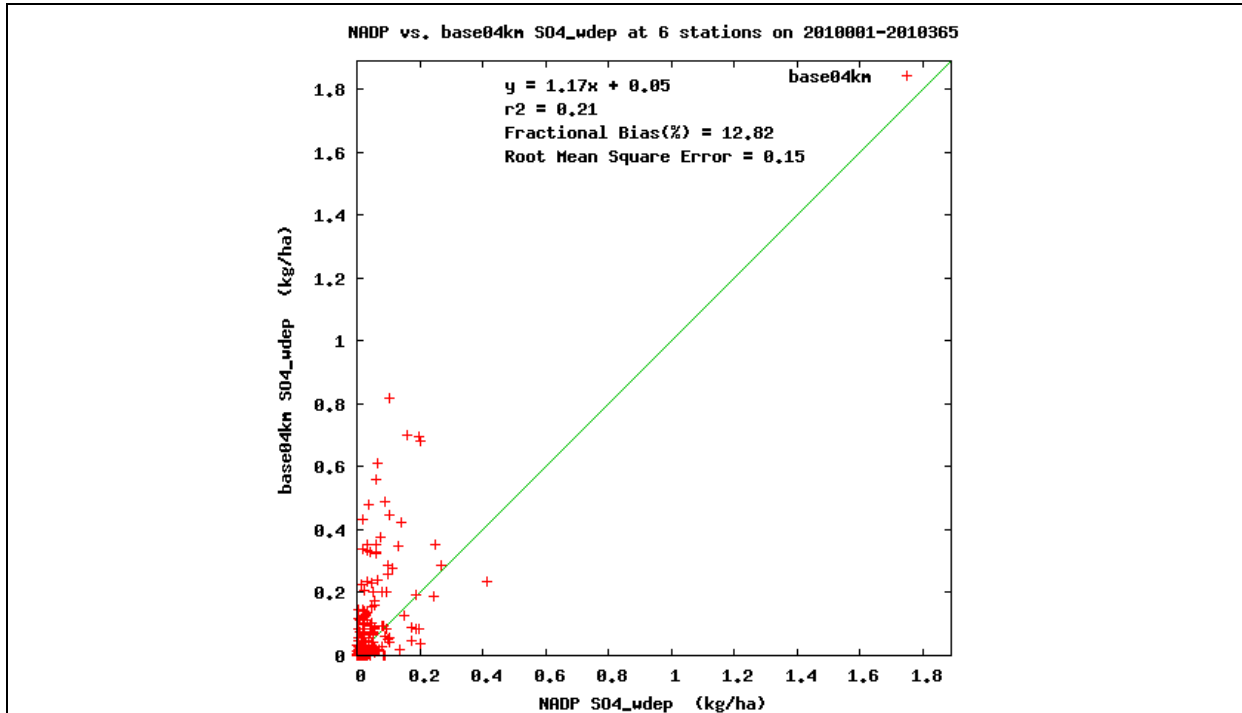
Figure 4.5-3   Scatter Plot for Sulfate Wet Deposition in the 4-km Domain
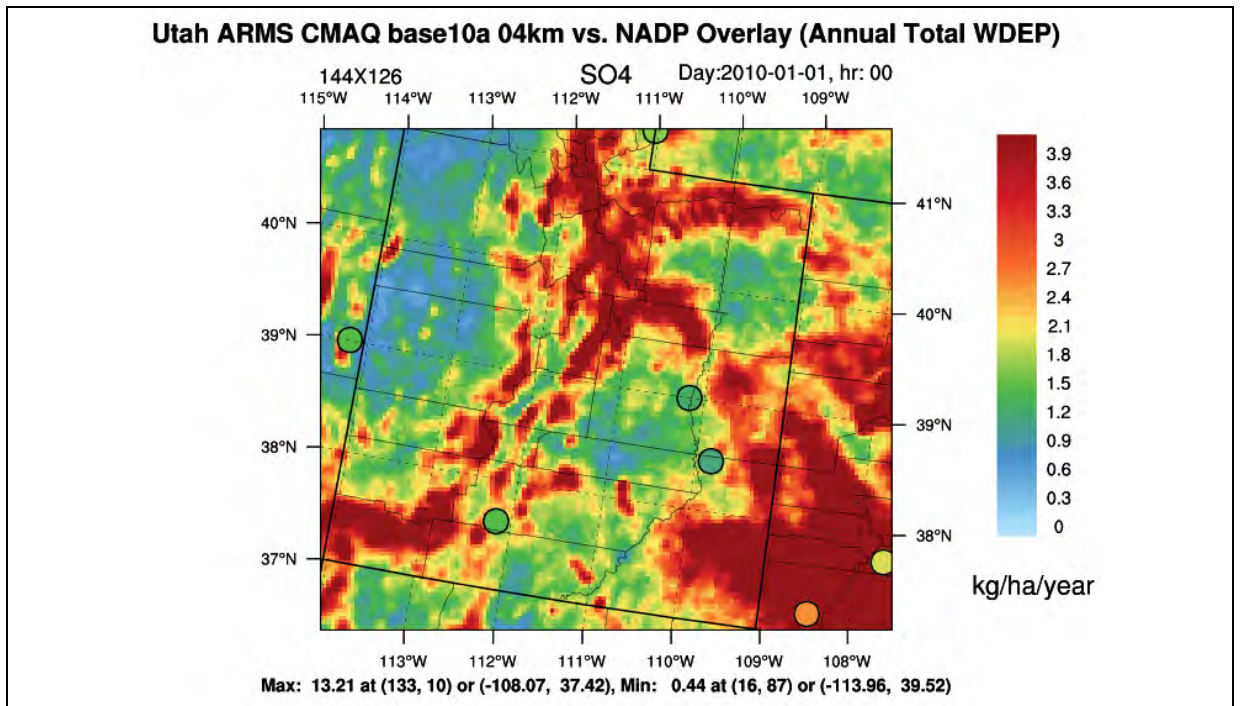
Figure 4.5-4   4-km Spatial Plot for Annual Sulfate Wet Deposition
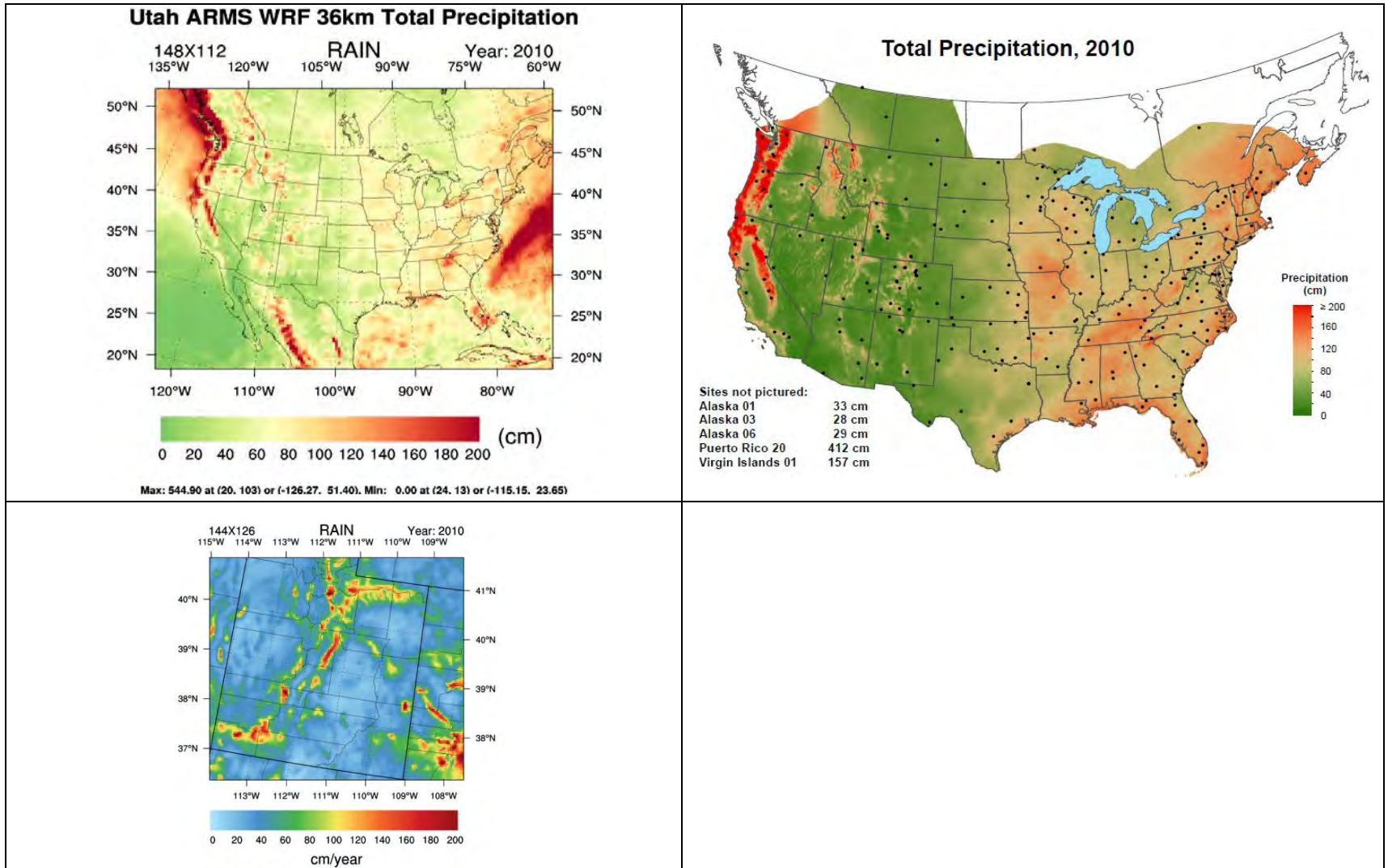
Source: NADP 2013.

Figure 4.5-5   Annual Precipitation from the CMAQ Model and NADP

Table 4.5-2 Model Performance Statistical Summary for Nitrate Wet Deposition

Monitoring Network	Statistic (percent)/ Concentration (kilogram per hectare [kg/ha])	36-km Domain					12-km Domain					4-km Domain				
		Annual	Winter	Spring	Summer	Fall	Annual	Winter	Spring	Summer	Fall	Annual	Winter	Spring	Summer	Fall
NADP (Annual/ Seasonal)	MFB	-7	3	2	-10	-24	-3	-9	20	29	-38	-27	-4	-2	-7	-70
	MFGE	75	83	69	71	79	96	101	87	84	101	99	97	102	82	105
	MNB	133	131	135	220	53	162	216	207	197	57	80	92	159	82	-5
	MNGE	186	180	180	274	118	221	278	250	234	138	153	148	218	139	96
	NMB	-3	34	2	-18	-13	23	25	31	39	-22	35	64	79	32	-29
	NME	65	84	62	61	63	96	106	94	97	81	95	97	124	92	64
	R^2	0.222	0.273	0.284	0.137	0.260	0.121	0.135	0.103	0.068	0.070	0.321	0.654	0.305	0.129	0.330
	Observed Mean Deposition (kg/ha)	0.15	0.10	0.15	0.22	0.12	0.10	0.08	0.11	0.15	0.07	0.09	0.07	0.06	0.19	0.07
	Predicted Mean Deposition (kg/ha)	0.15	0.14	0.16	0.18	0.10	0.13	0.10	0.14	0.21	0.06	0.12	0.11	0.11	0.25	0.05
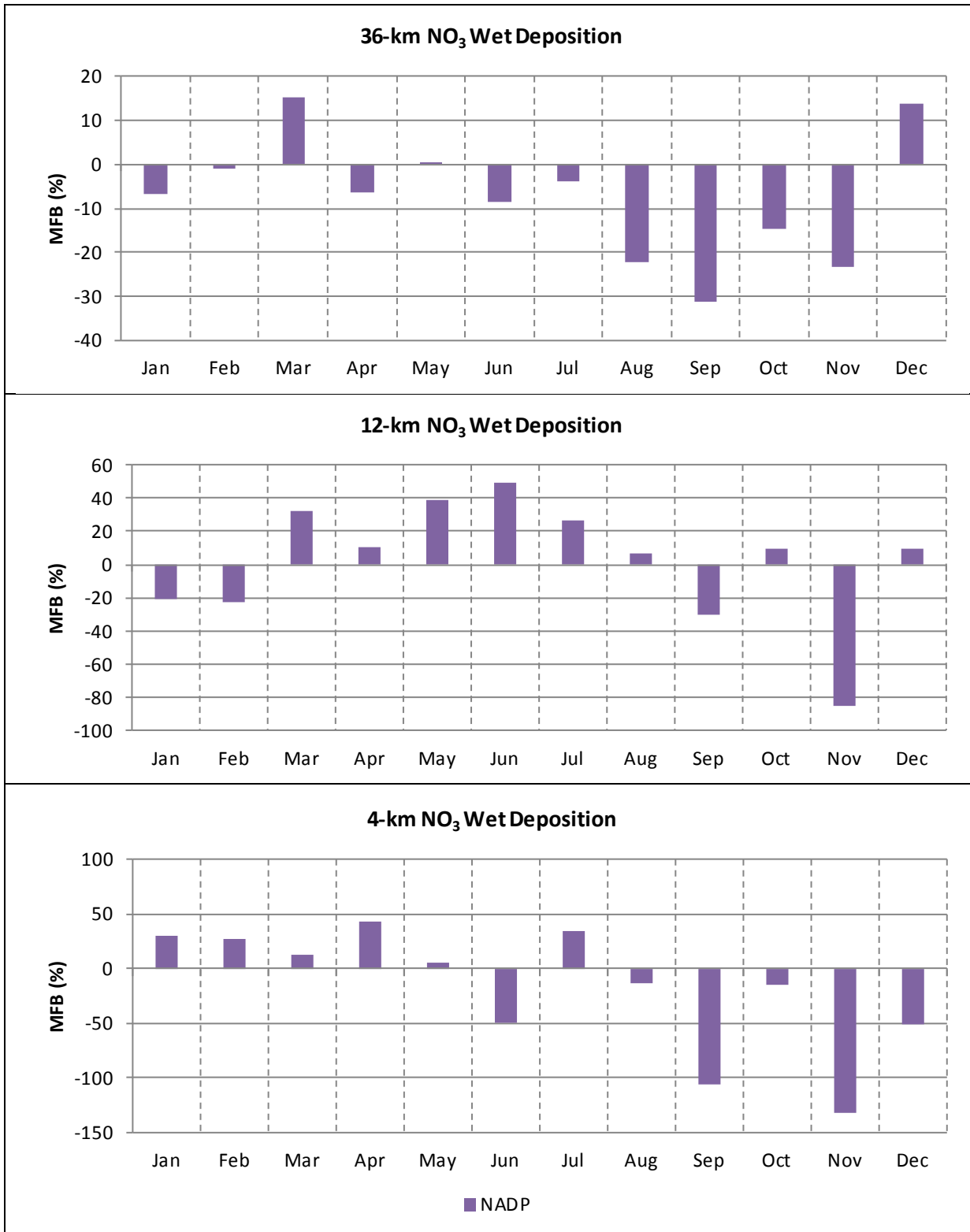
Figure 4.5-6   Monthly Normalized Mean Bias for Nitrate
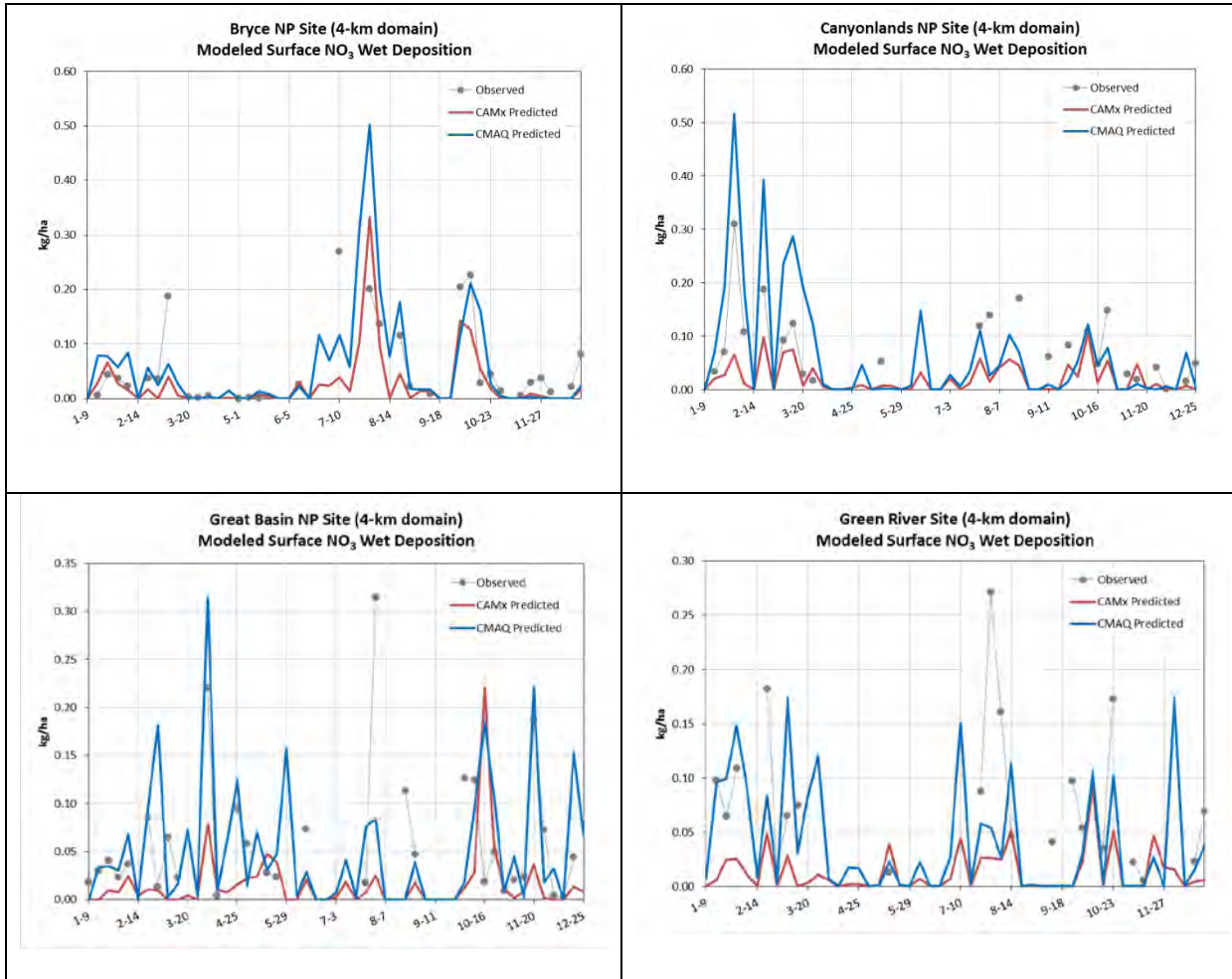
Figure 4.5-7   Annual Time Series for Nitrate at Selected NADP Sites
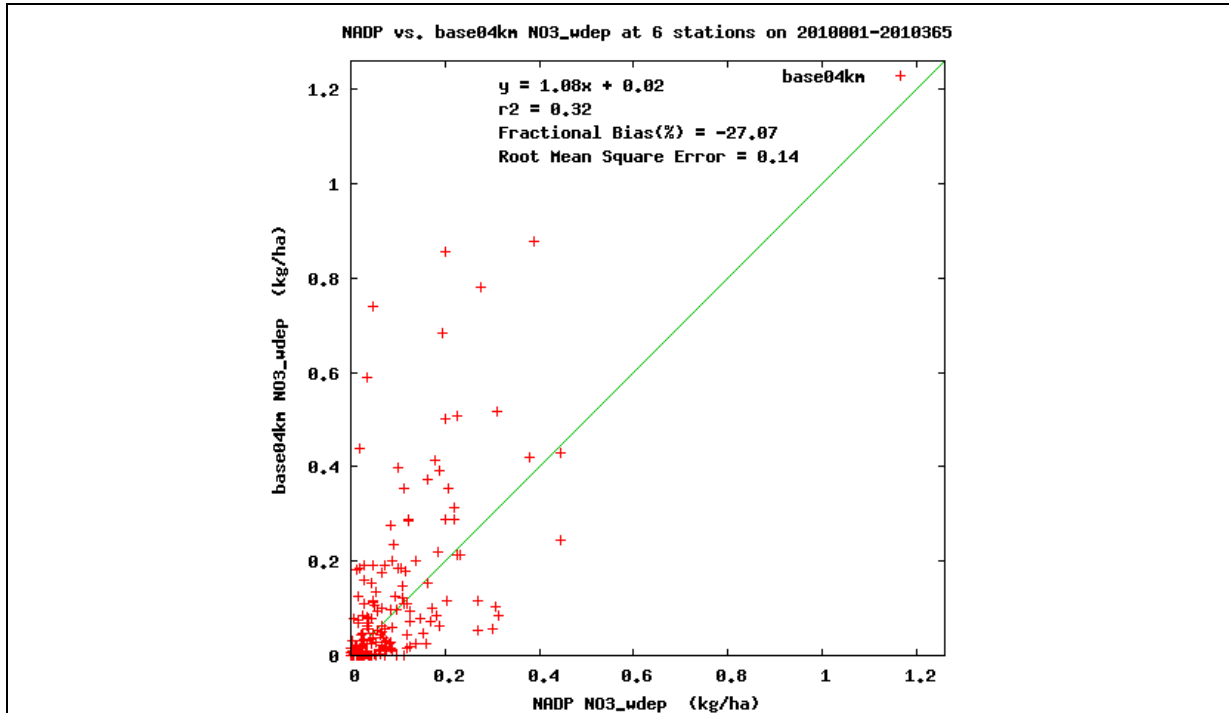
Figure 4.5-8   Scatter Plot for Nitrate Wet Deposition in the 4-km Domain
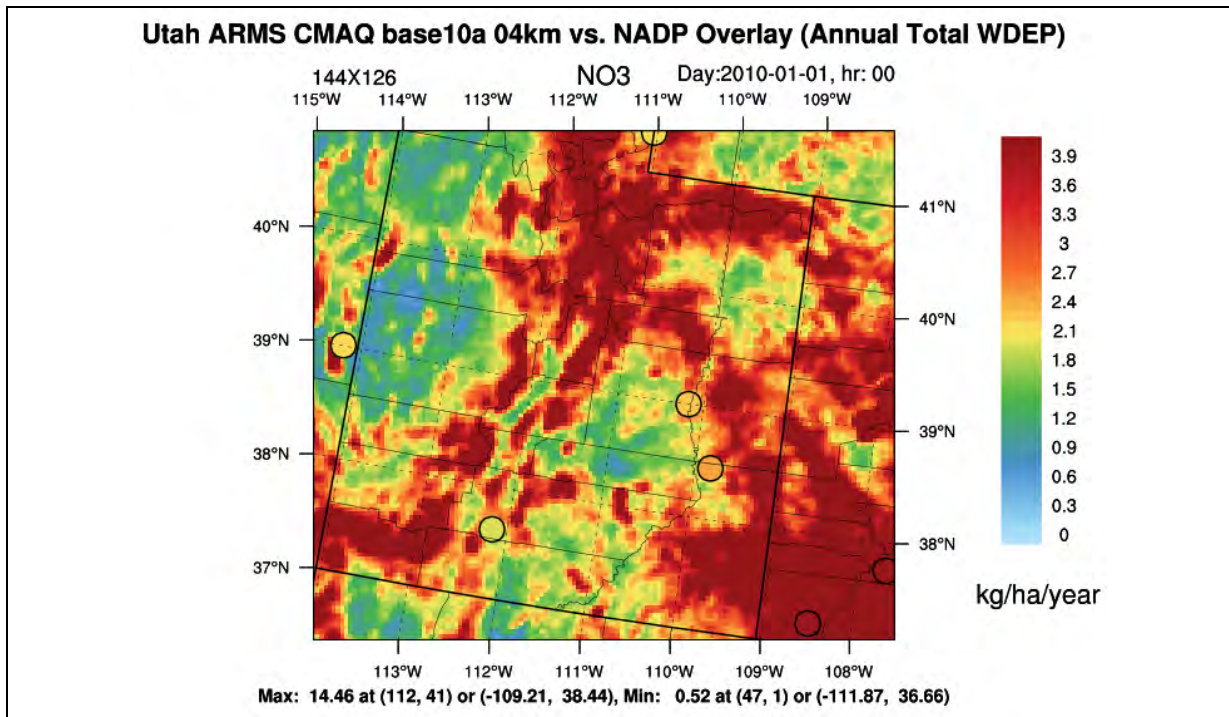
Figure 4.5-9   4-km Spatial Plot for Annual Nitrate Wet Deposition

Table 4.5-3   Model Performance Statistical Summary for Ammonium Wet Deposition

Monitoring Network	Statistic (percent)/ Concentration (kilogram per hectare [kg/ha])	36-km Domain					12-km Domain					4-km Domain				
		Annual	Winter	Spring	Summer	Fall	Annual	Winter	Spring	Summer	Fall	Annual	Winter	Spring	Summer	Fall
NADP (Annual/ Seasonal)	MFB	7	-7	11	32	-13	7	-14	30	50	-29	-6	-2	25	12	-53
	MFGE	83	88	76	84	82	106	116	100	98	105	108	110	116	93	102
	MNB	317	159	272	651	156	534	453	542	992	287	234	195	637	140	38
	MNGE	365	216	315	686	216	592	526	586	1023	366	299	260	686	189	127
	NMB	2	-3	-5	16	-18	38	41	40	64	-17	35	70	111	38	-23
	NME	72	76	63	80	65	115	140	112	126	85	108	126	153	113	68
	R^2	0.295	0.202	0.332	0.193	0.321	0.095	0.077	0.109	0.017	0.155	0.141	0.295	0.392	0.004	0.271
	Observed Mean Deposition (kg/ha)	0.05	0.03	0.07	0.08	0.05	0.03	0.02	0.04	0.04	0.02	0.02	0.01	0.01	0.05	0.03
	Predicted Mean Deposition (kg/ha)	0.05	0.02	0.06	0.09	0.04	0.04	0.03	0.05	0.07	0.02	0.03	0.02	0.03	0.07	0.02
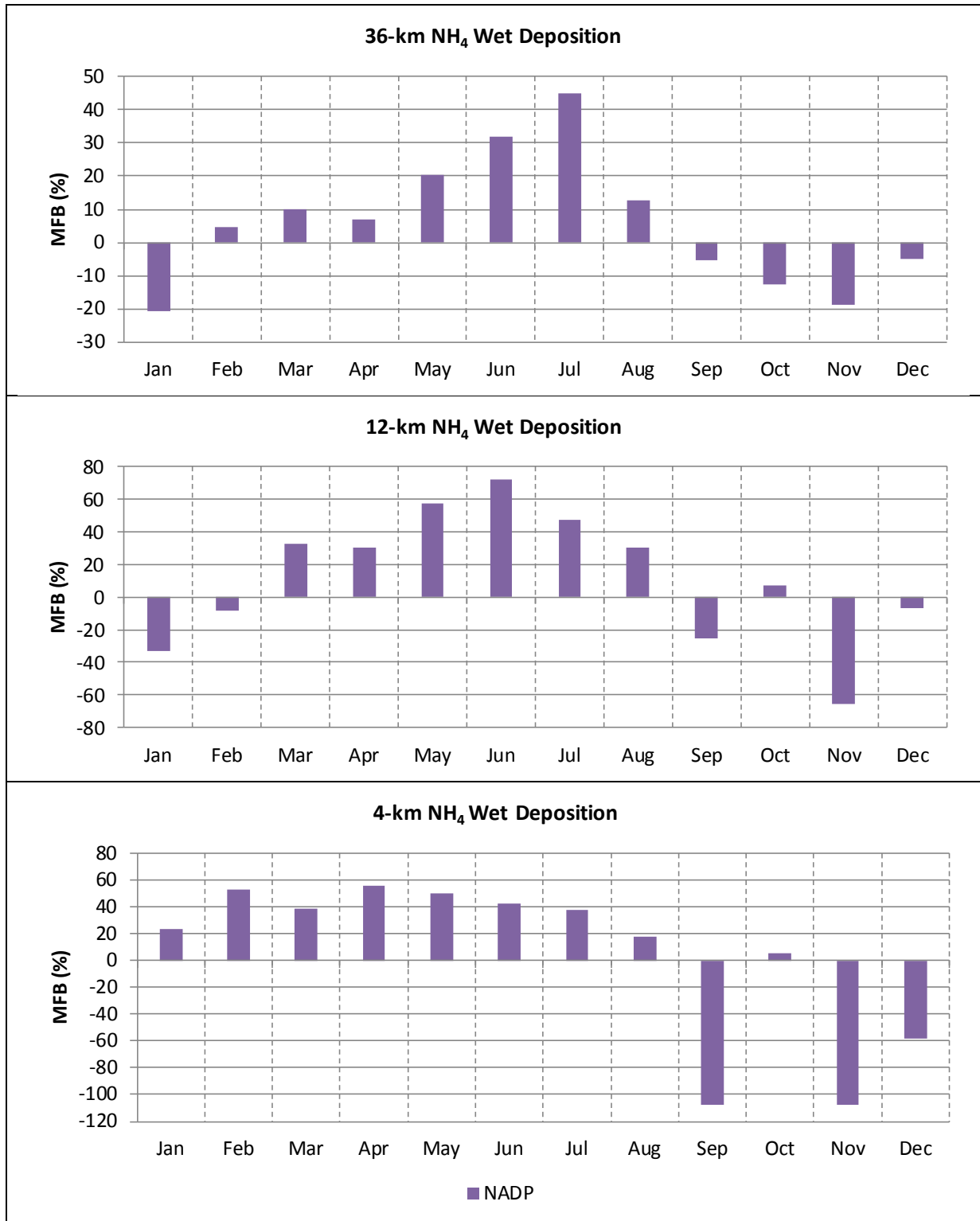
Figure 4.5-10   Monthly Normalized Mean Bias for Ammonium
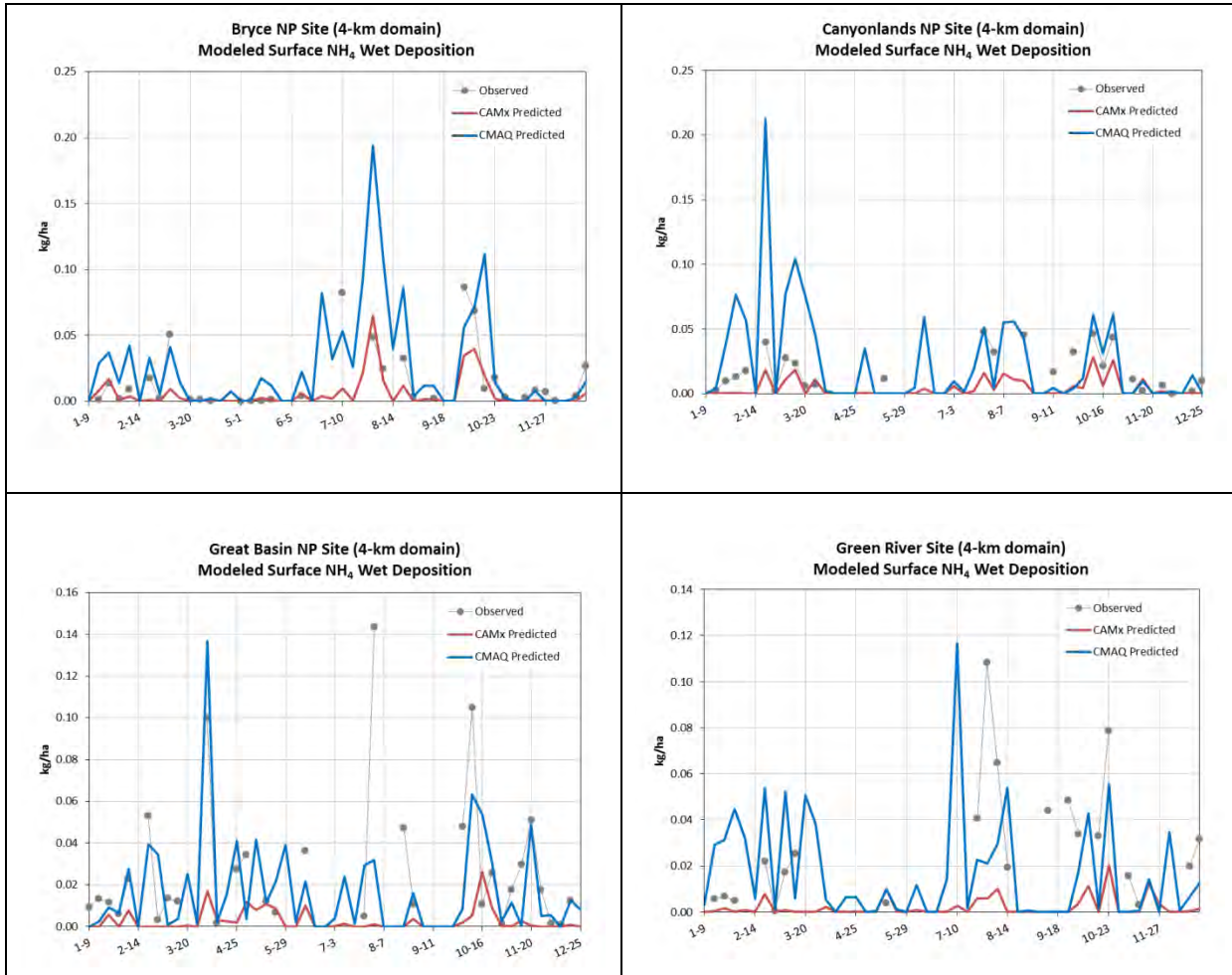
Figure 4.5-11   Annual Time Series for Ammonium at Selected NADP Sites
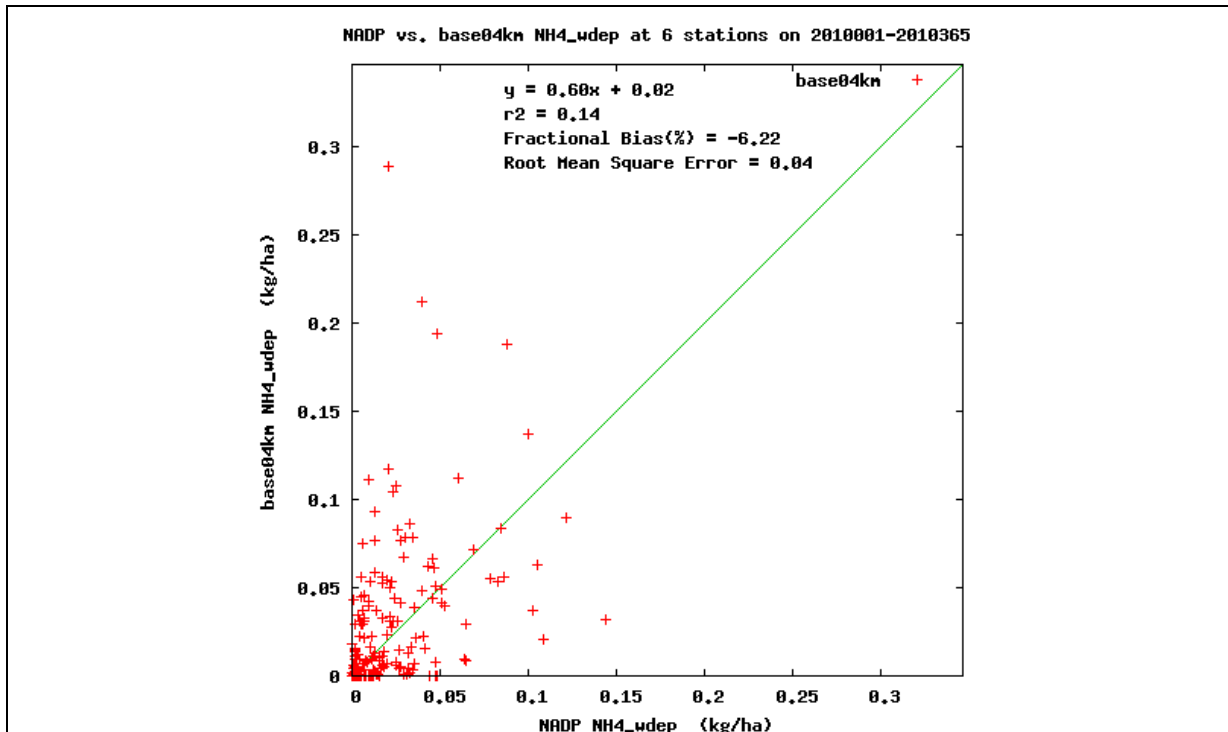
Figure 4.5-12   Scatter Plot for Ammonium Wet Deposition in the 4-km Domain
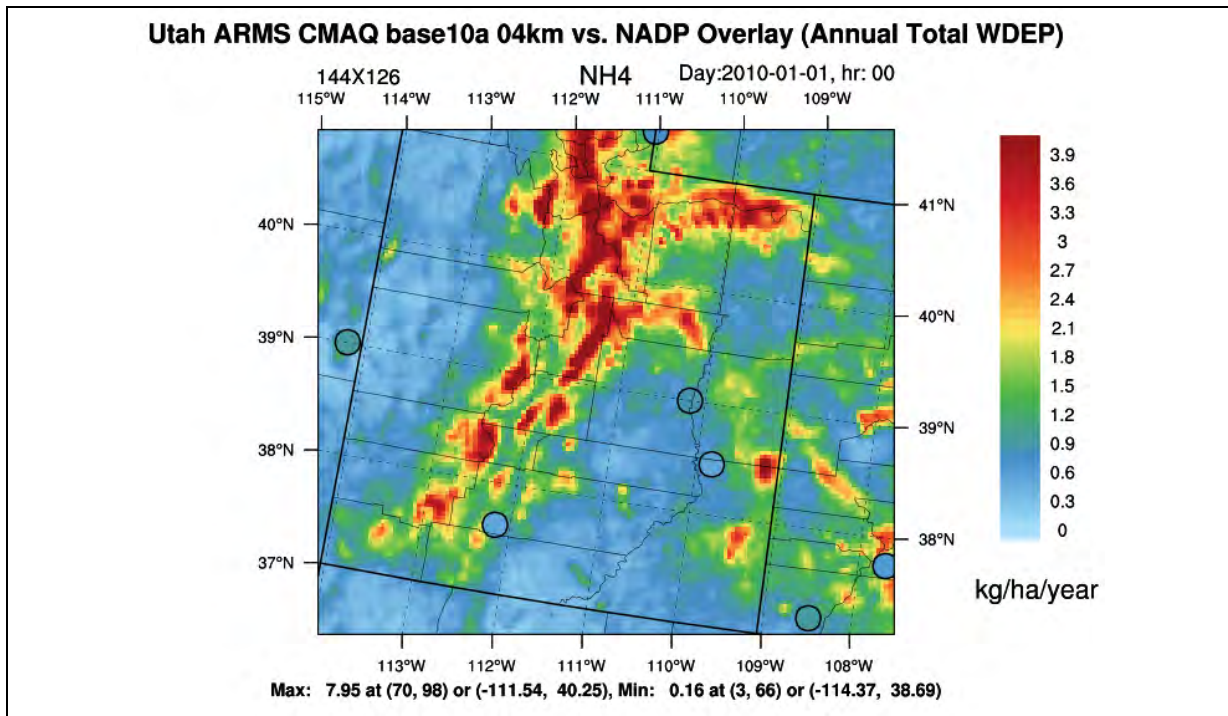
Figure 4.5-13   4-km Spatial Plot for Annual Ammonium Wet Deposition
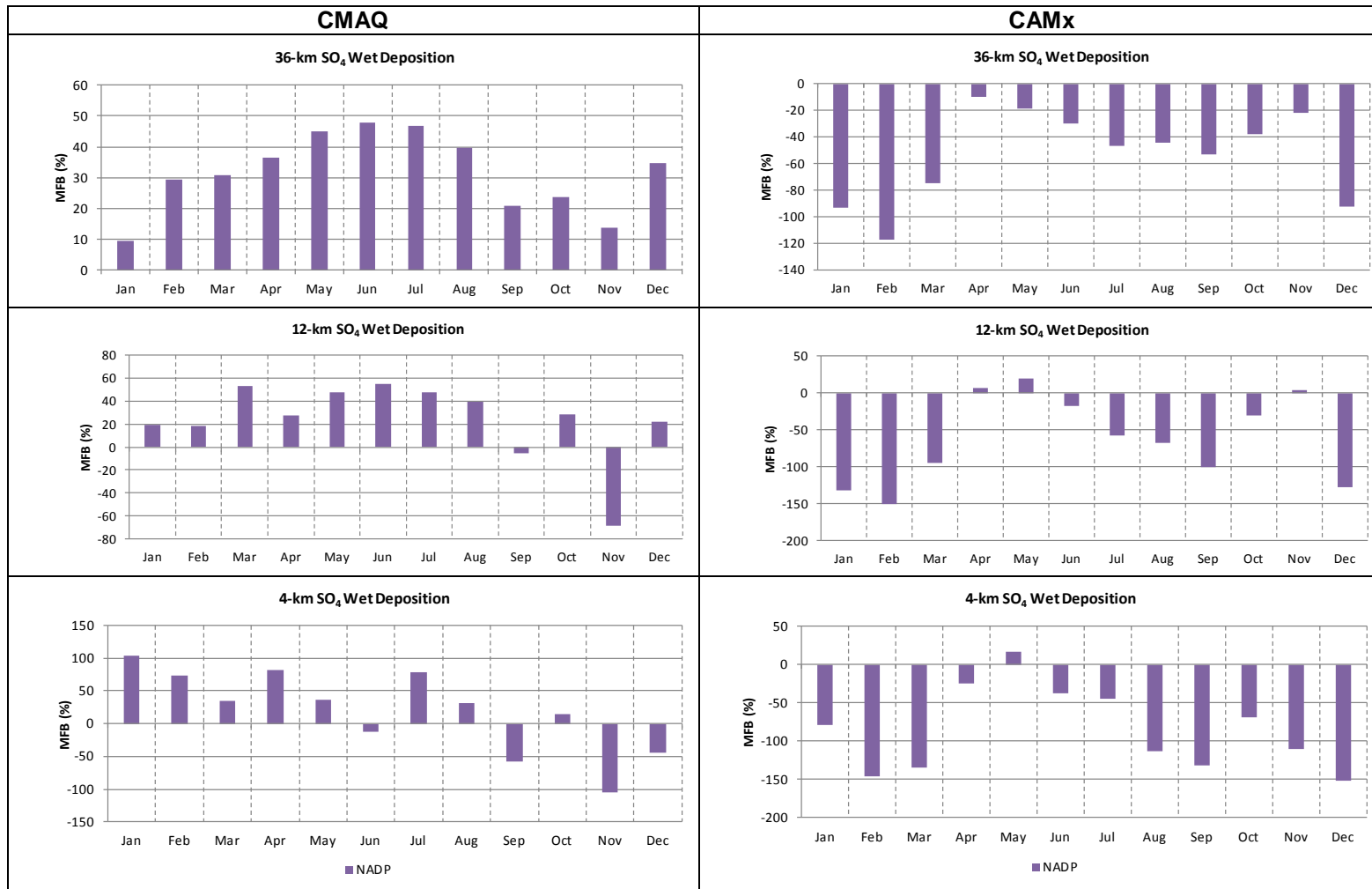
Figure 4.5-14   Mean Fractional Bias for sulfate wet deposition CMAQ (left) and CAMx (right)
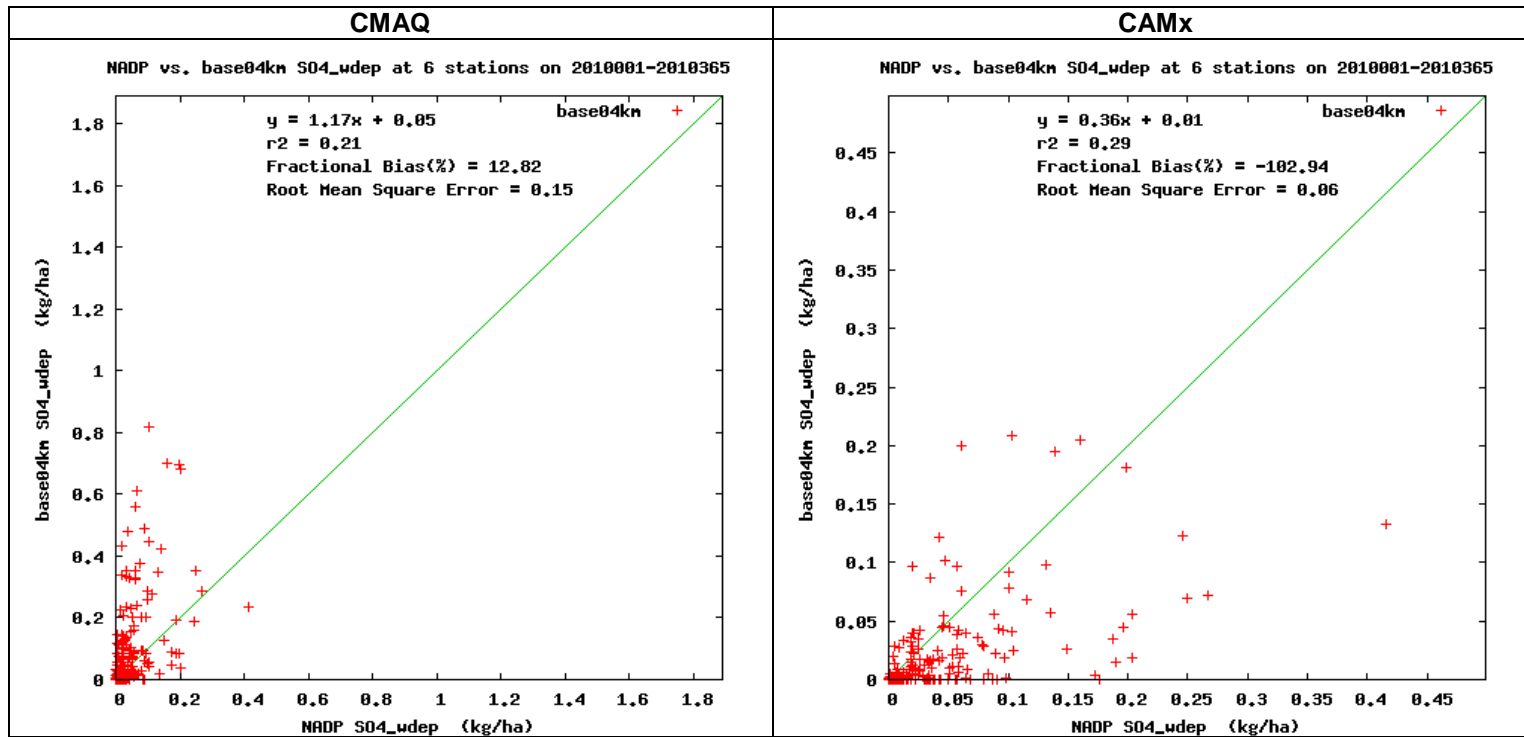
Figure 4.5-15   Scatterplot for sulfate wet deposition CMAQ (left) and CAMx (right)
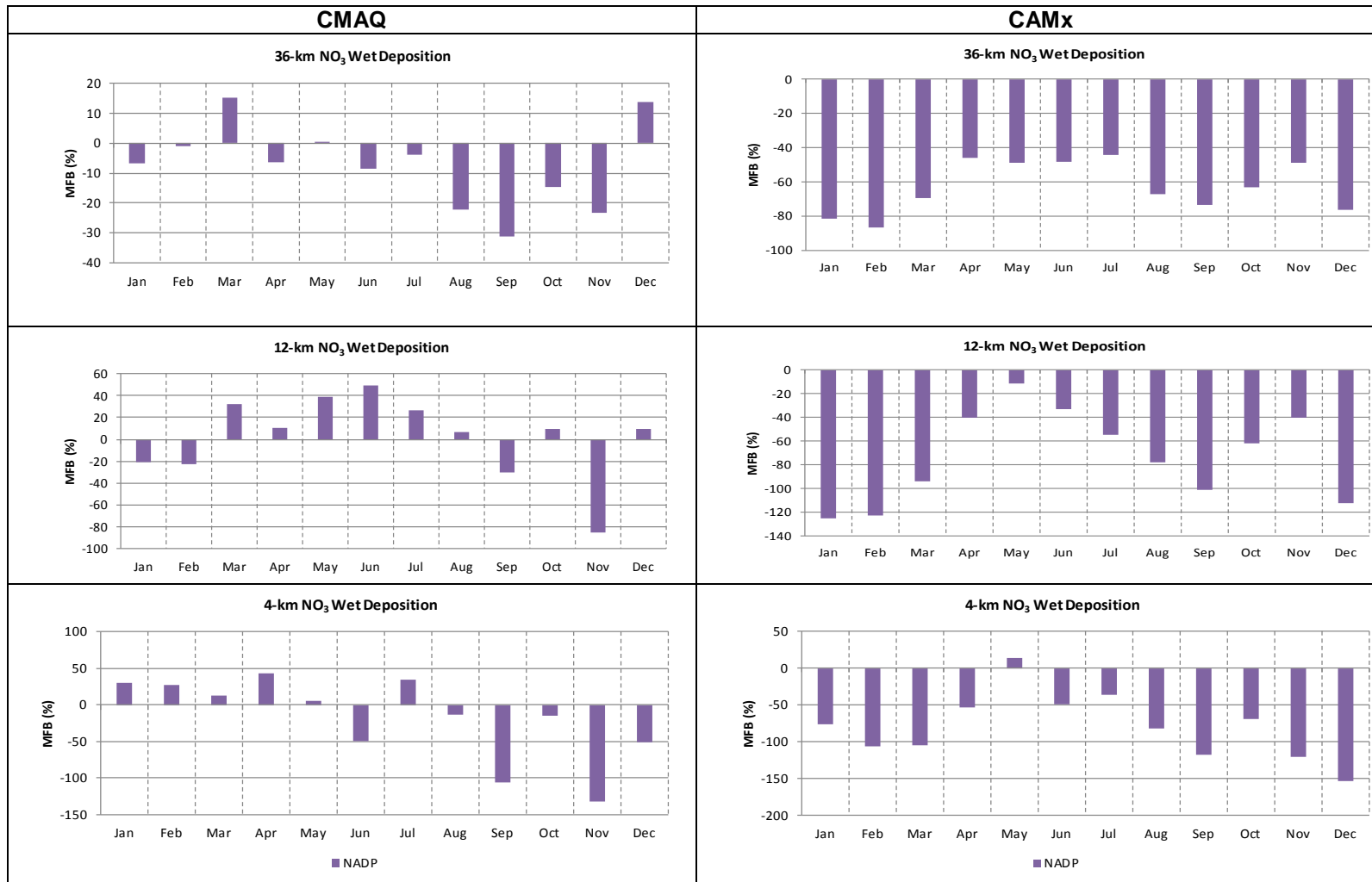
Figure 4.5-16   Mean Fractional Bias for nitrate wet deposition CMAQ (left) and CAMx (right)
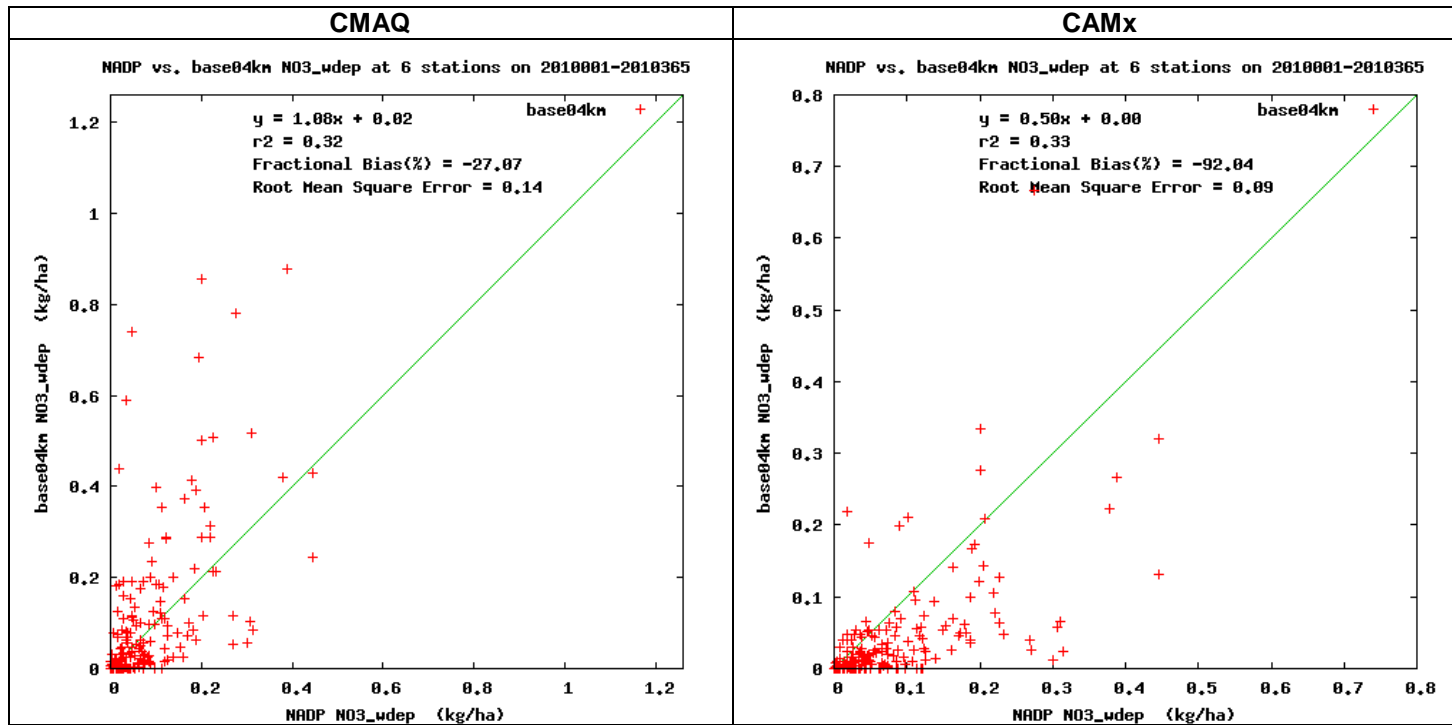
Figure 4.5-17   Scatterplot for nitrate wet deposition CMAQ (left) and CAMx (right)

Figure 4.5-18   Mean Fractional Bias for ammonium wet deposition CMAQ (left) and CAMx (right))
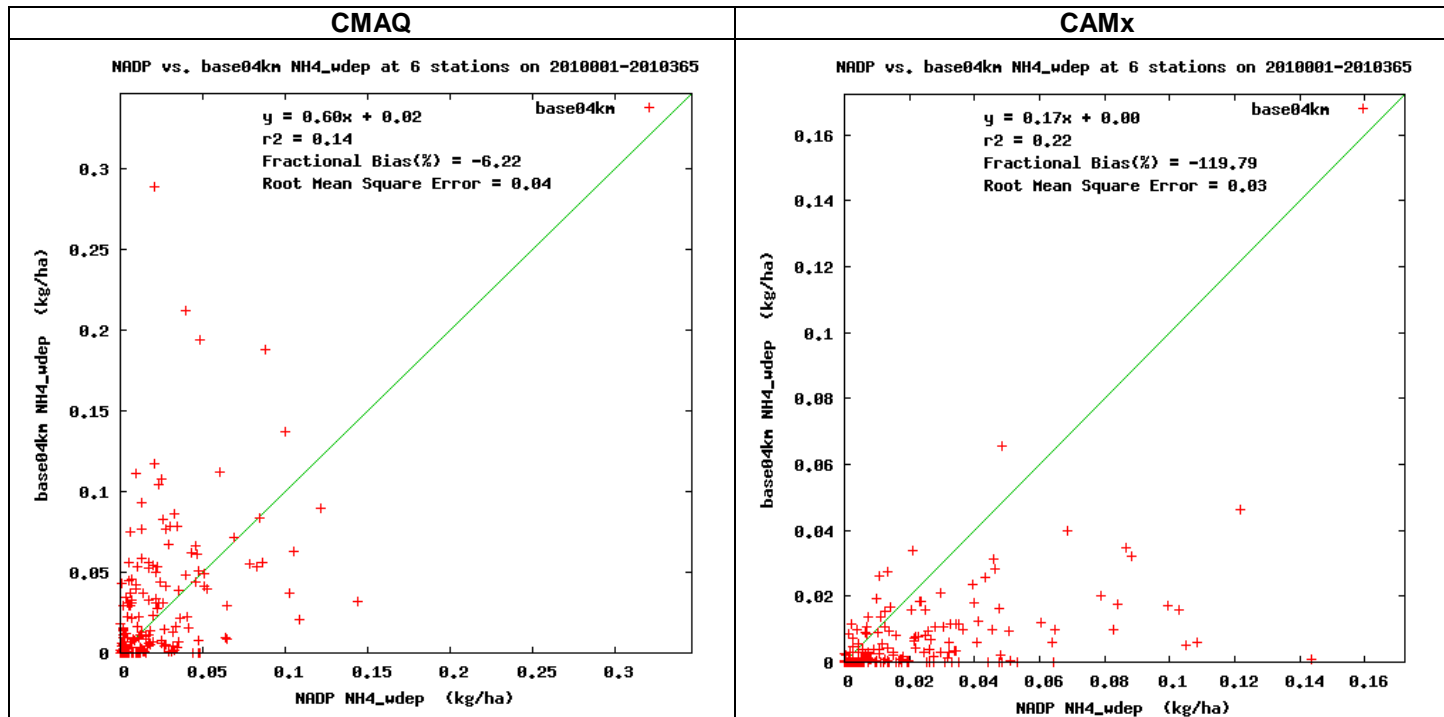
Figure 4.5-19   Scatter plot for ammonium wet deposition CMAQ (left) and CAMx (right)

5.0   Conclusions

The model performance is summarized below for applicable criteria air pollutants, as well as AQRVs for visibility and atmospheric deposition in order to provide an overview of the model errors and biases identified as part of this operational MPE. The discussion is focused on model limitations that could affect future studies that rely on the ARMS 2010 model platform. It is important to note that the USEPA (2007) does not consider regional photochemical grid models (PGM) appropriate for compliance demonstrations for most gas-phase criteria pollutants (excluding ozone); rather, their primary purpose of PGMs is for assessment of ozone, $PM_{2.5}$, and regional haze (visibility).

Following the summary of model performance for individual pollutants is a discussion of the atmospheric processes that influence the model performance for multiple pollutants that are chemically related. Of central importance to the evaluation of the overall model performance is an assessment of both the sources (either primary emissions or secondary formation processes) and the sinks (removal pathways and the corresponding atmospheric lifetimes) for individual pollutants. This information is then used to assess how these processes affect the model performance for chemically related pollutants. This approach is used to analyze and assess the overall model performance throughout the following sections.

Finally, this chapter provides a synthesis of CMAQ and CAMx similarities and differences. Based on evaluation and intercomparison of the models' performance, the CMAQ model is recommended for assessment of future impacts in the Uinta Basin, primarily since the CMAQ model is better able to replicate wintertime ozone formation and timing in the Uinta Basin.

5.1   Summary of Model Performance

5.1.1   Ozone

In general, the model performance for ozone was acceptable and meets the USEPA-recommended performance goals for all modeling domains, monitoring networks and seasons on a domain-wide basis, as supported by the MNB and MNGE model performance statistics for daily maximum 1-hour and daily maximum 8-hour average ozone with a 60 ppb threshold. While the daily maximum modeled concentrations compare well with the monitored daily maximum values, the MNB and MNGE values for the running 8-hour average ozone concentration (with the 60 ppb threshold applied) generally exceed USEPA performance criteria, indicating that although the model reproduces peak concentrations well, the timing of the daily peaks differs from monitored peaks. Importantly, in the context of assessing peak concentrations for comparison with AAQS, statistics computed from daily maximum 8-hour ozone concentration are most important for evaluating model performance and suitability.

The biases calculated when monitored values exceed 60 ppb suggest that the model generally under-predicts daily maximum 8-hour ozone concentrations, but over-predicts ozone concentrations within the 4-km domain during the summer and fall. While some measures of bias and error exceed the USEPA-recommended goals for the AQS monitoring network during the winter months modeled values relative to the CASTNET network are almost always within the USEPA-recommended goals throughout the year

Comparison of ozone modeling results with observations in the Uinta Basin shows the model is able to capture both episodic events and seasonal trends well, although the model consistently over-predicts ozone concentrations when observed values are below 30 ppb. Importantly, the model shows good agreement with periods of elevated winter ozone in the Uinta Basin, particularly relative to the Ouray monitor, which typically records the highest winter ozone concentrations in the Uinta Basin. The model is able to reproduce characteristics known to be important for winter ozone formation, namely the presence of snow cover; strong and persistent inversions; and light surface winds. Ozone precursor concentrations

generally follow expected spatial, temporal, and vertical trends, although there may be subtle spatial inaccuracies in the emissions sources that lead to under-predictions of ozone concentrations in the vicinity of Redwash and Dinosaur monitors. Two key differences between measured and modeled winter concentrations are that modeled peak ozone concentrations occur earlier in the day and decline more rapidly than measurements. Although limited monitoring data is available for comparison with the 2010 model results, modeled vertical ozone concentrations and spatial extent of surface maximums in the afternoon, when ozone concentrations peak, are generally consistent with observations during other years. The model under-predicts ozone concentrations in the nighttime and early morning hours during periods with elevated ozone.

In general, the model is able to capture the observed diurnal variation in ozone concentrations throughout the year, but tends to under-predict ozone peaks in winter and over-predict ozone peaks in summer. Given that the applicable AAQS and the tools used to predict future impacts are based on concentrations over 60 ppb, the model is considered to be suitable for assessment of both potential project-specific and cumulative ozone impacts. Importantly, any model biases for ozone are accounted for and minimized when the Model Attainment Test Software (MATS) tool is used in the assessment of future impacts.

5.1.2   Particulate Matter

In general, the model performs adequately for daily total $PM_{2.5}$ concentrations in most locations and seasons with a tendency to under-predict total $PM_{2.5}$ and PM_{10} concentrations. For the 12- and 4-km domain, the model systematically shows the largest under-predictions during the summer months while it tends to slightly over-predict $PM_{2.5}$ concentrations during the winter months. The model performance for total $PM_{2.5}$ is generally within the USEPA-established performance criteria for most months, monitoring networks and modeling domains. Although model $PM_{2.5}$ errors relative to hourly measurements often exceed USEPA-established performance criteria, the model performance relative to daily measurements are more relevant for comparison to AAQS which are for 24-hour or annual averaging periods. Given the good model performance for daily $PM_{2.5}$ relative to USEPA performance criteria, the model is considered suitable for cumulative $PM_{2.5}$ impact assessments.

Model estimates of total PM_{10} are under-predicted relative to observed concentrations for all modeling domains, time periods, and most monitoring networks except during the winter for IMPROVE. Seasonally, the model tends to be the most accurate in winter. The model performance for PM_{10} is frequently outside the USEPA-established performance criteria.

The overall performance for $PM_{2.5}$ and PM_{10} is related to the performance of their primary chemical constituents. There is variability in the model performance of these PM components; notably, the model tends to over-predict SO_4, NH_4, and SOIL and tends to under-predict NO_3, OC, EC, and CM in the 4-km domain. It is important to note that model biases for each chemical compound are accounted for and minimized when the MATS tool is used for predicting future impacts to $PM_{2.5}$ (AECOM 2012).

5.1.3   Other Gaseous Pollutants

Model performance for other gas-phase criteria pollutants was carefully analyzed to provide additional information for chemically related pollutants; however, PGMs are not intended to be used to assess impacts of gas-phase criteria pollutants with the exception of ozone (USEPA 2007).

Model results for NO_x show reasonable performance for all modeling domains, monitoring networks and seasons on a domain-wide basis. On the 4-km domain, the model under-predicts NO_x in the winter and fall and over-predicts NO_x in the spring and summer. In the Uinta Basin during winter, the model consistently under-predicts NO_x concentrations although performance is better at the Ouray site than at Redwash. In the Uinta Basin during summer, the model generally over-predicts peak nighttime NO_x concentrations at Ouray, under-predicts peak nighttime NO_x concentrations at Redwash, and performs well in the afternoon at both sites. Given that the model was able to reproduce the observed diurnal cycle

as well as the approximate magnitude of observed concentrations, the model is believed to be appropriate for ozone impact assessments. Model-predicted concentrations of short-term and annual NO_2 are not considered to be representative of maximum values, and a near-field modeling demonstration will be necessary for future site-specific analyses of potential impacts for comparison to applicable AAQS.

In general, the model tends to under-predict CO concentrations throughout the year for all the modeling domains. The NMB shows a general seasonal pattern for all modeling domains with the largest biases occurring in the winter and smallest in the summer. Spatial plots of modeled CO concentrations over two POIs indicated elevated CO concentrations in the Salt Lake City area and relatively low concentrations throughout the rest of the 4-km domain. Sparsely located monitors, however, indicate a general under-prediction of CO by the model throughout the 4-km domain. Model-predicted concentrations of CO are not considered to be representative of maximum values, and a near-field modeling demonstration will be necessary for future site-specific analyses of potential impacts for comparison to applicable AAQS.

In general, the model shows no clear trend of under-prediction or over-prediction for SO_2 concentrations relative to the AQS network, although the model systematically over-predicts SO_2 relative to CASTNet. The AQS monitors tend to be located in the Salt Lake City metropolitan area and therefore the statistical metrics based on the AQS network may not adequately represent SO_2 model performance throughout the entire 4-km domain or the Uinta Basin study area. The modeled spatial analysis indicated localized hotspots of SO_2 concentrations scattered throughout the 4-km domain that are likely attributable to emissions from electric generating units. While modeled SO_2 concentrations are low throughout the rest of the 4-km domain, the modeled values exhibit a high positive bias relative to the CASTNet network, indicating that monitored values are even lower in rural areas. Model-predicted short-term cumulative SO_2 values are usually not considered to be representative of maximum values, and near-field modeling demonstrations will be necessary to assess the potential impacts of specific sites for comparison to applicable AAQS.

5.1.4   Visibility

In general, the model performed well for total light extinction (b_{ext}) in both the 12- and 4-km domains. The model-predicted annual average total b_{ext} values are fairly consistent with reconstructed annual average b_{ext}. Based on the mean light extinction and MFB, the model tends to slightly over-predict the extinction during the winter and under-predict b_{ext} for all other seasons. The overall model performance for visibility is influenced by the contributions from individual PM species. The largest errors in the b_{ext} due to individual species are due to SS, followed by NO_3, CM, OC, SOIL, EC and SO_4 in decreasing order. In general, the model slightly over-predicts the contribution to the extinction from SO_4 in the 12-km and 4-km domains except during the summer. The model under-predicts b_{ext} for NO_3 in the 12-km except during the winter. For the 4-km domain, the model always over-predicts the NO_3 contributions except during the summer. The model always under-predicts the contributions to OC, EC, CM, and total PM_{10} throughout the year.

While the model was not able to reproduce maximum reconstructed b_{ext} values due to wildfire and windblown dust events, the model-predicted b_{ext} was similar to reconstructed b_{ext} during most seasons. Further analysis using stacked bar time series plots suggests that reconstructed b_{ext} during episodes of high b_{ext} was dominated by OC, which in the cases analyzed is an indicator of impacts from wildfire events, and CM, which is an indicator of windblown dust events. While the model predictions were not able to match the timing and magnitude of the observations during these fire and dust events, the impacts for the rest of the year were in general very similar to observations except during winter. The model is considered suitable for assessing visibility impacts for this study particularly since model biases for each chemical compound are accounted for and minimized by the MATS tool, which will be used for predicting future impacts to visibility.

5.1.5 Atmospheric Deposition

The modeled deposition performance was assessed for wet deposition, recognizing that dry deposition model performance is also important for assessing overall model performance. However, only wet deposition measurements are available for select species. In general, for the 12- and 4-km domains the model tends to over-predict SO_4 and NH_4 wet deposition for all three domains except in the fall and winter when it tends to under-predict the wet deposition of these ions. NO_3 wet deposition does not exhibit any particular seasonal trend for the bias that might indicate any systematic over- or under-prediction for its deposition values. A comparison between model predicted and spatially interpolated NADP annual precipitation was performed. This showed that the model spatial precipitation closely resembles the topographic features in the region like the Uinta Mountains, the Wasatch Range, the Pahvant Range and the Tushar Range. Generally, on an annual basis for the 4-km domain, the model is able to capture the spatial patterns as well as the magnitude of the observed precipitation. Annual time series comparison of CMAQ with SO_4, NH_4 and NO_3 wet deposition observations shows that the model is able to generally capture the correct magnitude and occasionally the correct timing of a significant number of deposition events within the 4-km domain. The spatial distribution of wet deposition from the model closely resembles the topographic features of the 4-km domain, since wet deposition is driven largely by precipitation. Based on the spatial variability of the wet deposition performance, the model is considered suitable for assessing wet deposition impacts; however since wet deposition impacts are only a portion of total deposition amounts, total modeled deposition results should be interpreted with care.

5.2 Assessment of the Model's Performance Limitations

5.2.1 Ozone

Ozone is a secondary pollutant that is photochemically formed in the atmosphere. The ozone concentrations in the troposphere are determined to a large extent by the concentrations of its precursors: volatile organic compounds (VOC) and nitrogen oxides (NO_x). The model ozone biases showed a fairly strong seasonal cycle for all networks in the 4-km domain where the model under-predicts concentrations from January to May and over-predicts them from June to October. The time series comparisons of modeled to observed ozone indicate the model generally was able to reproduce elevated ozone concentrations but not always the peak concentrations, particularly during winter months. Also the model is not able to accurately predict the lowest observed concentrations. The ability of the model to reproduce peak concentrations is important due to the use of peak 8-hour average values for AAQS.

Typically the highest observed ozone concentrations occur in the summer when higher temperatures and increased solar radiation favor ozone formation. However, the Uinta Basin study area experiences high ozone concentrations during the winter. During snowy winters in the Uinta Basin, NO_x and VOC precursors are able to form ozone under stagnant conditions with a strong temperature inversion. The presence of snow covered greatly enhances the surface albedo and therefore the photochemistry. The importance of HONO and heterogeneous reactions with the snow surfaces are not fully understood and could potentially play a role in ozone formation during winter episodes, particularly with respect to the model-predicted rapid decline in ozone concentrations in the afternoon. Based on a model sensitivity test, stratospheric ozone intrusions do not influence model results as described in **Appendix A**.

5.2.2 Nitrogen

When gaseous NO_x is emitted into the atmosphere there are several possible removal pathways, either by dry deposition or various chemical oxidation reactions leading to the formation of compounds such as nitric acid (HNO_3), particulate NO_3 and peroxyacetyl nitrate. HNO_3 is quickly removed from the atmosphere via dry deposition or by reaction with available NH_3 to form particulate ammonium nitrate. As a result of these rapid removal pathways, the typical atmospheric lifetime for NO_x is fairly short: approximately 1 day before it is removed or converted into a different compound.

The MPE results in the 4-km domain show that during the winter and fall the model slightly under-predicts NO_x concentrations while it slightly over-predicts concentrations during the summer. Additionally time series in the Uinta Basin study area for selected POI generally confirms these findings. Spatial overlay plots also illustrate the ability of the model to properly capture the spatial gradients of NO_x, however the location of AQS monitors around urban areas does not allow for a complete comparison with NO_x concentrations in remote and rural areas.

The MPE results show that the model performance for NO_x slightly over-predicts concentrations in the summer, which correlates with the largest over-predictions seen for nitric acid that occur in the spring and summer. Particulate NO_3 shows a different seasonal trend with the largest over-predictions occurring during the winter and fall and the largest under-predictions during the summer. When the total nitrate (HNO_3 combined with particulate NO_3) estimated from the model is compared with observations, the model performance generally improves, although the total NO_3 is over-predicted throughout the year and the over-prediction during winter is significant.

Combined, there is indication that during winter NO_x reaction products tend to be oxidized into NO_3 more rapidly than may occur in the atmosphere. If sufficient ammonia is available, the resulting NO_3 is likely to be in the form of particulate NO_3 during the winter season when temperatures are low and relative humidity is higher. During summer, NO_3 will tend to remain as gaseous HNO_3. The model tends to over-estimate the particulate concentration in the winter and under-estimate it during the summer. This same seasonal pattern is evident in the NH_4 model performance, although to a lesser extent. In addition, this seasonal bias affects AQRVs that are sensitive to ammonium nitrate concentrations.

In particular, the visibility MFB tend to follow the same seasonal trends as particulate NO_3 MFB, underestimating the contribution of particulate NO_3 to the total light extinction during the summer but overestimating it during the winter. Importantly, even with predicted particulate NO_3 concentrations being over-predicted in the winter, NO_3 wet deposition shows the largest under-prediction occurs during the winter (small under-predictions of NH_4 wet deposition also occur in winter). This could be due to the model not able to properly represent the wet removal processes during winter since wet deposition biases are a combination of both the concentration and precipitation fields. It is also possible that the overall nitrogen deposition (as the sum of both dry and wet deposition) could be more accurate than the wet deposition results might otherwise indicate because dry deposition of HNO_3 is very sensitive to HNO_3 concentrations.

5.2.3   Carbon Monoxide

The CO emissions are closely related to combustion sources and, therefore, strongly correlated to NO_x emissions. The MPE shows that modeled CO concentrations were systematically under-predicted throughout the year for all modeling domains, while NO_x concentrations are generally over-predicted during the summer months. CO is quite different from NO_x in that it is relatively unreactive and, thus, has a longer atmospheric lifetime of several months in the troposphere. Therefore, it seems more likely that CO is under-estimated in the emissions inventory and may not be suitable for use as a tracer.

5.2.4   Sulfur

Once gaseous SO_2 is emitted into the atmosphere there are several possible removal pathways, either by wet and dry deposition or various chemical reaction processes leading to the formation of particulate SO_4. The typical lifetime for SO_2 is approximately 1 day before it is removed or converted into particulate SO_4, while the typical lifetime of SO_4 in the troposphere is approximately 5 days before it is removed, primarily via wet deposition. Due to the longer lifetime, SO_4 generally is transported farther than SO_2, which has important implications when comparing model results to monitored values. While the SO_2 MPE is primarily a comparison of the model to locally emitted SO_2, the SO_4 MPE reflects performance for both SO_4 formed relatively close to the monitor as well as SO_4 that has been transported from upwind locations, potentially even from the boundary conditions.

The MPE shows that SO_2 biases varied between positive and negative values depending on the season and monitoring network. In particular, predicted 4-km SO_2 concentrations show no clear trend of under-prediction or over-prediction for SO_2 concentrations relative to the AQS network, while results were systematically over-predicted relative to CATNet. The location of monitors in the AQS network is meant to capture an anthropogenic/urban mix of pollutants, which could be an indication of potential shortcomings with the emissions inventories or the transport of SO_2 in urban areas. For CASTNet, the location of the monitors in the network tends to reflect a more rural atmosphere. For these rural networks, the model performance showed a systematic over-prediction of SO_2 concentrations throughout the year although both the modeled and monitored concentrations were very low. In some instances, the model overstated the SO_4 influence from wildfires, which is a reflection of how difficult it is to accurately model the transport of complex smoke plumes. Importantly, the model performance for particulate SO_4 is different from SO_2 and indicates good model performance for all monitoring networks and modeling domains, independent of season, albeit with slight over-prediction in winter.

The different model performance results between SO_2 and SO_4 is due, in part, to the different atmospheric lifetimes of these compounds.

5.2.5   Dust

Windblown dust from exposed surfaces and fugitive dust from surface disturbances are challenging sources to model due to temporal and spatial variability in site-specific factors including soil type, soil moisture, and wind gusts. During the spring, but particularly in April and May, a series of spring frontal systems affected the Southwestern US increasing the windblown dust. Importantly, only a small fraction of monitoring sites collects information necessary to assess the composition of PM and identify the fraction that is composed of crustal material (e.g., SOIL or CM). The model evaluation relative to SOIL and CM indicates that the model over-predicted SOIL (which is soil in the fine size mode) in the winter months and significantly under-predicted CM throughout the year. Dust also affects visibility conditions. In late spring in 2010, large light extinction values were observed in some areas (Mesa Verde NP and Weminuche WA in Colorado) cooincident with episodes of windblown dust. The model was not able to reproduce any of these monitored dust events. Altogether the model performance for dust in late spring and summer indicates large under-predictions which is attributable to the dust emissions inventory. The model tendency to under-predict CM and thus the total PM_{10} and windblown dust impacts to visibility will be qualified when reporting model predicted impacts.

5.2.6   Organic Particulates

Wildfires are a key contributor to air quality impacts and visibility impairment in the western U.S. The occurrence of wildfires influences the concentrations of ozone, particulates (primarily OC and EC as well as total $PM_{2.5}$ and PM_{10}), and visibility. During the summer and early fall, a series of wildfires affected the western U.S and in particular the state of Utah. The model is able to capture some instances in which particulate concentration increased and visibility was impacted due to wildfires. In some instances, the model overstated the influence from wildfires, which is a reflection of how difficult it is to accurately model the transport of complex smoke plumes.

5.3   Summary of Model Inter-comparison

A variety of statistical and graphical analyses were developed from both CMAQ and CAMx model results. These analyses were examined to understand how both models performed relative to USEPA performance benchmarks, and to each other. The analyses covered all of the key gaseous and particulate pollutant species. Model performance was analyzed on a domain-wide basis for all three modeling domains, with special attention paid to how the models performed within the Uinta Basin on the 4-km domain.

For ozone, both models performed well on a domain-wide basis for all three modeling domains, with biases and errors well within USEPA recommended performance criteria for all months except

December, when ozone monitoring data are limited. CMAQ biases were generally smaller in magnitude than in CAMx, except during the summer months in the 4-km domain. In the Uinta Basin, both models produced enhanced ozone concentrations during the observed winter ozone episodes. Although both models under-predicted peak daily ozone concentrations, CMAQ produced higher ozone concentrations and reproduced observed maximum concentrations better than CAMx when observed ozone concentrations were highest in the Uinta Basin. Both models under-predicted NO_x concentrations in the Uinta basin during the winter ozone episodes, though peak NO_x concentrations were sometimes higher in CMAQ. CAMx tends to have higher ozone dry deposition rates than CMAQ despite the fact that the CAMx ozone concentrations are generally lower than CMAQ for the periods included in the analysis. During the summer, both models performed well with respect to ozone in the Uinta Basin, with both models slightly over-predicting peak ozone concentrations.

For total $PM_{2.5}$, both models performed reasonably well on a domain-wide basis for all three modeling domains. For most months, biases and errors are within USEPA recommended performance criteria. However, on the 4-km domain, CMAQ did not meet these performance criteria during the summer, while CAMx did not meet the criteria during the winter. Both models tended to under-predict $PM_{2.5}$ concentrations during the summer and over-predict during the winter. In the Uinta Basin, CMAQ produced significantly higher $PM_{2.5}$ concentrations and reproduced observed concentrations better than CAMx during the winter air quality episodes. During the summer, both models significantly under-predicted $PM_{2.5}$ concentrations in the Uinta Basin, and neither model captured the fire-induced $PM_{2.5}$ enhancements observed in August. For individual particulate species, model performance tendencies varied depending on domain, season, species, and monitoring network. For both models, performance metrics consistently fell within USEPA recommended performance criteria for sulfate, nitrate, and ammonium, with CMAQ producing slightly smaller annual sulfate biases than CAMx. Both models struggled to meet model performance criteria during some seasons and monitoring networks for other particulate components, such as elemental carbon, organic carbon, and fine soil.

5.4   Summary

Based on the detailed model inter-comparison performed between CMAQ and CAMx, CMAQ is the recommended modeling system for the ARMS Modeling Platform. This recommendation is driven primarily by the fact that CMAQ provided superior performance for ozone and total $PM_{2.5}$ in the Uinta Basin during wintertime ozone episodes. CMAQ also provided slightly better overall domain-wide performance for ozone and wet deposition. Both models performed similarly well for total $PM_{2.5}$ concentration and visibility. In conclusion, the CMAQ model is considered suitable for assessing the impacts on certain pollutants (ozone, $PM_{2.5}$, regional haze [visibility], deposition). The model performance for these pollutants typically was within the USEPA-recommended performance criteria. While the model under-predicted concentrations of other gas-phase criteria pollutants, this is consistent with other studies and recognized limitations of the model. As part of ARMS future year impacts assessment, all results will be reported but results will be qualified based on the findings described in this MPE.

6.0   References

AECOM Environment (AECOM). 2013. Utah State BLM Emissions Inventory Technical Support Document. Prepared for Utah Bureau of Land Management. November 2013.

_____ . 2012. Utah Air Resource Management Strategy Air Quality Modeling and Assessment Protocol. Prepared for Utah Bureau of Land Management. January 2012.

AECOM and Sonoma Technology, Inc. (STI). 2013. Utah Air Resource Management Strategy Modeling Project: Meteorological Model Performance Evaluation. Prepared for Utah Bureau of Land Management. February 2013.

Ames, R. B. and W. C. Malm. 2001. Comparison of sulfate and nitrate particle mass concentrations measured by IMPROVE and the CDN, Atmos. Environ., 35, 905-916.

Boylan, J. W. and A. G. Russell. 2006. PM and Light Extinction Model Performance Metrics, Goals, and Criteria for Three-dimensional Air Quality Models. Atmospheric Environment 40(26):4946-4959.

Byun, D. and J. Ching. 1999. Science Algorithms of the USEPA Models-3 Community Multiscale Air Quality (CMAQ) Modeling System., USEPA Tech. Rep. USEPA-600/R-99/030. Available from USEPA/ORD, Washington, D.C. 20460.

Chien, C. J, G. S. Tonnesen, and B. Wang. 2005. Model Performance Evaluation Software User's Guide, Version 2.0.1, Air Quality Modeling Group, CE-CERT, University of California Riverside, Riverside, California.

Energy Dynamics Laboratory. 2011. Uinta Basin Winter Ozone and Air Quality Study Final Report. June 2011.

ENVIRON Corporation (ENVIRON). 2011. User's Guide: Comprehensive Air Quality Model with Extensions, Version 5.40, ENVIRON International Corporation. Novato, California. September 2011.

_____ . 2010. A Conceptual Model of Winter Ozone Episodes in Southwest Wyoming. Prepared for Air Quality Division of the Wyoming Department of Environmental Quality. January 2010.

Flanagan, J. B., R. K. M. Jayanty, E. E. Rickman, Jr., and M. R. Peterson. 2006. $PM_{2.5}$ Speciation Trends Network: Evaluation of Whole-System Uncertainties Using Data from Sites with Collocated Samplers, *J. Air & Waste Manage. Assoc.* 56, 492–499.

Gego, E. L., P. S. Porter, J. S. Irwin, C. Hogrefe, and S. T. Rao. 2005. Assessing Comparability of Ammonium, Nitrate, and Sulfate Concentrations Measured by Three Air Quality Monitoring Networks, *Pure Appl. Geophys.*, 162, 1919-1939, DOI 10.1007/s00024-005-2698-3.

Hand, J., L. and W. C. Malm. 2006. Review of the IMPROVE Equation for Estimating Ambient Light Extinction Coefficients. National Park Service. May, 2006. ISSN 0737-5352-71.

Lane, D. A., (ed.). 1999. Gas and Particle Phase Measurements of Atmospheric Organic Compounds, Advances in Environmental, Industrial, and Process Control Technologies, Volume 2, Gordon and Breach Science Publishers, 1999.

Liu, X., K. Chance, C. E. Sioris, T. P. Kurosu, R. J. D. Spurr, R. V. Martin, T. Fu, J. A. Logan,
    D. J. Jacob, P. I. Palmer, M. J. Newchurch, I. A. Megretskaia, and R. B. Chatfield. 2006. First
    Directly Retrieved Global Distribution of Tropospheric Column Ozone from GOME: Comparison
    with the GEOS-Chem Model. Journal of Geophysical Research, Atmospherics, 111, D02308,
    doi:10.1029/2005JD006564.

Malm, W. C., B. A. Schichtel, R. B. Ames, and K. A. Gebhart. 2002. A 10-year spatial and temporal trend
    of sulfate across the United States, *J. Geophys. Res.*, 107, 2002.

Malm, W. C., J. F. Sisler, D. Huffman, R. A. Eldred, and T. A. Cahill. 1994. Spatial and seasonal trends
    in particle concentration and optical extinction in the United States, *J. Geophys. Res.*, 99, D1,
    1347-1370.

National Aeronautics and Space Administration (NASA). 2013. Earth Observatory. Internet website:
    http://earthobservatory.nasa.gov/NaturalHazards/view.php?id=46199&eocn=image&eoci=relate
    d_image . Accessed December 2013.

National Atmospheric Deposition Program (NADP). 2013. Precipitation maps for year 2008. Internet
    website: http://nadp.sws.uiuc.edu/. Accessed April 2013.

National Oceanic and Atmospheric Administration. National Climatic Data Center (NOAA-NCDC). 2013.
    State of the Climate Wildfires June through September reports for 2010. Internet website:
    http://www.ncdc.noaa.gov/sotc/fire/2010/9 . Accessed December 2013.

Sickles, J. E. II, and D. S. Shadwick. 2008. Comparison of particulate sulfate and nitrate at collocated
    CASTNET and IMPROVE sites in the eastern US, Atmos. Environ., 42, 2062–2073, 2008.

Simon, H., Baker, K.R., Phillips, S. 2012. Compilation and interpretation of photochemical model
    performance statistics published between 2006 and 2012. Atmos. Environ., 61, 124-139, 2012.

The Smog Blog. 2013. U.S. Air Quality September 30, 2010.
    http://alg.umbc.edu/usaq/archives/2010_09.html . Accessed on December 2013.

Sonoma Technology, Inc. (STI). 2006. Regional and Local Contributions to Peak Local Ozone
    Concentrations in Six Western Cities by C. P. MacDonald, D. S. Miller, and S. M. Raffus.
    Prepared For Western States Air Resources Council. May 2006.

Tesche, T., R. Morris, G. Tonnesen, D. McNally, J. Boylan, and P. Brewer. 2005. CMAQ/CAMx Annual
    2002 Performance Evaluation over the Eastern U.S. Atmospheric Environment
    40(26):4906-4919.

Tonnesen, G., Z. Wang, M. Omary, and C. J Chien. 2006. Final Report for the Western Regional Air
    Partnership (WRAP) 2002 Visibility Model Performance Evaluation. Prepared for the Western
    Governors Association, Denver, Colorado. WGA Contract Number: 30203. February 24, 2006.

United States Environmental Protection Agency (USEPA). 2012. 2010 GEOS-Chem Simulation provided
    by USEPA (Akhtar) to AECOM (Chien) in November 2012.

_____ . 2007. Guidance on the Use of Models and Other Analyses for Demonstrating Attainment of Air
    Quality Goals for Ozone, PM$_{2.5}$, and Regional Haze. U.S. Environmental Protection Agency,
    Office of Air Quality and Planning Standards, Research Triangle Park, North Carolina.
    EPA-454/B-07-002. April 2007.

_____ . 2006. Office of Air Quality Planning & Standards, Outreach & Information Division, National Air Data Group, AQS Fundamentals, Version 1.0, Research Triangle Park, NC 27711 USA.

U.S. Geological Survey (USGS). 2013. Southwest Geographic Science Team Dust Detection. Internet website: http://sgst.wr.usgs.gov/dust_detection/dust-events/2010-2/ . Accessed December 2013.

U.S. Geological Survey (USGS). 2011. Physiographic Divisions of the Conterminous U.S. Internet website: http://water.usgs.gov/lookup/getgislist. Accessed January 17, 2011.

Utah Department of Environmental Quality. 2011. Uintah Basin Winter Ozone Study Plan and Budget: Draft Version 3.0. Prepared by B. LeBaron, G. Tonnessen, S. Hill, R. Martin, G. Petron, J. Roberts, R. Schnell, and P. Barickman for the Utah Department of Environmental Quality. October 2011.

Yarwood G., J. Jung, G. Heo, G. Whitten, J. Mellberg, and M. Estes. 2010. CB6 Version 6 of the Carbon Bond Mechanism. CMAS Conference, October 11-13, 2010, Chapel Hill, North Carolina.

Appendix A

Model Sensitivity Tests

Contents

List of Tables

List of Figures

A.0 Model Sensitivity Tests

A.1   Introduction

Observed ozone concentrations result from: 1) natural background ozone, 2) transported ozone generated from emissions from upwind urban centers and non-routine natural events such as wildfires, and 3) ozone generated from local anthropogenic emissions precursors (STI 2006). A model sensitivity study was conducted to evaluate the contribution of non-local sources of ozone (from natural and anthropogenic sources) to observed local ozone concentrations in the Uinta Basin study area. More specifically, the goals of the sensitivity study were to assess: 1) the contributions of ozone from the boundaries, 2) whether or not stratospheric ozone intrusions play a major role in modeled ozone concentrations, and 3) the influence of natural background conditions. The following two sets of model simulations were conducted for both CMAQ and CAMx for the sensitivity study:

- **Boundary Condition Sensitivity Test.** In this set of simulations, chemistry solvers and emissions inputs were turned off in both models to investigate the contribution of ozone transported into the modeling domains from the boundary conditions. In both the CMAQ and CAMx simulations, boundary conditions for the 36-km domain were obtained from the GEOS-Chem global model as described in Chapter 2 (USEPA 2013), while the boundary conditions for the nested domains were obtained from the 36-km model domain.

- **Natural Background Sensitivity Test.** In this set of simulations, the contribution of ozone from natural sources was investigated by turning on the chemistry solvers and deposition mechanisms, and by invoking a subset of emissions inputs in both models. Anthropogenic contributions within the modeling domains were zeroed-out in the emissions inputs for this test, leaving only naturally occurring emissions (e.g., biogenic emissions and wildfires).

To investigate important periods of interest in the Uinta Basin, while also considering computational efficiency, only one winter and one summer month (February 2010 and August 2010, respectively) were simulated for these tests. Both models have a two-week spin-up period for each simulation.

A.2   Boundary Condition Sensitivity Test

A.2.1   Boundary Condition Test Configuration

In order to evaluate the contribution of ozone transported into the modeling domains from the boundary conditions, a boundary condition test was performed with the initial conditions, natural emissions, and anthropogenic emissions set to zero. In addition, the chemistry solvers and deposition mechanisms were turned off, leaving transport and diffusion as the only physical processes that could affect ozone concentrations in the modeling systems. Pertinent CMAQ and CAMx model configuration options for this sensitivity test are listed in **Table A-1**. **Table A-1** shows only the options that differ from the Base Case modeling configurations selected for the full annual simulations shown in **Table 2-4**.

Table A-1   CMAQ and CAMx Configurations for Sensitivity Test Simulations

Parameter	CMAQ	CAMx
Initial Conditions	15 days spin-up for the 36-km domain and 7 days of spin-up for the 12-km and 4-km nested domain	
Boundary Conditions	2010 GEOS-Chem data for the 36-km domain, and extraction of boundary conditions from the 36-km domain for the finer resolution domain	
Horizontal Advection	YAMO scheme	PPM scheme

Table A-1   CMAQ and CAMx Configurations for Sensitivity Test Simulations

Parameter	CMAQ	CAMx
Vertical Advection	VWRF scheme	Implicit scheme with vertical velocity update
Horizontal Diffusion	Multiscale	K-theory 1st order closure with K_h grid size dependence
Vertical Diffusion	ACM2	K-theory approach
Boundary Condition Sensitivity Test		
Gas Phase Chemistry	None	
Aerosol Chemistry	None	
Cloud Chemistry	None	
Dry Deposition	None	
Wet Deposition	None	
Natural Background Source Sensitivity Test		
Gas Phase Chemistry	CB05-TU	CB6
Gas Phase Chemistry Solver	Euler Backward Iterative (EBI) solver[1]	EBI solver
Aerosol Chemistry	AERO5 and ISORROPIA2.1	SOAP and ISORROPIA1.6 with static 2-mode coarse/fine size distribution
Cloud Chemistry	RADM-type aqueous chemistry	RADM-type aqueous chemistry
Dry Deposition	CCTM in-line	Zhang scheme
Wet Deposition	CMAQ-specific	CAMx-specific

[1] EBI was used in the CMAQ sensitivity tests for all domains; however CMAQ 4-km domain base case annual simulation used the Rosenbrock solver to allow the model to be run with Process Analysis.

For the CAMx simulations, boundary ozone concentration inputs were tagged to provide additional information as part of this test. Ozone concentrations were tagged by the lateral boundary quadrant (north, south, east, and west 36-km domain boundary) and by vertical height. Vertical tagging was performed by grouping the vertical model layers into the six groups shown in **Table A-2**, which also indicates the approximate height above ground level (AGL) for each vertical group. By combining the lateral tagging with the vertical tagging, there are a total of 24 groups (i.e., 6 vertical layers for each of the four lateral boundaries) of unique ozone tracers. Information from these tracer groups are used to identify the origin of ozone coming from the model boundaries. Other pollutants, such as $PM_{2.5}$, were not tagged since this sensitivity test focused solely on ozone. To simplify the evaluation and for computational efficiency, this tagged boundary source attribution was not performed with the CMAQ model.

Table A-2   Vertical Grouping for CAMx Tagging Boundary Condition Test

Tagged Vertical Group	Altitude Range (AGL)	CAMx Vertical Model Layers
Layer 1	0 to 1 km	1 to 15
Layer 2	1 to 2 km	16 to 20
Layer 3	2 to 5 km	21 to 26
Layer 4	5 to 7.5 km	27 to 29
Layer 5	7.5 to 10.5 km	30 to 32
Layer 6	10.5 km to model top	33 to 36

A.2.2   Boundary Condition Test Results

Surface layer ozone concentrations were extracted from both the CMAQ and CAMx 4-km domain model outputs. Results were only extracted from grid cells containing the non-regulatory monitoring sites at Dinosaur National Monument (Dinosaur), Ouray, Utah (Ouray), and atop Deadman's Bench (Redwash), and the Rangely, Colorado golf course (Rangely). **Table A-3** summarizes information about available monitoring data in the Uinta Basin in 2010.

Table A-3   Summary of 2010 Monitoring Data in the Uinta Basin Study Area

Monitor ID	Description	Monitored Pollutants	Monitoring Period in 2010
081030006	Non-EPA federal site at Rangely, Colorado golf course (Rangely)	NO_x, ozone, $PM_{2.5}$	8/7/2010 - 12/31/2010
490471002	Non-regulatory site at Dinosaur National Monument (Dinosaur)	Ozone	4/13/2010 - 9/30/2010
490472002	Non-regulatory site atop Deadman's Bench (Redwash)	NO_x, ozone, $PM_{2.5}$	1/1/2010 - 12/31/2010
490472003	Non-regulatory site near Ouray, Utah (Ouray)	NO_x, ozone, $PM_{2.5}$	PM: 2/4/2010 - 12/31/2010, Other Pollutants: 1/1/2010 - 12/31/2010

Figure A-1 shows a time series comparison of the CMAQ and CAMx model results to the monitored surface ozone concentrations during the months of February and August 2010. Dates and times shown in the time series are relative to local times (i.e., Mountain Standard Time [MST] in February and Mountain Daylight Time [MDT] in August). As shown in **Figure A-1**, the CMAQ and CAMx results are similar to each other for both February and August, indicating that transport and diffusion processes affecting ozone concentrations in the Uinta Basin are not significantly different between the two models. The plots in **Figure A-1** show that model-predicted ozone concentrations are similar to measured peak observations in August, while they are typically much less than the peak observations in February. This indicates that the boundary conditions are potentially more important to local ozone concentrations in August than in February. Importantly, the modeled concentrations in February are around 40 ppb, indicating that model-predicted winter ozone from the boundary is near natural background levels. As seen in **Figure A-1**, the modeled ozone concentrations are higher and more variable in August than in February. This may be due to enhanced vertical transport and/or fire emissions outside the 36-km domain that are included in the boundary condition dataset.
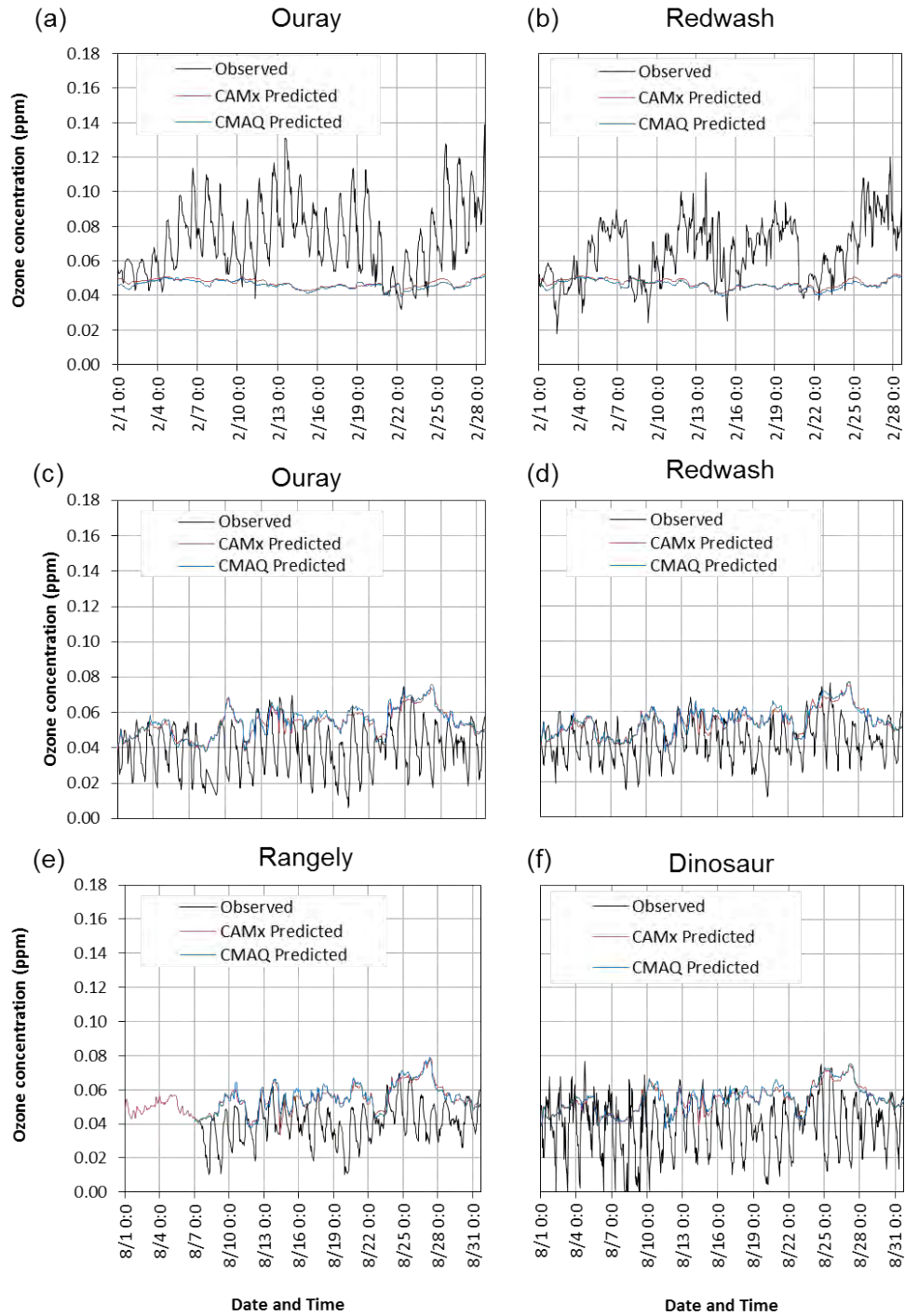
Figure A-1   Boundary Condition Ozone Results at the (a) Ouray and (b) Redwash sites during February 2010, and the (c) Ouray, (d) Redwash, (e) Rangely, and (f) Dinosaur sites during August 2010

Based on the tagged ozone species in the CAMx simulations (not shown here) ozone from the western boundary contributes the most to modeled ozone concentrations in Uinta Basin during February, while both the western and northern boundary contribute to ozone concentrations in Uinta Basin during August.

Results in panels (c) through (f) of **Figure A-1** show that the duration of modeled elevated ozone concentrations in August last longer than observations at all four monitoring sites in the Uinta Basin. This may be due to omission of ozone removal processes (either chemical processes or deposition) as configured for the boundary condition test. **Figure A-2** shows contour plots of CAMx-modeled ozone concentrations in the 36-km and 4-km modeling domains for August 27, 2010 at 1700 MDT, which coincides with one of the extended duration episodes when the model-predicted ozone concentrations exceed 70 ppb. Upon further examination of the CAMx boundary condition ozone tracer species, it was found that the modeled ozone during this event originated from the northern boundary at altitudes above 5 km AGL.
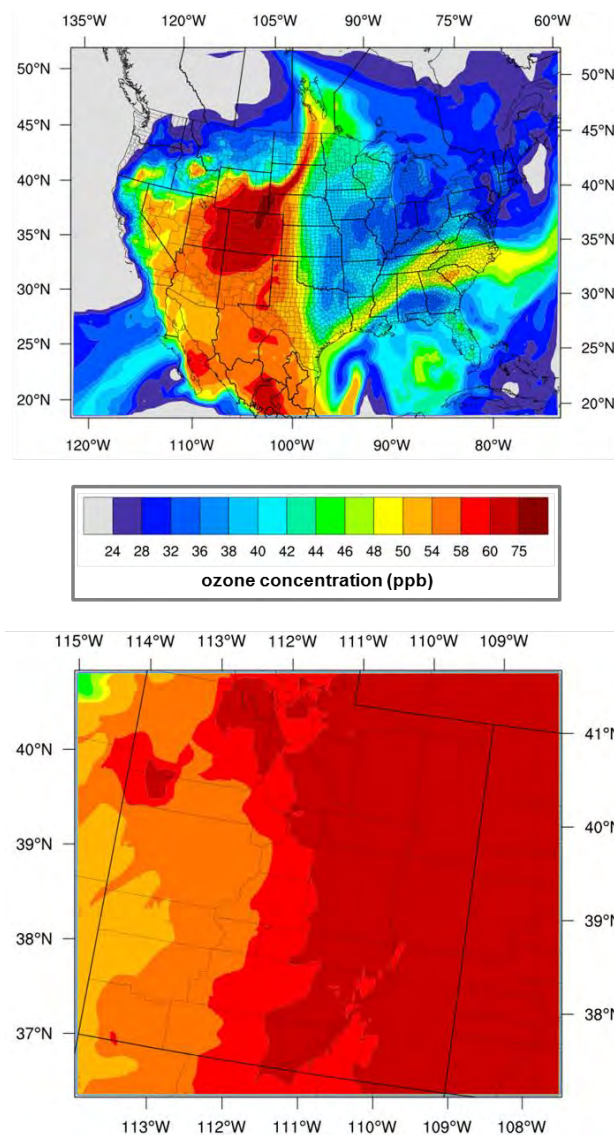
Figure A-2   CAMx 36-km domain (top) and 4-km domain (bottom) Boundary Condition ozone concentrations on August 27, 2010 at 1700 MDT

A.3   Natural Background Sensitivity Test

The main purpose of this sensitivity test was to evaluate the contribution of naturally occurring emissions sources (e.g., biogenic emissions and wildfire) to local ozone and $PM_{2.5}$ concentrations.

A.3.1   Natural Background Test Configuration

To isolate the contribution of non-anthropogenic emissions sources, CMAQ and CAMx simulations were configured without anthropogenic emissions and chemistry solvers and deposition mechanisms turned on. A set of emissions files was developed specifically for this test, which included only biogenic and fire emissions. Pertinent CMAQ and CAMx model configuration options for this sensitivity test are listed in **Table A-1**. **Table A-1** shows only the options that differ from the Base Case modeling configurations selected for the full annual simulations shown in Table 2-4 of the main document.

A.3.2   Natural Background Test Ozone Results

As in the boundary condition sensitivity test, surface layer ozone concentrations were extracted from the CMAQ and CAMx natural background simulation outputs for the 4-km domain grid cells containing the four monitoring sites in the Uinta Basin that are listed in **Table A-3**. **Figure A-3** shows time series plots of these concentrations in February and August 2010 along with the observed values. A comparison of **Figures A-3** to **A-1** shows that ozone concentrations predicted by both CMAQ and CAMx are significantly lower in the natural background sensitivity test than in the boundary condition test. Furthermore, the extended duration of some elevated ozone episodes seen in the August boundary condition test does not occur in this sensitivity test, supporting the hypothesis that removal mechanisms not invoked during the boundary condition test are important for the model to be able to reproduce the timing and duration of local ozone episodes.

While the CMAQ and CAMx results were very similar to each other in the boundary condition test during both February and July, CMAQ and CAMx natural background test results have notable differences during both February and July. While ozone concentrations predicted by CAMx are slightly higher than those predicted by CMAQ in February, the opposite is true, though to a lesser extent, in August. Since the boundary condition test indicated that the models were treating physical transport and dispersion similarly, and the input emissions for this test are identical for the two models, the differences in predicted ozone concentrations suggest that any differences between the model results in the base case simulation results is due to differences in the models' treatments of chemistry and deposition.

A comparison of the model results to monitored concentrations in **Figure A-3** show that the modeled boundary conditions plus natural background emissions modeled for the natural condition test are predicted to be a small contribution to the monitored ozone concentrations in the Uinta Basin during winter. On the other hand, they are predicted to contribute a significant fraction to the monitored ozone concentrations in the Uinta Basin during summer.

Figure A-4 shows spatial plots of CAMx-modeled ozone concentrations in the 36-km and 4-km modeling domains for August 24 at 1700 MDT, which occurs at the beginning of one of the ozone episodes.

A.3.3   Natural Background Test $PM_{2.5}$ Results

Surface layer $PM_{2.5}$ concentrations were extracted from the CMAQ and CAMx natural background simulation outputs for the 4-km domain grid cells containing the three relevant monitoring sites in the Uinta Basin that are listed in **Table A-2**. **Figure A-5** shows the time series plots of these concentrations in February and August 2010, along with the observed values. These plots show that, although concentrations of $PM_{2.5}$ predicted by CMAQ are less than those predicted by CAMx, both models predict very low concentrations of $PM_{2.5}$ from natural background emissions sources. The plots also indicate that those sources will not collectively be an important contributor to total $PM_{2.5}$ concentrations in the full base case simulations, and that anthropogenic sources likely account for a substantial amount of the observed

PM$_{2.5}$ concentrations. However, it also is possible that an important local or regional natural background source, such as wind blown dust, is not included in the modeled emissions. **Figure A-6** shows contour plots of CAMx-modeled PM$_{2.5}$ concentrations in the 36-km and 4-km modeling domains for August 24 at 1700 MDT.
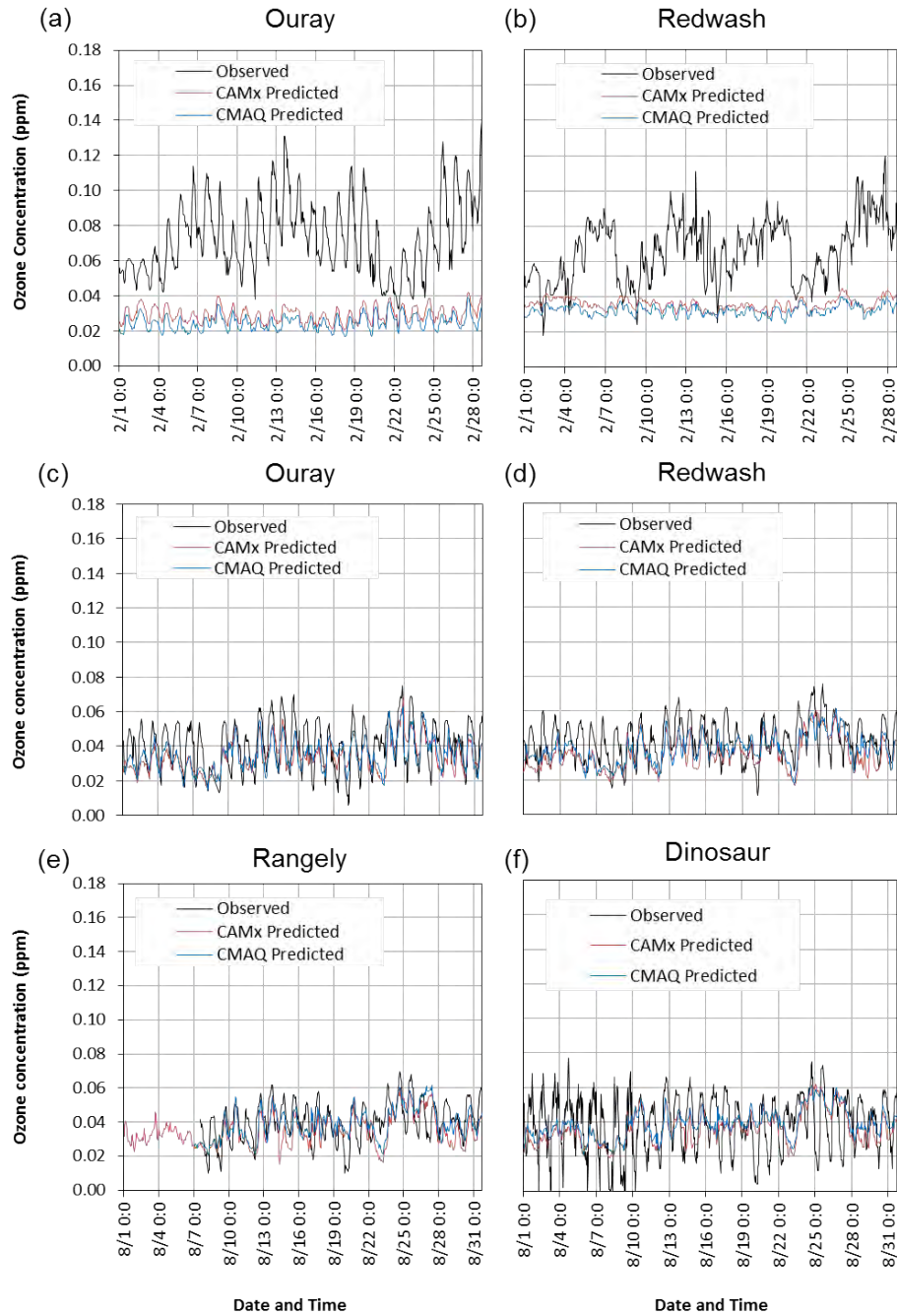
Figure A-3   Natural Background Test Ozone Results at the (a) Ouray and (b) Redwash sites during February 2010, and the (c) Ouray, (d) Redwash, (e) Rangely, and (f) Dinosaur sites during August 2010
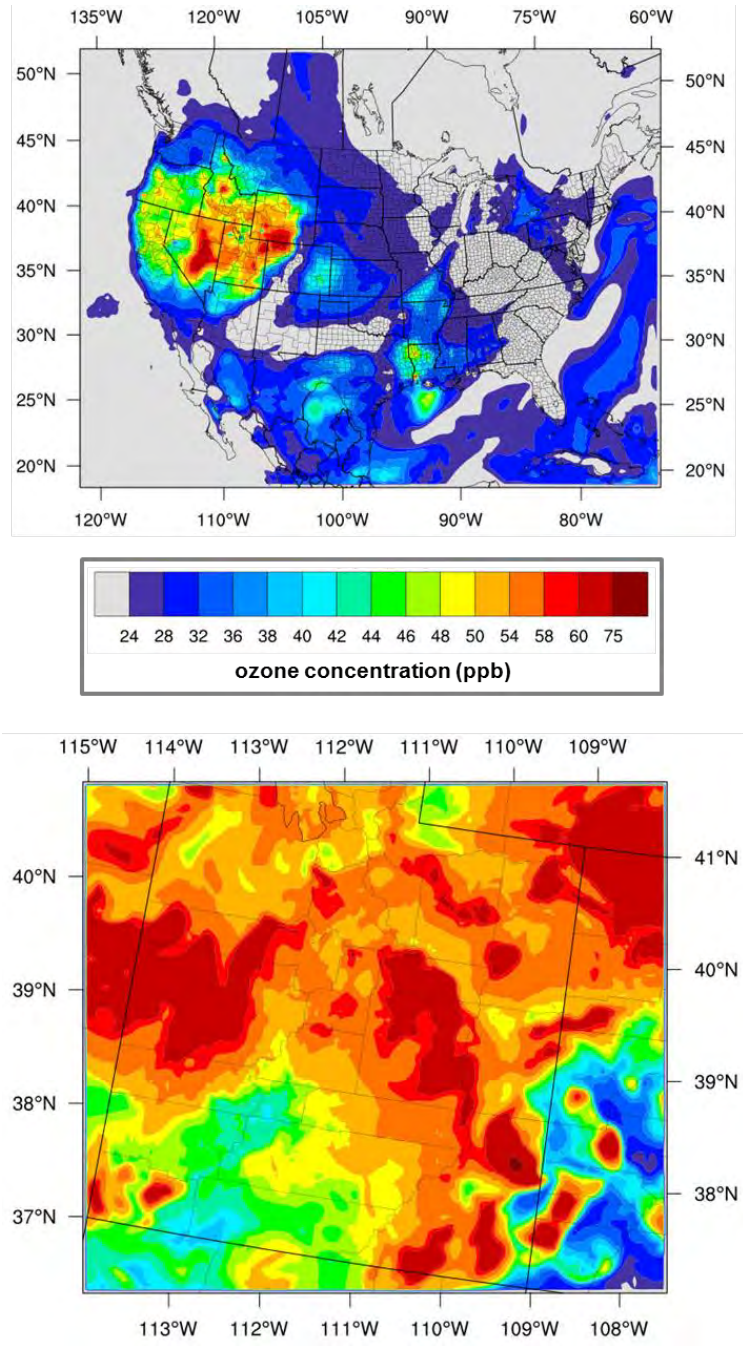
Figure A-4   CAMx Ozone 36-km domain (top) and 4-km domain (bottom) Natural Background Test on August 24, 2010 at 1700 MDT
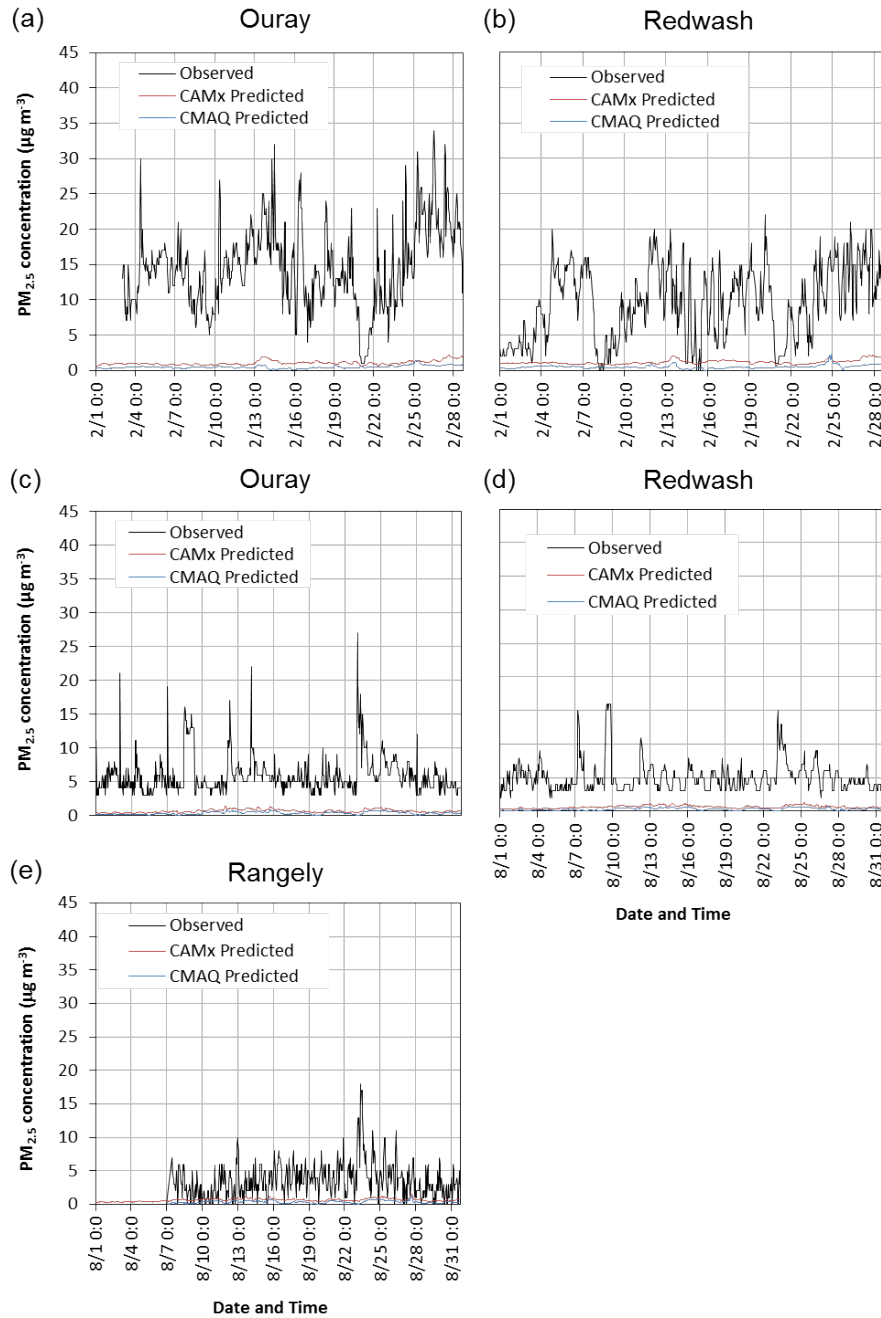
Figure A-5   Natural Background Test PM$_{2.5}$ Results at the (a) Ouray and (b) Redwash sites during February 2010, and the (c) Ouray, (d) Redwash and (e) Rangely sites during August 2010
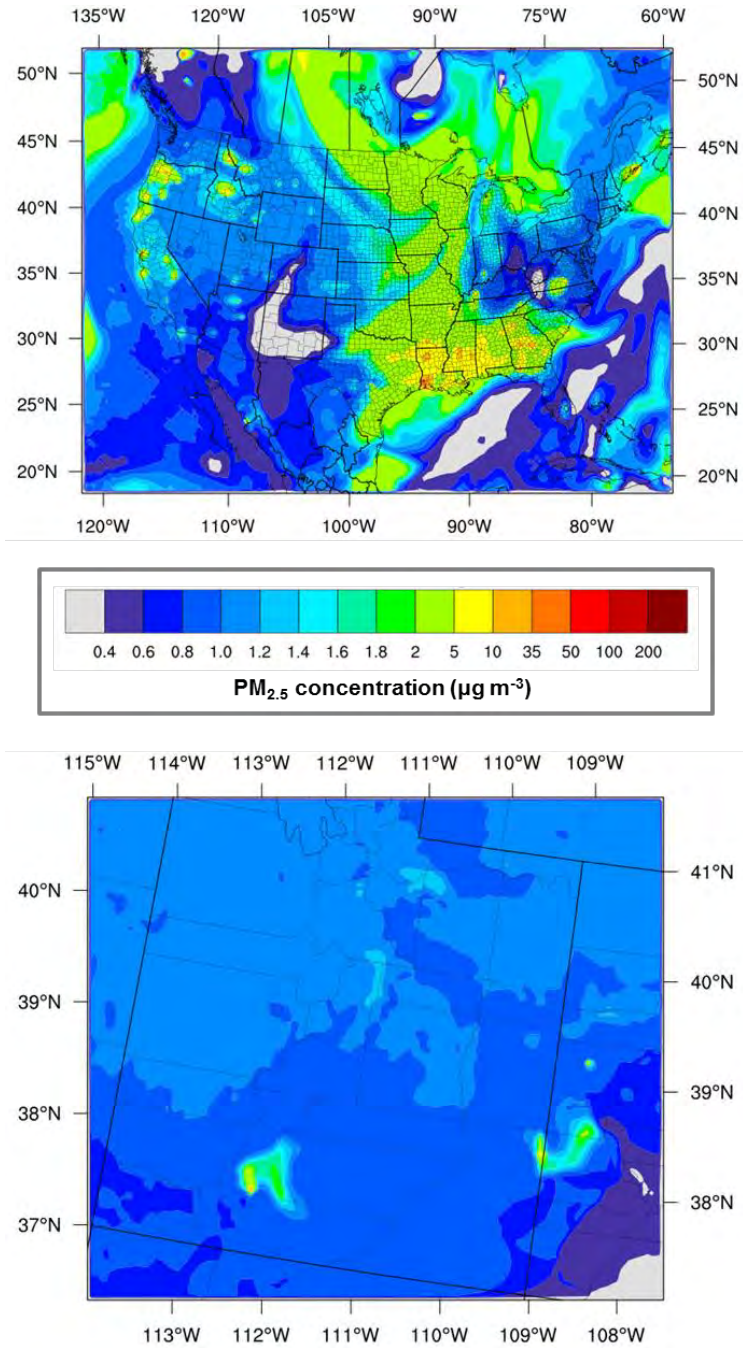
Figure A-6   CAMx PM$_{2.5}$ 36-km domain (top) and 4-km domain (bottom) Natural Background Test on August 24, 2010 at 1700 MDT

A.4   Summary

Results from the boundary condition sensitivity test indicate that transport and diffusion processes affecting ozone concentrations in the Uinta Basin are not significantly different between CMAQ and CAMx. Results also suggest that the boundary conditions are potentially more important to local ozone concentrations in summer than in winter. Additionally, ozone from the western boundary contributes the most to modeled ozone concentrations in Uinta Basin during February, while both the western and northern boundary contribute to ozone concentrations in Uinta Basin during August.

Results from the natural background source sensitivity test showed that activation of chemical transformations and deposition processes, which were turned off in the boundary condition test, were important for the model to be able to reproduce the timing and duration of local ozone episodes. Ozone concentrations predicted by CAMx were slightly higher than those predicted by CMAQ during the winter, but the opposite was true during the summer, indicating differences in chemistry and deposition treatment between the two models. Total $PM_{2.5}$ concentrations predicted by CMAQ were less than those predicted by CAMx, but both models predicted very low concentrations of $PM_{2.5}$ from natural background sources during both summer and winter.

A.5   Reference

Sonoma Technology, Inc. (STI). 2006. Regional and Local Contributions to Peak Local Ozone Concentrations in Six Western Cities by C. P. MacDonald, D. S. Miller, and S. M. Raffuse. Prepared For Western States Air Resources Council. May 2006.

Appendix B

CAMx Model Performance Evaluation

Contents

List of Tables

List of Figures

B.0 CAMx Model Performance Evaluation

This appendix presents supplemental material on the CAMx model performance evaluation. The statistical and graphical analyses presented here were used to help inform decisions that were made regarding the recommended air quality model for use in subsequent ARMS Modeling Project simulations. The organization of material in this appendix is similar to that in Chapter 4. Statistical tables and graphical summaries of CAMx model performance are presented for each of the key model species, including ozone, total $PM_{2.5}$, and other particulate and gaseous species. The Chapter concludes with supplemental material summarizing CAMx model performance for visibility and deposition. Additional spatial plots from the CAMx 4-km domain are included for ozone and total $PM_{2.5}$, but not for other species. Time series plots showing CAMx model performance within the Uinta Basin can be found throughout Chapter 4, plotted alongside corresponding CMAQ model output. Although this appendix provides no additional narratives of CAMx model performance results, important findings and conclusions from the model inter-comparison between CMAQ and CAMx can be found in Chapter 4.

B.1   Ozone

This section presents statistical tables and graphical summaries of CAMx model performance for ozone. Statistical results from the model performance evaluation are presented in **Table B-1** through **Table B-4.** A summary of monthly MNB for peak 8-hour ozone concentration in each domain is presented in **Figure B-1.** Selected spatial plots of CAMx ozone concentrations in the 4-km domain overlaid with AQS observations is presented in **Figures B-2** and **B-3.**

Table B-1   Table B-1CAMx Mean Normalized Bias Summary for Ozone

Monitoring Network	Pollutant	36-km Domain					12-km Domain					4-km Domain				
		Annual	Winter	Spring	Summer	Fall	Annual	Winter	Spring	Summer	Fall	Annual	Winter	Spring	Summer	Fall
AQS (Hourly)	1-hour O$_3$ (60 ppb threshold)	-12.1	-38.6	-12.8	-11.6	-9.6	-12.2	-36.3	-14.4	-10.9	-7.6	-12.9	-36.6	-15.7	-5.3	1.6
	1-hour O$_3$ (no threshold)	89.3	171.1	46.2	32.5	129.7	66.8	151.8	27.4	27.1	81.6	48.1	93.6	26.9	27.7	63.8
	Daily Max 1-hour O$_3$ (60 ppb threshold)	-4.8	-21.9	-7.4	-4.2	-1.7	-5.5	-23.6	-9.5	-3.7	-2.3	-4.1	-21.7	-9.8	-0.7	4.1
	Daily Max 1-hour O$_3$ (no threshold)	9.7	19.3	4.5	7.6	9.1	4.7	10.1	-0.4	5.1	4.7	5.9	19.6	-3.2	5.1	5.8
	8-hour O$_3$ (60 ppb threshold)	-34.7	-49.6	-33.2	-34.2	-38.0	-28.3	-44.6	-27.8	-27.8	-28.7	-26.7	-45.3	-25.7	-19.4	-21.7
	8-hour O$_3$ (no threshold)	71.3	190.7	28.1	17.5	76.2	58.0	162.1	19.5	16.9	56.7	59.7	170.5	34.2	22.5	54.3
	Daily Max 8-hour O$_3$ (60 ppb threshold)	-7.4	-24.8	-10.0	-6.3	-5.5	-8.3	-26.4	-12.0	-6.6	-4.6	-8.4	-25.3	-12.9	-2.8	0.4
	Daily Max 8-hour O$_3$ (no threshold)	14.2	32.9	4.7	10.2	12.5	7.3	18.5	-1.0	6.3	7.5	8.4	29.8	-3.8	5.6	8.3
CASTNET (Hourly)	1-hour O$_3$ (60 ppb threshold)	-2.9	-21.7	-8.6	0.9	2.1	-15.1	-21.5	-17.8	-13.6	-10.1	-10.9	-13.7	-17.1	-4.4	3.3
	1-hour O$_3$ (no threshold)	33.7	1.1	13.1	78.4	41.4	-2.2	-4.3	-8.9	4.7	-0.7	0.7	-0.3	-7.1	6.6	3.8
	Daily Max 1-hour O$_3$ (60 ppb threshold)	4.4	-16.6	-2.5	10.1	7.4	-10.5	-18.1	-13.3	-8.8	-6.0	-6.3	-9.7	-12.3	-1.2	6.5
	Daily Max 1-hour O$_3$ (no threshold)	9.3	-2.7	3.3	26.8	9.3	-2.8	-3.7	-7.2	0.5	-1.1	0.2	-2.5	-6.2	6.4	3.0
	8-hour O$_3$ (60 ppb threshold)	-17.6	-19.8	-21.4	-14.9	-14.7	-18.7	-19.4	-20.2	-17.9	-16.0	-13.6	NA	-19.3	-7.3	-2.4
	8-hour O$_3$ (no threshold)	34.5	5.7	12.1	75.4	44.5	-2.1	-4.2	-8.7	4.7	-0.8	0.5	-0.6	-7.0	6.5	3.3
	Daily Max 8-hour O$_3$ (60 ppb threshold)	1.8	-15.7	-5.4	7.0	6.3	-12.3	-19.2	-14.9	-10.9	-7.6	-8.6	NA	-14.2	-2.7	6.5
	Daily Max 8-hour O$_3$ (no threshold)	8.1	-4.1	0.7	27.0	8.4	-3.4	-3.7	-8.4	-0.1	-1.7	-0.3	-1.8	-6.8	4.7	2.6

Table B-2   CAMx Mean Normalized Gross Error Summary for Ozone

Monitoring Network	Pollutant	36-km Domain					12-km Domain					4-km Domain				
		Annual	Winter	Spring	Summer	Fall	Annual	Winter	Spring	Summer	Fall	Annual	Winter	Spring	Summer	Fall
AQS (Hourly)	1-hour O$_3$ (60 ppb threshold)	17.4	39.4	15.1	17.6	18.4	15.9	37.2	15.6	15.5	14.1	16.9	37.8	16.5	11.2	9.3
	1-hour O$_3$ (no threshold)	115.7	204.4	71.0	54.4	157.5	91.7	182.6	53.4	46.9	106.8	67.1	121.9	51.0	40.6	79.0
	Daily Max 1-hour O$_3$ (60 ppb threshold)	12.3	23.8	10.6	12.6	13.5	11.0	25.6	11.2	10.7	10.2	10.7	24.6	11.1	9.2	9.5
	Daily Max 1-hour O$_3$ (no threshold)	19.7	29.2	14.0	18.0	19.4	16.3	23.5	12.0	15.0	16.3	15.1	31.3	9.9	11.6	12.7
	8-hour O$_3$ (60 ppb threshold)	35.7	49.9	33.4	35.4	39.4	29.3	45.9	28.0	29.1	30.2	27.6	46.9	25.9	20.5	22.0
	8-hour O$_3$ (no threshold)	104.3	227.7	60.9	47.8	109.7	87.6	194.4	50.8	43.1	86.1	81.0	195.4	61.3	39.5	72.9
	Daily Max 8-hour O$_3$ (60 ppb threshold)	12.5	25.5	11.4	12.4	14.0	11.7	27.3	12.6	11.0	10.4	11.7	26.6	13.1	8.0	8.7
	Daily Max 8-hour O$_3$ (no threshold)	24.1	42.7	15.0	19.2	23.1	19.4	31.7	13.0	15.9	19.3	17.7	42.3	10.3	11.4	15.0
CASTNET (Hourly)	1-hour O$_3$ (60 ppb threshold)	18.1	21.7	15.4	21.4	17.6	16.9	21.5	18.1	16.4	13.6	13.8	13.7	17.4	9.8	7.0
	1-hour O$_3$ (no threshold)	55.1	34.1	37.2	88.0	60.5	16.5	14.2	14.8	20.1	16.3	13.5	13.0	12.7	14.2	13.9
	Daily Max 1-hour O$_3$ (60 ppb threshold)	15.6	16.6	11.0	20.2	15.8	13.0	18.1	13.9	12.4	11.7	11.0	9.7	13.0	8.5	13.8
	Daily Max 1-hour O$_3$ (no threshold)	20.1	15.0	14.3	31.9	18.9	11.6	10.3	11.2	13.5	11.4	10.0	9.2	9.7	11.3	9.7
	8-hour O$_3$ (60 ppb threshold)	22.9	19.8	23.6	23.1	20.9	20.3	19.4	20.6	20.4	17.9	15.2	NA	19.3	10.6	4.9
	8-hour O$_3$ (no threshold)	58.3	39.1	39.0	88.1	67.0	17.3	14.6	15.4	21.7	17.3	13.5	12.4	12.8	14.7	13.8
	Daily Max 8-hour O$_3$ (60 ppb threshold)	15.3	15.7	11.3	19.3	15.5	13.8	19.2	15.1	13.2	10.1	11.4	NA	14.2	8.4	6.5
	Daily Max 8-hour O$_3$ (no threshold)	20.6	16.1	14.4	32.3	19.3	11.5	10.4	11.3	13.1	11.1	9.7	9.5	9.8	10.2	9.4

Table B-3   CAMx Normalized Mean Bias Summary for Ozone

Monitoring Network	Pollutant	36-km Domain					12-km Domain					4-km Domain				
		Annual	Winter	Spring	Summer	Fall	Annual	Winter	Spring	Summer	Fall	Annual	Winter	Spring	Summer	Fall
AQS (Hourly)	1-hour O_3 (60 ppb threshold)	-12.7	-39.8	-13.1	-12.4	-10.1	-12.8	-37.2	-14.7	-11.6	-7.9	-14.2	-37.3	-16.4	-5.6	1.4
	1-hour O_3 (no threshold)	5.4	12.0	0.1	4.7	8.9	2.1	6.4	-4.1	3.3	5.4	5.4	2.3	-4.5	9.6	13.6
	Daily Max 1-hour O_3 (60 ppb threshold)	-5.9	-24.2	-7.9	-5.5	-2.8	-6.3	-25.1	-9.9	-4.9	-2.8	-5.1	-23.4	-10.5	-1.3	3.6
	Daily Max 1-hour O_3 (no threshold)	4.0	9.2	1.7	3.1	4.5	0.4	1.9	-2.7	1.6	1.3	1.9	3.3	-4.5	3.9	5.2
	8-hour O_3 (60 ppb threshold)	-35.6	-51.6	-33.6	-35.3	-38.6	-29.1	-46.5	-28.1	-28.6	-29.2	-28.4	-47.0	-26.7	-19.7	-21.7
	8-hour O_3 (no threshold)	0.3	6.1	-4.4	-0.1	3.1	-0.2	4.0	-6.0	1.0	2.5	4.8	3.7	-5.2	8.7	12.3
	Daily Max 8-hour O_3 (60 ppb threshold)	-8.1	-26.9	-10.4	-7.1	-6.2	-9.0	-28.0	-12.3	-7.4	-4.9	-9.5	-27.1	-13.5	-3.1	0.3
	Daily Max 8-hour O_3 (no threshold)	5.8	13.8	1.4	5.5	6.3	0.9	4.4	-3.7	2.2	2.1	2.3	3.6	-5.1	4.5	6.6
CASTNET (Hourly)	1-hour O_3 (60 ppb threshold)	-3.2	-21.8	-8.6	0.1	1.8	-15.6	-21.6	-17.9	-14.4	-10.4	-11.1	-13.7	-17.2	-4.6	3.2
	1-hour O_3 (no threshold)	5.8	-10.5	-2.8	27.4	7.8	-4.4	-5.4	-9.9	0.2	-2.4	-0.6	-1.6	-7.9	5.0	3.0
	Daily Max 1-hour O_3 (60 ppb threshold)	3.9	-16.8	-2.7	8.7	6.9	-11.4	-18.3	-13.7	-10.3	-6.7	-6.8	-9.7	-12.6	-1.6	6.3
	Daily Max 1-hour O_3 (no threshold)	7.7	-4.6	1.7	22.8	7.3	-4.1	-4.2	-8.1	-2.1	-1.7	-0.4	-3.1	-7.0	5.5	3.2
	8-hour O_3 (60 ppb threshold)	-18.1	-19.9	-21.5	-16.0	-15.2	-19.3	-19.4	-20.5	-18.9	-16.3	-13.7	NA	-19.4	-7.5	-2.3
	8-hour O_3 (no threshold)	5.8	-10.3	-2.8	27.4	7.6	-4.4	-5.3	-9.9	0.2	-2.5	-0.6	-1.6	-7.9	4.9	2.8
	Daily Max 8-hour O_3 (60 ppb threshold)	1.3	-15.7	-5.4	6.0	5.8	-12.8	-19.3	-15.1	-11.8	-7.9	-8.8	NA	-14.3	-3.1	6.5
	Daily Max 8-hour O_3 (no threshold)	6.4	-6.3	-0.7	23.2	6.2	-4.5	-4.2	-9.0	-2.2	-2.2	-0.9	-2.4	-7.4	4.0	2.7

Table B-4   CAMx Normalized Mean Error Summary for Ozone

Monitoring Network	Pollutant	36-km Domain					12-km Domain					4-km Domain				
		Annual	Winter	Spring	Summer	Fall	Annual	Winter	Spring	Summer	Fall	Annual	Winter	Spring	Summer	Fall
AQS (Hourly)	1-hour O$_3$ (60 ppb threshold)	17.8	40.5	15.3	18.0	18.5	16.4	38.0	15.8	16.0	14.2	18.0	38.4	17.1	11.4	9.4
	1-hour O$_3$ (no threshold)	31.1	43.2	25.3	27.3	36.0	26.8	36.7	22.6	23.9	29.5	24.4	33.6	20.2	22.2	27.2
	Daily Max 1-hour O$_3$ (60 ppb threshold)	12.8	25.7	10.9	13.2	13.8	11.5	26.8	11.6	11.3	10.4	11.3	25.8	11.7	9.4	9.5
	Daily Max 1-hour O$_3$ (no threshold)	15.7	20.5	12.5	15.9	15.9	13.2	16.7	10.9	13.2	13.3	12.3	19.9	9.9	11.2	11.9
	8-hour O$_3$ (60 ppb threshold)	36.6	51.9	33.8	36.4	39.9	30.0	47.5	28.3	29.8	30.6	29.2	48.3	26.9	20.8	22.1
	8-hour O$_3$ (no threshold)	38.5	48.7	33.0	36.1	42.6	33.4	41.1	29.2	31.7	36.0	29.4	36.3	25.0	28.0	32.8
	Daily Max 8-hour O$_3$ (60 ppb threshold)	12.9	27.5	11.7	12.9	14.3	12.1	28.7	12.9	11.5	10.6	12.7	28.2	13.7	8.1	8.7
	Daily Max 8-hour O$_3$ (no threshold)	17.1	25.6	12.8	16.3	17.9	14.0	19.6	11.3	13.2	14.3	12.8	22.2	10.1	10.7	13.1
CASTNET (Hourly)	1-hour O$_3$ (60 ppb threshold)	18.2	21.8	15.4	21.5	17.6	17.3	21.6	18.3	17.0	13.8	13.9	13.7	17.6	9.9	7.0
	1-hour O$_3$ (no threshold)	28.2	23.6	22.5	38.8	27.9	15.4	13.6	14.8	17.6	15.2	12.8	11.9	12.8	13.2	13.1
	Daily Max 1-hour O$_3$ (60 ppb threshold)	15.7	16.8	11.0	20.1	15.8	13.7	18.3	14.3	13.5	12.0	11.2	9.7	13.3	8.6	13.8
	Daily Max 1-hour O$_3$ (no threshold)	18.7	13.8	13.3	29.0	17.0	11.8	10.1	11.6	13.6	11.4	10.0	8.7	10.1	11.0	9.8
	8-hour O$_3$ (60 ppb threshold)	23.2	19.9	23.7	23.8	21.2	20.8	19.4	20.8	21.2	18.1	15.3	NA	19.5	10.7	4.8
	8-hour O$_3$ (no threshold)	32.5	25.6	27.3	43.4	33.2	16.5	13.9	15.4	19.6	16.4	13.0	11.6	13.0	13.7	13.4
	Daily Max 8-hour O$_3$ (60 ppb threshold)	15.4	15.7	11.3	19.4	15.4	14.1	19.3	15.3	13.9	10.2	11.5	NA	14.3	8.5	6.5
	Daily Max 8-hour O$_3$ (no threshold)	19.0	14.9	13.4	29.3	17.3	11.5	10.1	11.6	13.0	10.9	9.7	9.0	10.1	9.9	9.5
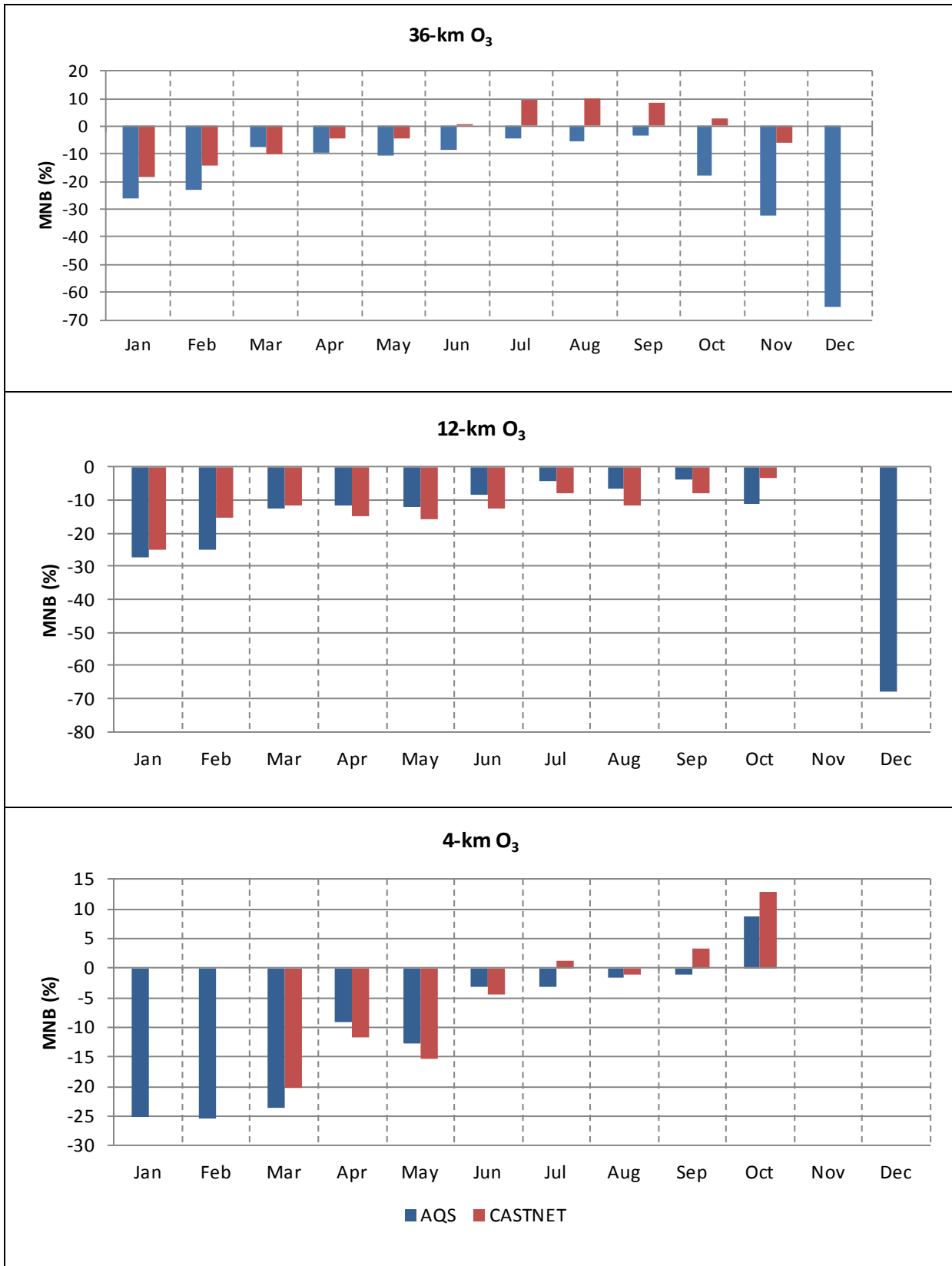
Figure B-1   CAMx Monthly Mean Normalized Bias for Ozone
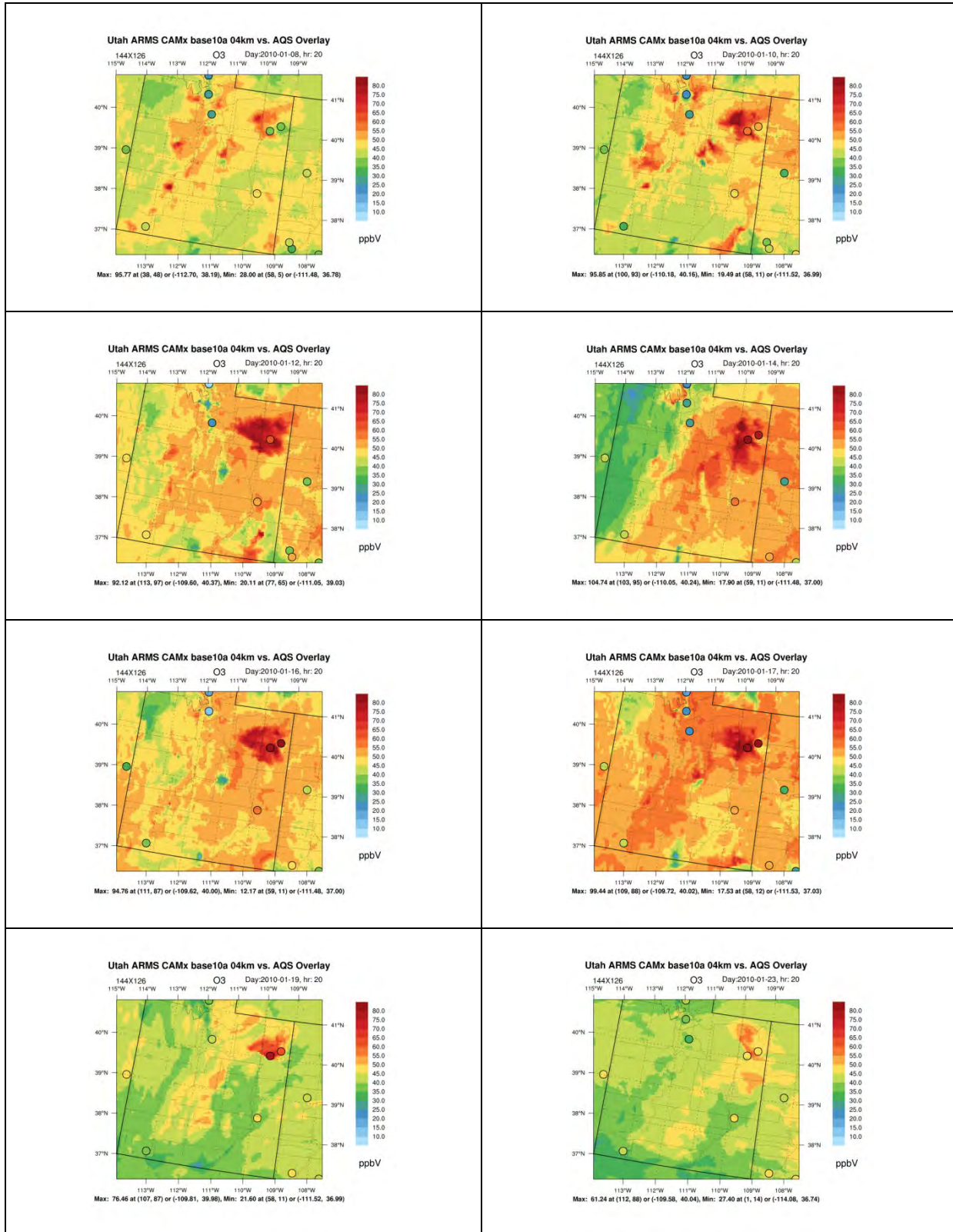
Figure B-2   CAMx 4-km Spatial Plots for Ozone during January 8 to January 23, 2010
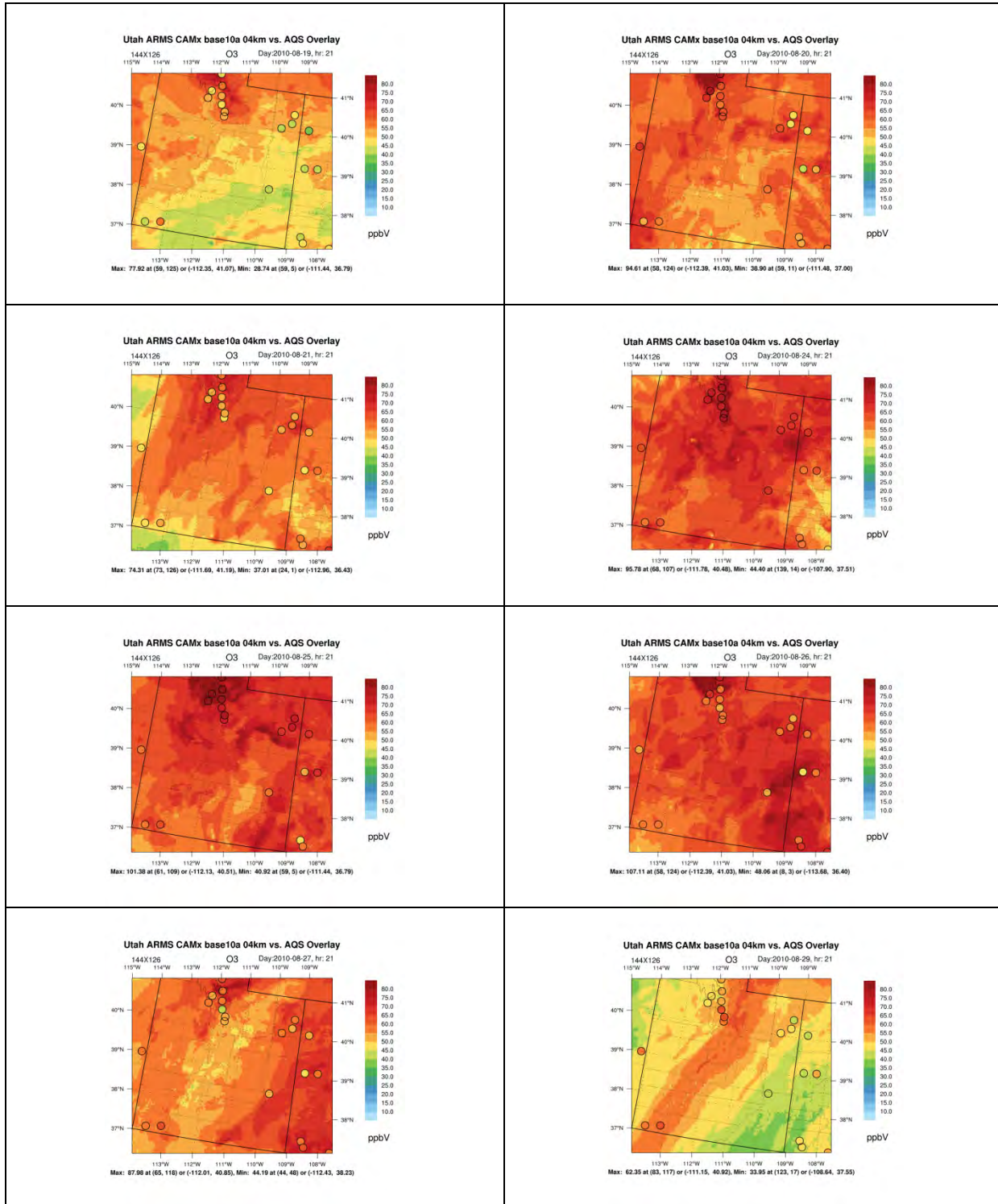
Figure B-3   CAMx 4-km Spatial Plots for Ozone during August 19 to August 29, 2010

B.2   Particulate Matter

The subsections that follow present supplementary CAMx model performance results for the various PM$_{2.5}$ components.

B.2.1   PM Composition

B.2.1.1 Sulfate

This section presents statistical tables and graphical summaries of CAMx model performance for sulfate. Statistical results from the model performance evaluation are presented in **Table B-5.** A summary of monthly mean fractional bias is presented in **Figure B-4**, while Bugle plots summarizing model performance in the context of recommended USEPA performance criteria are presented in **Figure B-5.**

Table B-5   CAMx Model Performance Statistical Summary for Sulfate

Monitoring Network	Statistic (%)/ Concentration (µg/m³)	36-km Domain					12-km Domain					4-km Domain				
		Annual	Winter	Spring	Summer	Fall	Annual	Winter	Spring	Summer	Fall	Annual	Winter	Spring	Summer	Fall
CASTNET (Weekly)	MFB	34	30	44	24	39	29	69	25	-3	31	27	59	21	1	30
	MFGE	45	49	48	39	44	40	70	32	25	40	37	62	32	20	38
	MNB	68	82	88	45	65	59	155	34	2	61	48	121	30	5	48
	MNGE	77	98	91	58	69	69	156	41	25	68	57	123	40	21	56
	NMB	36	28	64	33	22	23	84	25	-7	27	24	61	23	2	27
	NME	53	52	68	46	55	40	86	35	26	39	36	66	36	20	39
	R^2	0.056	0.453	0.536	0.541	0.011	0.348	0.581	0.155	0.379	0.403	0.321	0.602	0.003	0.234	0.382
	Observed Mean Concentration (µg/m³)	2.01	1.70	1.83	2.62	1.80	0.54	0.31	0.66	0.68	0.47	0.55	0.39	0.67	0.63	0.47
	Predicted Mean Concentration (µg/m³)	2.73	2.17	3.00	3.48	2.20	0.66	0.56	0.83	0.63	0.60	0.68	0.63	0.82	0.64	0.60
IMPROVE (Daily)	MFB	47	58	55	25	49	39	73	43	5	35	39	68	47	8	36
	MFGE	61	75	61	48	60	53	78	49	35	49	50	74	49	29	50
	MNB	172	306	147	113	135	93	186	96	17	74	86	188	82	16	67
	MNGE	183	319	152	131	143	104	190	101	41	86	95	193	84	34	78
	NMB	51	52	75	31	53	35	91	47	0	33	40	75	58	8	37
	NME	71	82	84	56	68	56	102	57	37	52	55	89	62	31	55
	R^2	0.475	0.370	0.466	0.545	0.549	0.267	0.327	0.244	0.298	0.271	0.227	0.326	0.123	0.287	0.179
	Observed Mean Concentration (µg/m³)	1.17	0.94	1.19	1.52	1.01	0.52	0.32	0.57	0.68	0.49	0.47	0.34	0.50	0.61	0.44
	Predicted Mean Concentration (µg/m³)	1.77	1.43	2.08	1.98	1.54	0.70	0.61	0.84	0.68	0.65	0.66	0.59	0.79	0.66	0.60

Table B-5   CAMx Model Performance Statistical Summary for Sulfate

Monitoring Network	Statistic (%)/ Concentration (μg/m^3)	36-km Domain					12-km Domain					4-km Domain				
		Annual	Winter	Spring	Summer	Fall	Annual	Winter	Spring	Summer	Fall	Annual	Winter	Spring	Summer	Fall
STN (Daily)	MFB	31	45	44	2	34	35	44	47	11	39	23	11	38	-8	46
	MFGE	56	69	56	45	54	55	67	56	45	55	43	56	41	20	49
	MNB	97	150	124	30	83	104	167	129	33	90	53	48	64	-5	91
	MNGE	115	167	134	63	99	120	184	136	59	103	68	82	67	17	94
	NMB	33	53	56	-4	37	23	33	42	-6	32	19	-10	41	-9	79
	NME	66	88	74	46	65	59	73	59	46	65	51	53	46	21	85
	R^2	0.255	0.292	0.327	0.258	0.302	0.224	0.063	0.420	0.405	0.166	0.019	0.035	0.168	0.127	0.058
	Observed Mean Concentration (μg/m^3)	1.25	1.16	1.20	1.55	1.08	0.89	0.80	0.83	1.09	0.82	0.75	1.08	0.68	0.71	0.52
	Predicted Mean Concentration (μg/m^3)	1.66	1.78	1.88	1.48	1.48	1.09	1.07	1.17	1.03	1.08	0.89	0.97	0.96	0.64	0.93
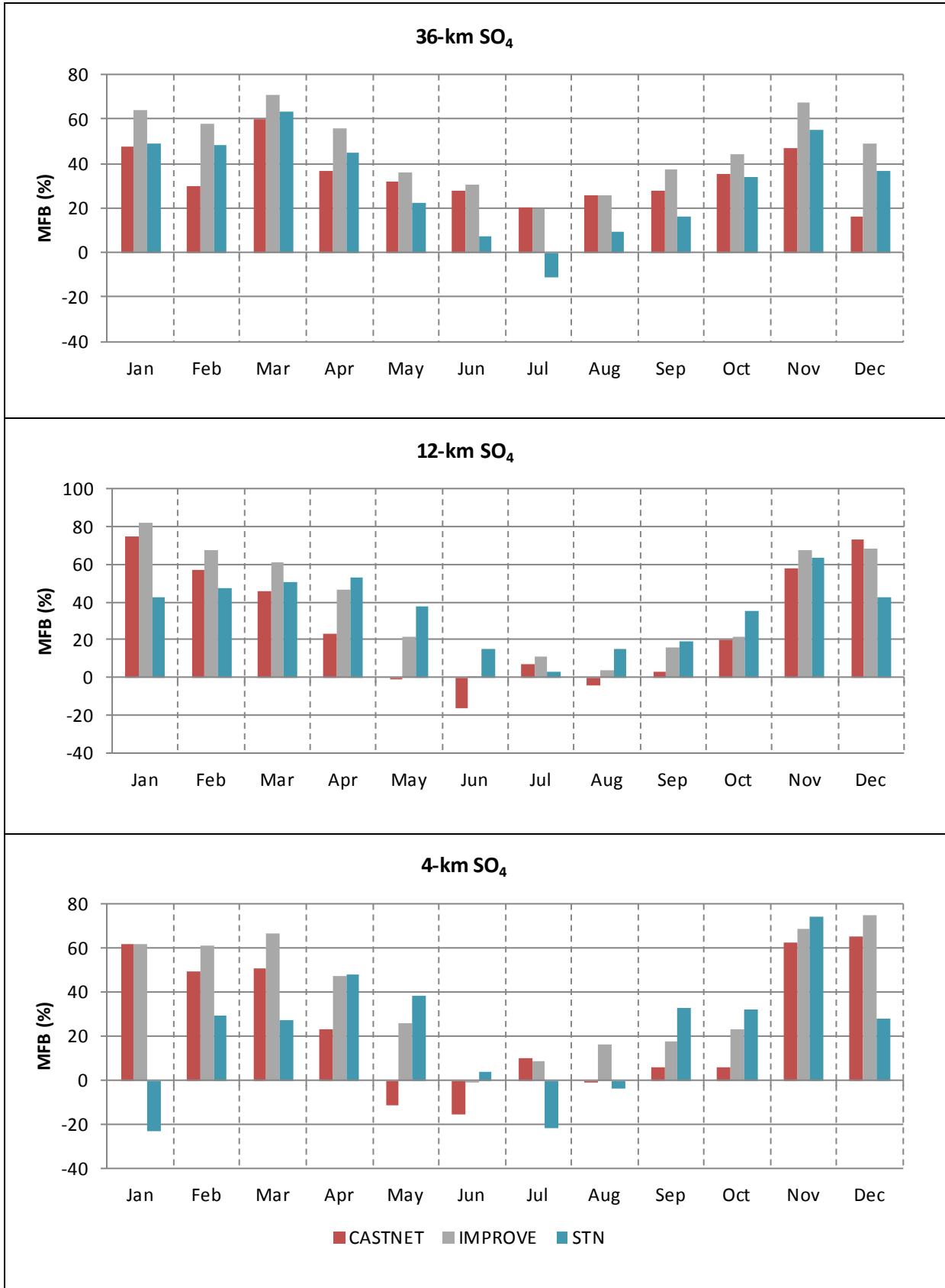
Figure B-4   CAMx Monthly Mean Fractional Bias for Sulfate
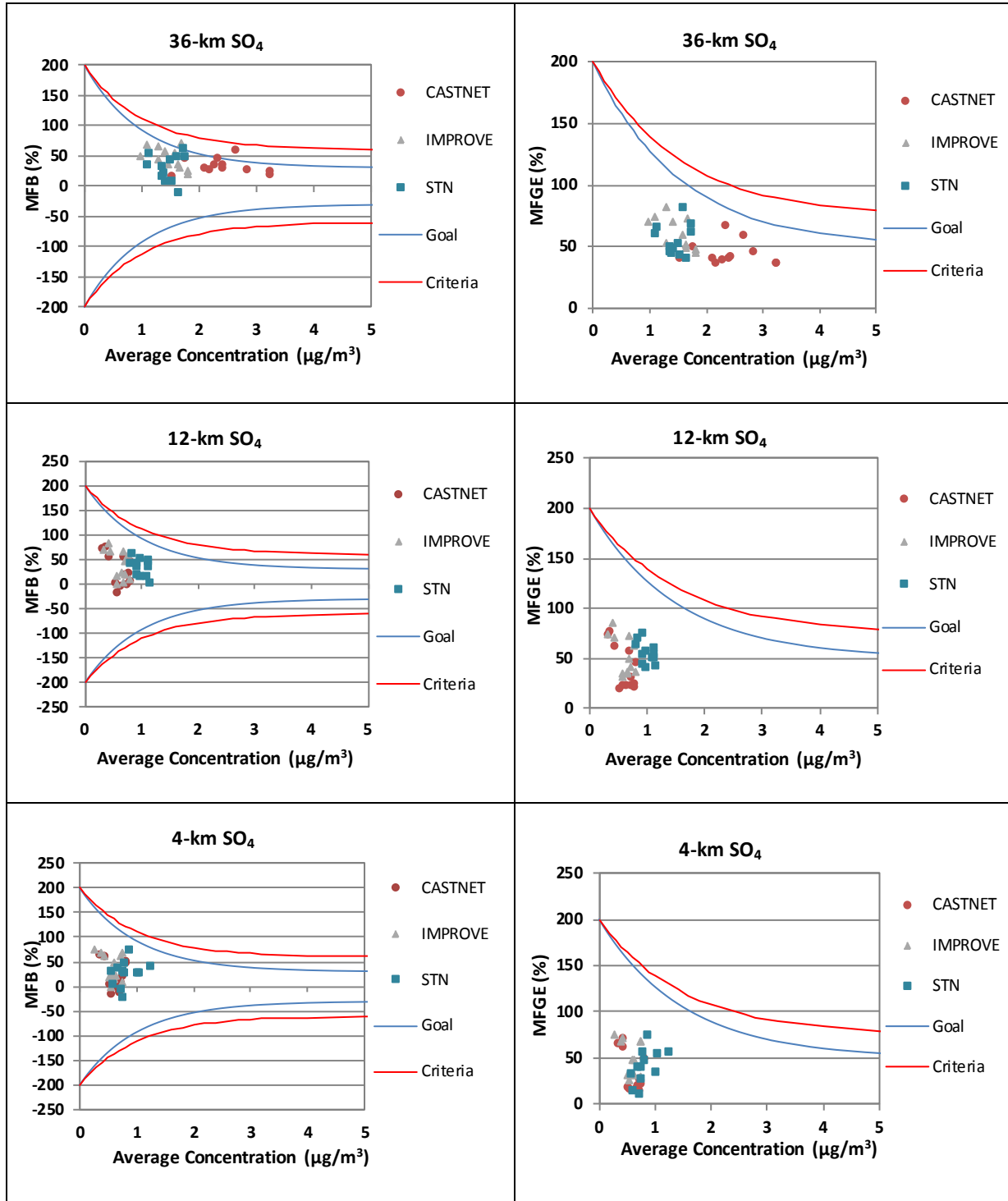
Note: Goals and criteria based on Boylan et al. (2006) and accepted by USEPA (2007).

Figure B-5   CAMx Bugle Plots of Sulfate Monthly Mean Fractional Bias and Mean Fractional Gross Error

B.2.1.2 Nitrate

This section presents statistical tables and graphical summaries of CAMx model performance for nitrate and nitric acid. Statistical results from the model performance evaluation are presented in **Table B-6** and **Table B-7.** A summary of monthly mean fractional bias is presented in **Figure B-6**, while Bugle plots summarizing model performance in the context of recommended USEPA performance criteria are presented in **Figure B-7**

Table B-6   CAMx Model Performance Statistical Summary for Nitrate

Monitoring Network	Statistic (%)/ Concentration (µg/m³)	36-km Domain					12-km Domain					4-km Domain				
		Annual	Winter	Spring	Summer	Fall	Annual	Winter	Spring	Summer	Fall	Annual	Winter	Spring	Summer	Fall
CASTNET (Weekly)	MFB	2	31	15	-26	-5	-82	38	-100	-156	-92	-73	36	-90	-143	-90
	MFGE	93	77	86	120	87	128	110	117	157	124	118	89	115	143	118
	MNB	124	195	115	131	67	46	391	-47	-85	-17	11	168	-39	-81	-14
	MNGE	177	226	159	212	121	165	435	81	86	107	123	203	84	81	107
	NMB	42	29	83	45	31	-49	74	-70	-92	-63	19	174	-45	-82	-30
	NME	92	62	120	158	95	100	154	84	92	92	122	190	86	82	94
	R²	0.215	0.658	0.618	0.003	0.032	0.008	0.163	0.005	0.017	0.010	0.463	0.689	0.001	0.032	0.005
	Observed Mean Concentration (µg/m³)	0.82	1.55	0.77	0.34	0.73	0.30	0.23	0.47	0.29	0.21	0.23	0.30	0.31	0.20	0.15
	Predicted Mean Concentration (µg/m³)	1.17	2.01	1.40	0.50	0.95	0.16	0.40	0.14	0.02	0.08	0.28	0.83	0.17	0.04	0.11
IMPROVE (Daily)	MFB	-39	5	-27	-96	-36	-86	-16	-89	-146	-85	-46	60	-46	-150	-47
	MFGE	117	101	105	142	120	134	126	119	158	135	132	124	107	163	135
	MNB	159	361	105	21	172	79	393	-21	-67	43	192	656	36	-66	176
	MNGE	246	417	180	149	258	198	471	96	93	161	287	691	122	98	274
	NMB	51	35	82	12	79	-25	71	-48	-80	-37	87	213	25	-77	80
	NME	112	86	132	140	147	105	156	82	89	105	159	230	102	93	165
	R²	0.423	0.448	0.489	0.054	0.278	0.088	0.153	0.124	0.122	0.041	0.396	0.409	0.339	0.001	0.219
	Observed Mean Concentration (µg/m³)	0.46	0.91	0.45	0.19	0.30	0.21	0.21	0.29	0.17	0.14	0.16	0.26	0.18	0.11	0.08
	Predicted Mean Concentration (µg/m³)	0.70	1.22	0.82	0.21	0.54	0.15	0.36	0.15	0.03	0.09	0.30	0.82	0.22	0.03	0.14

Table B-6   CAMx Model Performance Statistical Summary for Nitrate

Monitoring Network	Statistic (%)/ Concentration (μg/m³)	36-km Domain					12-km Domain					4-km Domain				
		Annual	Winter	Spring	Summer	Fall	Annual	Winter	Spring	Summer	Fall	Annual	Winter	Spring	Summer	Fall
STN (Daily)	MFB	-85	-70	-53	-137	-84	-95	-68	-53	-155	-104	-46	-55	9	-138	-20
	MFGE	117	93	96	153	126	111	88	83	157	117	75	68	40	140	65
	MNB	-14	-20	16	-54	-2	-40	0	-23	-83	-51	-16	-34	23	-75	10
	MNGE	99	77	103	99	114	78	98	59	85	73	58	50	47	77	63
	NMB	-47	-45	-23	-81	-51	-60	-59	-41	-93	-66	-47	-59	10	-75	-14
	NME	78	67	77	97	92	69	66	58	94	74	58	62	33	77	48
	R2	0.190	0.169	0.288	0.017	0.030	0.359	0.295	0.351	0.018	0.121	0.498	0.238	0.821	0.010	0.668
	Observed Mean Concentration (μg/m3)	1.82	3.61	1.39	1.06	1.35	1.82	4.26	1.26	0.85	1.16	2.78	8.37	1.24	0.29	0.96
	Predicted Mean Concentration (μg/m3)	0.97	2.00	1.08	0.20	0.66	0.72	1.76	0.75	0.06	0.40	1.48	3.45	1.36	0.07	0.83

Table B-7   CAMx Model Performance Statistical Summary for Nitric Acid and Total Nitrate for CASTNet Monitors

Chemical Compound	Statistic (percent) /b_{ext}	36-km Domain					12-km Domain					4-km Domain				
		Annual	Winter	Spring	Summer	Fall	Annual	Winter	Spring	Summer	Fall	Annual	Winter	Spring	Summer	Fall
HNO$_3$ (gas)	MFB	51	58	41	43	64	64	77	71	42	70	56	35	83	45	61
	MFGE	60	71	52	51	70	71	93	73	49	74	75	106	84	45	69
	MNB	121	162	92	90	155	154	246	157	74	164	141	174	211	66	132
	MNGE	128	172	101	96	159	159	257	159	80	168	153	217	213	66	138
	NMB	50	73	41	49	43	61	91	73	29	84	65	21	124	59	80
	NME	76	89	56	64	98	76	127	81	45	90	91	116	127	59	87
	R^2	0.011	0.389	0.393	0.145	0.003	0.622	0.120	0.687	0.785	0.671	0.151	0.006	0.288	0.436	0.614
	Reconstructed Mean	0.91	0.78	0.88	0.99	0.96	0.57	0.38	0.46	0.88	0.52	0.54	0.61	0.32	0.69	0.52
	Model-predicted Mean	1.36	1.36	1.23	1.48	1.38	0.92	0.73	0.80	1.13	0.95	0.89	0.74	0.72	1.09	0.94
Total NO$_3$	MFB	42	48	38	34	52	36	77	17	13	47	42	72	30	20	46
	MFGE	52	56	47	48	58	50	84	37	35	54	45	77	33	27	47
	MNB	82	105	66	65	99	82	199	33	26	90	70	146	44	27	69
	MNGE	90	112	74	77	103	93	205	50	44	97	74	150	47	34	70
	NMB	56	44	62	56	73	23	83	5	-2	41	51	72	41	27	54
	NME	66	55	69	72	78	51	99	42	35	53	57	88	45	34	54
	R^2	0.632	0.682	0.715	0.374	0.648	0.562	0.468	0.504	0.772	0.662	0.497	0.525	0.379	0.435	0.724
	Reconstructed Mean	1.61	2.34	1.61	1.25	1.34	0.86	0.61	0.87	1.16	0.73	0.77	0.91	0.62	0.87	0.68
	Model-predicted Mean	2.51	3.36	2.61	1.95	2.32	1.06	1.12	0.92	1.14	1.02	1.16	1.56	0.87	1.11	1.04
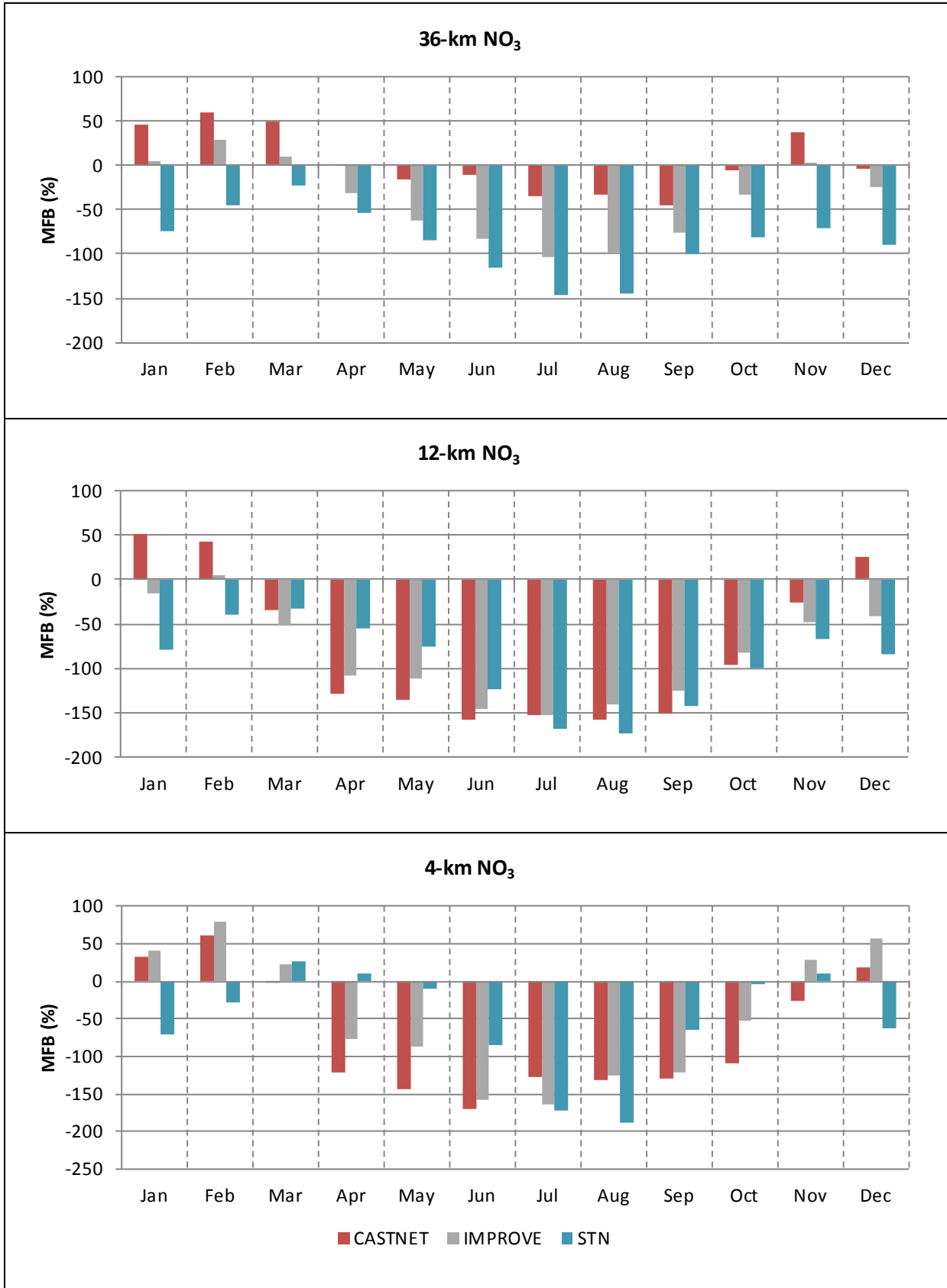
Figure B-6   CAMx Monthly Mean Fractional Bias for Nitrate
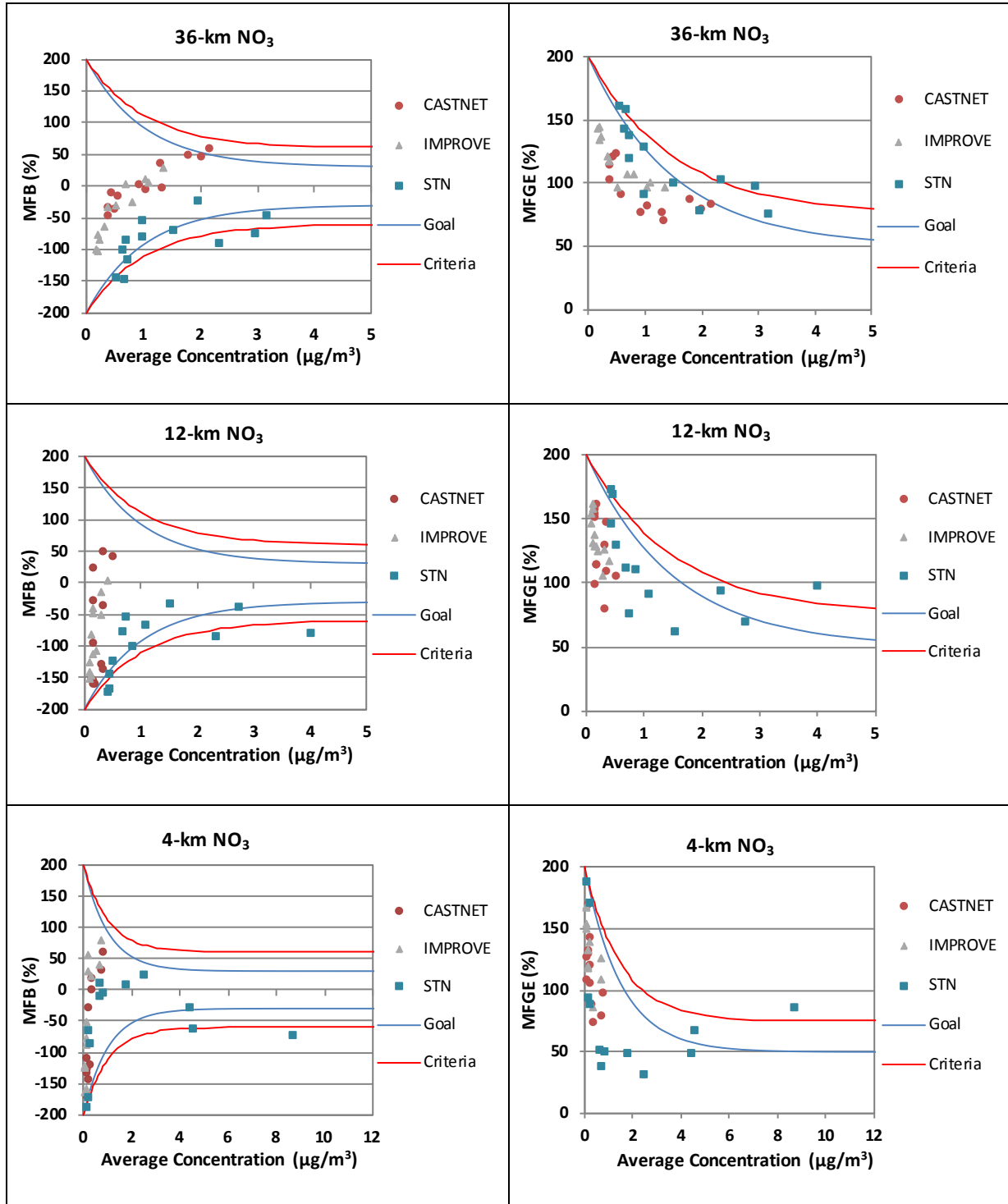
Note: Goals and criteria based on Boylan et al. (2006) and accepted by USEPA (2007).

Figure B-7   CAMx Bugle Plots of Nitrate Monthly Mean Fractional Bias and Mean Fractional Gross Error

B.2.1.3 Ammonium

This section presents statistical tables and graphical summaries of CAMx model performance for ammonium. Statistical results from the model performance evaluation are presented in **Table B-8** through **Table 2-7.** A summary of monthly mean fractional bias is presented in **Figure B-8**, while Bugle plots summarizing model performance in the context of recommended USEPA performance criteria are presented in **Figure B-9.**

Table B-8   CAMx Model Performance Statistical Summary for Ammonium

| Monitoring Network	Statistic (%)/ Concentration (µg/m³)	36-km Domain					12-km Domain					4-km Domain				
		Annual	Winter	Spring	Summer	Fall	Annual	Winter	Spring	Summer	Fall	Annual	Winter	Spring	Summer	Fall
CASTNET (Weekly)	MFB	45	39	61	30	52	23	68	23	-9	19	29	78	27	-7	26
	MFGE	53	52	63	43	57	40	74	34	23	36	42	78	36	20	39
	MNB	89	95	119	53	96	53	162	36	-5	41	62	168	45	-3	55
	MNGE	96	106	121	63	100	68	167	45	21	55	73	168	54	21	66
	NMB	53	29	105	44	49	22	97	22	-11	14	44	138	36	-6	26
	NME	69	46	107	56	80	44	110	39	23	34	58	138	47	19	42
	R^2	0.079	0.687	0.698	0.313	0.013	0.199	0.429	0.133	0.442	0.289	0.410	0.782	0.069	0.304	0.104
	Observed Mean Concentration (µg/m³)	0.78	0.94	0.66	0.84	0.67	0.21	0.15	0.23	0.24	0.19	0.20	0.19	0.21	0.23	0.17
	Predicted Mean Concentration (µg/m³)	1.19	1.20	1.36	1.21	0.99	0.25	0.29	0.28	0.22	0.21	0.29	0.44	0.28	0.21	0.22
IMPROVE (Daily)	MFB	27	45	31	3	32	12	52	6	-19	11	25	75	20	-17	24
	MFGE	55	66	53	47	54	47	67	39	40	42	50	81	41	33	45
	MNB	110	204	91	73	84	50	142	41	-8	33	76	233	43	-10	50
	MNGE	131	220	107	106	101	77	154	67	36	57	96	238	60	31	67
	NMB	30	28	52	6	39	4	66	-2	-24	3	33	118	25	-17	26
	NME	61	60	74	49	65	49	89	41	39	43	60	126	48	30	51
	R^2	0.462	0.529	0.457	0.497	0.466	0.222	0.313	0.277	0.369	0.218	0.260	0.500	0.197	0.288	0.099
	Observed Mean Concentration (µg/m³)	0.57	0.61	0.57	0.62	0.46	0.25	0.18	0.30	0.30	0.22	0.22	0.20	0.24	0.26	0.18
	Predicted Mean Concentration (µg/m³)	0.74	0.77	0.87	0.66	0.64	0.26	0.29	0.29	0.23	0.23	0.29	0.43	0.30	0.22	0.23

Table B-8   CAMx Model Performance Statistical Summary for Ammonium

Monitoring Network	Statistic (%)/ Concentration (µg/m³)	36-km Domain					12-km Domain					4-km Domain				
		Annual	Winter	Spring	Summer	Fall	Annual	Winter	Spring	Summer	Fall	Annual	Winter	Spring	Summer	Fall
STN (Daily)	MFB	31	16	49	18	40	27	0	53	19	33	26	-37	57	21	58
	MFGE	71	72	72	66	76	65	73	69	54	62	57	73	60	30	61
	MNB	250	106	506	133	232	100	61	144	59	127	77	1	137	36	122
	MNGE	279	146	523	168	257	127	114	157	85	148	100	77	140	44	125
	NMB	9	-13	51	-4	22	-15	-39	30	-13	2	-27	-54	55	20	52
	NME	78	65	91	76	92	63	64	65	56	63	62	63	60	31	64
	R^2	0.165	0.179	0.261	0.043	0.034	0.343	0.280	0.470	0.394	0.225	0.450	0.269	0.761	0.254	0.739
	Observed Mean Concentration (µg/m³)	0.77	1.35	0.63	0.58	0.57	0.68	1.45	0.47	0.43	0.47	1.01	2.92	0.45	0.20	0.37
	Predicted Mean Concentration (µg/m³)	0.84	1.17	0.95	0.56	0.70	0.58	0.88	0.60	0.37	0.48	0.73	1.34	0.70	0.24	0.56

Figure B-8   CAMx Monthly Mean Fractional Bias for Ammonium

Note: Goals and criteria based on Boylan et al. (2006) and accepted by USEPA (2007).

Figure B-9   CAMx Bugle Plots of Ammonium Monthly Mean Fractional Bias and Mean Fractional Gross Error

B.2.1.4 Organic Carbon

This section presents statistical tables and graphical summaries of CAMx model performance for organic carbon. Statistical results from the model performance evaluation are presented in **Table B-9**. A summary of monthly mean fractional bias is presented in **Figure B-10**, while Bugle plots summarizing model performance in the context of recommended USEPA performance criteria are presented in **Figure B-11.**

Table B-9   CAMx Model Performance Statistical Summary for Organic Carbon

Monitoring Network	Statistic (%)/ Concentration ($\mu g/m^3$)	36-km Domain					12-km Domain					4-km Domain				
		Annual	Winter	Spring	Summer	Fall	Annual	Winter	Spring	Summer	Fall	Annual	Winter	Spring	Summer	Fall
IMPROVE (Daily)	MFB	-11	-13	-1	-11	-19	-37	-34	-18	-48	-49	-29	-40	2	-36	-43
	MFGE	53	62	48	49	54	60	72	48	57	65	51	61	39	49	58
	MNB	55	105	53	24	46	13	75	13	-22	-13	-7	-19	27	-21	-14
	MNGE	101	157	89	68	98	81	146	61	53	67	51	49	55	41	58
	NMB	-10	-21	-2	-3	-16	-46	-54	-39	-44	-51	-38	-36	-8	-34	-56
	NME	51	56	52	49	51	56	70	54	48	58	49	49	37	43	60
	R^2	0.193	0.233	0.115	0.324	0.186	0.032	0.010	0.003	0.251	0.117	0.030	0.086	0.137	0.033	0.023
	Observed Mean Concentration ($\mu g/m^3$)	1.26	1.02	1.09	1.57	1.34	0.72	0.57	0.56	0.96	0.81	0.59	0.42	0.36	0.72	0.85
	Predicted Mean Concentration ($\mu g/m^3$)	1.13	0.80	1.07	1.53	1.12	0.39	0.26	0.34	0.54	0.40	0.36	0.27	0.33	0.47	0.37
STN (Daily)	MFB	-27	-40	-22	-16	-31	37	32	50	30	34	75	84	78	54	82
	MFGE	52	61	48	46	52	48	61	53	33	47	76	85	78	54	82
	MNB	-9	-19	-6	2	-15	68	84	88	44	57	144	191	145	79	150
	MNGE	47	49	45	48	45	77	106	92	47	67	144	192	145	79	150
	NMB	-20	-31	-11	-8	-25	50	50	76	40	41	126	138	134	74	137
	NME	47	50	44	43	47	68	79	82	44	63	128	141	134	74	137
	R^2	0.174	0.170	0.310	0.163	0.081	0.216	0.102	0.247	0.319	0.062	0.498	0.209	0.328	0.460	0.584
	Observed Mean Concentration ($\mu g/m^3$)	2.24	3.03	1.78	1.86	2.34	2.12	3.22	1.41	1.77	2.19	1.90	3.13	1.21	1.49	1.74
	Predicted Mean Concentration ($\mu g/m^3$)	1.78	2.10	1.58	1.71	1.75	3.17	4.82	2.48	2.48	3.09	4.30	7.44	2.84	2.60	4.14

Figure B-10   CAMx Monthly Mean Fractional Bias for Organic Carbon
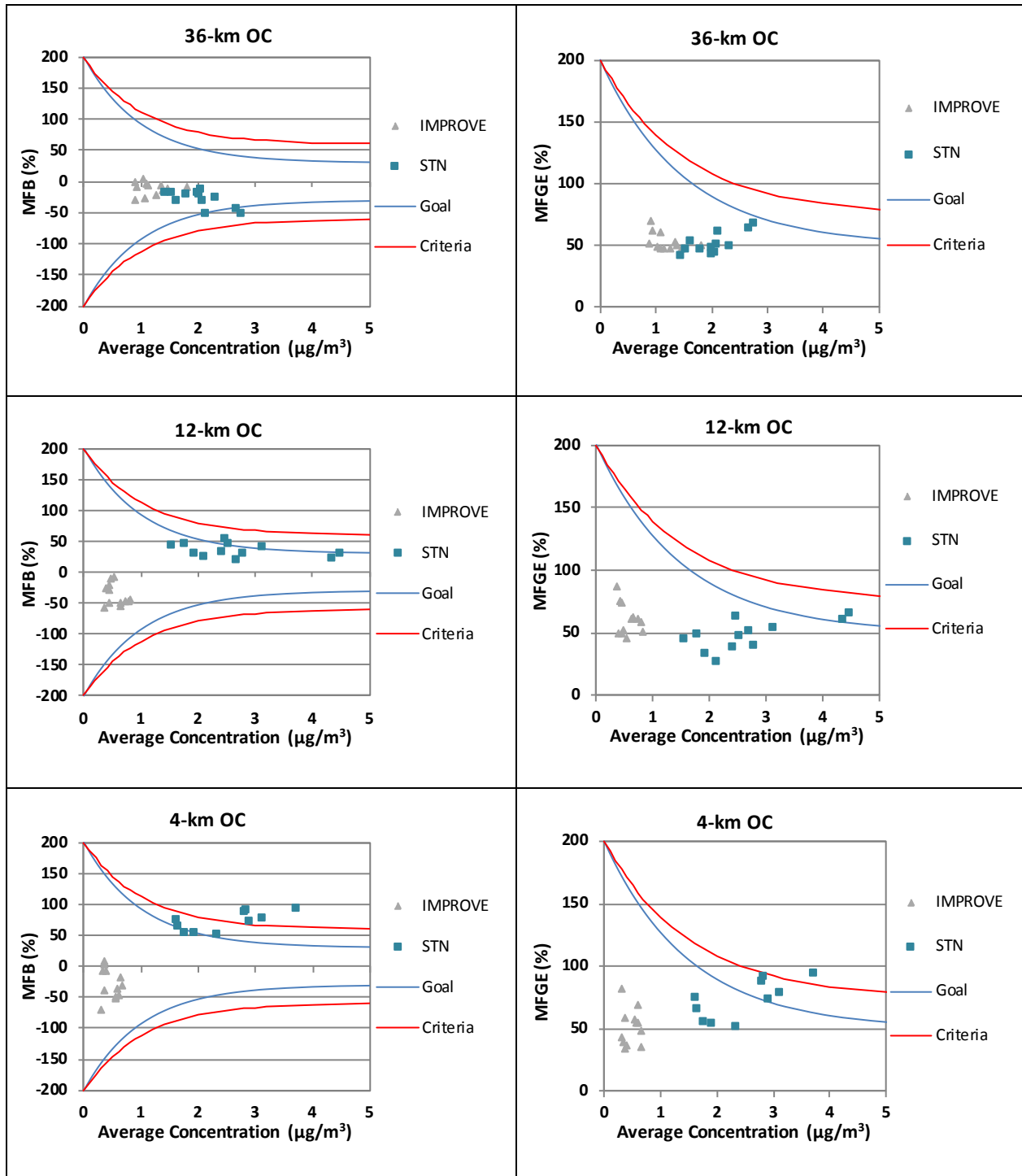
Note: Goals and criteria based on Boylan et al. (2006) and accepted by USEPA (2007).

Figure B-11   CAMx Bugle Plots of Organic Carbon Monthly Mean Fractional Bias and Mean Fractional Gross Error
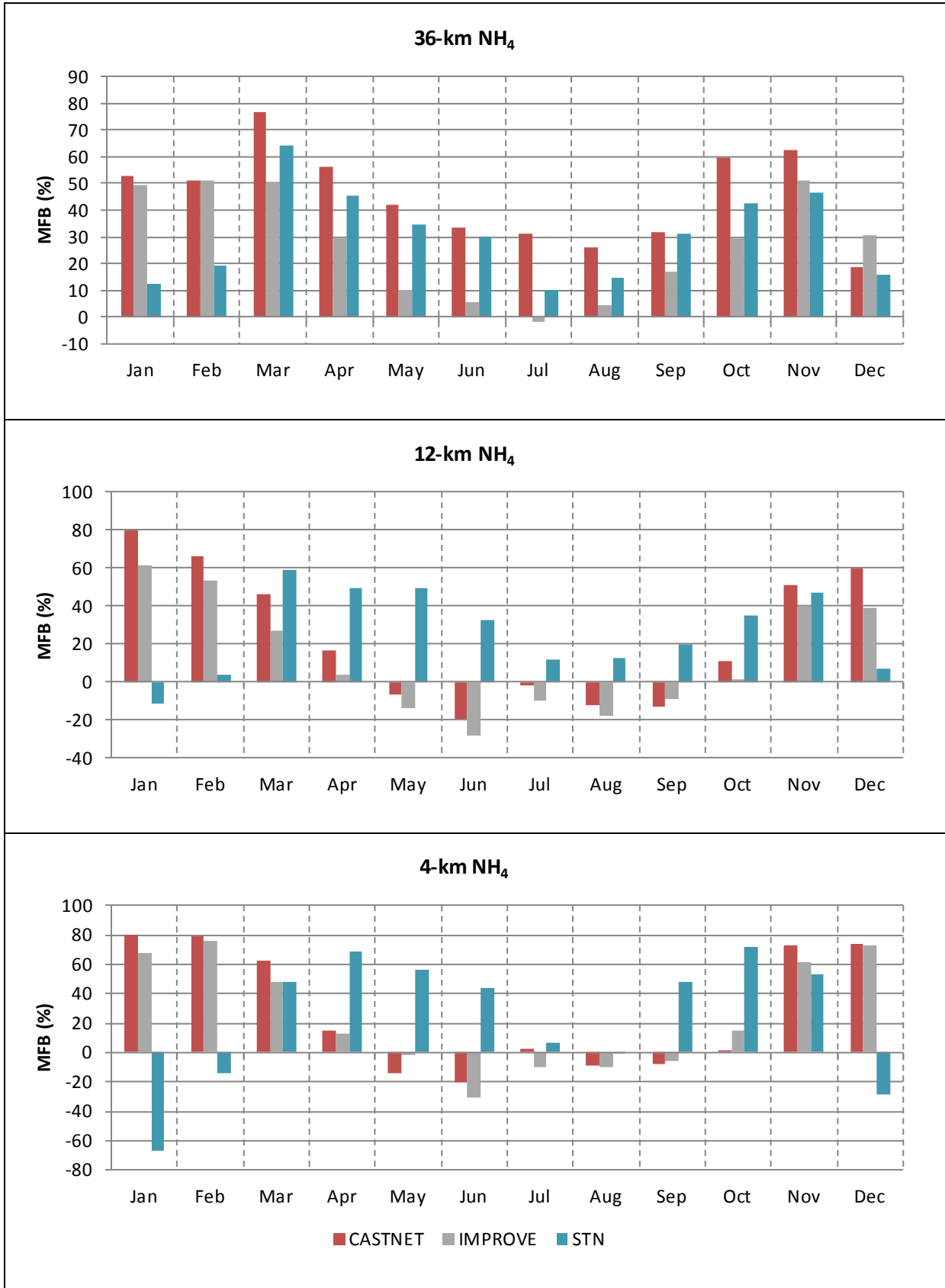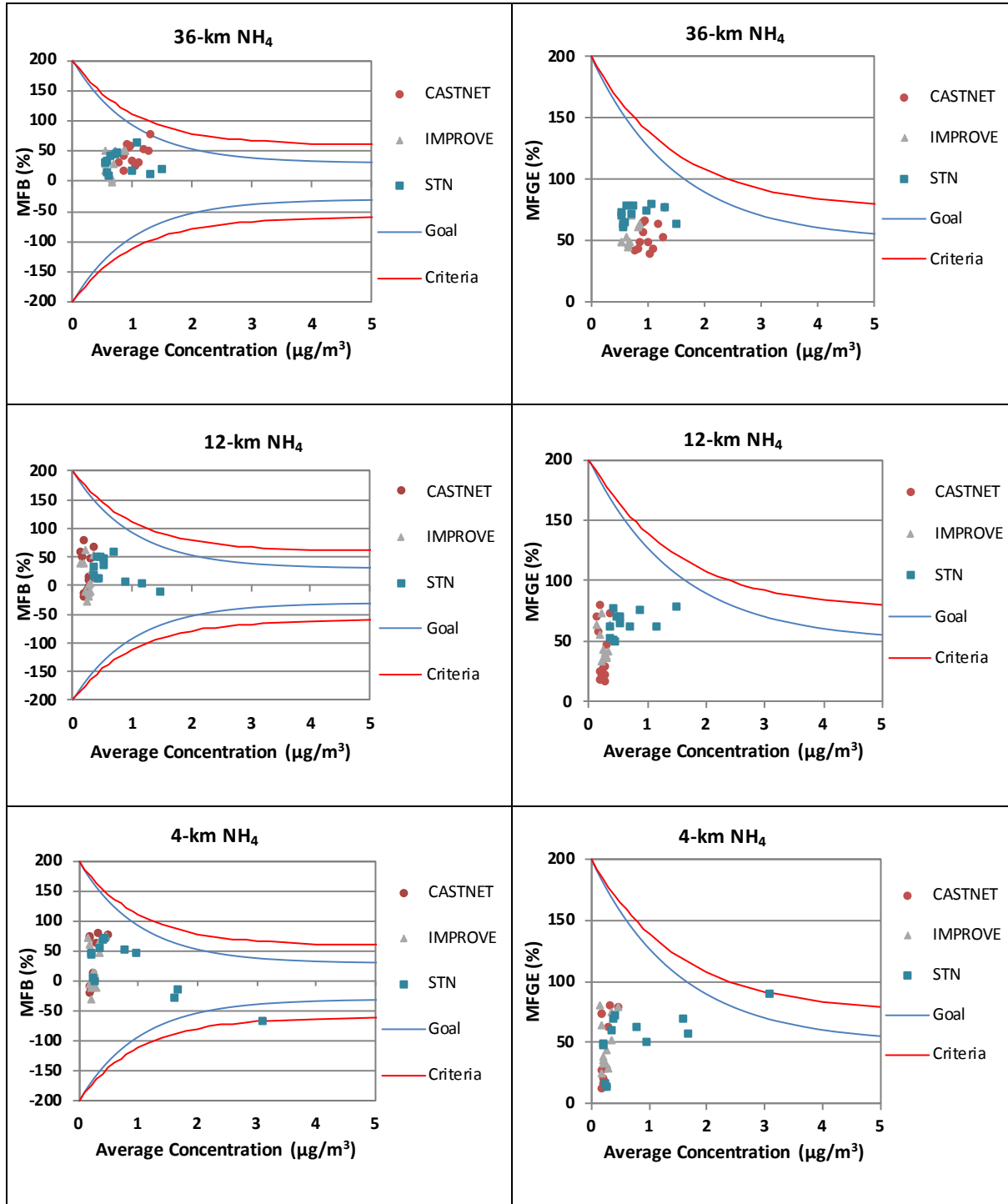
B.2.1.5 Elemental Carbon

This section presents statistical tables and graphical summaries of CAMx model performance for elemental carbon. Statistical results from the model performance evaluation are presented in **Table B-10**. A summary of monthly mean fractional bias is presented in **Figure B-12**, while Bugle plots summarizing model performance in the context of recommended USEPA performance criteria are presented in **Figure B-13.**

Table B-10   CAMx Model Performance Statistical Summary for Elemental Carbon

Monitoring Network	Statistic (%)/ Concentration (µg/m³)	36-km Domain					12-km Domain					4-km Domain				
		Annual	Winter	Spring	Summer	Fall	Annual	Winter	Spring	Summer	Fall	Annual	Winter	Spring	Summer	Fall
IMPROVE (Daily)	MFB	24	42	32	10	12	-4	12	12	-24	-21	6	8	35	-11	-8
	MFGE	61	74	59	56	55	56	74	50	49	54	52	66	51	42	47
	MNB	145	223	127	122	90	54	118	95	-5	9	67	90	149	11	13
	MNGE	171	246	147	156	121	99	161	123	48	62	100	131	162	52	54
	NMB	43	56	58	35	26	-20	-20	-12	-22	-26	-10	-2	29	-22	-25
	NME	80	92	92	73	67	57	71	57	46	55	51	63	52	42	49
	R²	0.284	0.483	0.200	0.274	0.342	0.077	0.060	0.017	0.330	0.130	0.047	0.076	0.218	0.019	0.039
	Observed Mean Concentration (µg/m³)	0.19	0.20	0.18	0.18	0.21	0.09	0.09	0.08	0.10	0.10	0.07	0.07	0.04	0.08	0.09
	Predicted Mean Concentration (µg/m³)	0.27	0.31	0.28	0.24	0.26	0.07	0.07	0.07	0.08	0.08	0.06	0.07	0.06	0.06	0.07
STN (Daily)	MFB	35	36	45	40	20	88	89	101	93	72	141	144	145	141	133
	MFGE	73	80	74	72	68	92	95	101	93	80	141	144	145	141	133
	MNB	122	143	136	130	80	220	246	262	216	160	565	678	616	514	440
	MNGE	149	173	158	154	113	222	250	262	216	166	565	678	616	514	440
	NMB	61	58	100	90	27	168	195	213	179	111	497	544	540	490	398
	NME	104	104	127	120	82	173	198	213	179	122	497	544	540	490	398
	R²	0.120	0.120	0.126	0.086	0.042	0.491	0.426	0.444	0.471	0.447	0.475	0.133	0.449	0.451	0.676
	Observed Mean Concentration (µg/m³)	0.46	0.68	0.31	0.29	0.57	0.52	0.81	0.33	0.36	0.63	0.50	0.85	0.31	0.29	0.53
	Predicted Mean Concentration (µg/m³)	0.74	1.08	0.62	0.56	0.72	1.41	2.38	1.04	1.00	1.33	2.99	5.50	1.98	1.71	2.63
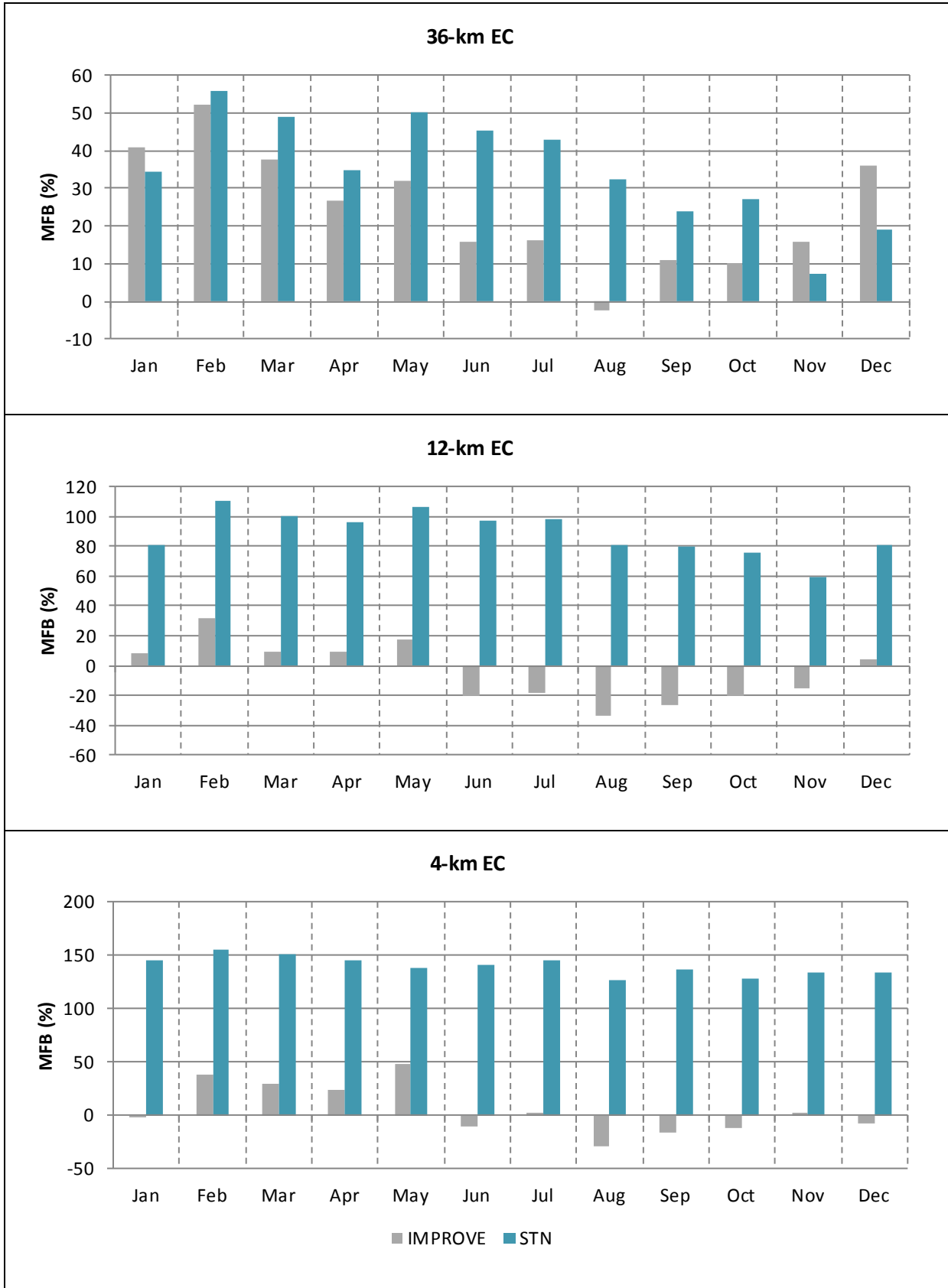
Figure B-12   CAMx Monthly Mean Fractional Bias for Elemental Carbon
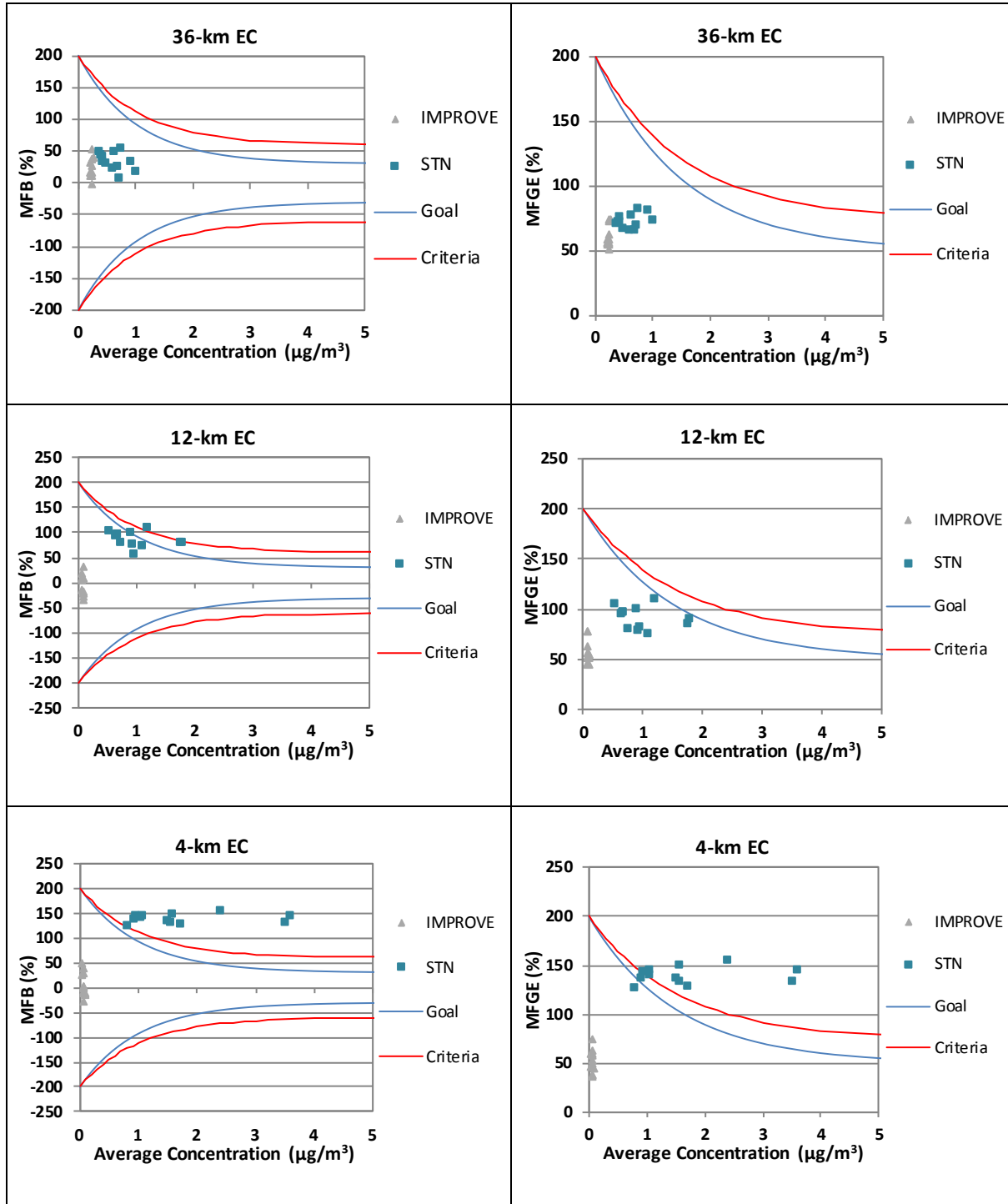
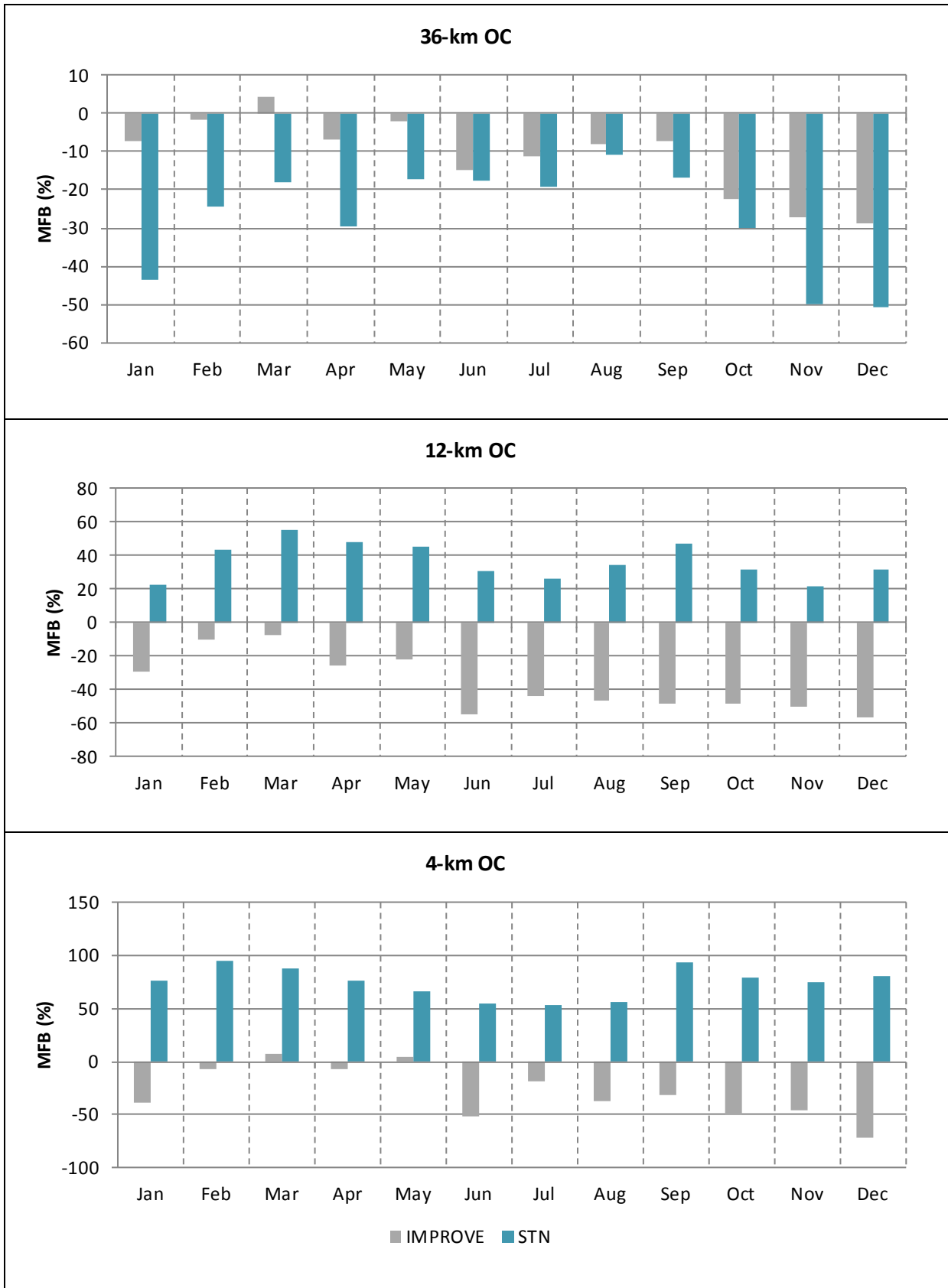Note: Goals and criteria based on Boylan et al. (2006) and accepted by USEPA (2007).

Figure B-13   CAMx Bugle Plots of Elemental Carbon Monthly Mean Fractional Bias and Mean Fractional Gross Error

B.2.1.6 Fine Soil

This section presents statistical tables and graphical summaries of CAMx model performance for fine soil. Statistical results from the model performance evaluation are presented in **Table B-11**. A summary of monthly mean fractional bias is presented in **Figure B-14**, while Bugle plots summarizing model performance in the context of recommended USEPA performance criteria are presented in **Figure B-15.**

Table B-11   CAMx Model Performance Statistical Summary for Fine Soil

Monitoring Network	Statistic (%)/ Concentration (µg/m^3)	36-km Domain					12-km Domain					4-km Domain				
		Annual	Winter	Spring	Summer	Fall	Annual	Winter	Spring	Summer	Fall	Annual	Winter	Spring	Summer	Fall
IMPROVE (Daily)	MFB	72	118	66	32	74	18	78	21	-39	12	18	83	14	-48	22
	MFGE	96	126	85	78	97	72	92	64	64	68	70	95	66	58	61
	MNB	497	929	313	332	441	109	286	87	-14	80	109	312	78	-30	83
	MNGE	514	934	326	365	457	146	296	117	56	119	145	321	114	45	111
	NMB	84	304	66	20	100	-20	111	-19	-50	-18	-30	121	-40	-54	6
	NME	140	341	118	92	151	72	144	69	63	71	72	146	75	57	61
	R^2	0.034	0.042	0.014	0.086	0.039	0.052	0.057	0.019	0.016	0.002	0.069	0.092	0.013	0.094	0.047
	Observed Mean Concentration (µg/m^3)	0.71	0.32	1.01	0.92	0.58	0.83	0.20	1.46	0.98	0.62	0.91	0.17	1.97	1.00	0.45
	Predicted Mean Concentration (µg/m^3)	1.31	1.28	1.68	1.10	1.17	0.66	0.43	1.18	0.49	0.51	0.64	0.38	1.19	0.46	0.48
STN (Daily)	MFB	96	133	103	59	92	123	158	127	91	118	130	167	118	79	145
	MFGE	110	137	111	84	108	127	158	131	100	121	135	167	131	85	145
	MNB	1517	915	4289	223	429	755	1418	616	365	682	808	1571	483	214	840
	MNGE	1526	918	4295	241	441	758	1419	619	371	685	811	1571	492	219	840
	NMB	175	481	178	64	138	274	779	236	127	222	314	1089	110	93	527
	NME	216	494	213	113	191	302	781	286	156	240	359	1089	205	109	527
	R^2	0.003	0.021	0.009	0.066	0.000	0.001	0.114	0.001	0.003	0.082	0.003	0.020	0.003	0.118	0.105
	Observed Mean Concentration (µg/m^3)	0.95	0.56	1.02	1.16	1.03	0.93	0.55	0.98	1.11	1.03	1.11	0.60	1.75	1.42	0.71
	Predicted Mean Concentration (µg/m^3)	2.61	3.25	2.83	1.90	2.47	3.47	4.84	3.31	2.52	3.31	4.59	7.09	3.69	2.74	4.46
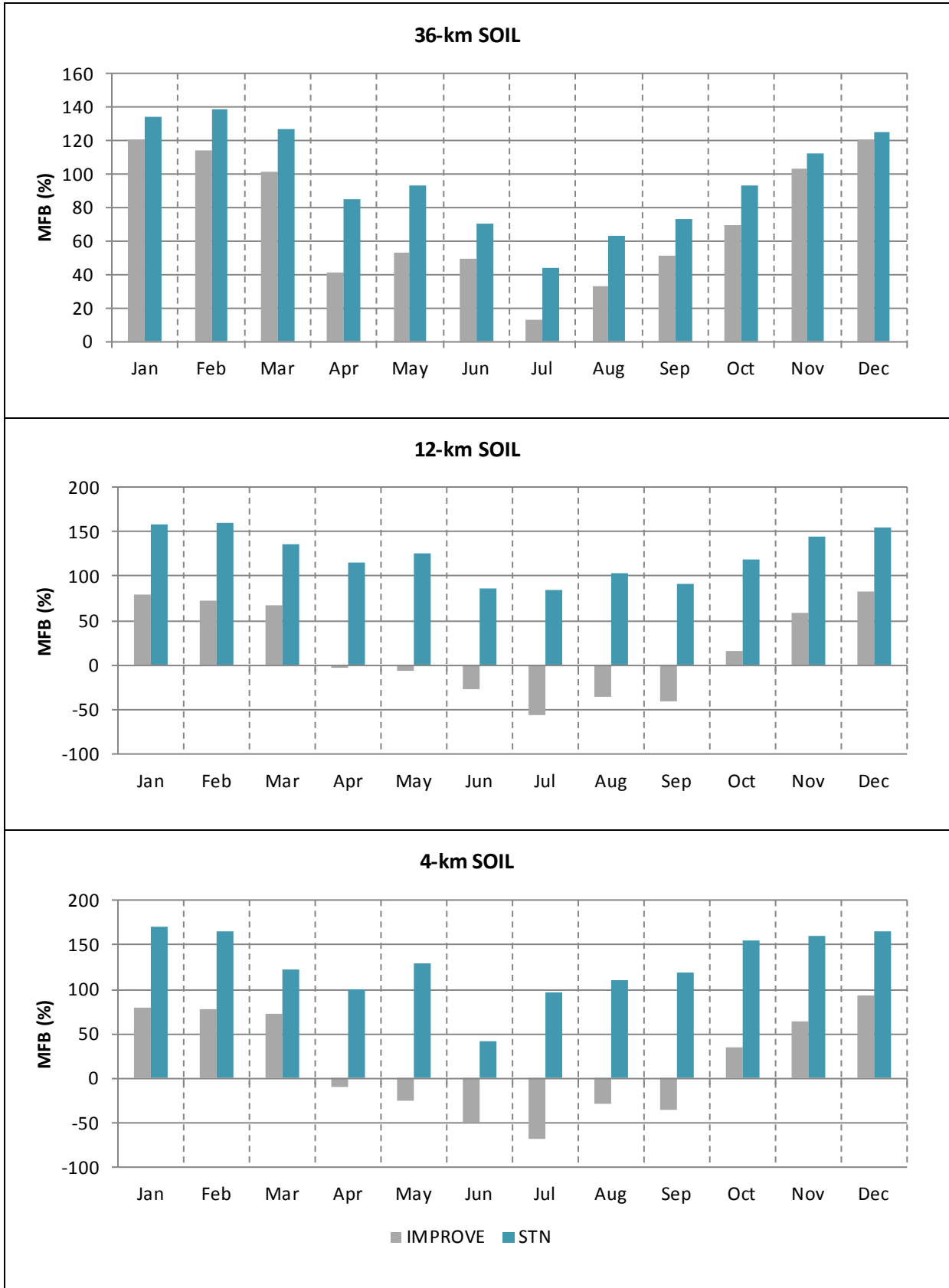
Figure B-14   CAMx Monthly Mean Fractional Bias for Fine Soil
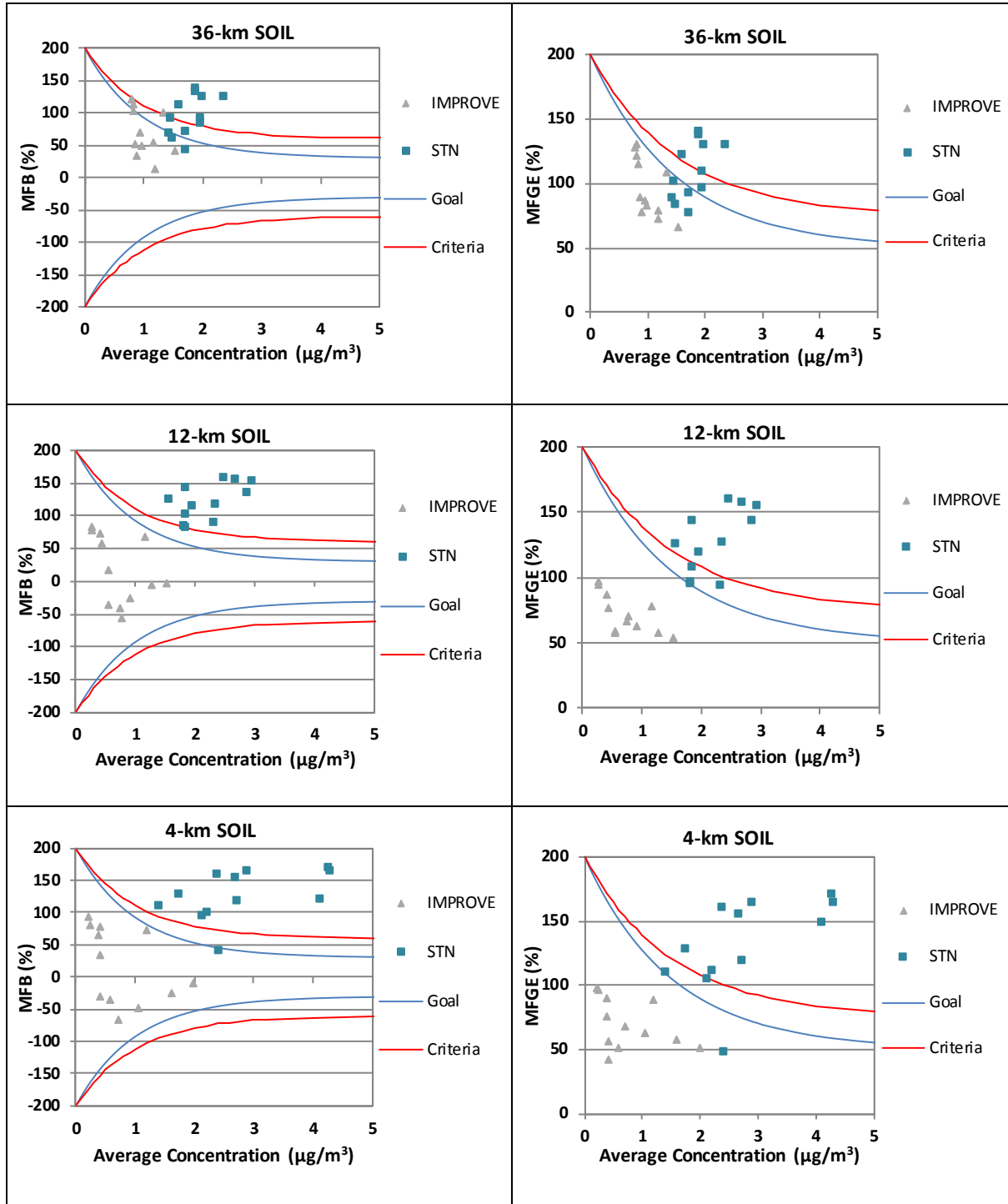
Note: Goals and criteria based on Boylan et al. (2006) and accepted by USEPA (2007).

Figure B-15   CAMx Bugle Plots of Fine Soil Monthly Mean Fractional Bias and Mean Fractional Gross Error

B.2.1.7 Coarse Mass

This section presents statistical tables and graphical summaries of CAMx model performance for coarse mass. Statistical results from the model performance evaluation are presented in **Table B-12**. A summary of monthly mean fractional bias is presented in **Figure B-16**, while Bugle plots summarizing model performance in the context of recommended USEPA performance criteria are presented in **Figure B-17**

Table B-12   CAMx Model Performance Statistical Summary for Coarse Mass

| Monitoring Network	Statistic (%)/ Concentration ($\mu g/m^3$)	36-km Domain					12-km Domain					4-km Domain				
		Annual	Winter	Spring	Summer	Fall	Annual	Winter	Spring	Summer	Fall	Annual	Winter	Spring	Summer	Fall
IMPROVE (Daily)	MFB	-50	-1	-24	-105	-68	-60	-18	-12	-129	-82	-65	-27	-19	-135	-89
	MFGE	88	78	72	111	91	95	77	73	130	99	94	71	74	135	99
	MNB	142	178	408	-59	-1	23	126	54	-75	-18	22	178	39	-79	-50
	MNGE	229	230	471	71	99	119	190	112	77	94	121	245	101	79	66
	NMB	-53	-15	-41	-72	-62	-62	-22	-44	-82	-71	-68	-35	-59	-83	-74
	NME	72	76	67	75	71	77	75	73	82	75	79	62	80	83	76
	R^2	0.067	0.139	0.039	0.086	0.144	0.031	0.089	0.008	0.151	0.027	0.037	0.092	0.004	0.134	0.024
	Observed Mean Concentration ($\mu g/m^3$)	4.87	2.62	5.20	6.05	5.39	3.72	1.06	4.66	5.28	3.59	3.67	0.78	6.20	4.74	2.91
	Predicted Mean Concentration ($\mu g/m^3$)	2.28	2.22	3.09	1.69	2.05	1.41	0.83	2.61	0.97	1.06	1.19	0.50	2.56	0.83	0.76
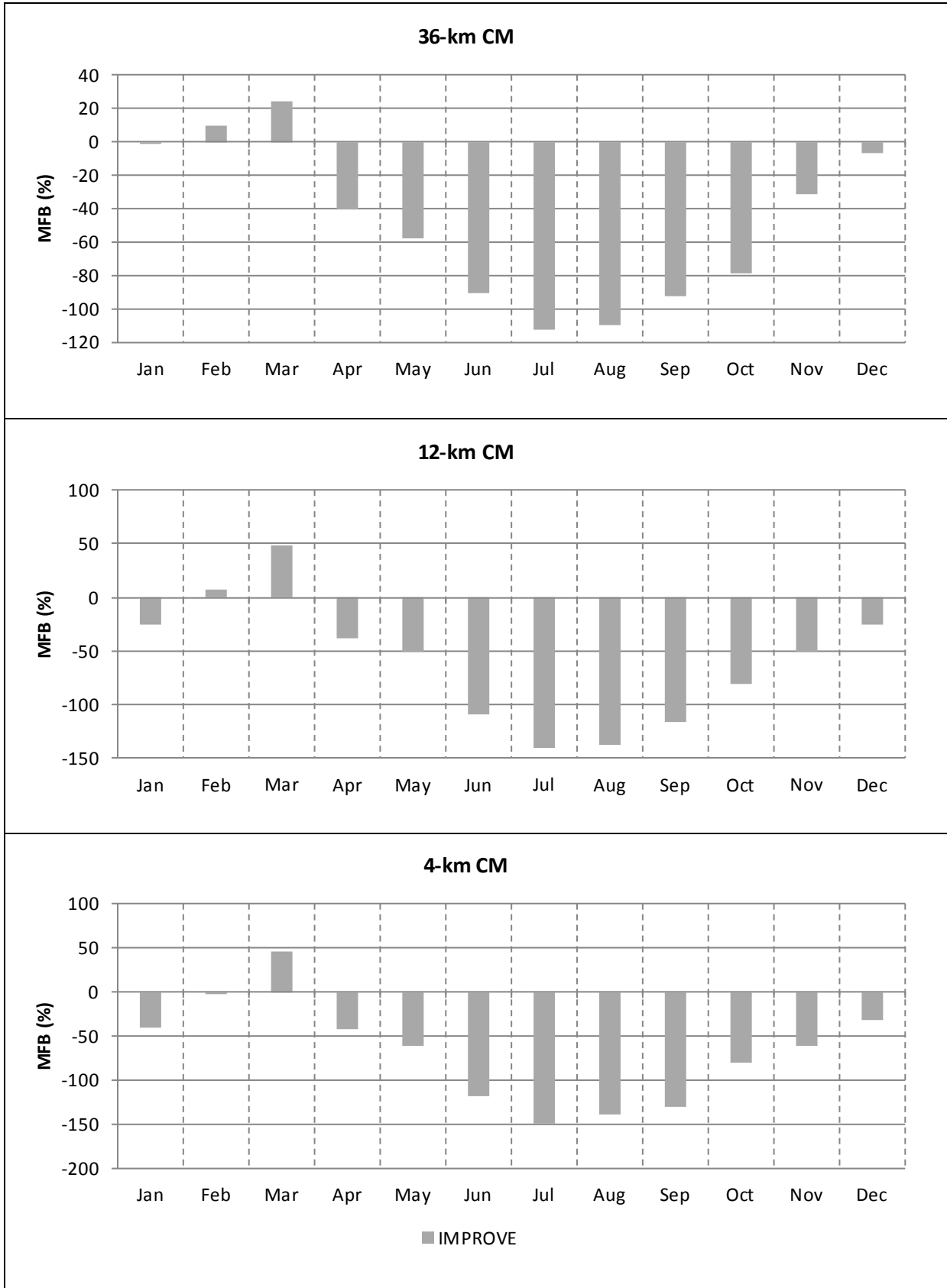
Figure B-16   CAMx Monthly Mean Fractional Bias for Coarse Mass
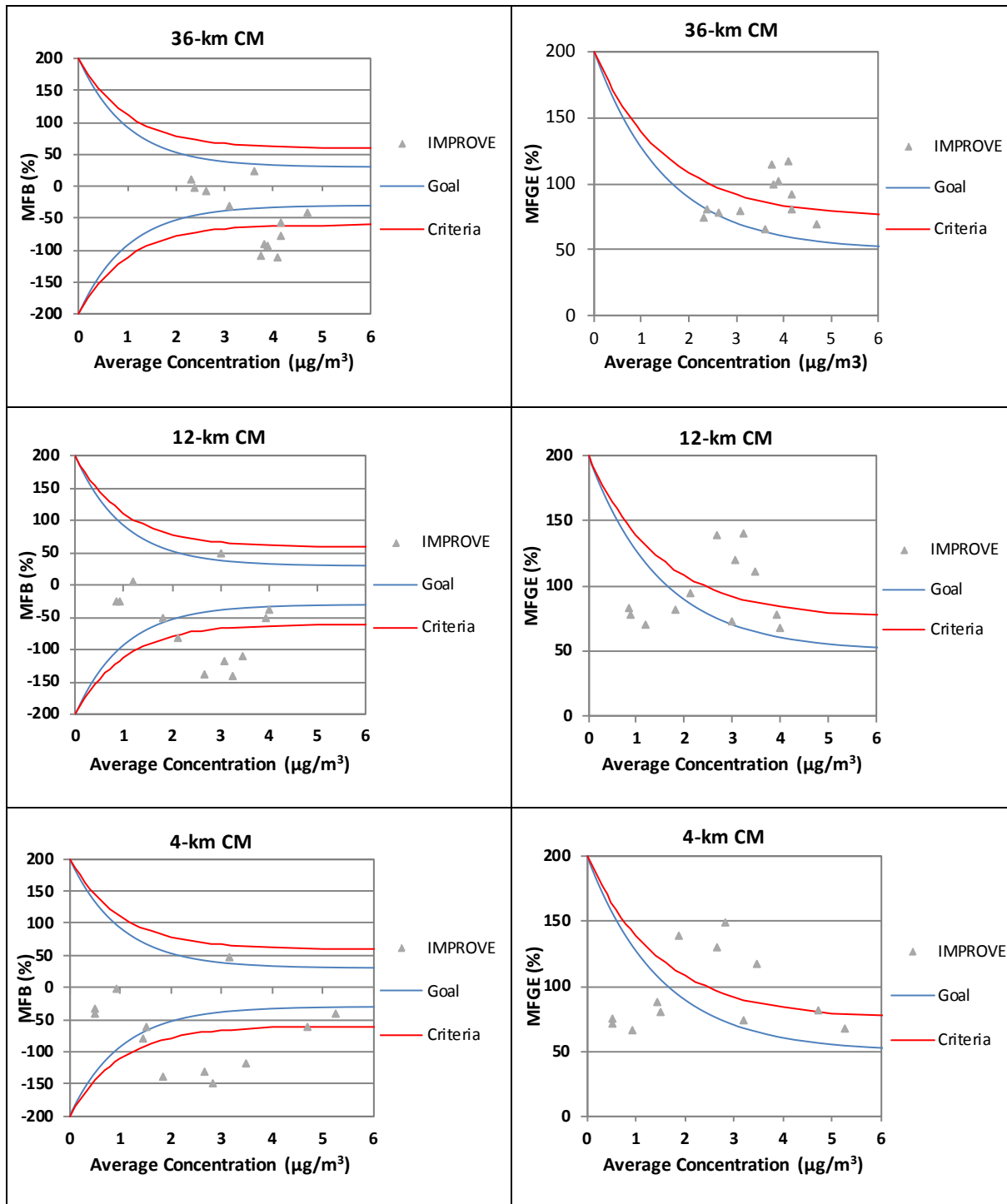
Note: Goals and criteria based on Boylan et al. (2006) and accepted by USEPA (2007).

Figure B-17   CAMx Bugle Plots of Coarse Mass Monthly Mean Fractional Bias and Mean Fractional Gross Error

B.2.2   Total PM$_{2.5}$

This section presents statistical tables and graphical summaries of CAMx model performance for total PM$_{2.5}$ mass. Statistical results from the model performance evaluation are presented in **Table B-13**. Summaries of monthly mean fractional bias, as well as Bugle plots summarizing model performance in the context of recommended USEPA performance criteria are presented in **Figure B-18** through **Figure B-21**. Finally, spatial plots of PM$_{2.5}$ concentrations on the CAMx 4-km domain overlaid with observations are presented for select dates in **Figure B-22** and **B-23.**

Table B-13   CAMx Model Performance Statistical Summary for Total PM$_{2.5}$

Monitoring Network	Statistic (%)/ Concentration (µg/m^3)	36-km Domain					12-km Domain					4-km Domain				
		Annual	Winter	Spring	Summer	Fall	Annual	Winter	Spring	Summer	Fall	Annual	Winter	Spring	Summer	Fall
AQS (Daily)	MFB	-31	-31	-9	-51	-34	-6	-3	15	-34	-4	3	-6	28	-31	19
	MFGE	53	62	42	56	50	52	65	46	50	47	50	55	51	47	46
	MNB	-13	-2	6	-35	-19	22	45	43	-19	17	27	26	57	-18	43
	MNGE	47	61	45	43	42	64	92	67	42	55	62	70	74	40	65
	NMB	-32	-36	-14	-42	-32	-6	-11	15	-28	1	-6	-21	18	-29	30
	NME	48	54	42	46	45	55	66	55	44	48	53	50	64	43	55
	R^2	0.227	0.197	0.166	0.277	0.205	0.150	0.095	0.085	0.093	0.174	0.262	0.245	0.032	0.016	0.291
	Observed Mean Concentration (µg/m^3)	8.55	12.00	6.77	7.77	7.79	7.28	11.22	5.74	6.30	6.00	8.85	16.46	6.36	6.87	6.13
	Predicted Mean Concentration (µg/m^3)	5.81	7.64	5.85	4.47	5.27	6.84	9.94	6.61	4.56	6.09	8.30	12.96	7.53	4.89	7.95
IMPROVE (Daily)	MFB	21	45	32	-10	17	-7	35	6	-50	-18	2	53	10	-47	-9
	MFGE	51	62	52	44	47	50	57	43	54	45	51	63	49	49	43
	MNB	69	139	81	14	47	20	89	30	-36	-3	33	128	40	-35	7
	MNGE	93	152	96	55	71	62	106	59	41	45	70	136	68	37	47
	NMB	27	46	47	-1	23	-18	41	-9	-44	-26	-11	81	-12	-41	-21
	NME	58	70	70	44	54	48	69	46	45	44	53	91	57	42	44
	R^2	0.378	0.439	0.324	0.430	0.431	0.102	0.197	0.060	0.270	0.099	0.019	0.400	0.003	0.096	0.017
	Observed Mean Concentration (µg/m^3)	4.71	4.03	4.64	5.75	4.31	2.73	1.43	3.14	3.62	2.66	2.58	1.39	3.26	3.23	2.39
	Predicted Mean Concentration (µg/m^3)	5.96	5.88	6.81	5.71	5.31	2.23	2.02	2.86	2.05	1.96	2.30	2.52	2.87	1.91	1.89

Table B-13   CAMx Model Performance Statistical Summary for Total PM$_{2.5}$

Monitoring Network	Statistic (%)/ Concentration (μg/m^3)	36-km Domain					12-km Domain					4-km Domain				
		Annual	Winter	Spring	Summer	Fall	Annual	Winter	Spring	Summer	Fall	Annual	Winter	Spring	Summer	Fall
STN (Daily)	MFB	-18	-17	-3	-36	-15	19	20	34	-3	24	50	45	53	9	81
	MFGE	50	52	46	55	48	45	55	48	32	44	63	62	64	39	81
	MNB	3	5	23	-20	2	44	57	64	7	45	102	116	95	21	154
	MNGE	52	54	60	46	48	64	84	75	35	61	112	130	102	44	154
	NMB	-15	-14	1	-31	-15	15	15	32	-7	20	48	33	52	4	129
	NME	50	52	48	48	50	50	58	55	32	47	76	66	88	41	129
	R^2	0.139	0.108	0.213	0.113	0.045	0.191	0.103	0.097	0.071	0.135	0.296	0.130	0.028	0.003	0.631
	Observed Mean Concentration (μg/m^3)	10.07	13.29	8.81	9.17	9.24	9.15	13.89	7.14	8.08	8.08	10.21	19.33	7.59	7.74	5.91
	Predicted Mean Concentration (μg/m^3)	8.60	11.45	8.88	6.35	7.83	10.51	15.95	9.43	7.49	9.68	15.07	25.78	11.53	8.07	13.50

Table B-13   CAMx Model Performance Statistical Summary for Total PM$_{2.5}$

Monitoring Network	Statistic (%)/ Concentration (µg/m³)	36-km Domain					12-km Domain					4-km Domain				
		Annual	Winter	Spring	Summer	Fall	Annual	Winter	Spring	Summer	Fall	Annual	Winter	Spring	Summer	Fall
AQS (Hourly)	MFB	-32	-26	-18	-50	-34	-19	-10	-2	-41	-20	-32	-16	-12	-72	-28
	MFGE	78	83	70	82	77	80	86	71	83	79	72	68	60	86	72
	MNB	2101	2918	2418	1439	1751	3061	4070	3475	2170	2635	24	43	50	-15	19
	MNGE	2180	2990	2479	1528	1826	3132	4134	3527	2254	2703	97	102	103	91	91
	NMB	-45	-42	-34	-55	-46	-30	-25	-19	-45	-30	-31	-22	-22	-57	-24
	NME	66	70	62	67	64	73	79	70	70	70	63	63	62	67	62
	R²	0.087	0.086	0.049	0.123	0.116	0.034	0.045	0.009	0.014	0.044	0.086	0.159	0.010	0.011	0.072
	Observed Mean Concentration (µg/m³)	9.00	10.61	7.90	8.96	8.64	7.52	9.56	6.75	7.13	6.79	8.41	12.80	7.78	7.64	5.94
	Predicted Mean Concentration (µg/m³)	5.00	6.20	5.18	4.03	4.71	5.27	7.19	5.46	3.89	4.76	5.84	9.93	6.04	3.28	4.53
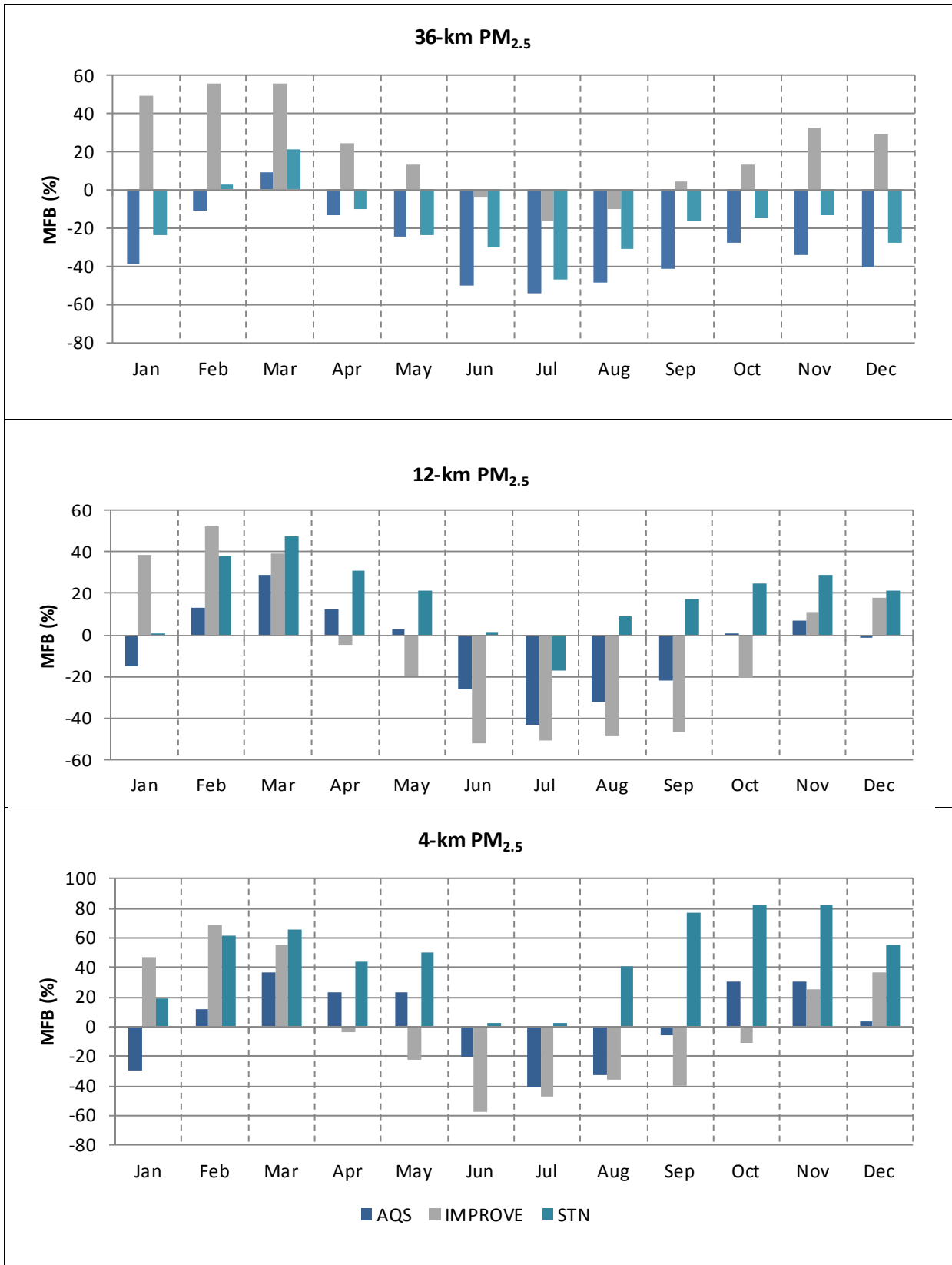
Figure B-18   CAMx Monthly Mean Fractional Bias for Total PM$_{2.5}$ (Daily)
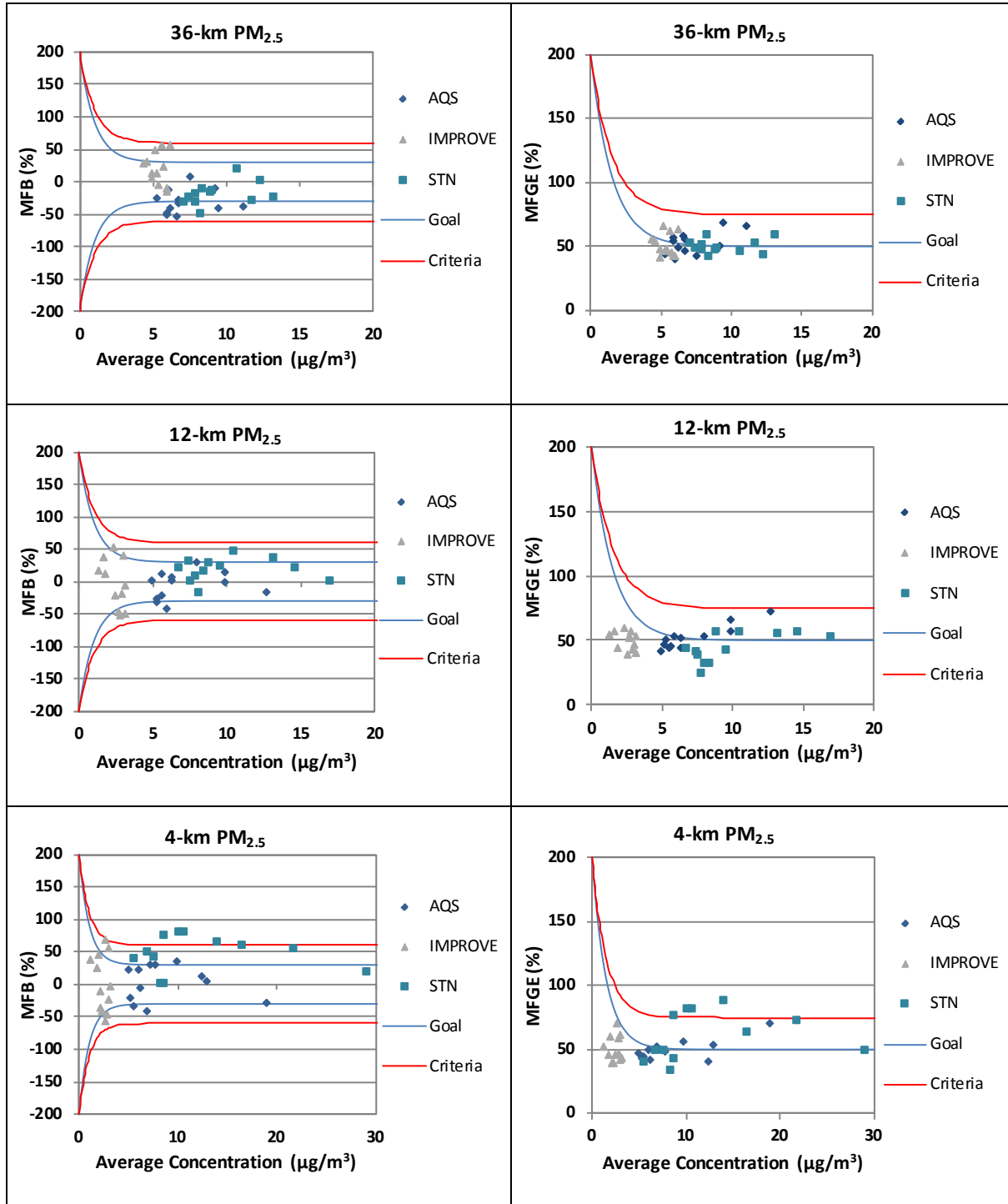
Note: Goals and criteria based on Boylan et al. (2006) and accepted by USEPA (2007).

Figure B-19   CAMx Bugle Plots of Total PM$_{2.5}$ (Daily) Monthly Mean Fractional Bias and Mean Fractional Gross Error
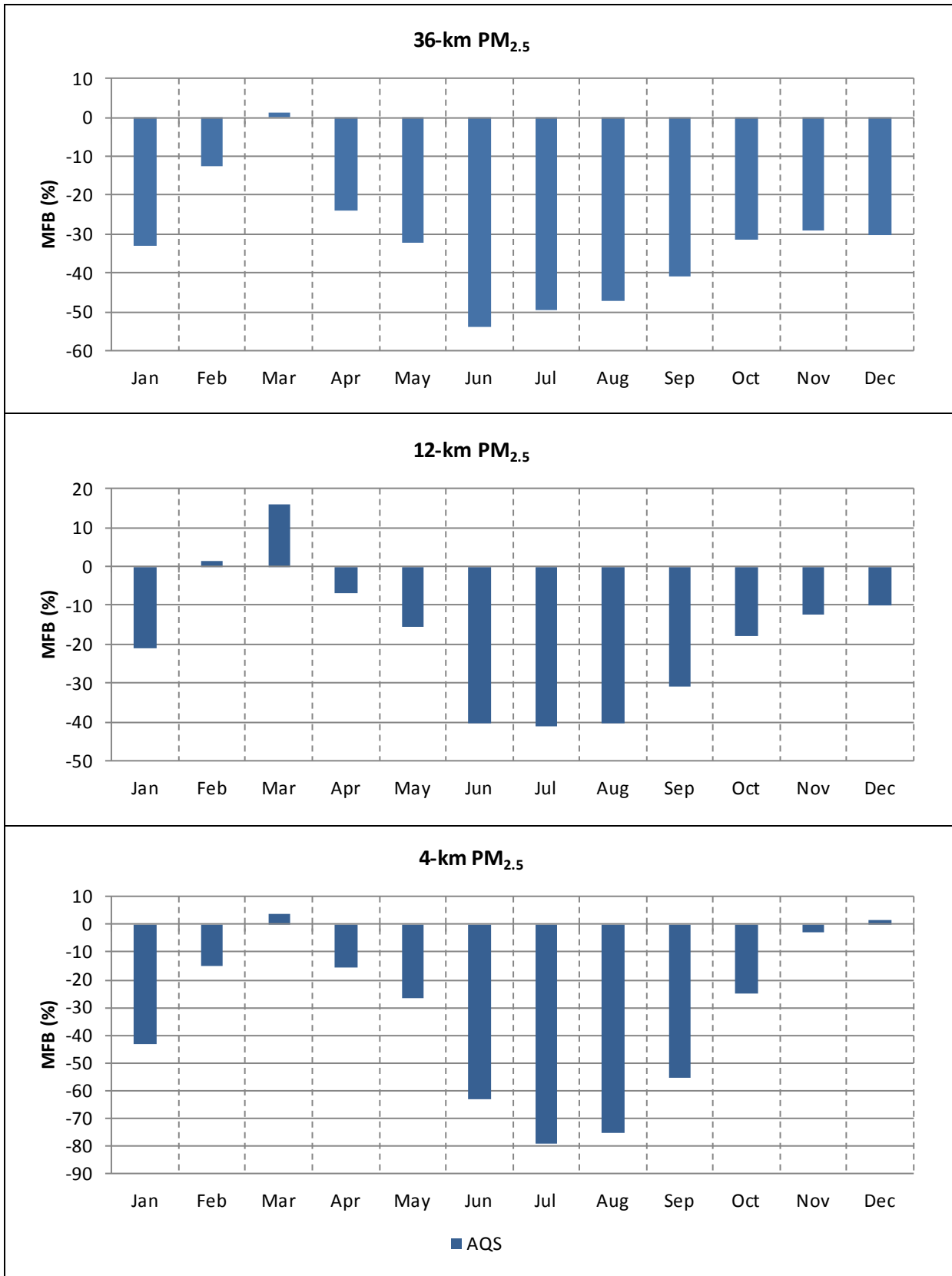
Figure B-20   CAMx Monthly Mean Fractional Bias for Total PM$_{2.5}$ (Hourly)

Note: Goals and criteria based on Boylan et al. (2006) and accepted by USEPA (2007).

Figure B-21   CAMx Bugle Plots of Total PM$_{2.5}$ (Hourly) Monthly Mean Fractional Bias and Mean Fractional Gross Error
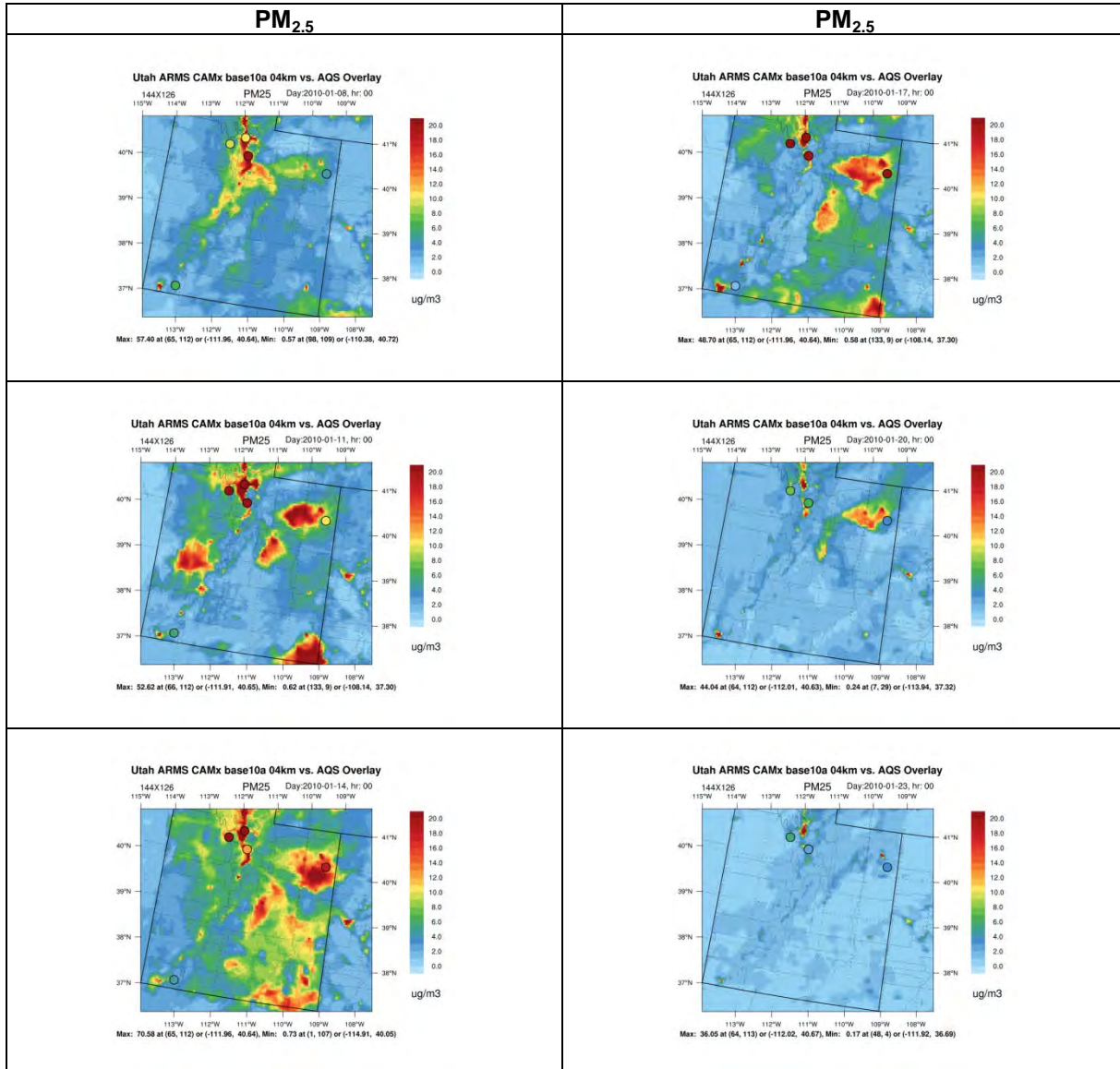
Figure B-22   CAMx 4-km Spatial Plots for Total PM$_{2.5}$ during January 8 to January 23, 2010

PM$_{2.5}$	PM$_{2.5}$
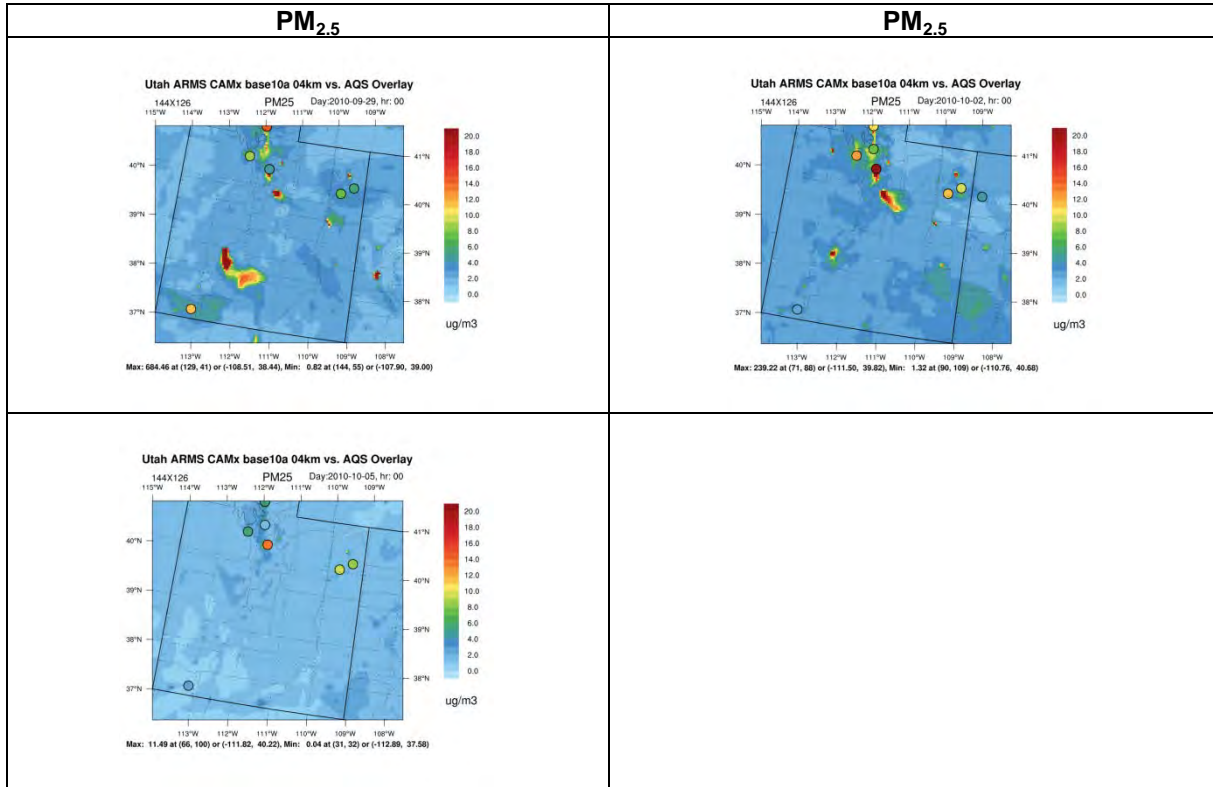
Figure B-23   CAMx 4-km Spatial Plots for Total PM$_{2.5}$ during September 27 to October 5, 2010

B.2.3   Total PM$_{10}$

This section presents statistical tables and graphical summaries of CAMx model performance for total PM$_{10}$ mass. Statistical results from the model performance evaluation are presented in **Table B-14** and **Table B-15**. A summary of monthly mean fractional bias is presented in **Figure B-24**, while Bugle plots summarizing model performance in the context of recommended USEPA performance criteria are presented in **Figure B-25**.

Table B-14   CAMx Model Performance Statistical Summary for Total PM$_{10}$ (Hourly)

Monitoring Network	Statistic (%)/ Concentration (µg/m^3)	36-km Domain					12-km Domain					4-km Domain				
		Annual	Winter	Spring	Summer	Fall	Annual	Winter	Spring	Summer	Fall	Annual	Winter	Spring	Summer	Fall
AQS (Hourly)	MFB	-75	-46	-58	-110	-87	-54	-19	-34	-95	-67	-112	NA	-113	-68	-89
	MFGE	99	87	85	117	105	98	94	85	111	103	112	NA	113	78	92
	MNB	-12	43	7	-62	-36	55	174	68	-42	20	-70	NA	-70	-40	-57
	MNGE	96	128	99	75	82	150	246	146	84	125	70	NA	71	57	60
	NMB	-62	-41	-56	-77	-68	-30	37	-27	-63	-44	-73	NA	-74	-57	-71
	NME	76	76	73	79	77	96	136	89	82	90	73	NA	75	61	72
	R^2	0.010	0.019	0.002	0.007	0.014	0.003	0.036	0.000	0.001	0.004	0.012	NA	0.012	0.100	0.001
	Observed Mean Concentration (µg/m^3)	22.51	19.05	22.84	24.24	23.93	19.42	14.83	19.91	22.33	20.31	27.16	NA	24.25	29.85	32.05
	Predicted Mean Concentration (µg/m^3)	8.63	11.22	9.97	5.65	7.61	13.68	20.38	14.57	8.30	11.41	7.24	NA	6.19	12.86	9.34

Table B-15   CAMx Model Performance Statistical Summary for Total PM$_{10}$ (Daily)

Monitoring Network	Statistic (%)/ Concentration (µg/m^3)	36-km Domain					12-km Domain					4-km Domain				
		Annual	Winter	Spring	Summer	Fall	Annual	Winter	Spring	Summer	Fall	Annual	Winter	Spring	Summer	Fall
AQS (Daily)	MFB	-85	-63	-64	-116	-95	-70	-47	-51	-103	-79	-65	-51	-50	-95	-63
	MFGE	94	82	75	117	100	87	79	72	107	90	78	71	68	98	76
	MNB	-49	-30	-38	-71	-57	-34	-9	-23	-61	-43	-37	-28	-24	-59	-36
	MNGE	64	64	54	72	66	66	73	59	68	65	57	56	55	63	56
	NMB	-66	-54	-64	-76	-69	-56	-36	-55	-69	-57	-57	-50	-61	-68	-48
	NME	70	64	68	76	71	68	66	68	72	66	63	57	69	69	57
	R^2	0.019	0.073	0.002	0.057	0.037	0.013	0.104	0.001	0.020	0.055	0.040	0.297	0.002	0.008	0.130
	Observed Mean Concentration (µg/m^3)	20.79	17.98	22.55	22.28	20.35	20.00	17.04	21.69	21.69	19.40	23.16	25.01	26.04	21.34	20.29
	Predicted Mean Concentration (µg/m^3)	7.00	8.20	8.20	5.29	6.34	8.88	10.89	9.71	6.67	8.33	10.03	12.56	10.16	6.89	10.51
IMPROVE (Daily)	MFB	-8	29	9	-48	-21	-30	20	-4	-88	-50	-25	31	-3	-88	-45
	MFGE	58	59	54	64	56	67	56	55	90	65	66	54	59	90	65
	MNB	38	108	48	-16	7	6	76	27	-58	-25	14	89	31	-59	-11
	MNGE	84	130	81	62	62	72	104	69	60	54	76	106	75	60	66
	NMB	-13	25	2	-37	-24	-42	20	-27	-66	-50	-43	42	-40	-66	-50
	NME	55	64	58	51	52	62	63	59	66	58	65	64	70	66	58
	R^2	0.166	0.352	0.098	0.182	0.229	0.052	0.178	0.018	0.187	0.062	0.022	0.327	0.002	0.135	0.024
	Observed Mean Concentration (µg/m^3)	9.48	6.45	9.74	11.92	9.65	6.39	2.37	7.66	9.11	6.24	6.09	2.14	9.08	7.83	5.27
	Predicted Mean Concentration (µg/m^3)	8.24	8.03	9.89	7.51	7.37	3.71	2.84	5.59	3.09	3.10	3.50	3.04	5.44	2.70	2.63
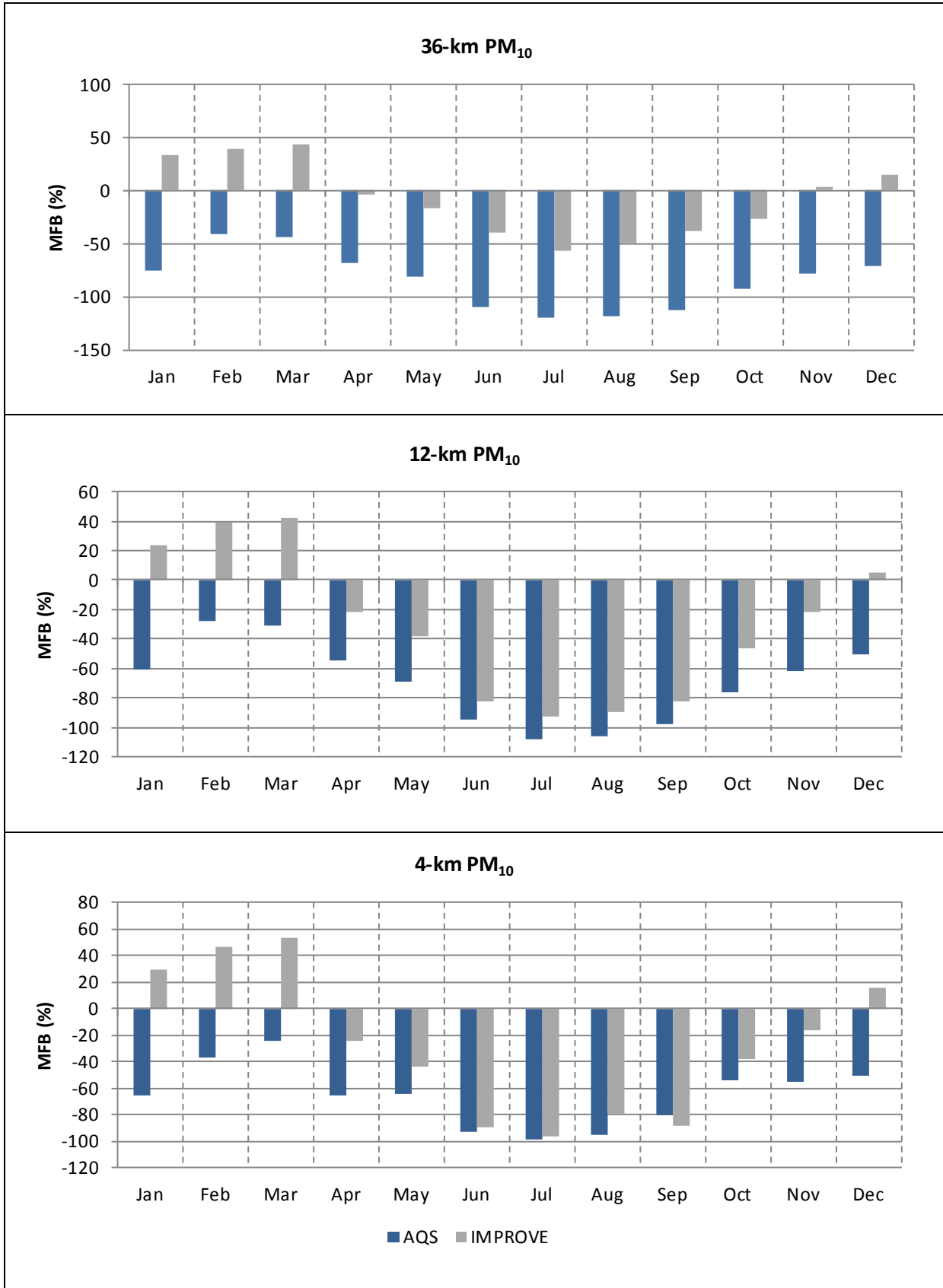
Figure B-24   CAMx Monthly Mean Fractional Bias for Total PM$_{10}$ (Daily)
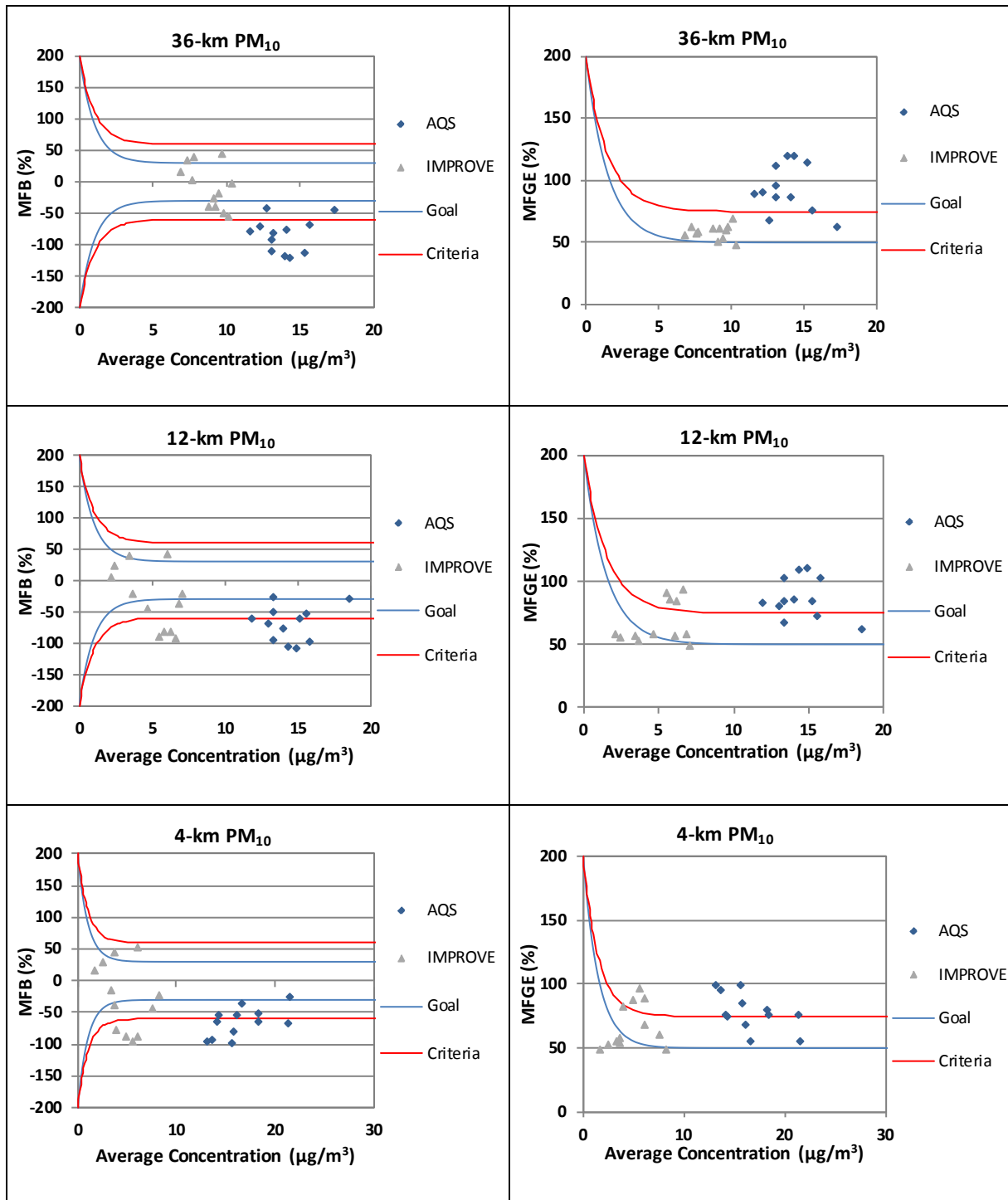
Note: Goals and criteria based on Boylan et al. (2006) and accepted by USEPA (2007).

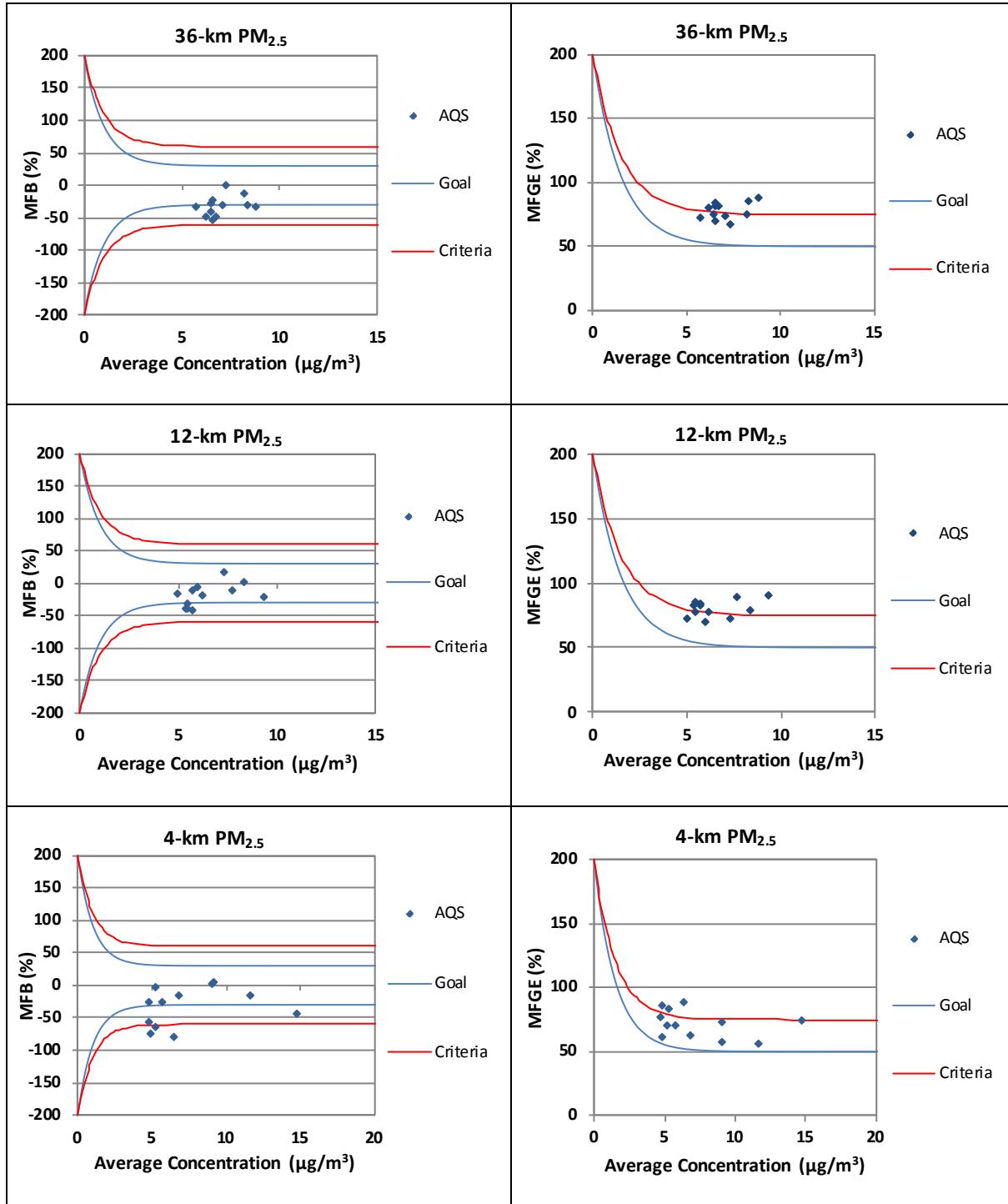**Figure B-25   CAMx Bugle Plots of PM$_{10}$ (Daily) Monthly Mean Fractional Bias and Mean Fractional Gross Error**

B.3   Other Gaseous Species

B.3.1   Nitrogen Oxides

This section presents statistical tables and graphical summaries of CAMx model performance for nitrogen oxides. Statistical results from the model performance evaluation are presented in **Table B-16**. A summary of monthly normalized mean bias is presented in **Figure B-26**.

Table B-16   CAMx Model Performance Statistical Summary for Nitrogen Oxides

Monitoring Network	Statistics (percent)/ Concentration (parts per million [ppm])	36-km Domain					12-km Domain					4-km Domain				
		Annual	Winter	Spring	Summer	Fall	Annual	Winter	Spring	Summer	Fall	Annual	Winter	Spring	Summer	Fall
AQS (Hourly)	MFB	-14	-20	-14	-10	-13	11	-12	22	17	14	16	-15	35	27	16
	MFGE	87	82	90	88	86	96	92	99	96	96	80	78	86	81	75
	MNB	36	29	29	44	41	43	33	46	41	50	101	83	134	102	86
	MNGE	105	98	102	113	109	108	106	109	103	113	146	144	172	142	129
	NMB	-22	-29	-19	-6	-24	-13	-25	2	8	-17	12	-9	49	67	1
	NME	74	70	76	79	74	77	76	81	76	75	89	82	110	116	71
	R^2	0.250	0.266	0.209	0.203	0.199	0.223	0.201	0.209	0.262	0.206	0.190	0.132	0.165	0.199	0.328
	Observed Mean Concentration (ppm)	0.013	0.020	0.010	0.007	0.014	0.011	0.019	0.007	0.006	0.010	0.015	0.032	0.011	0.007	0.013
	Predicted Mean Concentration (ppm)	0.010	0.014	0.008	0.007	0.011	0.009	0.014	0.008	0.007	0.009	0.017	0.029	0.016	0.012	0.013

1

2

Figure B-26   CAMx Monthly Normalized Mean Bias for Nitrogen Oxides
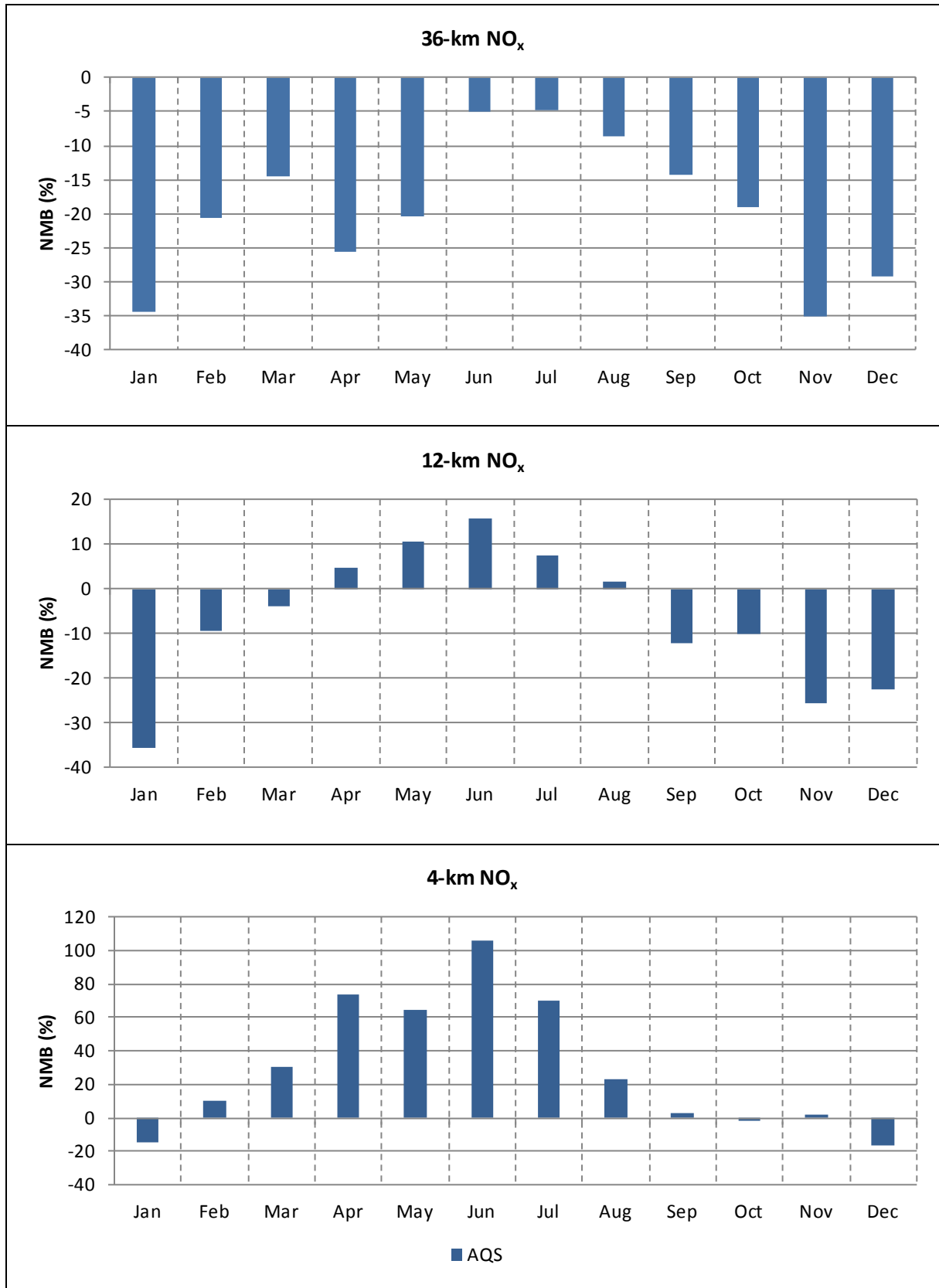
B.3.2   Carbon Monoxide

This section presents statistical tables and graphical summaries of CAMx model performance for carbon monoxide. Statistical results from the model performance evaluation are presented in **Table B-17**. A summary of monthly normalized mean bias is presented in **Figure B-27**.

Table B-17   CAMx Model Performance Statistical Summary for Carbon Monoxide

Monitoring Network	Statistics (percent)/ Concentration (parts per million [ppm])	36-km Domain					12-km Domain					4-km Domain				
		Annual	Winter	Spring	Summer	Fall	Annual	Winter	Spring	Summer	Fall	Annual	Winter	Spring	Summer	Fall
AQS (Hourly)	MFB	-32	-44	-25	-26	-32	-15	-25	-10	-9	-15	-16	-31	-21	6	-18
	MFGE	70	73	65	70	72	68	70	61	70	70	65	65	58	74	64
	MNB	1	-15	-9	14	14	8	3	7	7	14	11	-3	1	38	9
	MNGE	73	66	58	84	87	69	70	61	68	76	71	66	60	91	70
	NMB	-39	-46	-32	-33	-37	-20	-28	-13	-12	-18	-16	-17	-16	-3	-23
	NME	60	61	57	59	61	64	66	61	66	64	61	63	56	70	56
	R^2	0.127	0.128	0.091	0.046	0.110	0.101	0.075	0.071	0.037	0.134	0.124	0.070	0.082	0.025	0.123
	Observed Mean Concentration (ppm)	0.40	0.54	0.32	0.29	0.41	0.37	0.52	0.31	0.27	0.38	0.40	0.62	0.35	0.25	0.38
	Predicted Mean Concentration (ppm)	0.24	0.29	0.22	0.19	0.26	0.30	0.37	0.27	0.24	0.31	0.34	0.51	0.30	0.24	0.29
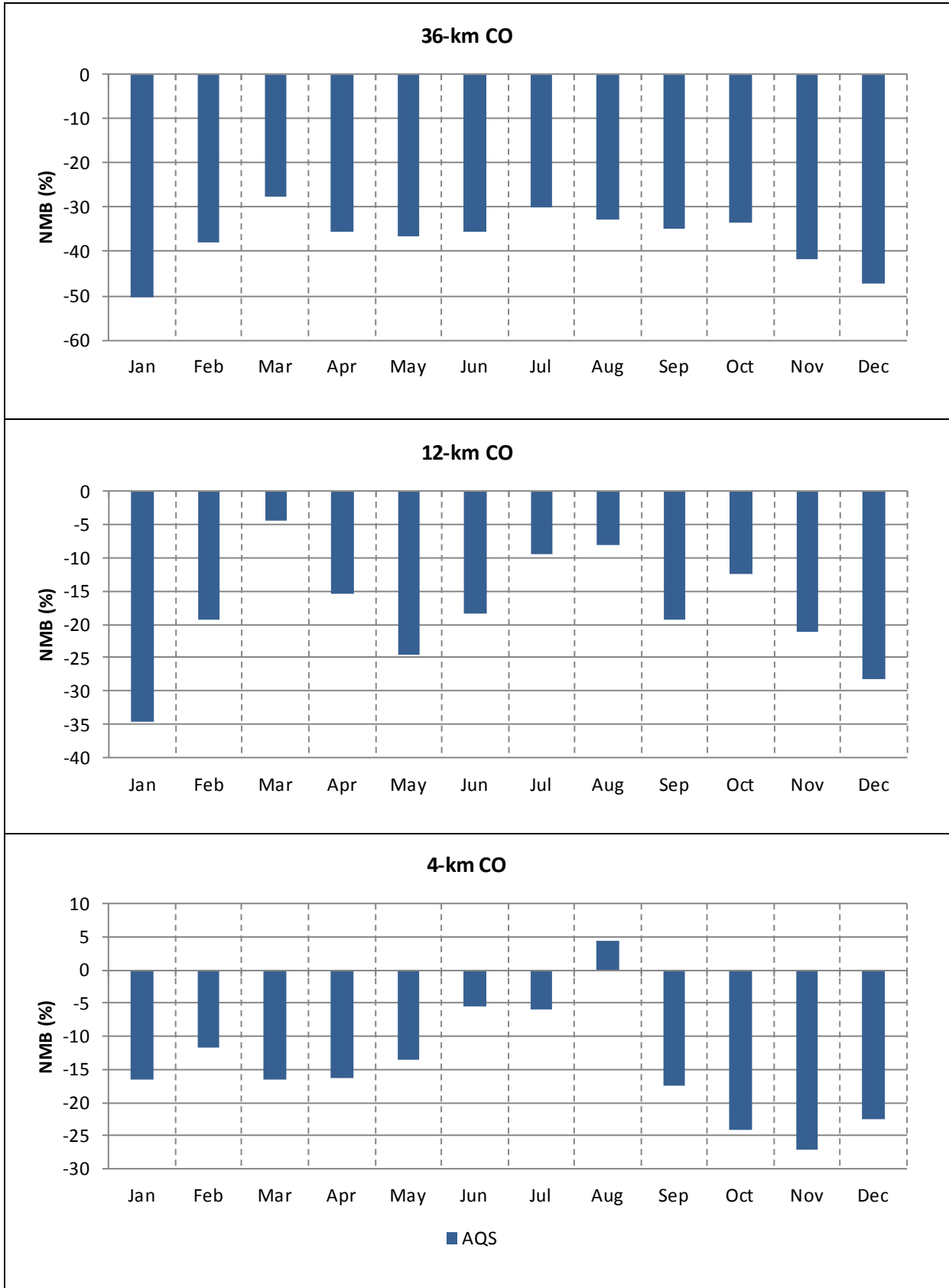
Figure B-27   CAMx Monthly Normalized Mean Bias for Carbon Monoxide

B.4   Visibility

This section presents statistical tables and graphical summaries of CAMx model performance for visibility. Statistical results from the model performance evaluation for total light extinction, as well as light extinction for individual chemical compounds are presented in **Table B-18** and **Table B-19**. A summary of monthly biases and errors for light extinction coefficients are presented in **Figure B-28** and **Figure B-29**. Finally, reconstructed versus Model-predicted Light Extinction Coefficients at IMPROVE sites within the CAMx 4-km domain are presented in **Figure B-30** through **B-36**.

Table B-18   CAMx Model Performance Statistical Summary for Total Light Extinction

Monitoring Network	Statistic (percent) /b_{ext}	12-km Domain					4-km Domain				
		Annual	Winter	Spring	Summer	Fall	Annual	Winter	Spring	Summer	Fall
IMPROVE (Daily)	MFB	-7	14	-2	-29	-12	0	26	4	-24	-7
	MFGE	26	28	24	31	24	26	32	25	26	21
	MNB	-1	23	3	-23	-8	7	39	10	-20	-4
	MNGE	26	34	24	26	22	28	44	26	22	20
	NMB	-11	13	-6	-28	-16	-2	37	-3	-23	-15
	NME	29	35	26	29	26	31	44	31	24	27
	R^2	0.112	0.093	0.183	0.503	0.072	0.018	0.431	0.004	0.112	0.000
	Reconstructed Mean	21.07	17.72	22.14	23.41	20.88	19.30	17.36	20.52	19.97	19.35
	Model-predicted Mean	18.83	20.06	20.73	16.90	17.51	19.01	23.77	19.95	15.45	16.47

Table B-19   CAMx Model Performance Statistical Summary for Individual Chemical Compound Light Extinction Coefficients

| Chemical Compound	Statistic (percent) /b_{ext}	12-km Domain					4-km Domain				
		Annual	Winter	Spring	Summer	Fall	Annual	Winter	Spring	Summer	Fall
SO$_4$	MFB	40	75	45	4	36	40	69	49	7	36
	MFGE	54	79	51	36	51	52	75	51	30	50
	MNB	170	197	376	17	77	92	194	87	15	69
	MNGE	182	200	381	42	89	101	199	89	35	80
	NMB	42	97	52	-2	37	48	75	64	8	40
	NME	63	109	62	39	57	62	90	67	32	59
	R^2	0.261	0.286	0.371	0.383	0.225	0.250	0.340	0.201	0.390	0.132
	Reconstructed Mean	3.41	2.62	3.85	3.93	3.20	2.92	2.97	3.07	3.02	2.60
	Model-predicted Mean	4.83	5.17	5.84	3.86	4.39	4.30	5.21	5.02	3.26	3.65

Table B-19   CAMx Model Performance Statistical Summary for Individual Chemical

Chemical Compound	Statistic (percent) /b_{ext}	12-km Domain					4-km Domain				
		Annual	Winter	Spring	Summer	Fall	Annual	Winter	Spring	Summer	Fall
NO$_3$	MFB	-84	-14	-88	-146	-85	-44	63	-45	-150	-45
	MFGE	135	130	120	158	136	133	127	108	163	136
	MNB	76	373	-19	-66	37	204	665	40	-64	185
	MNGE	196	454	98	94	155	299	702	126	99	282
	NMB	-14	73	-47	-78	-33	125	216	38	-73	101
	NME	111	161	84	89	108	182	239	108	95	180
	R^2	0.108	0.136	0.152	0.174	0.050	0.444	0.378	0.423	0.001	0.247
	Reconstructed Mean	1.50	1.82	2.13	1.02	0.99	1.15	2.38	1.15	0.52	0.49
	Model-predicted Mean	1.28	3.16	1.14	0.22	0.66	2.58	7.54	1.58	0.14	0.99
OC	MFB	-55	-45	-37	-71	-70	-51	-61	-20	-59	-66
	MFGE	76	86	61	77	83	64	72	46	66	75
	MNB	-12	37	-11	-40	-32	-28	-38	-1	-40	-34
	MNGE	78	124	60	61	70	52	51	48	48	63
	NMB	-63	-68	-59	-58	-66	-57	-52	-29	-50	-73
	NME	68	79	68	60	70	60	56	41	54	74
	R^2	0.011	0.002	0.000	0.243	0.083	0.010	0.084	0.139	0.033	0.007
	Reconstructed Mean	3.04	2.49	2.45	3.78	3.48	2.40	1.59	1.33	2.76	4.02
	Model-predicted Mean	1.13	0.79	1.00	1.58	1.17	1.04	0.77	0.94	1.37	1.09
EC	MFB	-4	14	13	-23	-20	6	9	35	-11	-8
	MFGE	57	74	50	48	55	52	65	51	42	47
	MNB	56	119	98	-4	9	67	90	149	11	13
	MNGE	99	161	126	49	62	100	130	162	52	54
	NMB	-20	-17	-12	-21	-26	-10	-3	29	-22	-25
	NME	57	72	57	46	55	51	63	52	42	49
	R^2	0.076	0.059	0.017	0.333	0.130	0.047	0.071	0.218	0.019	0.039
	Reconstructed Mean	0.93	0.86	0.76	1.04	1.05	0.70	0.68	0.44	0.81	0.87
	Model-predicted Mean	0.74	0.71	0.67	0.82	0.78	0.63	0.66	0.57	0.64	0.65

Compound Light Extinction Coefficients

Table B-19   CAMx Model Performance Statistical Summary for Individual Chemical Compound Light Extinction Coefficients

Chemical Compound	Statistic (percent) /b_{ext}	12-km Domain					4-km Domain				
		Annual	Winter	Spring	Summer	Fall	Annual	Winter	Spring	Summer	Fall
SOIL	MFB	18	78	21	-38	11	21	83	17	-43	24
	MFGE	72	93	63	63	68	69	96	63	54	62
	MNB	108	285	87	-13	80	109	292	79	-26	89
	MNGE	146	295	116	56	120	143	300	111	43	117
	NMB	-18	117	-16	-49	-19	-23	122	-32	-49	7
	NME	72	150	68	63	72	70	147	73	54	63
	R^2	0.052	0.050	0.021	0.014	0.002	0.068	0.090	0.012	0.097	0.051
	Reconstructed Mean	0.82	0.20	1.41	0.97	0.63	0.83	0.17	1.75	0.91	0.44
	Model-predicted Mean	0.67	0.44	1.18	0.49	0.51	0.64	0.38	1.19	0.46	0.47
SS	MFB	-151	-104	-148	-190	-159	-136	-51	-151	-195	-149
	MFGE	176	161	172	192	177	175	155	172	197	177
	MNB	6	158	-11	-94	-25	31	280	-45	-97	-17
	MNGE	174	298	155	100	148	191	390	123	100	151
	NMB	-98	-94	-98	-100	-98	-95	-86	-98	-100	-95
	NME	100	103	100	100	100	101	104	99	100	102
	R^2	0.024	0.015	0.048	0.015	0.025	0.008	0.025	0.001	0.001	0.029
	Reconstructed Mean	0.09	0.06	0.14	0.10	0.05	0.04	0.04	0.05	0.05	0.02
	Model-predicted Mean	0.00	0.00	0.00	0.00	0.00	0.00	0.01	0.00	0.00	0.00
CM	MFB	-53	3	-10	-126	-81	-60	-20	-13	-131	-87
	MFGE	97	87	75	130	99	95	74	77	136	99
	MNB	24	144	54	-75	-16	22	167	39	-79	-50
	MNGE	120	205	112	77	95	121	233	101	79	66
	NMB	-62	-13	-44	-81	-71	-67	-33	-58	-82	-74
	NME	77	81	73	82	75	80	63	81	83	76
	R^2	0.034	0.093	0.009	0.166	0.026	0.037	0.100	0.004	0.142	0.024
	Reconstructed Mean	2.19	0.59	2.79	3.15	2.16	2.17	0.45	3.63	2.81	1.74
	Model-predicted Mean	0.84	0.51	1.57	0.59	0.64	0.71	0.30	1.53	0.49	0.46
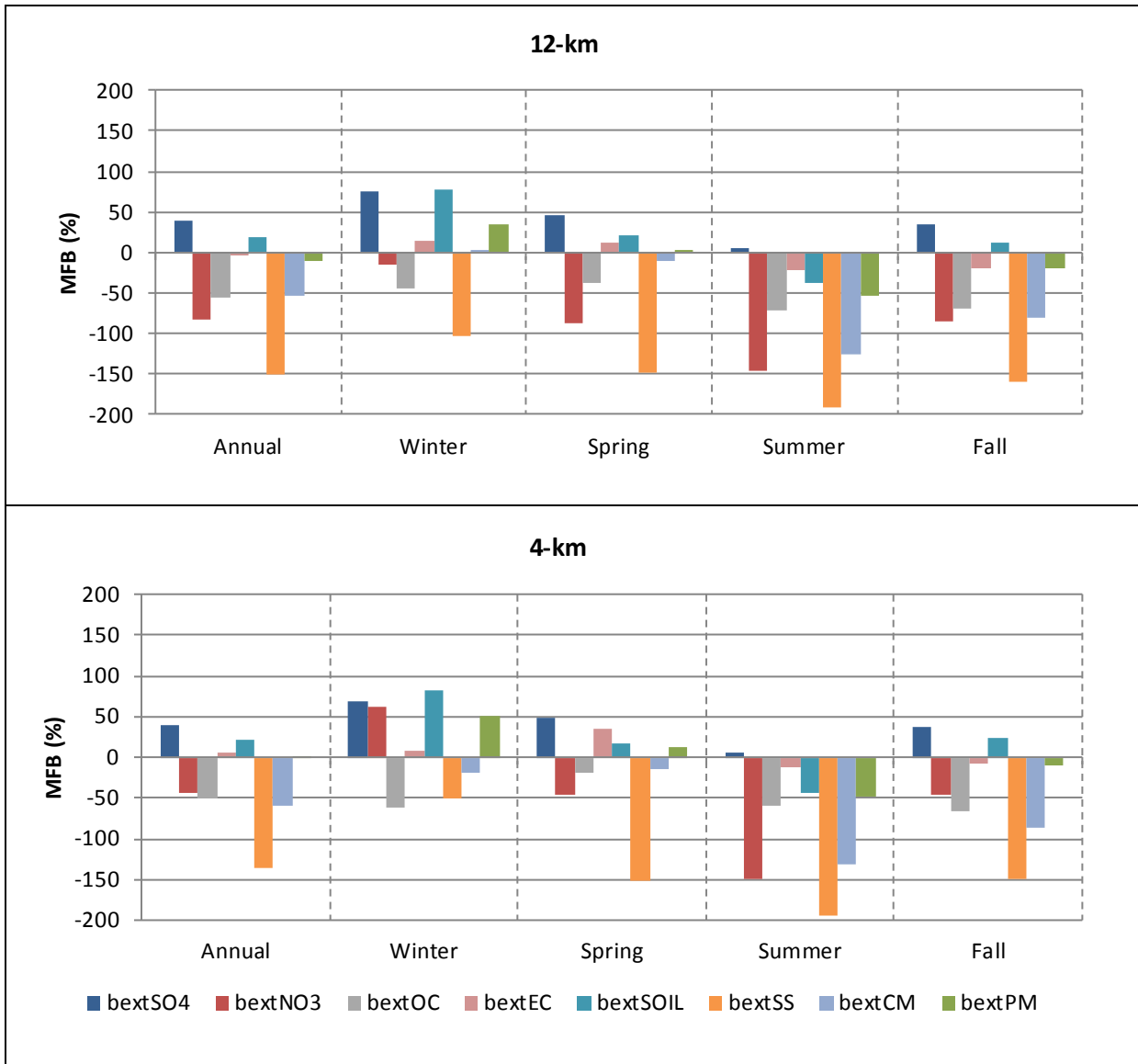
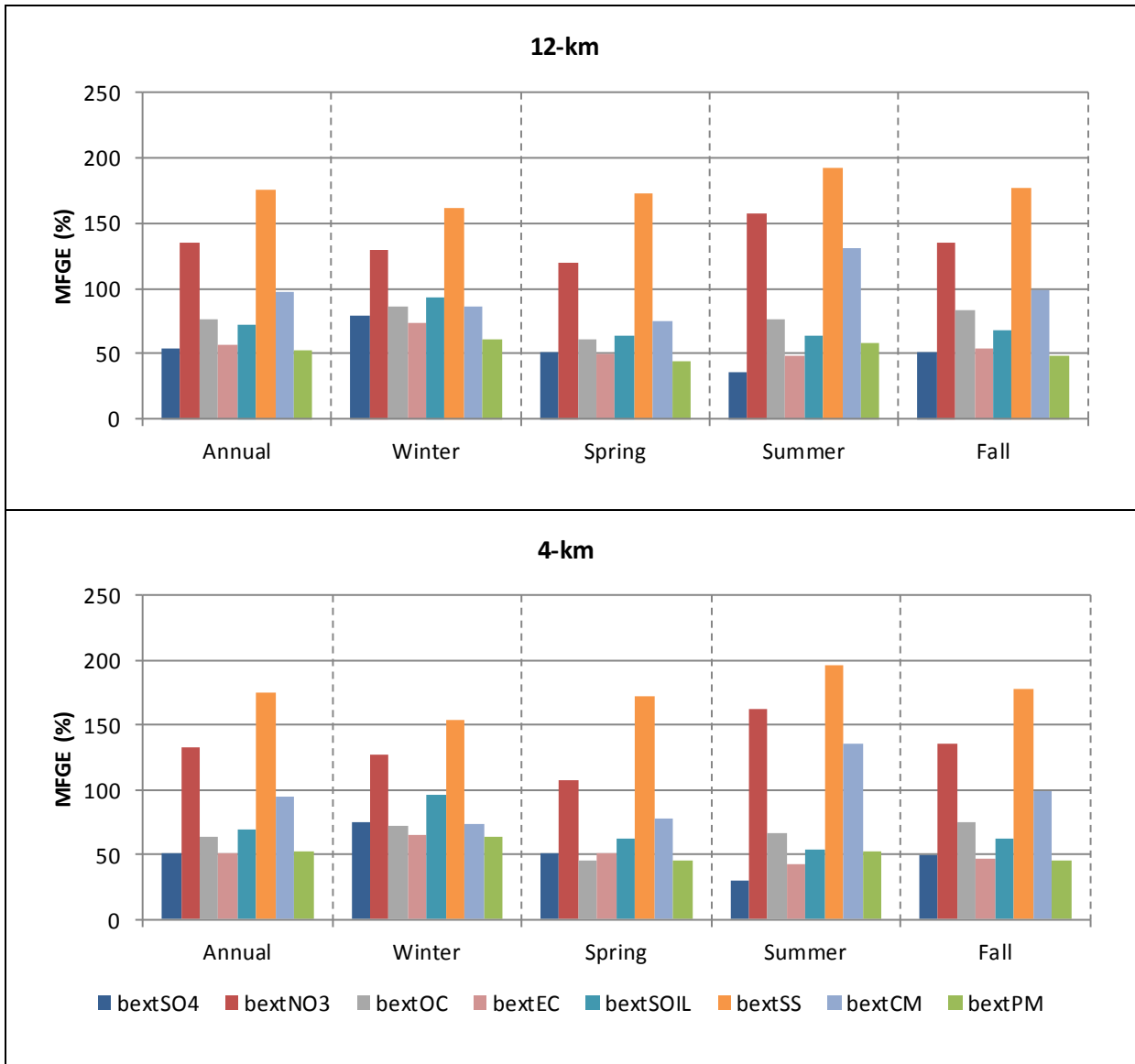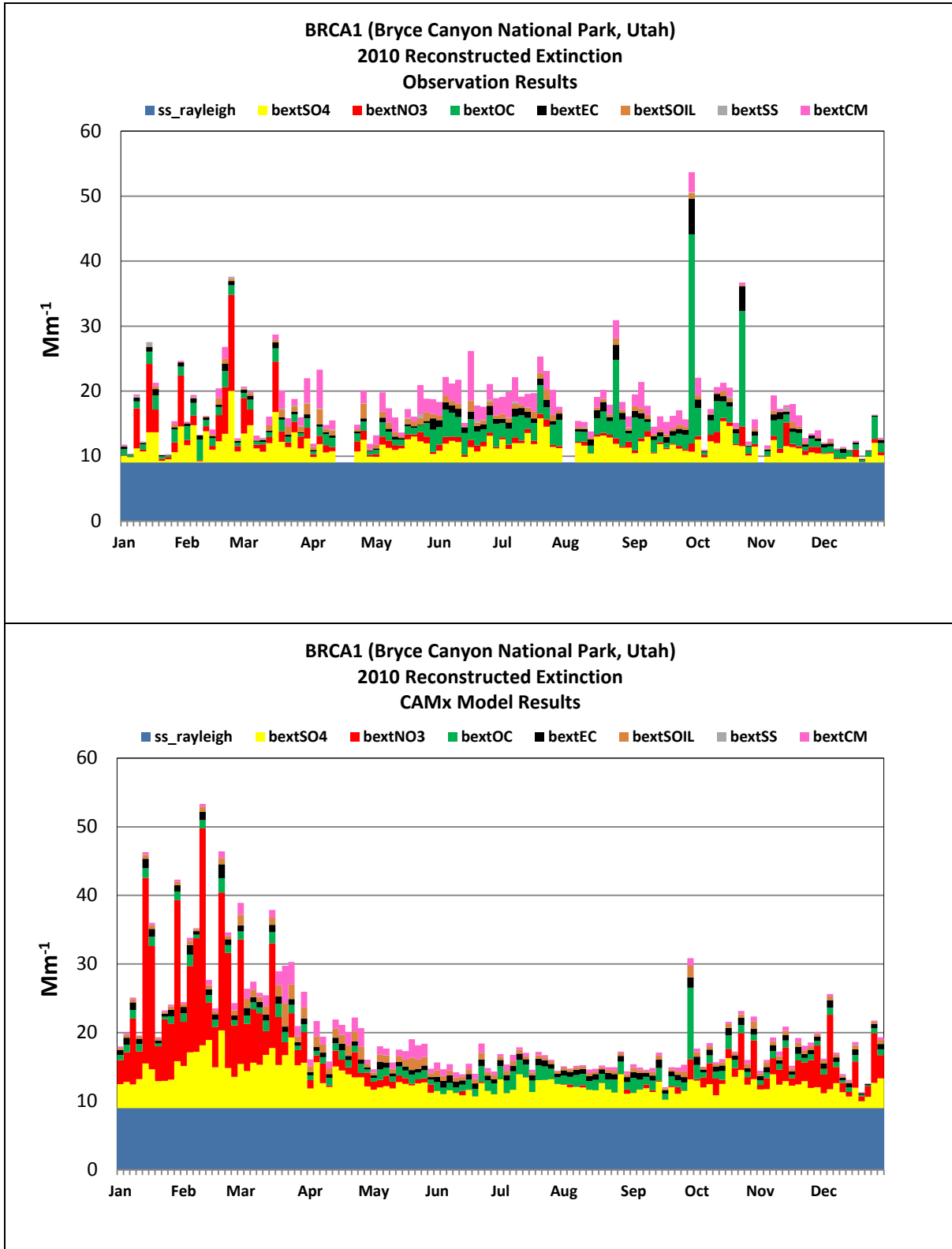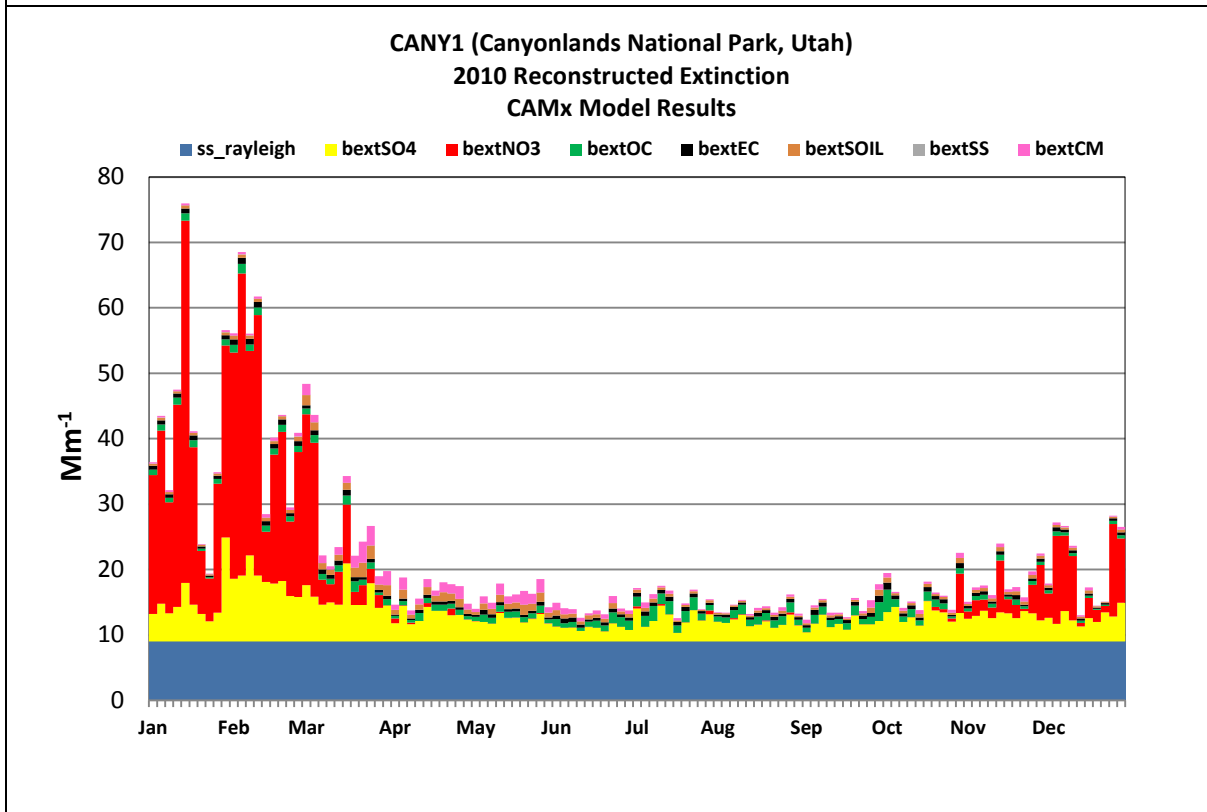**Figure B-28   CAMx Mean Fractional Bias for Light Extinction Coefficients**
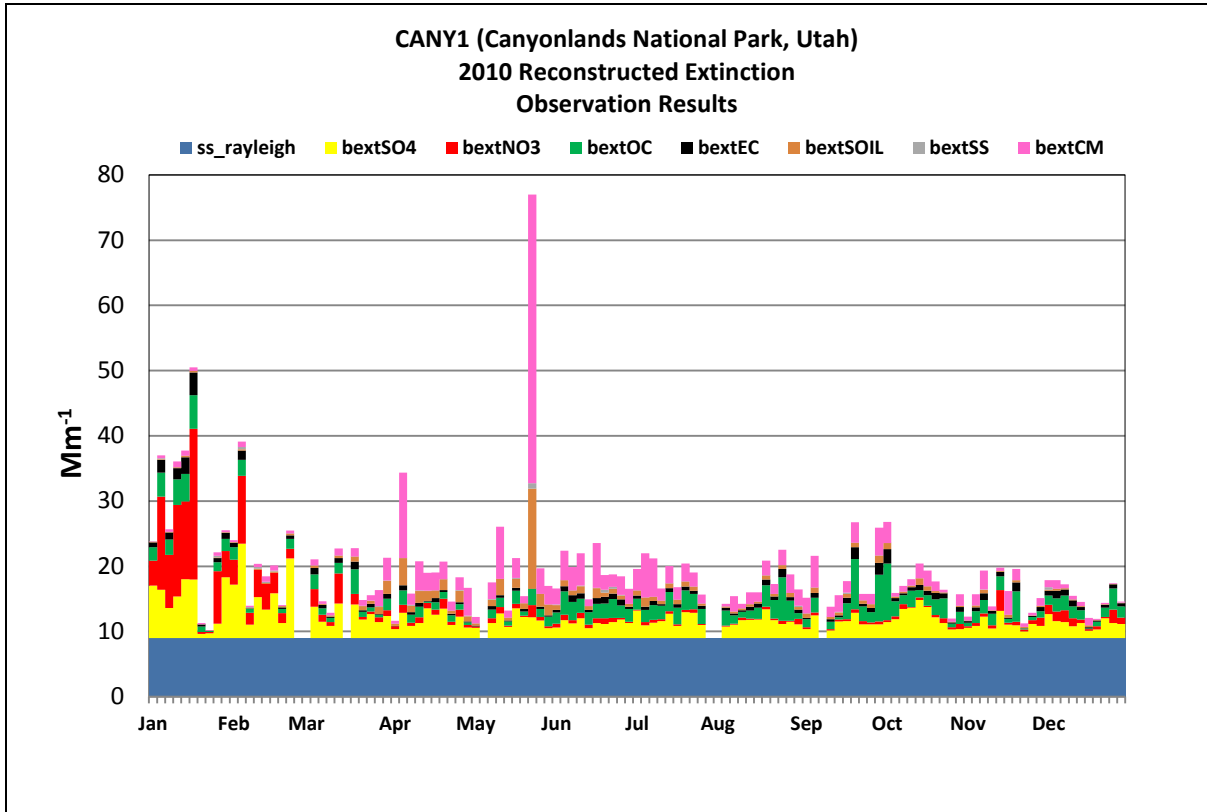
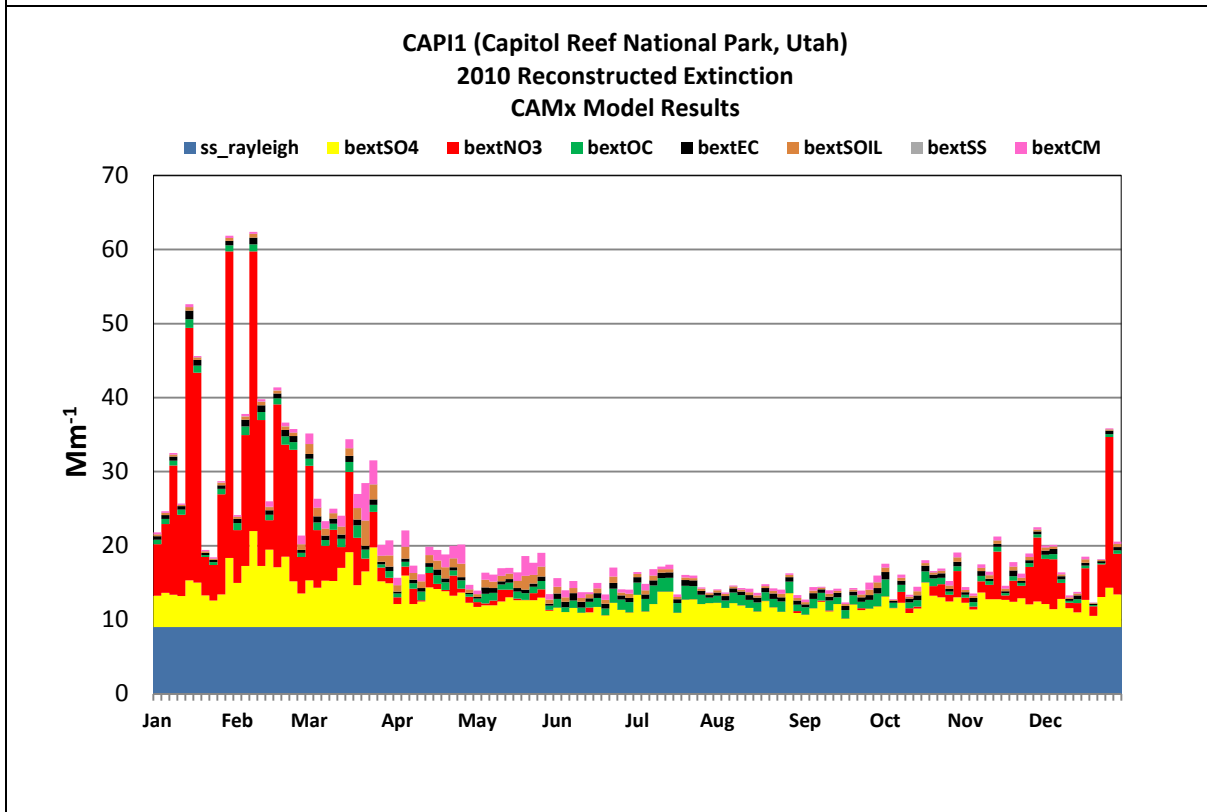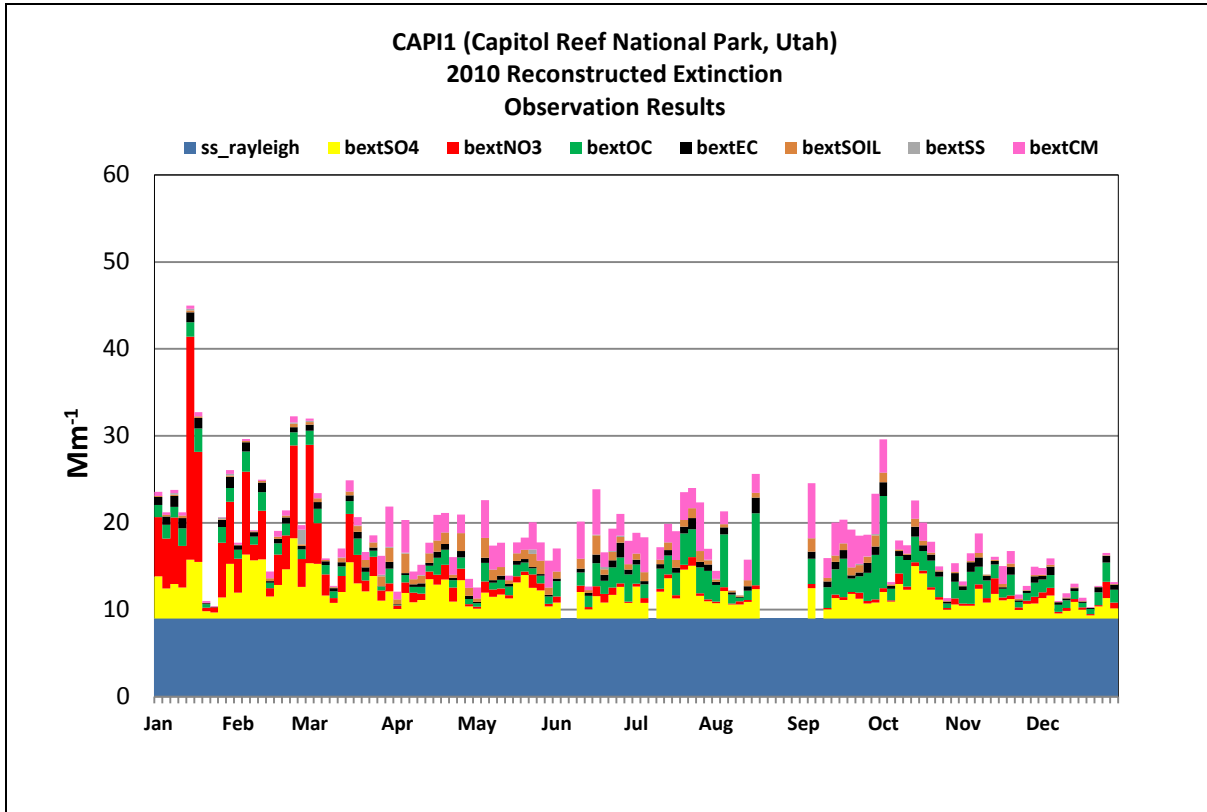**Figure B-29   CAMx Mean Fractional Gross Error for Light Extinction Coefficients**
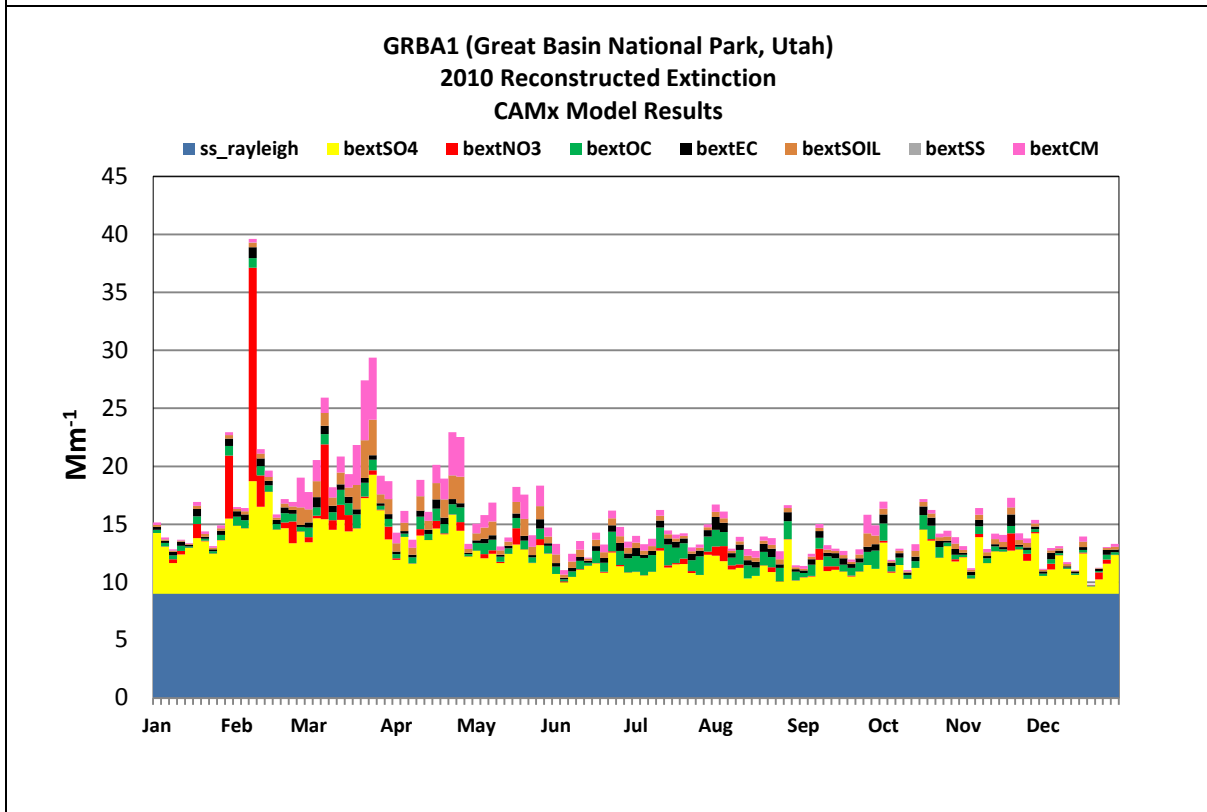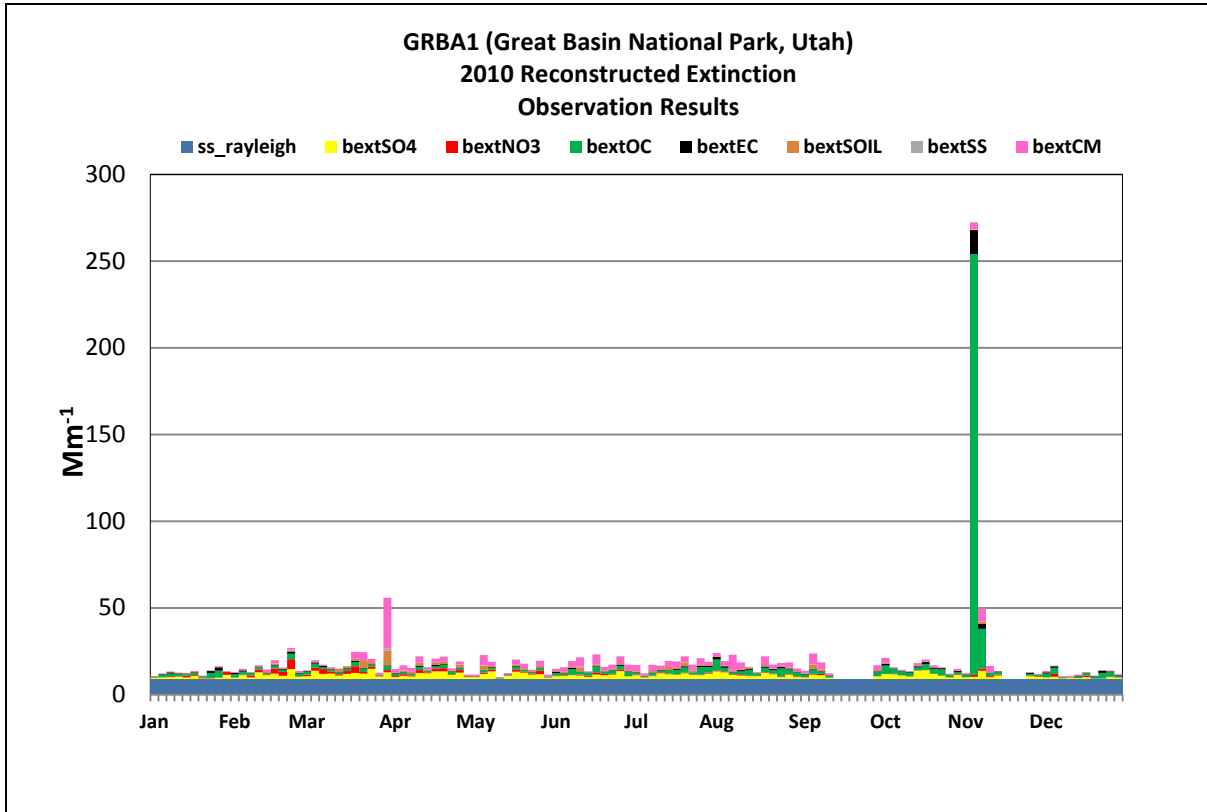
Figure B-30   CAMx Reconstructed versus Model-predicted Light Extinction Coefficients at Bryce Canyon National Park, Utah
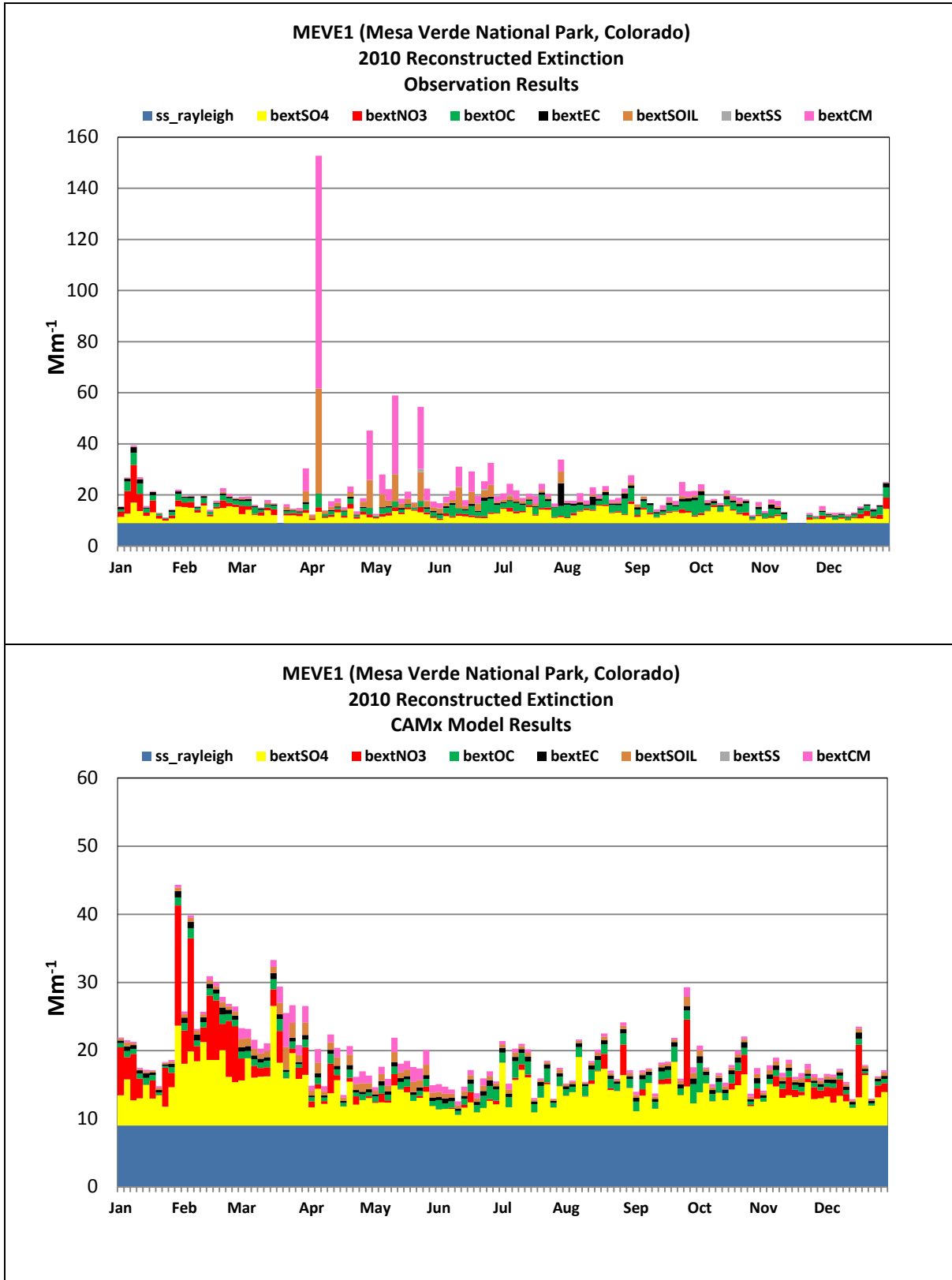
Figure B-31   CAMx Reconstructed versus Model-predicted Light Extinction Coefficients at Canyonlands National Park, Utah

Figure B-32   CAMx Reconstructed versus Model-predicted Light Extinction Coefficients at Capitol Reef National Park, Utah
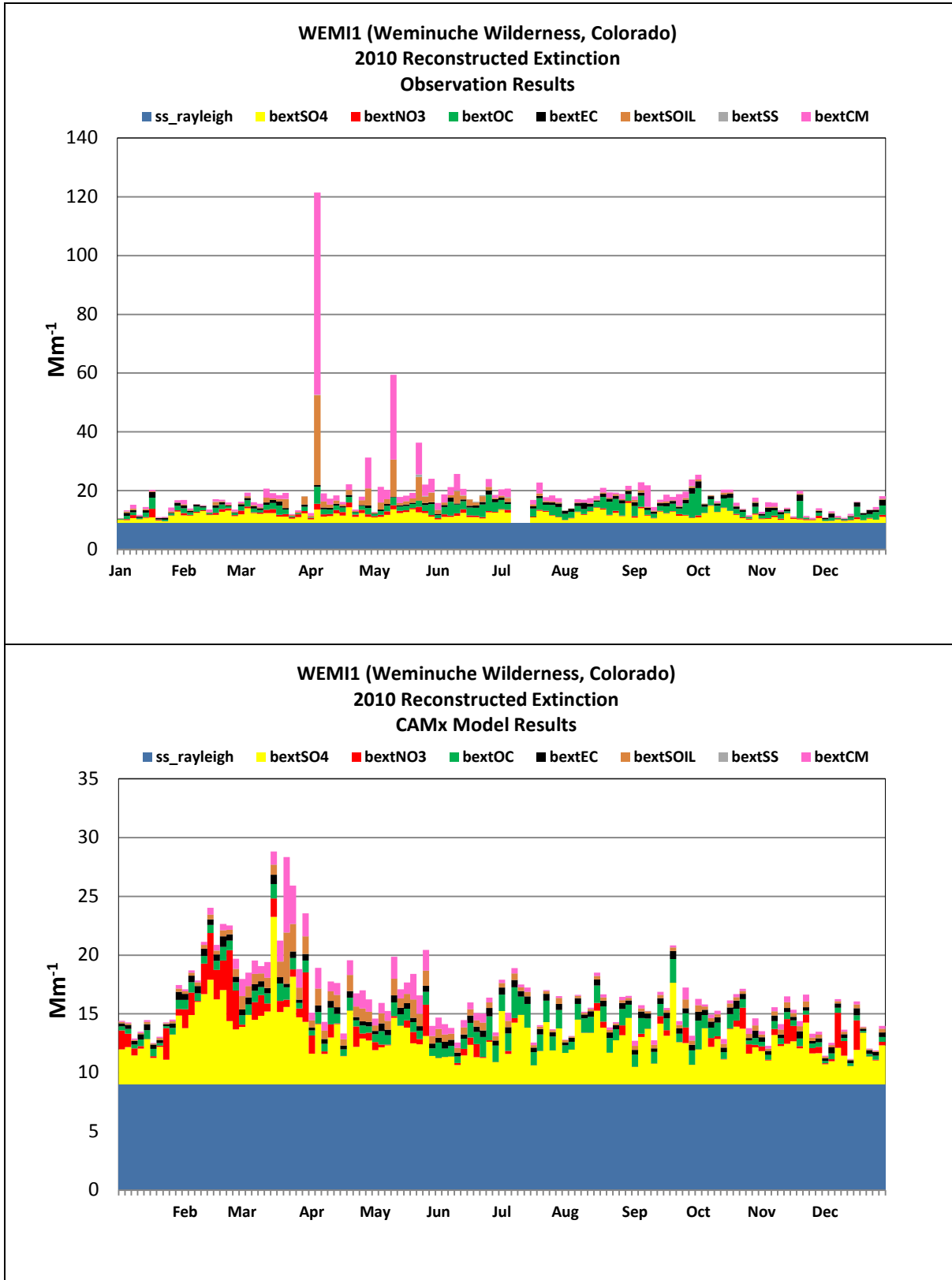
Figure B-33   CAMx Reconstructed versus Model-predicted Light Extinction Coefficients at Great Basin National Park, Utah

Figure B-34   CAMx Reconstructed versus Model-predicted Light Extinction Coefficients at Mesa Verde National Park, Colorado

Figure B-35   CAMx Reconstructed versus Model-predicted Light Extinction Coefficients at Weminuche Wilderness, Colorado
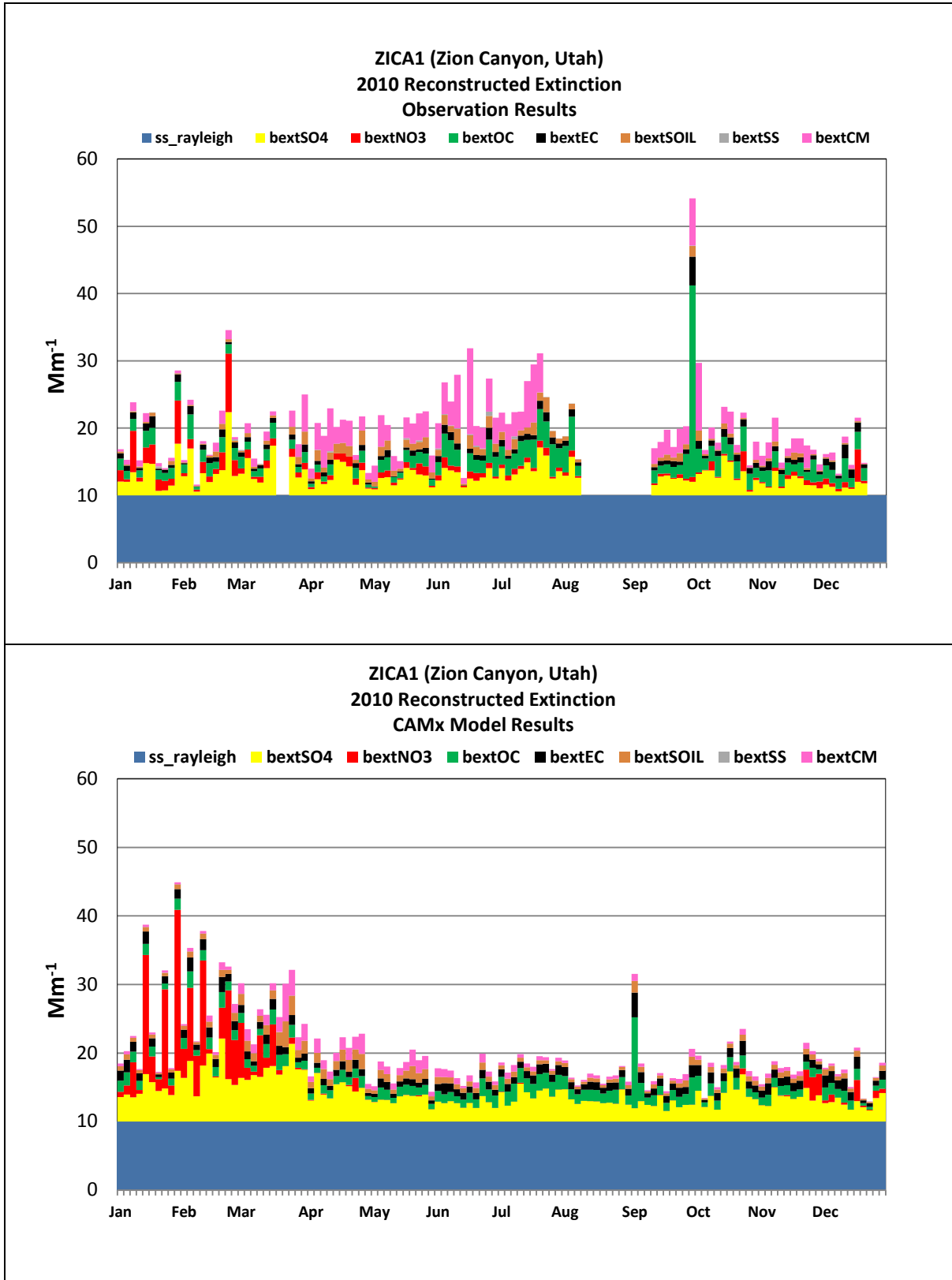
Figure B-36   CAMx Reconstructed versus Model-predicted Light Extinction Coefficients at Zion Canyon, Utah

B.5   Deposition

The following subsections present supplemental material for the CAMx model performance evaluation for wet deposition.

B.5.1   Sulfate

This section presents statistical tables and graphical summaries of CAMx model performance for sulfate wet deposition. Statistical results from the model performance evaluation for sulfate wet deposition are presented in **Table B-20**. A summary of monthly mean fractional bias for sulfate deposition is presented in **Figure B-37**. Finally, a scatterplot of modeled and observed sulfate wet deposition in the CAMx 4-km domain is presented in **Figure B-38**.

Table B-20   CAMx Model Performance Statistical Summary for Sulfate Wet Deposition

| Monitoring Network	Statistic (percent)/ Concentration (kilogram per hectare [kg/ha])	36-km Domain					12-km Domain					4-km Domain				
		Annual	Winter	Spring	Summer	Fall	Annual	Winter	Spring	Summer	Fall	Annual	Winter	Spring	Summer	Fall
NADP (Annual/ Seasonal)	MFB	-54	-101	-39	-39	-39	-68	-137	-39	-42	-48	-103	-127	-87	-69	-100
	MFGE	106	126	94	101	101	119	151	101	103	114	125	142	127	97	118
	MNB	49	-28	46	86	81	74	-54	72	42	128	-40	-56	-10	-23	-45
	MNGE	140	97	124	167	162	177	99	153	125	220	87	89	107	74	79
	NMB	-17	-42	-18	-10	-12	-37	-75	-40	-14	-31	-51	-45	-63	-39	-59
	NME	75	64	68	83	76	84	85	83	83	84	72	72	76	70	71
	R^2	0.195	0.432	0.193	0.145	0.220	0.030	0.113	0.011	0.060	0.113	0.286	0.456	0.403	0.031	0.457
	Observed Mean Deposition (kg/ha)	0.16	0.10	0.18	0.23	0.13	0.07	0.04	0.11	0.08	0.05	0.05	0.03	0.04	0.09	0.06
	Predicted Mean Deposition (kg/ha)	0.13	0.06	0.15	0.21	0.11	0.04	0.01	0.06	0.07	0.04	0.02	0.02	0.02	0.05	0.02
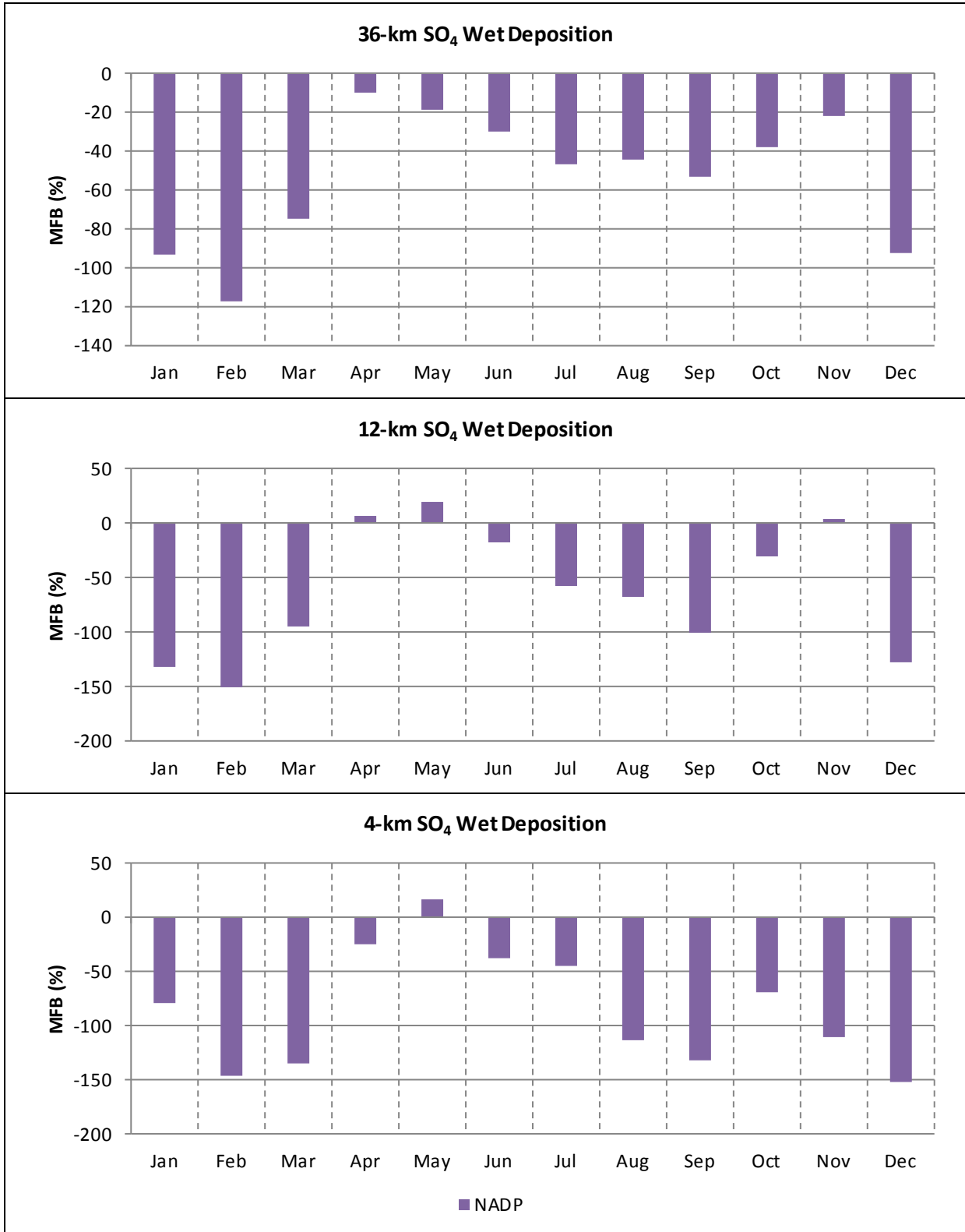
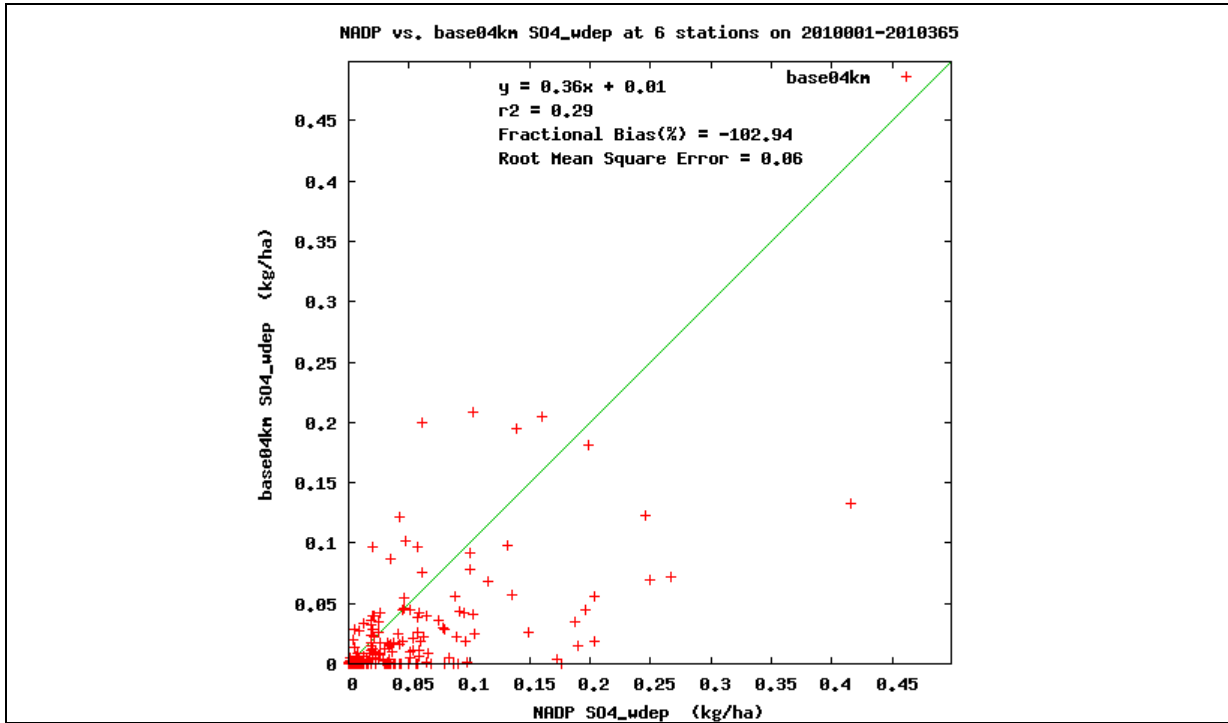**Figure B-37   CAMx Monthly Mean Fractional Bias for Sulfate**

Figure B-38   CAMx Scatter Plot for Sulfate Wet Deposition in the 4-km Domain

B.5.2   Nitrate

This section presents statistical tables and graphical summaries of CAMx model performance for nitrate wet deposition. Statistical results from the model performance evaluation for nitrate wet deposition are presented in **Table B-21**. A summary of monthly mean fractional bias for nitrate wet deposition is presented in **Figure B-39**. Finally, a scatterplot of modeled and observed nitrate wet deposition in the CAMx 4-km domain is presented in **Figure B-40**.

Table B-21   CAMx Model Performance Statistical Summary for Nitrate Wet Deposition

Monitoring Network	Statistic (percent)/ Concentration (kilogram per hectare [kg/ha])	36-km Domain					12-km Domain					4-km Domain				
		Annual	Winter	Spring	Summer	Fall	Annual	Winter	Spring	Summer	Fall	Annual	Winter	Spring	Summer	Fall
NADP (Annual/ Seasonal)	MFB	-63	-81	-58	-52	-62	-78	-119	-61	-52	-72	-92	-116	-72	-64	-96
	MFGE	94	102	88	88	96	109	135	95	90	111	111	124	108	90	113
	MNB	25	-26	9	94	17	19	-38	-4	-5	53	-36	-59	-14	-24	-30
	MNGE	119	81	98	180	111	127	103	90	80	159	82	78	92	70	90
	NMB	-38	-47	-39	-37	-33	-54	-77	-51	-41	-53	-49	-58	-60	-35	-56
	NME	63	61	59	64	65	73	81	70	64	80	67	61	70	66	71
	R^2	0.240	0.310	0.309	0.134	0.239	0.119	0.099	0.131	0.100	0.070	0.329	0.622	0.405	0.165	0.150
	Observed Mean Deposition (kg/ha)	0.15	0.10	0.15	0.22	0.12	0.10	0.08	0.11	0.15	0.07	0.09	0.07	0.06	0.19	0.07
	Predicted Mean Deposition (kg/ha)	0.09	0.05	0.09	0.14	0.08	0.05	0.02	0.05	0.09	0.03	0.05	0.03	0.02	0.12	0.03
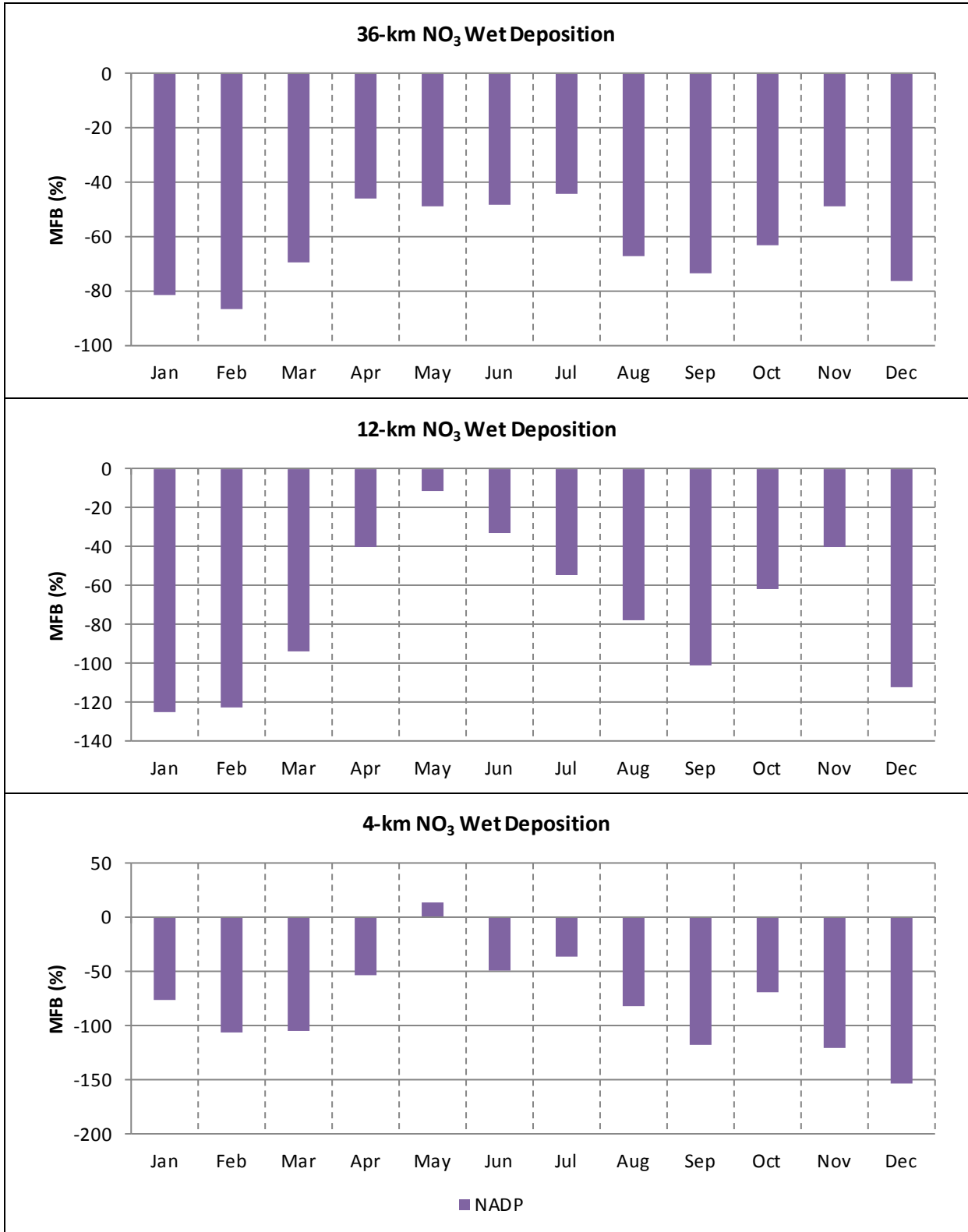
Figure B-39   CAMx Monthly Mean Fractional Bias for Nitrate

NADP vs. base04km NO3_wdep at 6 stations on 2010001-2010365

y = 0.50x + 0.00
r2 = 0.33
Fractional Bias(%) = -92.04
Root Mean Square Error = 0.09
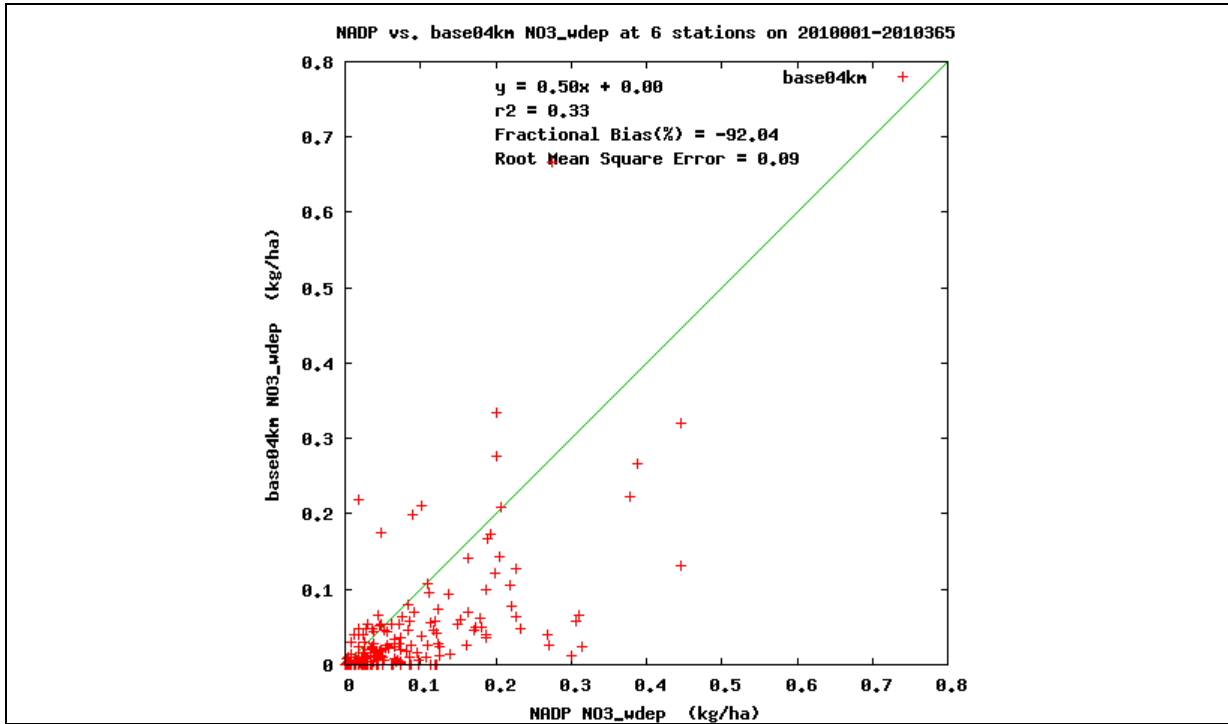
Note: 4-km data shown in red.

Figure B-40   CAMx Scatter Plot for Nitrate Wet Deposition

B.5.3   Ammonium

This section presents statistical tables and graphical summaries of CAMx model performance for ammonium wet deposition. Statistical results from the model performance evaluation for ammonium wet deposition are presented in **Table B-22**. A summary of monthly mean fractional bias for ammonium wet deposition is presented in **Figure B-41**. Finally, a scatterplot of modeled and observed ammonium wet deposition in the CAMx 4-km domain is presented in **Figure B-42**.

Table B-22   CAMx Model Performance Statistical Summary for Ammonium Wet Deposition

Monitoring Network	Statistic (percent)/ Concentration (kilogram per hectare [kg/ha])	36-km Domain					12-km Domain					4-km Domain				
		Annual	Winter	Spring	Summer	Fall	Annual	Winter	Spring	Summer	Fall	Annual	Winter	Spring	Summer	Fall
NADP (Annual/ Seasonal)	MFB	-89	-128	-75	-78	-81	-84	-148	-49	-67	-70	-120	-140	-95	-107	-115
	MFGE	118	140	106	113	113	127	161	109	113	123	137	151	129	119	135
	MNB	30	-58	8	135	13	89	-65	97	135	126	-49	-63	-7	-56	-50
	MNGE	147	89	113	245	124	206	99	188	237	234	92	95	115	73	90
	NMB	-59	-72	-56	-59	-59	-57	-84	-46	-55	-57	-72	-72	-69	-71	-73
	NME	74	78	69	75	75	80	90	78	77	83	78	77	77	77	81
	R^2	0.217	0.277	0.273	0.137	0.175	0.105	0.105	0.140	0.018	0.129	0.215	0.303	0.296	0.015	0.221
	Observed Mean Deposition (kg/ha)	0.05	0.03	0.07	0.08	0.05	0.03	0.02	0.04	0.04	0.02	0.02	0.01	0.01	0.05	0.03
	Predicted Mean Deposition (kg/ha)	0.02	0.01	0.03	0.03	0.02	0.01	0.00	0.02	0.02	0.01	0.01	0.00	0.00	0.01	0.01

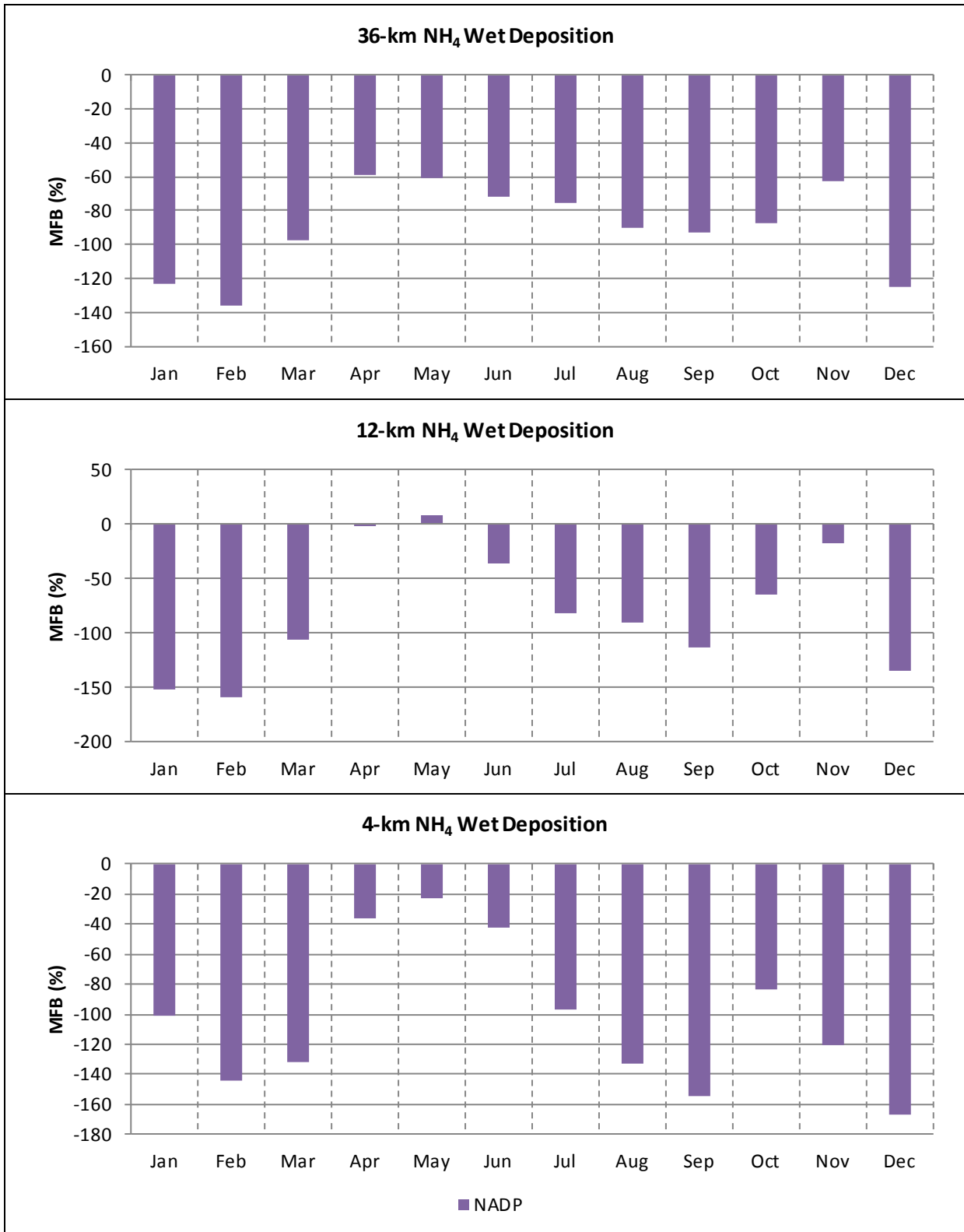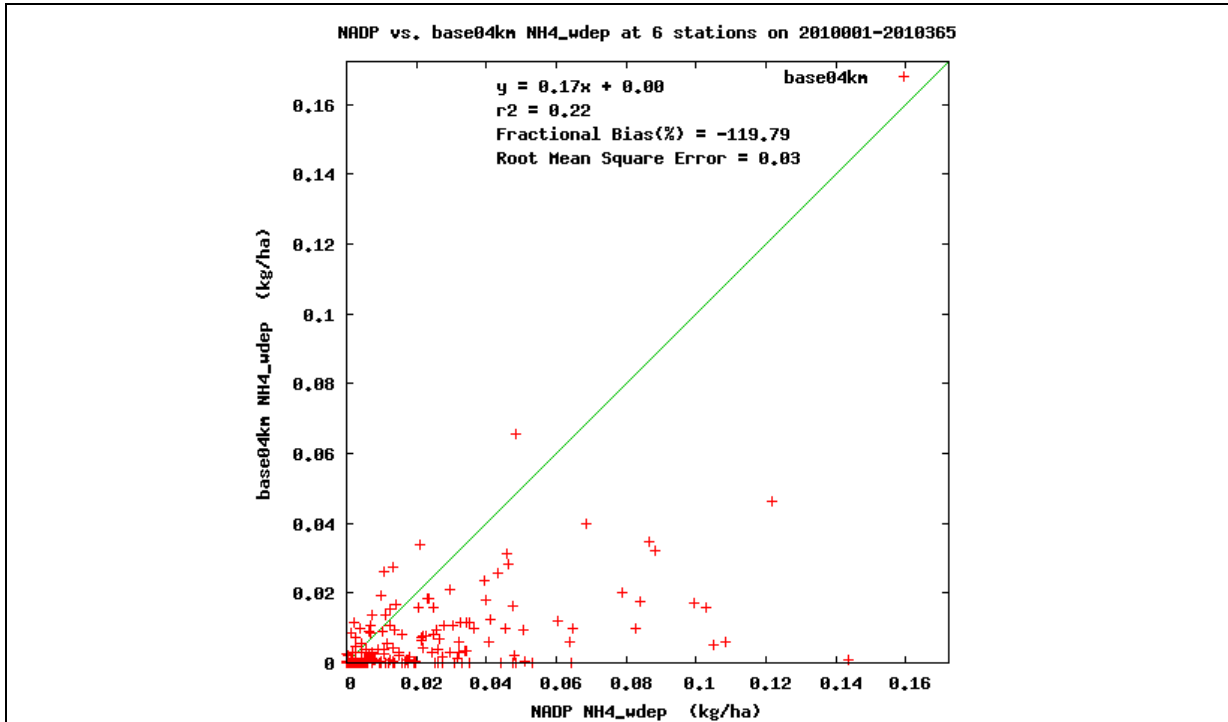**Figure B-41   CAMx Monthly Mean Fractional Bias for Ammonium**

Note: 4-km data shown in red.

Figure B-42   CAMx Scatter Plot for Ammonium Wet Deposition